Health Risk and Exposure Assessment for Ozone

Final Report

Chapter 4 Appendices

This page left intentionally blank

EPA-452/R-14-004b
August 2014

Health Risk and Exposure Assessment for Ozone

Final Report

Chapter 4 Appendices

U.S. Environmental Protection Agency
Office of Air and Radiation
Office of Air Quality Planning and Standards
Health and Environmental Impacts Division
Risk and Benefits Group
Research Triangle Park, North Carolina 27711

DISCLAIMER

This final document has been prepared by staff from the Risk and Benefits Group, Health and Environmental Impacts Division, Office of Air Quality Planning and Standards, U.S. Environmental Protection Agency. Any findings and conclusions are those of the authors and do not necessarily reflect the views of the Agency.

Questions related to this document should be addressed to Dr. Bryan Hubbell, U.S. Environmental Protection Agency, Office of Air Quality Planning and Standards, C539-07, Research Triangle Park, North Carolina 27711 (email: hubbell.bryan@epa.gov).

CHAPTER 4 APPENDICES

	Title	Pages
APPENDIX 4A:	Ambient Air Quality Monitoring Data	(4A-1 to 4A-37)
APPENDIX 4B:	Modeling Technical Support Document for the 2013 Ozone Risk and Exposure Assessment	(4B-1 to 4B-73)
APPENDIX 4C:	Air Quality Spatial Fields for the National Mortality Risk Burden Assessment	(4C-1 to 4C-18)
APPENDIX 4D:	Model-based Air Quality Adjustment Using the Higher-order Decoupled Direct Method (HDDM)	(4D-1 to 4D-179)
APPENDIX 4E:	Evaluation of Seattle Air Quality	(4E-1 to 4E-8)

This page left intentionally blank

APPENDIX 4A

Ambient Air Quality Monitoring Data

Table of Contents

4A-1. AMBIENT OZONE MONITORING AND AIR QUALITY DATA 4A-1

4A-1.1 Overview of Ambient Ozone Monitoring 4A-1

4A-1.2 Ambient Ozone Concentration Data 4A-3

4A-1.3 Data Handling 4A-5

4A-2. AIR QUALITY INPUTS FOR THE EXPOSURE AND CLINICAL-BASED RISK ASSESSMENTS 4A-9

4A-2.1 Urban Case Study Areas 4A-9

4A-2.2 Air Quality Inputs to the Air Pollutants Exposure (APEX) Model 4A-10

4A-2.3 Evaluation of Air Quality Spatial Field Techniques 4A-27

4A-3. AIR QUALITY INPUTS FOR THE EPIDEMIOLOGY-BASED RISK ASSESSMENT ……4A-31

4A-3.1 Urban Case Study Areas 4A-31

4A-3.2 Air Quality Inputs to the Benefits Mapping and Analysis Program (BenMAP)……..... 4A-33

4A-4. REFERENCES 4A-37

List of Tables

Table 4A-1. Information on the 15 Urban Case Study Areas in the Exposure and Clinical Risk Assessments. 4A-10
Table 4A-2. Information on the 12 Urban Case Study Areas in the Epidemiology Based Risk Assessment. 4A-32
Table 4A-3. Summary of the air quality inputs to BenMAP. 4A-36

List of Figures

Figure 4A-1. Map of U.S. ambient O_3 monitoring sites in operation during the 2006-2010 period. 4A-3
Figure 4A-2. Map of monitored 8-hour O_3 design values for the 2006-2008 period. 4A-8
Figure 4A-3. Map of monitored 8-hour O_3 design values for the 2008-2010 period. 4A-9
Figure 4A-4. Numerical example of the Voronoi Neighbor Averaging (VNA) technique.. 4A-11
Figure 4A-5. Maps of design values and May – September average MDA8 values based on VNA spatial fields for Atlanta. 4A-13
Figure 4A-6. Maps of design values and May – September average MDA8 values based on VNA spatial fields for Baltimore. 4A-14
Figure 4A-7. Maps of design values and May – September average MDA8 values based on VNA spatial fields for Boston. 4A-15
Figure 4A-8. Maps of design values and May – September average MDA8 values based on VNA spatial fields for Chicago. 4A-16
Figure 4A-9. Maps of design values and May – September average MDA8 values based on VNA spatial fields for Cleveland. 4A-17
Figure 4A-10. Maps of design values and May – September average MDA8 values based on VNA spatial fields for Dallas. 4A-18
Figure 4A-11. Maps of design values and May – September average MDA8 values based on VNA spatial fields for Denver. 4A-19
Figure 4A-12. Maps of design values and May – September average MDA8 values based on VNA spatial fields for Detroit. 4A-20
Figure 4A-13. Maps of design values and May – September average MDA8 values based on VNA spatial fields for Houston. 4A-21
Figure 4A-14. Maps of design values and May – September average MDA8 values based on VNA spatial fields for Los Angeles. 4A-22
Figure 4A-15. Maps of design values and May – September average MDA8 values based on VNA spatial fields for New York. 4A-23
Figure 4A-16. Maps of design values and May – September average MDA8 values based on VNA spatial fields for Philadelphia. 4A-24
Figure 4A-17. Maps of design values and May – September average MDA8 values based on VNA spatial fields for Sacramento. 4A-25

Figure 4A-18. Maps of design values and May – September average MDA8 values based on VNA spatial fields for St. Louis. 4A-26
Figure 4A-19. Maps of design values and May – September average MDA8 values based on VNA spatial fields for Washington, D.C. 4A-27
Figure 4A-20. Maps of monitored values (left), nearest neighbor spatial fields (center), and VNA spatial fields (right) for selected hours in Atlanta (top), and Philadelphia (bottom)……...4A-28
Figure 4A-21. Density scatter plots and performance statistics for the cross-validation analysis of nearest neighbor (NN; left) and Voronoi Neighbor Averaging (VNA; right) spatial field techniques applied to monitored hourly O_3 concentrations in Atlanta, 2005…..... 4A-29
Figure 4A-22. Density scatter plots and performance statistics for the cross-validation analysis of nearest neighbor (NN; left) and Voronoi Neighbor Averaging (VNA; right) spatial field techniques applied to monitored hourly O_3 concentrations in Detroit, 2005…..... 4A-30
Figure 4A-23. Density scatter plots and performance statistics for the cross-validation analysis of nearest neighbor (NN; left) and Voronoi Neighbor Averaging (VNA; right) spatial field techniques applied to monitored hourly O_3 concentrations in Philadelphia, 2005..... 4A-30

4A-1. AMBIENT OZONE MONITORING AND AIR QUALITY DATA

This section provides a brief overview of ambient O_3 monitoring in the U.S. (Section 4A-1.1), the ambient O_3 concentration data extracted for use in the risk and exposure assessments (Section 4A-1.2), and the data handling procedures used for determining compliance with the existing and potential alternative standards as well as some other relevant air quality metrics (Section 4A-1.3).

4A-1.1 Overview of Ambient Ozone Monitoring

The Clean Air Act establishes air quality monitoring requirements to provide information on ambient concentrations for six criteria pollutants, including O_3, and makes provisions for the collection of other ambient air quality measurements, such as O_3 precursors. The federal regulations for ambient air quality monitoring, including establishment and periodic assessment of local monitoring networks, approved monitoring methods, operating schedules, and protocols for data reporting, quality assurance, and certification, are in Part 58 of the Code of Federal Regulations.

There were over 1,300 ambient O_3 monitoring sites actively operating in the U.S. in 2010. These monitoring sites are operated by over 100 federal, state, local, and tribal agencies, and can be grouped into one of the following networks:

1) State and Local Air Monitoring Stations (SLAMS): Monitoring sites operated by state, local, and tribal governments for the purposes of determining compliance with the National Ambient Air Quality Standards (NAAQS), and providing ambient air quality information to help state and local public health agencies evaluate and implement air quality control programs. There were over 1,100 SLAMS O_3 monitoring sites operating in 2010, making up over 80% of the U.S. ambient O_3 monitoring network. There are two important subcategories of SLAMS monitors:
    a. National Multi-pollutant Monitoring Network (NCore): Approximately 80 monitoring sites (60 urban and 20 rural) operated by state and local agencies. These sites monitor six criteria pollutants (CO, NO_2, O_3, SO_2, PM_{10}, and $PM_{2.5}$) and other important parameters for the purposes of assessing multi-pollutant impacts on public health, and supporting air quality forecasting.
    b. Photochemical Assessment Monitoring Stations (PAMS): Approximately 80 monitoring sites operated by state and local agencies with EPA funding. These sites monitor O_3 and its precursors, including NO, NO_2, total NO_x, total reactive nitrogen (NO_y), and over 60 volatile organic compounds (VOCs) for the purposes of understanding O_3 chemistry and transport, aiding photochemical modeling, and

evaluating O_3 precursor emissions control strategies in areas designated nonattainment for the O_3 NAAQS. Some PAMS monitoring sites are co-located with NCore monitoring sites.

2) Clean Air Status and Trends Network (CASTNET): Approximately 80 O_3 monitoring sites operated year-round by EPA and the National Park Service (NPS) for the purpose of determining O_3 levels in national parks and other rural areas.
3) Special Purpose Monitoring Stations (SPMS): These monitoring sites are used to support various air quality monitoring objectives, such as specific public health and welfare impacts studies, model evaluation, or monitoring network assessments. These monitoring sites are often operated on a temporary basis (up to 24 months), and are generally not used to determine compliance with the NAAQS. Some of these monitoring sites may be operated by local industry or other private interest groups.

SLAMS monitoring sites are required to monitor for O_3 only during the required O_3 monitoring season, which is defined for each state in Table D-3 of 40 CFR Part 58. Many states also operate their O_3 monitors outside of the required O_3 monitoring season. States that are required to operate some or all of their O_3 monitors on a year-round basis include Arizona, California, Hawaii, Louisiana, New Mexico, and Texas. EPA regional offices may approve waivers effectively shortening the length of the required O_3 monitoring season for some individual monitoring sites (e.g. rural monitoring sites which may be inaccessible during the winter months). CASTNET and NCore monitoring sites are typically operated on a year-round basis.

The Federal Reference Method (FRM) for O_3 measurement is the Chemiluminescence Method (CLM). The first ultraviolet (UV) absorption photometric analyzers were approved as Federal Equivalent Methods (FEMs) in 1977 and gained rapid acceptance for NAAQS compliance purposes due to ease of operation, relatively low cost, and reliability. All SLAMS and CASTNET O_3 monitoring sites in the U.S. have been operating UV analyzers since 2005.

Figure 4A-1 shows the locations of the ambient O_3 monitoring sites used in the risk and exposure assessments. Gray dots represent SLAMS monitoring sites, green dots represent CASTNET sites, blue dots represent NCore and/or PAMS monitoring sites, and black dots represent SPMS and other monitoring sites for which data were available.

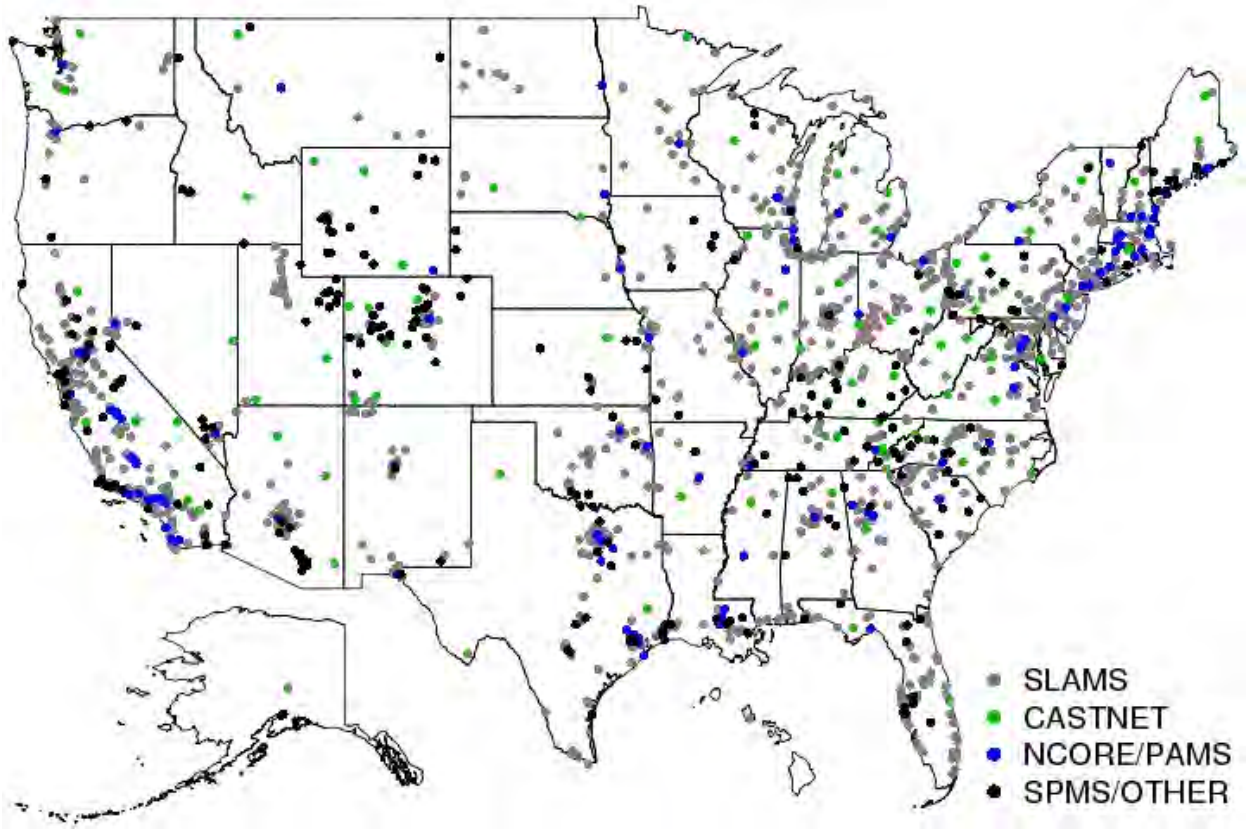

Figure 4A-1. Map of U.S. ambient O_3 monitoring sites in operation during the 2006-2010 period.

4A-1.2 Ambient Ozone Concentration Data

EPA's Air Quality System (AQS) database is a national repository for many types of air quality and related monitoring data. AQS contains monitoring data for the six criteria pollutants dating back to the 1970's, as well as more recent additions such as $PM_{2.5}$ speciation, air toxics, and meteorology data. As of 2010, over 100 federal, state, local, and tribal agencies submitted hourly O_3 concentration data collected from over 1,300 ambient monitoring sites to AQS.

Air quality monitoring data from 1,468 ambient O_3 monitoring sites in the U.S. were extracted for use in the risk and exposure assessments. The initial dataset consisted of hourly O_3 concentrations in ppb collected from these monitors between 1/1/2006 and 12/31/2010. Data for nearly 1,400 of these monitors were extracted from the AQS database in October 2012, and the remaining data were extracted from the CASTNET database at the same time. CASTNET monitors operated by the National Park Service were included in the data extracted from AQS, but the CASTNET monitors operated by EPA did not begin reporting data to AQS until 2011. Data collected from these EPA operated CASTNET monitors prior to 2011 did not meet EPA's quality assurance requirements, but the data were subject to quality assurance criteria, and it is

generally agreed that data collected from CASTNET monitors prior to 2011 is of comparable quality to the regulatory data stored in AQS.

There were a number of subtle, yet noteworthy differences between the air quality data used in the 1st draft REA and the air quality data used in this draft.

1. In the 1st draft REA, multiple AQS data extractions were used for the air quality inputs to various parts of the risk and exposure assessments. In this draft, all air quality inputs were derived from the data extraction described above.
2. In the 1st draft REA, data collected from EPA operated CASTNET sites and other non-regulatory monitoring sites were not included in the air quality inputs to the risk and exposure assessments. In this draft, these monitors were included, but were not used to make determinations of meeting the existing standard or the potential alternative standards.
3. In the 1st draft REA, data collected with O_3 analyzers not using federal reference or equivalent methods were not included in the air quality inputs to the risk and exposure assessments. In this draft, these monitors were included, but were not used to make determinations of meeting the existing standard or the potential alternative standards.
4. In the 1st draft REA, reported hourly O_3 concentrations lower than the minimum detection limit (MDL, 5 ppb for most O_3 analyzers) were replaced with a value of ½ MDL. This is called the "standard sample value" for criteria pollutant data extracted from AQS. In this draft, the actual reported sample values were used, effectively allowing concentrations down to 0 ppb.
5. In the 1st draft REA, hourly O_3 concentrations flagged by the monitoring agencies and concurred by EPA as having been affected by exceptional events were removed from the air quality inputs to the risk and exposure assessments. In this draft, these data were included, but were not used to make determinations of meeting the existing standard or the potential alternative standards, which is consistent with EPA's exceptional events policy.
6. In this draft, missing data gaps of 1 or 2 hours in length were filled in using linear interpolation. These short gaps often occur at regular intervals in the ambient data due to an EPA requirement for monitoring agencies to perform routine quality control checks on their O_3 monitors. Quality control checks are typically performed between midnight and 6:00 AM when O_3 concentrations are low. Missing data gaps of 3 hours or more in length were not replaced, and interpolated values were not used to make determinations of meeting the existing standard or the potential alternative standards.
7. In this draft, hourly O_3 concentrations from 7 monitoring sites where multiple O_3 analyzers were operated simultaneously in the same physical location were combined to

create a single hourly site record using the highest reported hourly concentration in each hour.

8. In some instances, EPA regional offices may approve the data combinations for pairs of nearby O_3 monitoring sites affected by short distance site relocations for the purpose of making NAAQS determinations. In this draft, hourly O_3 concentrations from 12 such pairs of monitoring sites were combined to create a single hourly site record for each pair.

4A-1.3 Data Handling

To determine whether or not the NAAQS have been met at an ambient air quality monitoring site, a statistic commonly referred to as a "design value" must be calculated based on 3 consecutive years of data collected from that site. The form of the existing O_3 NAAQS design value statistic is the 3-year average of the annual 4th highest daily maximum 8-hour O_3 concentration in ppb, with all decimal digits truncated. The existing O_3 NAAQS are met at an ambient monitoring site when the design value is less than or equal to 75 ppb. The data handling protocols for calculating design values for the existing O_3 NAAQS are in 40 CFR Part 50, Appendix P. In counties or other geographic areas with multiple monitors, the area-wide design value is defined as the design value at the highest individual monitoring site, and the area is said to have met the NAAQS if all monitors in the area are meeting the NAAQS. The initial hourly O_3 concentration dataset was split into two design value periods, 2006-2008 and 2008-2010, and subsequent analyses were conducted independently for these two periods. The following daily summary statistics were calculated from the hourly O_3 concentrations:

1. Daily Maximum 8-hour Average (MDA8) Concentration: There are 24 consecutive 8-hour periods in each day (midnight – 8:00 AM, 1:00 AM – 9:00 AM, ..., 11:00 PM – 7:00 AM). Rolling 8-hour averages were calculated for each period with 6, 7, or 8 hours of data available, using 6, 7, or 8 as the divisor, respectively, and 8-hour periods with fewer than 6 hours of data available were not used. The 8-hour average values were stored in the 1st, or start, hour of the 8-hour period. The MDA8 value is the highest of the 8-hour average values for each day, and the MDA8 values for two consecutive days may have some hours in common. MDA8 values were considered to be valid if there were sufficient data available to calculate at least 18 of 24 possible 8-hour averages, or, if used for design value calculations, if the MDA8 value is greater than the level of the standard. This is the daily metric used in design values and the Smith et al. (2009) short-term mortality study.
2. Daily 10:00 AM – 6:00 PM Mean Concentration: This is the rolling 8-hour average value as defined above for the 8-hour period starting at 10:00 AM. This is the daily metric used in the Zanobetti and Schwartz, 2008 short-term mortality study.

3. Daily Maximum 1-hour Concentration: This is the highest hourly O_3 concentration reported during a given day. Daily Maximum 1-hour values were considered to be valid if there were at least 18 hourly O_3 concentrations reported in a given day. This is the daily metric used in the Jerrett et al. (2009) long-term mortality study.
4. Daily 24-hour Average Concentration: This is the simple arithmetic average of the hourly O_3 concentrations reported during a given day. Daily 24-hour average values were considered to be valid if there were at least 18 hourly O_3 concentrations reported in a given day. This is the daily metric used in the Bell et al. (2004) short-term mortality study.

The daily summary statistics described above were then used to calculate the following annual summary statistics:

1. Annual 4th Highest MDA8 Concentration: This is the 4th highest valid MDA8 value measured at a given monitoring site in a given year. The 4th highest MDA8 values were considered to be valid if there were valid MDA8 values available for at least 75% of the days in the required O_3 monitoring season, or, if used for design value calculations, if the 4th highest MDA8 value was greater than the level of the standard. Data collected outside of the required O_3 monitoring season were used in determining the 4th highest MDA8 value, but were not used in determining validity.
2. May – September Average MDA8: This is the average of all available valid MDA8 values at a given monitoring site during the May – September period (153 days). The May – September average MDA8 values were considered to be valid if valid MDA8 values were available for at least 114 days (75%) in May – September of a given year. Three-year averages of these values were calculated for the 2006-2008 period and used to create the May – September average MDA8 national fused air quality surface described in Appendix 4C. This surface was then used in the national-scale risk assessment based on Smith et al. (2009) described in the Health Risk and Exposure Assessment (HREA) Chapter 8.
3. June – August Average Daily 10:00 AM – 6:00 PM Mean: This is the average of all available daily 10:00 AM – 6:00 PM mean values at a given monitoring site during the June – August period (92 days). The June – August average daily mean values were considered to be valid if daily 10:00 AM – 6:00 PM mean values were available for at least 70 days (75%) in June – August of a given year. Three-year averages of these values were calculated for the 2006-2008 period and used to create the June – August average daily 10:00 AM – 6:00 PM mean national fused air quality surface described in

Appendix 4C. This surface was then used in the national-scale risk assessment based on Zanobetti and Schwartz (2008) described in HREA Chapter 8.

4. April – September Average Daily Maximum 1-hour Concentration: This is the average of all available valid daily maximum 1-hour values at a given monitoring site during the April – September period. The April – September average daily maximum 1-hour values were considered to be valid if valid daily maximum 1-hour values were available for at least 137 days (75%) in April – September of a given year. Three-year averages of these values were calculated for the 2006-2008 period and used to create the April - September average daily maximum 1-hour national fused air quality surface described in Appendix 4C. This surface was then used in the national-scale risk assessment based on Jerrett et al. (2009) described in HREA Chapter 8.

The design value statistic for the existing O_3 standard is the 3-year average of the annual 4th highest MDA8 values described above. Design values greater than the level of the existing standard (76 ppb or higher) are automatically valid. Design values less than or equal to the level of the existing standard must be based on 3 valid 4th highest MDA8 values, with the additional requirement that the 3-year average of the annual data completeness statistics (percent of valid MDA8 values within the required O_3 monitoring season) must be at least 90%. These same criteria were chosen to determine design values for the potential alternative standards. The implications of this choice are that in some cases, a monitoring site may have different design values based on the level of the standard. This may occur for one of two reasons:

1. A monitoring site with insufficient data to determine a design value at higher standard level may have sufficient data to show a violation at a lower standard level. For example, if a monitoring site has a 3-year average annual 4th highest MDA8 value of 72 ppb, but does not meet the data completeness criteria described above, then the site has a design value of 72 ppb for the potential alternative standards of 70 ppb, 65 ppb, and 60 ppb, but does not have a design value for the existing standard of 75 ppb.
2. EPA's current practice is to use only "valid" MDA8 values when determining the annual 4th highest MDA8 value. A valid MDA8 value is either based on at least 18 of 24 possible 8-hour average values, or it is greater than the level of the standard. This can cause the design value to change based on the level of the standard, due to whether certain days are considered valid or not. For example, suppose the five highest MDA8 values at a particular monitoring site for a given year are 78 ppb, 76 ppb, 75 ppb, 74 ppb, and 70 ppb, but the 4th highest value is based on only 12 valid 8-hour averages. Then for the existing standard, the 4th highest MDA8 value is 70 ppb, but for the 70 ppb alternative standard, the 4th highest MDA8 value is 74 ppb.

Figure 4A-2 and Figure 4A-3 show the design values for the existing O_3 NAAQS for all regulatory monitoring sites in the U.S. for the 2006-2008 and 2008-2010 periods, respectively. In general, O_3 design values were lower in 2008-2010 than in 2006-2008, especially in the Eastern U.S. There were 518 O_3 monitors in the U.S. with design values above the existing standard in 2006-2008, compared to only 179 in 2008-2010.

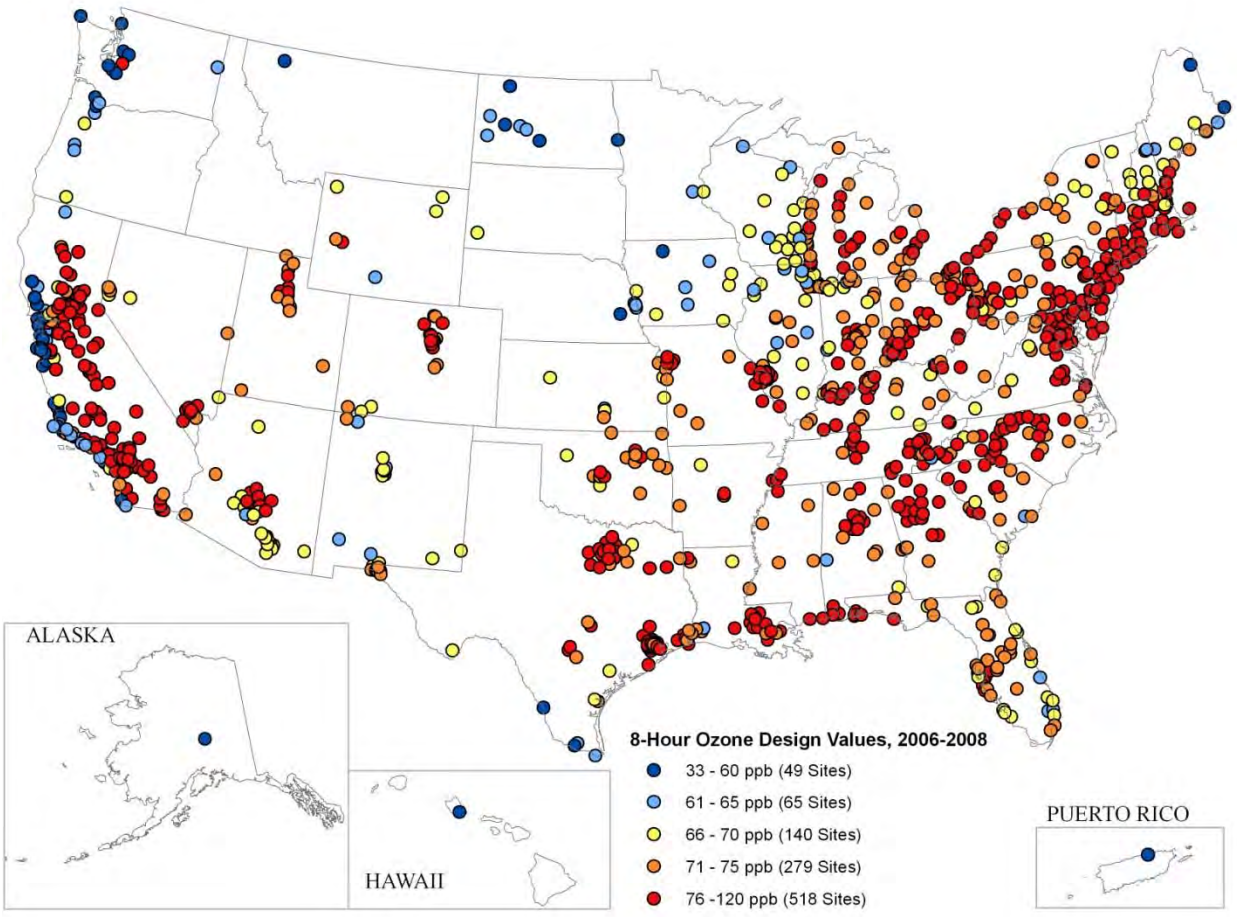

Figure 4A-2. Map of monitored 8-hour O_3 design values for the 2006-2008 period.

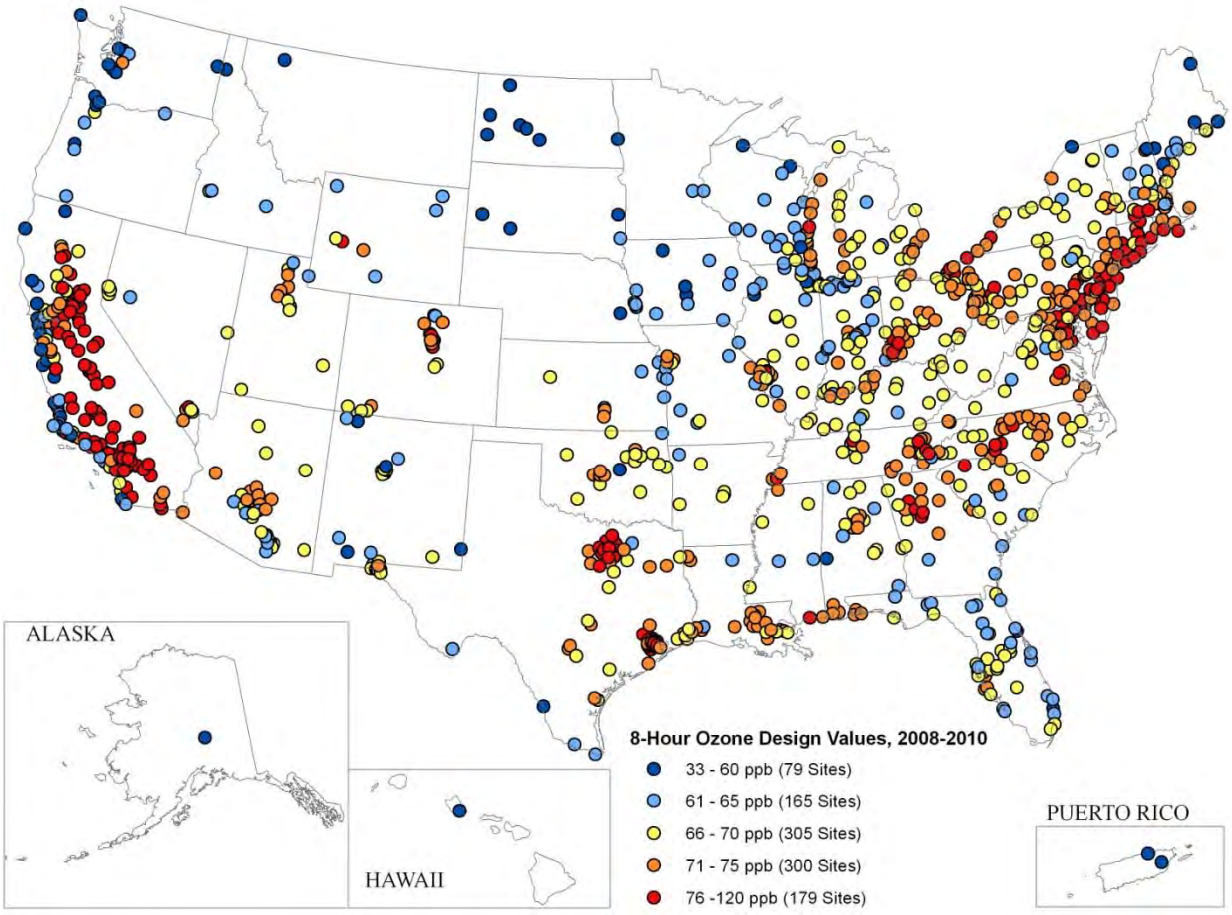

Figure 4A-3. Map of monitored 8-hour O_3 design values for the 2008-2010 period.

4A-2. AIR QUALITY INPUTS FOR THE EXPOSURE AND CLINICAL-BASED RISK ASSESSMENTS

This section describes the 15 urban case study areas used in the exposure and clinical risk assessments described in the HREA Chapters 5 and 6 (Section 4A-2.1), the hourly O_3 concentration spatial fields used as inputs to the Air Pollutants Exposure Model (APEX; Section 4A-2.2), and some methods evaluations supporting the change from nearest neighbor to the Voronoi Neighbor Averaging (VNA) technique for generating the spatial fields (Section 4A-2.3).

4A-2.1 Urban Case Study Areas

The 15 urban case study areas in the exposure (HREA Chapter 5) and clinical risk (HREA Chapter 6) assessments covered a large spatial extent, with boundaries generally similar to those covered by the respective Combined Statistical Areas (CSA) defined by the U.S. Census Bureau. Table 4A-1 gives some basic information about the 15 urban case study areas in the

exposure and clinical risk assessments, including the number of counties, number of ambient O_3 monitoring sites, the required O_3 monitoring season, and the 2006-2008 and 2008-2010 design values. All 15 urban case study areas had 8-hour O_3 design values above the existing standard in 2006-2008, while 13 areas had 8-hour O_3 design values above the existing standard in 2008-2010. Chicago (74 ppb) and Detroit (75 ppb) had design values meeting the existing standard during the 2008-2010 period. The design values in the 15 urban areas decreased by an average of 6 ppb between 2006-2008 and 2008-2010, ranging from no change in Sacramento to a decrease of 15 ppb in Atlanta.

Table 4A-1. Information on the 15 Urban Case Study Areas in the Exposure and Clinical Risk Assessments.

Area Name	# of Counties	# of O_3 Monitors	Population (2010)	Required O_3 Monitoring Season	2006-2008 DV (ppb)	2008-2010 DV (ppb)
Atlanta	33	13	5,618,431	March - October	95	80
Baltimore	7	7	2,710,489	April - October	91	89
Boston	10	14	5,723,468	April - September	83	77
Chicago	16	26	9,686,021	April - October	78	74
Cleveland	8	13	2,881,937	April - October	82	77
Dallas	11	20	6,366,542	January - December	89	86
Denver	13	26	3,390,504	March - September	86	77
Detroit	9	12	5,218,852	April - September	81	75
Houston	10	22	5,946,800	January - December	91	85
Los Angeles	5	54	17,877,006	January - December	119	112
New York	27	31	21,056,173	April - October	90	84
Philadelphia	15	19	7,070,622	April - October	92	83
Sacramento	7	26	2,755,972	January - December	102	102
St. Louis	17	17	2,837,592	April - October	85	77
Washington	26	22	5,838,518	April - October	87	81

4A-2.2 Air Quality Inputs to the Air Pollutants Exposure (APEX) Model

The Air Pollutants Exposure Model (APEX) described in HREA Chapter 5 requires spatial fields of air quality concentrations with no missing values as inputs. In the 1st draft REA, the spatial fields were generated using hourly O_3 concentrations from the nearest available monitoring site for each census tract in four of the 15 urban case study areas (Atlanta, Denver, Los Angeles, and New York). Here, the spatial fields were generated with hourly O_3 concentrations interpolated using the Voronoi Neighbor Averaging (VNA; Gold, 1997; Chen et al., 2004) technique described below for each census tract in the 15 urban case study areas. The following paragraphs provide a numerical example of VNA used to estimate an O_3 concentration value for census tract "E" in Figure 4A-4 below.

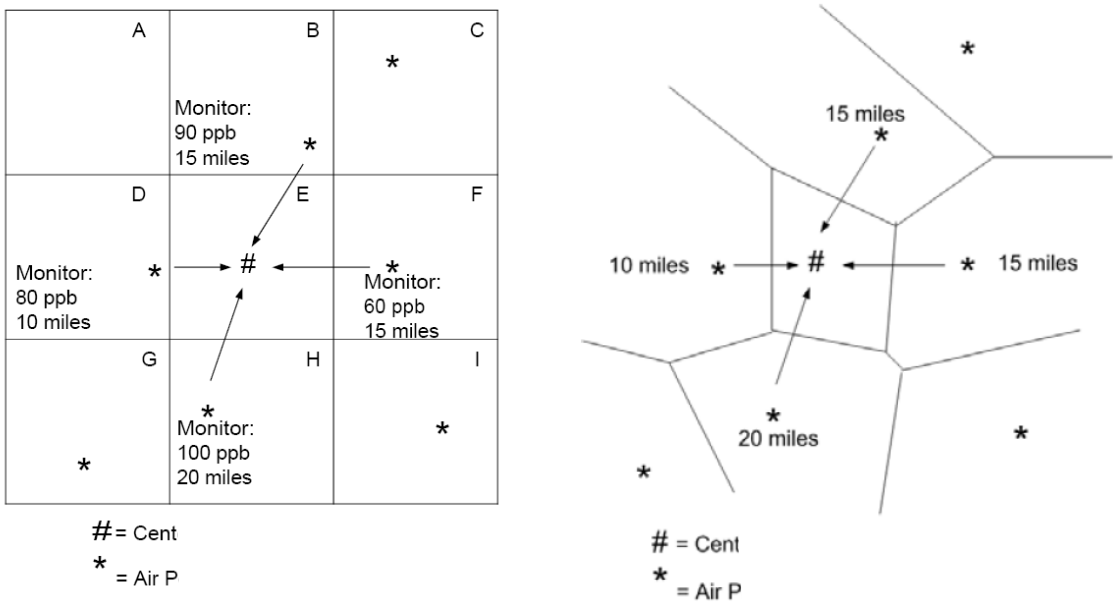

Figure 4A-4. Numerical example of the Voronoi Neighbor Averaging (VNA) technique.

The first step in the VNA technique is to identify the set of nearest monitors for each census tract. The left-hand panel of Figure 4A-4 presents a numerical example with nine census tracts (squares) and seven monitoring sites (stars), with the focus on identifying the set of nearest neighboring sites to census tract "E" in the center of the panel. The Delaunay triangulation algorithm identifies the set of nearest neighboring monitors by drawing a set of polygons called the "Voronoi diagram" around the census tract "E" centroid and each of the monitoring sites. Voronoi diagrams have the special property that each edge of each of the polygons are the same distance from the two closest points, as shown in the right-hand panel of Figure 4A-4.

The VNA technique then chooses the monitoring sites whose polygons share a boundary with the census tract "E" centroid. These monitors are the "Voronoi neighbors", which are used to estimate the concentration value for census tract "E". The VNA estimate of the concentration value in census tract "E" is the inverse distance squared weighted average of the four monitored concentrations. The further the monitor is from the center of census tract "E", the smaller the weight. For example, the weight for the monitor in census tract "D" 10 miles from the census tract "E" centroid is calculated as follows:

$$\frac{1/10^2}{1/10^2+1/15^2+1/15^2+1/20^2} = \mathbf{0.4675} \qquad \text{Equation (4A-1)}$$

The weights for the other monitors are calculated in a similar fashion. The final VNA estimate for census tract "E" is calculated as follows:

$$VNA(E) = 0.4675 * 80 + 0.2078 * 90 + 0.2078 * 60 + 0.1169 * 100 = 80.3\ ppb$$

Equation (4A-2)

The observed hourly O_3 concentrations in the 15 urban case study areas were used to calculate VNA estimates for approximately 24,935 census tracts * 43,824 hours ≈ 1.1 billion values. The actual number of values was lower than this, because values were not calculated for hours outside the required monitoring season. However, the same VNA procedure was also used to create hourly spatial surfaces based on air quality adjusted to meet the existing standard of 75 ppb, and air quality adjusted to meet the potential alternative standards of 70 ppb, 65 ppb, 60 ppb, and 55 ppb, which effectively increased the total number of VNA estimates by roughly a factor of 5. The computations were executed using the R statistical computing program (R, 2012), with the Delaunay triangulation algorithm implemented in the "deldir" package (Turner, 2012).

Figure 4A-5 through Figure 4A-19 show maps of the 2006-2008 and 2008-2010 design values and May–September "seasonal" average MDA8 values in the 15 urban case study areas based on the VNA spatial fields. The top panels in each figure show the design values, while the bottom panels show the seasonal average values. The left-hand panels in each figure show the 2006-2008 values, while the right-hand panels show the 2008-2010 values. The colored circles in each panel represent census tract centroids, and the colored squares represent monitoring sites. In each panel, counties colored pink indicate the study area boundaries used in the Zanobetti and Schwartz (2008) and/or Smith et al. (2009b) epidemiology studies[1], where applicable. Counties colored gray indicate additional counties within the CBSA boundaries, and counties colored peach indicate any additional counties included in the exposure and lung function risk assessments. Note that the maps show some monitors outside of the study area boundaries. This is because the VNA surfaces were generated using data from monitors within a 50 km radius of the study area boundaries, in addition to the monitors inside the study areas.

[1] The Zanobetti and Schwartz (2008) and Smith et al. (2009) study area boundaries were identical for 6 of the 12 urban case study areas, and had at least one county in common for all 12 urban case study areas. The counties colored pink in Figures 4A-5 through 4A-19 refer to counties included in either of those two studies.

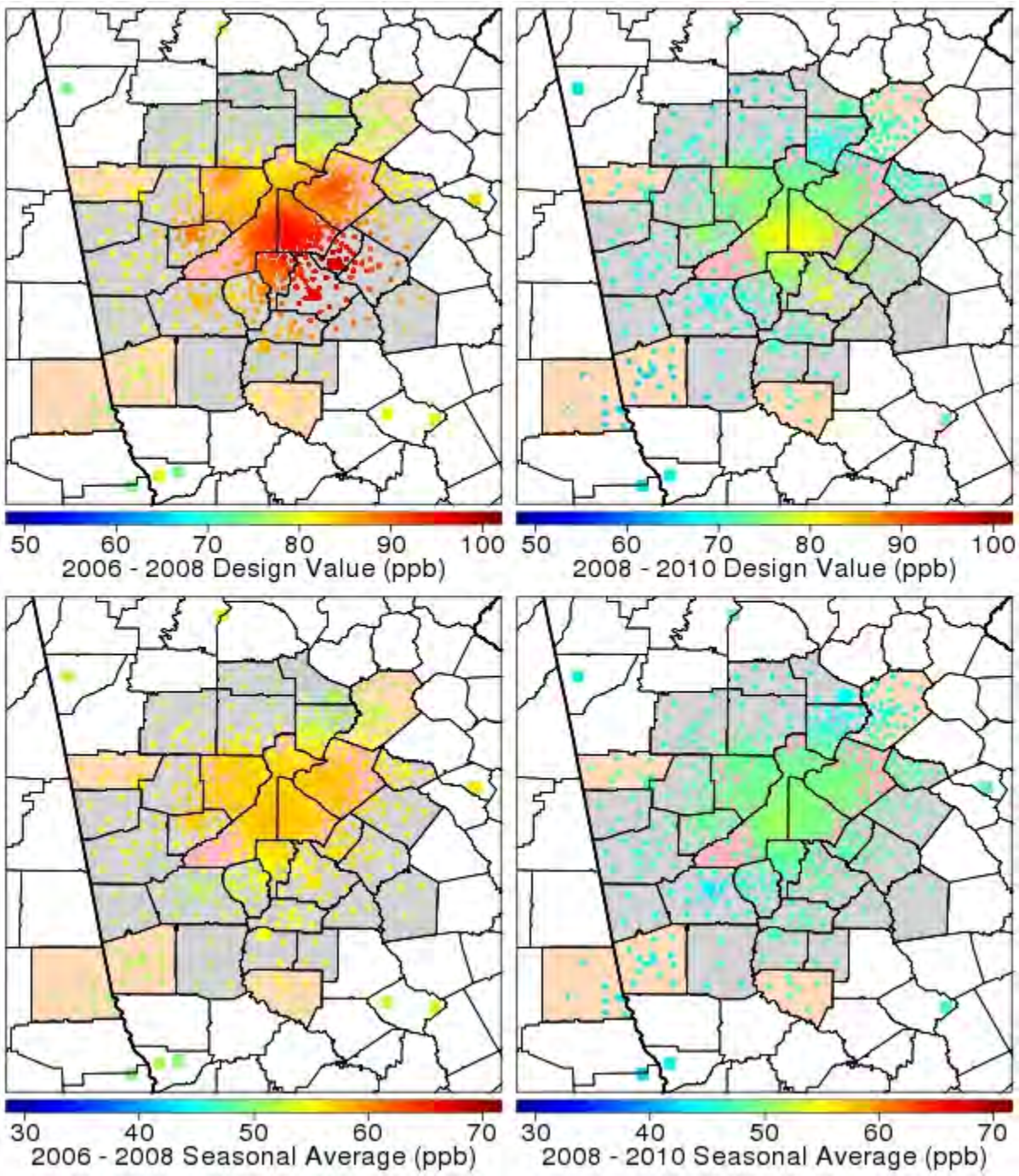

Figure 4A-5. Maps of design values and May – September average MDA8 values based on VNA spatial fields for Atlanta.

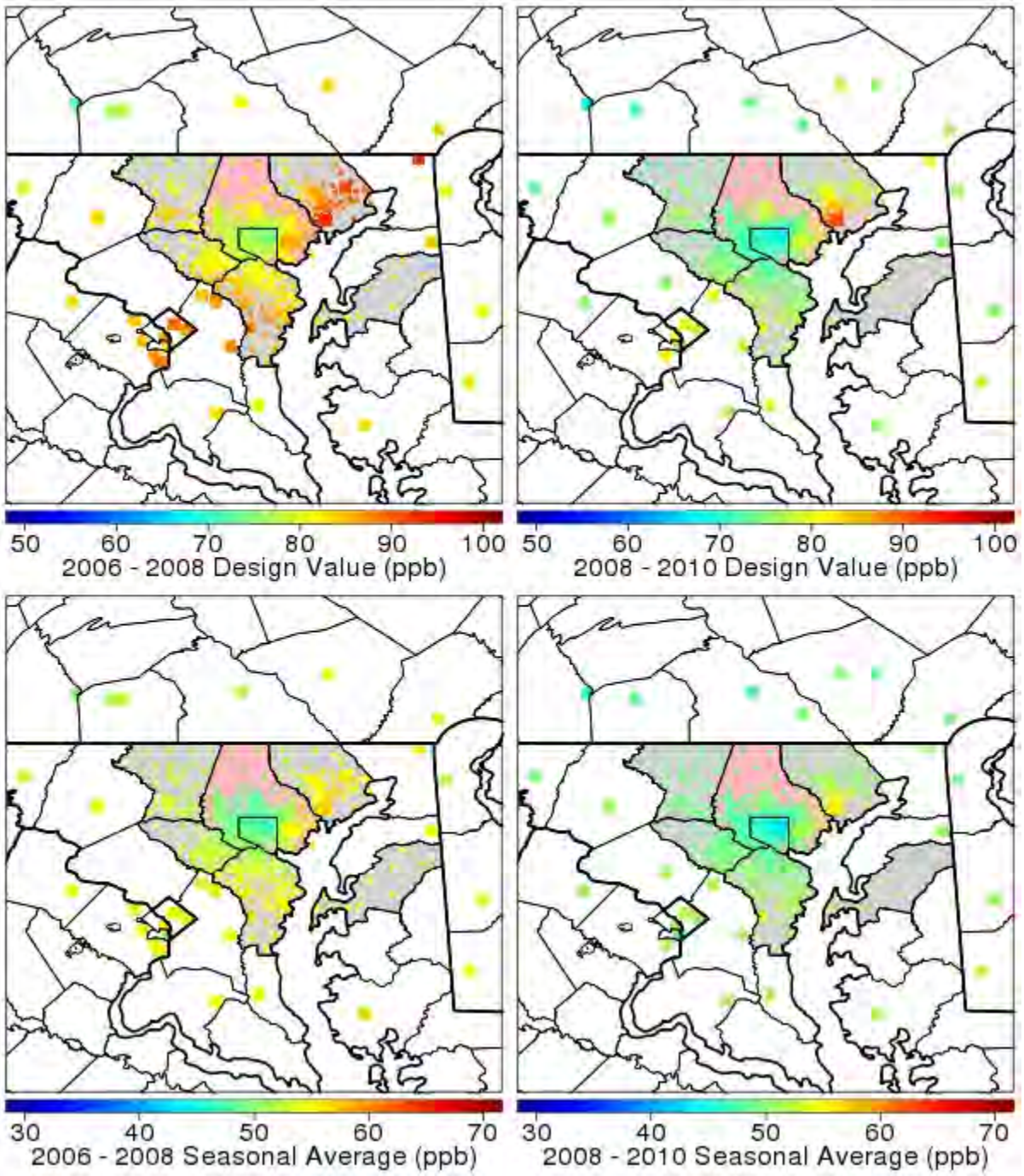

Figure 4A-6. Maps of design values and May – September average MDA8 values based on VNA spatial fields for Baltimore.

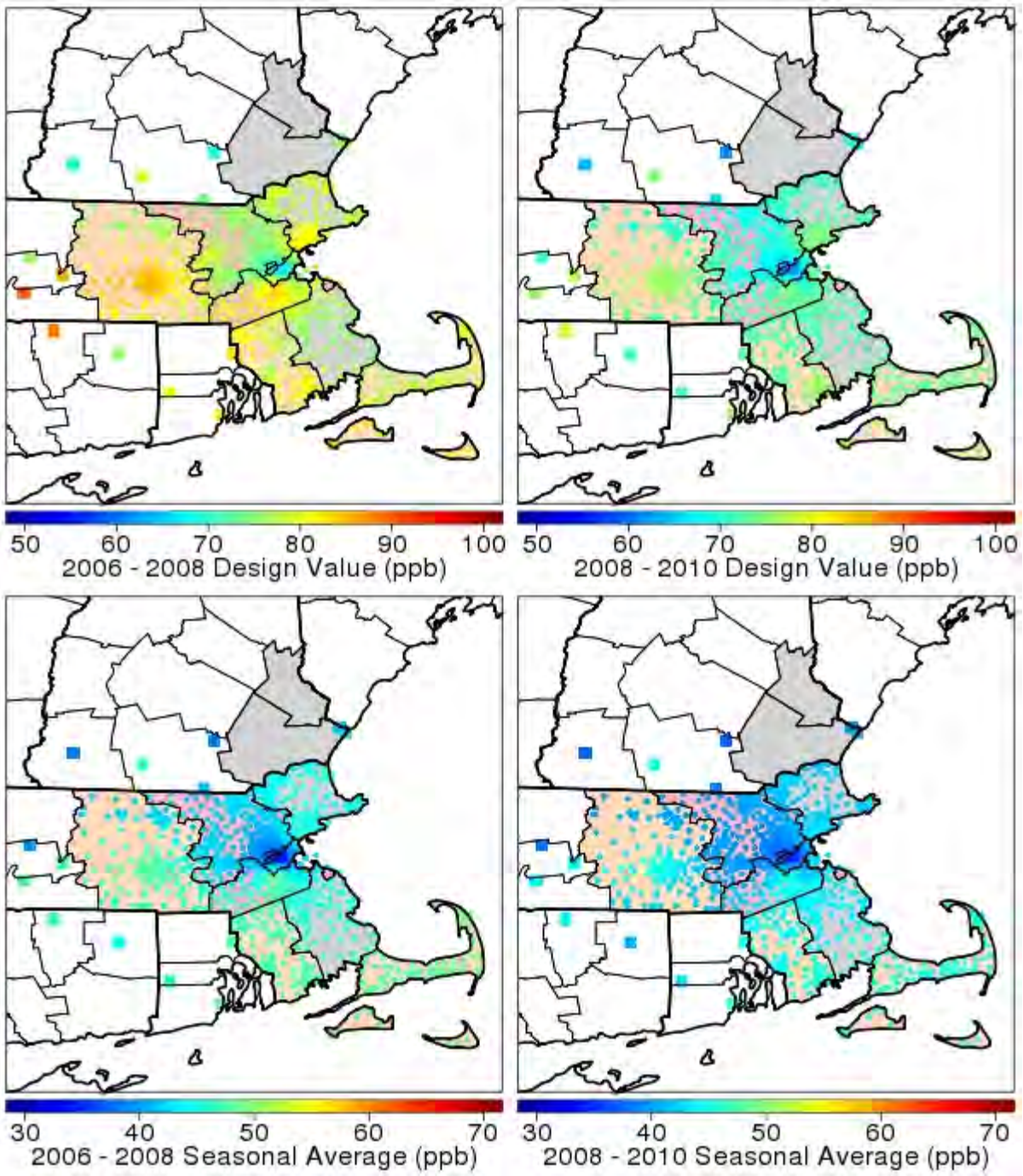

Figure 4A-7. Maps of design values and May – September average MDA8 values based on VNA spatial fields for Boston.

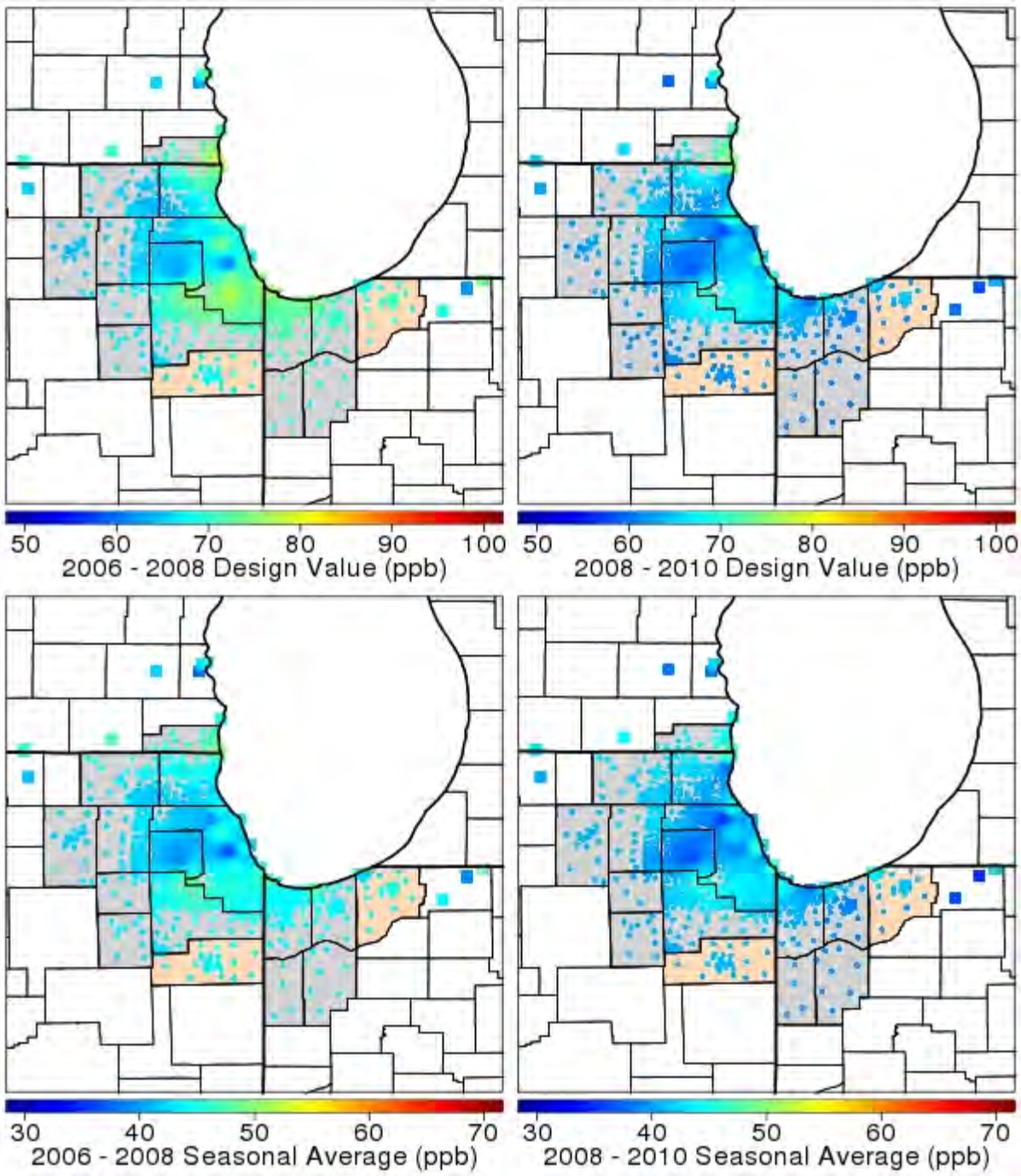

Figure 4A-8. Maps of design values and May – September average MDA8 values based on VNA spatial fields for Chicago.

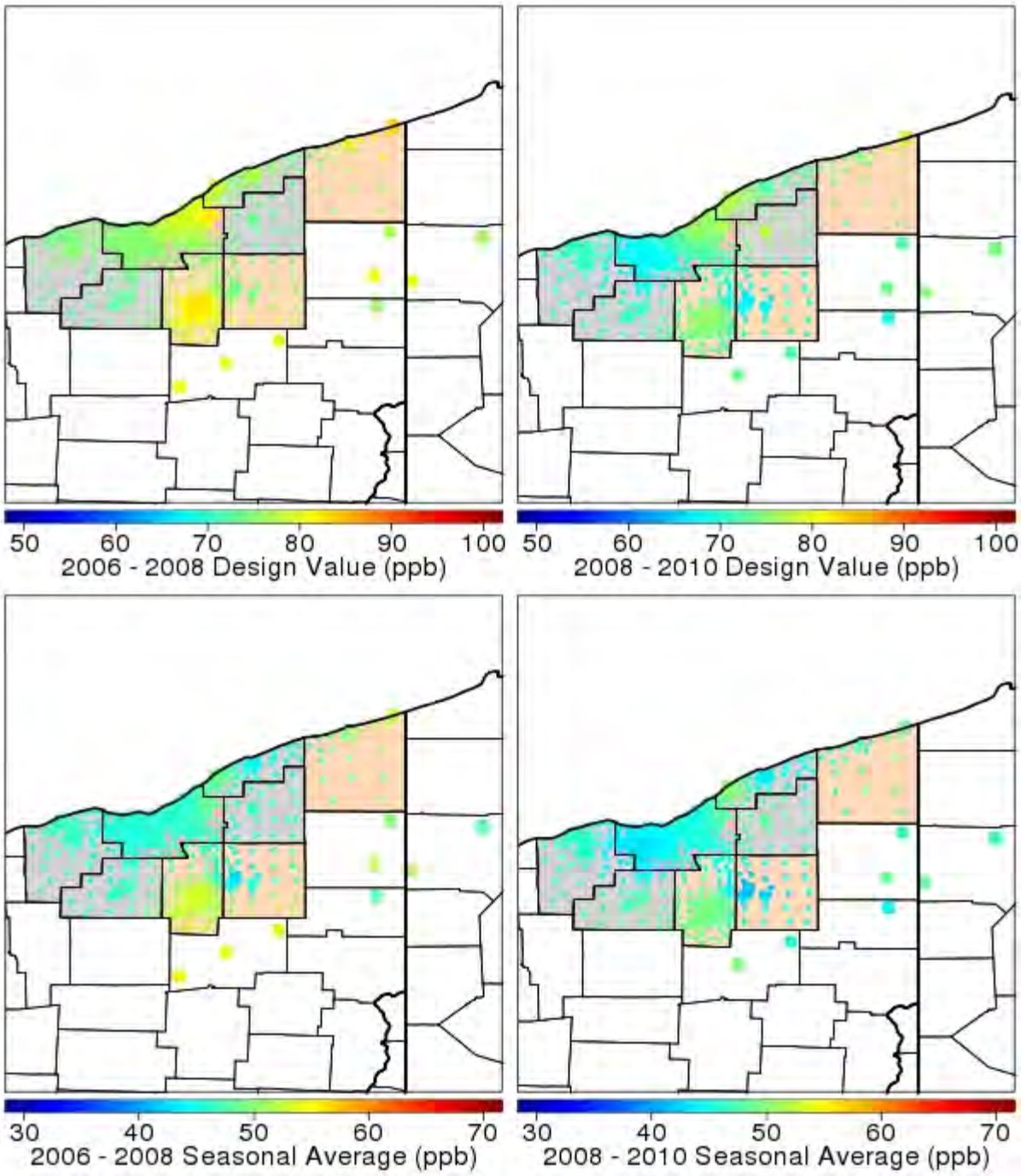

Figure 4A-9. Maps of design values and May – September average MDA8 values based on VNA spatial fields for Cleveland.

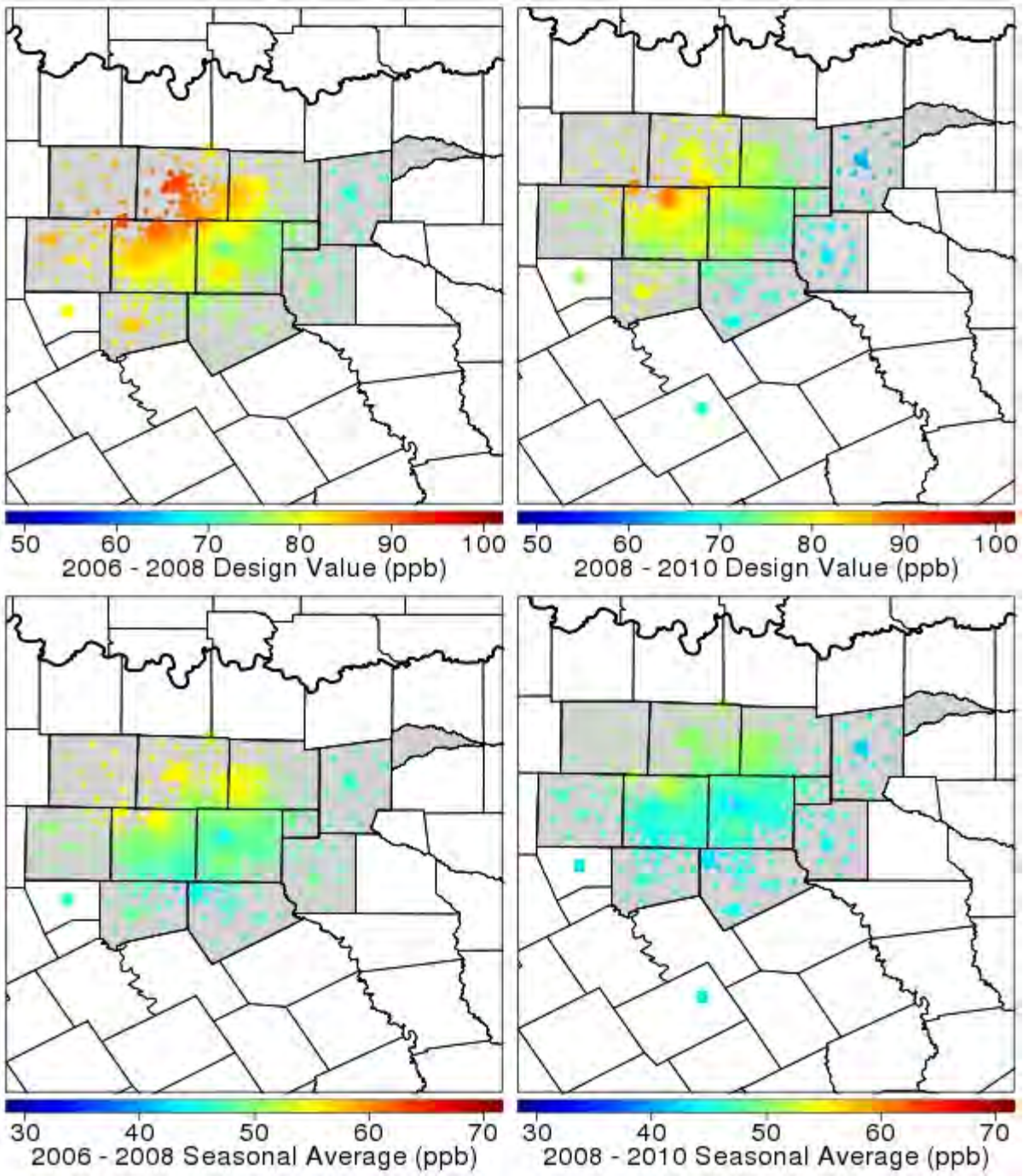

Figure 4A-10. Maps of design values and May – September average MDA8 values based on VNA spatial fields for Dallas.

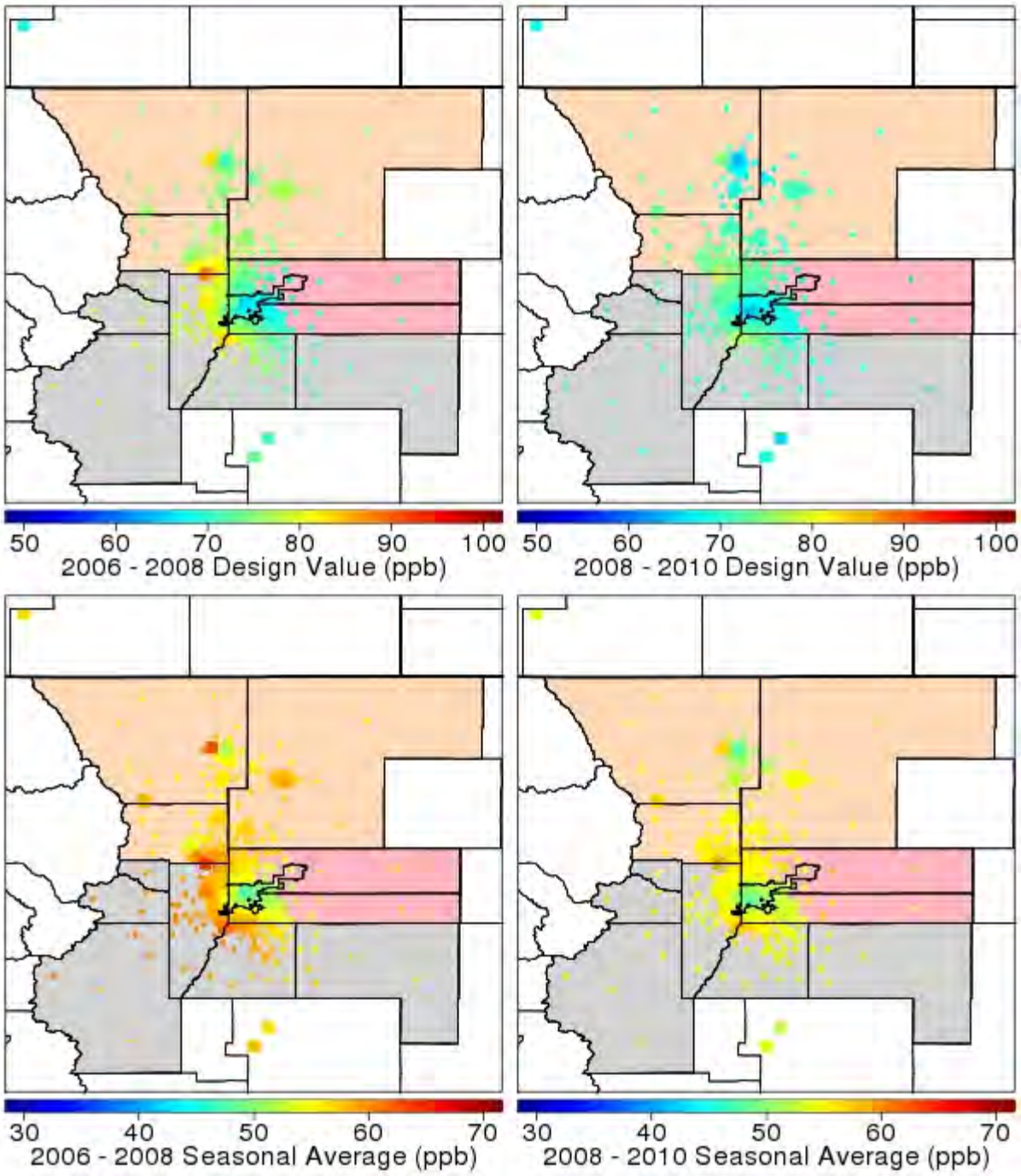

Figure 4A-11. Maps of design values and May – September average MDA8 values based on VNA spatial fields for Denver.

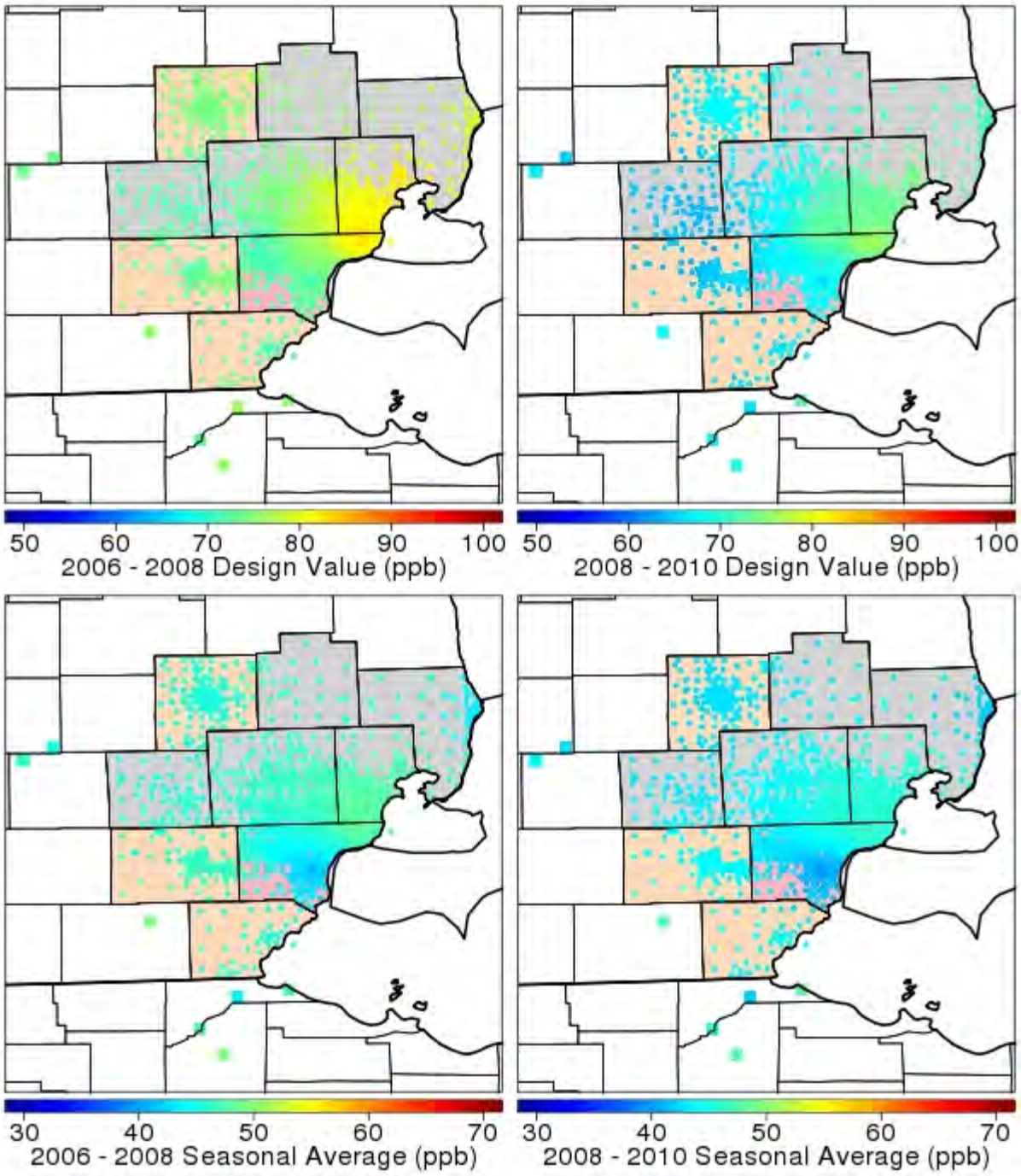

Figure 4A-12. Maps of design values and May – September average MDA8 values based on VNA spatial fields for Detroit.

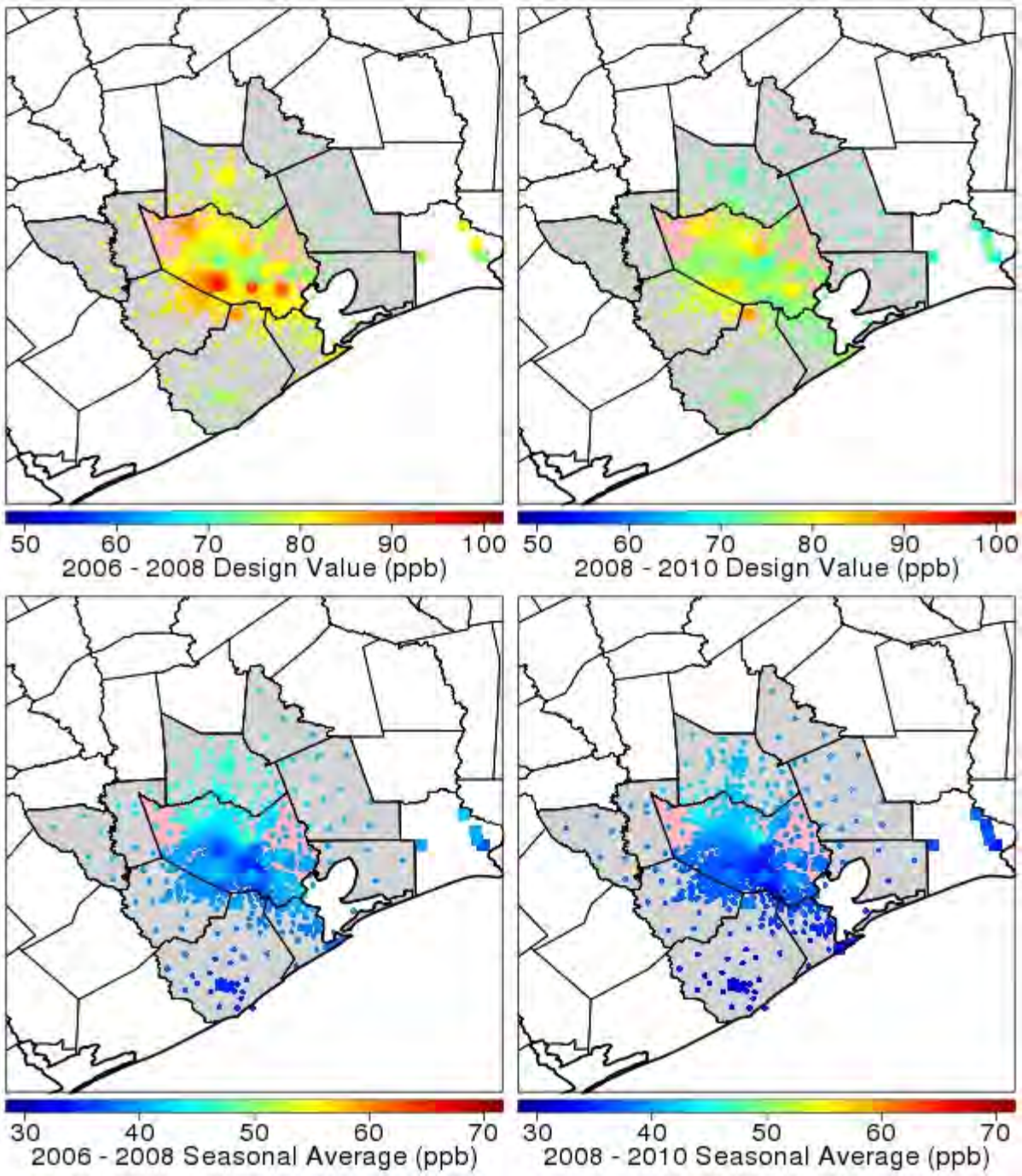

Figure 4A-13. Maps of design values and May – September average MDA8 values based on VNA spatial fields for Houston.

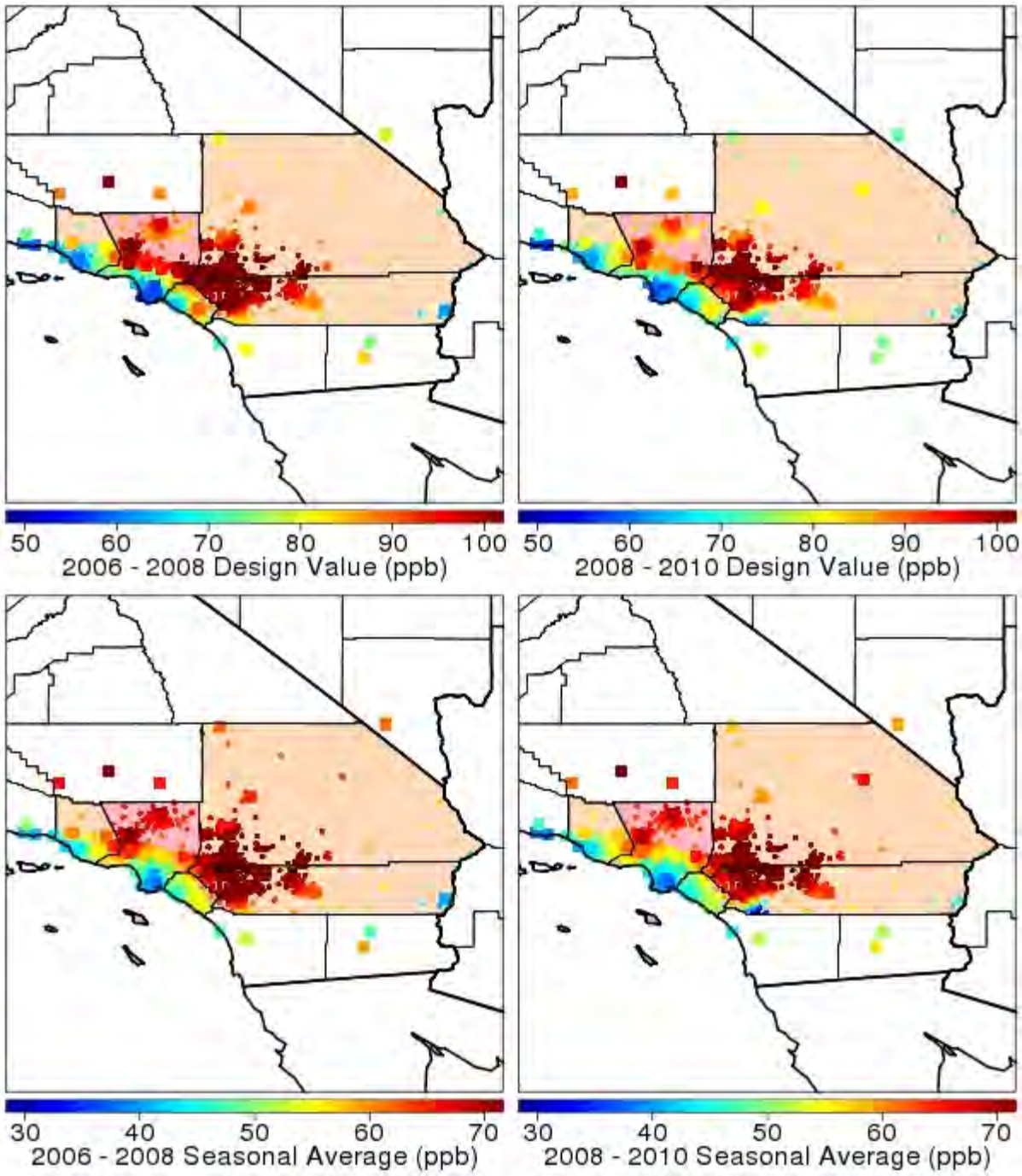

Figure 4A-14. Maps of design values and May – September average MDA8 values based on VNA spatial fields for Los Angeles.

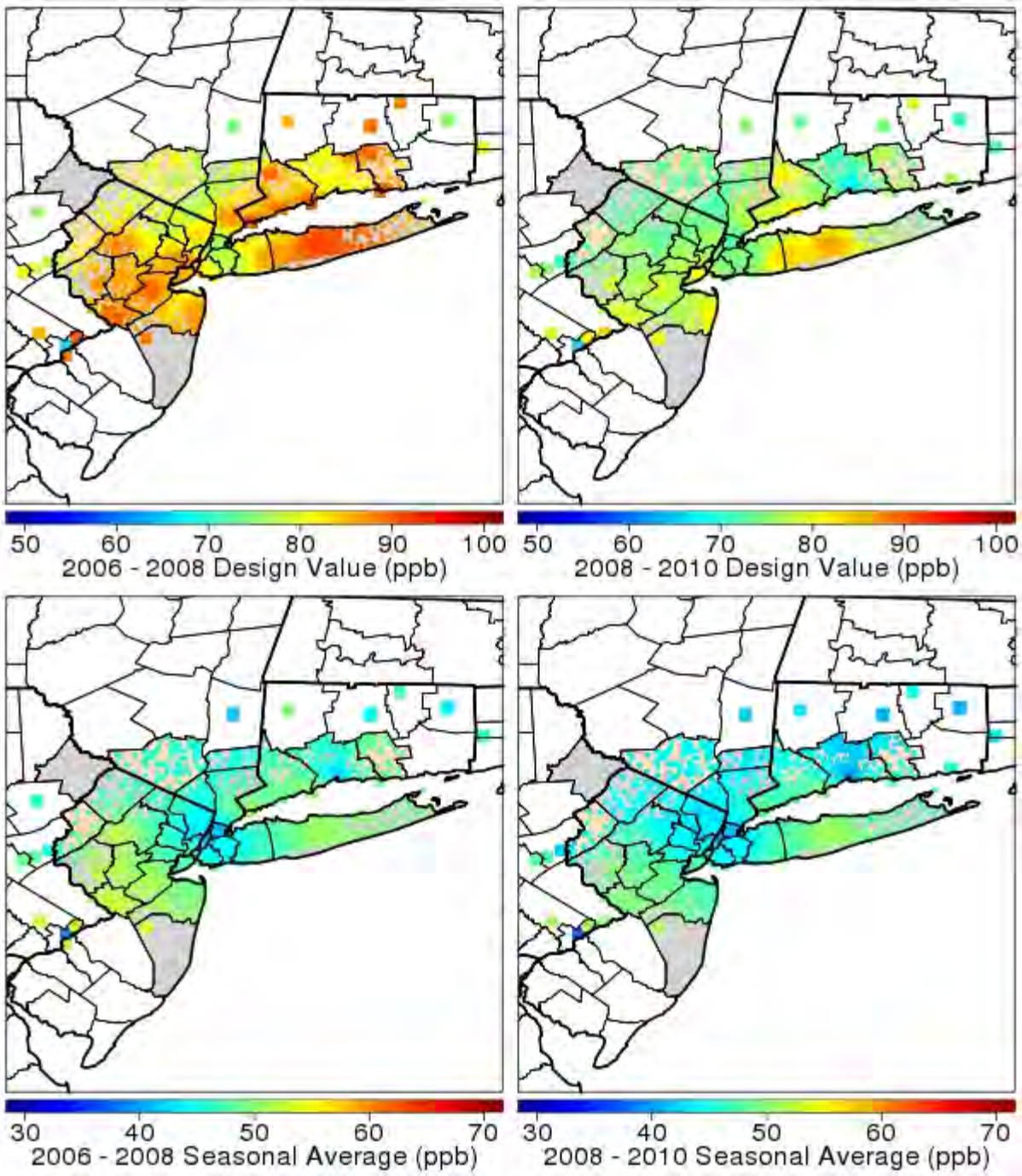

Figure 4A-15. Maps of design values and May – September average MDA8 values based on VNA spatial fields for New York.

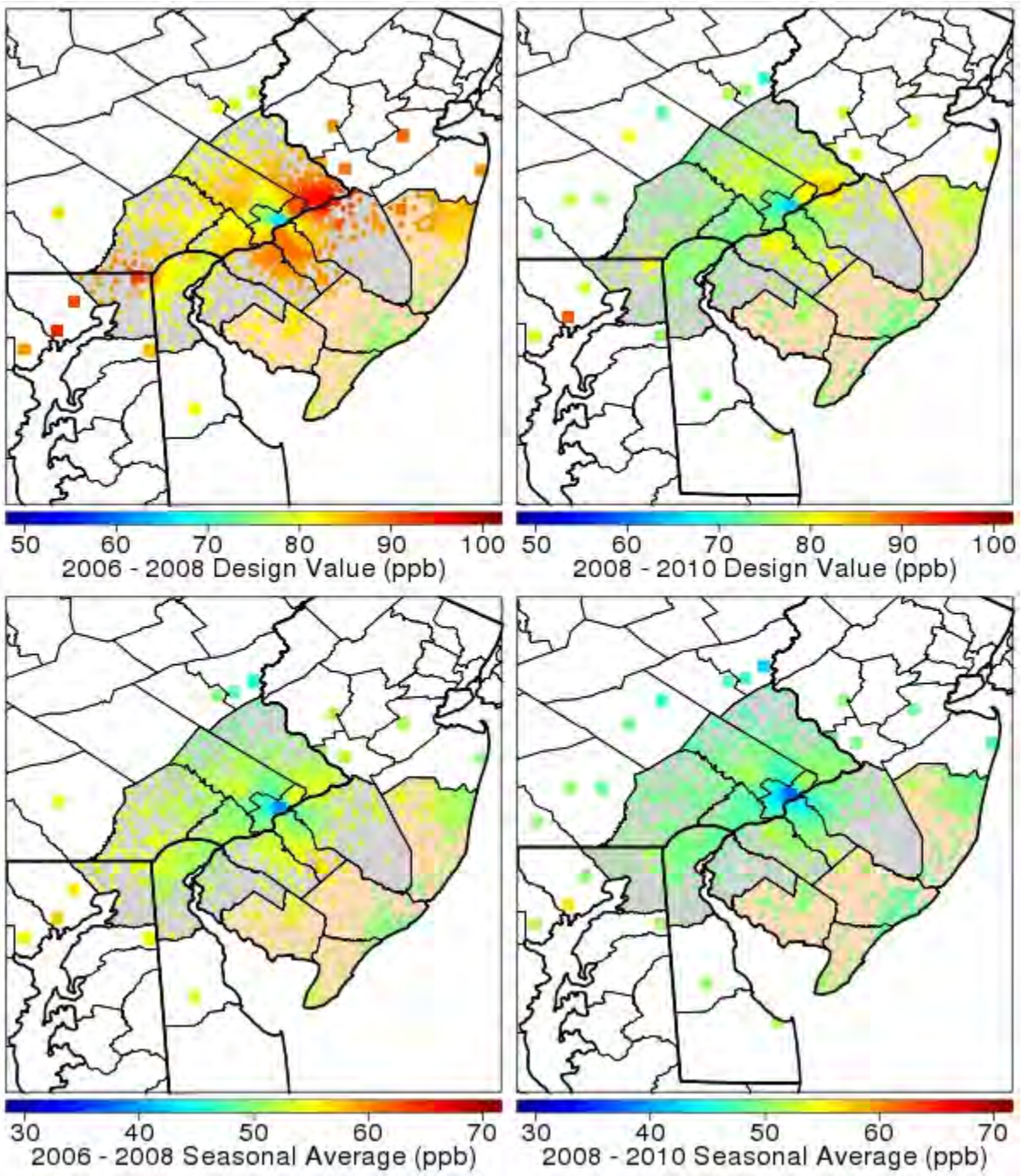

Figure 4A-16. Maps of design values and May – September average MDA8 values based on VNA spatial fields for Philadelphia.

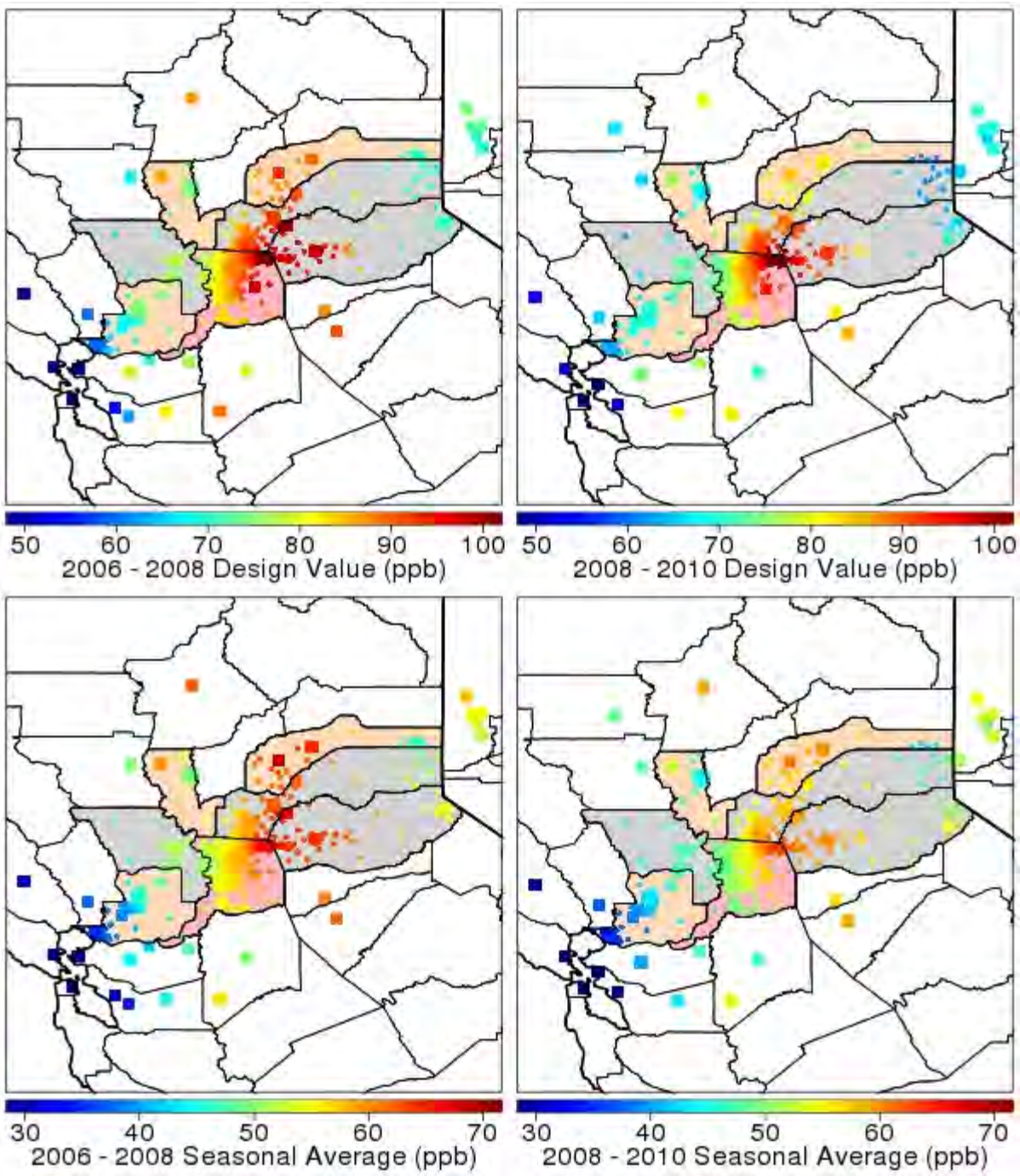

Figure 4A-17. Maps of design values and May – September average MDA8 values based on VNA spatial fields for Sacramento.

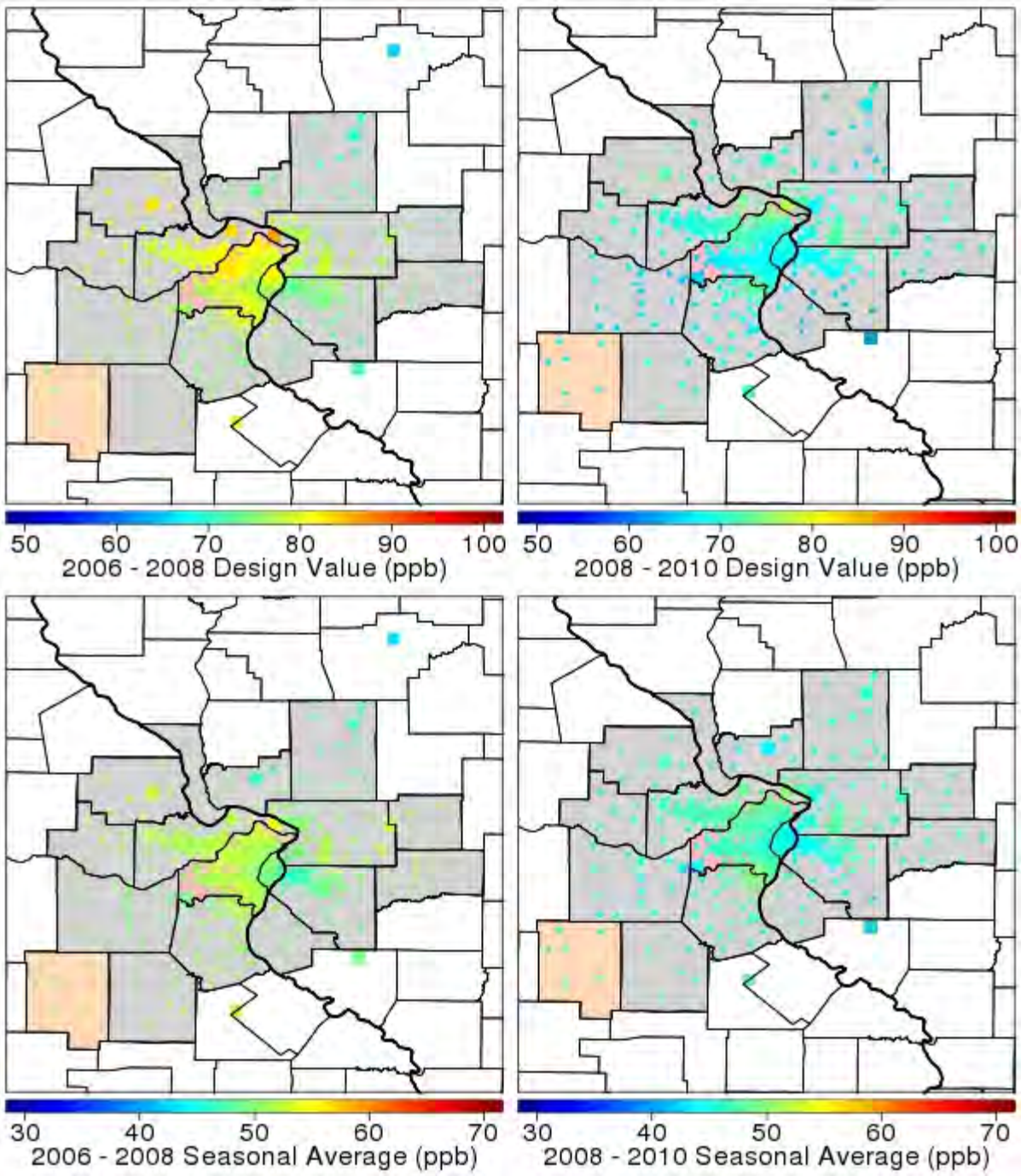

Figure 4A-18. Maps of design values and May – September average MDA8 values based on VNA spatial fields for St. Louis.

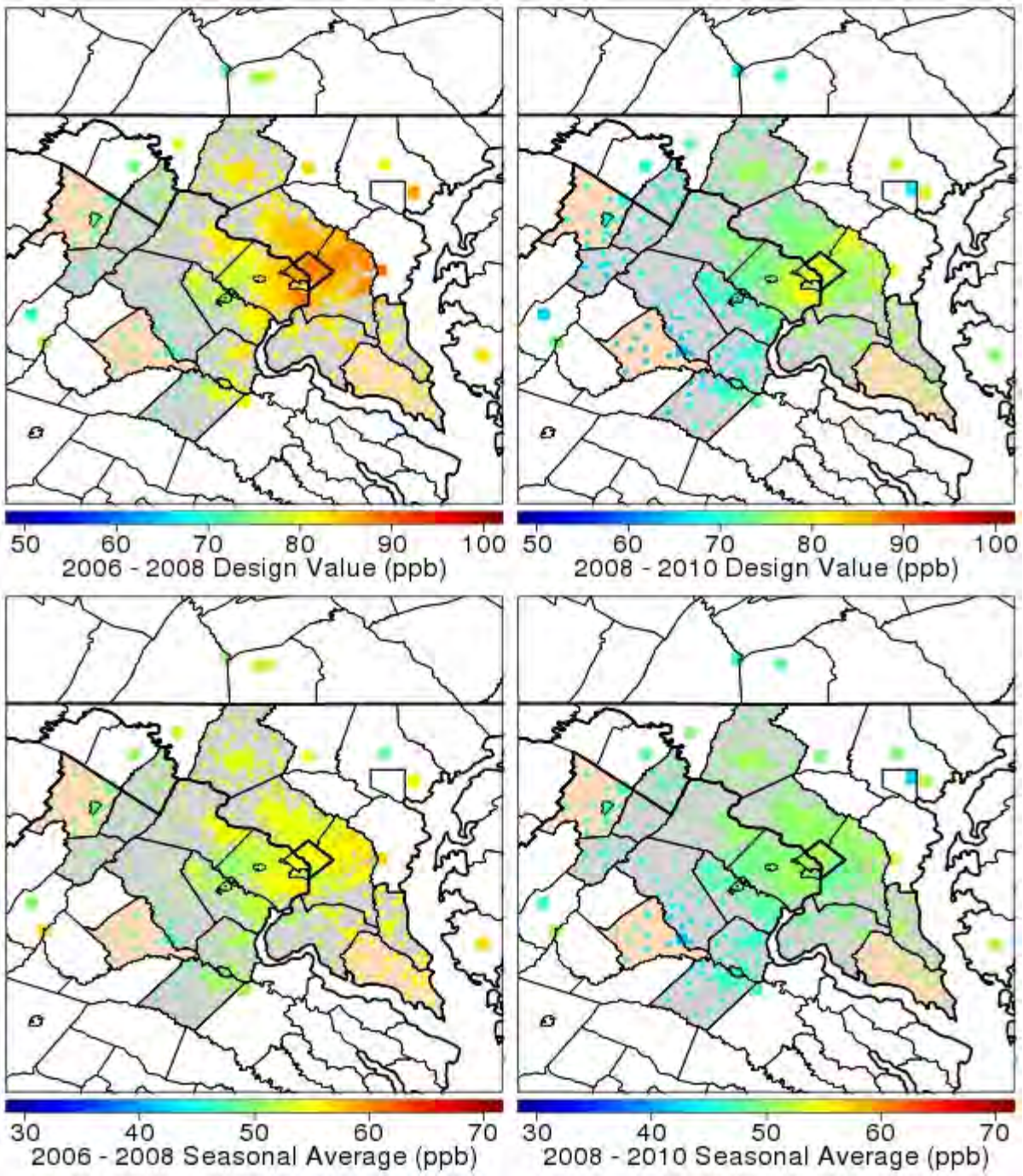

Figure 4A-19. Maps of design values and May – September average MDA8 values based on VNA spatial fields for Washington, D.C.

4A-2.3 Evaluation of Air Quality Spatial Field Techniques

As mentioned previously, in the 1st draft REA the air quality spatial fields used as inputs to APEX were based on hourly O_3 concentrations from the nearest monitoring site, while in this

draft the spatial fields were based on the VNA technique described in the previous section. This section presents an evaluation comparing the relative accuracy of the nearest neighbor (NN) and VNA techniques for generating spatial fields of hourly O_3 concentrations.

The evaluations were conducted over 4km gridded domains in Atlanta, Detroit, and Philadelphia using monitored hourly O_3 concentrations from 2005. Due to potential discrepancies in the availability of data, only data collected within the required O_3 monitoring seasons for each area (March – October for Atlanta; April – September for Detroit; April – October for Philadelphia) were considered. Figure 4A-20 below shows maps of the monitored values (AQS, left), NN values (center), and VNA values (right) in Atlanta (top) and Philadelphia (bottom) for a single selected hour in each area. These maps show an extreme example of the differences in the NN and VNA spatial fields. The NN fields (center column) have very sharp breaks between air quality monitors, while the VNA fields (right column) tend to produce much smoother surfaces. The NN fields also have a tendency to spread concentrations out over a large area if the monitoring network is sparse. For example, the highest concentration at the monitor in southern Atlanta is spread out over a large area in the NN fields, but this effect is somewhat mitigated in the VNA fields.

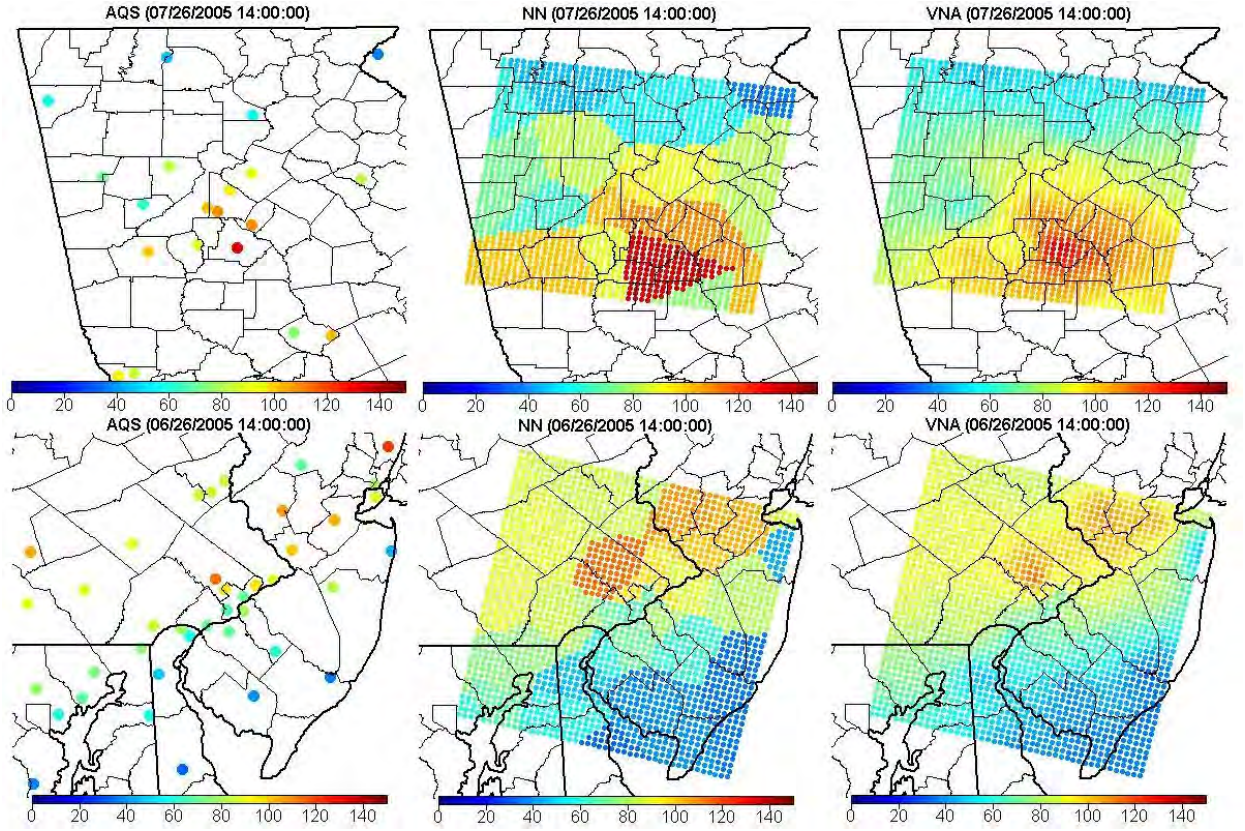

Figure 4A-20. Maps of monitored values (left), nearest neighbor spatial fields (center), and VNA spatial fields (right) for selected hours in Atlanta (top), and Philadelphia (bottom).

A cross-validation analysis was performed to evaluate the relative accuracy of the estimates from these two methods. For each hour in the required O_3 season, the concentrations from each monitor in the 4 km gridded domain were withheld (one at a time) from the input dataset, and the concentrations from the remaining monitors were used to estimate the concentration at the monitoring site that was withheld using NN and VNA. Additional monitoring sites within a 50 km radius of the 4 km gridded domain were used in the estimates, but were not included in the set of monitors that were withheld from the analysis. The estimated values were then compared to the respective monitored concentrations that were withheld, and the relative accuracy of NN and VNA were assessed using three summary statistics: the coefficient of variation (R^2), the mean bias, and the root mean squared error (RMSE).

Figure 4A-21 (Atlanta), Figure 4A-22 (Detroit), and Figure 4A-23 (Philadelphia) show density scatter plots and performance statistics for the NN and VNA spatial fields based on the cross-validation analysis described above for the three urban areas. Each figure shows the monitored hourly O_3 concentrations in ppb (AQS; x-axis) from the monitors which were withheld from the analysis, versus the respective values estimated using the NN (left panel) and VNA (right panel) techniques. In each panel, the plot region was split into 2 ppb x 2 ppb squares, with the colors indicating the number of points falling into each square. The diagonal line in each panel is a one-to-one reference line, and performance statistics for each method are included in the upper left-hand corner. High R^2 values, low mean bias values, and low RMSE values are indicative of good performance.

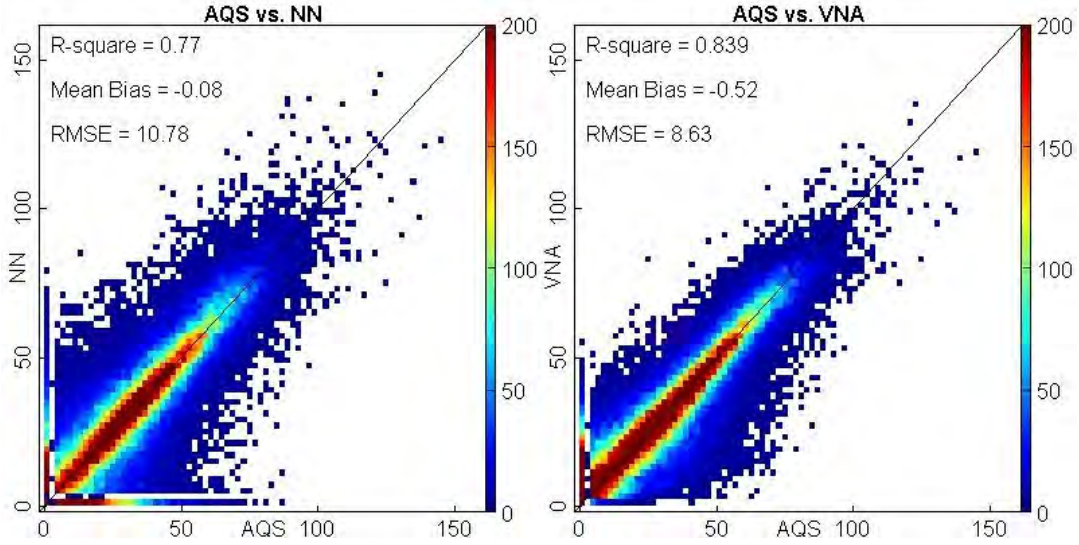

Figure 4A-21. Density scatter plots and performance statistics for the cross-validation analysis of nearest neighbor (NN; left) and Voronoi Neighbor Averaging (VNA; right) spatial field techniques applied to monitored hourly O_3 concentrations in Atlanta, 2005.

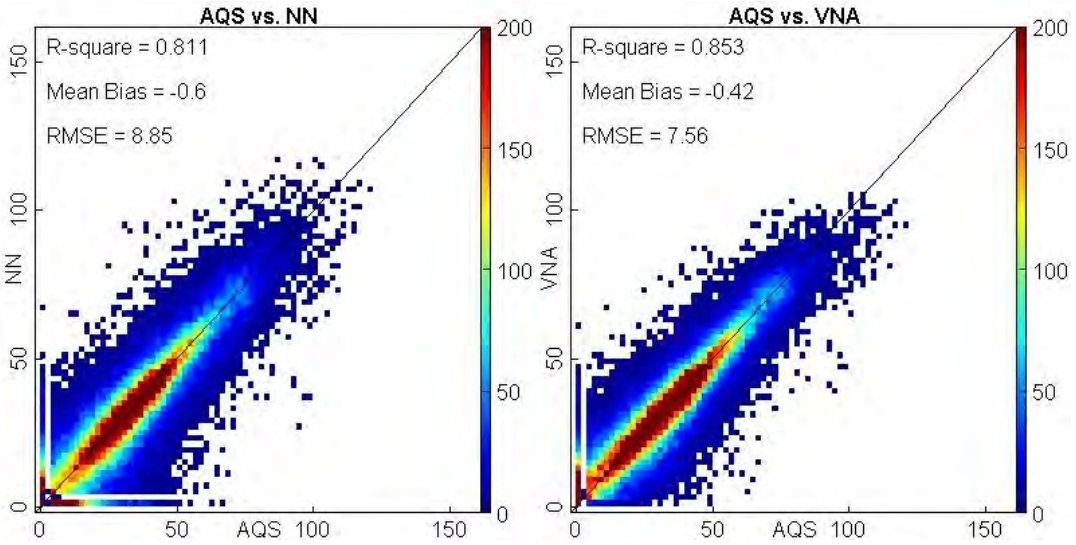

Figure 4A-22. Density scatter plots and performance statistics for the cross-validation analysis of nearest neighbor (NN; left) and Voronoi Neighbor Averaging (VNA; right) spatial field techniques applied to monitored hourly O_3 concentrations in Detroit, 2005.

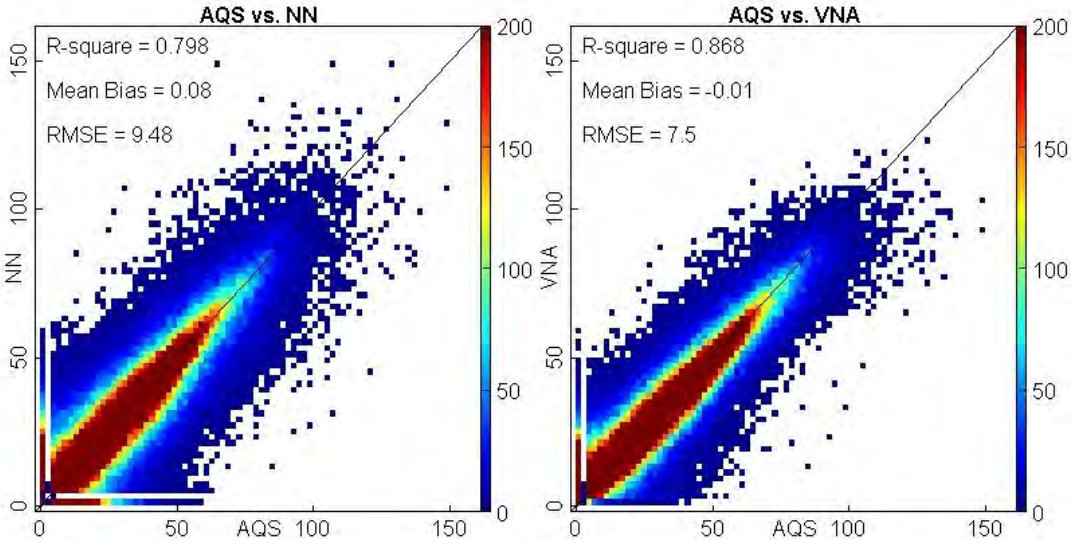

Figure 4A-23. Density scatter plots and performance statistics for the cross-validation analysis of nearest neighbor (NN; left) and Voronoi Neighbor Averaging (VNA; right) spatial field techniques applied to monitored hourly O_3 concentrations in Philadelphia, 2005.

Both techniques had relatively low mean bias statistics in all three urban areas (< 1 ppb in all cases). However, the VNA estimates had higher R^2 statistics and lower RMSE statistics than the NN estimates in all three urban areas, both of which indicate that the VNA technique consistently produces more accurate estimates than NN. This is also reflected by the fact that there is generally less scatter in the density plots based on the VNA estimates than those based

on the NN estimates. From a physical perspective, the VNA technique is also more appealing since it does not produce sharp breakpoints in the estimated values between adjacent monitors when the reported concentrations are different.

4A-3. AIR QUALITY INPUTS FOR THE EPIDEMIOLOGY-BASED RISK ASSESSMENT

This section describes the 12 urban case study areas for the epidemiology-based risk assessment described in HREA Chapter 7 (Section 7.4A-3.1), and the spatially averaged "composite monitor" values used as inputs to the Benefits Mapping and Analysis Program (BenMAP; Section 4A-3.2).

4A-3.1 Urban Case Study Areas

Three distinct sets of boundaries were considered for the 12 urban case study areas in the epidemiology-based risk assessment:

1. Core Based Statistical Areas[2] ("CBSA" boundaries)
2. Area boundaries defined in the Zanobetti and Schwartz (2008) study ("Z & S" boundaries)
3. Area boundaries defined in Smith et al. (2009) study ("Smith" boundaries)

In the 1st draft REA, the short-term mortality risk estimates were based on the concentration response functions estimated in the Zanobetti and Schwartz (2008) study using the Z & S boundaries. Here, the primary set of short-term and long-term mortality risk estimates described in HREA Chapter 7 are based on the concentration response functions estimated in the Smith et al, 2009 study using the CBSA boundaries. The other two sets of boundaries are used in sensitivity analyses. The first sensitivity analysis uses the Z & S boundaries to assess the impact of changing from the quadratic rollback method used to adjust air quality in the 1st draft REA to the HDDM adjustment method described in HREA Chapter 4 and Appendix 4D. The second sensitivity analysis uses the Smith boundaries to assess the impact of pairing air quality information based on the CBSA boundaries with the concentration-response functions which were derived from air quality information based on the Smith boundaries.

Table 4A-2 gives some basic information about the 12 urban case study areas in the epidemiology-based risk assessment for each set of boundaries. In general, the Z & S and Smith areas were generally smaller and more focused on the urban population centers than the CBSAs.

[2] Core Based Statistical Areas (CBSAs) are used by the Office of Management and Budget (OMB) to group U.S. counties into urbanized areas. These groupings are updated by OMB every 5 years. The CBSAs used in the epidemiology based risk assessment are based on the OMB delineations from 2008. For more information see: http://www.whitehouse.gov/sites/default/files/omb/assets/bulletins/b10-02.pdf

The Z & S and Smith areas were identical in 6 of the 12 urban case study areas, and had at least one county in common for all 12 study areas. The CBSAs were typically smaller than the respective study areas described in Section 4A-2.1 for the exposure and clinical risk assessments, with the exceptions of Baltimore, Dallas, and Houston, where the areas were identical. The final two columns of Table 4A-2 show the annual 4th highest MDA8 values in ppb based on monitors within the three sets of boundaries for 2007 and 2009, the two years upon which the risk estimates in HREA Chapter 7 are focused.

Table 4A-2. Information on the 12 Urban Case Study Areas in the Epidemiology Based Risk Assessment.

Area Name	Boundary Definition	# of Counties	# of O_3 Monitors	Population (2010)	2007 4th high (ppb)	2009 4th high (ppb)
Atlanta	CBSA	28	13	5,268,860	102	77
	Z & S	4	5	3,105,873	98	77
	Smith	2	3	1,612,474	98	77
Baltimore	CBSA	7	7	2,710,489	92	83
	Z & S	2	3	1,425,990	83	71
	Smith	1	1	620,961	73	66
Boston	CBSA	7	11	4,552,402	89	75
	Z & S	3	5	2,895,958	88	75
	Smith	1	2	722,023	72	75
Cleveland	CBSA	5	10	2,077,240	83	72
	Z & S	1	4	1,280,122	83	71
	Smith	1	4	1,280,122	83	71
Denver	CBSA	10	16	2,543,482	97	79
	Z & S	1	3	600,158	76	63
	Smith	3	6	1,613,764	76	72
Detroit	CBSA	6	8	4,296,250	93	73
	Z & S	1	4	1,820,584	92	73
	Smith	1	4	1,820,584	92	73
Houston	CBSA	10	22	5,946,800	90	91
	Z & S	1	17	4,092,459	90	86
	Smith	1	17	4,092,459	90	86
Los Angeles	CBSA	2	21	12,828,837	105	108
	Z & S	1	17	9,818,605	105	108
	Smith	1	17	9,818,605	105	108
New York	CBSA	23	22	18,897,109	94	81
	Z & S	5	6	8,175,133	83	78
	Smith	6	7	9,124,246	94	78
Philadelphia	CBSA	11	15	5,965,343	102	74
	Z & S	1	4	1,526,006	95	72
	Smith	1	4	1,526,006	95	72
Sacramento	CBSA	4	17	2,149,127	93	96
	Z & S	1	8	1,418,788	90	96
	Smith	1	8	1,418,788	90	96
St. Louis	CBSA	16	17	2,812,896	94	74
	Z & S	2	5	1,318,248	94	70
	Smith	1	2	319,294	91	65

Since O_3 is not emitted directly but formed indirectly through photochemical reactions, precursor emissions may continue to react and form O_3 downwind of emissions sources, and thus the highest O_3 concentrations are often measured downwind of the highest concentration of precursor emissions in the urban population center. This phenomenon is reflected in Table 4A-2, where the highest monitored value in the CBSA occurs outside of the Smith boundaries in 9 of 12 areas in 2007, and in 7 of 12 areas in 2009. In addition, there were some instances where the highest monitored O_3 concentrations occurred outside of the CBSAs, but within the respective study areas used in the exposure and clinical risk assessments, which were designed to always include the monitor associated with the highest area-wide design value. For example, in Los Angeles, the CBSA includes Los Angeles County, CA and Orange County, CA, but the highest O_3 concentrations are typically measured further downwind in Riverside County, CA and San Bernardino County, CA.

4A-3.2 Air Quality Inputs to the Benefits Mapping and Analysis Program (BenMAP)

The air quality monitoring data used as inputs to the Benefits Mapping and Analysis Program (BenMAP) were daily time-series of spatially averaged "composite monitor" values for the 12 urban case study areas based on monitored air quality data. These composite monitor values were calculated by taking hour-by-hour spatial averages of the hourly O_3 concentrations for all monitors within a given study area, then calculating the four daily metrics described in Section 4A-1.3:

1. Daily Maximum 8-hour Average (MDA8) Concentration
2. Daily 10:00 AM – 6:00 PM Mean Concentration
3. Daily Maximum 1-hour Concentration
4. Daily 24-hour Average Concentration

These four daily metrics were calculated based on each of the three sets of urban case study area boundaries listed in the previous section, for a total of 12 daily metric/area boundary combinations. Although these 12 values were provided based on available monitoring data for each day in the 2006-2010 period, only a subset of these data were used for the air quality inputs to BenMAP. Since the BenMAP software is designed to run for only one year at a time, we chose to focus on air quality data from 2007 and 2009. In most cases, the 2007 data was meant to represent a year with high O_3 levels, while 2009 was meant to represent a year with low O_3 levels. In some areas, the data were also subset to a particular "O_3 season", either to match the period used in the respective epidemiology study, or to avoid the potential disparity in data availability which could arise if the air quality data included months outside of the required O_3 monitoring season. Appendix 4D contains "box and whisker" plots showing the distribution of

composite monitor values in each area for current air quality, air quality adjusted to meet the existing O_3 standard, and air quality adjusted to meet the potential alternative standards of 70 ppb, 65 ppb, and 60 ppb. These plots are stratified to show the effects of varying spatial extents (CBSAs vs. Z & S areas), O_3 season lengths (June – August vs. April – October), and years (2007 vs. 2009).

Table 4A-3 gives a list of the air quality inputs to the various BenMAP outputs discussed in HREA Chapter 7, including the health endpoints modeled, the epidemiology studies from which the concentration-response functions were derived, which urban case study areas were modeled, which air quality metrics were used, which O_3 season was modeled, and which set of boundaries were used in calculating the composite monitor values. Rows shaded pink represent air quality inputs used in primary risk estimates, while rows shaded blue represent air quality inputs for risk estimates included as sensitivity analyses.

Table 4A-3. Summary of the air quality inputs to BenMAP.

Health Endpoint	Epidemiology Study	Urban Case Study Area(s)	Air Quality Metric	O_3 Season	Study Area Boundaries
Emergency Room Visits, Respiratory	Darrow et al. (2011)	Atlanta, GA	MDA8	March - October	CBSA
Asthma Exacerbation, Wheeze	Gent et al. (2003)	Boston, MA	1-Hour Max	April - September	CBSA
Asthma Exacerbation, Wheeze	Gent et al. (2004)	Boston, MA	MDA8	April - September	CBSA
Emergency Room Visits, Asthma	Ito et al. (2007)	New York, NY	MDA8	April - September	CBSA
Mortality, Long-Term (Total and Respiratory)	Jerrett et al. (2009)	all 12 areas	Seasonal Average[3]	April - September	CBSA
Hospital Admissions, All Respiratory	Katsouyanni et al. (2009)	Detroit, MI	1-Hour Max	June - August	CBSA
Hospital Admissions, All Respiratory	Lin et al. (2000)	Los Angeles, CA	24-Hour Average	June - August	CBSA
Hospital Admissions, Chronic Lung Disease	Lin et al. (2008)	New York, NY	1-Hour Max	April - October	CBSA
Hospital Admissions, Chronic Lung Disease	Medina-Ramon et al. (2006)	all 12 areas	MDA8	May - September	CBSA
Hospital Admissions, Asthma	Silverman and Ito (2010)	New York, NY	MDA8	April - August	CBSA
Mortality, Non-Accidental	Smith et al. (2009)	all 12 areas	MDA8	Required O_3 season	CBSA
Mortality, Non-Accidental	Smith et al. (2009)	all 12 areas	MDA8	April - October	CBSA
Mortality, Non-Accidental	Smith et al. (2009)	all 12 areas	MDA8	June - August	CBSA
Mortality, Non-Accidental	Smith et al. (2009)	all 12 areas	MDA8	Required O_3 season	Smith
Emergency Room Visits, Respiratory	Strickland et al. (2010)	Atlanta, GA	MDA8	May - October	CBSA
Emergency Room Visits, Respiratory	Tolbert et al. (2007)	Atlanta, GA	MDA8	March - October	CBSA
Mortality, All Cause	Zanobetti and Schwartz (2008)	all 12 areas	10AM-6PM Mean	June - August	CBSA
Mortality, All Cause	Zanobetti and Schwartz (2008)	all 12 areas	10AM-6PM Mean	June - August	Z & S

[3] For the Jerrett et al. (2009) long-term mortality study, the air quality inputs were based on an annual metric instead of a daily metric. The annual metric was the April – September average of the daily maximum 1-hour concentrations.

4A-4. REFERENCES

Abt Associates, Inc. (2010). Environmental Benefits and Mapping Program (Version 4.0). Bethesda, MD. Prepared for U.S. Environmental Protection Agency, Office of Air Quality Planning and Standards, Research Triangle Park, NC. Available on the Internet at: http://www.epa.gov/air/benmap.

Bell, M.L., McDermott, A., Zeger S.L., Samet, J.M., Dominici, F. (2004). Ozone and Short-Term Mortality in 95 U.S. Urban Communities, 1987-2000. Journal of the Air and Waste Management Association, 292:2372-2378.

Chen, J., Zhao, R., Li, Z. (2004). Voronoi-based k-order Neighbor Relations for Spatial Analysis. Journal of Photogrammetry and Remote Sensing, 59(1-2), 60-72.

Gold, C. (1997). Voronoi methods in GIS. In: Algorithmic Foundation of Geographic Information Systems (va Kereveld M., Nievergelt, J., Roos, T., Widmayer, P., eds.). Lecture Notes in Computer Science, Vol 1340. Berlin: Springer-Verlag, 21-35.

Jerrett, M., Burnett, R.T., Pope III C.A., Ito, K., Thurston, G., Krewski, D., Shi, Y., Calle, E., Thun, M. (2009). Long-Term O_3 Exposure and Mortality. New England Journal of Medicine, 360:1085-1095.

R Core Team (2012). R: A language and environment for statistical computing. R Foundation for Statistical Computing, Vienna, Austria. http://www.R-project.org/.

Smith, R.L.; Xu, B., Switzer, P. (2009). Reassessing the Relationship between Ozone and Short-Term Mortality in 95 U.S. Urban Communities. Inhalation Toxicology, 21: 37-61.

Turner, R. (2012). deldir: Delaunay Triangulation and Dirichlet (Voronoi) Tessellation. R package version 0.0-19. http://CRAN.R-project.org/package=deldir

U.S. Environmental Protection Agency. (2012a). Integrated Science Assessment for Ozone and Related Photochemical Oxidants: Final Report. U.S. Environmental Protection Agency, Research Triangle Park, NC. EPA/600/R-10/076C. Available on the Internet at: http://www.epa.gov/ttn/naaqs/standards/ozone/s_o3_2008_isa.html

U.S. Environmental Protection Agency. (2012b). Health Risk and Exposure Assessment for Ozone, First External Review Draft. U.S. Environmental Protection Agency, Research Triangle Park, NC. EPA/600/R-10/076C. Available on the Internet at: http://www.epa.gov/ttn/naaqs/standards/ozone/s_o3_2008_rea.html

U.S. Environmental Protection Agency. (2012c). Total Risk Integrated Methodology (TRIM) - Air Pollutants Exposure Model (APEX) Documentation (TRIM-Expo / APEX, Version 4.4). Available on the Internet at: http://www.epa.gov/ttn/fera/human_apex.html

Wells, B., Wesson, K., Jenkins, S. (2012). Analysis of Recent U.S. Ozone Air Quality Data to Support the O_3 NAAQS Review and Quadratic Rollback Simulations to Support the First Draft of the Risk and Exposure Assessment. Available on the Internet at: http://www.epa.gov/ttn/naaqs/standards/ozone/s_o3_td.html

Zanobetti, A., and J. Schwartz (2008). Mortality Displacement in the Association of Ozone with Mortality: An Analysis of 48 Cities in the United States. American Journal of Respiratory and Critical Care Medicine, 177:184-189.

APPENDIX 4B

Modeling Technical Support Document for the 2013 Ozone Risk and Exposure Assessment

Table of Contents

4B-1. MODEL SET-UP AND SIMULATION 4B-1

4B-1.1 Model Domain 4B-1

4B-1.2 Model Time Period 4B-2

4B-1.3 Model Inputs: Meteorology 4B-3

4B-1.4 Model Inputs: Emissions 4B-4

4B-1.5 Model Inputs: Boundary and Initial conditions 4B-6

4B-2. EVALUATION OF MODELED OZONE CONCENTRATIONS 4B-7

4B-2.1 Operational Evaluation in the Northeast U.S. 4B-9

4B-2.2 Operational Evaluation in the Southeast U.S. 4B-27

4B-2.3 Operational Evaluation in the Midwest 4B-34

4B-2.4 Operational Evaluation in the Central U.S. 4B-45

4B-2.5 Operational Evaluation in the Western U.S. 4B-57

4B-3. REFERENCES 4B-71

List of Tables

Table 4B-1. Geographic elements of domain used in the CMAQ/HDDM modeling..... 4B-2
Table 4B-2. Vertical layer structure for 2007 WRF and CMAQ simulations. 4B-4
Table 4B-3. Summary of emissions totals by sector for the 12km Eastern U.S. domain… 4B-6
Table 4B-4. Summary of CMAQ model performance at AQS monitoring sites in the Northeastern U.S. 4B-10
Table 4B-5. Summary of CMAQ model performance at AQS monitoring sites in the Boston area. 4B-15
Table 4B-6. Summary of CMAQ model performance at AQS monitoring sites in the New York area. 4B-17
Table 4B-7. Summary of CMAQ model performance at AQS monitoring sites in the Philadelphia area. 4B-20
Table 4B-8. Summary of CMAQ model performance at AQS monitoring sites in the Baltimore area. 4B-22
Table 4B-9. Summary of CMAQ model performance at AQS monitoring sites in the Washington D.C. area. 4B-25
Table 4B-10. Summary of CMAQ model performance at AQS monitoring sites in the Southeastern U.S. 4B-28
Table 4B-11. Summary of CMAQ model performance at AQS monitoring sites in the Atlanta area. 4B-32
Table 4B-12. Summary of CMAQ model performance at AQS monitoring sites in the Midwest. 4B-35
Table 4B-13. Summary of CMAQ model performance at AQS monitoring sites in the Chicago area. 4B-39
Table 4B-14. Summary of CMAQ model performance at AQS monitoring sites in the Cleveland area. 4B-41
Table 4B-15: Summary of CMAQ model performance at AQS monitoring sites in the Detroit area. 4B-43
Table 4B-16. Summary of CMAQ model performance at AQS monitoring sites in the central U.S. 4B-46
Table 4B-17. Summary of CMAQ model performance at AQS monitoring sites in the Saint Louis area 4B-50
Table 4B-18. Summary of CMAQ model performance at AQS monitoring sites in the Dallas area. 4B-52
Table 4B-19. Summary of CMAQ model performance at AQS monitoring sites in the Houston area 4B-55
Table 4B-20. Summary of CMAQ model performance at AQS monitoring sites in the western U.S. 4B-58
Table 4B-21. Summary of CMAQ model performance at AQS monitoring sites in the Denver area. 4B-63
Table 4B-22. Summary of CMAQ model performance at AQS monitoring sites in the Sacramento area. 4B-65
Table 4B-23. Summary of CMAQ model performance at AQS monitoring sites in the Los Angeles area. 4B-67

List of Figures

Figure 4B-1. Map of the CMAQ modeling domain. 4B-2
Figure 4B-2. Map of normalized mean bias for MDA8 O_3 concentrations in the Northeastern U.S. for winter months in 2007. ..... 4B-11
Figure 4B-3. Map of normalized mean bias for MDA8 O_3 concentrations in the Northeastern U.S. for spring months in 2007. ..... 4B-12
Figure 4B-4. Map of normalized mean bias for MDA8 O_3 concentrations in the Northeastern U.S. for summer months in 2007. ..... 4B-13
Figure 4B-5. Map of normalized mean bias for MDA8 O_3 concentrations in the Northeastern U.S. for fall months in 2007 ..... 4B-14
Figure 4B-6. Time series of 8-hr daily maximum O_3 concentrations at Boston monitoring sites for April-October 2007. Observed values shown in black and modeled values shown in red. 4B-15
Figure 4B-7. Time series of hourly O_3 concentrations at Boston monitoring sites for January 2007. Observed values shown in black and modeled values shown in red. 4B-16
Figure 4B-8. Time series of hourly O_3 concentrations at Boston monitoring sites for April 2007. Observed values shown in black and modeled values shown in red. 4B-16
Figure 4B-9. Time series of hourly O_3 concentrations at Boston monitoring sites for July 2007. Observed values shown in black and modeled values shown in red. 4B-16
Figure 4B-10. Time series of hourly O_3 concentrations at Boston monitoring sites for October 2007. Observed values shown in black and modeled values shown in red. 4B-17
Figure 4B-11. Time series of 8-hr daily maximum O_3 concentrations at New York monitoring sites for April-October 2007. Observed values shown in black and modeled values shown in red. 4B-18
Figure 4B-12. Time series of hourly O_3 concentrations at New York monitoring sites for January 2007. Observed values shown in black and modeled values shown in red. 4B-18
Figure 4B-13. Time series of hourly O_3 concentrations at New York monitoring sites for April 2007. Observed values shown in black and modeled values shown in red. 4B-18
Figure 4B-14. Time series of hourly O_3 concentrations at New York monitoring sites for July 2007. Observed values shown in black and modeled values shown in red. 4B-19
Figure 4B-15. Time series of hourly O_3 concentrations at New York monitoring sites for October 2007. Observed values shown in black and modeled values shown in red. 4B-19
Figure 4B-16. Time series of 8-hr daily maximum O_3 concentrations at Philadelphia monitoring sites for April-October 2007. Observed values shown in black and modeled values shown in red. 4B-20
Figure 4B-17. Time series of hourly O_3 concentrations at Philadelphia monitoring sites for January 2007. Observed values shown in black and modeled values shown in red. 4B-21
Figure 4B-18. Time series of hourly O_3 concentrations at Philadelphia monitoring sites for April 2007. Observed values shown in black and modeled values shown in red. 4B-21
Figure 4B-19. Time series of hourly O_3 concentrations at Philadelphia monitoring sites for July 2007. Observed values shown in black and modeled values shown in red. 4B-21
Figure 4B-20. Time series of hourly O_3 concentrations at Philadelphia monitoring sites for October 2007. Observed values shown in black and modeled values shown in red. 4B-22

Figure 4B-21. Time series of 8-hr daily maximum O_3 concentrations at Baltimore monitoring sites for April-October 2007. Observed values shown in black and modeled values shown in red. 4B-23
Figure 4B-22. Time series of hourly O_3 concentrations at Baltimore monitoring sites for January 2007. Observed values shown in black and modeled values shown in red. 4B-23
Figure 4B-23. Time series of hourly O_3 concentrations at Baltimore monitoring sites for April 2007. Observed values shown in black and modeled values shown in red. 4B-23
Figure 4B-24. Time series of hourly O_3 concentrations at Baltimore monitoring sites for July 2007. Observed values shown in black and modeled values shown in red. 4B-24
Figure 4B-25. Time series of hourly O_3 concentrations at Baltimore monitoring sites for October 2007. Observed values shown in black and modeled values shown in red. 4B-24
Figure 4B-26. Time series of 8-hr daily maximum O_3 concentrations at Washington D.C. monitoring sites for April-October 2007. Observed values shown in black and modeled values shown in red. 4B-25
Figure 4B-27. Time series of hourly O_3 concentrations at Washington D.C. monitoring sites for January 2007. Observed values shown in black and modeled values shown in red. 4B-26
Figure 4B-28. Time series of hourly O_3 concentrations at Washington D.C. monitoring sites for April 2007. Observed values shown in black and modeled values shown in red. 4B-26
Figure 4B-29. Time series of hourly O_3 concentrations at Washington D.C. monitoring sites for July 2007. Observed values shown in black and modeled values shown in red.4B-26
Figure 4B-30. Time series of hourly O_3 concentrations at Washington D.C. monitoring sites for October 2007. Observed values shown in black and modeled values shown in red. 4B-27
Figure 4B-31. Map of normalized mean bias for MDA8 O_3 concentrations in the Southeastern U.S. for winter months in 2007. ..... 4B-28
Figure 4B-32. Map of normalized mean bias for MDA8 O_3 concentrations in the Southeastern U.S. for spring months in 2007. ..... 4B-29
Figure 4B-33. Map of normalized mean bias for MDA8 O_3 concentrations in the Southeastern U.S. for summer months in 2007. ..... 4B-30
Figure 4B-34. Map of normalized mean bias for MDA8 O_3 concentrations in the Southeastern U.S. for fall months in 2007. ..... 4B-31
Figure 4B-35. Time series of 8-hr daily maximum O_3 concentrations at Atlanta monitoring sites for April-October 2007. Observed values shown in black and modeled values shown in red. 4B-32
Figure 4B-36. Time series of hourly O_3 concentrations at Atlanta monitoring sites for April 2007. Observed values shown in black and modeled values shown in red. 4B-33
Figure 4B-37. Time series of hourly O_3 concentrations at Atlanta monitoring sites for July 2007. Observed values shown in black and modeled values shown in red. 4B-33
Figure 4B-38. Time series of hourly O_3 concentrations at Atlanta monitoring sites for October 2007. Observed values shown in black and modeled values shown in red. 4B-33
Figure 4B-39. Map of normalized mean bias for MDA8 O_3 concentrations in the Midwest for winter months in 2007. ..... 4B-35

Figure 4B-40. Map of normalized mean bias for MDA8 O_3 concentrations in the Midwest for spring months in 2007. ..... 4B-36
Figure 4B-41. Map of normalized mean bias for MDA8 O_3 concentrations in the Midwest for summer months in 2007. ..... 4B-37
Figure 4B-42. Map of normalized mean bias for MDA8 O_3 concentrations in the Midwest for fall months in 2007. ..... 4B-38
Figure 4B-43. Time series of 8-hr daily maximum O_3 concentrations at Chicago monitoring sites for April-October 2007. Observed values shown in black and modeled values shown in red. 4B-39
Figure 4B-44. Time series of hourly O_3 concentrations at Chicago monitoring sites for January 2007. Observed values shown in black and modeled values shown in red. 4B-40
Figure 4B-45. Time series of hourly O_3 concentrations at Chicago monitoring sites for April 2007. Observed values shown in black and modeled values shown in red. 4B-40
Figure 4B-46. Time series of hourly O_3 concentrations at Chicago monitoring sites for July 2007. Observed values shown in black and modeled values shown in red. 4B-40
Figure 4B-47. Time series of hourly O_3 concentrations at Chicago monitoring sites for October 2007. Observed values shown in black and modeled values shown in red. 4B-41
Figure 4B-48. Time series of 8-hr daily maximum O_3 concentrations at Cleveland monitoring sites for April-October 2007. Observed values shown in black and modeled values shown in red. 4B-42
Figure 4B-49. Time series of hourly O_3 concentrations at Cleveland monitoring sites for April 2007. Observed values shown in black and modeled values shown in red. 4B-42
Figure 4B-50. Time series of hourly O_3 concentrations at Cleveland monitoring sites for July 2007. Observed values shown in black and modeled values shown in red. 4B-42
Figure 4B-51. Time series of hourly O_3 concentrations at Cleveland monitoring sites for October 2007. Observed values shown in black and modeled values shown in red. 4B-43
Figure 4B-52. Time series of 8-hr daily maximum O_3 concentrations at Detroit monitoring sites for April-October 2007. Observed values shown in black and modeled values shown in red. 4B-44
Figure 4B-53. Time series of hourly O_3 concentrations at Detroit monitoring sites for April 2007. Observed values shown in black and modeled values shown in red. 4B-44
Figure 4B-54. Time series of hourly O_3 concentrations at Detroit monitoring sites for July 2007. Observed values shown in black and modeled values shown in red. 4B-44
Figure 4B-55. Map of normalized mean bias for MDA8 O_3 concentrations in the Central U.S. for winter months in 2007. ..... 4B-46
Figure 4B-56. Map of normalized mean bias for MDA8 O_3 concentrations in the Central U.S. for spring months in 2007. ..... 4B-47
Figure 4B-57. Map of normalized mean bias for MDA8 O_3 concentrations in the Central U.S. for summer months in 2007. ..... 4B-48
Figure 4B-58. Map of normalized mean bias for MDA8 O_3 concentrations in the Central U.S. for fall months in 2007. ..... 4B-49
Figure 4B-59. Time series of 8-hr daily maximum O_3 concentrations at Saint Louis monitoring sites for April-October 2007. Observed values shown in black and modeled values shown in red. 4B-50

Figure 4B-60. Time series of hourly O_3concentrations at Saint Louis monitoring sites for January 2007. Observed values shown in black and modeled values shown in red. 4B-51
Figure 4B-61. Time series of hourly O_3 concentrations at Saint Louis monitoring sites for April 2007. Observed values shown in black and modeled values shown in red. 4B-51
Figure 4B-62. Time series of hourly O_3 concentrations at Saint Louis monitoring sites for July 2007. Observed values shown in black and modeled values shown in red. 4B-51
Figure 4B-63. Time series of hourly O_3 concentrations at Saint Louis monitoring sites for October 2007. Observed values shown in black and modeled values shown in red. 4B-52
Figure 4B-64. Time series of 8-hr daily maximum O_3 concentrations at Dallas monitoring sites for April-October 2007. Observed values shown in black and modeled values shown in red. 4B-53
Figure 4B-65. Time series of hourly O_3 concentrations at Dallas monitoring sites for January 2007. Observed values shown in black and modeled values shown in red. 4B-53
Figure 4B-66. Time series of hourly O_3 concentrations at Dallas monitoring sites for April 2007. Observed values shown in black and modeled values shown in red. 4B-53
Figure 4B-67. Time series of hourly O_3 concentrations at Dallas monitoring sites for July 2007. Observed values shown in black and modeled values shown in red. 4B-54
Figure 4B-68. Time series of hourly O_3 concentrations at Dallas monitoring sites for October 2007. Observed values shown in black and modeled values shown in red. 4B-54
Figure 4B-69. Time series of 8-hr daily maximum O_3 concentrations at Houston monitoring sites for April-October 2007. Observed values shown in black and modeled values shown in red. 4B-55
Figure 4B-70. Time series of hourly O_3 concentrations at Houston monitoring sites for January 2007. Observed values shown in black and modeled values shown in red. 4B-56
Figure 4B-71. Time series of hourly O_3 concentrations at Houston monitoring sites for April 2007. Observed values shown in black and modeled values shown in red. 4B-56
Figure 4B-72. Time series of hourly O_3 concentrations at Houston monitoring sites for July 2007. Observed values shown in black and modeled values shown in red. 4B-56
Figure 4B-73. Time series of hourly O_3 concentrations at Houston monitoring sites for October 2007. Observed values shown in black and modeled values shown in red. 4B-57
Figure 4B-74. Map of normalized mean bias for MDA8 O_3 concentrations in the Western U.S. for winter months in 2007. ..... 4B-59
Figure 4B-75. Map of normalized mean bias for MDA8 O_3 concentrations in the Western U.S. for spring months in 2007. ..... 4B-60
Figure 4B-76. Map of normalized mean bias for MDA8 O_3 concentrations in the Western U.S. for summer months in 2007. ..... 4B-61
Figure 4B-77. Map of normalized mean bias for MDA8 O_3 concentrations in the Western U.S. for fall months in 2007. ..... 4B-62
Figure 4B-78. Time series of 8-hr daily maximum O_3 concentrations at Denver monitoring sites for April-October 2007. Observed values shown in black and modeled.... values shown in red. 4B-63
Figure 4B-79. Time series of hourly O_3 concentrations at Denver monitoring sites for April 2007. Observed values shown in black and modeled values shown in red. 4B-64

Figure 4B-80. Time series of hourly O_3 concentrations at Denver monitoring sites for July 2007. Observed values shown in black and modeled values shown in red. 4B-64
Figure 4B-81. Time series of hourly O_3 concentrations at Denver monitoring sites for October 2007. Observed values shown in black and modeled values shown in red. 4B-64
Figure 4B-82. Time series of 8-hr daily maximum O_3 concentrations at Sacramento monitoring sites for April-October 2007. Observed values shown in black and modeled values shown in red..... 4B-65
Figure 4B-83. Time series of hourly O_3concentrations at Sacramento monitoring sites for January 2007. Observed values shown in black and modeled values shown in red. 4B-66
Figure 4B-84. Time series of hourly O_3 concentrations at Sacramento monitoring sites for April 2007. Observed values shown in black and modeled values shown in red. 4B-66
Figure 4B-85. Time series of hourly O_3 concentrations at Sacramento monitoring sites for July 2007. Observed values shown in black and modeled values shown in red. 4B-66
Figure 4B-86. Time series of hourly O_3 concentrations at Sacramento monitoring sites for October 2007. Observed values shown in black and modeled values shown in red. 4B-67
Figure 4B-87. Time series of 8-hr daily maximum O_3 concentrations at Los Angeles monitoring sites for April-October 2007. Observed values shown in black and modeled values shown in red..... 4B-68
Figure 4B-88. Time series of hourly O_3 concentrations at Los Angeles monitoring sites for January 2007. Observed values shown in black and modeled values shown in red. 4B-68
Figure 4B-89. Time series of hourly O_3 concentrations at Los Angeles monitoring sites for April 2007. Observed values shown in black and modeled values shown in red. 4B-68
Figure 4B-90. Time series of hourly O_3 concentrations at Los Angeles monitoring sites for July 2007. Observed values shown in black and modeled values shown in red. 4B-69
Figure 4B-91. Time series of hourly O_3 concentrations at Los Angeles monitoring sites for October 2007. Observed values shown in black and modeled values shown in red. 4B-69
Figure 4B-92. Map of mean observed MDA8 O_3 concentrations at Los Angeles monitoring sites for summer months (June, July, Aug) 2007..... 4B-70
Figure 4B-93. Map of normalized mean bias for MDA8 O_3 concentrations at Los Angeles monitoring sites for summer months (June, July, Aug) 2007..... 4B-70

4B-1. MODEL SET-UP AND SIMULATION

The air quality modeling underlying the HDDM adjustment methodology described in the Health Risk and Exposure Assessment (HREA) Chapter 4 and Appendix 4D was performed using CMAQv4.7.1 with HDDM for ozone (O_3) (www.cmaq-model.org). A modified version of CMAQ-HDDM-3D was used that tracked species concentrations through all modeled processes, but tracked O_3 sensitivities through the chemistry, transport, and dry deposition subroutines only and did not account for the effects of aerosol and cloud processing due to the uncertainties in these model processes with respect to O_3 sensitivity as well as to conserve computational costs. CMAQ was run using the carbon bond 2005 (CB05) gas-phase chemical mechanism (Gery et al., 1989; Yarwood et al., 2005) and the AERO5 aerosol module which includes ISORROPIA for gas-particle partitioning of inorganic species (Nenes et al., 1998) and secondary organic aerosol treatment as described in Carlton et al. (2010).

4B-1.1 Model Domain

For this analysis, all CMAQ/HDDM runs were performed for a domain that covers the 48 contiguous states included portions of southern Canada and Northern Mexico with a 12 x 12 km resolution (Figure 4B-1). The CMAQ simulations were performed with 24 vertical layers with a top at about 17,600 meters, or 50 millibars (mb). Table 4B-1 and Table 4B-2 provides some basic geographic information regarding the CMAQ domain and vertical layer structure, respectively. Results from the lowest layer of the model were used for analyses to support the O_3 HREA.

Figure 4B-1. Map of the CMAQ modeling domain.

Table 4B-1. Geographic elements of domain used in the CMAQ/HDDM modeling.

Element	CMAQ Modeling Configuration: National Grid
Map Projection	Lambert Conformal Projection
Grid Resolution	12 km
True Latitudes	33 deg N and 45 deg N
Dimensions	396 x 246 x 24
Vertical extent	24 Layers: Surface to 50 millibar level (Table 4B-2)

4B-1.2 Model Time Period

The CMAQ/HDDM modeling was performed for January and April-October of 2007. The simulations included 10 day "ramp-up" periods from December 22-31, 2006 and from March 22-31 2007 to minimize the effects of initial conditions. The ramp-up days were not considered in the analysis for the HDDM results.

4B-1.3 Model Inputs: Meteorology

CMAQ model simulations require inputs of meteorological fields, emissions, and initial and boundary conditions. The gridded meteorological data for the entire year of 2007 at the 12 km continental United States scale domain was derived from version 3.1 of the Weather Research and Forecasting Model (WRF), Advanced Research WRF (ARW) core (Skamarock et al., 2008). The WRF Model is a next-generation mesoscale numerical weather prediction system developed for both operational forecasting and atmospheric research applications (http://wrf-model.org). The 2007 WRF simulation included the physics options of the Pleim-Xiu land surface model (LSM), Asymmetric Convective Model version 2 planetary boundary layer (PBL) scheme, Morrison double moment microphysics, Kain-Fritsch cumulus parameterization scheme and the RRTMG long-wave radiation (LWR) scheme (Gilliam and Pleim, 2010).

The WRF meteorological outputs were processed to create model-ready inputs for CMAQ using the Meteorology-Chemistry Interface Processor (MCIP) package (Otte et al., 2010), version 3.6, to derive the specific inputs to CMAQ: horizontal wind components (i.e., speed and direction), temperature, moisture, vertical diffusion rates, and rainfall rates for each grid cell in each vertical layer. The WRF simulation used the same CMAQ map projection, a lambert conformal projection centered at (-97, 40) with true latitudes at 33 and 45 degrees north. The 12 km WRF domain consisted of 459 by 299 grid cells. The WRF simulation utilized 34 vertical layers with a surface layer of approximately 38 meters. Table 4B-2 shows the vertical layer structure used in WRF and the layer collapsing approach to generate the CMAQ meteorological inputs. CMAQ resolved the vertical atmosphere with 24 layers, preserving greater resolution in the PBL.

In terms of the 2007 WRF meteorological model performance evaluation, an approach which included a combination of qualitative and quantitative analyses was used to assess the adequacy of the WRF simulated fields (U.S. EPA, 2011). The qualitative aspects involved comparisons of the model-estimated synoptic patterns against observed patterns from historical weather chart archives. Additionally, the evaluations compared spatial patterns of monthly average rainfall and monthly maximum planetary boundary layer (PBL) heights. The statistical portion of the evaluation examined the model bias and error for temperature, water vapor mixing ratio, solar radiation, and wind fields. These statistical values were calculated on a monthly basis.

Table 4B-2. Vertical layer structure for 2007 WRF and CMAQ simulations.

Layer Top Height (m)	Pressure (mb)	WRF	Depth (m)	CMAQ	Depth (m)
17,145	50	34	2,655	24	4,552
14,490	95	33	1,896		
12,593	140	32	1,499	23	2,749
11,094	185	31	1,250		
9,844	230	30	1,078	22	2,029
8,766	275	29	951		
7,815	320	28	853	21	1,627
6,962	365	27	775		
6,188	410	26	711	20	1,368
5,477	455	25	657		
4,820	500	24	612	19	1,185
4,208	545	23	573		
3,635	590	22	539	18	539
3,095	635	21	509	17	509
2,586	680	20	388	16	388
2,198	716	19	281	15	281
1,917	743	18	273	14	273
1,644	770	17	178	13	178
1,466	788	16	174	12	174
1,292	806	15	171	11	171
1,121	824	14	168	10	168
952	842	13	165	9	165
787	860	12	82	8	163
705	869	11	81		
624	878	10	80	7	160
544	887	9	80		
465	896	8	79	6	157
386	905	7	78		
307	914	6	78	5	78
230	923	5	77	4	77
153	932	4	38	3	76
114	937	3	38		
76	941	2	38	2	38
38	946	1	38	1	38

4B-1.4 Model Inputs: Emissions

The emissions data used are based on the 2007 Version 5 emissions modeling platform developed for the Particulate Matter (PM) NAAQS rule (U.S. EPA 2012a, U.S. EPA 2012b). Some small updates to the 2007v5 platform are enumerated below. First we give a general summary of the emissions processing performed for the PM NAAQS 2007 modeling emissions inputs (more details are available in U.S. EPA 2012a, 2012b, and in the PM NAAQS section of http://www.epa.gov/ttn/chief/emch/index.html). The 2008 National Emissions Inventory,

Version 2 (http://www.epa.gov/ttn/chief/net/2008inventory.html) was the starting point for these emissions, with updates to specific source categories made where necessary to better represent the year 2007. Emissions were processed to photochemical model inputs with the SMOKE modeling system version 3.1 (Houyoux et al., 2000). For this analysis, emissions from wildfires and prescribed burns are estimated based on a multi-year average of data from 2003 through 2010. Electric generating utilities (EGUs) emissions for 2007 are temporalized based on average temporal profiles from 3 years of data. In addition, U.S. emissions are included from other point sources, area sources, agricultural sources (ammonia only), anthropogenic fugitive dust sources, nonroad mobile sources, onroad mobile sources, and biogenic sources. Onroad mobile sources were created using EPA's MOVES 2010b model (www.epa.gov/otaq/models/moves), except that California emissions were adjusted to match the county total emissions obtained directly from the California Air Resources Board. Biogenic emissions were estimated using the Biogenic Emissions Inventory System version 3.14 (BEISv3.14) (Pierce et al., 1998). Other North American emissions are based on a 2006 Canadian inventory and 2008 Mexican inventory. Emissions totals within the 12 km Eastern domain are summarized in Table 4B-3 for CO, NH3, NO_x, PM_{10}, $PM_{2.5}$, SO_2, and VOC.

There are a few differences between the emissions data used for this analysis and the data documented in the PM NAAQS 2007v5 platform technical support document (TSD). First, the years used to compute the average fires were 2003-2010, versus 2003-2009 for the PM NAAQS. Second, point source emissions for South Dakota were updated with more recent data. Finally, a correction was made the spatial surrogates used for oil and gas emissions in the Western Regional Air Partnership states and updated spatial surrogates for gas stations and dry cleaners were used.

Table 4B-3. Summary of emissions totals by sector for the 12km Eastern U.S. domain.

Sector Name	Sector description	Emissions (1000 tons/year)						
		CO	NH_3	NO_X	PM_{10}	$PM_{2.5}$	SO_2	VOC
afdust	Anthropogenic fugitive dust				5,854	825		
ag	Agricultural sources		3,595					
c1c2rail	Locomotive and marine mobile sources (except C3 marine)	219	0.6	1,338	44	41	49	60
avefire	Average year fire emissions	15,598	256	216	1,589	1,347	118	2,797
nonpt	Area sources	4,335	155	1,229	768	676	402	6,671
nonroad	Off road equipment	17,834	1.9	1,878	188	178	101	2,781
onroad	Onroad mobile vehicles	36,757	145	7,561	363	277	40	3,186
othar	Canada and Mexico area sources	4,225	671	918	1,510	451	154	1,815
othon	Canada and Mexico onroad mobile sources	5,173	25	631	23	18	11	405
othpt	Canada and Mexico point sources	1,331	21	1,280	241	159	2,504	626
ptipm	Point sources: electric generation units	704	25	3,357	437	330	9,136	43
ptnonipm	Point sources other than electric generating units	2,934	68	2,077	583	409	1,589	1,074
c3marine US	C3 marine vessels within 4 miles of the U.S. coast	13		138	12	11	105	5.1
c3marine non US	C3 marine vessels more than 4 miles off the U.S. coast	86		1,047	87	80	646	38
beis	Biogenic emissions	8,211		1,931				48,616
total US anthro	Total U.S. anthropogenic emissions used in HDDM (NO_x and VOC only)			17,578				13,819
total	Domain-wide total	97,420	4,964	23,602	11,699	4,802	14,854	68,117

4B-1.5 Model Inputs: Boundary and Initial conditions

The lateral boundary concentrations for the 12km US2 domain are provided by a three-dimensional global atmospheric chemistry model, the GEOS-CHEM (Yantosca, 2004) model (standard version 8-03-02 with version 8-02-03 chemistry). The global GEOS-CHEM model simulates atmospheric chemical and physical processes driven by assimilated meteorological observations from the NASA's Goddard Earth Observing System (GEOS-5). This model was

run for 2007 with a grid resolution of 2.0 degree x 2.5 degree (latitude-longitude) and 46 vertical layers up to 0.01 hPa. The predictions were processed using the GEOS-2-CMAQ tool (Akhtar et al., 2012, Henderson et al., 2013) and used to provide one-way dynamic boundary conditions at one-hour intervals. The O_3 from these GEOS-Chem runs was evaluated by comparing to satellite vertical profiles and ground-based measurements and found acceptable model performance (Akhtar et al., 2012; Henderson et al., 2013).

Initial conditions were extracted from a slightly older model simulation using GEOS-CHEM (Yantosca, 2004) version 8-02-03. The model simulation from which the initial conditions were extracted was also run with a grid resolution of 2.0 of 2.0 degree x 2.5 degree (latitude-longitude) and 47 vertical layers. A GEOS-Chem evaluation was conducted for the purpose of validating the 2007 GEOS-Chem simulation outputs for their use as inputs to the CMAQ modeling system. This evaluation included reproducing GEOS-Chem evaluation plots reported in the literature for previous versions of the model (Lam, 2010).

4B-2. EVALUATION OF MODELED OZONE CONCENTRATIONS

CMAQ is a peer-reviewed, community air quality model that simulates the formation and fate of photochemical oxidants, aerosol concentrations, acid deposition, and air toxics, over multiple scales for given input sets of meteorological conditions and emissions. In order to assure that CMAQ is an appropriate tool to estimate the AQ changes expected to result from a given set of emissions reductions, the model is typically evaluated for each new application. This evaluation consists of assessments of the model itself and an assessment of this particular application of the model.

An independent panel consisting of academic and government experts assessed the science within the CMAQ model version 4.7.1 in September 2011 (http://www.epa.gov/AMD/Reviews/2011_CMAQ_Review_FinalReport.pdf). Among the conclusions of this peer-review report was the finding that the CMAQ science and evaluation efforts was of “very high quality” and have provided a “foundation for the more reliable use of the CMAQ modeling system”.

As CMAQ model version 4.7.1 was being developed, a series of incremental diagnostic tests were performed to assess how model performance varied across a variety of model improvements. This analysis is summarized in Foley et al. (2010) as well as Godowitch et al., (2011). While time and resource intensive, this systematic incremental testing shows “the effect of each scientific improvement on the simulated fields.” This evaluation allowed for a clear comparison with previous model versions and provided assurance that CMAQ v4.7.1 yielded equivalent or improved performance relative to previous CMAQ versions.

Numerous dynamic evaluations of CMAQ's ability to simulate the change in air quality resulting from emissions reductions have been conducted and summarized in the peer-reviewed literature. For instance, Napelenok et al. (2011) concluded that the CMAQ model "is able to reproduce the observed change in daily maximum 8-hour O_3 levels" at the majority of locations when emissions uncertainty is considered. Other dynamic evaluations (Zhou et al., 2013, Godowitch et al., 2010, Gilliland et al., 2008, Godowitch et al., 2007) have suggested that CMAQ may be a conservative estimate of the air quality improvements resulting from emissions reductions.

This TSD summarizes the ability of the model to reproduce 2007 conditions simulated using specific emissions, meteorological, initial conditions and boundary conditions inputs described above. This operational evaluation shows that the CMAQ model predictions for 2007 are equivalent or better than typical regional modeling simulations as summarized in Simon et al. (2012).

In the following sections we present general model performance statistics and plots for five regions of the U.S. We compare model predictions of maximum daily 8-hr average (MDA8) O_3 concentrations to measurements reported in EPA's Air Quality System (AQS) which is a repository of air pollution measurements made by EPA, state, local, and tribal agencies. For the 2007 model performance evaluation, we ran CMAQ for 2007 using the same emissions as those used for the 2007 HDDM runs, except that we included actual wild fires instead of average fires and we used CEM data to for hourly EGU emissions (U.S. EPA, 2012b) instead of the multi-year average temporal method used for the HDDM runs.

The model statistics presented here include mean bias, mean error, normalized mean bias, and normalized mean error as calculated in Simon et al. (2012). Our analysis focuses on regional model evaluation statistics from five U.S. regions as well as evaluations of the 15 urban areas included in the Risk and Exposure Assessment. The five regions are defined as follows: Northeast (Connecticut, Delaware, District of Columbia, Maine, Maryland, Massachusetts, New Hampshire, New Jersey, New York, Pennsylvania, Rhode Island, Vermont), Southeast (Alabama, Florida, Georgia, Kentucky, Mississippi, North Carolina, South Carolina, Tennessee, Virginia, West Virginia), Midwest (Illinois, Indiana, Michigan, Ohio, Wisconsin), Central (Arkansas, Iowa, Kansas, Louisiana, Minnesota, Missouri, Nebraska, Oklahoma, Texas), and West (Arizona, California, Colorado, Idaho, Nevada, New Mexico, Oregon, Utah, Wyoming). Statistics for model performance in these regions and urban areas are shown by season in Table 4B-4 through Table 4B-23 for observed days with MDA8 O_3 values >= 60 ppb, observed days with MDA8 O_3 < 60 ppb, and for all observed days. Plots are provided to show regional maps of Normalized Mean Bias by season and time series of modeled and measured O_3 concentrations in each urban area. Time series are provided for MDA8 O_3 from April-October 2007 and for

hourly O_3 from one month from each season in 2007 (January, April, July, October) where monitoring data is available. Note that time series show average concentrations across all monitors within each urban area and the number of monitors included in this average sometimes changes by season since different monitors within each area take measurements over different periods of the year.

4B-2.1 Operational Evaluation in the Northeast U.S.

Table 4B-4 shows that in the Northeastern U.S., model mean bias was generally less than 6 ppb and normalized mean bias was less than 15% in most cases. High O_3 days and summertime days were more likely to be under-estimated by the model while low O_3 days and wintertime days were more likely to be over-estimated by the model. Performance was best in the spring and fall and had the largest errors in the winter. Five of the 15 urban areas evaluated were in the Northeast: Boston, New York, Philadelphia, Baltimore, and Washington D.C.

Model performance at Boston area monitoring sites (Table 4B-5) was similar to that at other Northeastern U.S. sites. The time series plots show that the model has skill at reproducing measured day-to-day variability in MDA8 O_3 concentrations (Figure 4B-6). Hourly daytime and nighttime O_3 concentrations are also well modeled in all seasons with exception of a few 2-3 day periods in July in which the model over-estimates daytime and nighttime O_3 with some over-estimates of daytime peaks in October (Figure 4B-7 through Figure 4B-10).[1]

Bulk performance statistics for MDA8 model estimates in New York (Table 4B-6) also look equivalent to both the Boston statistics and those of the Northeast as a whole. Again, the 7-month time series of MDA8 O_3 at NY area sites shows that the model captures synoptic variations in O_3 concentrations (Figure 4B-11). Hourly New York area O_3 in January is generally well captured by the model, although CMAQ does somewhat under-estimate the daytime peaks (Figure 4B-12). The April time series (Figure 4B-13) shows that the model captures the range of measured daytime and nighttime O_3 values but has a 3-day period of over-estimates in early April and a week-long period of under-estimates later in the month. July and October O_3 is well captured by the model on both low and high O_3 days and at night (Figure 4B-14 and Figure 4B-15).

Bulk model performance statistics for Philadelphia (Table 4B-7) are equivalent to those for the Northeast as a whole. The time series plots show that variations of MDA8 are well captured in Philadelphia (Figure 4B-16) and that the model does a reasonable job of estimating day to night O_3 changes in all seasons but has some under-estimates of daytime O_3 in January (Figure 4B-17) and some over-estimates of daytime and nighttime O_3 in October (Figure 4B-20).

[1] Note that the Y-axis scale for the various time series are not consistent

Baltimore MDA8 O_3 performance (Table 4B-8) is generally similar to O_3 performance in the rest of the Northeast except for summertime values which are somewhat more overestimated in Baltimore (8 ppb MB in Baltimore versus 4 ppb MB in the Northeast). Still, these bias and error statistics are well within the range of state-of-the-science model performance described by Simon et al. (2012). As shown by the time series in Figure 4B-21, most model overestimates in this area occur from late July to late August. Outside of that time period, the MDA8 variations from April-October are well captured by the model. The hourly time series plots for Baltimore generally show reasonable agreement between the observed and modeled values although the period of over-estimated daytime O_3 concentrations in July is apparent in Figure 4B-24.

Bulk statistics for Washington D.C. sites (Table 4B-9) are similar to statistics for the rest of the Northeast region. The period of overestimated MDA8 values in late July through August which was seen in nearby Baltimore is less pronounced in Washington D.C. (Figure 4B-26). Hourly time series generally show reasonable performance with some overestimates of nighttime O_3 in October (Figure 4B-30).

Table 4B-4. Summary of CMAQ model performance at AQS monitoring sites in the Northeastern U.S.

Season	MDA8	No. of Days	MB (ppb)	NMB (%)	ME (ppb)	NME (%)
Winter	< 60 ppb	5085	-4.65	-17.0	5.83	21.2
	≥ 60 ppb	0	NA	NA	NA	NA
	All Days	5085	-4.65	-17.0	5.83	21.2
Spring	< 60 ppb	10420	-0.69	-1.4	5.63	13.2
	≥ 60 ppb	1856	-6.34	-9.1	8.25	11.8
	All Days	12276	-1.47	-3.1	6.03	12.9
Summer	< 60 ppb	11859	5.58	13.4	7.99	19.2
	≥ 60 ppb	4114	-0.51	-0.7	7.78	10.9
	All Days	15973	4.01	8.2	7.93	16.1
Fall	< 60 ppb	10036	2.86	8.1	6.23	17.7
	≥ 60 ppb	1030	-4.21	-6.1	8.06	11.7
	All Days	11066	2.21	5.8	6.40	16.7

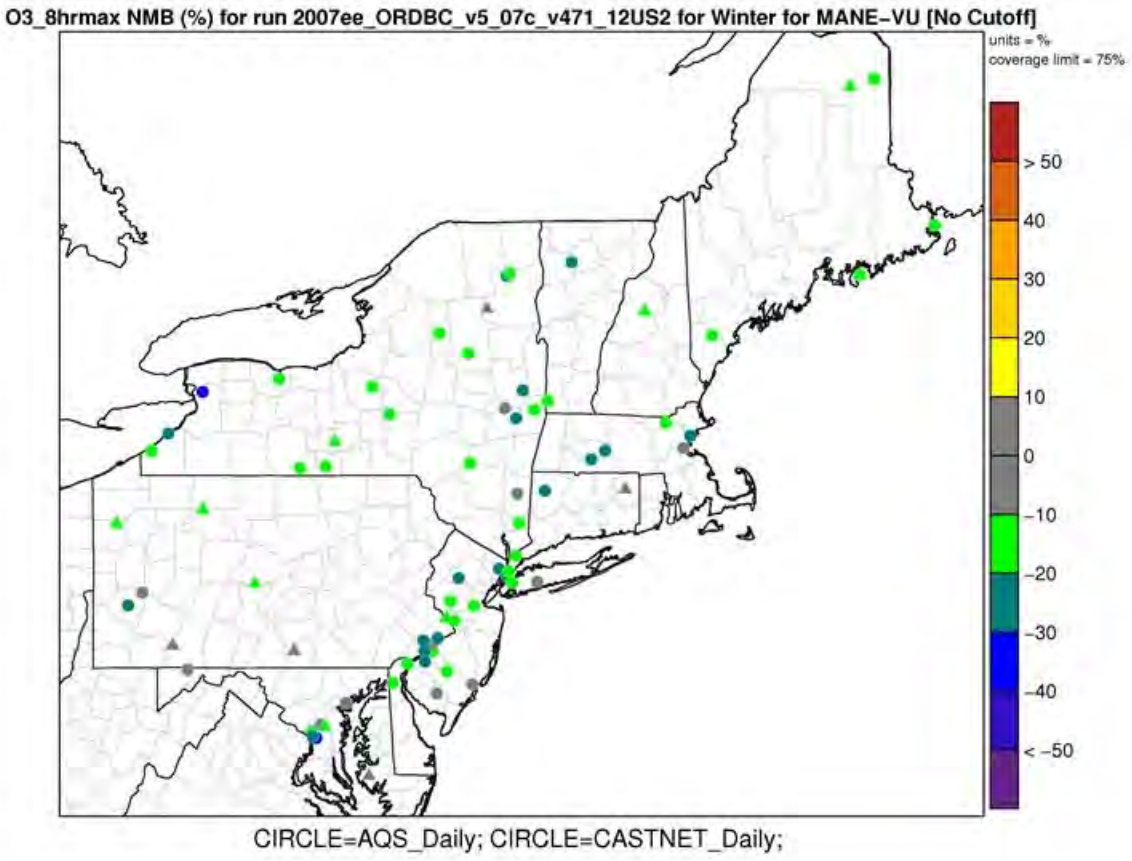

Figure 4B-2. Map of normalized mean bias for MDA8 O_3 concentrations in the Northeastern U.S. for winter months in 2007.

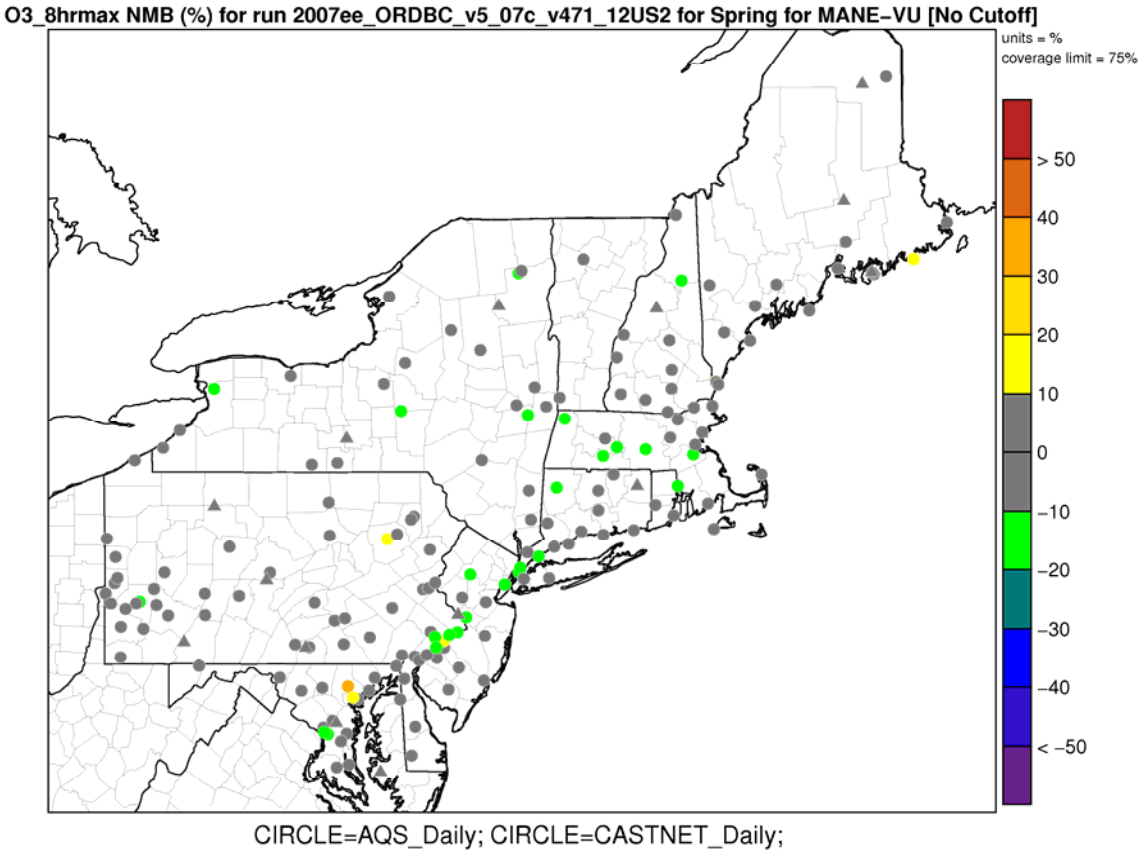

Figure 4B-3. Map of normalized mean bias for MDA8 O_3 concentrations in the Northeastern U.S. for spring months in 2007.

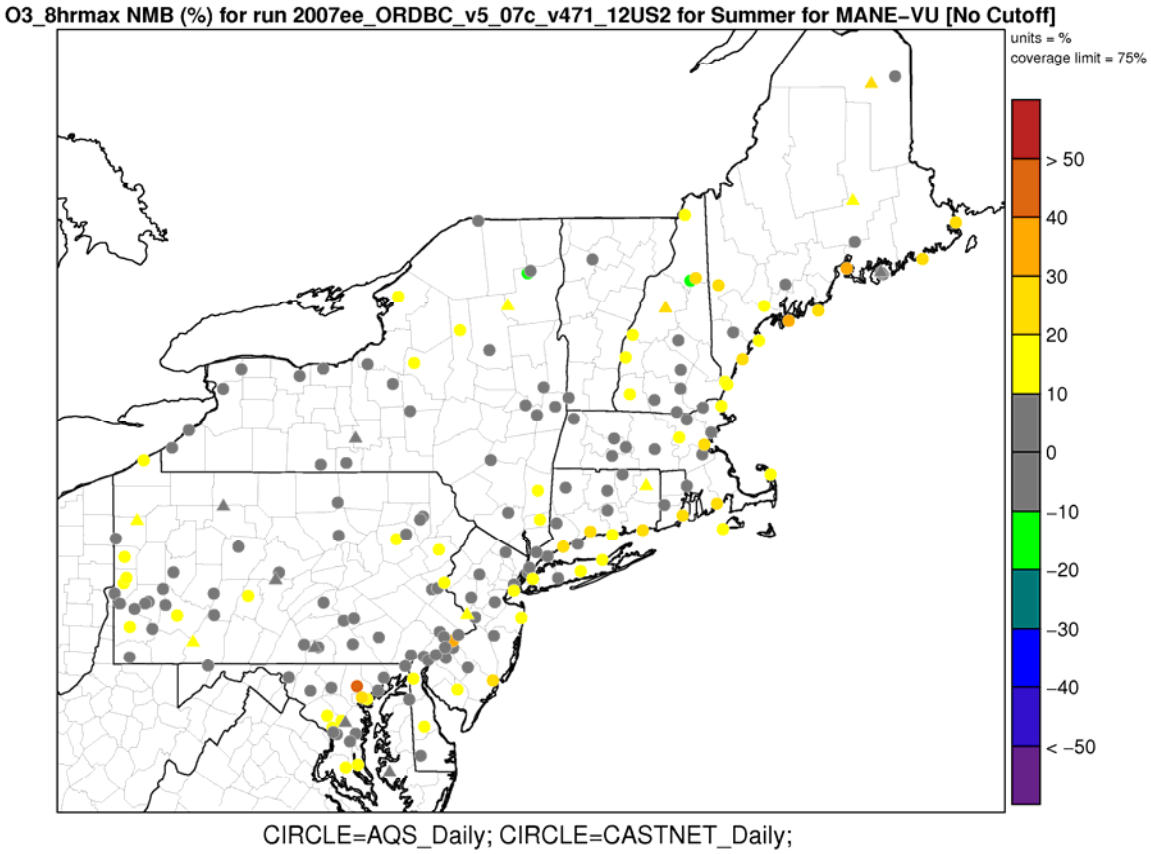

Figure 4B-4. Map of normalized mean bias for MDA8 O_3 concentrations in the Northeastern U.S. for summer months in 2007.

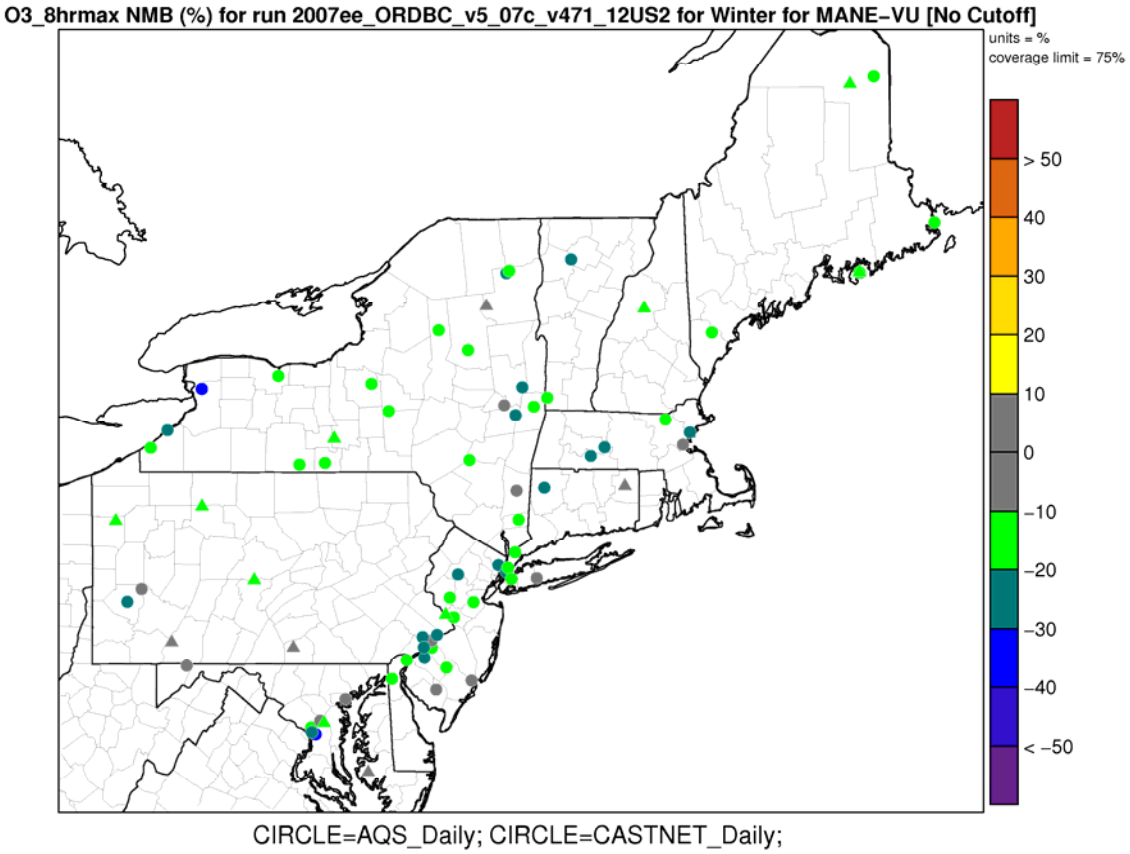

Figure 4B-5. Map of normalized mean bias for MDA8 O_3 concentrations in the Northeastern U.S. for fall months in 2007.

Table 4B-5. Summary of CMAQ model performance at AQS monitoring sites in the Boston area.

Season	MDA8	No. of Days	MB (ppb)	NMB (%)	ME (ppb)	NME (%)
Winter	< 60 ppb	265	-3.91	-15.1	5.40	20.9
	≥ 60 ppb	0	NA	NA	NA	NA
	All Days	265	-3.91	-15.1	5.40	20.9
Spring	< 60 ppb	680	-1.32	-3.1	5.73	13.5
	≥ 60 ppb	87	-4.95	-7.0	8.46	11.9
	All Days	767	-1.73	-3.8	6.04	13.2
Summer	< 60 ppb	784	6.71	16.5	8.47	20.8
	≥ 60 ppb	210	-2.88	-4.0	8.76	12.1
	All Days	994	4.69	9.9	8.53	18.0
Fall	< 60 ppb	433	3.69	11.3	6.22	19.0
	≥ 60 ppb	62	-6.48	-9.1	9.92	13.9
	All Days	495	2.42	6.4	6.68	17.8

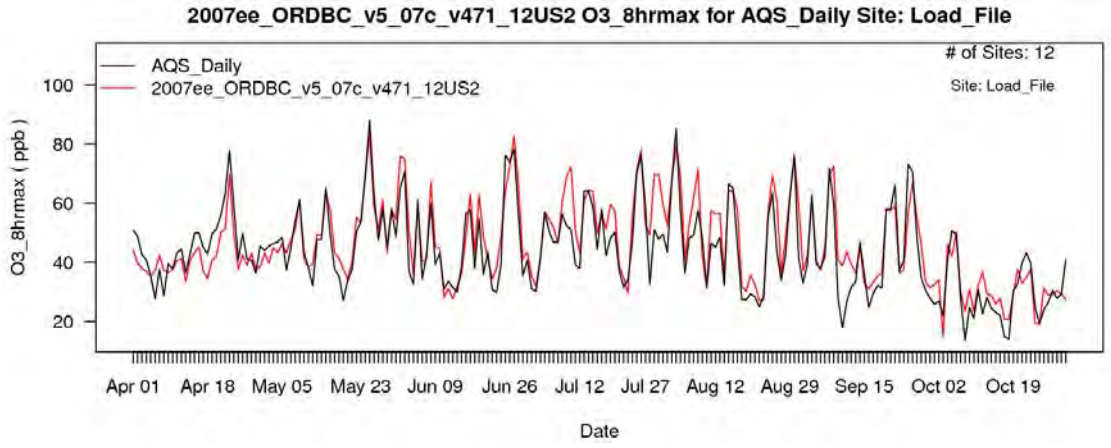

Figure 4B-6. Time series of 8-hr daily maximum O_3 concentrations at Boston monitoring sites for April-October 2007. Observed values shown in black and modeled values shown in red.

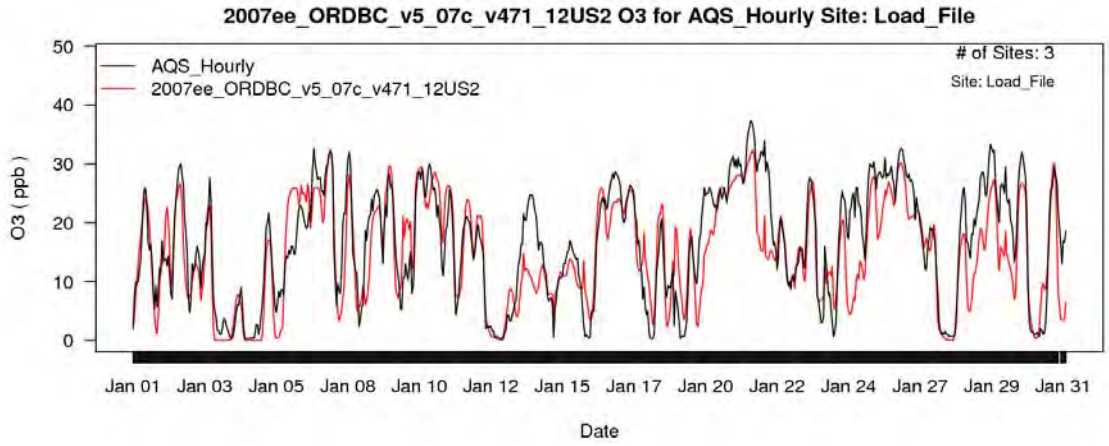

Figure 4B-7. Time series of hourly O_3 concentrations at Boston monitoring sites for January 2007. Observed values shown in black and modeled values shown in red.

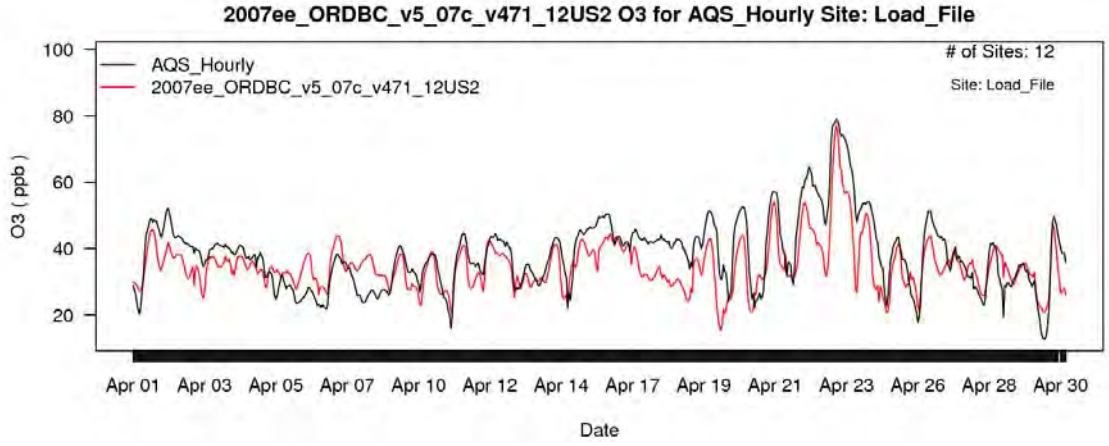

Figure 4B-8. Time series of hourly O_3 concentrations at Boston monitoring sites for April 2007. Observed values shown in black and modeled values shown in red.

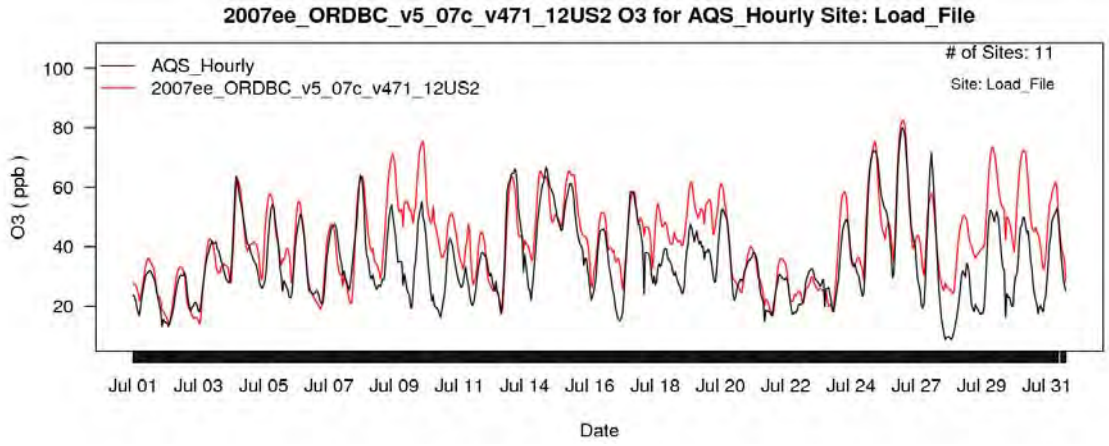

Figure 4B-9. Time series of hourly O_3 concentrations at Boston monitoring sites for July 2007. Observed values shown in black and modeled values shown in red.

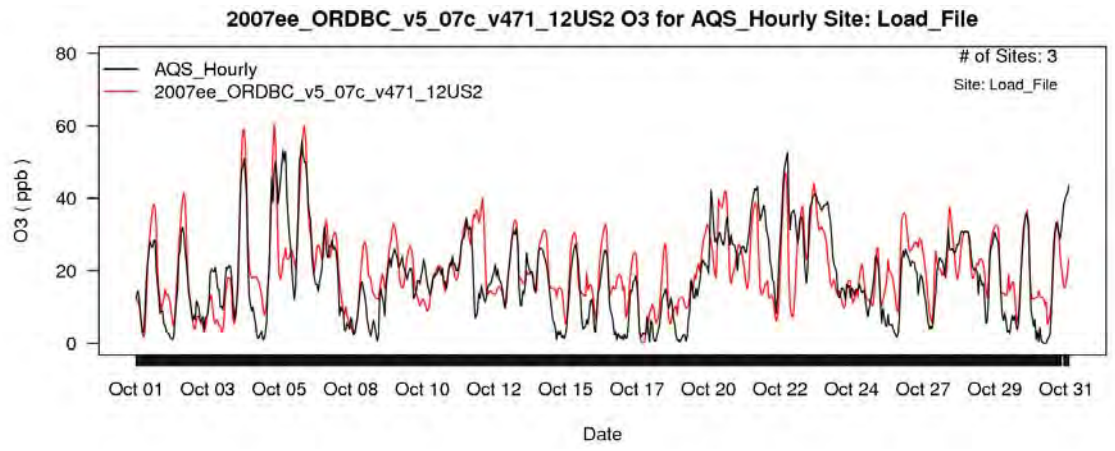

Figure 4B-10. Time series of hourly O_3 concentrations at Boston monitoring sites for October 2007. Observed values shown in black and modeled values shown in red.

Table 4B-6. Summary of CMAQ model performance at AQS monitoring sites in the New York area.

Season	MDA8	No. of Days	MB (ppb)	NMB (%)	ME (ppb)	NME (%)
Winter	< 60 ppb	916	-4.14	-17.8	5.34	22.9
	≥ 60 ppb	0	NA	NA	NA	NA
	All Days	916	-4.14	-17.8	5.34	22.9
Spring	< 60 ppb	1547	-1.20	-3.0	6.04	15.0
	≥ 60 ppb	200	-6.05	-8.5	9.45	13.2
	All Days	1747	-1.75	-4.0	6.43	14.7
Summer	< 60 ppb	1469	5.16	12.3	8.53	20.4
	≥ 60 ppb	635	1.48	2.0	9.25	12.7
	All Days	2104	4.05	7.9	8.75	17.1
Fall	< 60 ppb	1443	2.01	6.2	6.40	19.7
	≥ 60 ppb	108	-5.60	-8.1	8.90	12.8
	All Days	1551	1.48	4.2	6.58	18.7

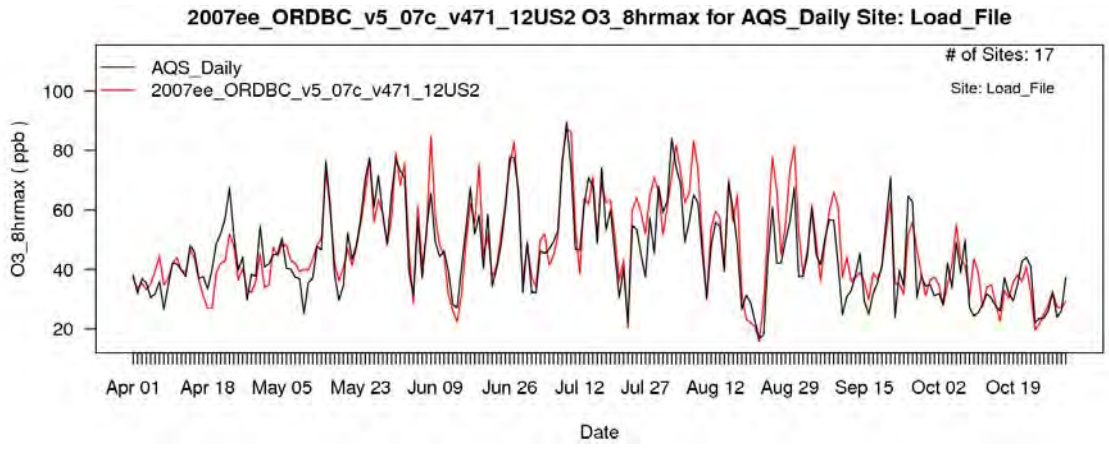

Figure 4B-11. Time series of 8-hr daily maximum O_3 concentrations at New York monitoring sites for April-October 2007. Observed values shown in black and modeled values shown in red.

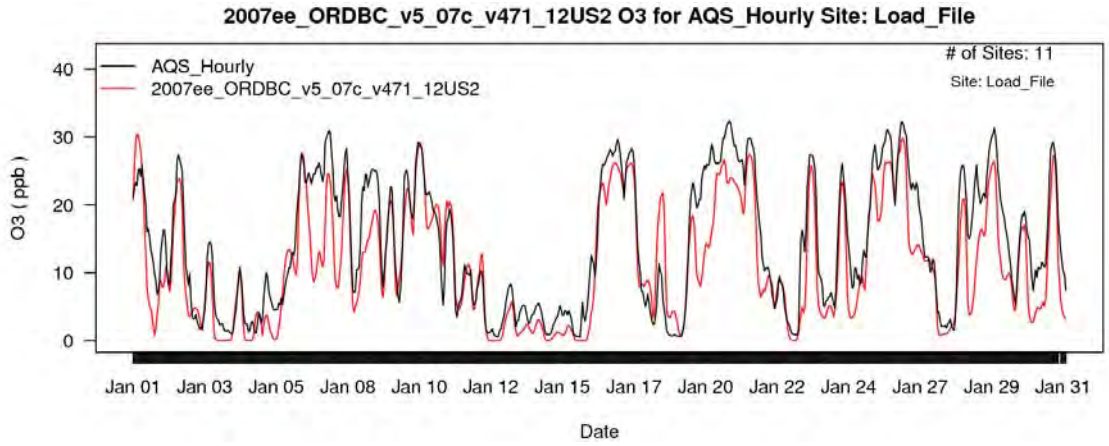

Figure 4B-12. Time series of hourly O_3 concentrations at New York monitoring sites for January 2007. Observed values shown in black and modeled values shown in red.

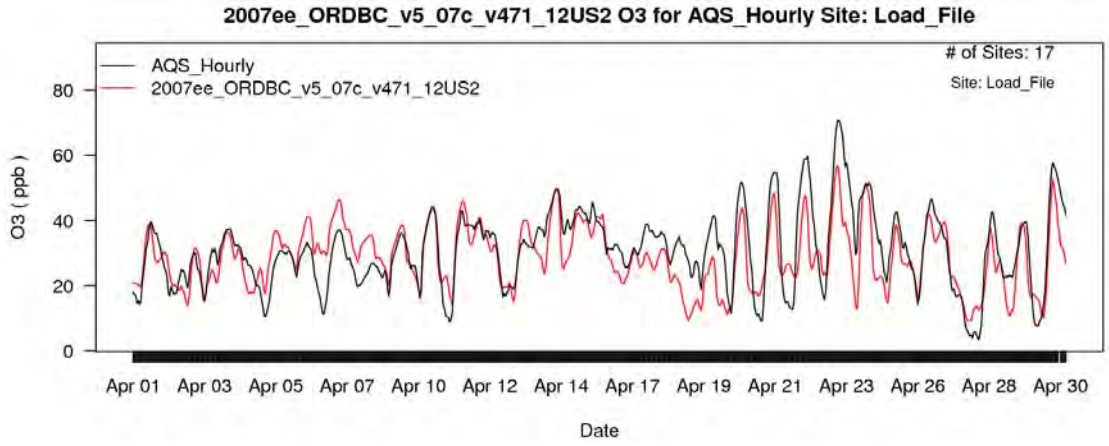

Figure 4B-13. Time series of hourly O_3 concentrations at New York monitoring sites for April 2007. Observed values shown in black and modeled values shown in red.

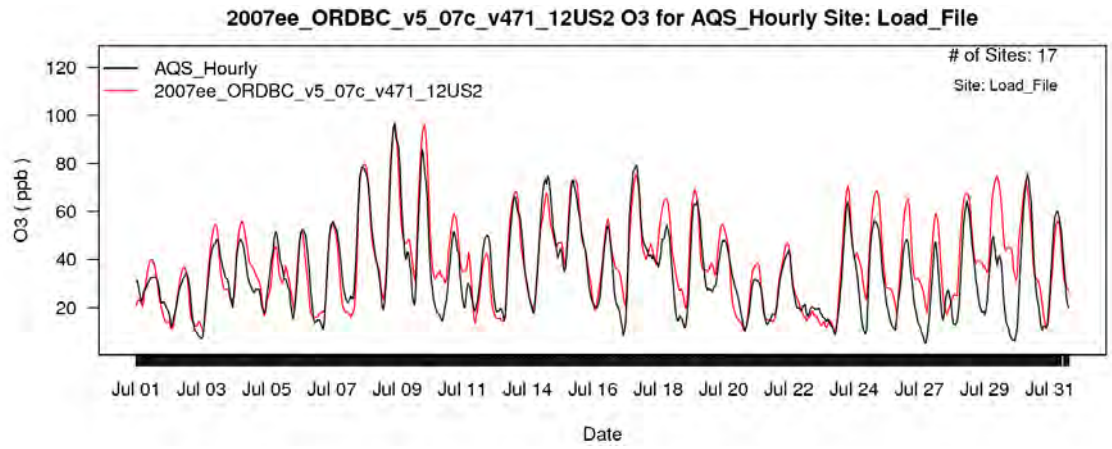

Figure 4B-14. Time series of hourly O_3 concentrations at New York monitoring sites for July 2007. Observed values shown in black and modeled values shown in red.

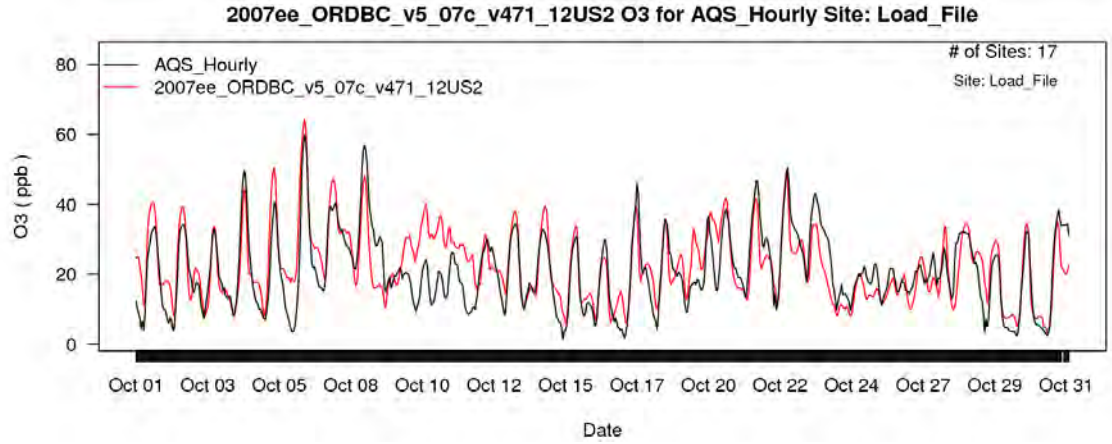

Figure 4B-15. Time series of hourly O_3 concentrations at New York monitoring sites for October 2007. Observed values shown in black and modeled values shown in red.

Table 4B-7. Summary of CMAQ model performance at AQS monitoring sites in the Philadelphia area.

Season	MDA8	No. of Days	MB (ppb)	NMB (%)	ME (ppb)	NME (%)
Winter	< 60 ppb	684	-3.48	-14.4	5.15	21.3
	≥ 60 ppb	0	NA	NA	NA	NA
	All Days	684	-3.48	-14.4	5.15	21.3
Spring	< 60 ppb	942	-0.80	-1.9	5.93	14.1
	≥ 60 ppb	204	-7.01	-9.9	8.6	12.1
	All Days	1146	-1.91	-4.0	6.40	13.5
Summer	< 60 ppb	778	6.25	9.44	14.1	21.3
	≥ 60 ppb	507	1.23	1.7	7.80	10.8
	All Days	1285	4.27	7.7	8.79	15.9
Fall	< 60 ppb	1005	2.69	7.8	6.01	17.4
	≥ 60 ppb	103	-4.51	-6.7	7.68	11.4
	All Days	1108	2.02	5.4	6.16	16.4

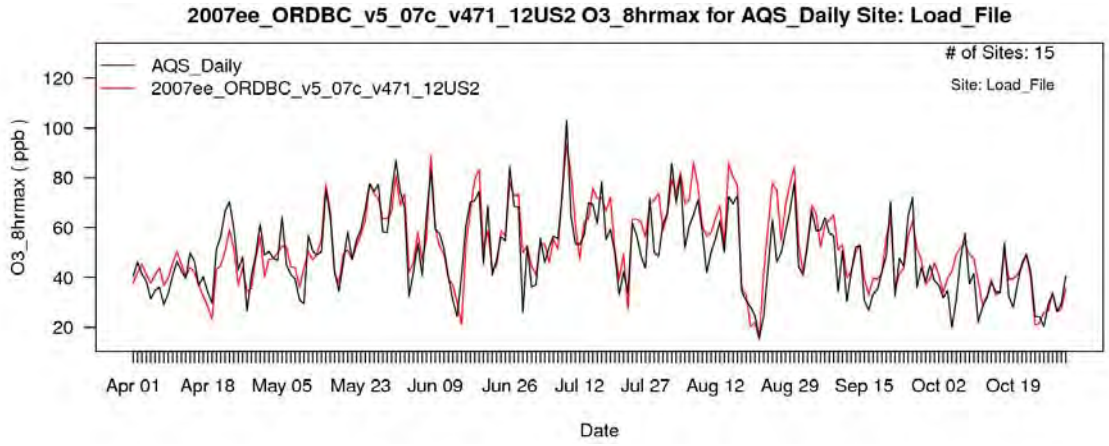

Figure 4B-16. Time series of 8-hr daily maximum O_3 concentrations at Philadelphia monitoring sites for April-October 2007. Observed values shown in black and modeled values shown in red.

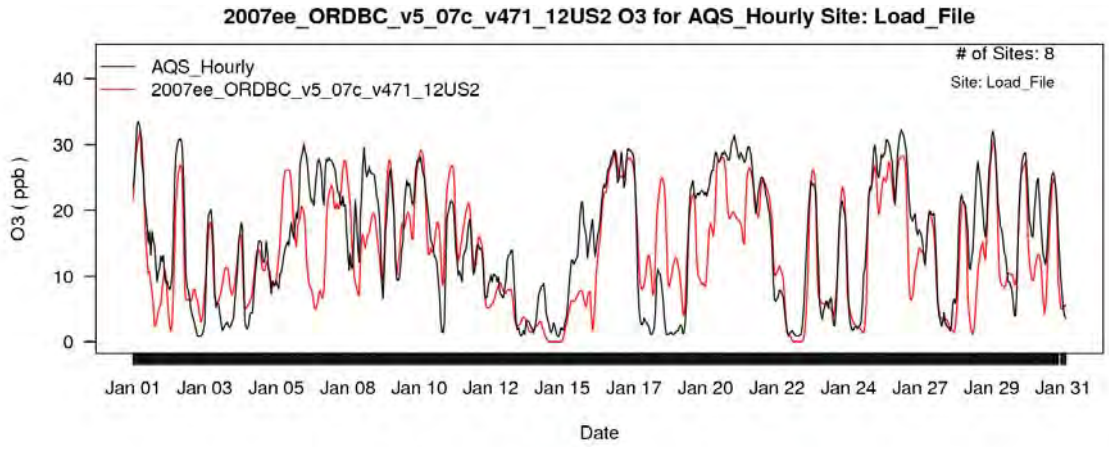

Figure 4B-17. Time series of hourly O_3 concentrations at Philadelphia monitoring sites for January 2007. Observed values shown in black and modeled values shown in red.

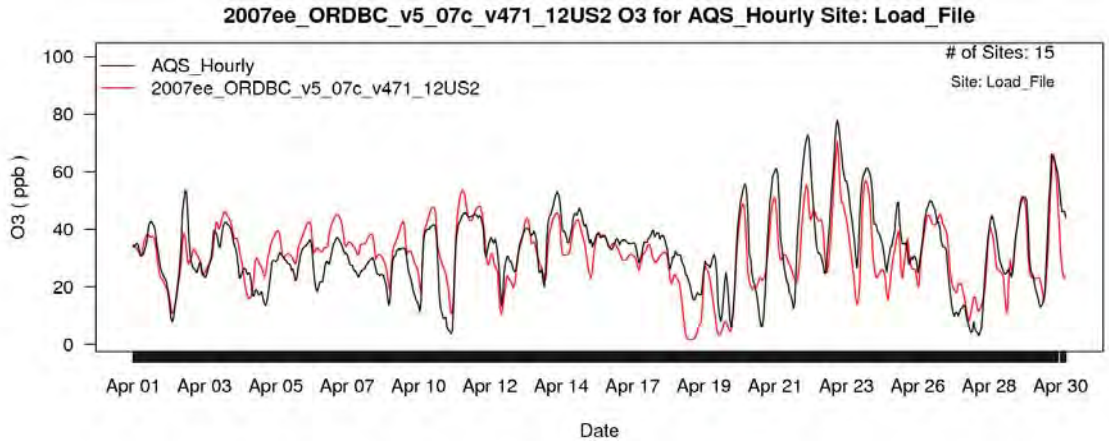

Figure 4B-18. Time series of hourly O_3 concentrations at Philadelphia monitoring sites for April 2007. Observed values shown in black and modeled values shown in red.

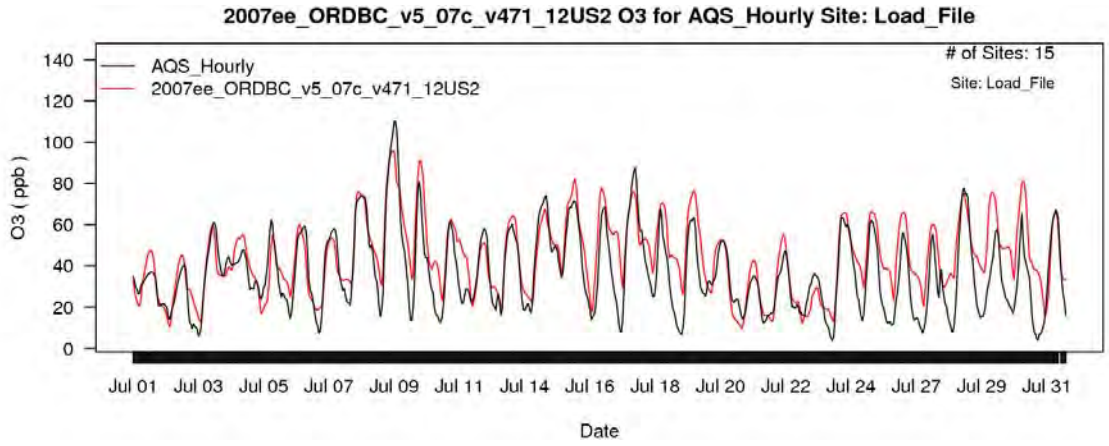

Figure 4B-19. Time series of hourly O_3 concentrations at Philadelphia monitoring sites for July 2007. Observed values shown in black and modeled values shown in red.

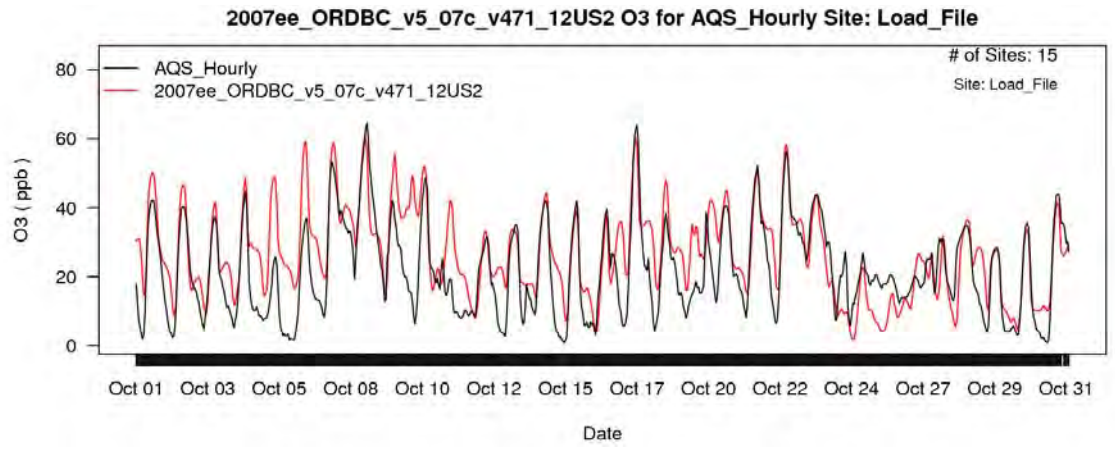

Figure 4B-20. Time series of hourly O_3 concentrations at Philadelphia monitoring sites for October 2007. Observed values shown in black and modeled values shown in red.

Table 4B-8. Summary of CMAQ model performance at AQS monitoring sites in the Baltimore area.

Season	MDA8	No. of Days	MB (ppb)	NMB (%)	ME (ppb)	NME (%)
Winter	< 60 ppb	78	-1.50	-7.0	4.63	21.5
	≥ 60 ppb	0	NA	NA	NA	NA
	All Days	78	-1.50	-7.0	4.63	21.5
Spring	< 60 ppb	358	4.62	11.1	6.81	16.3
	≥ 60 ppb	92	-0.86	-1.2	5.92	8.5
	All Days	450	3.50	7.4	6.62	14.0
Summer	< 60 ppb	382	10.40	23.2	11.60	25.8
	≥ 60 ppb	255	4.18	5.7	8.95	12.3
	All Days	637	7.90	14.1	10.50	18.8
Fall	< 60 ppb	389	6.63	17.9	8.35	22.5
	≥ 60 ppb	51	-1.07	-1.5	7.67	11.0
	All Days	440	5.74	14.1	8.27	20.2

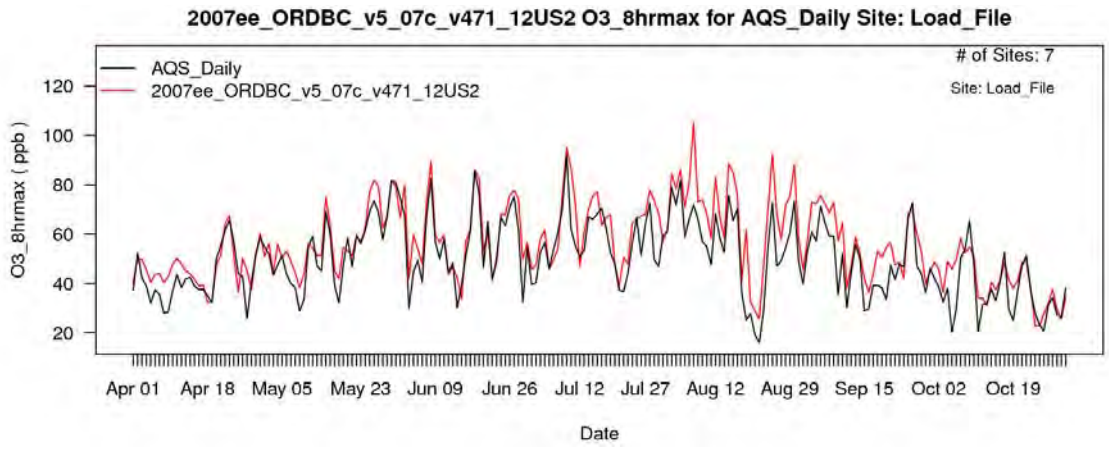

Figure 4B-21. Time series of 8-hr daily maximum O_3 concentrations at Baltimore monitoring sites for April-October 2007. Observed values shown in black and modeled values shown in red.

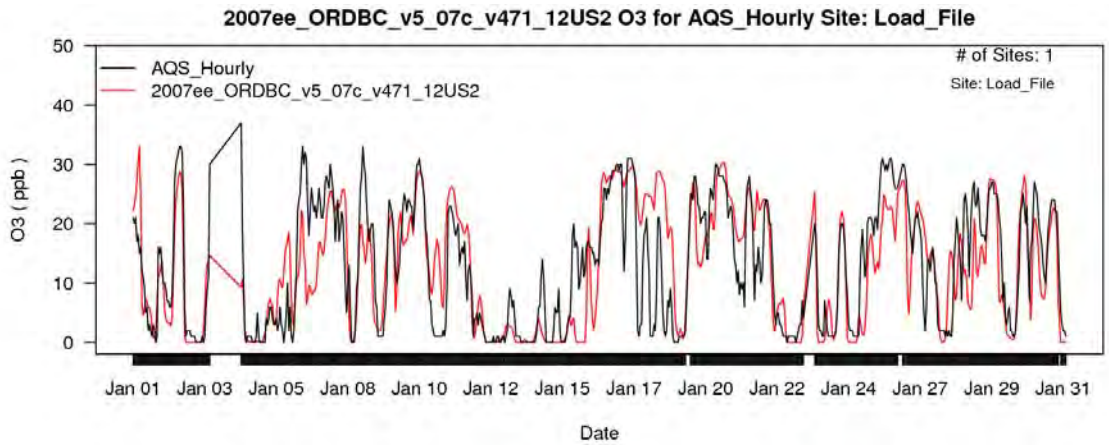

Figure 4B-22. Time series of hourly O_3 concentrations at Baltimore monitoring sites for January 2007. Observed values shown in black and modeled values shown in red.

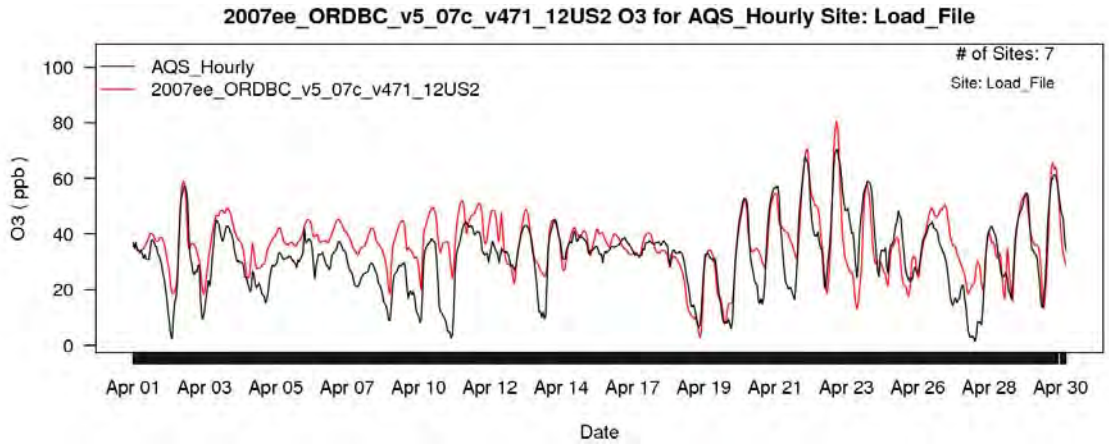

Figure 4B-23. Time series of hourly O_3 concentrations at Baltimore monitoring sites for April 2007. Observed values shown in black and modeled values shown in red.

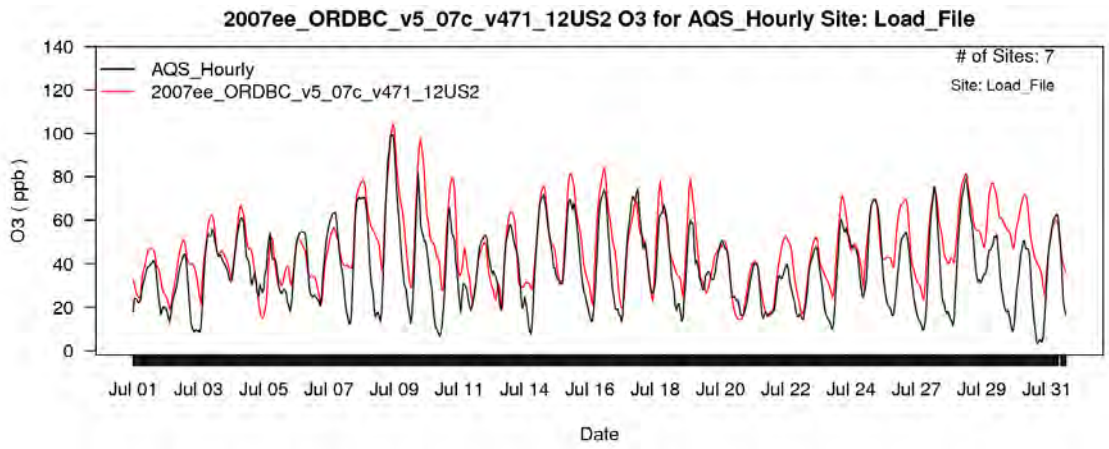

Figure 4B-24. Time series of hourly O_3 concentrations at Baltimore monitoring sites for July 2007. Observed values shown in black and modeled values shown in red.

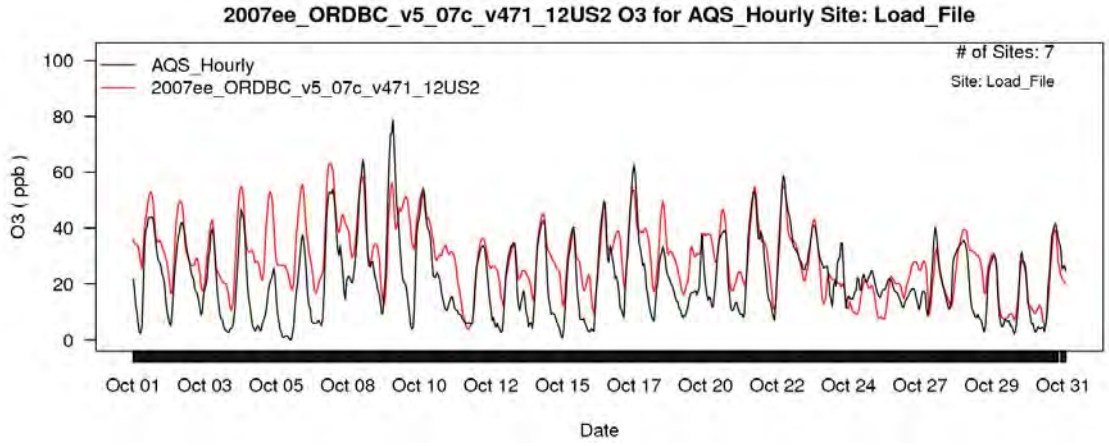

Figure 4B-25. Time series of hourly O_3 concentrations at Baltimore monitoring sites for October 2007. Observed values shown in black and modeled values shown in red.

Table 4B-9. Summary of CMAQ model performance at AQS monitoring sites in the Washington D.C. area.

Season	MDA8	No. of Days	MB (ppb)	NMB (%)	ME (ppb)	NME (%)
Winter	< 60 ppb	565	-4.97	-20.5	6.12	25.2
	≥ 60 ppb	0	NA	NA	NA	NA
	All Days	565	-4.97	-20.5	6.12	25.2
Spring	< 60 ppb	1120	-0.95	-2.2	6.11	14.2
	≥ 60 ppb	334	-4.98	-7.3	7.00	10.2
	All Days	1454	-1.88	-3.8	6.31	12.9
Summer	< 60 ppb	1066	6.55	13.9	8.24	17.5
	≥ 60 ppb	819	2.36	3.3	7.13	10.2
	All Days	1885	4.73	8.3	7.76	13.6
Fall	< 60 ppb	1188	2.07	5.4	7.22	19.0
	≥ 60 ppb	106	-2.03	-3.0	8.37	12.4
	All Days	1394	1.46	3.5	7.39	17.4

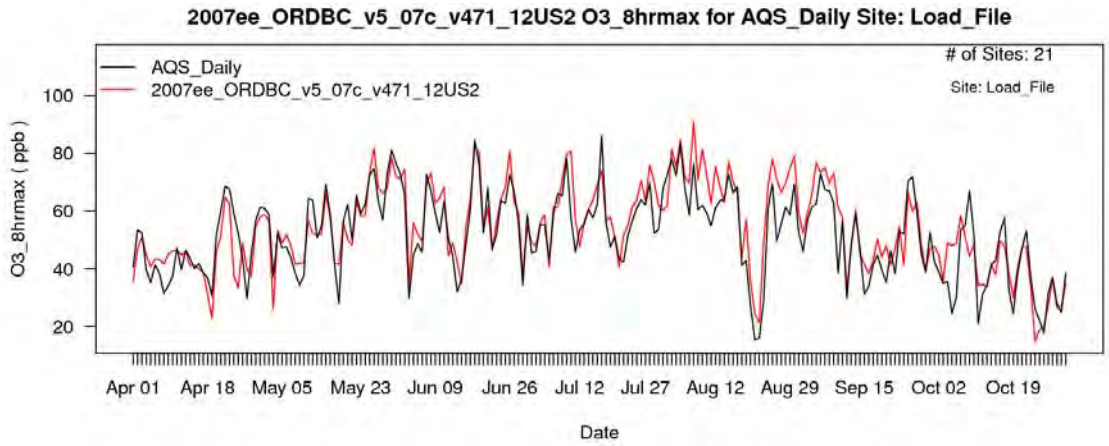

Figure 4B-26. Time series of 8-hr daily maximum O_3 concentrations at Washington D.C. monitoring sites for April-October 2007. Observed values shown in black and modeled values shown in red.

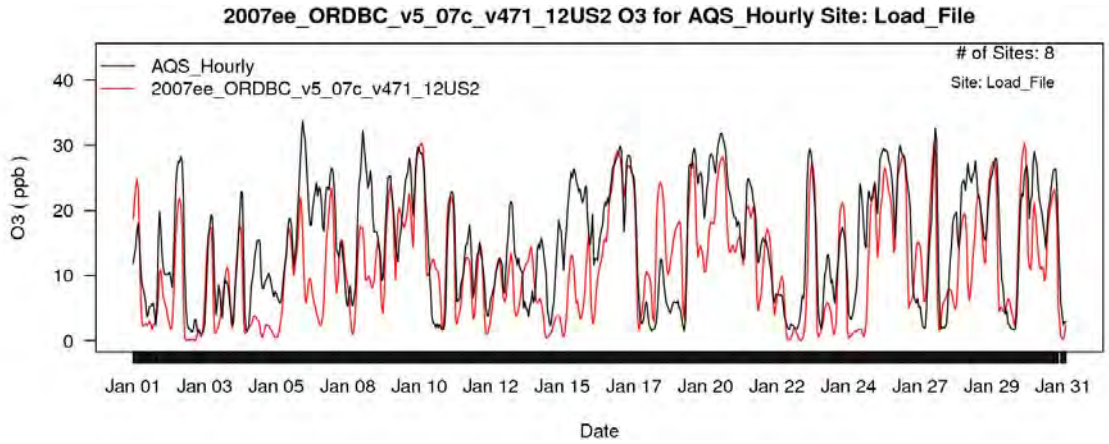

Figure 4B-27. Time series of hourly O_3 concentrations at Washington D.C. monitoring sites for January 2007. Observed values shown in black and modeled values shown in red.

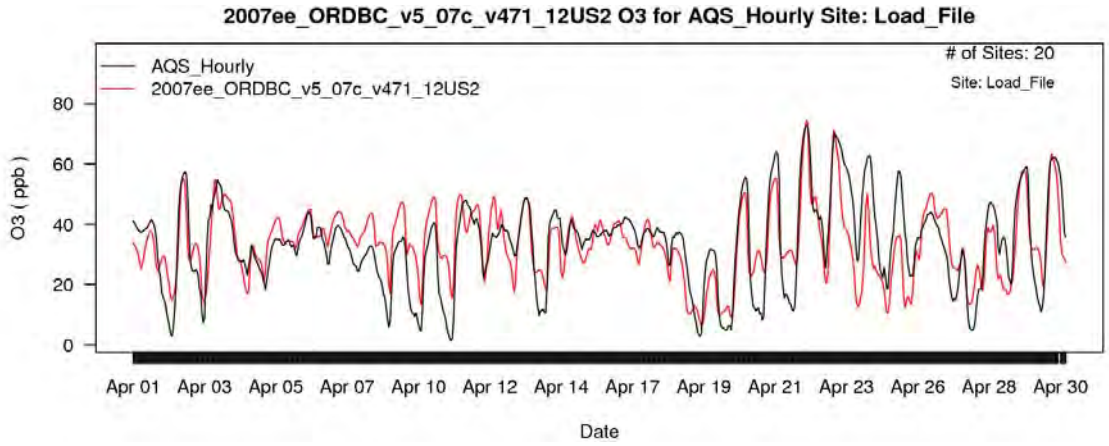

Figure 4B-28. Time series of hourly O_3 concentrations at Washington D.C. monitoring sites for April 2007. Observed values shown in black and modeled values shown in red.

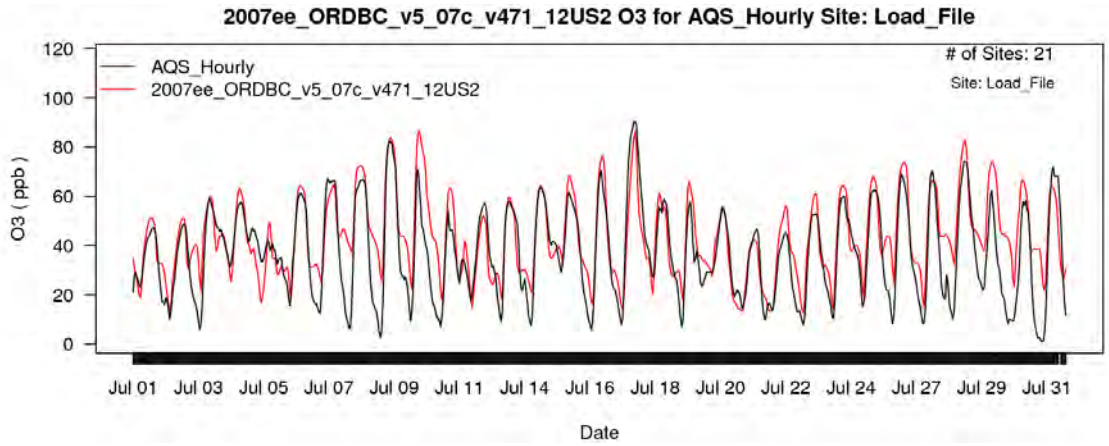

Figure 4B-29. Time series of hourly O_3 concentrations at Washington D.C. monitoring sites for July 2007. Observed values shown in black and modeled values shown in red.

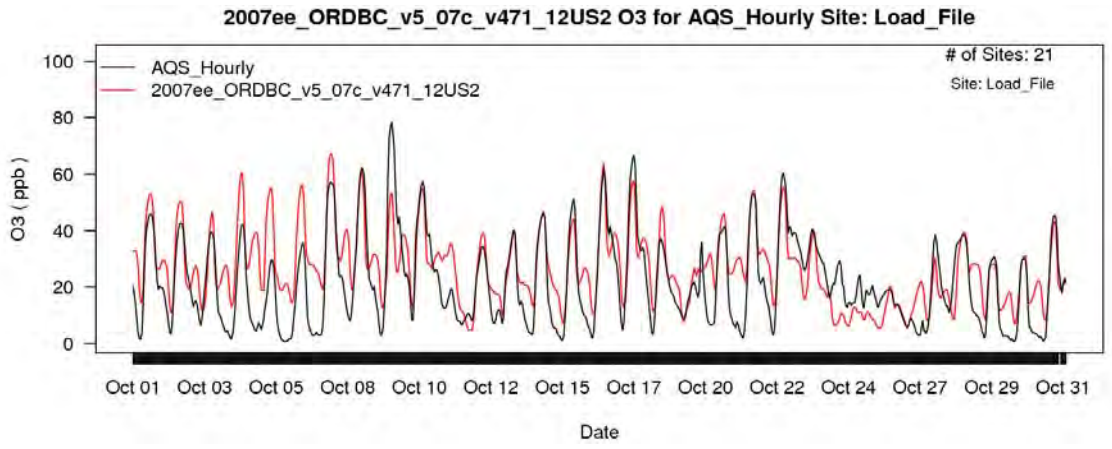

Figure 4B-30. Time series of hourly O_3 concentrations at Washington D.C. monitoring sites for October 2007. Observed values shown in black and modeled values shown in red.

4B-2.2 Operational Evaluation in the Southeast U.S.

Model performance in the Southeastern U.S. was in the range of reported performance for state of the science models (Simon et al., 2012). Mean bias for MDA8 O_3 was less than 5 ppb at most sites in the winter and spring and less than 10 ppb at most sites in the summer and fall seasons. Normalized mean bias was generally less than 10% at most sites in the winter and spring and less than 25% at most sites in the summer and fall. Also, there were very few days above 60 ppb in the winter season (4 days at two sites and 0,1, or 2 days at all other sites), but the model generally had trouble capturing O_3 on those days and had mean biases in the range of -5 to -15 ppb on those days. The higher biases in the summer and fall are most pronounced along the Gulf coast and at sites in Florida. Atlanta was the only one of the 15 urban study areas from the HREA which was located in the Southeast region.

There were no O_3 measurements in the Atlanta area during the winter season. Mean bias and normalized mean bias at Atlanta sites for the spring, summer, and fall months were typical of performance throughout the Southeast region. The April to June MDA8 O_3 time series (Figure 4B-35) shows that the model does a good job of capturing the variability between high and low O_3 days. The hourly time series plots for April (Figure 4B-36), July (Figure 4B-37), and October (Figure 4B-38) show reasonable model performance during daytime hours but some persistent overestimates of nighttime O_3, especially in April and July.

Table 4B-10. Summary of CMAQ model performance at AQS monitoring sites in the Southeastern U.S.

Season	MDA8	No. of Days	MB (ppb)	NMB (%)	ME (ppb)	NME (%)
Winter	< 60 ppb	6378	0.13	0.4	5.32	15.7
	≥ 60 ppb	53	-10.40	-16.1	11.10	17.2
	All Days	6431	0.04	0.1	5.37	15.7
Spring	< 60 ppb	13326	1.10	2.3	5.22	10.8
	≥ 60 ppb	5190	-4.94	-7.4	6.45	9.6
	All Days	18516	-0.60	-1.1	5.57	10.4
Summer	< 60 ppb	14129	10.3	23.2	11.2	25.3
	≥ 60 ppb	6336	0.3	0.5	6.7	9.6
	All Days	20465	7.20	13.8	9.82	18.8
Fall	< 60 ppb	14105	5.43	13.9	7.67	19.7
	≥ 60 ppb	1743	-1.44	-2.1	6.40	9.5
	All Days	15848	4.67	11.1	7.53	17.9

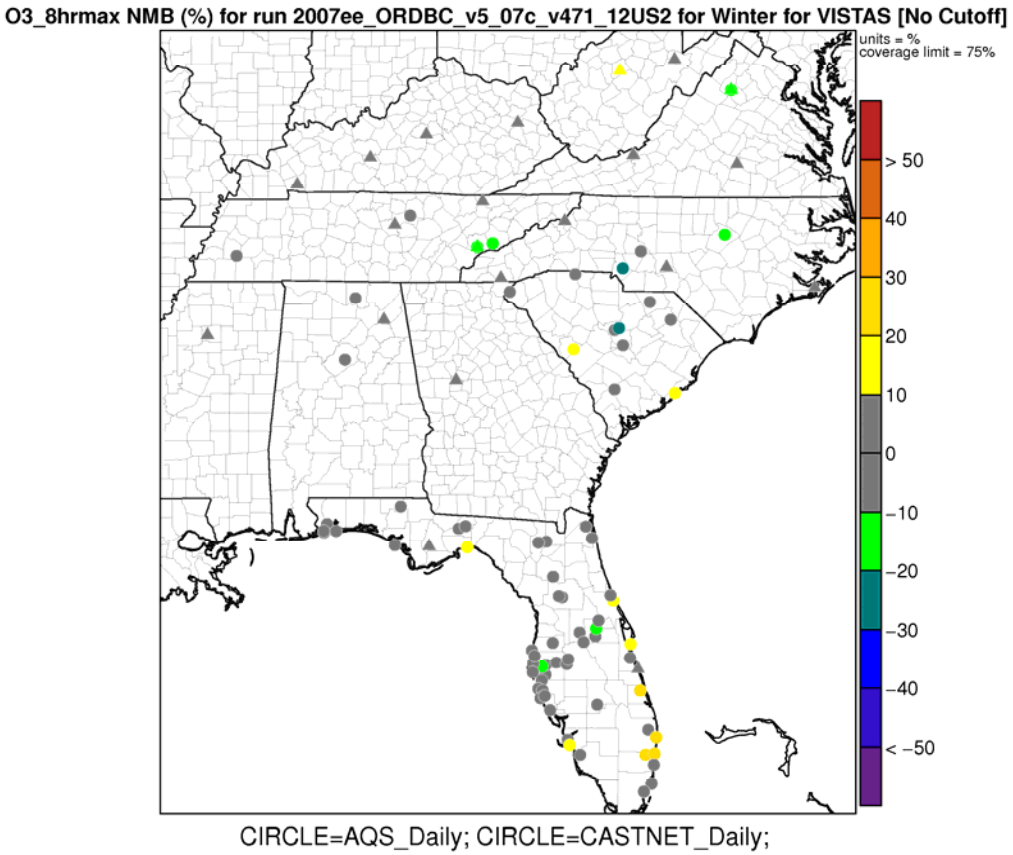

Figure 4B-31. Map of normalized mean bias for MDA8 O_3 concentrations in the Southeastern U.S. for winter months in 2007.

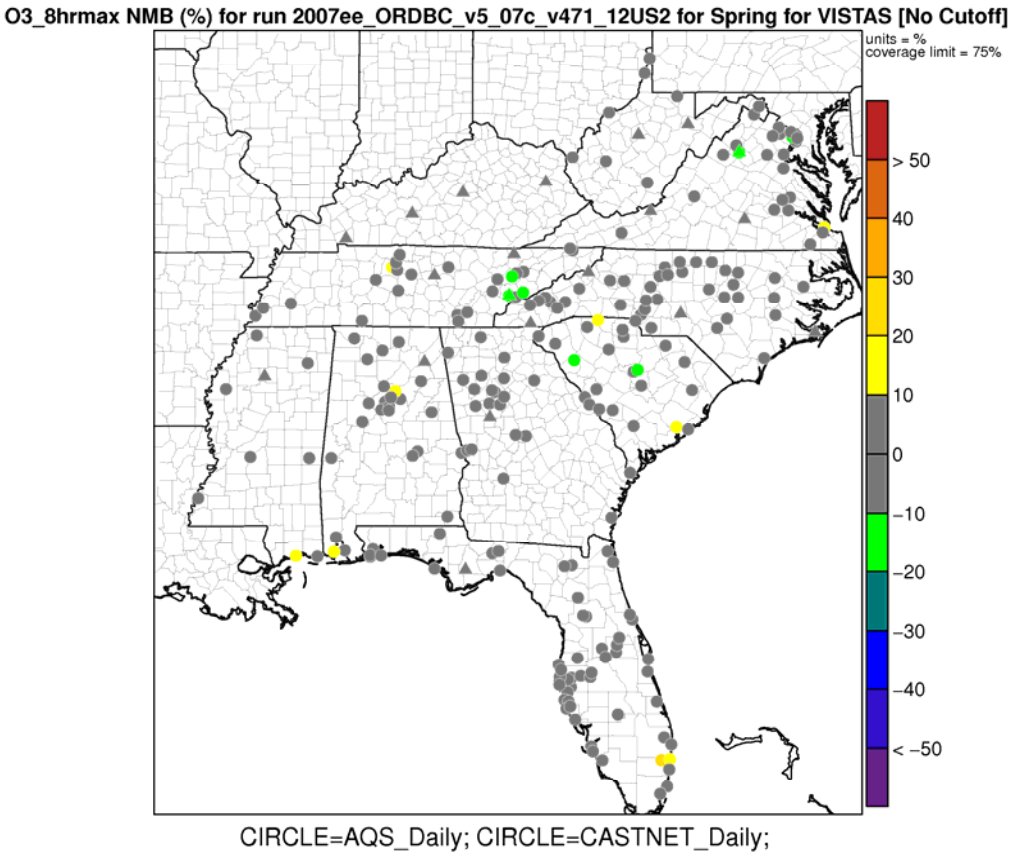

Figure 4B-32. Map of normalized mean bias for MDA8 O_3 concentrations in the Southeastern U.S. for spring months in 2007.

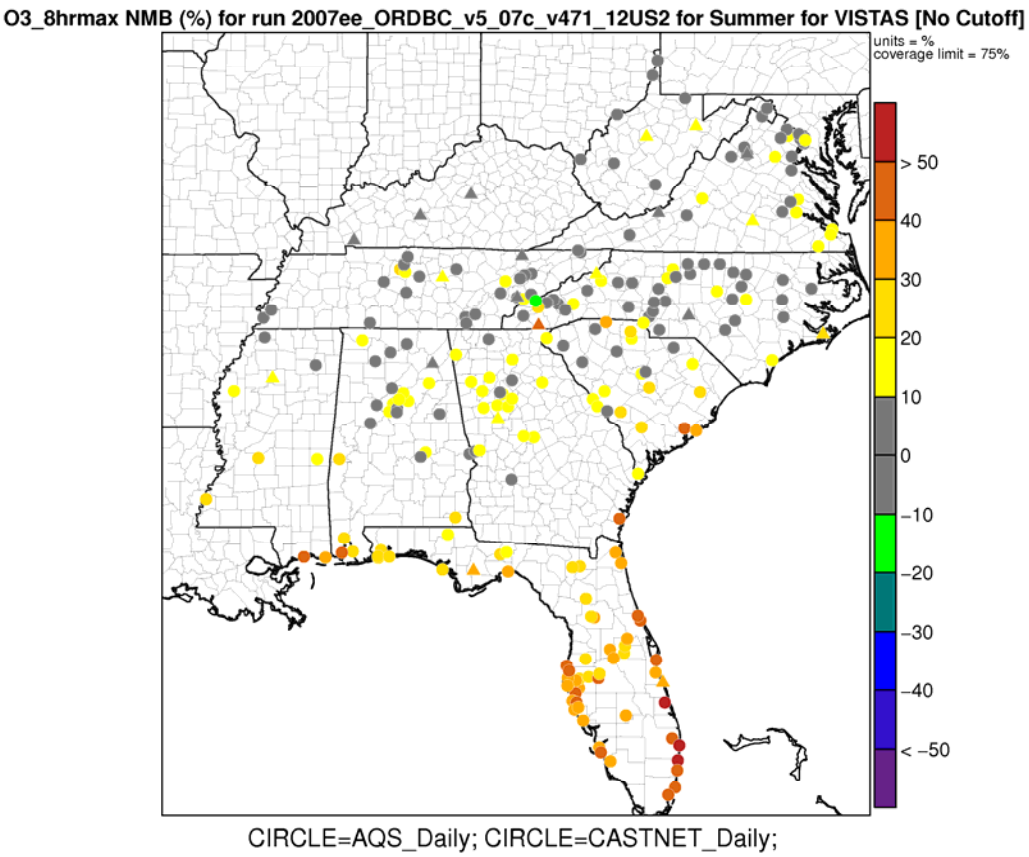

Figure 4B-33. Map of normalized mean bias for MDA8 O_3 concentrations in the Southeastern U.S. for summer months in 2007.

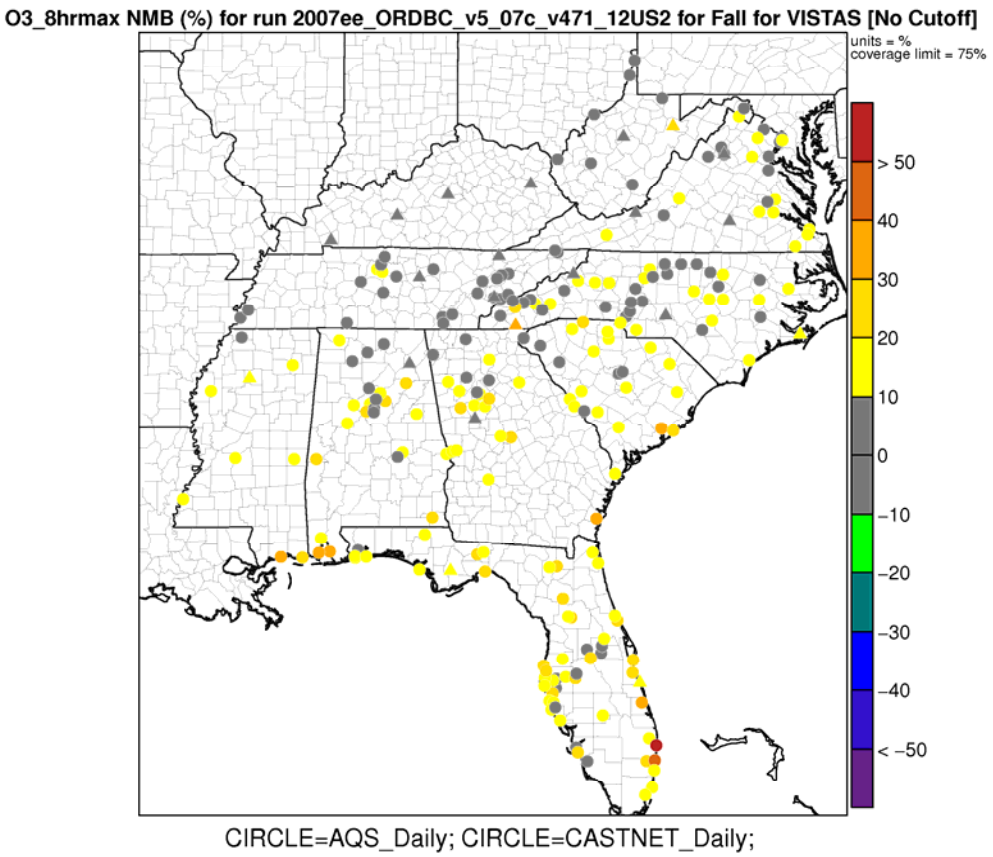

Figure 4B-34. Map of normalized mean bias for MDA8 O_3 concentrations in the Southeastern U.S. for fall months in 2007.

Table 4B-11. Summary of CMAQ model performance at AQS monitoring sites in the Atlanta area.

Season	MDA8	No. of Days	MB (ppb)	NMB (%)	ME (ppb)	NME (%)
Winter	< 60 ppb	0	NA	NA	NA	NA
	≥ 60 ppb	0	NA	NA	NA	NA
	All Days	0	NA	NA	NA	NA
Spring	< 60 ppb	703	0.52	1.1	5.99	12.5
	≥ 60 ppb	295	-3.08	-4.6	6.03	9.0
	All Days	998	-0.54	-1.0	6.00	11.2
Summer	< 60 ppb	510	10.00	21.7	11.50	24.8
	≥ 60 ppb	467	3.77	5.2	8.46	11.5
	All Days	977	7.04	11.9	10.00	17.0
Fall	< 60 ppb	575	5.45	13.7	7.72	19.4
	≥ 60 ppb	87	4.01	5.9	6.27	9.2
	All Days	662	5.26	12.1	7.53	17.3

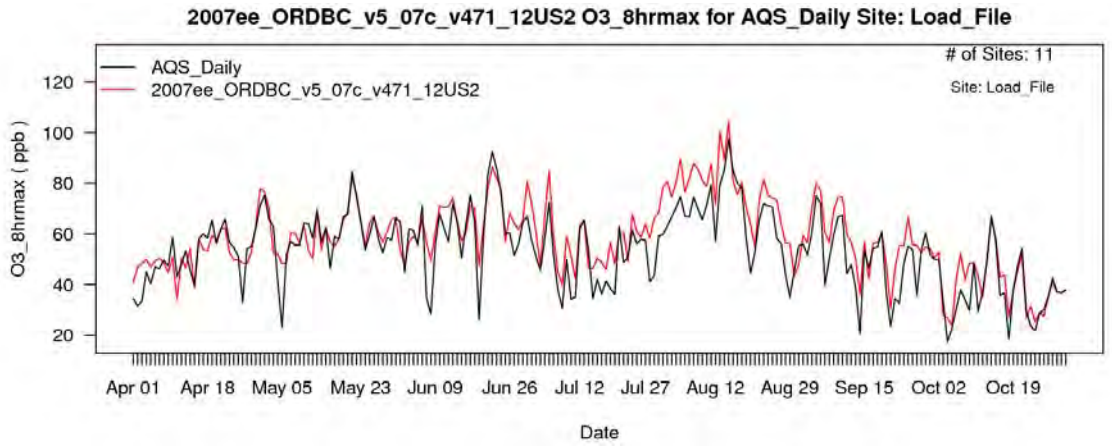

Figure 4B-35. Time series of 8-hr daily maximum O_3 concentrations at Atlanta monitoring sites for April-October 2007. Observed values shown in black and modeled values shown in red.

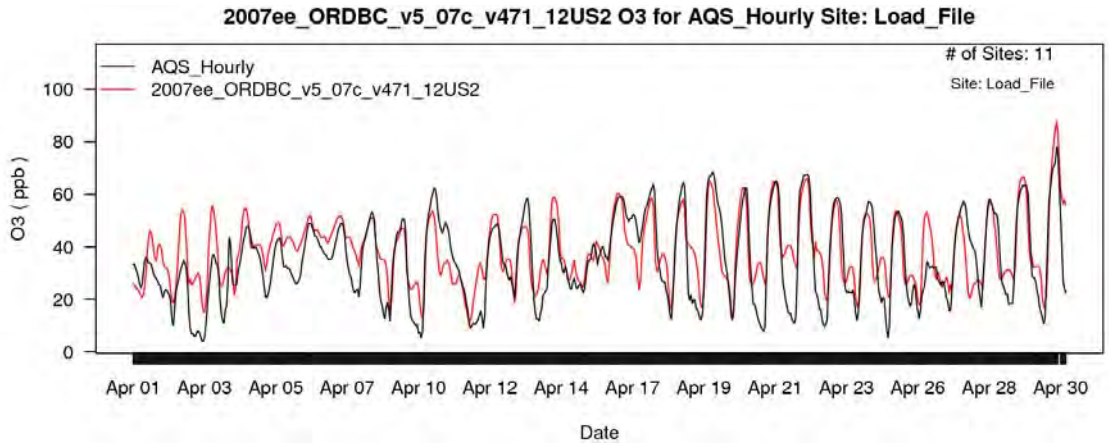

Figure 4B-36. Time series of hourly O_3 concentrations at Atlanta monitoring sites for April 2007. Observed values shown in black and modeled values shown in red.

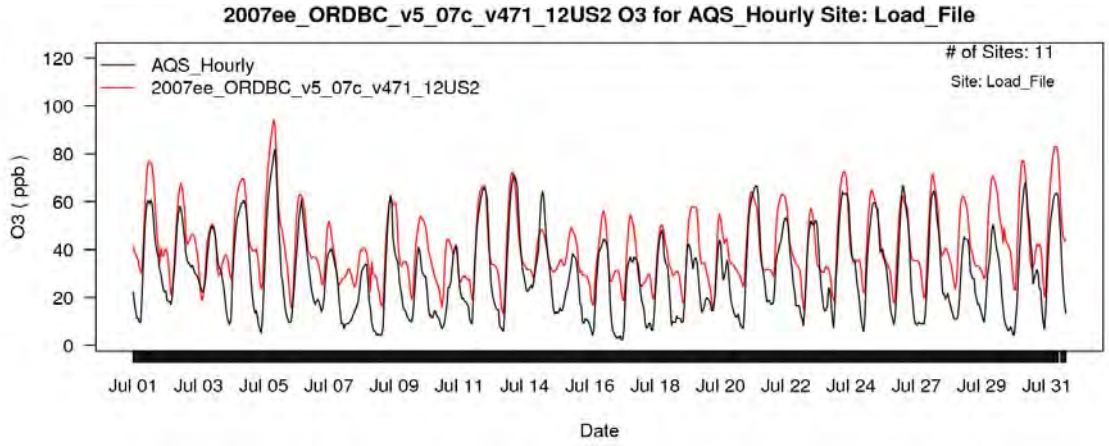

Figure 4B-37. Time series of hourly O_3 concentrations at Atlanta monitoring sites for July 2007. Observed values shown in black and modeled values shown in red.

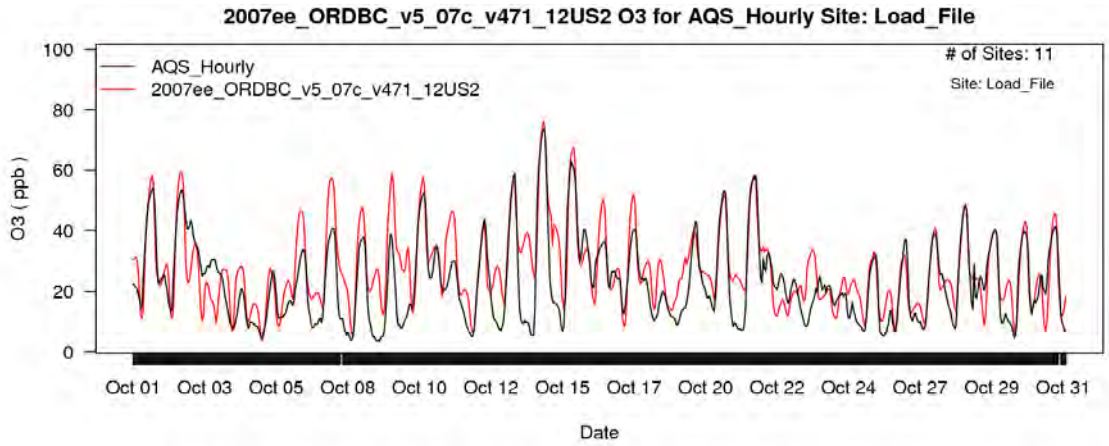

Figure 4B-38. Time series of hourly O_3 concentrations at Atlanta monitoring sites for October 2007. Observed values shown in black and modeled values shown in red.

4B-2.3 Operational Evaluation in the Midwest

The model performed well compared to observed O_3 concentrations in the Midwest. Mean bias for MDA8 O_3 was around 5 ppb or less at most sites in the winter, spring, and fall and less than 7 ppb at most sites in the summer. Normalized mean bias for MDA8 O_3 was less than 15% at most sites except in the winter when it was somewhat higher (less than 20% at most sites) due to lower observed O_3 concentrations. The model was more likely to be biased high on low O_3 days and biased low on higher O_3 days. No distinct spatial trends are apparent from the maps of normalized mean bias (Figure 4B-39 through Figure 4B-42). Three urban areas in the Midwest were examined more closely for this evaluation: Chicago, Cleveland, and Detroit.

Chicago performance statistics for MDA8 O_3 were similar to those of the rest of the region. The time series of MDA8 O_3 from Apr-Oct 2007 (Figure 4B-43) as well as the hourly time series for January, April, July, and October (Figure 4B-44 through Figure 4B-47) all show that the model does a good job of capturing synoptic variations in O_3 observed in Chicago and reasonably captures both day and nighttime measured concentrations.

No measurements were made during the winter season in Cleveland. MB for MDA8 O_3 on high days ($\geq$ 60 ppb) was similar to MB in the rest of the region, but MB on low O_3 days was somewhat higher than was typically seen in the Midwest (4 ppb vs. 1 ppb in the spring, 11 ppb vs. 6 ppb in the summer, and 4 ppb vs. 3 ppb in the fall). The time series plots for Cleveland sites show good correlation with observed O_3, although a period of moderate model over-estimates in daytime O_3 is depicted in July (Figure 4B-48 and Figure 4B-50). Nighttime O_3 concentrations are often overestimated by the model except in the time series shown for April, July, and October the latter portion of October, 2007.

Detroit area sites did not report any O_3 measurements during the winter of 2007. Detroit performance statistics for MDA8 O_3 were similar to those from the rest of the Midwest; however under-estimates on high O_3 days were more pronounced in Detroit than in the rest of the region. The time series shows that the model accurately estimates both day and nighttime hourly O_3 in Detroit in April and July and generally captures the variations in MDA8 O_3 across the April-October time period.

Table 4B-12. Summary of CMAQ model performance at AQS monitoring sites in the Midwest.

Season	MDA8	No. of Days	MB (ppb)	NMB (%)	ME (ppb)	NME (%)
Winter	< 60 ppb	2824	-3.76	-15.1	5.36	21.5
	≥ 60 ppb	0	NA	NA	NA	NA
	All Days	2824	-3.76	-15.1	5.36	21.5
Spring	< 60 ppb	9447	1.11	2.6	5.55	12.8
	≥ 60 ppb	2403	-6.19	-8.9	7.38	10.6
	All Days	11850	-0.37	-0.8	5.92	12.2
Summer	< 60 ppb	12478	6.31	14.2	8.39	18.8
	≥ 60 ppb	4114	-1.19	-1.7	7.56	10.8
	All Days	16592	4.45	8.8	8.18	16.1
Fall	< 60 ppb	8207	2.94	8.2	6.22	17.3
	≥ 60 ppb	1382	-4.48	-6.5	7.72	11.1
	All Days	9589	1.87	4.6	6.44	15.8

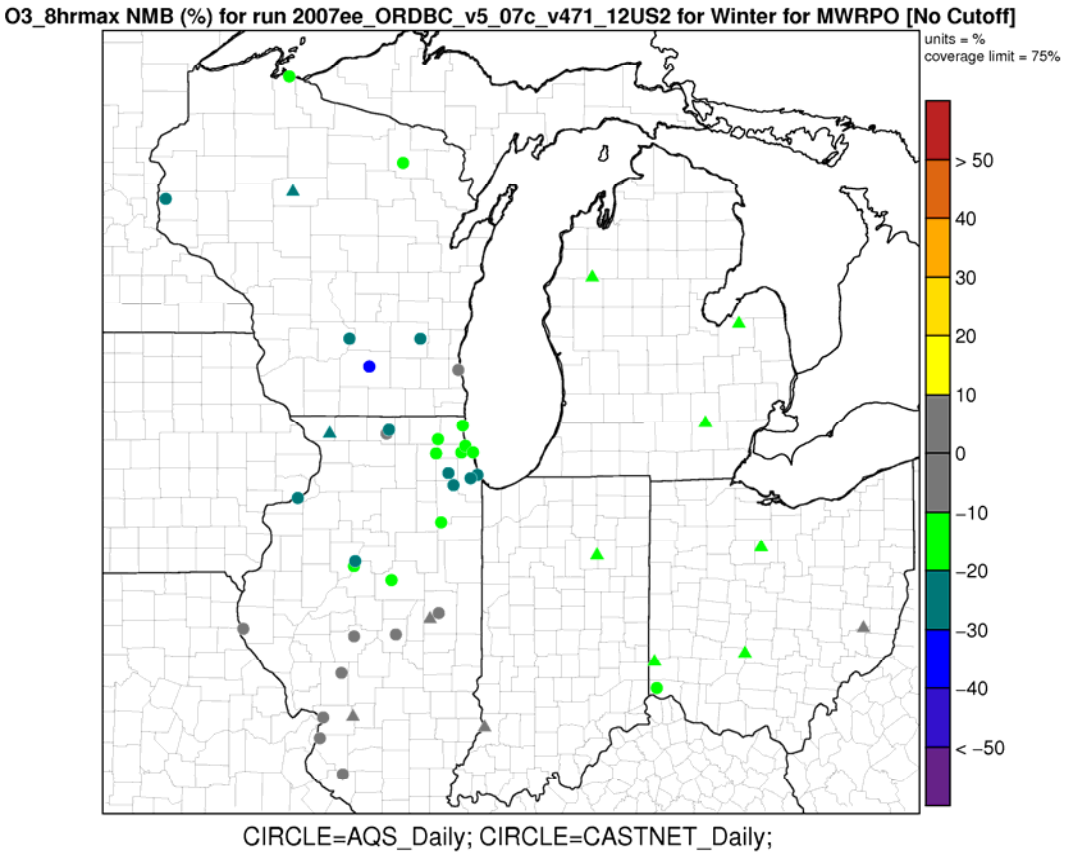

Figure 4B-39. Map of normalized mean bias for MDA8 O_3 concentrations in the Midwest for winter months in 2007.

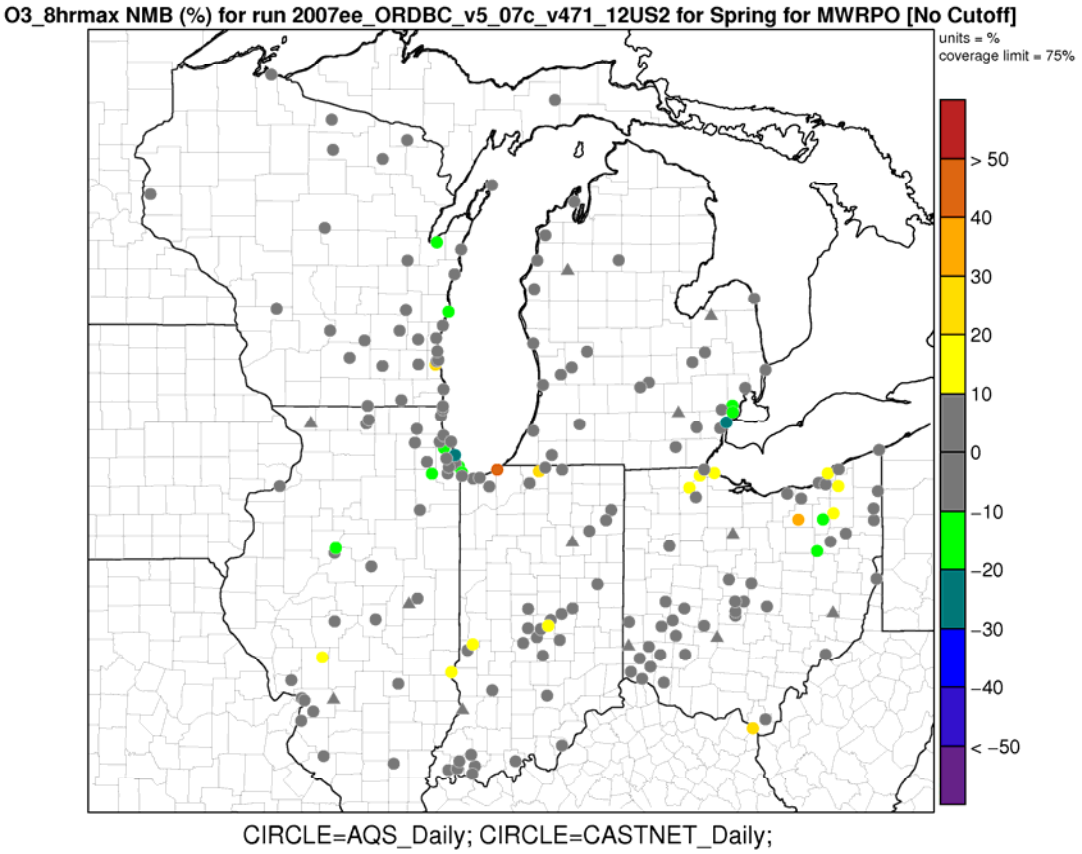

Figure 4B-40. Map of normalized mean bias for MDA8 O_3 concentrations in the Midwest for spring months in 2007.

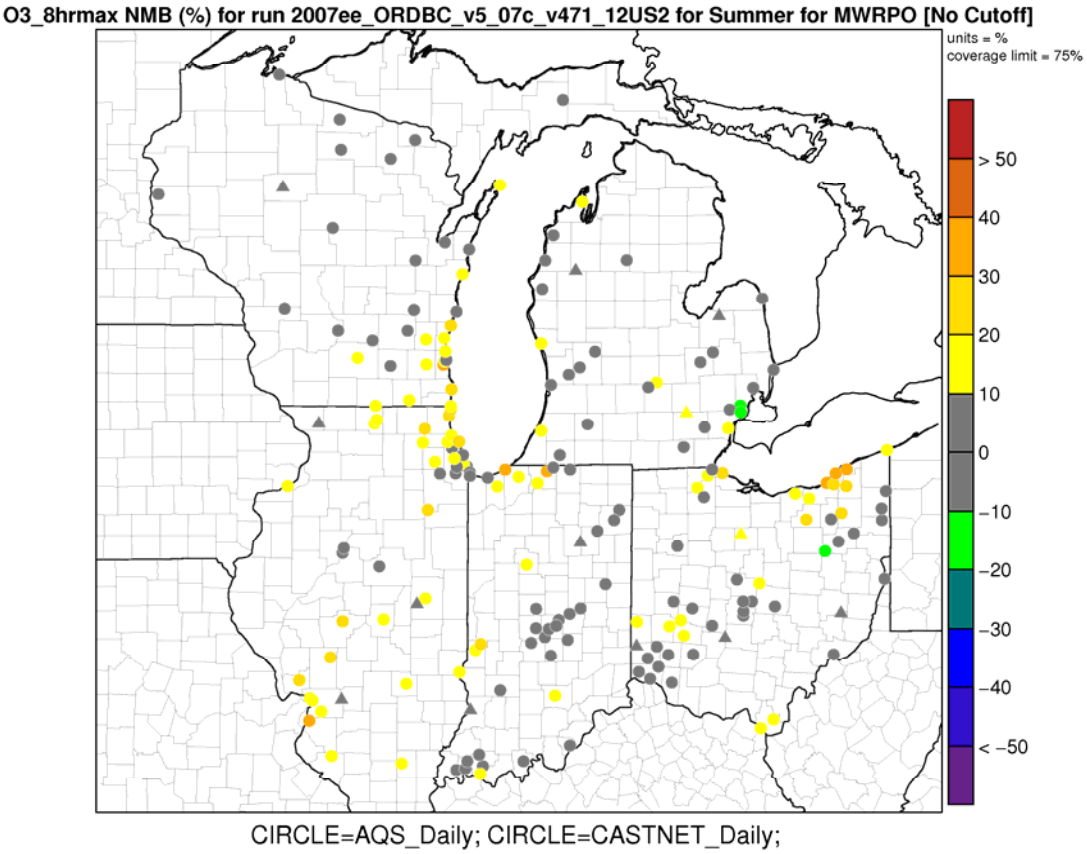

Figure 4B-41. Map of normalized mean bias for MDA8 O_3 concentrations in the Midwest for summer months in 2007.

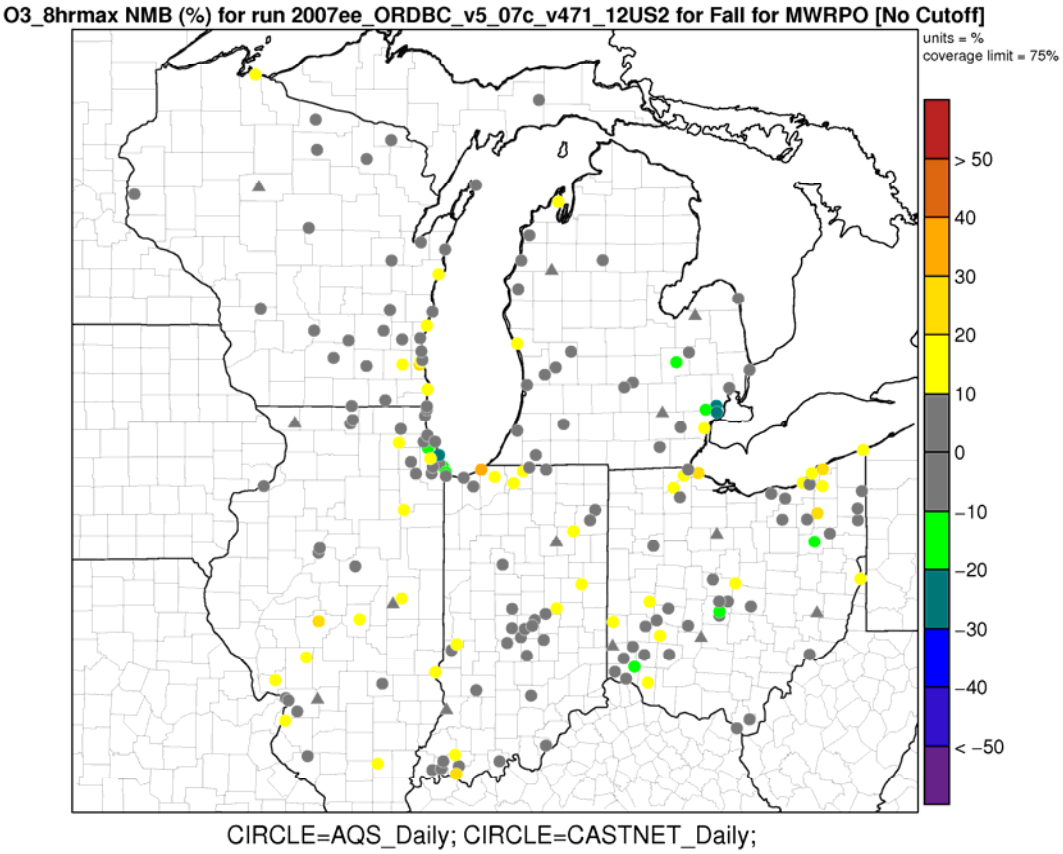

Figure 4B-42. Map of normalized mean bias for MDA8 O_3 concentrations in the Midwest for fall months in 2007.

Table 4B-13. Summary of CMAQ model performance at AQS monitoring sites in the Chicago area.

Season	MDA8	No. of Days	MB (ppb)	NMB (%)	ME (ppb)	NME (%)
Winter	< 60 ppb	963	-3.93	-17.5	5.13	22.9
	≥ 60 ppb	0	NA	NA	NA	NA
	All Days	963	-3.93	-17.5	5.13	22.9
Spring	< 60 ppb	1510	0.70	1.7	6.02	15.1
	≥ 60 ppb	218	-5.55	-8.1	6.62	9.7
	All Days	1728	-0.09	-0.2	6.1	14.0
Summer	< 60 ppb	1700	8.10	18.8	10.0	23.2
	≥ 60 ppb	448	1.70	2.5	8.65	12.5
	All Days	2148	6.76	13.9	9.74	20.0
Fall	< 60 ppb	1375	1.93	6.1	5.62	17.8
	≥ 60 ppb	136	-4.61	-6.7	9.05	13.2
	All Days	1511	1.34	3.8	5.93	17.0

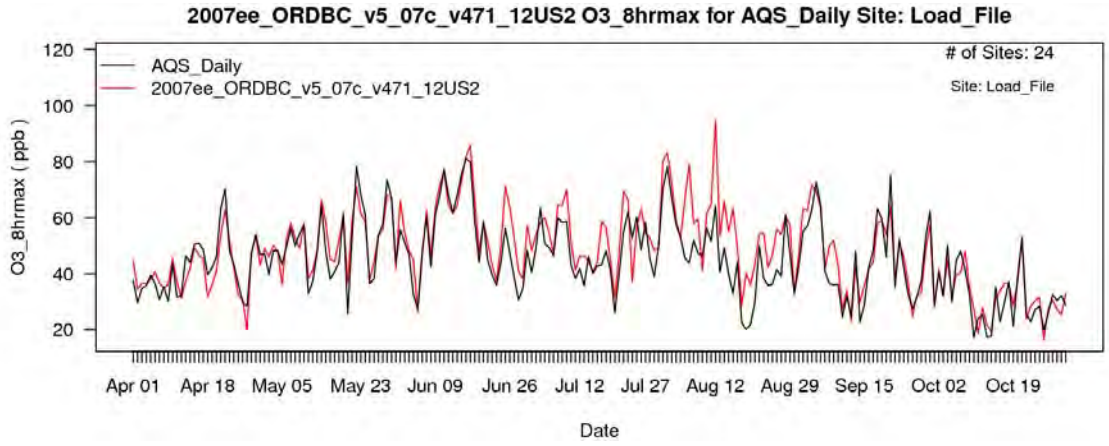

Figure 4B-43. Time series of 8-hr daily maximum O_3 concentrations at Chicago monitoring sites for April-October 2007. Observed values shown in black and modeled values shown in red.

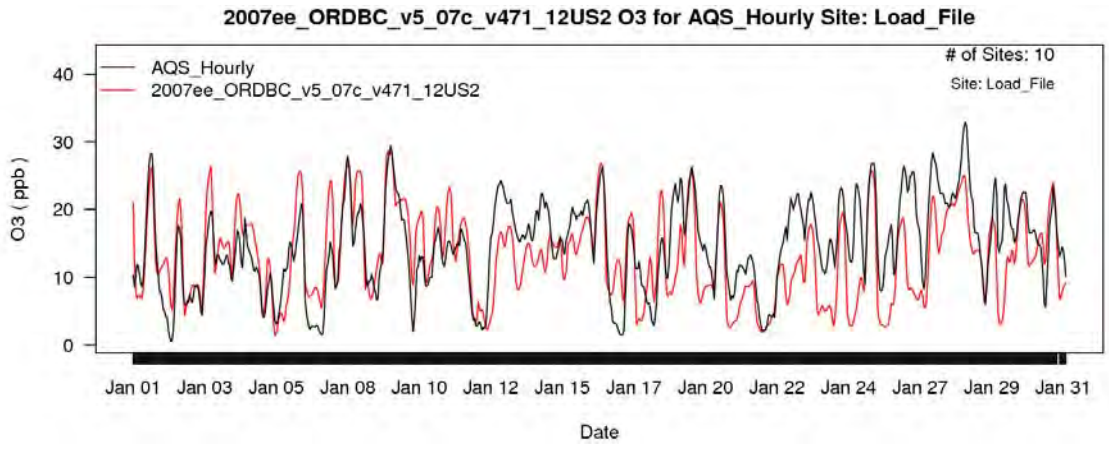

Figure 4B-44. Time series of hourly O_3 concentrations at Chicago monitoring sites for January 2007. Observed values shown in black and modeled values shown in red.

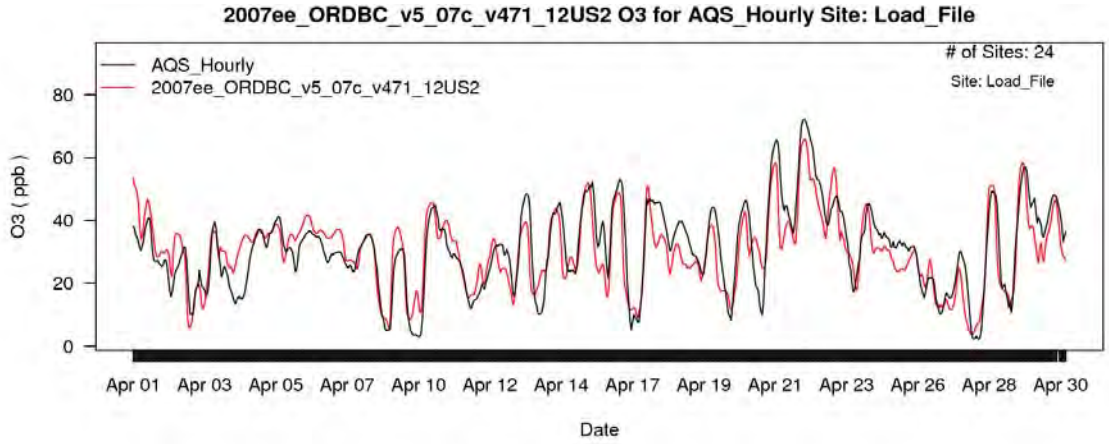

Figure 4B-45. Time series of hourly O_3 concentrations at Chicago monitoring sites for April 2007. Observed values shown in black and modeled values shown in red.

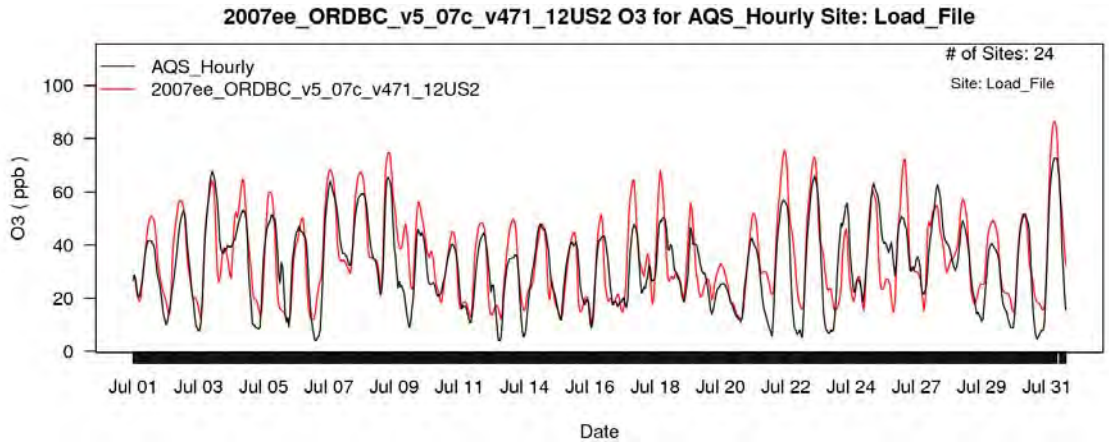

Figure 4B-46. Time series of hourly O_3 concentrations at Chicago monitoring sites for July 2007. Observed values shown in black and modeled values shown in red.

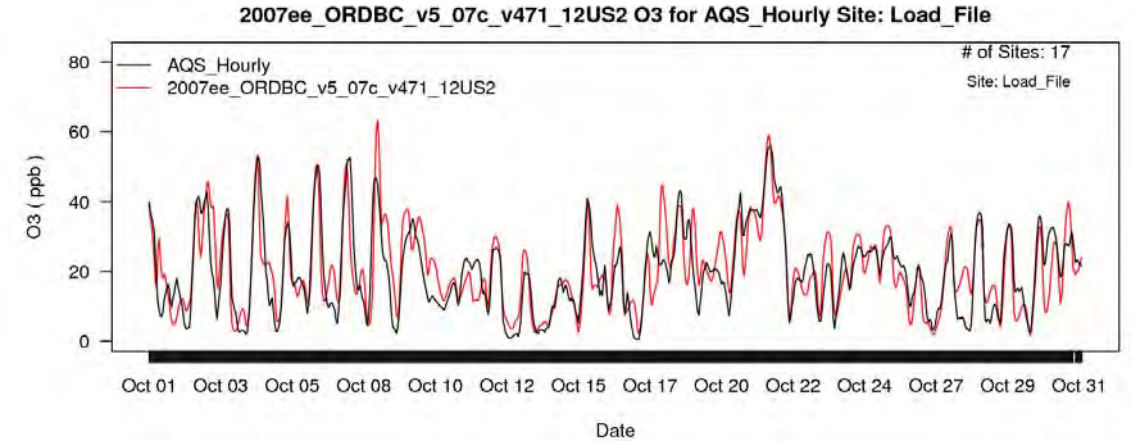

Figure 4B-47. Time series of hourly O_3 concentrations at Chicago monitoring sites for October 2007. Observed values shown in black and modeled values shown in red.

Table 4B-14. Summary of CMAQ model performance at AQS monitoring sites in the Cleveland area.

Season	MDA8	No. of Days	MB (ppb)	NMB (%)	ME (ppb)	NME (%)
Winter	< 60 ppb	0	NA	NA	NA	NA
	≥ 60 ppb	0	NA	NA	NA	NA
	All Days	0	NA	NA	NA	NA
Spring	< 60 ppb	491	4.35	10.5	7.03	17.0
	≥ 60 ppb	113	-4.80	-6.7	8.46	11.7
	All Days	604	2.64	5.6	7.30	15.5
Summer	< 60 ppb	714	11.00	25.8	12.90	30.3
	≥ 60 ppb	187	2.25	3.2	9.48	13.6
	All Days	901	9.16	19.0	12.20	25.3
Fall	< 60 ppb	543	4.41	11.6	7.38	19.4
	≥ 60 ppb	60	-4.48	-6.5	8.97	13.1
	All Days	603	3.52	8.6	7.54	18.4

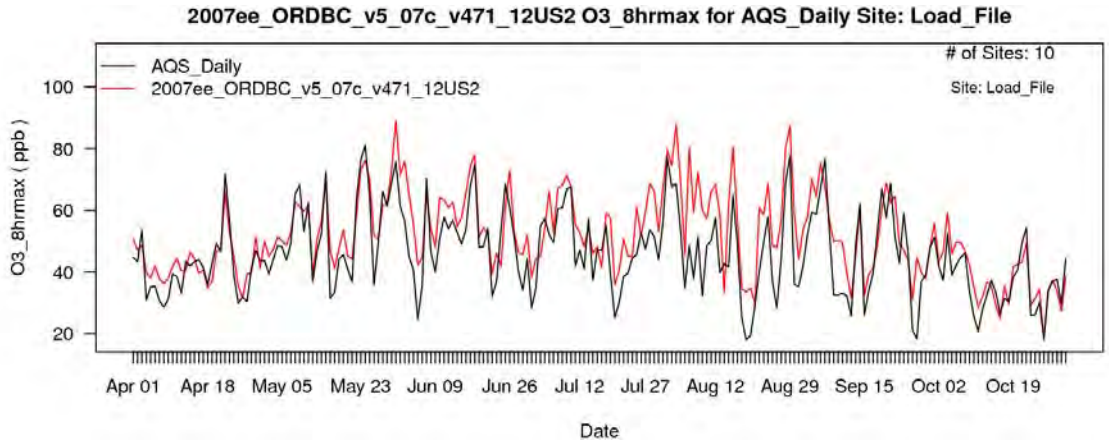

Figure 4B-48. Time series of 8-hr daily maximum O_3 concentrations at Cleveland monitoring sites for April-October 2007. Observed values shown in black and modeled values shown in red.

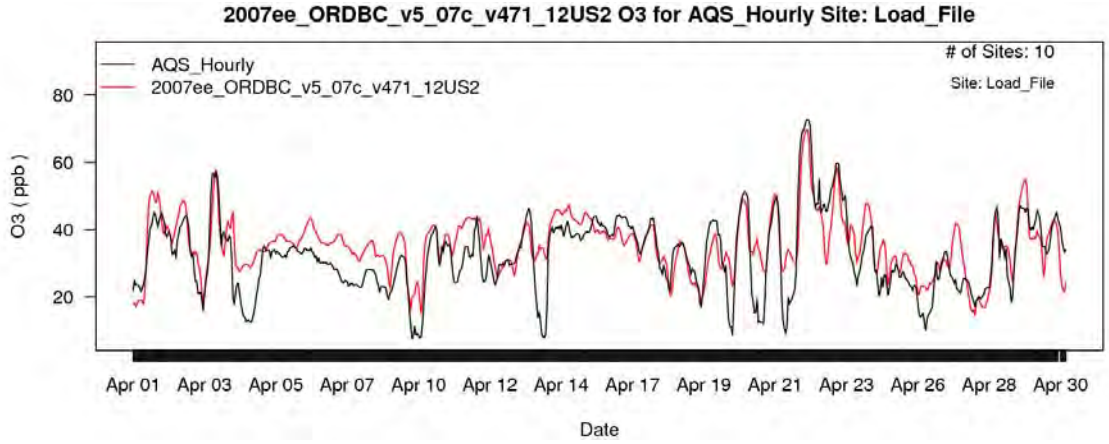

Figure 4B-49. Time series of hourly O_3 concentrations at Cleveland monitoring sites for April 2007. Observed values shown in black and modeled values shown in red.

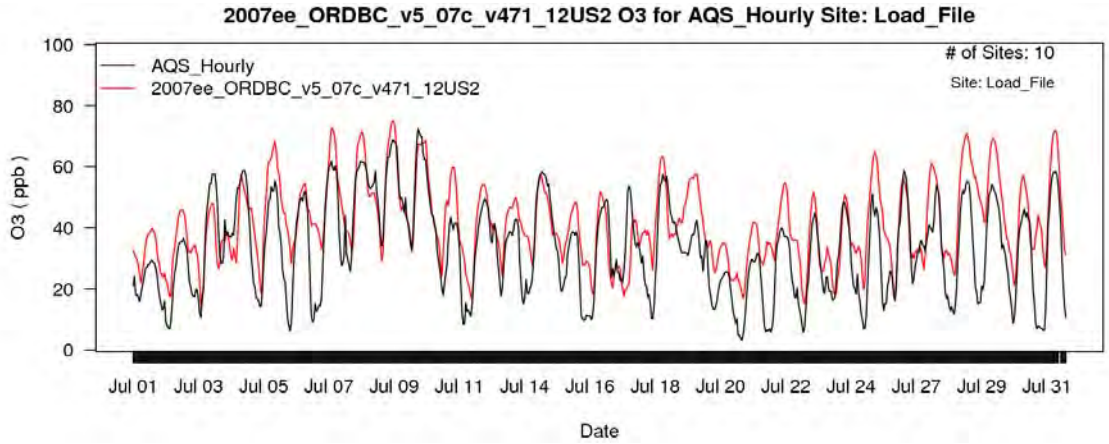

Figure 4B-50. Time series of hourly O_3 concentrations at Cleveland monitoring sites for July 2007. Observed values shown in black and modeled values shown in red.

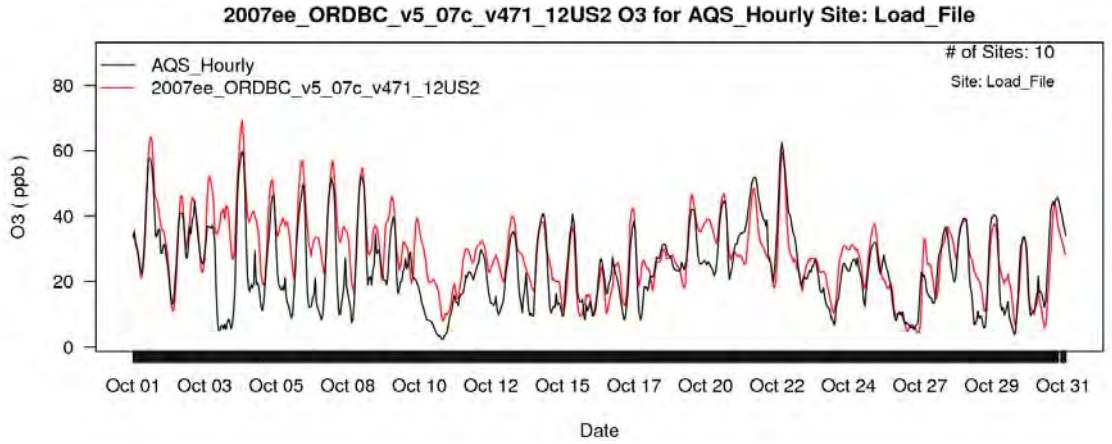

Figure 4B-51. Time series of hourly O_3 concentrations at Cleveland monitoring sites for October 2007. Observed values shown in black and modeled values shown in red.

Table 4B-15: Summary of CMAQ model performance at AQS monitoring sites in the Detroit area.

Season	MDA8	No. of Days	MB (ppb)	NMB (%)	ME (ppb)	NME (%)
Winter	< 60 ppb	0	NA	NA	NA	NA
	≥ 60 ppb	0	NA	NA	NA	NA
	All Days	0	NA	NA	NA	NA
Spring	< 60 ppb	443	-1.04	-2.5	4.93	11.7
	≥ 60 ppb	90	-8.61	-11.7	9.15	12.4
	All Days	533	-2.32	-4.9	5.64	11.9
Summer	< 60 ppb	614	1.65	3.9	7.19	16.7
	≥ 60 ppb	191	-7.16	-9.9	10.9	15.1
	All Days	805	-0.44	-0.8	8.07	16.2
Fall	< 60 ppb	220	-1.01	-2.6	6.65	17.1
	≥ 60 ppb	46	-14.70	-21.2	15.6	22.6
	All Days	166	-3.38	-7.7	8.2	18.6

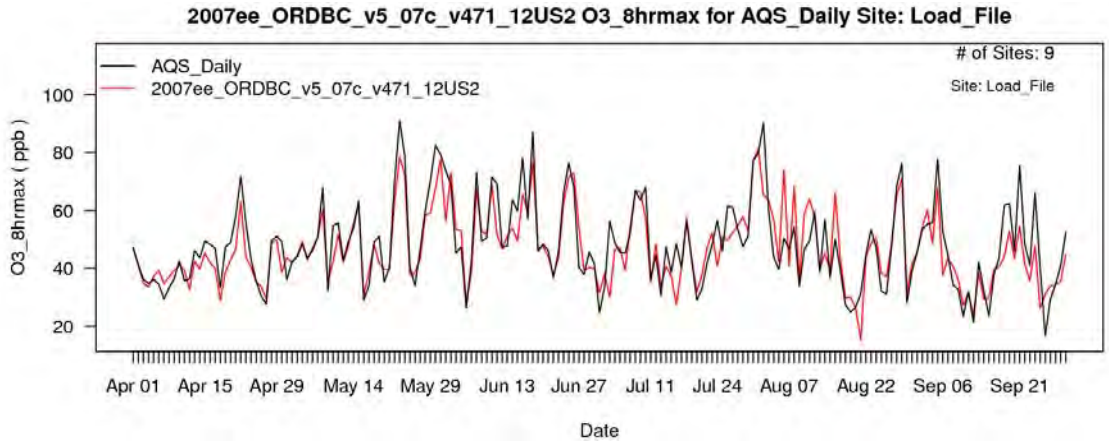

Figure 4B-52. Time series of 8-hr daily maximum O_3 concentrations at Detroit monitoring sites for April-October 2007. Observed values shown in black and modeled values shown in red.

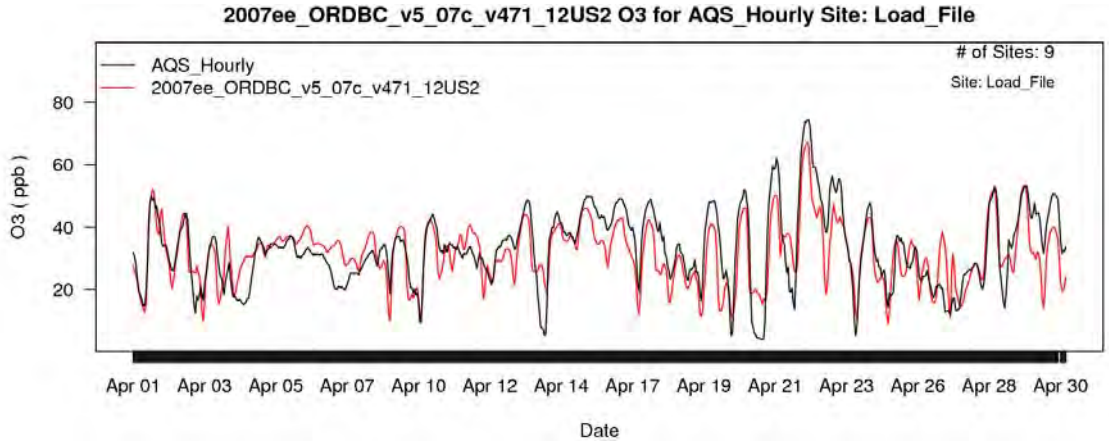

Figure 4B-53. Time series of hourly O_3 concentrations at Detroit monitoring sites for April 2007. Observed values shown in black and modeled values shown in red.

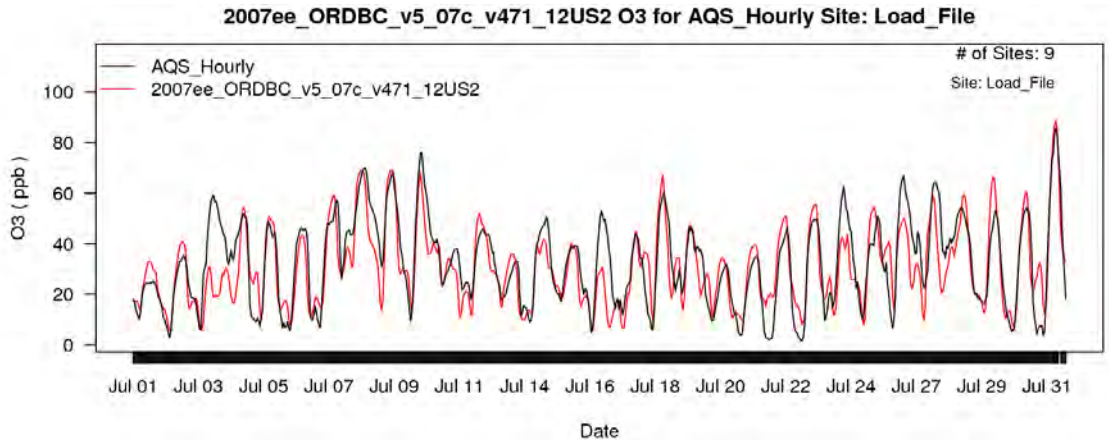

Figure 4B-54. Time series of hourly O_3 concentrations at Detroit monitoring sites for July 2007. Observed values shown in black and modeled values shown in red.

4B-2.4 Operational Evaluation in the Central U.S.

Mean bias for MDA8 O_3 concentrations were in the range of 4 ppb or less at Central U.S. monitoring sites during the winter and spring and less than 13 ppb and 6 ppb in the summer and fall respectively. Normalized mean bias was less than 15% at most sites in winter, spring, and fall and less than 35% at most sites in the summer. Summertime model overestimates were primarily located along the Gulf coast of Texas and Louisiana, mostly occurring on days with MDA8 O_3 concentrations less than 60 ppb. This is similar to summertime overestimates reported for the Southern U.S. which also were more pronounced along the Gulf Coast. Houston, Dallas, and Saint Louis were the three cities from the 15 urban study areas which were located in the Central U.S. region.

Saint Louis mean bias for MDA8 was moderately better than mean bias in the rest of the region for winter and spring periods and substantially better than the mean bias in the rest of the Central region in the summer and fall. The time series plots show that the model does a good job of replicating the observed variations in O_3 (both MDA8 and hourly). Nighttime O_3 is generally well simulated with the exception of a few several day periods in July when nighttime concentrations were overestimated by the model.

Dallas performance statistics for MDA8 O_3 were very similar to those presented for the Central region as a whole with the exception of comparisons made for the fall season which showed that Dallas performed substantially better than average for the region. The time series plot of MDA8 O_3 modeled and measured values (Figure 4B-64) demonstrate consistent high bias on very low O_3 days in May through early September but not in April or October. Hourly O_3 is fairly well replicated in January (Figure 4B-65), April (Figure 4B-66), and October (Figure 4B-68) but is overestimated during July both on low O_3 days and at night (Figure 4B-67).

As mentioned above, the largest summertime overestimates in MDA8 O_3 in the Central U.S. occur along the Texas Gulf coast. This is demonstrated by the Houston model performance statistics. Houston model performance is relatively good and is equivalent to that in the rest of the Central U.S. during the winter, spring, and fall seasons and on high days during the summer. However summertime MDA8 O_3 is overestimated by 15 ppb and 48% on summer days with observed levels less than 60 ppb in the Houston area. This summertime overestimate of low O_3 days is demonstrated in the time series plots in Figure 4B-69 and Figure 4B-72.

Table 4B-16. Summary of CMAQ model performance at AQS monitoring sites in the central U.S.

Season	MDA8	No. of Days	MB (ppb)	NMB (%)	ME (ppb)	NME (%)
Winter	< 60 ppb	11190	-0.42	-1.4	5.61	18.7
	≥ 60 ppb	33	-13.9	-21.5	14.5	22.4
	All Days	11223	-0.46	-1.5	5.64	18.7
Spring	< 60 ppb	13077	2.88	6.7	6.35	14.7
	≥ 60 ppb	2137	-6.68	-10.0	8.26	12.4
	All Days	15214	1.54	3.3	6.62	14.2
Summer	< 60 ppb	14142	11.4	29.7	12.6	32.8
	≥ 60 ppb	2477	0.60	0.9	7.77	11.1
	All Days	16619	9.82	22.8	11.9	27.5
Fall	< 60 ppb	13209	4.39	11.8	7.54	20.3
	≥ 60 ppb	1359	-3.33	-4.9	7.04	10.4
	All Days	14568	3.67	9.2	7.49	18.7

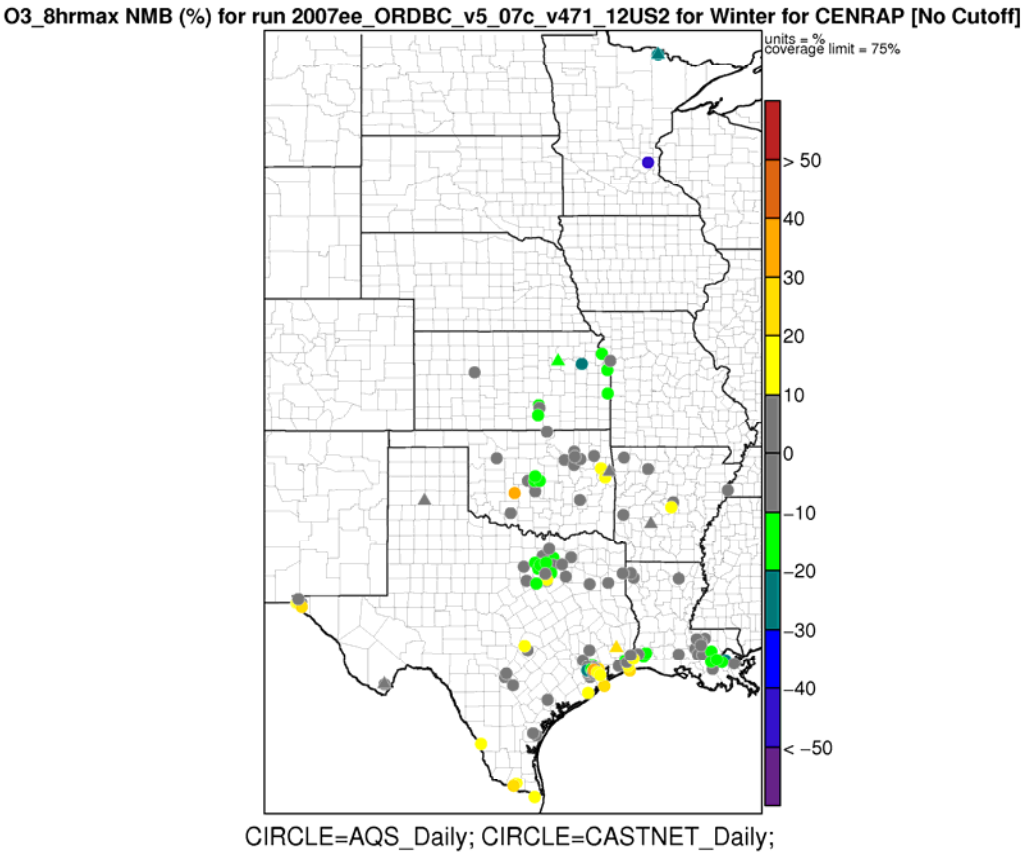

Figure 4B-55. Map of normalized mean bias for MDA8 O_3 concentrations in the Central U.S. for winter months in 2007.

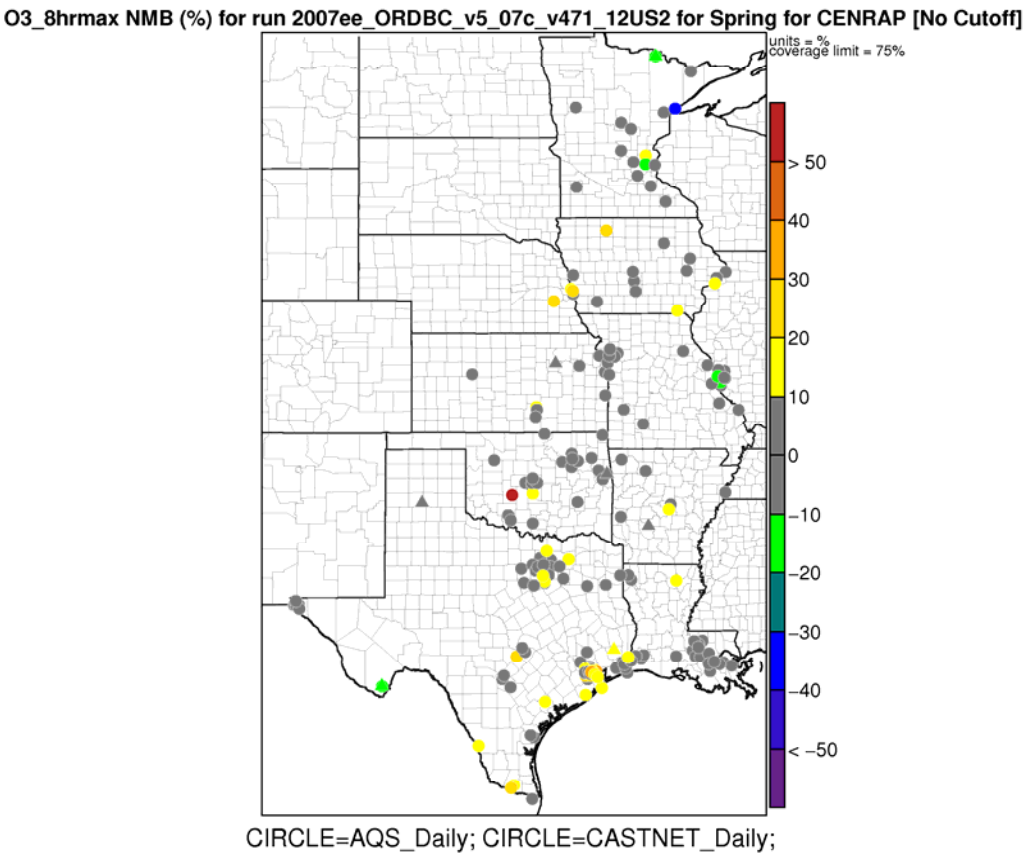

Figure 4B-56. Map of normalized mean bias for MDA8 O_3 concentrations in the Central U.S. for spring months in 2007.

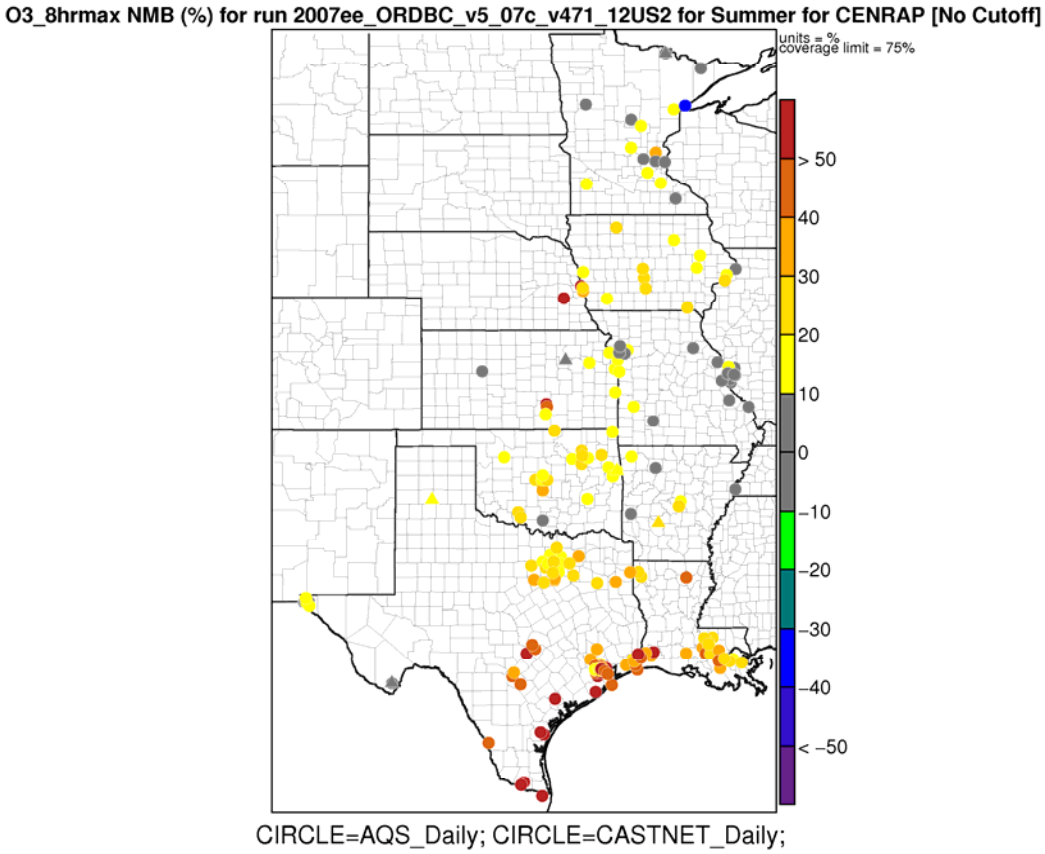

Figure 4B-57. Map of normalized mean bias for MDA8 O_3 concentrations in the Central U.S. for summer months in 2007.

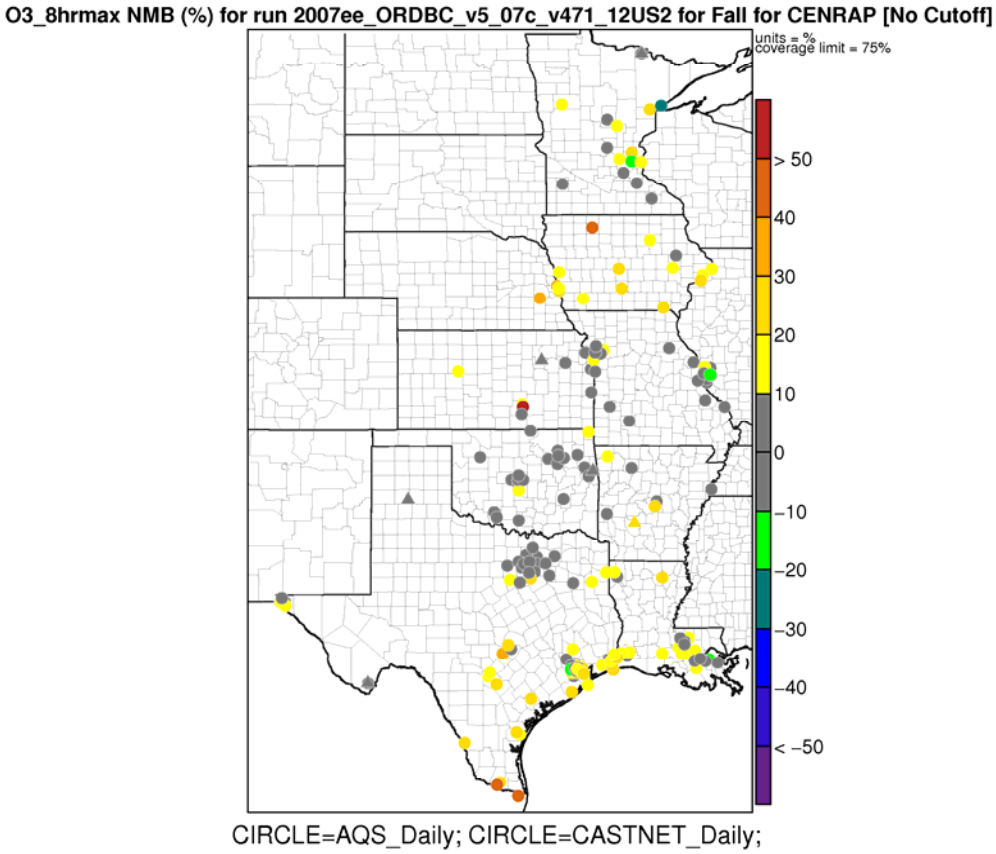

Figure 4B-58. Map of normalized mean bias for MDA8 O_3 concentrations in the Central U.S. for fall months in 2007.

Table 4B-17. Summary of CMAQ model performance at AQS monitoring sites in the Saint Louis area.

Season	MDA8	No. of Days	MB (ppb)	NMB (%)	ME (ppb)	NME (%)
Winter	< 60 ppb	266	-0.16	-0.7	4.10	18.1
	≥ 60 ppb	0	NA	NA	NA	NA
	All Days	266	-0.16	-0.7	4.10	18.1
Spring	< 60 ppb	812	1.09	2.5	5.31	11.9
	≥ 60 ppb	139	-6.93	-10.6	7.85	12.0
	All Days	951	-0.08	-0.2	5.68	11.9
Summer	< 60 ppb	834	8.71	18.9	9.83	21.4
	≥ 60 ppb	447	0.66	0.9	9.34	12.7
	All Days	1281	5.90	10.6	9.66	17.4
Fall	< 60 ppb	829	2.38	6.6	6.34	17.6
	≥ 60 ppb	113	-6.19	-8.8	8.46	12.1
	All Days	942	1.35	3.4	6.60	16.4

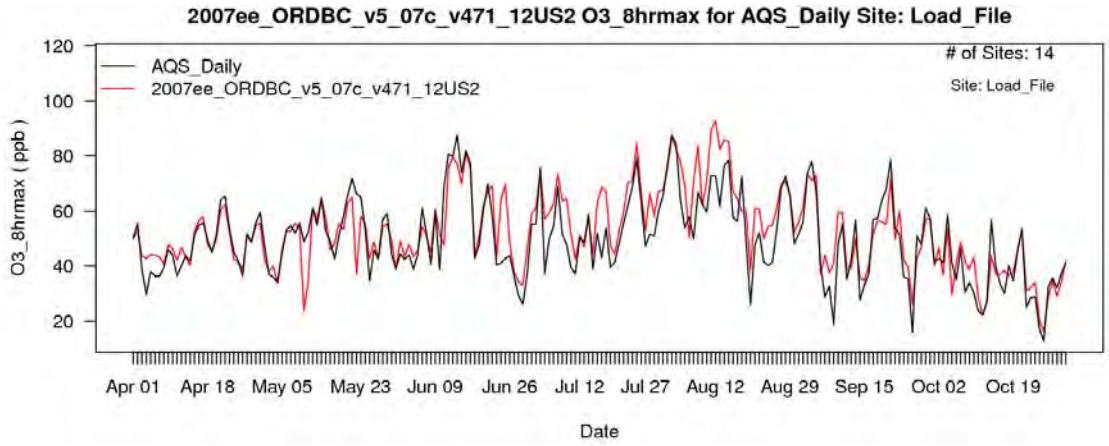

Figure 4B-59. Time series of 8-hr daily maximum O_3 concentrations at Saint Louis monitoring sites for April-October 2007. Observed values shown in black and modeled values shown in red.

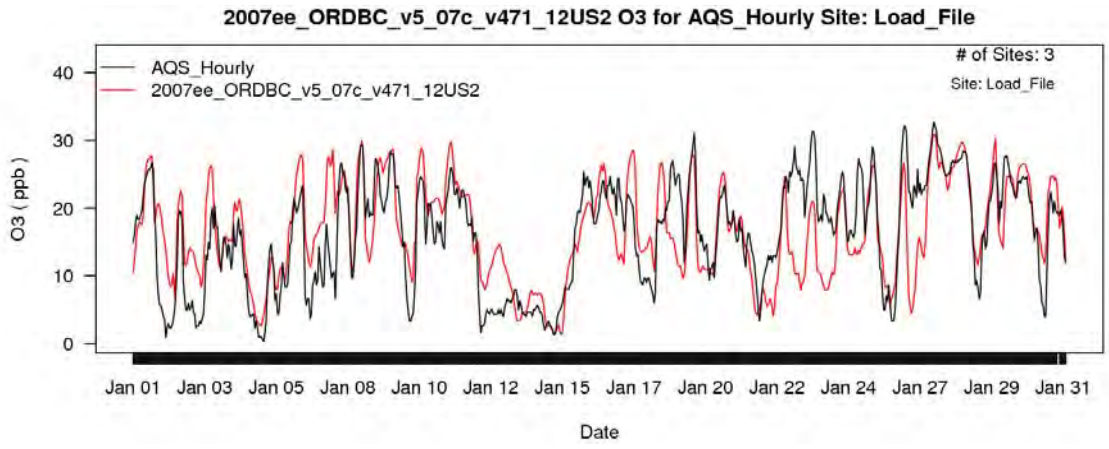

Figure 4B-60. Time series of hourly O_3 concentrations at Saint Louis monitoring sites for January 2007. Observed values shown in black and modeled values shown in red.

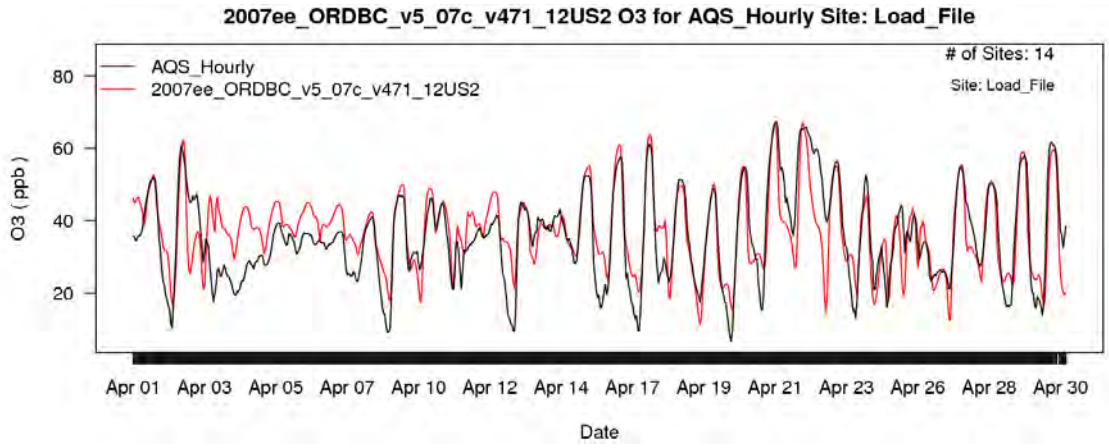

Figure 4B-61. Time series of hourly O_3 concentrations at Saint Louis monitoring sites for April 2007. Observed values shown in black and modeled values shown in red.

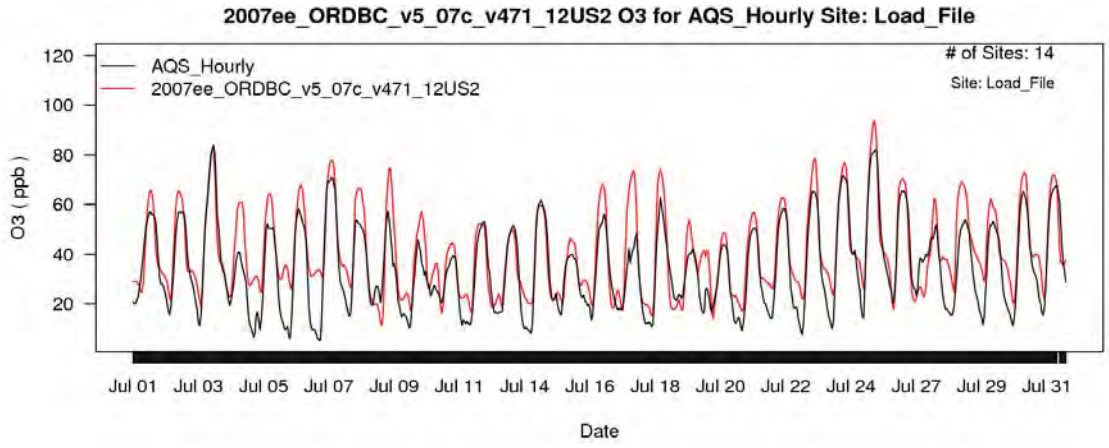

Figure 4B-62. Time series of hourly O_3 concentrations at Saint Louis monitoring sites for July 2007. Observed values shown in black and modeled values shown in red.

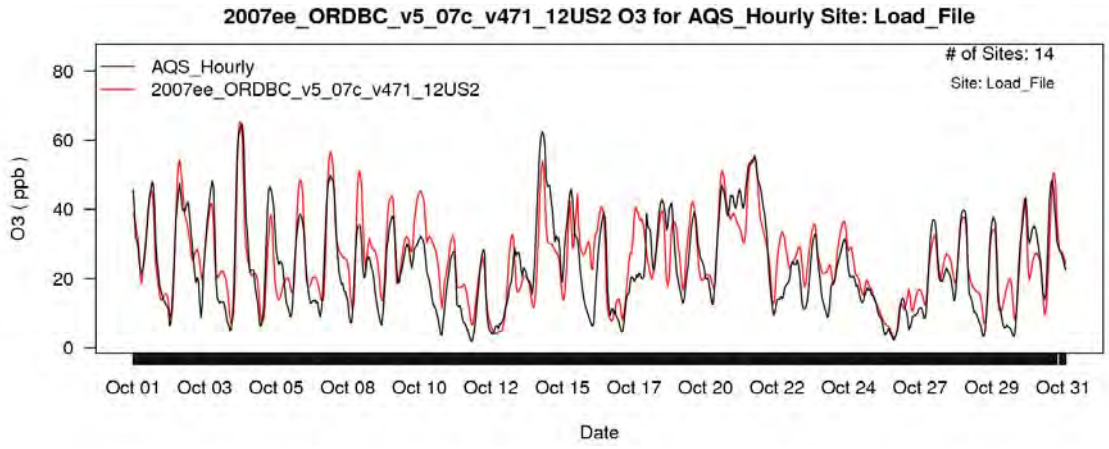

Figure 4B-63. Time series of hourly O_3 concentrations at Saint Louis monitoring sites for October 2007. Observed values shown in black and modeled values shown in red.

Table 4B-18. Summary of CMAQ model performance at AQS monitoring sites in the Dallas area.

Season	MDA8	No. of Days	MB (ppb)	NMB (%)	ME (ppb)	NME (%)
Winter	< 60 ppb	1483	-2.12	-7.4	5.30	18.6
	≥ 60 ppb	0	NA	NA	NA	NA
	All Days	1483	-2.12	-7.4	5.30	18.6
Spring	< 60 ppb	1360	2.92	7.0	6.77	16.2
	≥ 60 ppb	168	-8.10	-12.3	9.38	14.2
	All Days	1528	1.71	3.8	7.05	15.8
Summer	< 60 ppb	1289	11.10	28.3	12.30	31.5
	≥ 60 ppb	260	3.35	4.7	8.59	12.0
	All Days	1549	9.77	21.9	11.70	26.3
Fall	< 60 ppb	1306	1.67	4.3	6.89	17.8
	≥ 60 ppb	223	-2.77	-4.1	6.69	9.8
	All Days	1529	1.02	2.4	6.86	15.9

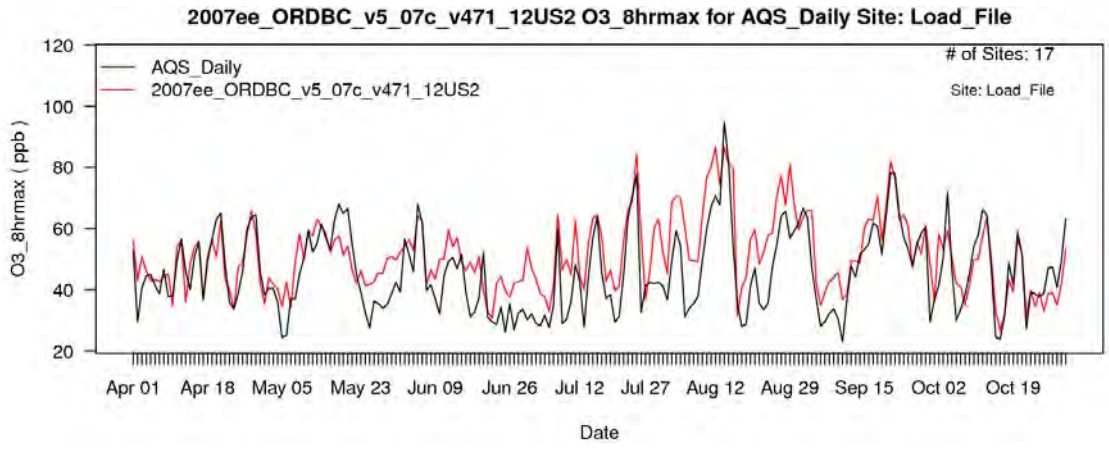

Figure 4B-64. Time series of 8-hr daily maximum O_3 concentrations at Dallas monitoring sites for April-October 2007. Observed values shown in black and modeled values shown in red.

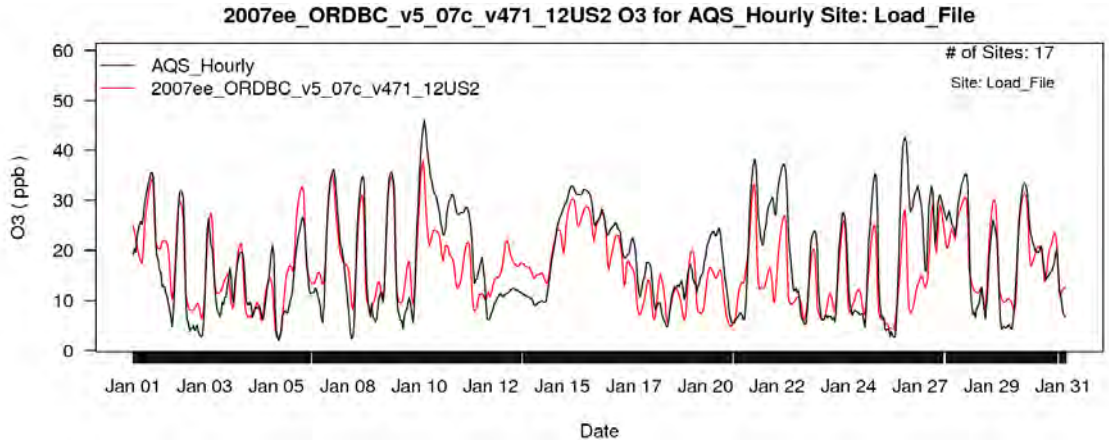

Figure 4B-65. Time series of hourly O_3 concentrations at Dallas monitoring sites for January 2007. Observed values shown in black and modeled values shown in red.

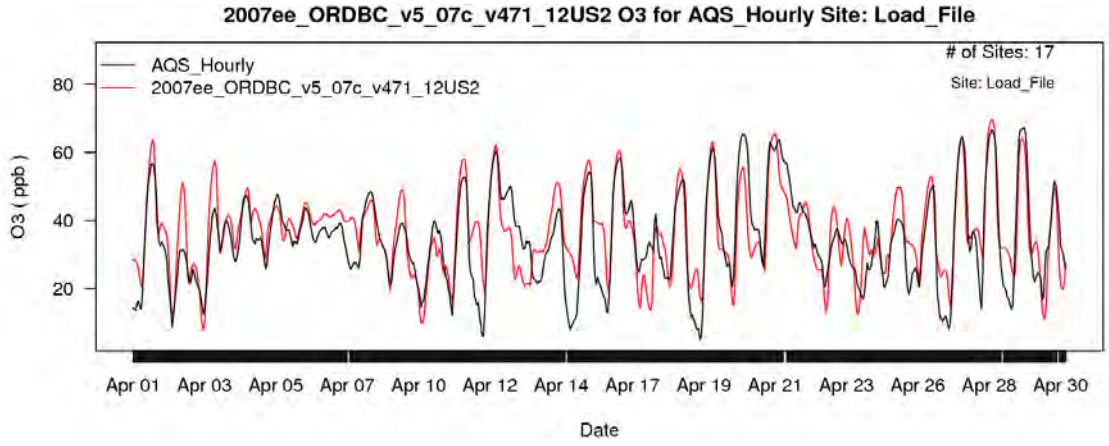

Figure 4B-66. Time series of hourly O_3 concentrations at Dallas monitoring sites for April 2007. Observed values shown in black and modeled values shown in red.

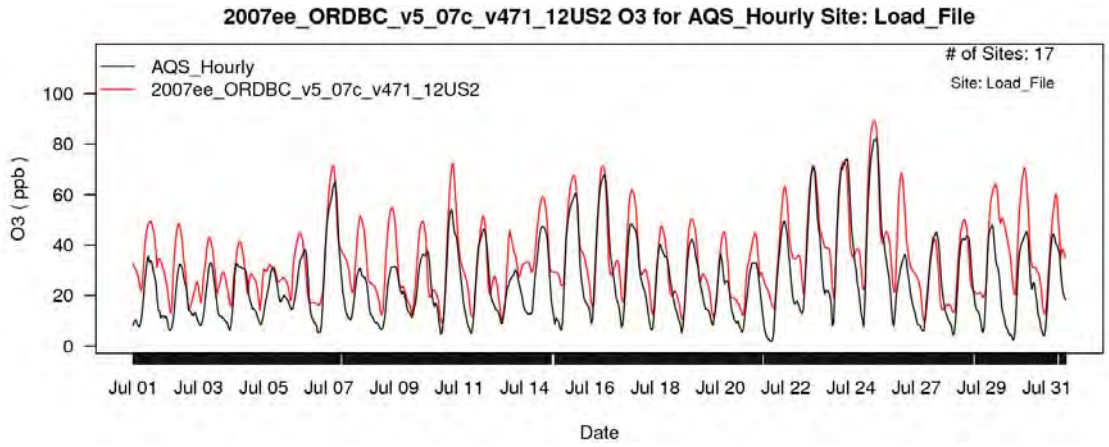

Figure 4B-67. Time series of hourly O_3 concentrations at Dallas monitoring sites for July 2007. Observed values shown in black and modeled values shown in red.

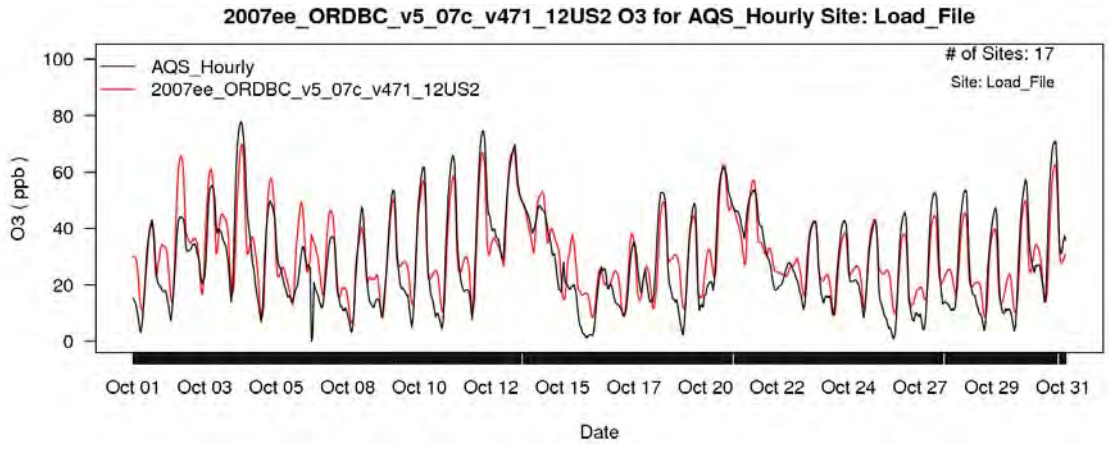

Figure 4B-68. Time series of hourly O_3 concentrations at Dallas monitoring sites for October 2007. Observed values shown in black and modeled values shown in red.

Table 4B-19. Summary of CMAQ model performance at AQS monitoring sites in the Houston area.

Season	MDA8	No. of Days	MB (ppb)	NMB (%)	ME (ppb)	NME (%)
Winter	< 60 ppb	1772	0.48	1.8	5.97	22.2
	≥ 60 ppb	0	NA	NA	NA	NA
	All Days	1772	0.48	1.8	5.97	22.2
Spring	< 60 ppb	1569	5.82	14.5	9.05	22.5
	≥ 60 ppb	276	-5.23	-7.7	10.40	15.2
	All Days	1845	4.17	9.4	9.25	20.8
Summer	< 60 ppb	1706	15.00	48.4	16.8	54.2
	≥ 60 ppb	165	1.71	2.5	11.00	15.8
	All Days	1871	13.80	40.2	16.30	47.3
Fall	< 60 ppb	1608	5.41	14.9	8.73	24.1
	≥ 60 ppb	259	-3.38	-4.8	9.05	12.8
	All Days	1867	4.19	10.2	8.78	21.4

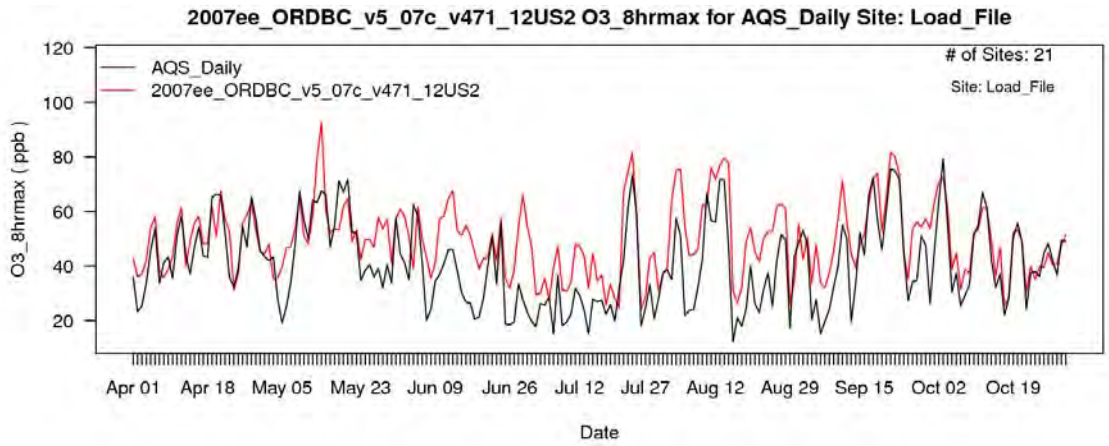

Figure 4B-69. Time series of 8-hr daily maximum O_3 concentrations at Houston monitoring sites for April-October 2007. Observed values shown in black and modeled values shown in red.

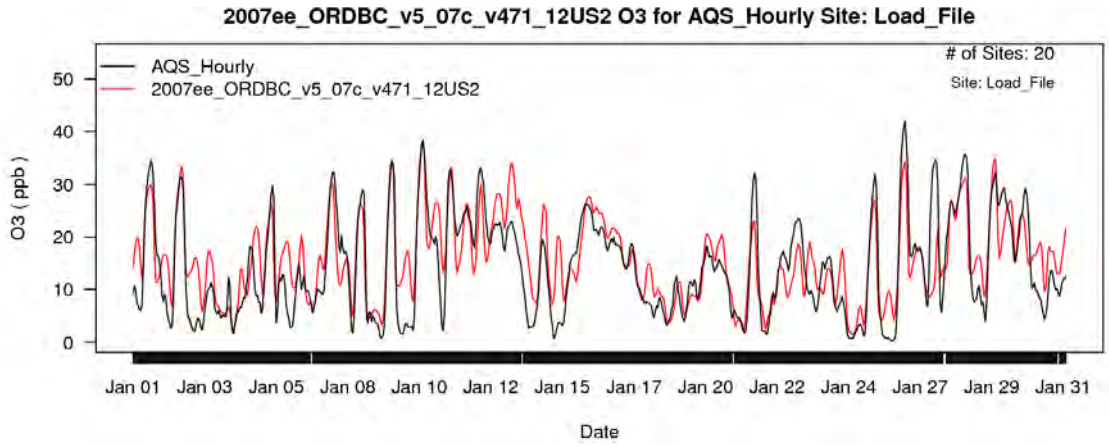

Figure 4B-70. Time series of hourly O_3 concentrations at Houston monitoring sites for January 2007. Observed values shown in black and modeled values shown in red.

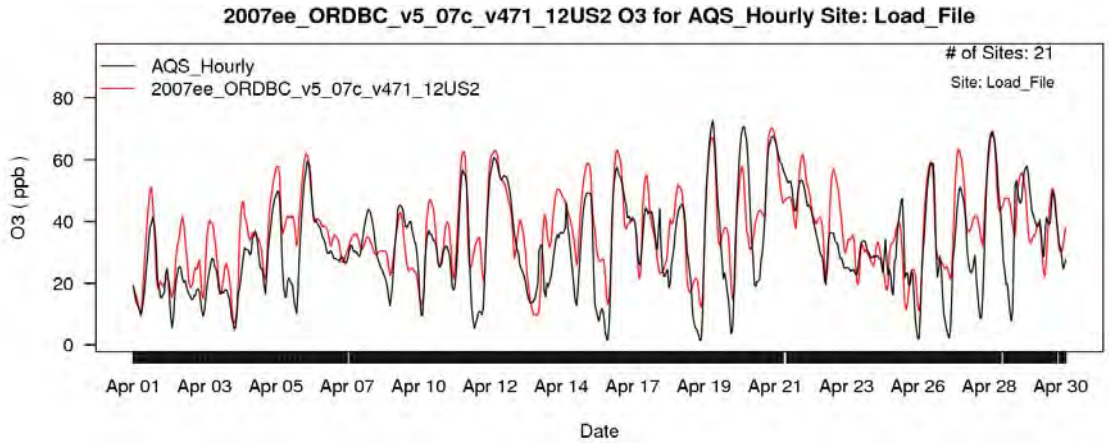

Figure 4B-71. Time series of hourly O_3 concentrations at Houston monitoring sites for April 2007. Observed values shown in black and modeled values shown in red.

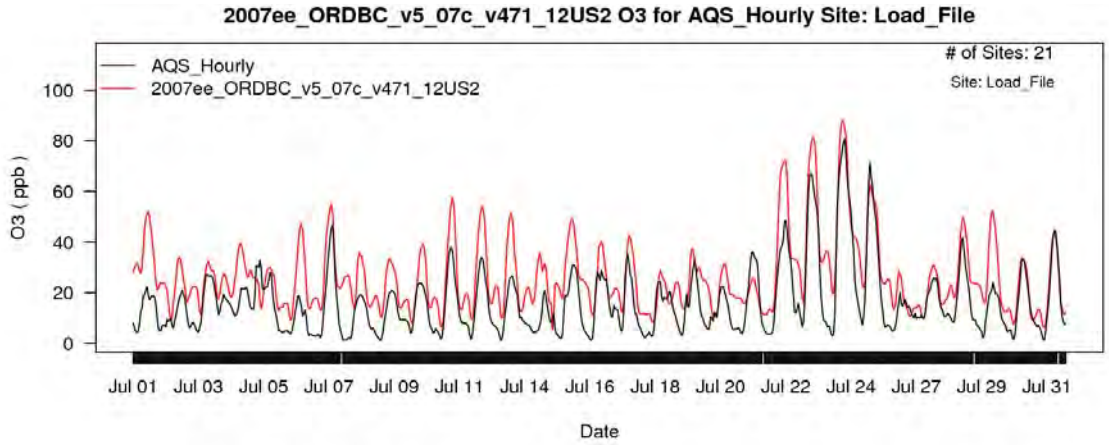

Figure 4B-72. Time series of hourly O_3 concentrations at Houston monitoring sites for July 2007. Observed values shown in black and modeled values shown in red.

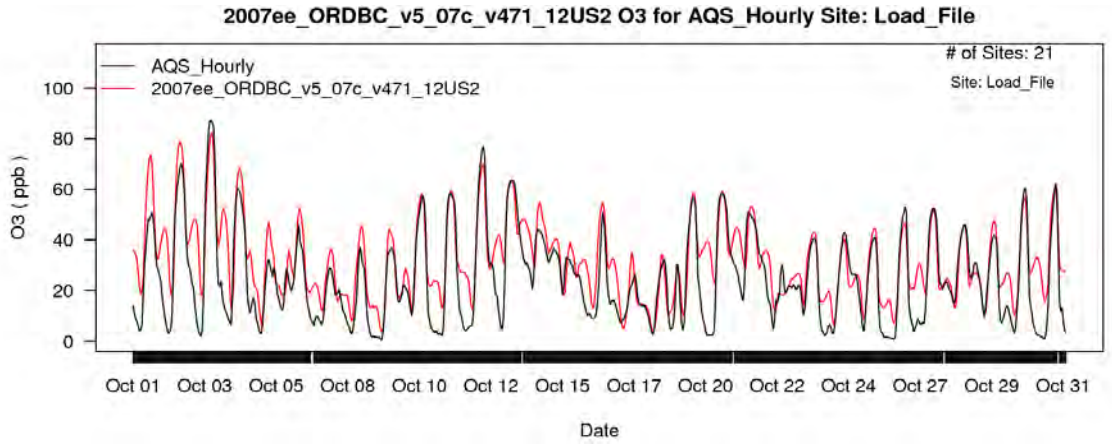

Figure 4B-73. Time series of hourly O_3 concentrations at Houston monitoring sites for October 2007. Observed values shown in black and modeled values shown in red.

4B-2.5 Operational Evaluation in the Western U.S.

Again model statistics for MDA8 O_3 in the Western U.S. are in the range of what has been reported for state of the science model performance in the literature (Simon et al., 2012). Mean bias at most sites was less than 6 ppb in the winter, spring, and fall and less than 10 ppb in the summer. Normalized mean bias at most monitoring locations was less than 10% in the winter and spring, less than 20% in the summer and less than 15% in the fall. Only 3 sites in the West recorded O_3 concentrations equal to or above 60 ppb in winter (a Riverside California site reported 13 days and the other two sites in Sacramento, CA and Sublette county WY reported only 2 and 3 days above 60 ppb). These high wintertime observations were substantially underestimated by the model with an average MB of -34.5 ppb but likely for different reasons. The high days in Riverside California are probably due to traditionally understood O_3 formation that occurs on warm sunny days. The high O_3 concentrations in Wyoming are an example of wintertime O_3 formation that occurs during cold pool meteorology events which have substantial snow cover and extreme temperature inversions and are still an active area of research. Some spatial trends in normalized mean bias are apparent in the winter (Figure 4B-74) and in the summer (Figure 4B-76). Wintertime O_3 is more likely to be overestimated on the West Coast and more likely to be underestimated in the Intermountain West. Summertime model overestimates are greatest along the Southern Coast of California in locations that generally have low observed O_3 concentrations. Three urban study areas from the HREA are located in the Western U.S. and are evaluated in this section: Denver, Sacramento, and Los Angeles.

Denver area model performance was generally comparable to model performance in the rest of the Western U.S. although summertime overestimates of MDA8 were greater in Denver. These summertime overestimates can be seen on many days in Figure 4B-78 and Figure 4B-80.

Figure 4B-79 shows that the model generally captures measured hourly O_3 concentrations in the Denver area on mid to high O_3 days but often overestimates very low O_3 days in the spring. Fall hourly O_3 estimates from the model are reasonably well captured in Figure 4B-81.

Sacramento area model performance for MDA8 O_3 values was reasonably good in all seasons except for the 2 days with high observed O_3 in the winter. The model underestimated those high wintertime concentrations by 32 ppb. Other than those days, model bias was generally less than 10% in the Sacramento area. The time series figures of MDA8 and hourly O_3 concentrations show that the model does well at capturing the day to day and day to night O_3 variations in all seasons.

Los Angeles generally had reasonable model performance with low normalized mean bias number (0-8%) with two exceptions. The 13 high wintertime O_3 days measured in central Riverside County were not captured by the model which had a mean bias for those days at that site of -36 ppb and -45%. Also, the model tended to overestimate O_3 on summertime days with observed concentrations below 60 ppb (15 ppb mean bias). These low summer O_3 concentrations generally occurred along the coast (Figure 4B-92). A map of summertime normalized mean bias (Figure 4B-93) shows that the low O_3 sites are the locations with the largest model bias. Monitors away from the coast generally had fairly low bias (0-20%) with the exception of two sites in western Riverside County. The summer O_3 overestimates shown in the MDA8 time series (Figure 4B-87) are therefore due to performance at those coastal sites. The hourly time series for January (Figure 4B-88), April (Figure 4B-89), and October (Figure 4B-90) generally show good hourly O_3 performance during the day but model overestimates at night.

Table 4B-20. Summary of CMAQ model performance at AQS monitoring sites in the western U.S.

Season	MDA8	No. of Days	MB (ppb)	NMB (%)	ME (ppb)	NME (%)
Winter	< 60 ppb	23890	1.31	4.1	5.79	17.9
	≥ 60 ppb	18	-34.5	-45.8	34.5	45.8
	All Days	23908	1.29	4.0	5.81	17.9
Spring	< 60 ppb	22670	0.61	1.3	5.61	12.1
	≥ 60 ppb	5101	-4.84	-7.2	7.30	10.9
	All Days	27771	-0.40	-0.8	5.92	11.8
Summer	< 60 ppb	21098	7.50	17.0	9.96	22.6
	≥ 60 ppb	9708	1.29	2.8	8.94	12.8
	All Days	30806	5.74	11.0	9.64	18.5
Fall	< 60 ppb	26055	3.40	8.9	7.08	18.4
	≥ 60 ppb	1691	-3.32	-4.9	9.81	14.4
	All Days	27746	2.99	7.4	7.25	18.0

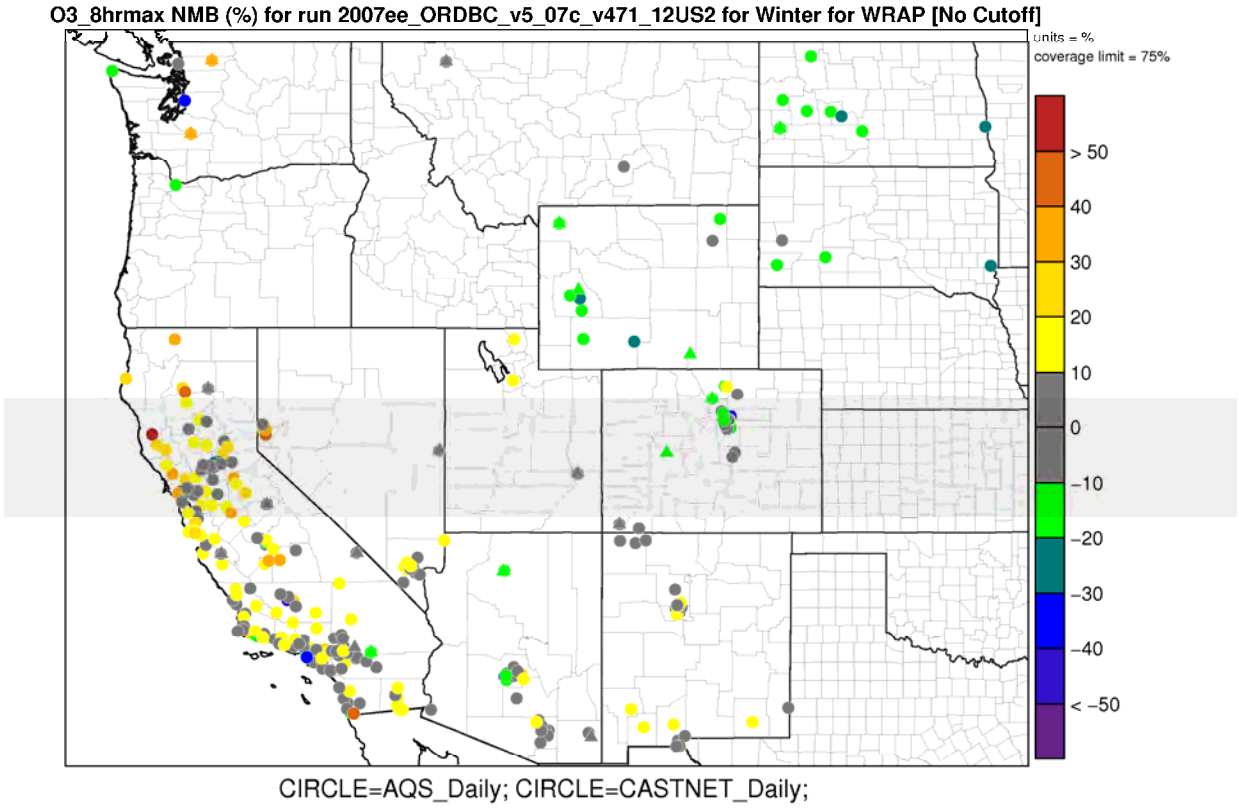

Figure 4B-74. Map of normalized mean bias for MDA8 O_3 concentrations in the Western U.S. for winter months in 2007.

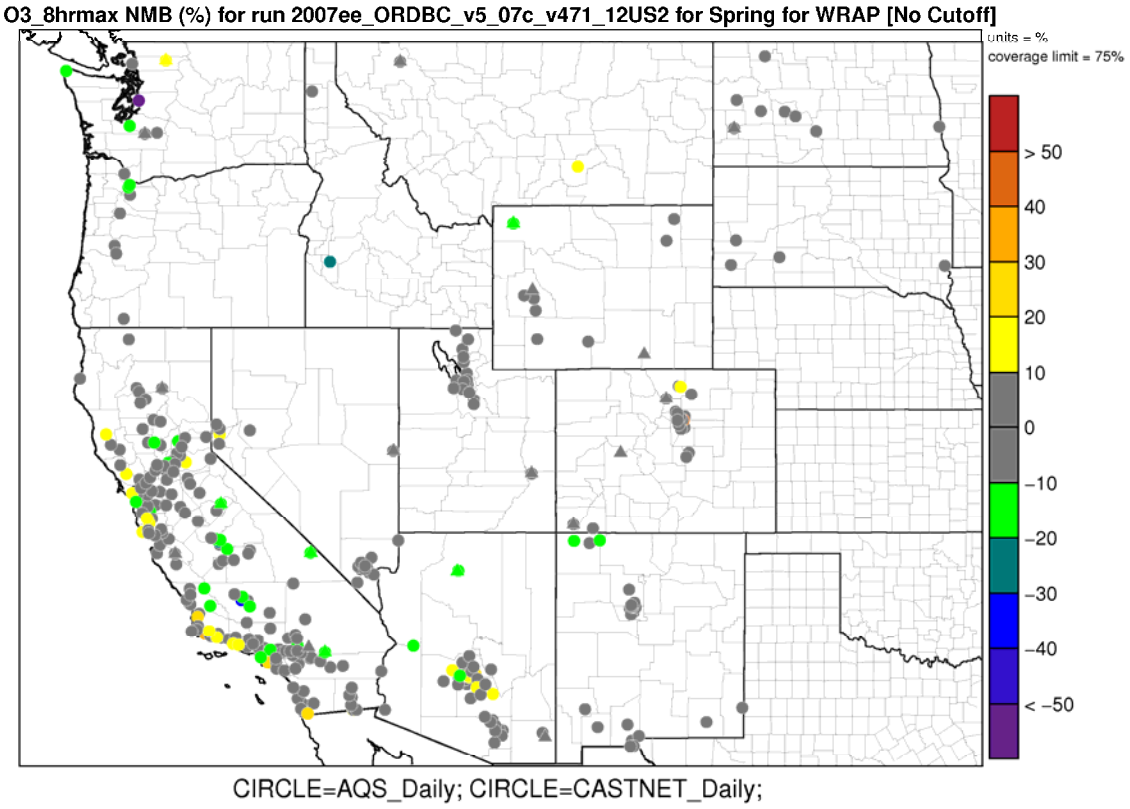

Figure 4B-75. Map of normalized mean bias for MDA8 O_3 concentrations in the Western U.S. for spring months in 2007.

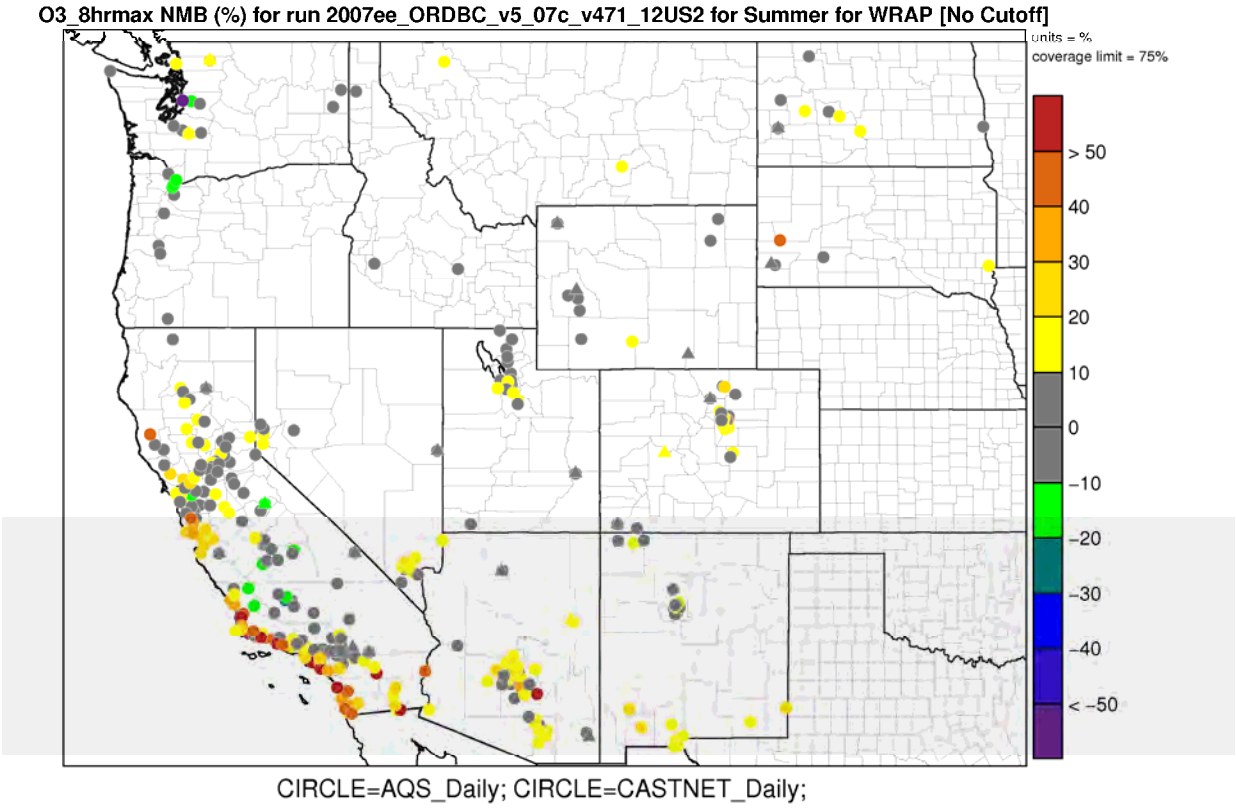

Figure 4B-76. Map of normalized mean bias for MDA8 O_3 concentrations in the Western U.S. for summer months in 2007.

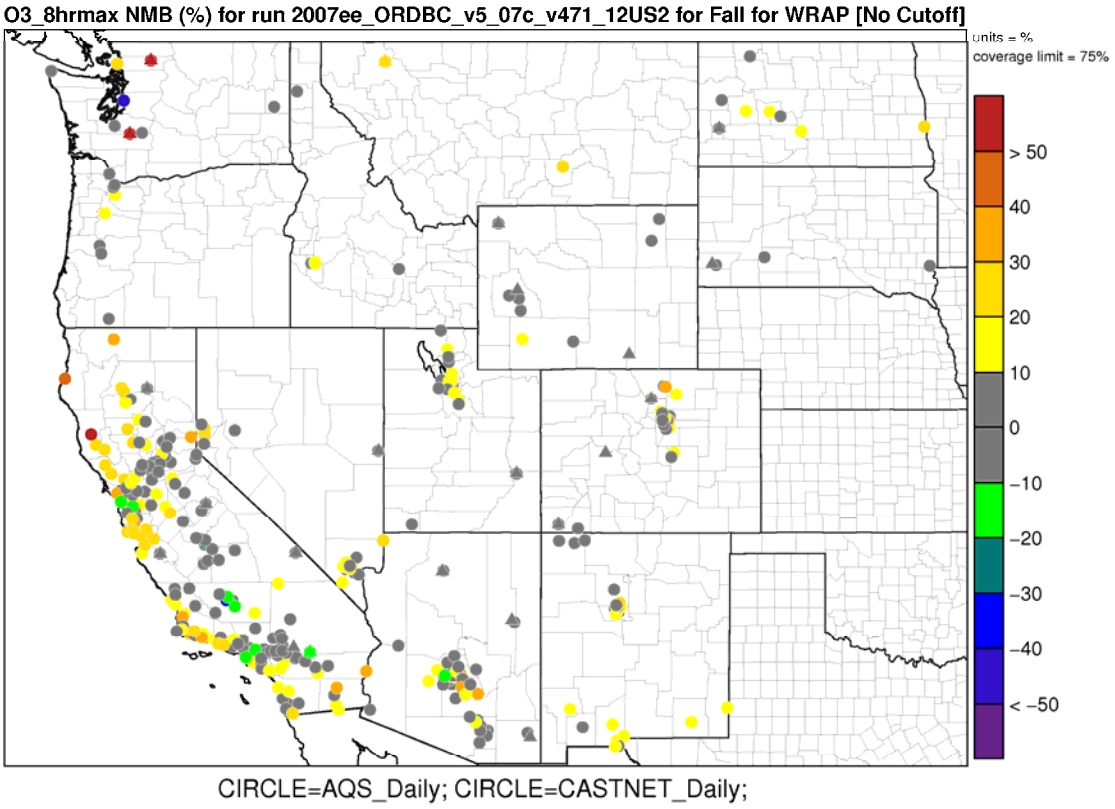

Figure 4B-77. Map of normalized mean bias for MDA8 O_3 concentrations in the Western U.S. for fall months in 2007.

Table 4B-21. Summary of CMAQ model performance at AQS monitoring sites in the Denver area.

Season	MDA8	No. of Days	MB (ppb)	NMB (%)	ME (ppb)	NMB (%)
Winter	< 60 ppb	1006	-3.84	-11.5	7.23	21.6
	≥ 60 ppb	0	NA	NA	NA	NA
	All Days	1006	-3.84	-11.5	7.23	21.6
Spring	< 60 ppb	893	3.36	7.3	6.24	13.7
	≥ 60 ppb	182	-2.42	-3.7	6.06	9.4
	All Days	1075	2.38	4.9	6.21	12.7
Summer	< 60 ppb	427	10.2	19.4	11.5	21.9
	≥ 60 ppb	653	4.94	7.2	8.18	11.9
	All Days	1080	7.02	11.3	9.49	15.2
Fall	< 60 ppb	993	3.19	8.4	6.47	17.0
	≥ 60 ppb	53	-1.59	-2.5	6.38	9.8
	All Days	1046	2.95	7.5	6.46	16.4

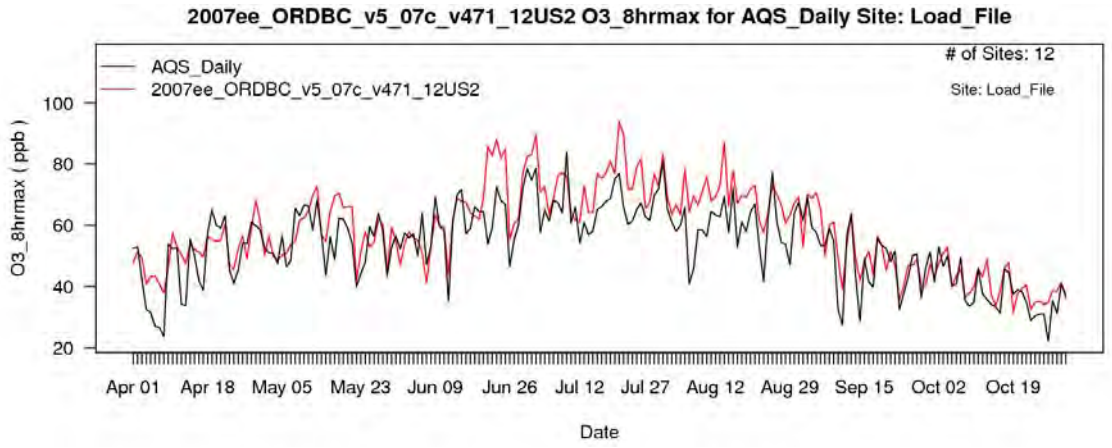

Figure 4B-78. Time series of 8-hr daily maximum O_3 concentrations at Denver monitoring sites for April-October 2007. Observed values shown in black and modeled values shown in red.

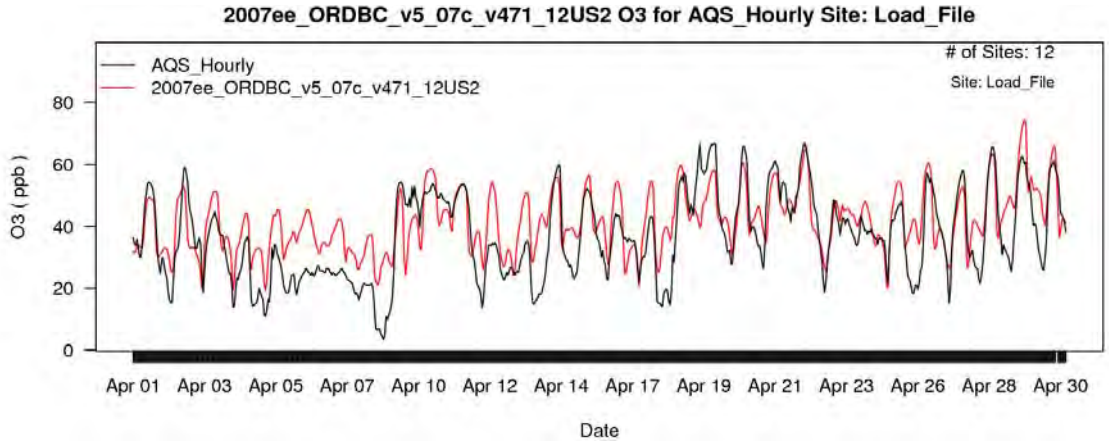

Figure 4B-79. Time series of hourly O_3 concentrations at Denver monitoring sites for April 2007. Observed values shown in black and modeled values shown in red.

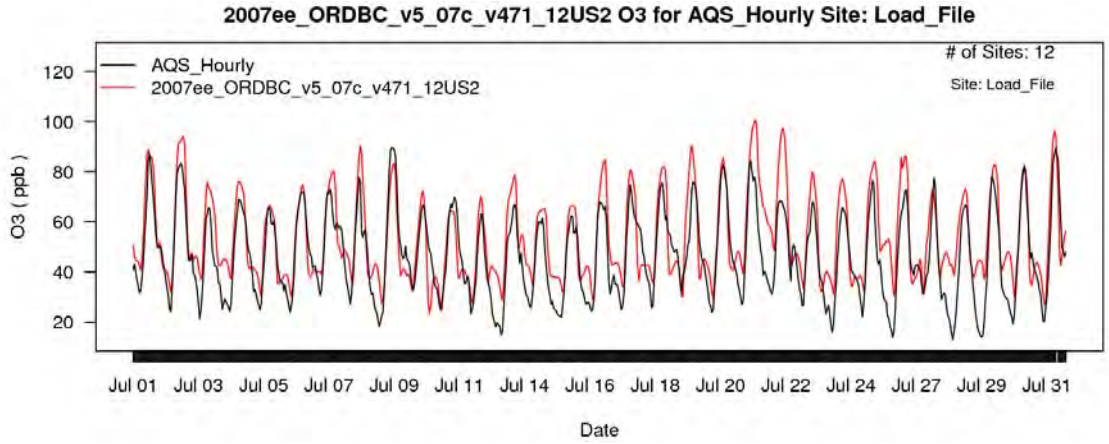

Figure 4B-80. Time series of hourly O_3 concentrations at Denver monitoring sites for July 2007. Observed values shown in black and modeled values shown in red.

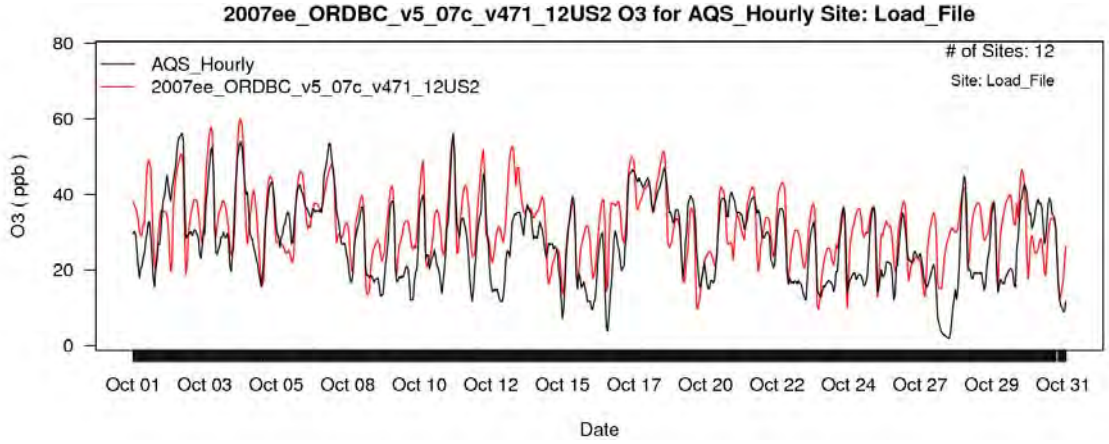

Figure 4B-81. Time series of hourly O_3 concentrations at Denver monitoring sites for October 2007. Observed values shown in black and modeled values shown in red.

Table 4B-22. Summary of CMAQ model performance at AQS monitoring sites in the Sacramento area.

Season	MDA8	No. of Days	MB (ppb)	NMB (%)	ME (ppb)	NME (%)
Winter	< 60 ppb	1374	1.04	3.5	5.41	18.4
	≥ 60 ppb	2	-31.80	-49.8	31.80	49.8
	All Days	1376	0.99	3.4	5.45	18.5
Spring	< 60 ppb	1516	-0.89	-2.0	5.28	11.8
	≥ 60 ppb	239	-4.83	-7.1	6.37	9.3
	All Days	1755	-1.42	-3.0	5.43	11.3
Summer	< 60 ppb	1443	4.10	9.1	6.58	14.6
	≥ 60 ppb	619	-1.39	-2.0	7.81	11.2
	All Days	2062	2.45	4.7	6.95	13.2
Fall	< 60 ppb	1809	1.80	4.8	6.30	16.7
	≥ 60 ppb	150	-7.82	-11.1	10.10	14.3
	All Days	1959	1.06	2.6	6.59	16.4

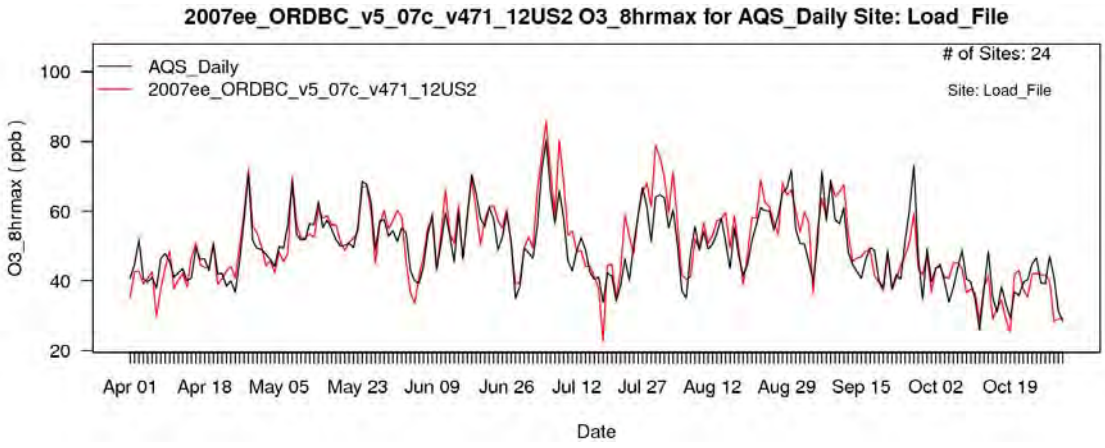

Figure 4B-82. Time series of 8-hr daily maximum O_3 concentrations at Sacramento monitoring sites for April-October 2007. Observed values shown in black and modeled values shown in red.

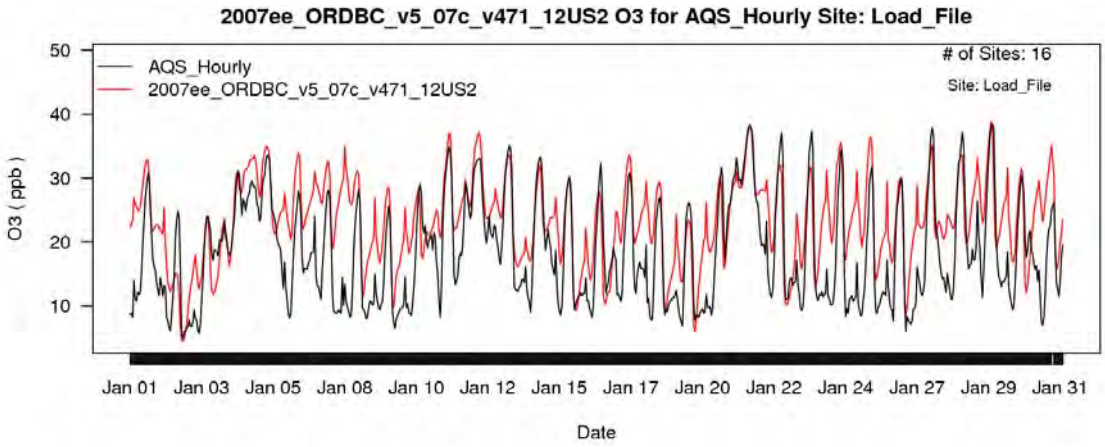

Figure 4B-83. Time series of hourly O_3 concentrations at Sacramento monitoring sites for January 2007. Observed values shown in black and modeled values shown in red.

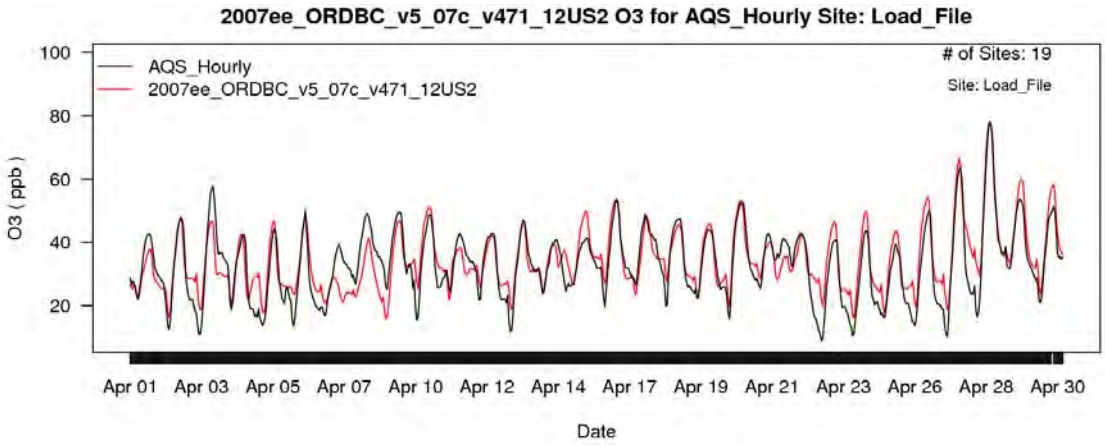

Figure 4B-84. Time series of hourly O_3 concentrations at Sacramento monitoring sites for April 2007. Observed values shown in black and modeled values shown in red.

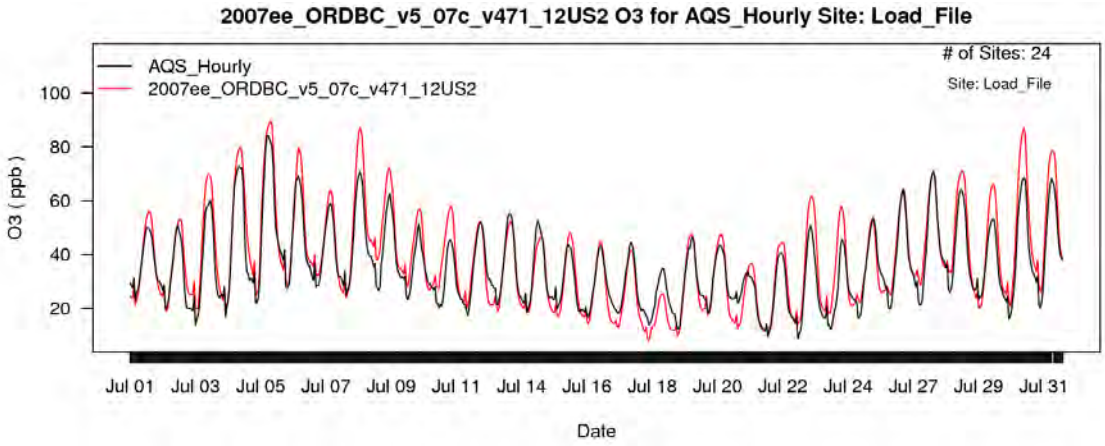

Figure 4B-85. Time series of hourly O_3 concentrations at Sacramento monitoring sites for July 2007. Observed values shown in black and modeled values shown in red.

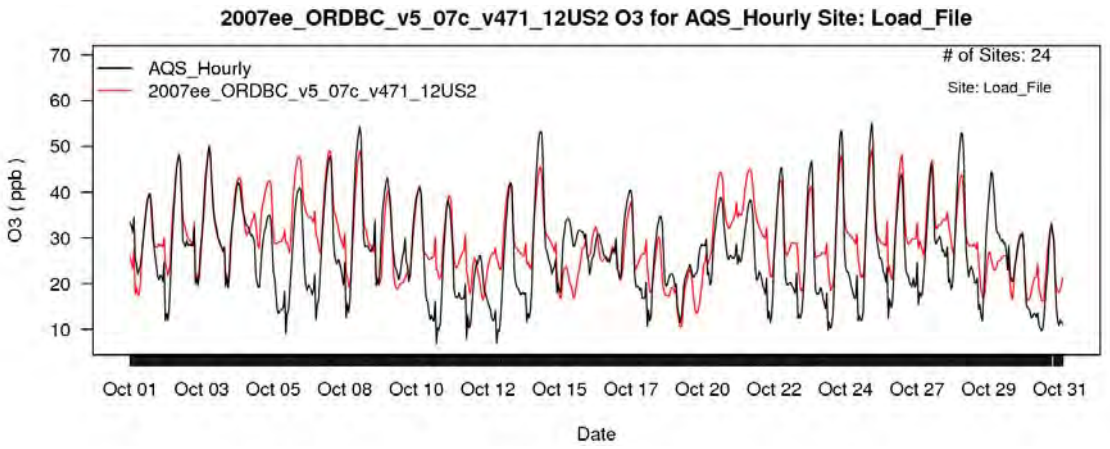

Figure 4B-86. Time series of hourly O_3 concentrations at Sacramento monitoring sites for October 2007. Observed values shown in black and modeled values shown in red.

Table 4B-23. Summary of CMAQ model performance at AQS monitoring sites in the Los Angeles area.

Season	MDA8	No. of Days	MB (ppb)	NMB (%)	ME (ppb)	NME (%)
Winter	< 60 ppb	3710	1.40	4.4	5.39	16.9
	≥ 60 ppb	13	-35.60	-44.9	35.6	44.9
	All Days	3723	1.27	4.0	5.49	17.2
Spring	< 60 ppb	2911	1.55	3.3	6.12	13.0
	≥ 60 ppb	968	-3.76	-5.4	7.20	10.4
	All Days	3879	0.22	0.4	6.39	12.2
Summer	< 60 ppb	1972	15.0	32.7	16.2	35.3
	≥ 60 ppb	1896	3.35	4.4	10.4	13.7
	All Days	3868	9.27	15.4	13.3	22.1
Fall	< 60 ppb	3461	2.95	7.7	8.30	21.5
	≥ 60 ppb	335	-2.66	-3.8	10.60	15.1
	All Days	3796	2.46	5.9	8.51	20.5

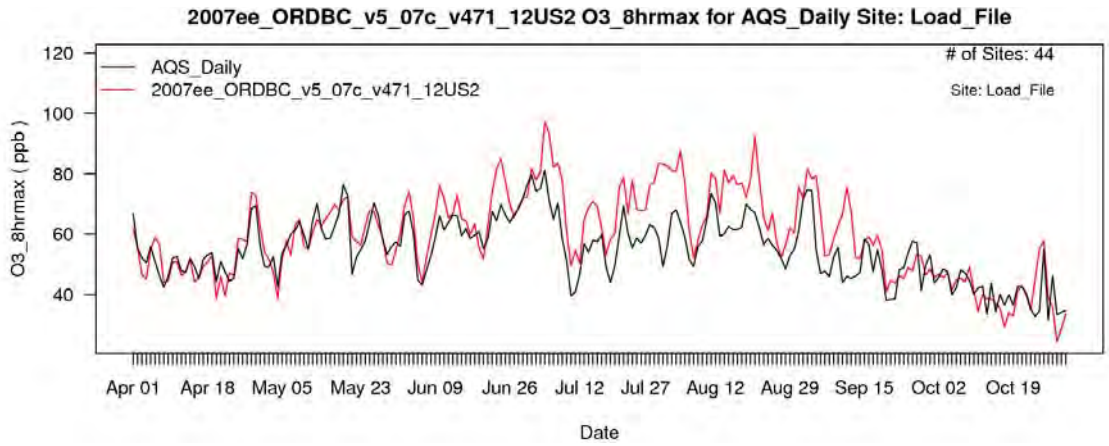

Figure 4B-87. Time series of 8-hr daily maximum O_3 concentrations at Los Angeles monitoring sites for April-October 2007. Observed values shown in black and modeled values shown in red.

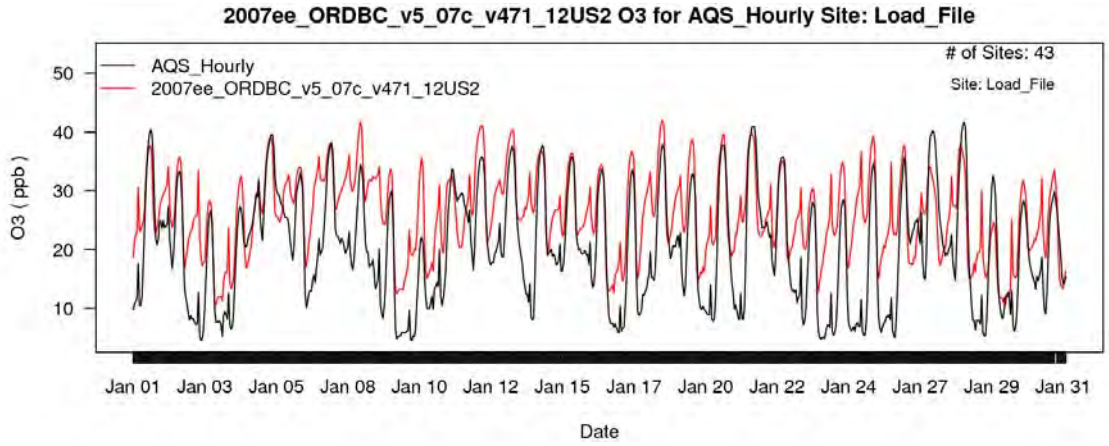

Figure 4B-88. Time series of hourly O_3 concentrations at Los Angeles monitoring sites for January 2007. Observed values shown in black and modeled values shown in red.

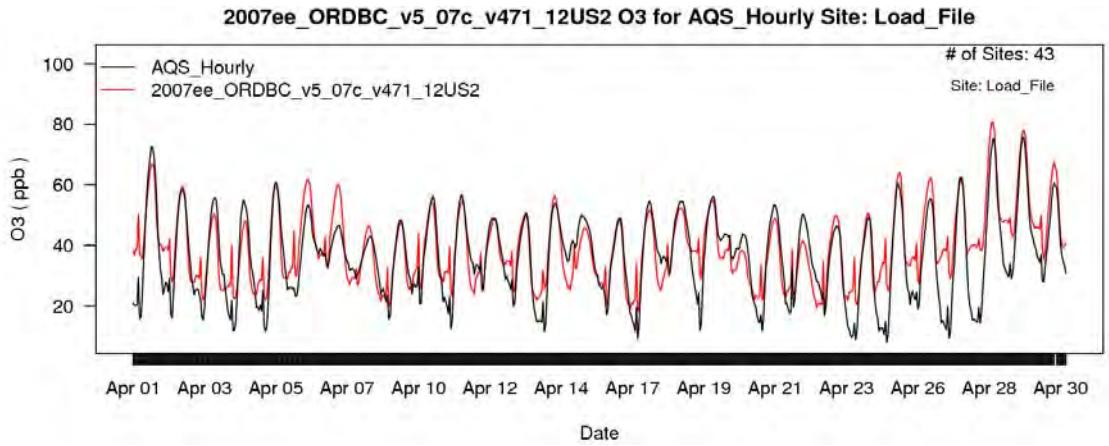

Figure 4B-89. Time series of hourly O_3 concentrations at Los Angeles monitoring sites for April 2007. Observed values shown in black and modeled values shown in red.

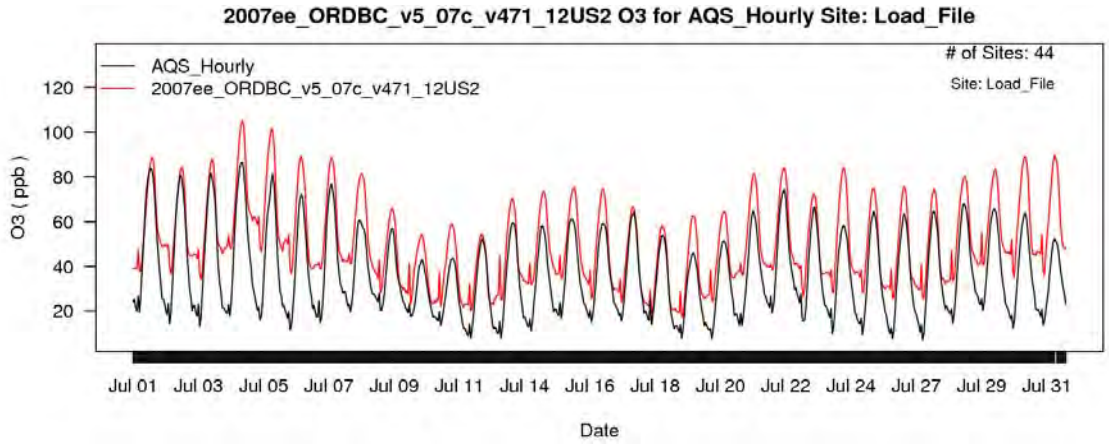

Figure 4B-90. Time series of hourly O_3 concentrations at Los Angeles monitoring sites for July 2007. Observed values shown in black and modeled values shown in red.

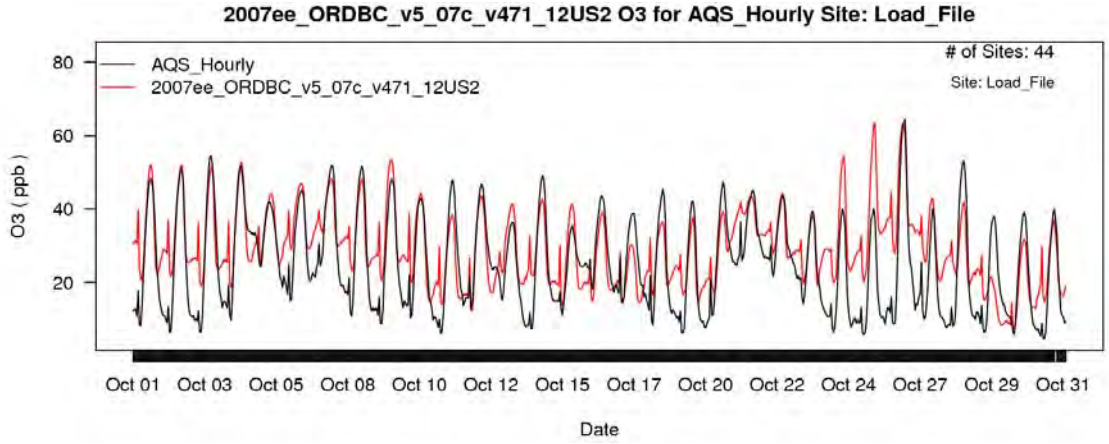

Figure 4B-91. Time series of hourly O_3 concentrations at Los Angeles monitoring sites for October 2007. Observed values shown in black and modeled values shown in red.

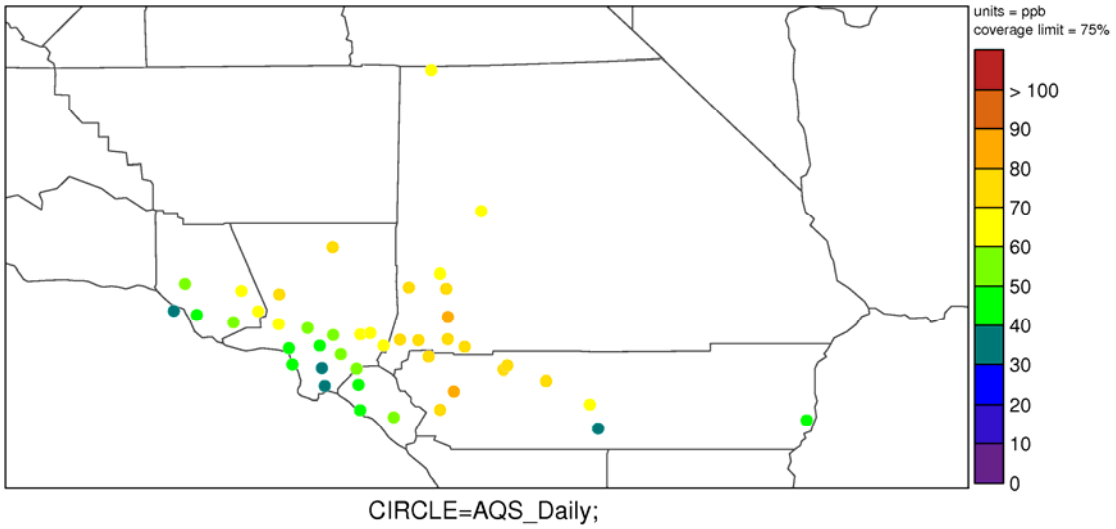

Figure 4B-92. Map of mean observed MDA8 O_3 concentrations at Los Angeles monitoring sites for summer months (June, July, Aug) 2007.

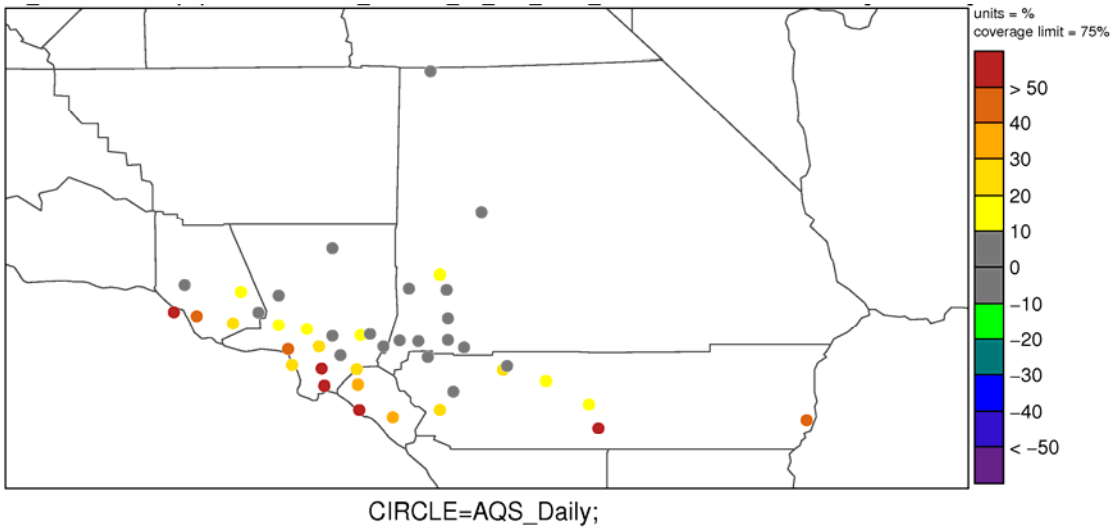

Figure 4B-93. Map of normalized mean bias for MDA8 O_3 concentrations at Los Angeles monitoring sites for summer months (June, July, Aug) 2007.

4B-3. REFERENCES

Akhtar, F., Henderson, B., Appel, W., Napelenok, S., Hutzell, B., Pye, H., Foley, K. (2012). Multiyear Boundary Conditions for CMAQ 5.0 from GEOS-Chem with Secondary Organic Aerosol Extensions, 11th annual Community Modeling and Analysis System conference, Chapel Hill, NC, October 2012.

Carlton, A.G., Bhave, P.V., Napelenok, S.L., Edney, E.D., Sarwar, G., Pinder, R.W., Pouliot, G.A., Houyoux, M. (2010). Model Representation of Secondary Organic Aerosol in CMAQv4.7. *Environmental Science & Technology*, 44: 8553-8560.

Foley, K.M., Roselle, S.J., Appel, K.W., Bhave, P.V., Pleim, J.E., Otte, T.L., Mathur, R., Sarwar, G., Young, J.O., Gilliam, R.C., Nolte, C.G., Kelly, J.T., Gilliland, A.B., Bash, J.O. (2010). Incremental testing of the Community Multiscale Air Quality (CMAQ) modeling system version 4.7, *Geoscientific Model Development*, 3: 205-226.

Gery, M.W., Whitten, G.Z., Killus, J.P., Dodge, M.C. (1989). A photochemical kinetics mechanism for urban and regional scale computer modeling. *Journal of Geophysical Research-Atmospheres*, 94: 12925-12956.

Gilliam, R.C., Pleim, J.E. (2010). Performance Assessment of New Land Surface and Planetary Boundary Layer Physics in the WRF-ARW. *Journal of Applied Meteorology and Climatology*, 49: 760-774.

Gilliland, A.B., Hogrefe, C., Pinder, R.W., Godowitch, J.M., Foley, K.L., Rao, S.T. (2008). Dynamic evaluation of regional air quality models: assessing changes in O3 stemming from changes in emission and meteorology. *Atmospheric Environment*, 42: 5110-5123.

Godowitch, J.M, Gilliam, R.C., Rao, S.T. (2011). Diagnostic evaluation of ozone production and horizontal transport in a regional photochemical air quality modeling system. *Atmospheric Environment*, 45: 3977-3987.

Godowitch, J.M., Pouliot, G.A., Rao, S.T. (2010). Assessing multi-year changes in modeled and observed urban NOx concentrations from a dynamic model evaluation perspective. *Atmospheric Environment*, 44: 2894-2901.

Godowitch, J.M., Hogrefe, C., Rao, S.T. (2008). Diagnostic analysis of a regional air quality model: changes in modeled processes affecting ozone and chemical-transport indicators form NOx point source emissions reductions. *Journal of Geophysical Research-Atmospheres*, 113(D19): D19303, DOI: 10.1029/2007JD009537.

Grell, G. A., Dudhia, A. J., and Stauffer, D. R. (1994). A description of the Fifth-Generation Penn State/NCAR Mesoscale Model (MM5). NCAR Technical Note NCAR/TN-398+STR. Available at http://www.mmm.ucar.edu/mm5/doc1.html.

Henderson, B.H., Akhtar, F., Pye, H.O.T., Napelenok, S.L., Hutzell, W.T. (2013) A database and tool for boundary conditions for regional air quality modeling: description and evaluation, Geoscientific Model Development Discussions, 6, 4665-4704.

Henze, D.K., J.H. Seinfeld, N.L. Ng, J.H. Kroll, T-M. Fu, D.J. Jacob, C.L. Heald (2008). Global modeling of secondary organic aerosol formation from aromatic hydrocarbons: High- vs. low-yield pathways. *Atmos. Chem. Phys*., 8: 2405-2420.

Lam, Y.F., Fu, J.S., Jacob, D.J., Jang, C., Dolwick, P., 2010 2006-2008 GEOS-Chem for CMAQ Initial and Boundary Conditions. 9th Annual CMAS Conference, October 11-13, 2010, Chapel Hill, NC.

Nenes, A., Pandis, S.N., Pilinis, C. (1998). ISORROPIA: A new thermodynamic equilibrium model for multiphase multicomponent inorganic aerosols. *Aquatic Geochemistry*, 4: 123-152.

Napelenok, S.L., Foley, K.M, Kang. D.W., Mathur, R., Pierce, T., Rao, S.T. (2011). Dynamic evaluation of regional air quality model's response to emission reduction in the presence of uncertain emission inventories. *Atmospheric Environment*, 45: 4091-4098.

Otte T.L., Pleim, J.E. (2010). The Meteorology-Chemistry Interface Processor (MCIP) for the CMAQ modeling system: updates through v3.4.1. *Geoscientific Model Development*, 3: 243-256.

Simon, H., Baker, K.R., Phillips, S. (2012). Compilation and interpretation of photochemical model performance statistics published between 2006 and 2012. *Atmospheric Environment*, 61: 124-139.

Skamarock, W.C., Klemp, J.B., Dudhia, J., Gill, D.O., Barker, D.M., Dudia, M.G., Huang, X., Wang, W., Powers, J.G. (2008). A Description of the Advanced Research WRF Version 3.

U.S. EPA (2011). Meteorological Model Performance for Annual 2007 Simulations, Office of Air Quality Planning and Standards, Research Triangle Park, NC., 27711, EPA-454/R-11-007.

U.S. EPA (2012a), Air Quality Modeling Technical Support Document for the Regulatory Impact Analysis for the Revisions of the National Ambient Air Quality Standard for Particulate Matter. Office of Air Quality Planning and Standards, Research Triangle Park, NC, December 2012. Available at: http://www.epa.gov/ttn/naaqs/standards/pm/data/201212aqm.pdf

U.S. EPA (2012b). Technical Support Document: Preparation of Emissions Inventories of the Version 5, 2007-based Platform. Office of Air Quality Planning and Standards, Research Triangle Park, NC. December 2012.

Yantosca, B. (2004). GEOS-CHEMv7-01-02 User's Guide, Atmospheric Chemistry Modeling Group, Harvard University, Cambridge, MA, October 15, 2004.

Yarwood, G., Rao, S., Yocke, M., Whitten, G.Z. (2005). Updates to the Carbon Bond chemical mechanism: CB05. Final Report to the US EPA, RT-0400675, December 8, 2005: http://www.camx.com/publ/pdfs/CB05_Final_Report_120805.pdf.

Zhou, W., Cohan, D.S., Napelenok, S.L. (2013). Reconciling NOx emissions reductions and ozone trends in the U.S., 2002-2006, *Atmospheric Environment*, 70: 236-244.

This page left intentionally blank

APPENDIX 4C

Air Quality Spatial Fields for the National Mortality Risk Burden Assessment

Table of Contents

4C-1. OVERVIEW 4C-1

4C-2. AIR QUALITY SPATIAL FIELD TECHNIQUES 4C-2

4C-2.1 Voronoi Neighbor Averaging (VNA) 4C-2

4C-2.2 Community Multi-scale Air Quality (CMAQ) Model 4C-3

4C-2.3 Enhanced Voronoi Neighbor Averaging (eVNA) 4C-4

4C-2.4 Downscaler (DS) 4C-5

4C-3. EVALUATION OF AIR QUALITY SPATIAL FIELD TECHNIQUES 4C-7

4C-3.1 Data 4C-7

4C-3.2 Methods 4C-7

4C-3.3 Results 4C-9

4C-4. AIR QUALITY INPUTS TO THE NATIONAL-SCALE MORTALITY RISK BURDENT ASSESSMENT 4C-12

4C-5. REFERENCES 4C-16

List of Tables

Table 4C-1. Summary of the cross-validation performance metrics for the four air quality spatial field techniques. 4C-12

List of Figures

Figure 4C-1. Numerical example of the Voronoi Neighbor Averaging (VNA) technique applied to a model grid domain. 4C-3
Figure 4C-2. Numerical example of the Enhanced Voronoi Neighbor Averaging (eVNA) technique applied to a model grid domain 4C-5
Figure 4C-3. Example of the "4-fold" cross-validation scheme used in the evaluation of the air quality spatial field techniques for the southern Lake Michigan area. 4C-9
Figure 4C-4. Cross-validation results for the 2007 annual 4th highest daily maximum O_3 concentrations. 4C-10
Figure 4C-5. Cross-validation results for the 2007 May-September mean of the daily maximum 8-hour O_3 concentrations. 4C-11
Figure 4C-6. May-September average daily maximum 8-hour O_3 concentrations in ppb, based on a Downscaler fusion of 2006-2008 average monitored values with a 2007 CMAQ model simulation. 4C-13
Figure 4C-7. June-August average daily 10am-6pm mean O_3 concentrations in ppb, based on a Downscaler fusion of 2006-2008 average monitored values with a 2007 CMAQ model simulation. 4C-14
Figure 4C-8. April-September average daily maximum 1-hour O_3 concentrations in ppb, based on a Downscaler fusion of 2006-2008 average monitored values with a 2007 CMAQ model simulation. 4C-15

4C-1. OVERVIEW

The need for greater spatial and temporal coverage of air quality concentration estimates has grown in recent years as epidemiology and exposure studies that link air quality to health effects have become more robust and as regulatory needs have increased. These health studies have historically relied upon direct measurements of air quality concentrations, but prohibitive logistics and costs limit the spatial coverage and temporal resolution of available ambient monitoring networks. Numerical methods of interpolation, which predict unknown values from data observed at known locations, have historically been used by researchers to extend the spatial coverage of these monitoring networks with a high degree of confidence to inform exposure studies. However, simple kriging approaches such as Voronoi Neighbor Averaging (VNA) do not take advantage of the greater availability of model predictions of air quality concentrations that can enhance the predictive capabilities of numerical methods. Such "data fusion" methods employ both ambient air quality monitoring data and air quality modeling simulation data as inputs, and therefore take advantage of the measurement data's accuracy at specific locations and the air quality model's spatial coverage to generate more robust spatial predictions. For regulatory purposes, the enhanced Voronoi Neighbor Averaging (eVNA) has been the preferred method used by EPA to make spatial predictions of ozone (O_3) as part of conducting health benefit assessments (U.S. EPA, 2010). Given the interest and value of these methods, research and development efforts have focused on improving their predictive capabilities. This includes the Office of Research and Development's development of the Downscaler (DS) model that can potentially provide predictions that are improved over those of eVNA (Berrocal et al., 2011).

This Appendix describes the methods, evaluation, and results of four different techniques for predicting air quality concentrations. These four techniques are:

1) VNA (interpolating the monitoring data),

2) CMAQ (using the absolute modeled air quality concentrations),

3) eVNA, and

4) Downscaler

EPA used the method with the best performance based on the evaluation to generate national air quality spatial fields of seasonally averaged O_3 concentrations as inputs to the national mortality risk burden assessment in Chapter 8 of the O_3 Health Risk and Exposure Assessment (HREA).

Air quality spatial fields are also used in two other applications for the risk and exposure assessments. In Appendix 4A of the HREA, we describe the methodology used to create urban-scale spatial fields of hourly O_3 concentrations for use in the exposure modeling. In Appendix 4A to the Welfare Risk and Exposure Assessment (WREA), we evaluate these same four spatial

field techniques for use in creating national-scale air quality spatial fields for the W126 exposure metric.

4C-2. AIR QUALITY SPATIAL FIELD TECHNIQUES

This section briefly describes the methodology of each of the four techniques considered for generating air quality spatial fields as inputs to the national risk mortality burden analyses described in the HREA Chapter 8.

4C-2.1 Voronoi Neighbor Averaging (VNA)

The Voronoi Neighbor Averaging (VNA; Gold, 1997; Chen et al., 2004) interpolation technique uses inverse distance squared weighted averages of the ambient concentrations from a set of nearest neighboring monitors to estimate the concentration at a specified location (in this case CMAQ grid cell centers). VNA identifies the nearest neighboring monitors for the center of each grid cell using a Delaunay triangulation algorithm, then takes the inverse distance squared weighted average of the hourly O_3 concentrations from each neighboring monitor to estimate an hourly O_3 concentration value for the center of the grid cell. The following paragraphs provide a numerical example of the VNA technique applied to a model grid domain.

The first step in VNA is to identify the set of nearest monitors for each grid cell in the domain. The left-hand panel of Figure 4C-1 below presents a numerical example with nine model grid cells and seven monitoring sites, with the focus on identifying the set of nearest neighboring sites to the center of grid cell "E", the center cell. The Delaunay triangulation algorithm identifies the set of nearest neighboring monitors by drawing a set of polygons called the "Voronoi diagram" around the center of grid cell "E" and each of the monitoring sites. Voronoi diagrams have the special property that the each edge of the polygons are the same distance from the two closest points, as shown in the right-hand panel below.

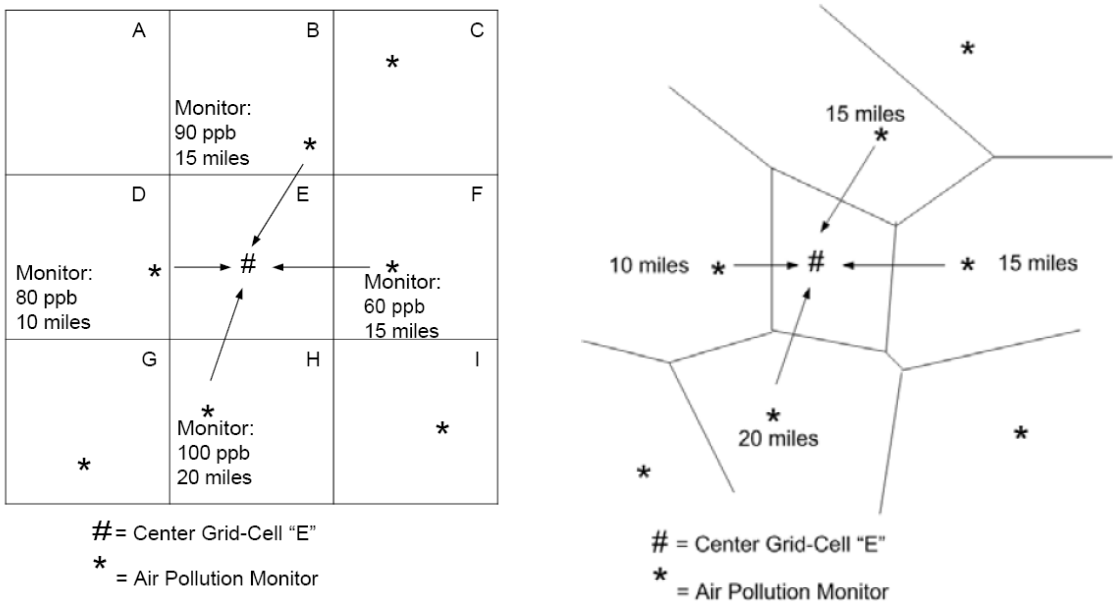

Figure 4C-1. Numerical example of the Voronoi Neighbor Averaging (VNA) technique applied to a model grid domain.

VNA then chooses the monitoring sites that share a boundary with the center of grid cell "E". These are the nearest neighboring sites, which are used to estimate the concentration value for grid cell "E". The VNA estimate of the concentration value in grid cell "E" is the inverse distance squared weighted average of the four monitored concentrations. The further the monitor is from grid cell "E", the smaller the weight.

For example, the weight for the monitor in grid cell "D" 10 miles from the center of grid cell "E" is calculated as follows:

$$\frac{1/10^2}{1/10^2+1/15^2+1/15^2+1/20^2} = 0.4675 \qquad \text{Equation (4C-1)}$$

The weights for the other monitors are calculated in a similar fashion. The final VNA estimate for grid cell "E" is calculated as follows:

$$VNA(E) = 0.4675 * 80 + 0.2078 * 90 + 0.2078 * 60 + 0.1169 * 100 = 80.3\ ppb$$

Equation (4C-2)

4C-2.2 Community Multi-scale Air Quality (CMAQ) Model

For more than a decade, the EPA's Community Multi-scale Air Quality (CMAQ; Foley et al., 2010) model has been a valuable computational tool used by EPA and states to inform air quality management programs. The CMAQ system simultaneously models multiple air

pollutants, including O_3, particulate matter, and a variety of air toxics to help regulators determine the best air quality management scenarios for their communities, states, and countries. CMAQ is also used by states to assess implementation actions needed to attain National Ambient Air Quality Standards.

The CMAQ system includes emissions, meteorology, and photochemical modeling components. Research continues in all of these areas to reduce biases and uncertainties in model simulations. CMAQ is a multi-scale system that has been applied over continental, national, regional, and urban modeling domains with progressively finer resolution in a series of nested grids. The CMAQ modeling community includes researchers, regulators, and forecasters in academia, government, and the private sector with thousands of users worldwide.

Modeled air quality concentrations from CMAQ simulations have a twofold purpose in the generation and analysis of air quality spatial fields. First, the modeled concentrations are "fused" with the ambient measurement data using the eVNA and DS techniques. Second, the original modeled concentrations are evaluated against the resulting concentration estimates from the other spatial field techniques, to ensure that those techniques successfully reduce biases in the modeled air quality fields.

4C-2.3 Enhanced Voronoi Neighbor Averaging (eVNA)

Enhanced Voronoi Neighbor Averaging (eVNA; Timin et al., 2010) is a direct extension of VNA used to combine monitored and modeled air quality concentration data. Continuing from the previous numerical example for VNA, suppose the model grid cells containing monitors are associated with modeled concentrations as shown in Figure 4C-2 below. The modeled concentrations are used to weight the VNA estimates relative to the modeled concentration gradient:

$$eVNA(E) = \sum_{i=1}^{n_i} Weight_i * Monitor_i * \frac{Model_E}{Model_i} \qquad \text{Equation (4C-3)}$$

where $Monitor_i$ represents the monitored concentration for a nearest neighboring monitor,
$Weight_i$ represents the inverse distance squared weight for $Monitor_i$,
$Model_E$ represents the modeled concentration for grid cell "E", and
$Model_i$ represents the modeled concentration in the grid cell containing $Monitor_i$.

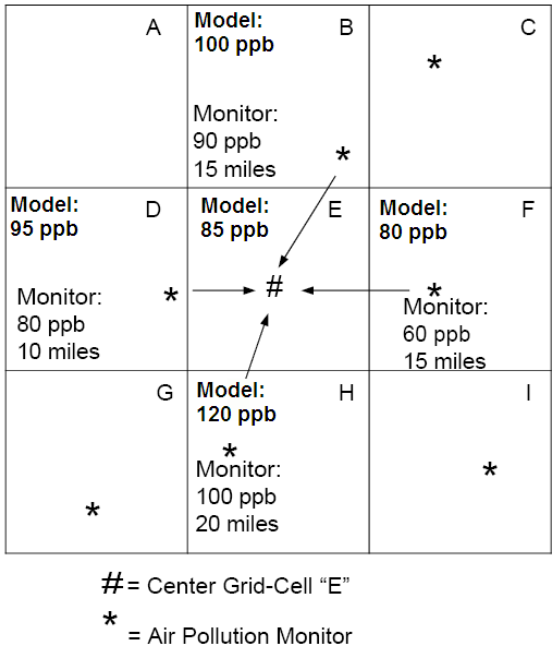

Figure 4C-2. Numerical example of the Enhanced Voronoi Neighbor Averaging (eVNA) technique applied to a model grid domain

Based on the values shown in Figure 4C-2, the eVNA estimate for grid cell "E" is calculated as follows:

$$eVNA(E) = \left(0.4675 * 80 * \frac{85}{95}\right) + \left(0.2078 * 90 * \frac{85}{100}\right) + \left(0.2078 * 60 * \frac{85}{80}\right) + \left(0.1169 * 100 * \frac{85}{120}\right) = 70.9\ ppb$$

Equation (4C-4)

In this example, eVNA adjusts the modeled concentration in grid cell "E" downward to reflect the tendency for the model to over-predict the monitored concentrations. In general, the eVNA method attempts to use the monitored concentrations to adjust for model biases, while preserving local gradients in the modeled concentration fields. The computations for VNA and eVNA were executed using the R statistical computing program (R, 2012), with the Delaunay triangulation algorithm implemented in the "deldir" package (Turner, 2012).

4C-2.4 Downscaler (DS)

The Downscaler (DS) model is EPA's most recently developed "data fusion" method for spatially predicting air pollution concentrations. Downscaler essentially operates by calibrating CMAQ data to the observational data, and then uses the resulting relationship to predict "observed" concentrations at new spatial points in the domain. Although similar in principle to a linear regression, spatial modeling aspects have been incorporated for improving the model fit,

and a Bayesian[1] approaching to fitting is used to generate an uncertainty value associated with each concentration prediction. The uncertainties that DS produces are a major distinguishing feature from earlier fusion methods previously used by EPA such as the "Hierarchical Bayesian" (HB) model (McMillan et al., 2009). The term "downscaler" refers to the fact that DS takes grid-averaged predictions from an air quality model such as CMAQ for input and produces point-based estimates, thus "scaling down" the area of data representation. Although this allows air pollution concentration estimates to be made at point locations where no observations exist, caution is needed when interpreting any within-grid cell spatial gradients generated by DS since they may not exist in the input datasets. The theory, development, and initial evaluation of DS can be found in the earlier papers of Berrocal, Gelfand, and Holland (2009, 2010, and 2011).

Downscaler develops a relationship between observed and modeled concentrations, and then uses that relationship to spatially predict what measurements would be at new locations in the spatial domain based on the input data. This process is separately applied for each time step (daily in this work) of data, and for each of the pollutants under study (O_3 and fine particulate matter, $PM_{2.5}$). In its most general form, the model can be expressed in an equation similar to that of linear regression:

$$Y(s,t) = \sim\beta_0(s,t) + \beta_1(t) * \sim x(s,t) + \varepsilon(s,t) \qquad \text{Equation (4C-5)}$$

where $Y(s,t)$ is the observed concentration at point s and time t,

$\sim x(s,t)$ is the CMAQ concentration at point s and time t, (This value is a weighted average of both the grid cell containing the monitor and neighboring grid cells.)

$\sim\beta_0(s,t)$ is the intercept, composed of global and local components,

$\beta_1(t)$ is the global slope, (Local components of the slope are contained in the $\sim x(s,t)$ term),

$\varepsilon(s,t)$ is the model residual error.

Downscaler has additional properties that differentiate it from linear regression:

1) Rather than just finding a single optimal solution to Equation (4C-5), DS uses a Bayesian approach so that uncertainties can be generated along with each concentration prediction. This involves drawing random samples of model parameters from built-in "prior" distributions and assessing their fit on the data on the order of thousands of times. After each iteration, properties of the prior distributions are adjusted to try to improve the fit of the next iteration. The resulting collection of $\sim\beta_0$ and β_1 values at each space-time point are the

[1] Bayesian statistical modeling refers to methods that are based on Bayes' theorem, and model the world in terms of probabilities based on previously acquired knowledge.

"posterior" distributions, and the means and standard distributions of these are used to predict concentrations and associated uncertainties at new spatial points.

2) The model is "hierarchical" in structure, meaning that the top level parameters in Equation (4C-5) (i.e., $\sim\beta_0(s,t)$, $\beta_1(t)$, $\sim x(s,t)$) are actually defined in terms of further parameters and sub-parameters in the DS code. For example, the overall slope and intercept is defined to be the sum of a global (one value for the entire spatial domain) and local (values specific to each spatial point) component. This gives more flexibility in fitting a model to the data to optimize the fit (i.e. minimize $\varepsilon(s,t)$).

EPA has recently used DS in other applications, such as providing spatial predictions of national daily 8-hour O_3 and $PM_{2.5}$ concentrations at a census tract resolution to the Centers for Disease Control (CDC) for the Public Health Air Surveillance Evaluation (PHASE) project as part of their Environmental Public Health Tracking (EPHT) program.

4C-3. EVALUATION OF AIR QUALITY SPATIAL FIELD TECHNIQUES

This section describes the data, methods, and results of an evaluation that was performed in order to assess the relative accuracy of the predictions generated by the four air quality spatial field techniques described in the previous section.

4C-3.1 Data

The evaluation was designed to assess the relative ability of each spatial field technique to reproduce monitored concentrations for two annual air quality metrics: 1) the 4th highest daily maximum 8-hour O_3 concentration (henceforth referred to as the "4th max"), and 2) the May – September mean of the daily maximum 8-hour O_3 concentrations (henceforth referred to as the "seasonal mean"). For the ambient monitoring data, these two metrics were calculated for all monitors in the contiguous U.S. with complete data for 2007 based on the initial dataset and the data completeness criteria described in HREA Appendix 4A. For the air quality modeling data, the two metrics were calculated from hourly O_3 concentrations based on a CMAQ simulation with a 12 km gridded domain covering the contiguous U.S., and 2007 emissions and meteorology inputs (EPA, 2012b).

4C-3.2 Methods

Cross-validation is a method commonly used to evaluate the ability of statistical models to make accurate predictions. In a cross-validation analysis, the data are split into two subsets, the "calibration" subset, and the "validation" subset. The calibration subset is used to "fit" the model, usually by estimating parameters which establish a relationship between the variable of interest and one or more dependent variables. The resulting model fit is then applied to the

dependent variable(s) in the validation subset, and the predictive ability of the model is assessed by how accurately it is able to reproduce the variable of interest in the validation subset.

The evaluation used a systematic "4-fold" cross-validation scheme based on the CMAQ modeling domain (e.g., 12 km x 12 km grid covering the continental U.S.). The CMAQ modeling domain was divided into four groups, or "folds", so that each 2x2 block of 12 km grid cells had one member in each fold. Figure 4C-3 shows an example of the resulting four folds with O_3 monitor locations for the area surrounding southern Lake Michigan. Four cross-validations were performed using VNA, eVNA, and DS, for both the 4th max and seasonal mean metrics. The calibration subset in the first cross-validation consisted of the monitors in folds 2, 3, and 4 as shown in Figure 4C-3 (blue dots), while the validation subset consisted of the monitors in fold 1 (red dots). The remaining cross-validations were performed in a similar manner, with three of the four folds used as the calibration subset and the final fold used as the validation subset. Thus, this method resulted in four cross-validation partitions, each with approximately 75% of the monitoring data used in the calibration subset, and the remaining 25% used in the validation subset. Each monitor was included in the validation subset exactly once, resulting in a validation dataset of observed 4th max and seasonal mean values paired with VNA, eVNA, and DS predictions of those values at monitor locations. The CMAQ predictions were simply the modeled 4th max and seasonal mean values for the 12 km grid cells containing O_3 monitors.

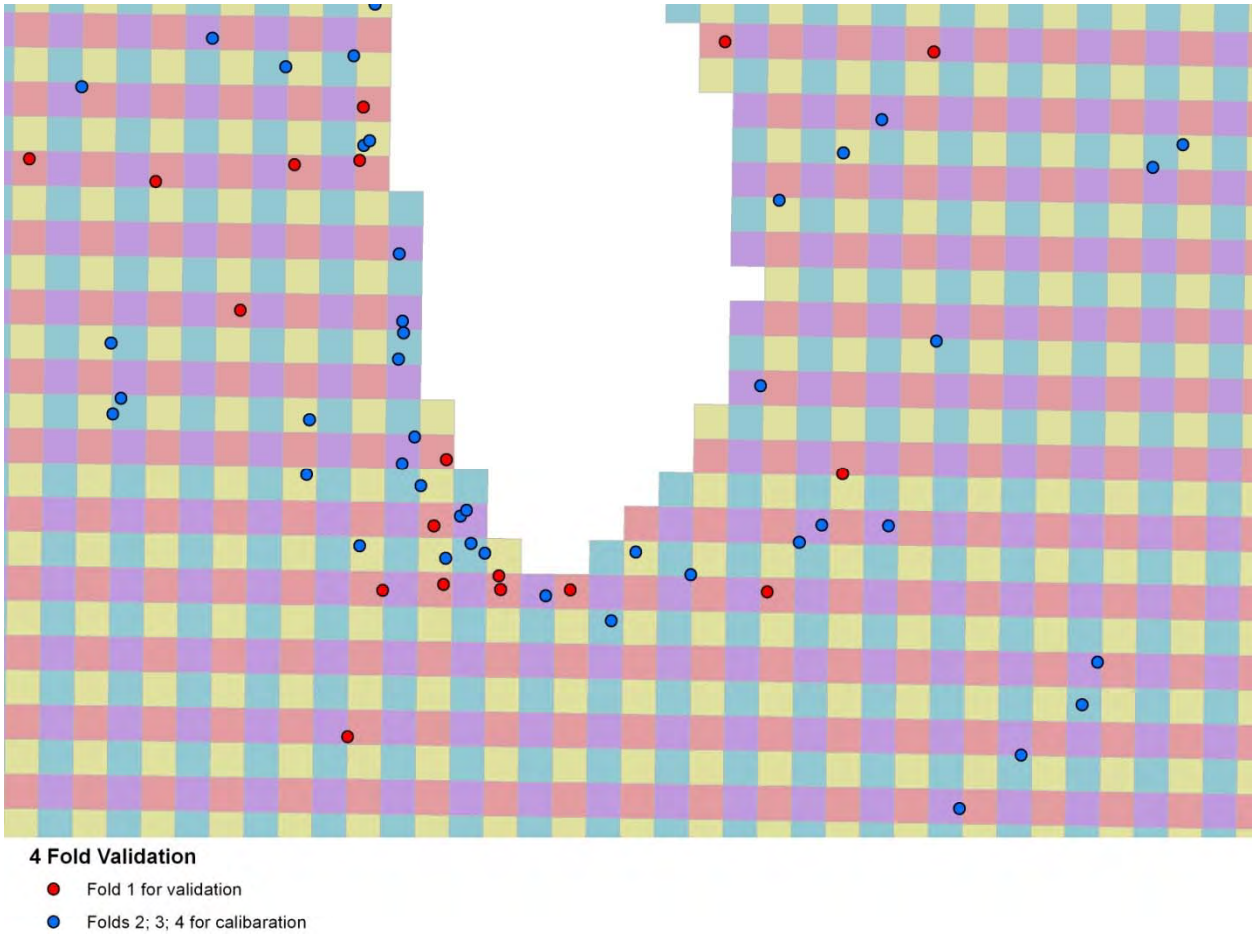

Figure 4C-3. Example of the "4-fold" cross-validation scheme used in the evaluation of the air quality spatial field techniques for the southern Lake Michigan area.

4C-3.3 Results

The cross-validation predictions based on the four air quality spatial field techniques were compared with the observed 4th max and seasonal mean values based on the ambient data. The comparison focused on three performance metrics: 1) the root mean squared error (RMSE), 2) the coefficient of variation (R^2), and 3) the mean bias (MB). The results of these comparisons are shown in Figure 4C-4 (4th max) and Figure 4C-5 (seasonal mean), and Table 4C-1 contains a summary of the three performance metrics for each technique.

The cross-validation results clearly showed that VNA, eVNA, and DS more accurately predict monitored 4th max and seasonal mean concentrations than the CMAQ model. The scatter plots and the mean bias statistics indicated that both eVNA and DS were effective at reducing the amount of bias present in the modeled concentrations. The differences between VNA, eVNA, and DS were much smaller, but the performance statistics consistently indicated that overall DS was able to most accurately reproduce the observed values. DS had the highest R^2 values, and the lowest RMSE and MB values of the four techniques for both air quality metrics. In contrast

to eVNA, DS seemed to be an improvement over VNA, which did not make use of the modeled concentration data. Based on these results, DS was deemed the most appropriate technique for generating spatial fields of seasonal mean O_3 concentrations for the national risk mortality burden analyses.

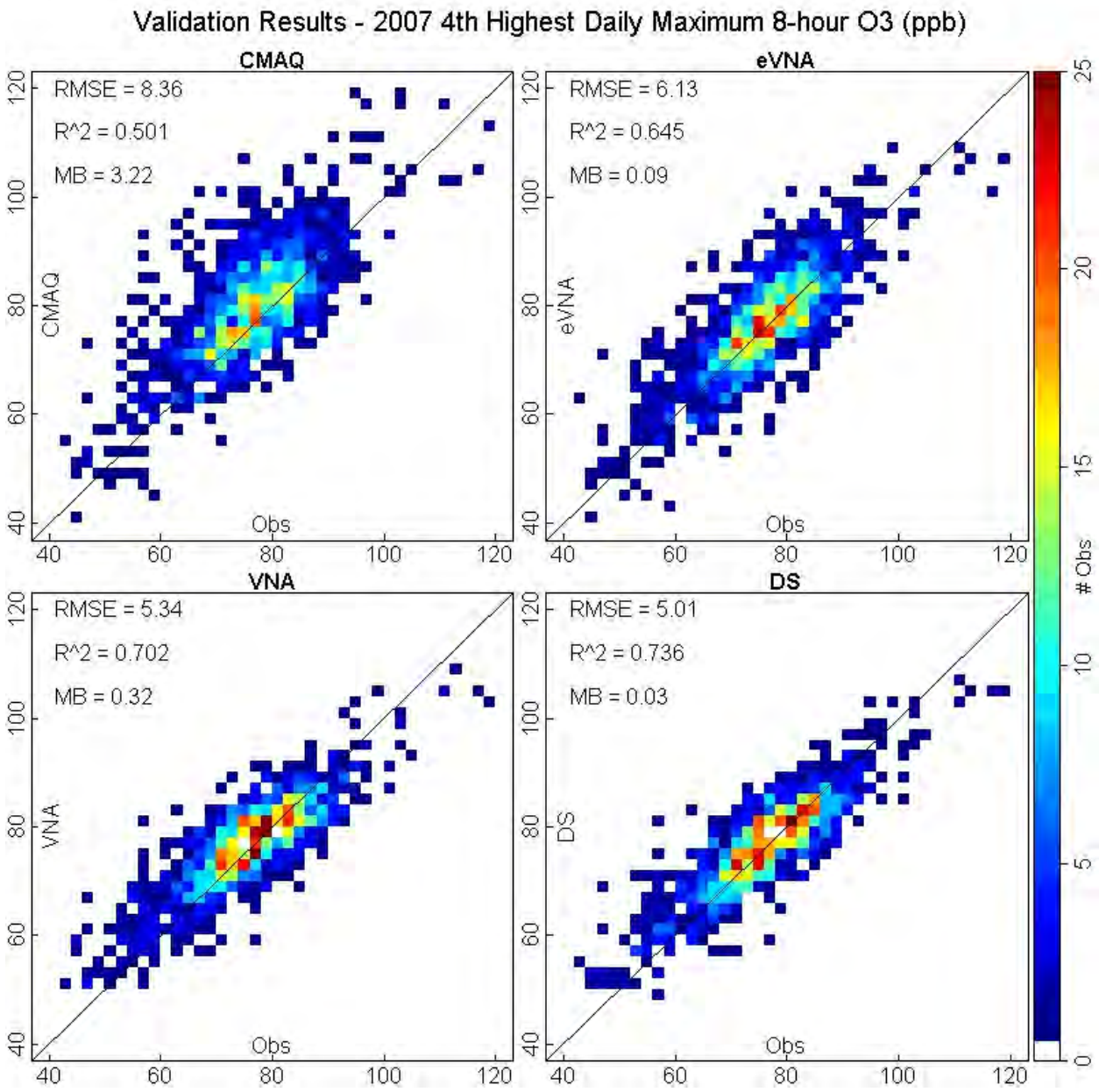

Figure 4C-4. Cross-validation results for the 2007 annual 4th highest daily maximum O_3 concentrations.

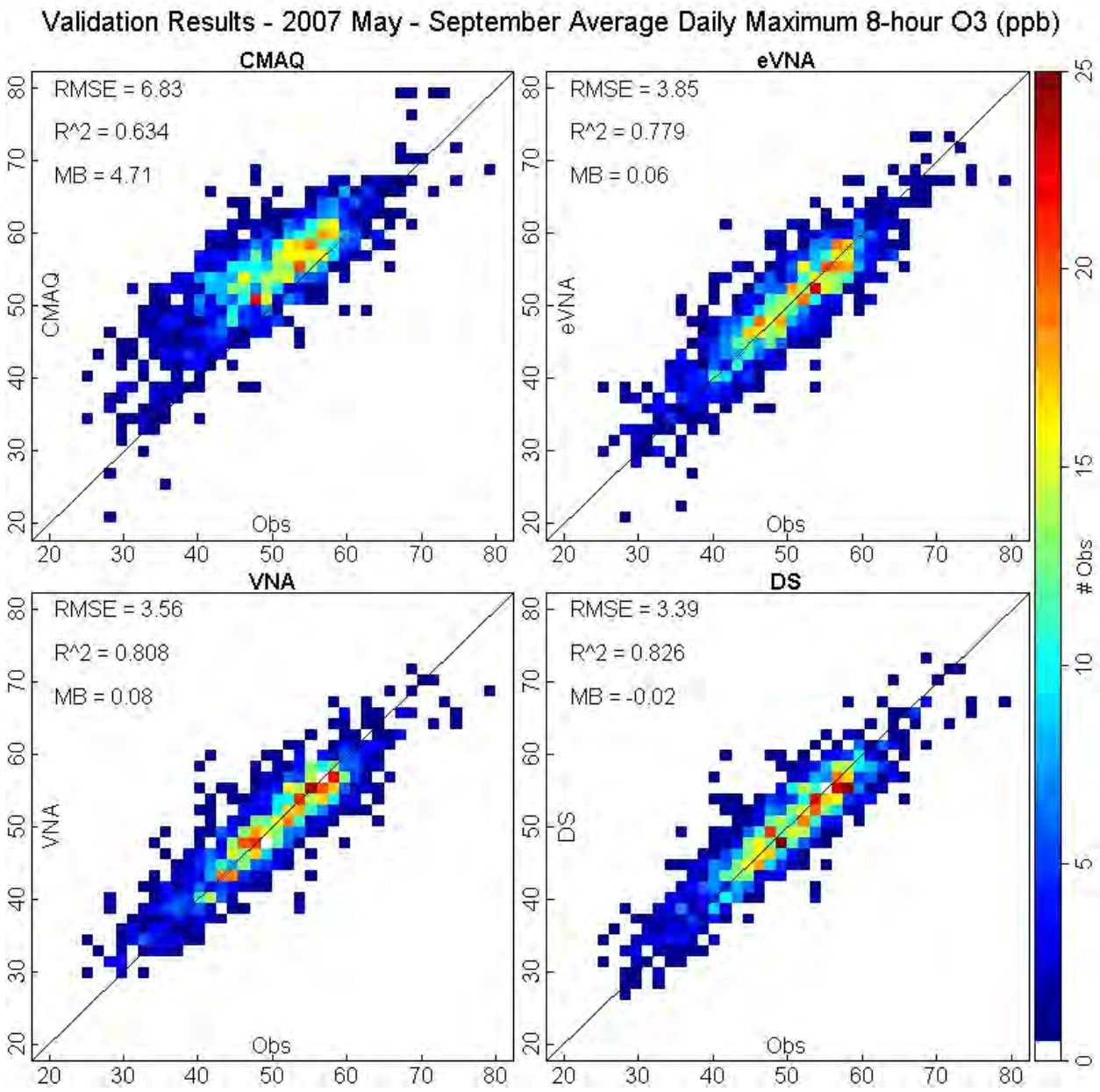

Figure 4C-5. Cross-validation results for the 2007 May-September mean of the daily maximum 8-hour O_3 concentrations.

Table 4C-1. Summary of the cross-validation performance metrics for the four air quality spatial field techniques.

Performance Metric	O_3 Metric	VNA	CMAQ	eVNA	DS
RMSE	4^{th} max	5.34	8.36	6.13	5.01
RMSE	seasonal mean	3.56	6.83	3.85	3.39
R^2	4^{th} max	0.702	0.501	0.645	0.736
R^2	seasonal mean	0.808	0.634	0.779	0.826
MB	4^{th} max	0.32	3.22	0.09	0.03
MB	seasonal mean	0.08	4.71	0.06	-0.02

4C-4. AIR QUALITY INPUTS TO THE NATIONAL-SCALE MORTALITY RISK BURDENT ASSESSMENT

Three air quality spatial fields were created using DS as inputs to the national mortality risk burden analyses. These fields were based on three seasonal mean O_3 metrics:

1) May-September average daily maximum 8-hour O_3 concentration (consistent with the metric used by Smith et al., 2009);
2) June-August average daily 10am-6pm mean O_3 concentration (consistent with the metric used by Zanobetti and Schwartz, 2008); and
3) April-September average daily maximum 1-hour O_3 concentration (consistent with the metric used by Jerrett et al., 2009).

For the ambient monitoring data, the 2006-2008 average of these annual metrics were calculated for all monitors in the contiguous U.S. with complete data for 2006-2008 based on the initial dataset and the data completeness criteria described in HREA Appendix 4A. For the air quality modeling data, these metrics were calculated from hourly O_3 concentrations based on a CMAQ simulation with a 12 km gridded domain covering the contiguous U.S., and 2007 emissions and meteorology inputs. This simulation differed from the one used for the evaluations in that the wildfire and power plant emissions inputs were based on multi-year averages instead of year-specific estimates. Appendix 4B contains a complete description of this CMAQ simulation and provides relevant model evaluation results.

Figure 4C-6, Figure 4C-7, and Figure 4C-8 show maps of the DS air quality spatial fields for the May-September average daily maximum 8-hour O_3 concentrations, the June-August average daily 10am-6pm mean O_3 concentrations, and the April-September average daily maximum 1-hour O_3 concentrations, respectively. The overall spatial pattern seen in these three fields is very similar, with the highest concentration values for each metric occurring in Southern California.

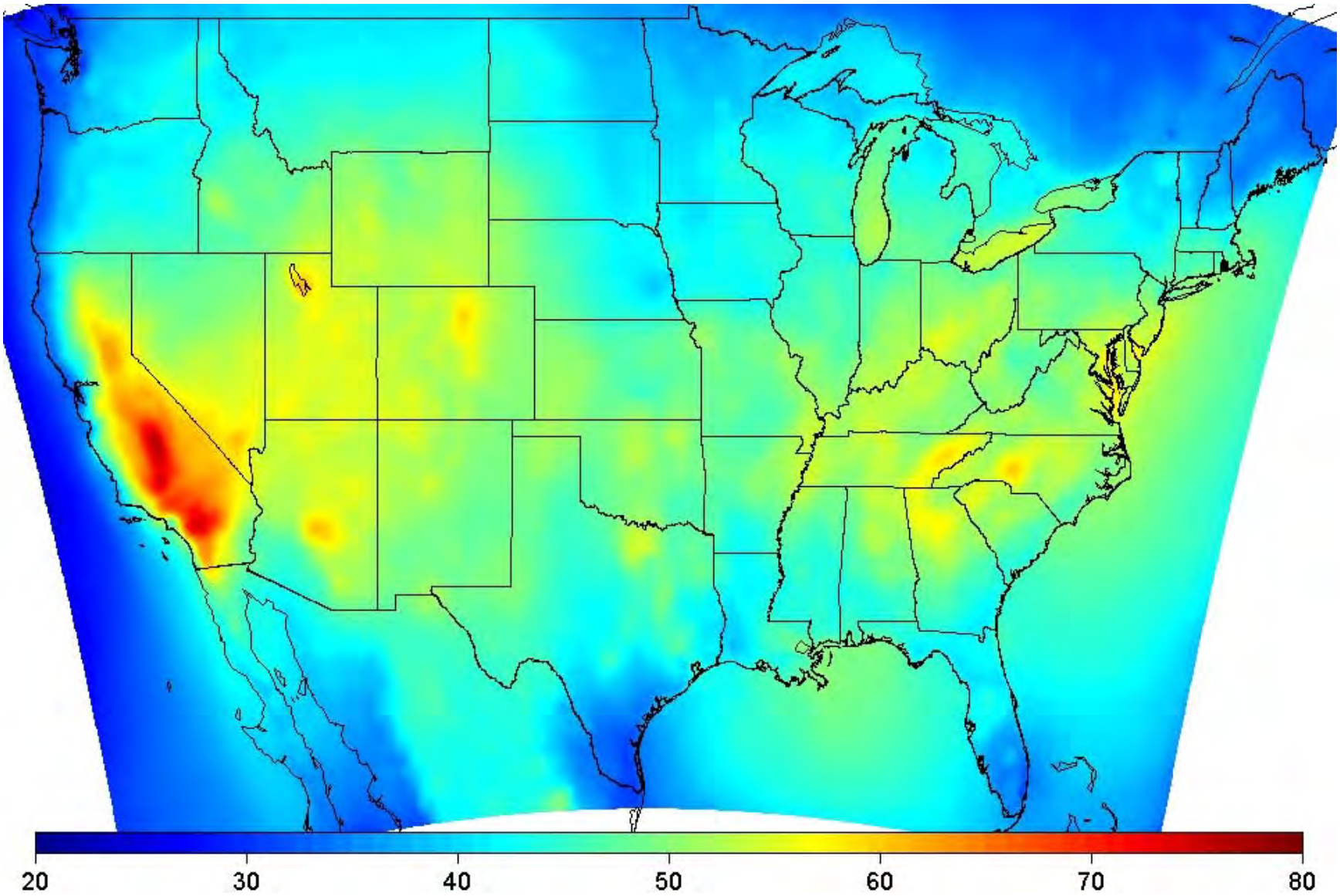

Figure 4C-6. May-September average daily maximum 8-hour O_3 concentrations in ppb, based on a Downscaler fusion of 2006-2008 average monitored values with a 2007 CMAQ model simulation.

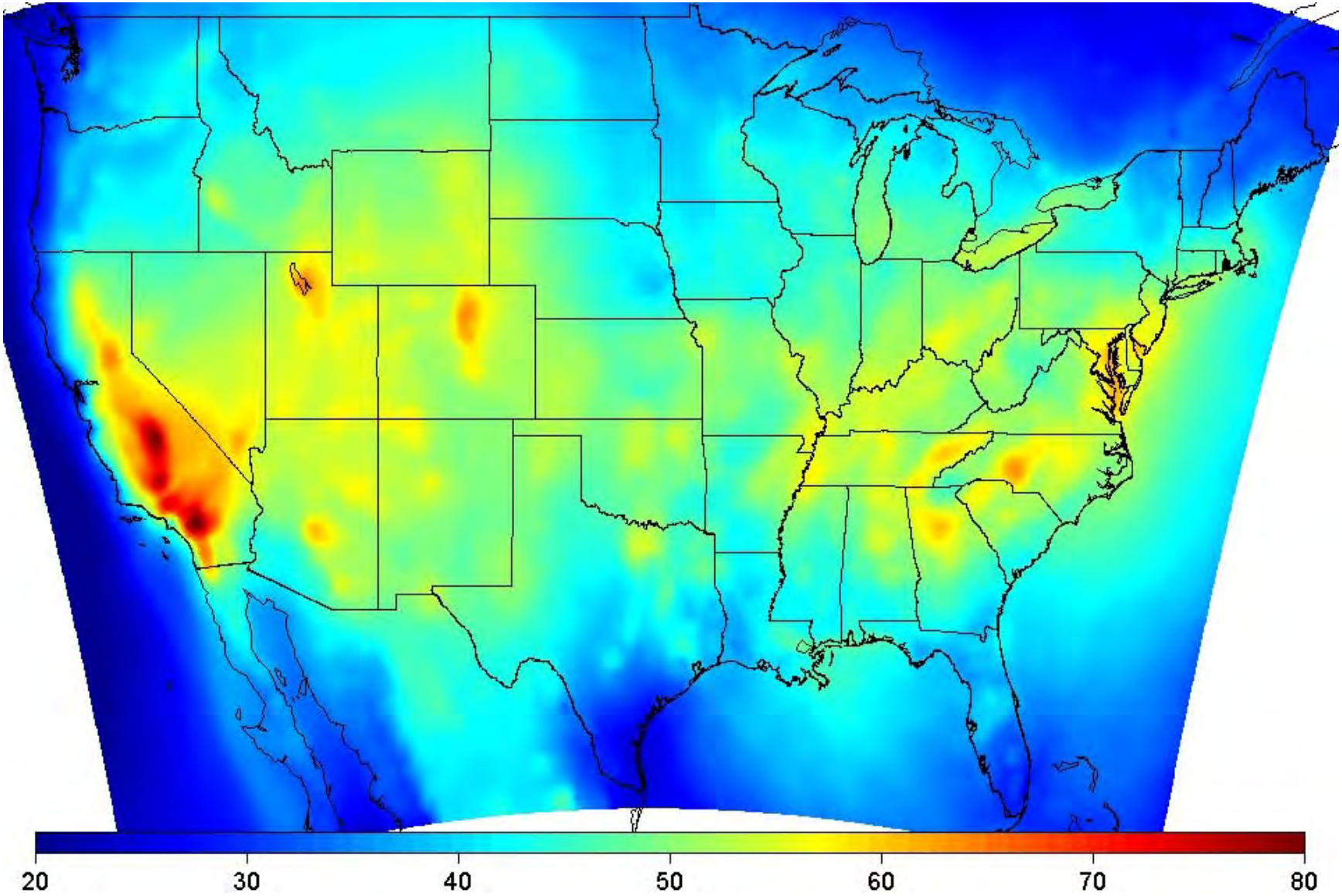

Figure 4C-7. June-August average daily 10am-6pm mean O_3 concentrations in ppb, based on a Downscaler fusion of 2006-2008 average monitored values with a 2007 CMAQ model simulation.

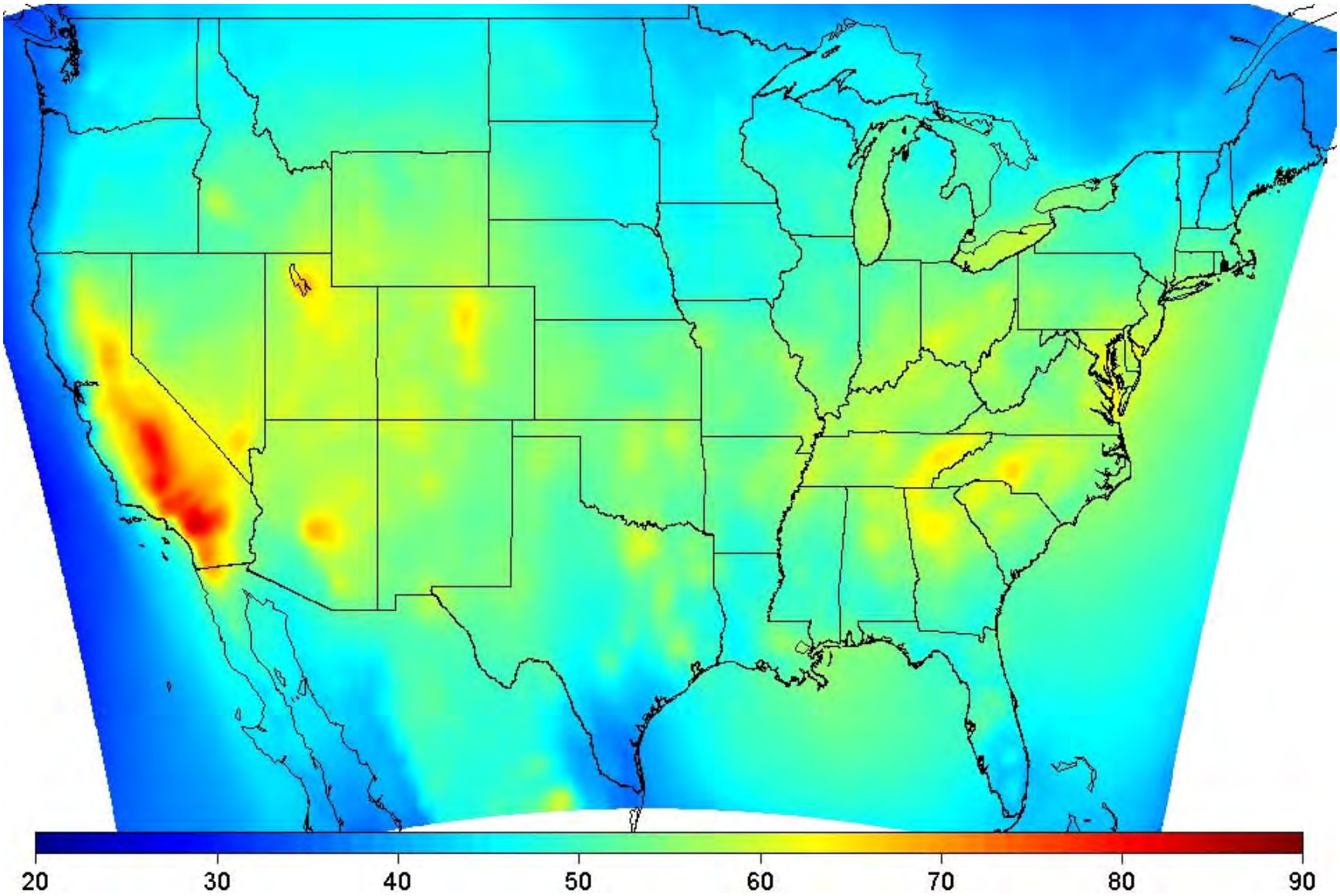

Figure 4C-8. April-September average daily maximum 1-hour O_3 concentrations in ppb, based on a Downscaler fusion of 2006-2008 average monitored values with a 2007 CMAQ model simulation.

4C-5. REFERENCES

Abt Associates, Inc. (2010). Environmental Benefits and Mapping Program (Version 4.0). Bethesda, MD. Prepared for U.S. Environmental Protection Agency Office of Air Quality Planning and Standards. Research Triangle Park, NC. Available on the Internet at <http://www.epa.gov/air/benmap>.

Berrocal, V.J., Gelfand, A.E., Holland, D.M. (2009). A Spatio-Temporal Downscaler for Output from Numerical Models. Journal of Agricultural, Biological, and Environmental Statistics, 15(2), 176–197.

Berrocal, V.J., Gelfand, A.E., Holland, D.M. (2010). A Bivariate Space-Time Downscaler Under Space and Time Misalignment. Annals of Applied Statistics, 4(4), 1942-1975.

Berrocal, V.J., Gelfand, A.E., Holland, D.M. (2011). Space-Time Data Fusion Under Error in Computer Model Output: An Application to Modeling Air Quality. Biometrics, 68(3), 837-848.

Chen, J., Zhao, R., Li, Z. (2004). Voronoi-based k-order neighbor relations for spatial analysis. ISPRS J Photogrammetry Remote Sensing, 59(1-2), 60-72.

Foley, K.M., Roselle, S.J., Appel, K.W., Pleim, J.E., Otte, T.L., Mathur, R., Sarwar, G., Young, J.O., Gilliam, R.C., Nolte, C.G., Kelly, J.T., Gilliland, A.B., Bash, J.O. (2010). Incremental testing of the Community Multiscale Air Quality (CMAQ) modeling system version 4.7. Geoscientific Model Development, 3, 205-226.

Gold, C. (1997). Voronoi methods in GIS. In: Algorithmic Foundation of Geographic Information Systems (va Kereveld M., Nievergelt, J., Roos, T., Widmayer, P., eds.). Lecture Notes in Computer Science, Vol 1340. Berlin: Springer-Verlag, 21-35.

Hall, E., Eyth, A., Phillips, S. (2012). Hierarchical Bayesian Model (HBM)-Derived Estimates of Air Quality for 2007: Annual Report. EPA/600/R-12/538. Available on the Internet at: http://www.epa.gov/heasd/sources/projects/CDC/AnnualReports/2007_HBM.pdf

Jerrett, M., R.T. Burnett, C.A. Pope III, K. Ito, G. Thurston, D. Krewski, Y. Shi, E. Calle, M. Thun. (2009). Long-term O3 exposure and mortality. N. Eng. J. Med., 360:1085-1095.

McMillan, N.J., Holland, D.M., Morara, M., Feng, J. (2009). Combining Numerical Model Output and Particulate Data using Bayesian Space-Time Modeling. Environmetrics, Vol. 21, 48-65.

R Core Team. (2012). R: A language and environment for statistical computing. R Foundation for Statistical Computing, Vienna, Austria. http://www.R-project.org/.

Smith, RL; Xu, B; Switzer, P. (2009). Reassessing the relationship between ozone and short-term mortality in U.S. urban communities. Inhal Toxicol 21: 37-61.

Timin B, Wesson K, Thurman J. (2010). Application of Model and Ambient Data Fusion Techniques to Predict Current and Future Year $PM_{2.5}$ Concentrations in Unmonitored Areas. Pp. 175-179 in Steyn DG, Rao St (eds.). Air Pollution Modeling and Its Application XX. Netherlands: Springer.

Turner, R. (2012). deldir: Delaunay Triangulation and Dirichlet (Voronoi) Tessellation. R package version 0.0-19. http://CRAN.R-project.org/package=deldir

U.S. EPA. (2012a). Health Risk and Exposure Assessment for Ozone, First External Review Draft. Available on the Internet at: http://www.epa.gov/ttn/naaqs/standards/ozone/s_o3_2008_rea.html

U.S. EPA. (2012b). Air Quality Modeling Technical Support Document for the Regulatory Impact Analysis for the Revisions to the National Ambient Air Quality Standards for Particulate Matter. Available on the Internet at: http://www.epa.gov/ttn/naaqs/standards/pm/data/201212aqm.pdf

Wells, B., Wesson, K., Jenkins, S. (2012). Analysis of Recent U.S. Ozone Air Quality Data to Support the O3 NAAQS Review and Quadratic Rollback Simulations to Support the First Draft of the Risk and Exposure Assessment. Available on the Internet at: http://www.epa.gov/ttn/naaqs/standards/ozone/s_o3_td.html

Zanobetti, A., and J. Schwartz. (2008). Mortality Displacement in the Association of Ozone with Mortality: An Analysis of 48 Cities in the United States. American Journal of Respiratory and Critical Care Medicine, 177, 184-189.

This page left intentionally blank

APPENDIX 4D

Model-based Air Quality Adjustment Using the Higher-order Decoupled Direct Method (HDDM)

Table of Contents

4D-1. MOTIVATION FOR AN NEW TECHNIQUE TO SIMULATE OZONE CONCENTRATIONS UNDER ALTERNATIVE STANDARDS 4D-1

4D-2. HIGHER-ORDER DECOUPLED DIRECT METHOD (HDDM) 4D-2

4D-2.1 Capabilities 4D-2

4D-2.2 Limitations 4D-4

4D-3. APPLYING HDDM/CMAQ TO ADJUST OZONE TO JUST MEET EXISTING AND ALTERNATIVE STANDARDS: METHODOLOGY 4D-5

4D-3.1 Conceptual Framework 4D-5

4D-3.2 Application to Measured O_3 Concentrations in 15 Urban Areas 4D-6

4D-3.2.1 Multi-step Application of HDDM Sensitivities 4D-7

4D-3.2.2 Relationships between HDDM Sensitivities and Modeled O_3 Concentrations 4D-16

4D-3.2.3 Application of Sensitivity Regressions to Ambient Data 4D-24

4D-3.2.4 Alternate Methodologies 4D-25

4D-4. APPLYING HDDM/CMAQ TO ADJUST OZONE TO JUST MEET EXISTING AND ALTERNATIVE STANDARDS: RESULTS 4D-26

4D-4.1 Emission Reductions Applied to Meet Alternative Standards 4D-26

4D-4.2 Design Values 4D-28

4D-4.3 Distribution of Hourly O_3 Concentrations 4D-40

4D-4.4 Standard Errors for Predicted Hourly and Daily 8-hr Maximum O_3 Concentrations 4D-71

4D-4.5 Air Quality Inputs for the Epidemiology-Based Risk Assessment 4D-90
4D-4.6 Air Quality Inputs for the Exposure and Clinical Risk Assessment 4D-99
4D-4.7 Comparing Air Quality Adjustments Based on NO_x Reductions Only to Air Quality Adjustments Based on NO_x and VOC Reductions 4D-162
4D-5. REFERENCES 4D-177

List of Tables

Table 4D-1. X and Y cutpoints used in Equations (4D-4) and (4D-8). Note: the NO_x/VOC sensitivity case was only performed in two cities. 4D-12
Table 4D-2. Percent emissions reductions used for each urban area to obtain each standard. 27
Table 4D-3. Design values for the Atlanta area regulatory monitors from observed data and for adjustments to meet the existing and potential alternative standards in 2006-2008 and 2008-2010. ..... 4D-29
Table 4D-4. Design values for the Baltimore area regulatory monitors from observed data and for adjustments to meet the existing and potential alternative standards in 2006-2008 and 2008-2010. ..... 4D-29
Table 4D-5. Design values for the Boston area regulatory monitors from observed data and for adjustments to meet the existing and potential alternative standards in 2006-2008 and 2008-2010. ..... 4D-30
Table 4D-6. Design values for the Chicago area regulatory monitors from observed data and for adjustments to meet the existing and potential alternative standards using NO_x and VOC emissions reductions in 2006-2008 and 2008-2010. ..... 4D-30
Table 4D-7. Design values for the Cleveland area regulatory monitors from observed data and for adjustments to meet the existing and potential alternative standards in 2006-2008 and 2008-2010. ..... 4D-31
Table 4D-8. Design values for the Dallas area regulatory monitors from observed data and for adjustments to meet the existing and potential alternative standards in 2006-2008 and 2008-2010. ..... 4D-32
Table 4D-9. Design values for the Denver area regulatory monitors from observed data and for adjustments to meet the existing and potential alternative standards using NO_x and VOC emissions reductions in 2006-2008 and 2008-2010. ..... 4D-33
Table 4D-10. Design values for the Detroit area regulatory monitors from observed data and for adjustments to meet the existing and potential alternative standards in 2006-2008 and 2008-2010. ..... 4D-33
Table 4D-11. Design values for the Houston area regulatory monitors from observed data and for adjustments to meet the existing and potential alternative standards in 2006-2008 and 2008-2010. ..... 4D-34
Table 4D-12. Design values for the Los Angeles area regulatory monitors from observed data and for adjustments to meet the existing and potential alternative standards using the lower bound of the 95^{th} percent confidence interval of estimated hourly O_3 in 2006-2008 and 2008-2010. ..... 4D-35
Table 4D-13. Design values for the New York area regulatory monitors from observed data and for adjustments to meet the existing and potential alternative standards using the lower bound of the 95^{th} percent confidence interval of estimated hourly O_3 in 2006-2008 and 2008-2010. ..... 4D-36
Table 4D-14. Design values for the Philadelphia area regulatory monitors from observed data and for adjustments to meet the existing and potential alternative standards in 2006-2008 and 2008-2010. ..... 4D-37
Table 4D-15. Design values for the Sacramento area regulatory monitors from observed data and for adjustments to meet the existing and potential alternative standards in 2006-2008 and 2008-2010. ..... 4D-38

Table 4D-16. Design values for the Saint Louis area regulatory monitors from observed data and for adjustments to meet the existing and potential alternative standards in 2006-2008 and 2008-2010. ..... 4D-39
Table 4D-17. Design values for the Washington D.C. area regulatory monitors from observed data and for adjustments to meet the existing and potential alternative standards in 2006-2008 and 2008-2010. ..... 4D-39
Table 4D-18. Mean standard error (ppb) in adjusted hourly O_3 concentration in each urban area for each standard. 4D-74
Table 4D-19. 95th percentile standard error (ppb) in adjusted hourly O_3 concentration in each urban area for each standard. 4D-75
Table 4D-20. Comparison of NO_x-only and NO_x/VOC emission reductions applied in sensitivity analyses for nine urban areas. 4D-163

List of Figures

Figure 4D-1. Flow diagram demonstrating DDM model-based O_3 adjustment approach. .. 4D-6
Figure 4D-2. Conceptual picture of 3-step application of HDDM sensitivities. 4D-9
Figure 4D-3. Comparison of brute force and 3-step HDDM O_3 estimates for 50% NO_x cut conditions: Atlanta, Baltimore, Boston, Chicago, Cleveland, Dallas, Denver, and Detroit. 4D-13
Figure 4D-4. Comparison of brute force and 3-step HDDM O_3 estimates for 50% NO_x cut conditions: Houston, Los Angeles, New York, Philadelphia, Sacramento, St. Louis, and Washington D.C. 4D-14
Figure 4D-5. Comparison of brute force and 3-step HDDM O_3 estimates for 90% NO_x cut conditions: Atlanta, Baltimore, Boston, Chicago, Cleveland, Dallas, Denver, and Detroit. 4D-15
Figure 4D-6. Comparison of brute force and 3-step HDDM O_3 estimates for 90% NO_x cut conditions: Houston, Los Angeles, New York, Philadelphia, Sacramento, St. Louis, and Washington D.C. 4D-16
Figure 4D-7. Relationship between S_{NOx} and hourly O_3 at a NO_x-limited site downwind of Atlanta (summer). Relationships are shown for one nighttime hour, one morning rush-hour hour, one daytime hour, and one evening rush-hour hour. The solid blue line show the linear regression for these points and the dotted blue line shows the floor value used for S_{NOx} based on the 5th percentile modeled value. 4D-19
Figure 4D-8. Relationship between S_{NOx} and hourly O_3 at a NO_x-saturated site in Queens County, NY (autumn). Relationships are shown for one nighttime hour, one morning rush-hour hour, one daytime hour, and one evening rush-hour hour. The solid blue line show the linear regression for these points and the dotted blue line shows the floor value used for S_{NOx} based on the 5th percentile modeled value. 4D-20
Figure 4D-9. Relationship between S_{NOx} and hourly O_3 at a NO_x-saturated site in Suffolk County, NY on Long Island (spring). Relationships are shown for one nighttime hour, one morning rush-hour hour, one daytime hour, and one evening rush-hour hour. The solid blue line show the linear regression for these points and the

dotted blue line shows the floor value used for S_{NOx} based on the 5th percentile modeled value. 4D-21
Figure 4D-10. Relationship between S^2_{NOx} and S_{NOx} at a NO_x-limited site downwind of Atlanta (summer). Relationships are shown for one nighttime hour, one morning rush-hour hour, one daytime hour, and one evening rush-hour hour. The solid blue line shows the linear regression for these points. 4D-22
Figure 4D-11. Relationship between S^2_{NOx} and S_{NOx} at a NO_x-saturated site in Queens County, NY (autumn). Relationships are shown for one nighttime hour, one morning rush-hour hour, one daytime hour, and one evening rush-hour hour. The solid blue line shows the linear regression for these points..... 4D-23
Figure 4D-12. Relationship between S^2_{NOx} and S_{NOx} at a NO_x-saturated site in Suffolk County, NY on Long Island (spring). Relationships are shown for one nighttime hour, one morning rush-hour hour, one daytime hour, and one evening rush-hour hour. The solid blue line shows the linear regression for these points..... 4D-24
Figure 4D-13. Hourly O_3 distributions at Atlanta area regulatory monitoring sites for observed air quality, and air quality adjusted to meet the existing (75 ppb) and alternative (65 ppb) standards for 2006-2008 (left) and 2008-2010 (right). White boxes (black whiskers/dots) show the observed distribution of hourly O_3 concentrations, red boxes (pink whiskers/dots) show the predicted distribution of hourly O_3 concentrations for the 75 ppb adjustment scenarios and blue boxes (light blue whiskers/dots) show the predicted distribution of hourly O_3 concentrations for the 65 ppb adjustment scenario. Boxes show the interquartile range, whiskers extend to 1.5 × the interquartile range and dots depict outlier values. 4D-42
Figure 4D-14. Hourly O_3 distributions at Baltimore area regulatory monitoring sites for observed air quality, and air quality adjusted to meet the existing (75 ppb) and alternative (65 ppb) standards for 2006-2008 (left) and 2008-2010 (right). White boxes (black whiskers/dots) show the observed distribution of hourly O_3 concentrations, red boxes (pink whiskers/dots) show the predicted distribution of hourly O_3 concentrations for the 75 ppb adjustment scenarios and blue boxes (light blue whiskers/dots) show the predicted distribution of hourly O_3 concentrations for the 65 ppb adjustment scenario. Boxes show the interquartile range, whiskers extend to 1.5 × the interquartile range and dots depict outlier values. 4D-43
Figure 4D-15. Hourly O_3 distributions at Boston area regulatory monitoring sites for observed air quality, and air quality adjusted to meet the existing (75 ppb) and alternative (65 ppb) standards for 2006-2008 (left) and 2008-2010 (right). White boxes (black whiskers/dots) show the observed distribution of hourly O_3 concentrations, red boxes (pink whiskers/dots) show the predicted distribution of hourly O_3 concentrations for the 75 ppb adjustment scenarios and blue boxes (light blue whiskers/dots) show the predicted distribution of hourly O_3 concentrations for the 65 ppb adjustment scenario. Boxes show the interquartile range, whiskers extend to 1.5 × the interquartile range and dots depict outlier values. 4D-44
Figure 4D-16. Hourly O_3 distributions at Chicago area regulatory monitoring sites for observed air quality, and air quality adjusted to meet the existing (75 ppb) and alternative (65 ppb) standards for 2006-2008 (left) and 2008-2010 (right). White boxes (black whiskers/dots) show the observed distribution of hourly O_3 concentrations, red boxes (pink whiskers/dots) show the predicted distribution of hourly O_3

concentrations for the 75 ppb adjustment scenarios and blue boxes (light blue whiskers/dots) show the predicted distribution of hourly O_3 concentrations for the 65 ppb adjustment scenario. Boxes show the interquartile range, whiskers extend to 1.5 × the interquartile range and dots depict outlier values. 4D-45
Figure 4D-17. Hourly O_3 distributions at Cleveland area regulatory monitoring sites for observed air quality, and air quality adjusted to meet the existing (75 ppb) and alternative (65 ppb) standards for 2006-2008 (left) and 2008-2010 (right). White boxes (black whiskers/dots) show the observed distribution of hourly O_3 concentrations, red boxes (pink whiskers/dots) show the predicted distribution of hourly O_3 concentrations for the 75 ppb adjustment scenarios and blue boxes (light blue whiskers/dots) show the predicted distribution of hourly O_3 concentrations for the 65 ppb adjustment scenario. Boxes show the interquartile range, whiskers extend to 1.5 × the interquartile range and dots depict outlier values. 4D-46
Figure 4D-18. Hourly O_3 distributions at Dallas area regulatory monitoring sites for observed air quality, and air quality adjusted to meet the existing (75 ppb) and alternative (65 ppb) standards for 2006-2008 (left) and 2008-2010 (right). White boxes (black whiskers/dots) show the observed distribution of hourly O_3 concentrations, red boxes (pink whiskers/dots) show the predicted distribution of hourly O_3 concentrations for the 75 ppb adjustment scenarios and blue boxes (light blue whiskers/dots) show the predicted distribution of hourly O_3 concentrations for the 65 ppb adjustment scenario. Boxes show the interquartile range, whiskers extend to 1.5 × the interquartile range and dots depict outlier values. 4D-47
Figure 4D-19. Hourly O_3 distributions at Denver area regulatory monitoring sites for observed air quality, and air quality adjusted to meet the existing (75 ppb) and alternative (65 ppb) standards for 2006-2008 (left) and 2008-2010 (right). White boxes (black whiskers/dots) show the observed distribution of hourly O_3 concentrations, red boxes (pink whiskers/dots) show the predicted distribution of hourly O_3 concentrations for the 75 ppb adjustment scenarios and blue boxes (light blue whiskers/dots) show the predicted distribution of hourly O_3 concentrations for the 65 ppb adjustment scenario. Boxes show the interquartile range, whiskers extend to 1.5 × the interquartile range and dots depict outlier values. 4D-48
Figure 4D-20. Hourly O_3 distributions at Detroit area regulatory monitoring sites for observed air quality, and air quality adjusted to meet the existing (75 ppb) and alternative (65 ppb) standards for 2006-2008 (left) and 2008-2010 (right). White boxes (black whiskers/dots) show the observed distribution of hourly O_3 concentrations, red boxes (pink whiskers/dots) show the predicted distribution of hourly O_3 concentrations for the 75 ppb adjustment scenarios and blue boxes (light blue whiskers/dots) show the predicted distribution of hourly O_3 concentrations for the 65 ppb adjustment scenario. Boxes show the interquartile range, whiskers extend to 1.5 × the interquartile range and dots depict outlier values. 4D-49
Figure 4D-21. Hourly O_3 distributions at Houston area regulatory monitoring sites for observed air quality, and air quality adjusted to meet the existing (75 ppb) and alternative (65 ppb) standards for 2006-2008 (left) and 2008-2010 (right). White boxes (black whiskers/dots) show the observed distribution of hourly O_3 concentrations, red boxes (pink whiskers/dots) show the predicted distribution of hourly O_3 concentrations for the 75 ppb adjustment scenarios and blue boxes (light blue

whiskers/dots) show the predicted distribution of hourly O_3 concentrations for the 65 ppb adjustment scenario. Boxes show the interquartile range, whiskers extend to 1.5 × the interquartile range and dots depict outlier values. 4D-50
Figure 4D-22. Hourly O_3 distributions at Los Angeles area regulatory monitoring sites for observed air quality, and air quality adjusted to meet the existing (75 ppb) and alternative (65 ppb) standards for 2006-2008 (left) and 2008-2010 (right). White boxes (black whiskers/dots) show the observed distribution of hourly O_3 concentrations, red boxes (pink whiskers/dots) show the predicted distribution of hourly O_3 concentrations for the 75 ppb adjustment scenarios and blue boxes (light blue whiskers/dots) show the predicted distribution of hourly O_3 concentrations for the 65 ppb adjustment scenario. Boxes show the interquartile range, whiskers extend to 1.5 × the interquartile range and dots depict outlier values. 4D-51
Figure 4D-23. Hourly O_3 distributions at New York area regulatory monitoring sites for observed air quality, and air quality adjusted to meet the existing (75 ppb) and alternative (65 ppb) standards for 2006-2008 (left) and 2008-2010 (right). White boxes (black whiskers/dots) show the observed distribution of hourly O_3 concentrations, red boxes (pink whiskers/dots) show the predicted distribution of hourly O_3 concentrations for the 75 ppb adjustment scenarios and blue boxes (light blue whiskers/dots) show the predicted distribution of hourly O_3 concentrations for the 65 ppb adjustment scenario. Boxes show the interquartile range, whiskers extend to 1.5 × the interquartile range and dots depict outlier values. 4D-52
Figure 4D-24. Hourly O_3 distributions at Philadelphia area regulatory monitoring sites for observed air quality, and air quality adjusted to meet the existing (75 ppb) and alternative (65 ppb) standards for 2006-2008 (left) and 2008-2010 (right). White boxes (black whiskers/dots) show the observed distribution of hourly O_3 concentrations, red boxes (pink whiskers/dots) show the predicted distribution of hourly O_3 concentrations for the 75 ppb adjustment scenarios and blue boxes (light blue whiskers/dots) show the predicted distribution of hourly O_3 concentrations for the 65 ppb adjustment scenario. Boxes show the interquartile range, whiskers extend to 1.5 × the interquartile range and dots depict outlier values. 4D-53
Figure 4D-25. Hourly O_3 distributions at Sacramento area regulatory monitoring sites for observed air quality, and air quality adjusted to meet the existing (75 ppb) and alternative (65 ppb) standards for 2006-2008 (left) and 2008-2010 (right). White boxes (black whiskers/dots) show the observed distribution of hourly O_3 concentrations, red boxes (pink whiskers/dots) show the predicted distribution of hourly O_3 concentrations for the 75 ppb adjustment scenarios and blue boxes (light blue whiskers/dots) show the predicted distribution of hourly O_3 concentrations for the 65 ppb adjustment scenario. Boxes show the interquartile range, whiskers extend to 1.5 × the interquartile range and dots depict outlier values. 4D-54
Figure 4D-26. Hourly O_3 distributions at St. Louis area regulatory monitoring sites for observed air quality, and air quality adjusted to meet the existing (75 ppb) and alternative (65 ppb) standards for 2006-2008 (left) and 2008-2010 (right). White boxes

(black whiskers/dots) show the observed distribution of hourly O_3 concentrations, red boxes (pink whiskers/dots) show the predicted distribution of hourly O_3 concentrations for the 75 ppb adjustment scenarios and blue boxes (light blue whiskers/dots) show the predicted distribution of hourly O_3 concentrations for the 65 ppb adjustment scenario. Boxes show the interquartile range, whiskers extend to 1.5 × the interquartile range and dots depict outlier values. 4D-55
Figure 4D-27. Hourly O_3 distributions at Washington, D.C. area regulatory monitoring sites for observed air quality, and air quality adjusted to meet the existing (75 ppb) and alternative (65 ppb) standards for 2006-2008 (left) and 2008-2010 (right). White boxes (black whiskers/dots) show the observed distribution of hourly O_3 concentrations, red boxes (pink whiskers/dots) show the predicted distribution of hourly O_3 concentrations for the 75 ppb adjustment scenarios and blue boxes (light blue whiskers/dots) show the predicted distribution of hourly O_3 concentrations for the 65 ppb adjustment scenario. Boxes show the interquartile range, whiskers extend to 1.5 × the interquartile range and dots depict outlier values. 4D-56
Figure 4D-28. Monthly O_3 distributions at Atlanta area regulatory monitoring sites for observed air quality, and air quality adjusted to meet the existing (75 ppb) and alternative (65 ppb) standards for 2006-2008 (left) and 2008-2010 (right). White boxes (black whiskers/dots) show the observed distribution of hourly O_3 concentrations, red boxes (pink whiskers/dots) show the predicted distribution of hourly O_3 concentrations for the 75 ppb adjustment scenarios and blue boxes (light blue whiskers/dots) show the predicted distribution of hourly O_3 concentrations for the 65 ppb adjustment scenario. Boxes show the interquartile range, whiskers extend to 1.5 × the interquartile range and dots depict outlier values. 4D-57
Figure 4D-29. Monthly O_3 distributions at Baltimore area regulatory monitoring sites for observed air quality, and air quality adjusted to meet the existing (75 ppb) and alternative (65 ppb) standards for 2006-2008 (left) and 2008-2010 (right). White boxes (black whiskers/dots) show the observed distribution of hourly O_3 concentrations, red boxes (pink whiskers/dots) show the predicted distribution of hourly O_3 concentrations for the 75 ppb adjustment scenarios and blue boxes (light blue whiskers/dots) show the predicted distribution of hourly O_3 concentrations for the 65 ppb adjustment scenario. Boxes show the interquartile range, whiskers extend to 1.5 × the interquartile range and dots depict outlier values. 4D-58
Figure 4D-30. Monthly O_3 distributions at Boston area regulatory monitoring sites for observed air quality, and air quality adjusted to meet the existing (75 ppb) and alternative (65 ppb) standards for 2006-2008 (left) and 2008-2010 (right). White boxes (black whiskers/dots) show the observed distribution of hourly O_3 concentrations, red boxes (pink whiskers/dots) show the predicted distribution of hourly O_3 concentrations for the 75 ppb adjustment scenarios and blue boxes (light blue whiskers/dots) show the predicted distribution of hourly O_3 concentrations for the 65 ppb adjustment scenario. Boxes show the interquartile range, whiskers extend to 1.5 × the interquartile range and dots depict outlier values. 4D-59
Figure 4D-31. Monthly O_3 distributions at Chicago area regulatory monitoring sites for observed air quality, and air quality adjusted to meet the existing (75 ppb) and alternative

(65 ppb) standards for 2006-2008 (left) and 2008-2010 (right). White boxes (black whiskers/dots) show the observed distribution of hourly O_3 concentrations, red boxes (pink whiskers/dots) show the predicted distribution of hourly O_3 concentrations for the 75 ppb adjustment scenarios and blue boxes (light blue whiskers/dots) show the predicted distribution of hourly O_3 concentrations for the 65 ppb adjustment scenario. Boxes show the interquartile range, whiskers extend to 1.5 × the interquartile range and dots depict outlier values. 4D-60

Figure 4D-32. Monthly O_3 distributions at Cleveland area regulatory monitoring sites for observed air quality, and air quality adjusted to meet the existing (75 ppb) and alternative (65 ppb) standards for 2006-2008 (left) and 2008-2010 (right). White boxes (black whiskers/dots) show the observed distribution of hourly O_3 concentrations, red boxes (pink whiskers/dots) show the predicted distribution of hourly O_3 concentrations for the 75 ppb adjustment scenarios and blue boxes (light blue whiskers/dots) show the predicted distribution of hourly O_3 concentrations for the 65 ppb adjustment scenario. Boxes show the interquartile range, whiskers extend to 1.5 × the interquartile range and dots depict outlier values. 4D-61

Figure 4D-33. Monthly O_3 distributions at Dallas area regulatory monitoring sites for observed air quality, and air quality adjusted to meet the existing (75 ppb) and alternative (65 ppb) standards for 2006-2008 (left) and 2008-2010 (right). White boxes (black whiskers/dots) show the observed distribution of hourly O_3 concentrations, red boxes (pink whiskers/dots) show the predicted distribution of hourly O_3 concentrations for the 75 ppb adjustment scenarios and blue boxes (light blue whiskers/dots) show the predicted distribution of hourly O_3 concentrations for the 65 ppb adjustment scenario. Boxes show the interquartile range, whiskers extend to 1.5 × the interquartile range and dots depict outlier values. 4D-62

Figure 4D-34. Monthly O_3 distributions at Denver area regulatory monitoring sites for observed air quality, and air quality adjusted to meet the existing (75 ppb) and alternative (65 ppb) standards for 2006-2008 (left) and 2008-2010 (right). White boxes (black whiskers/dots) show the observed distribution of hourly O_3 concentrations, red boxes (pink whiskers/dots) show the predicted distribution of hourly O_3 concentrations for the 75 ppb adjustment scenarios and blue boxes (light blue whiskers/dots) show the predicted distribution of hourly O_3 concentrations for the 65 ppb adjustment scenario. Boxes show the interquartile range, whiskers extend to 1.5 × the interquartile range and dots depict outlier values. 4D-63

Figure 4D-35. Monthly O_3 distributions at Detroit area regulatory monitoring sites for observed air quality, and air quality adjusted to meet the existing (75 ppb) and alternative (65 ppb) standards for 2006-2008 (left) and 2008-2010 (right). White boxes (black whiskers/dots) show the observed distribution of hourly O_3 concentrations, red boxes (pink whiskers/dots) show the predicted distribution of hourly O_3 concentrations for the 75 ppb adjustment scenarios and blue boxes (light blue whiskers/dots) show the predicted distribution of hourly O_3 concentrations for the 65 ppb adjustment scenario. Boxes show the interquartile range, whiskers extend to 1.5 × the interquartile range and dots depict outlier values. 4D-64

Figure 4D-36. Monthly O_3 distributions at Houston area regulatory monitoring sites for observed air quality, and air quality adjusted to meet the existing (75 ppb) and alternative

(65 ppb) standards for 2006-2008 (left) and 2008-2010 (right). White boxes (black whiskers/dots) show the observed distribution of hourly O_3 concentrations, red boxes (pink whiskers/dots) show the predicted distribution of hourly O_3 concentrations for the 75 ppb adjustment scenarios and blue boxes (light blue whiskers/dots) show the predicted distribution of hourly O_3 concentrations for the 65 ppb adjustment scenario. Boxes show the interquartile range, whiskers extend to 1.5 × the interquartile range and dots depict outlier values. 4D-65

Figure 4D-37. Monthly O_3 distributions at Los Angeles area regulatory monitoring sites for observed air quality, and air quality adjusted to meet the existing (75 ppb) and alternative (65 ppb) standards for 2006-2008 (left) and 2008-2010 (right). White boxes (black whiskers/dots) show the observed distribution of hourly O_3 concentrations, red boxes (pink whiskers/dots) show the predicted distribution of hourly O_3 concentrations for the 75 ppb adjustment scenarios and blue boxes (light blue whiskers/dots) show the predicted distribution of hourly O_3 concentrations for the 65 ppb adjustment scenario. Boxes show the interquartile range, whiskers extend to 1.5 × the interquartile range and dots depict outlier values. 4D-66

Figure 4D-38. Monthly O_3 distributions at New York area regulatory monitoring sites for observed air quality, and air quality adjusted to meet the existing (75 ppb) and alternative (65 ppb) standards for 2006-2008 (left) and 2008-2010 (right). White boxes (black whiskers/dots) show the observed distribution of hourly O_3 concentrations, red boxes (pink whiskers/dots) show the predicted distribution of hourly O_3 concentrations for the 75 ppb adjustment scenarios and blue boxes (light blue whiskers/dots) show the predicted distribution of hourly O_3 concentrations for the 65 ppb adjustment scenario. Boxes show the interquartile range, whiskers extend to 1.5 × the interquartile range and dots depict outlier values. 4D-67

Figure 4D-39. Monthly O_3 distributions at Philadelphia area regulatory monitoring sites for observed air quality, and air quality adjusted to meet the existing (75 ppb) and alternative (65 ppb) standards for 2006-2008 (left) and 2008-2010 (right). White boxes (black whiskers/dots) show the observed distribution of hourly O_3 concentrations, red boxes (pink whiskers/dots) show the predicted distribution of hourly O_3 concentrations for the 75 ppb adjustment scenarios and blue boxes (light blue whiskers/dots) show the predicted distribution of hourly O_3 concentrations for the 65 ppb adjustment scenario. Boxes show the interquartile range, whiskers extend to 1.5 × the interquartile range and dots depict outlier values. 4D-68

Figure 4D-40. Monthly O_3 distributions at Sacramento area regulatory monitoring sites for observed air quality, and air quality adjusted to meet the existing (75 ppb) and alternative (65 ppb) standards for 2006-2008 (left) and 2008-2010 (right). White boxes (black whiskers/dots) show the observed distribution of hourly O_3 concentrations, red boxes (pink whiskers/dots) show the predicted distribution of hourly O_3 concentrations for the 75 ppb adjustment scenarios and blue boxes (light blue whiskers/dots) show the predicted distribution of hourly O_3 concentrations for the 65 ppb adjustment scenario. Boxes show the interquartile

range, whiskers extend to 1.5 × the interquartile range and dots depict outlier values. 4D-69
Figure 4D-41. Monthly O_3 distributions at St. Louis area regulatory monitoring sites for observed air quality, and air quality adjusted to meet the existing (75 ppb) and alternative (65 ppb) standards for 2006-2008 (left) and 2008-2010 (right). White boxes (black whiskers/dots) show the observed distribution of hourly O_3 concentrations, red boxes (pink whiskers/dots) show the predicted distribution of hourly O_3 concentrations for the 75 ppb adjustment scenarios and blue boxes (light blue whiskers/dots) show the predicted distribution of hourly O_3 concentrations for the 65 ppb adjustment scenario. Boxes show the interquartile range, whiskers extend to 1.5 × the interquartile range and dots depict outlier values. 4D-70
Figure 4D-42. Monthly O_3 distributions at Washington, D.C. area regulatory monitoring sites for observed air quality, and air quality adjusted to meet the existing (75 ppb) and alternative (65 ppb) standards for 2006-2008 (left) and 2008-2010 (right). White boxes (black whiskers/dots) show the observed distribution of hourly O_3 concentrations, red boxes (pink whiskers/dots) show the predicted distribution of hourly O_3 concentrations for the 75 ppb adjustment scenarios and blue boxes (light blue whiskers/dots) show the predicted distribution of hourly O_3 concentrations for the 65 ppb adjustment scenario. Boxes show the interquartile range, whiskers extend to 1.5 × the interquartile range and dots depict outlier values. 4D-71
Figure 4D-43. Mean standard error in maximum daily 8-hr O_3 concentrations at each monitoring location in Atlanta for the 75 ppb adjustment scenario (top row) and the 60 ppb adjustment scenario (bottom row) for the 2006-2008 time period (left column) and the 2008-2010 time period (right column). 4D-76
Figure 4D-44. Mean standard error in maximum daily 8-hr O_3 concentrations at each monitoring location in Baltimore for the 75 ppb adjustment scenario (top row) and the 60 ppb adjustment scenario (bottom row) for the 2006-2008 time period (left column) and the 2008-2010 time period (right column). 4D-77
Figure 4D-45. Mean standard error in maximum daily 8-hr O_3 concentrations at each monitoring location in Boston for the 75 ppb adjustment scenario (top row) and the 60 ppb adjustment scenario (bottom row) for the 2006-2008 time period (left column) and the 2008-2010 time period (right column). 4D-78
Figure 4D-46. Mean standard error in maximum daily 8-hr O_3 concentrations at each monitoring location in Chicago for the 75 ppb adjustment scenario (top row) and the 60 ppb adjustment scenario (bottom row) for the 2006-2008 time period (left column) and the 2008-2010 time period (right column). 4D-79
Figure 4D-47. Mean standard error in maximum daily 8-hr O_3 concentrations at each monitoring location in Cleveland for the 75 ppb adjustment scenario (top row) and the 60 ppb adjustment scenario (bottom row) for the 2006-2008 time period (left column) and the 2008-2010 time period (right column). 4D-80
Figure 4D-48. Mean standard error in maximum daily 8-hr O_3 concentrations at each monitoring location in Dallas for the 75 ppb adjustment scenario (top row) and the 60 ppb adjustment scenario (bottom row) for the 2006-2008 time period (left column) and the 2008-2010 time period (right column). 4D-81

Figure 4D-49. Mean standard error in maximum daily 8-hr O_3 concentrations at each monitoring location in Washington D.C. for the 75 ppb adjustment scenario (top row) and the 60 ppb adjustment scenario (bottom row) for the 2006-2008 time period (left column) and the 2008-2010 time period (right column)..... 4D-82
Figure 4D-50. Mean standard error in maximum daily 8-hr O_3 concentrations at each monitoring location in Denver for the 75 ppb adjustment scenario (top row) and the 60 ppb adjustment scenario (bottom row) for the 2006-2008 time period (left column) and the 2008-2010 time period (right column)..... 4D-83
Figure 4D-51. Mean standard error in maximum daily 8-hr O_3 concentrations at each monitoring location in Detroit for the 75 ppb adjustment scenario (top row) and the 60 ppb adjustment scenario (bottom row) for the 2006-2008 time period (left column) and the 2008-2010 time period (right column)..... 4D-84
Figure 4D-52. Mean standard error in maximum daily 8-hr O_3 concentrations at each monitoring location in Houston for the 75 ppb adjustment scenario (top row) and the 60 ppb adjustment scenario (bottom row) for the 2006-2008 time period (left column) and the 2008-2010 time period (right column)..... 4D-85
Figure 4D-53. Mean standard error in maximum daily 8-hr O_3 concentrations at each monitoring location in Los Angele for the 75 ppb adjustment scenario (top row) and the 60 ppb adjustment scenario (bottom row) for the 2006-2008 time period (left column) and the 2008-2010 time period (right column)..... 4D-86
Figure 4D-54. Mean standard error in maximum daily 8-hr O_3 concentrations at each monitoring location in New York for the 75 ppb adjustment scenario (top row) and the 60 ppb adjustment scenario (bottom row) for the 2006-2008 time period (left column) and the 2008-2010 time period (right column)..... 4D-87
Figure 4D-55. Mean standard error in maximum daily 8-hr O_3 concentrations at each monitoring location in Philadelphia for the 75 ppb adjustment scenario (top row) and the 60 ppb adjustment scenario (bottom row) for the 2006-2008 time period (left column) and the 2008-2010 time period (right column)..... 4D-88
Figure 4D-56. Mean standard error in maximum daily 8-hr O_3 concentrations at each monitoring location in Sacramento for the 75 ppb adjustment scenario (top row) and the 60 ppb adjustment scenario (bottom row) for the 2006-2008 time period (left column) and the 2008-2010 time period (right column)..... 4D-89
Figure 4D-57. Mean standard error in maximum daily 8-hr O_3 concentrations at each monitoring location in St. Louis for the 75 ppb adjustment scenario (top row) and the 60 ppb adjustment scenario (bottom row) for the 2006-2008 time period (left column) and the 2008-2010 time period (right column)..... 4D-90
Figure 4D-58. Composite monitor daily maximum 8-hour O_3 values for Atlanta based on observed and adjusted air quality. Boxes represent the median and quartiles, x's represent mean values, whiskers extend up to 1.5x the inter-quartile range from the boxes, and circles represent outliers. 4D-93
Figure 4D-59. Composite monitor daily maximum 8-hour O_3 values for Baltimore based on observed and adjusted air quality. Boxes represent the median and quartiles, x's represent mean values, whiskers extend up to 1.5x the inter-quartile range from the boxes, and circles represent outliers. 4D-93
Figure 4D-60. Composite monitor daily maximum 8-hour O_3 values for Boston based on observed and adjusted air quality. Boxes represent the median and quartiles, x's

represent mean values, whiskers extend up to 1.5x the inter-quartile range from the boxes, and circles represent outliers. 4D-94
Figure 4D-61. Composite monitor daily maximum 8-hour O_3 values for Cleveland based on observed and adjusted air quality. Boxes represent the median and quartiles, x's represent mean values, whiskers extend up to 1.5x the inter-quartile range from the boxes, and circles represent outliers. 4D-94
Figure 4D-62. Composite monitor daily maximum 8-hour O_3 values for Denver based on observed and adjusted air quality. Boxes represent the median and quartiles, x's represent mean values, whiskers extend up to 1.5x the inter-quartile range from the boxes, and circles represent outliers. 4D-95
Figure 4D-63. Composite monitor daily maximum 8-hour O_3 values for Detroit based on observed and adjusted air quality. Boxes represent the median and quartiles, x's represent mean values, whiskers extend up to 1.5x the inter-quartile range from the boxes, and circles represent outliers. 4D-95
Figure 4D-64. Composite monitor daily maximum 8-hour O_3 values for Houston based on observed and adjusted air quality. Boxes represent the median and quartiles, x's represent mean values, whiskers extend up to 1.5x the inter-quartile range from the boxes, and circles represent outliers. 4D-96
Figure 4D-65. Composite monitor daily maximum 8-hour O_3 values for Los Angeles based on observed and adjusted air quality. Boxes represent the median and quartiles, x's represent mean values, whiskers extend up to 1.5x the inter-quartile range from the boxes, and circles represent outliers. 4D-96
Figure 4D-66. Composite monitor daily maximum 8-hour O_3 values for New York based on observed and adjusted air quality. Boxes represent the median and quartiles, x's represent mean values, whiskers extend up to 1.5x the inter-quartile range from the boxes, and circles represent outliers. 4D-97
Figure 4D-67. Composite monitor daily maximum 8-hour O_3 values for Philadelphia based on observed and adjusted air quality. Boxes represent the median and quartiles, x's represent mean values, whiskers extend up to 1.5x the inter-quartile range from the boxes, and circles represent outliers. 4D-97
Figure 4D-68. Composite monitor daily maximum 8-hour O_3 values for Sacramento based on observed and adjusted air quality. Boxes represent the median and quartiles, x's represent mean values, whiskers extend up to 1.5x the inter-quartile range from the boxes, and circles represent outliers. 4D-98
Figure 4D-69. Composite monitor daily maximum 8-hour O_3 values for St. Louis based on observed and adjusted air quality. Boxes represent the median and quartiles, x's represent mean values, whiskers extend up to 1.5x the inter-quartile range from the boxes, and circles represent outliers. 4D-98
Figure 4D-70. Change in VNA estimates of the daily maximum 8-hour average (MDA8) O_3 concentrations based on HDDM adjustments in Atlanta. 4D-102
Figure 4D-71. Change in VNA estimates of the daily maximum 8-hour average (MDA8) O_3 concentrations based on HDDM adjustments in Baltimore. 4D-103
Figure 4D-72. Change in VNA estimates of the daily maximum 8-hour average (MDA8) O_3 concentrations based on HDDM adjustments in Boston. 4D-104
Figure 4D-73. Change in VNA estimates of the daily maximum 8-hour average (MDA8) O_3 concentrations based on HDDM adjustments in Chicago. 4D-105

Figure 4D-74. Change in VNA estimates of the daily maximum 8-hour average (MDA8) O_3 concentrations based on HDDM adjustments in Cleveland. 4D-106
Figure 4D-75. Change in VNA estimates of the daily maximum 8-hour average (MDA8) O_3 concentrations based on HDDM adjustments in Dallas. 4D-107
Figure 4D-76. Change in VNA estimates of the daily maximum 8-hour average (MDA8) O_3 concentrations based on HDDM adjustments in Denver. 4D-108
Figure 4D-77. Change in VNA estimates of the daily maximum 8-hour average (MDA8) O_3 concentrations based on HDDM adjustments in Detroit. 109
Figure 4D-78. Change in VNA estimates of the daily maximum 8-hour average (MDA8) O_3 concentrations based on HDDM adjustments in Houston. 4D-110
Figure 4D-79. Change in VNA estimates of the daily maximum 8-hour average (MDA8) O_3 concentrations based on HDDM adjustments in Los Angeles..... 4D-111
Figure 4D-80. Change in VNA estimates of the daily maximum 8-hour average (MDA8) O_3 concentrations based on HDDM adjustments in New York. 4D-112
Figure 4D-81. Change in VNA estimates of the daily maximum 8-hour average (MDA8) O_3 concentrations based on HDDM adjustments in Philadelphia..... 4D-113
Figure 4D-82. Change in VNA estimates of the daily maximum 8-hour average (MDA8) O_3 concentrations based on HDDM adjustments in Sacramento. 4D-114
Figure 4D-83. Change in VNA estimates of the daily maximum 8-hour average (MDA8) O_3 concentrations based on HDDM adjustments in St. Louis. 4D-115
Figure 4D-84. Change in VNA estimates of the daily maximum 8-hour average (MDA8) O3 concentrations based on HDDM adjustments in Washington, D.C. 4D-116
Figure 4D-85. Changes in annual 4th highest MDA8 and May-September average MDA8 values based on HDDM adjustments for Atlanta, 2006-2008. The points are colored according to the change in ppb, and values falling outside the range in the color bar were set to the nearest value within the color bar. 4D-117
Figure 4D-86. Changes in annual 4th highest MDA8 and May-September average MDA8 values based on HDDM adjustments for Atlanta, 2008-2010. The points are colored according to the change in ppb, and values falling outside the range in the color bar were set to the nearest value within the color bar. 4D-118
Figure 4D-87. Changes in annual 4th highest MDA8 and May-September average MDA8 values based on HDDM adjustments for Baltimore, 2006-2008. The points are colored according to the change in ppb, and values falling outside the range in the color bar were set to the nearest value within the color bar. 4D-119
Figure 4D-88. Changes in annual 4th highest MDA8 and May-September average MDA8 values based on HDDM adjustments for Baltimore, 2008-2010. The points are colored according to the change in ppb, and values falling outside the range in the color bar were set to the nearest value within the color bar. 4D-120
Figure 4D-89. Changes in annual 4th highest MDA8 and May-September average MDA8 values based on HDDM adjustments for Boston, 2006-2008. The points are colored according to the change in ppb, and values falling outside the range in the color bar were set to the nearest value within the color bar. 4D-121
Figure 4D-90. Changes in annual 4th highest MDA8 and May-September average MDA8 values based on HDDM adjustments for Boston, 2008-2010. The points are colored according to the change in ppb, and values falling outside the range in the color bar were set to the nearest value within the color bar. 4D-122

Figure 4D-91. Changes in annual 4th highest MDA8 and May-September average MDA8 values based on HDDM adjustments for Chicago, 2006-2008. The points are colored according to the change in ppb, and values falling outside the range in the color bar were set to the nearest value within the color bar. 4D-123
Figure 4D-92. Changes in annual 4th highest MDA8 and May-September average MDA8 values based on HDDM adjustments for Chicago, 2008-2010. The points are colored according to the change in ppb, and values falling outside the range in the color bar were set to the nearest value within the color bar. 4D-124
Figure 4D-93. Changes in annual 4th highest MDA8 and May-September average MDA8 values based on HDDM adjustments for Cleveland, 2006-2008. The points are colored according to the change in ppb, and values falling outside the range in the color bar were set to the nearest value within the color bar. 4D-125
Figure 4D-94. Changes in annual 4th highest MDA8 and May-September average MDA8 values based on HDDM adjustments for Cleveland, 2008-2010. The points are colored according to the change in ppb, and values falling outside the range in the color bar were set to the nearest value within the color bar. 4D-126
Figure 4D-95. Changes in annual 4th highest MDA8 and May-September average MDA8 values based on HDDM adjustments for Dallas, 2006-2008. The points are colored according to the change in ppb, and values falling outside the range in the color bar were set to the nearest value within the color bar. 4D-127
Figure 4D-96. Changes in annual 4th highest MDA8 and May-September average MDA8 values based on HDDM adjustments for Dallas, 2008-2010. The points are colored according to the change in ppb, and values falling outside the range in the color bar were set to the nearest value within the color bar. 4D-128
Figure 4D-97. Changes in annual 4th highest MDA8 and May-September average MDA8 values based on HDDM adjustments for Denver, 2006-2008. The points are colored according to the change in ppb, and values falling outside the range in the color bar were set to the nearest value within the color bar. 4D-129
Figure 4D-98. Changes in annual 4th highest MDA8 and May-September average MDA8 values based on HDDM adjustments for Denver, 2008-2010. The points are colored according to the change in ppb, and values falling outside the range in the color bar were set to the nearest value within the color bar. 4D-130
Figure 4D-99. Changes in annual 4th highest MDA8 and May-September average MDA8 values based on HDDM adjustments for Detroit, 2006-2008. The points are colored according to the change in ppb, and values falling outside the range in the color bar were set to the nearest value within the color bar. 4D-131
Figure 4D-100. Changes in annual 4th highest MDA8 and May-September average MDA8 values based on HDDM adjustments for Detroit, 2008-2010. The points are colored according to the change in ppb, and values falling outside the range in the color bar were set to the nearest value within the color bar. 4D-132
Figure 4D-101. Changes in annual 4th highest MDA8 and May-September average MDA8 values based on HDDM adjustments for Houston, 2006-2008. The points are colored according to the change in ppb, and values falling outside the range in the color bar were set to the nearest value within the color bar. 4D-133
Figure 4D-102. Changes in annual 4th highest MDA8 and May-September average MDA8 values based on HDDM adjustments for Houston, 2008-2010. The points are colored

according to the change in ppb, and values falling outside the range in the color bar were set to the nearest value within the color bar. 4D-134
Figure 4D-103. Changes in annual 4th highest MDA8 and May-September average MDA8 values based on HDDM adjustments for Los Angeles, 2006-2008. The points are colored according to the change in ppb, and values falling outside the range in the color bar were set to the nearest value within the color bar. 4D-135
Figure 4D-104. Changes in annual 4th highest MDA8 and May-September average MDA8 values based on HDDM adjustments for Los Angeles, 2008-2010. The points are colored according to the change in ppb, and values falling outside the range in the color bar were set to the nearest value within the color bar. 4D-136
Figure 4D-105. Changes in annual 4th highest MDA8 and May-September average MDA8 values based on HDDM adjustments for New York, 2006-2008. The points are colored according to the change in ppb, and values falling outside the range in the color bar were set to the nearest value within the color bar. 4D-137
Figure 4D-106. Changes in annual 4th highest MDA8 and May-September average MDA8 values based on HDDM adjustments for New York, 2008-2010. The points are colored according to the change in ppb, and values falling outside the range in the color bar were set to the nearest value within the color bar. 4D-138
Figure 4D-107. Changes in annual 4th highest MDA8 and May-September average MDA8 values based on HDDM adjustments for Philadelphia, 2006-2008. The points are colored according to the change in ppb, and values falling outside the range in the color bar were set to the nearest value within the color bar. 4D-139
Figure 4D-108. Changes in annual 4th highest MDA8 and May-September average MDA8 values based on HDDM adjustments for Philadelphia, 2008-2010. The points are colored according to the change in ppb, and values falling outside the range in the color bar were set to the nearest value within the color bar. 4D-140
Figure 4D-109. Changes in annual 4th highest MDA8 and May-September average MDA8 values based on HDDM adjustments for Sacramento, 2006-2008. The points are colored according to the change in ppb, and values falling outside the range in the color bar were set to the nearest value within the color bar. 4D-141
Figure 4D-110. Changes in annual 4th highest MDA8 and May-September average MDA8 values based on HDDM adjustments for Sacramento, 2008-2010. The points are colored according to the change in ppb, and values falling outside the range in the color bar were set to the nearest value within the color bar. 4D-142
Figure 4D-111. Changes in annual 4th highest MDA8 and May-September average MDA8 values based on HDDM adjustments for St. Louis, 2006-2008. The points are colored according to the change in ppb, and values falling outside the range in the color bar were set to the nearest value within the color bar. 4D-143
Figure 4D-112. Changes in annual 4th highest MDA8 and May-September average MDA8 values based on HDDM adjustments for St. Louis, 2008-2010. The points are colored according to the change in ppb, and values falling outside the range in the color bar were set to the nearest value within the color bar. 4D-144
Figure 4D-113. Changes in annual 4th highest MDA8 and May-September average MDA8 values based on HDDM adjustments for Washington, D.C., 2006-2008. The points are colored according to the change in ppb, and values falling outside the range in the color bar were set to the nearest value within the color bar. 4D-145

Figure 4D-114. Changes in annual 4th highest MDA8 and May-September average MDA8 values based on HDDM adjustments for Washington D.C., 2008-2010. The points are colored according to the change in ppb, and values falling outside the range in the color bar were set to the nearest value within the color bar..... 4D-146
Figure 4D-115. Changes in VNA estimates of annual 4th highest MDA8 and May – September average MDA8 based on HDDM adjustments for Atlanta versus population and population density..... 4D-147
Figure 4D-116. Changes in VNA estimates of annual 4th highest MDA8 and May – September average MDA8 based on HDDM adjustments for Baltimore versus population and population density..... 4D-148
Figure 4D-117. Changes in VNA estimates of annual 4th highest MDA8 and May – September average MDA8 based on HDDM adjustments for Boston versus population and population density..... 4D-149
Figure 4D-118. Changes in VNA estimates of annual 4th highest MDA8 and May – September average MDA8 based on HDDM adjustments for Chicago versus population and population density..... 4D-150
Figure 4D-119. Changes in VNA estimates of annual 4th highest MDA8 and May – September average MDA8 based on HDDM adjustments for Cleveland versus population and population density..... 4D-151
Figure 4D-120. Changes in VNA estimates of annual 4th highest MDA8 and May – September average MDA8 based on HDDM adjustments for Dallas versus population and population density..... 4D-152
Figure 4D-121. Changes in VNA estimates of annual 4th highest MDA8 and May – September average MDA8 based on HDDM adjustments for Denver versus population and population density..... 4D-153
Figure 4D-122. Changes in VNA estimates of annual 4th highest MDA8 and May – September average MDA8 based on HDDM adjustments for Detroit versus population and population density..... 4D-154
Figure 4D-123. Changes in VNA estimates of annual 4th highest MDA8 and May – September average MDA8 based on HDDM adjustments for Houston versus population and population density..... 4D-155
Figure 4D-124. Changes in VNA estimates of annual 4th highest MDA8 and May – September average MDA8 based on HDDM adjustments for Los Angeles versus population and population density..... 4D-156
Figure 4D-125. Changes in VNA estimates of annual 4th highest MDA8 and May – September average MDA8 based on HDDM adjustments for New York versus population and population density..... 4D-157
Figure 4D-126. Changes in VNA estimates of annual 4th highest MDA8 and May – September average MDA8 based on HDDM adjustments for Philadelphia versus population and population density..... 4D-158
Figure 4D-127. Changes in VNA estimates of annual 4th highest MDA8 and May – September average MDA8 based on HDDM adjustments for Sacramento versus population and population density..... 4D-159
Figure 4D-128. Changes in VNA estimates of annual 4th highest MDA8 and May – September average MDA8 based on HDDM adjustments for St. Louis versus population and population density..... 4D-160

Figure 4D-129. Changes in VNA estimates of annual 4th highest MDA8 and May – September average MDA8 based on HDDM adjustments for Washington, D.C. versus population and population density. 4D-161
Figure 4D-130. Composite monitor daily maximum 8-hour O_3 values for Denver based on observed and adjusted air quality for the NO_x-only and NO_x/VOC scenarios. Boxes represent the median and quartiles, x's represent mean values, whiskers extend up to 1.5x the inter-quartile range from the boxes, and circles represent outliers..... 4D-165
Figure 4D-131. Composite monitor daily maximum 8-hour O_3 values for Detroit based on observed and adjusted air quality for the NO_x-only and NO_x/VOC scenarios. Boxes represent the median and quartiles, x's represent mean values, whiskers extend up to 1.5x the inter-quartile range from the boxes, and circles represent outliers..... 4D-165
Figure 4D-132. Composite monitor daily maximum 8-hour O_3 values for Houston based on observed and adjusted air quality for the NO_x-only and NO_x/VOC scenarios. Boxes represent the median and quartiles, x's represent mean values, whiskers extend up to 1.5x the inter-quartile range from the boxes, and circles represent outliers..... 4D-166
Figure 4D-133. Composite monitor daily maximum 8-hour O_3 values for Los Angeles based on observed and adjusted air quality for the NO_x-only and NO_x/VOC scenarios. Boxes represent the median and quartiles, x's represent mean values, whiskers extend up to 1.5x the inter-quartile range from the boxes, and circles represent outliers..... 4D-166
Figure 4D-134. Composite monitor daily maximum 8-hour O_3 values for New York based on observed and adjusted air quality for the NO_x-only and NO_x/VOC scenarios. Boxes represent the median and quartiles, x's represent mean values, whiskers extend up to 1.5x the inter-quartile range from the boxes, and circles represent outliers..... 4D-167
Figure 4D-135. Composite monitor daily maximum 8-hour O_3 values for Philadelphia based on observed and adjusted air quality for the NO_x-only and NO_x/VOC scenarios. Boxes represent the median and quartiles, x's represent mean values, whiskers extend up to 1.5x the inter-quartile range from the boxes, and circles represent outliers..... 4D-167
Figure 4D-136. Composite monitor daily maximum 8-hour O_3 values for Sacramento based on observed and adjusted air quality for the NO_x-only and NO_x/VOC scenarios. Boxes represent the median and quartiles, x's represent mean values, whiskers extend up to 1.5x the inter-quartile range from the boxes, and circles represent outliers..... 4D-168
Figure 4D-137. April-October seasonal average of daily maximum 8-hour O_3 values at Denver area monitor locations for observed 2006-2008 conditions (left panel), 75 ppb adjustment scenarios (middle panels), and 65 ppb adjustment scenarios (right panels). NO_x-only adjustments are shown in top panels, NO_x/VOC adjustments are shown in bottom panels..... 4D-170
Figure 4D-138. April-October seasonal average of daily maximum 8-hour O_3 values at Detroit area monitor locations for observed 2006-2008 conditions (left panel), 75 ppb adjustment scenarios (middle panels), and 65 ppb adjustment scenarios (right

panels). NO_x-only adjustments are shown in top panels, NO_x/VOC adjustments are shown in bottom panels..... 4D-171
Figure 4D-139. April-October seasonal average of daily maximum 8-hour O_3 values at Houston area monitor locations for observed 2006-2008 conditions (left panel), 75 ppb adjustment scenarios (middle panels), and 65 ppb adjustment scenarios (right panels). NO_x-only adjustments are shown in top panels, NO_x/VOC adjustments are shown in bottom panels..... 4D-172
Figure 4D-140. April-October seasonal average of daily maximum 8-hour O_3 values at Los Angeles area monitor locations for observed 2006-2008 conditions (left panel), 75 ppb adjustment scenarios (middle panels), and 65 ppb adjustment scenarios (right panels). NO_x-only adjustments are shown in top panels, NO_x/VOC adjustments are shown in bottom panels..... 4D-173
Figure 4D-141. April-October seasonal average of daily maximum 8-hour O_3 values at New York area monitor locations for observed 2006-2008 conditions (left panel), 75 ppb adjustment scenarios (middle panels), and 65 ppb adjustment scenarios (right panels). NO_x-only adjustments are shown in top panels, NO_x/VOC adjustments are shown in bottom panels..... 4D-174
Figure 4D-142. April-October seasonal average of daily maximum 8-hour O_3 values at Philadelphia area monitor locations for observed 2006-2008 conditions (left panel), 75 ppb adjustment scenarios (middle panels), and 65 ppb adjustment scenarios (right panels). NO_x-only adjustments are shown in top panels, NO_x/VOC adjustments are shown in bottom panels..... 4D-175
Figure 4D-143. April-October seasonal average of daily maximum 8-hour O_3 values at Sacramento area monitor locations for observed 2006-2008 conditions (left panel), 75 ppb adjustment scenarios (middle panels), and 65 ppb adjustment scenarios (right panels). NO_x-only adjustments are shown in top panels, NO_x/VOC adjustments are shown in bottom panels..... 4D-176

4D-1. MOTIVATION FOR AN NEW TECHNIQUE TO SIMULATE OZONE CONCENTRATIONS UNDER ALTERNATIVE STANDARDS

As part of the reviews of the National Ambient Air Quality Standards (NAAQS) for ozone (O_3), EPA estimates health risks after O_3 has been adjusted to just meet the existing standard and potential alternative standards. The first draft documents for this review rely upon the quadratic rollback method used in previous reviews to adjust or "roll back" hourly O_3 concentrations in urban areas. Although the quadratic rollback method simulates historical patterns of air quality changes more closely than some alternative methods (e.g. simply shaving peak concentrations off at the NAAQS level), its implementation requires some assumptions that may not always hold true. Specifically, the quadratic rollback method assumes that all monitors in an urban area will have the same response to emissions changes not allowing for temporally varying response depending on time of day. In addition, it assumes that O3 concentrations never increase in response to emissions reductions. However, during NO_x-saturated (i.e. VOC limited) conditions, NO_x reductions can result in O_3 increases (Seinfeld and Pandis, 1998). Finally, since the quadratic rollback method is purely a mathematical technique and does not account for physical and chemical atmospheric processes or the sources of emissions precursors that lead to O_3 formation, a backstop or "floor" must be used to ensure that predicted O_3 is not reduced below "background" concentrations[1].

EPA has received comments during past O_3 NAAQS reviews and during the January 9-10, 2012 and Sep 11-13, 2013 Clean Air Scientific Advisory Committee (CASAC) meetings for this O_3 NAAQS review which encourage the use of alternate methods to quadratic rollback. In addition, the National Research Council of the National Academies (NRC, 2008) recommended that EPA explore how emissions reductions might affect temporal and spatial variations in O_3 concentrations, and that EPA include information on how NO_x versus VOC control strategies might affect risk and exposure to O_3.

Photochemical modeling can simulate the O_3 response to emission reductions while avoiding the limitations presented by the quadratic rollback method. While there are uncertainties inherent in any modeling exercise due to uncertainties in inputs and model parameters, photochemical modeling provides a more representative characterization of the spatial and temporal responses of O_3 to emissions reductions. In this document we present a

[1] Background O_3 has been characterized in previous reviews of the O_3 NAAQS as "policy relevant background" or PRB, defined as O_3 concentrations that would exist in the absence of North American anthropogenic emissions. In the current review, we have refined the concept of background O_3 to recognize that there are several possible definitions of background O_3, reflecting both the geographic source of emissions, e.g. U.S., North American, Global non-U.S., and whether emissions are anthropogenic or natural in origin. In the cases described in this document, "background" refers to O_3 that would exist in absence of U.S. anthropogenic emissions.

model-based O_3 adjustment methodology that allows for adjustments to O_3 concentrations. This new approach is firmly rooted in the latest atmospheric modeling science and was peer reviewed in Simon et al. (2012). This analysis uses EPA's Community Multi-scale Air Quality (CMAQ) photochemical model (www.cmaq-model.org) instrumented with the Higher order Direct Decoupled Method (HDDM) - a tool that generates modeled sensitivities of O_3 to emissions changes - to estimate the distribution of O_3 concentrations associated with achievement of the existing O_3 standard and alternative standards for multiple urban areas. The HDDM sensitivities are applied to ambient measurements of O_3 to estimate how O_3 concentrations would respond to changes in U.S. anthropogenic emissions. We use this methodology to estimate O_3 concentrations meeting the existing and potential alternative standards in the health risk and exposure assessment (HREA) and the policy assessment (PA). The photochemical modeling incorporates emissions from non-anthropogenic sources and anthropogenic emissions from sources in the U.S and in portions of Canada and Mexico. Pollution from sources in other locations within and outside of North America is included as transport into the boundary of the modeling domain. Because the application of the model-based approach focuses on reductions in U.S. anthropogenic emissions while holding constant those emissions that influence U.S. background, all changes in O_3 will be relative to U.S. background. This does not mean that background O_3 concentrations will be constant between recent ambient O_3 conditions and after just meeting the existing or alternative standard levels, because of nonlinearities in the formation of O_3.

4D-2. HIGHER-ORDER DECOUPLED DIRECT METHOD (HDDM)

4D-2.1 Capabilities

Chemical transport models, such as CMAQ, simulate the effects of physical and chemical processes in the atmosphere to predict 3-D gridded pollutant concentrations (Foley et al., 2010, Appel et al., 2008, Appel et al., 2007, Byun and Schere, 2006). These models account for the impacts of emissions, transport, chemistry, and deposition on spatially and temporally varying pollutant concentrations. Required model inputs include time-varying emissions and meteorology fields, time varying concentrations of pollutants at the boundaries of the model domain (i.e. boundary conditions), and a characterization of the 3-D field of chemical concentrations to initialize the model (i.e. initial conditions).

Beyond modeling the concentrations of ambient O_3, chemical transport models can be used to estimate the response of ambient O_3 concentrations to changes in emissions. One technique to simulate the response of O_3 to emissions changes, the brute force method, requires the modeler to explicitly model this response by directly altering the emissions inputs in the model simulation. This technique provides an estimate of the O_3 concentration at the altered

emission level, but often does not provide accurate information regarding the response of O_3 to other levels of emissions since the chemistry for O_3 formation is nonlinear. Therefore, when using only brute force techniques a new model simulation would need to be performed for every emissions scenario under consideration.

Other analytical techniques have been developed to estimate the O_3 response to emissions changes without performing multiple simulations. One such method is termed the Decoupled Direct Method (DDM) (Dunker, 1984). DDM, solves for sensitivity coefficients which are defined as the partial derivative of the atmospheric diffusion equations that underly the model calculations, Equations (4D-1) and (4D-2).

$$s_{ij}(t) = \frac{\partial C_i(t)}{\partial p_j}$$

Equation (4D-1)

$$S_{ij}(t) = \tilde{P}_j \frac{\partial C_i(t)}{\partial p_j} = \tilde{P}_j \frac{\partial C_i(t)}{\partial (\epsilon_j \tilde{P}_j)} = \frac{\partial C_i(t)}{\partial \epsilon_j}$$

Equation (4D-2)

Here, $S_{ij}(t)$, the sensitivity, gives the change in model concentration, C_i, (for instance O_3 concentration) with an incremental change in any input parameter, p_j (in this case emissions). Equation (4D-2) allows us to normalize the sensitivity coefficient, $S_{ij}(t)$, so that it shows response in relative terms for the input rather than in absolute units. Therefore, $\tilde{P}_j$ (x,t) is the normalized input and ε_j is a scaling variable (Yang et al., 1997). In general terms, the sensitivity coefficient tells us how a model output (O_3 concentration) will change if a model input (emissions of NO_x or VOC) is varied. This first order sensitivity coefficient, $S_{ij}(t)$ is quite suitable for small changes, but gives a linear response which is unlikely to represent the results of large changes in very nonlinear chemical environments. Second (and third) order derivatives can be calculated to give higher order sensitivity coefficients (Hakami et al., 2003). Higher order sensitivity coefficients give the curvature and inflection points for the response curve and can capture the nonlinearities in the response of O_3 to emissions changes. Using Higher order DDM (HDDM) allows for the sensitivities to be more appropriately applied over larger emissions changes. Hakami et al. (2003) report that for an application in California, HDDM gave reasonable approximations of O_3 changes compared to brute force results for emission changes up to 50% using the first three terms of the Taylor series expansion, Equation (4D-3).

$$C(+\Delta\epsilon) = C(0) + \Delta\epsilon S(0) + \frac{\Delta\epsilon^2}{2} S^2(0) + \ ... + \frac{\Delta\epsilon^n}{n!} S^n(0) + R_{n+1}$$

Equation (4D-3)

Here $\Delta\epsilon$ represents the relative change in emissions (for instance $\Delta\epsilon$ = -0.2 would be equivalent to reducing emissions by 20%), $S^n(0)$ is the n^{th} order sensitivity coefficient, C(0) is the concentration under baseline conditions (no change in emissions) and R_{n+1} is a remainder term.

A variant of DDM called DDM-3D has been implemented into several chemical transport models, including CMAQ, for both O_3 and particulate matter (PM) predictions (Dunker, 1984; Yang et al., 1997; Hakami et al., 2003; Cohan et al., 2005; Napelenok et al., 2006; Koo et al., 2010; Zhang et al., 2012). These implementations allow the modeler to define the parameters for which first and higher order sensitivities will be calculated. For instance, the sensitivity can be calculated for emissions from a specific source type, for emissions in a specific geographic region, and for emissions of a single O_3 precursor or for multiple O_3 precursors. In addition, sensitivities can be calculated to boundary conditions, initial conditions, and various other model inputs. Sensitivities to different sets of parameters can be calculated in a single model simulation but computation time increases as the number of sensitivities increases. Outputs from an HDDM simulation consist of time varying 3-D fields of first and second order sensitivities.

For the purposes of the O_3 NAAQS analysis, HDDM provides an improved approach compared to existing quadratic rollback techniques for several reasons. First, it captures non-linearity of O_3 response to emissions changes, representing both increases and decreases in O_3 concentrations resulting from emissions reductions. Second, HDDM characterizes different O_3 response at different locations (downtown urban versus downwind suburban) and at different times of day allowing us to incorporate temporal and spatial variations in response into the O_3 adjustment methodology. Finally, HDDM eliminates the need to use "background" O_3 as a floor for rollback since predicted sensitivities are based on model formulations that explicitly account for background sources.

4D-2.2 Limitations

In addition to the many potential benefits of using HDDM to understand and characterize O_3 response to emissions changes, there are several limitations. First, HDDM encompasses all of the uncertainties of the base photochemical model formulation and inputs. So uncertainties in how the physical and chemical processes are treated in the model and in the model inputs propagate to the HDDM results. Also, HDDM can capture response to larger emissions changes than DDM but it is still most accurate for small changes. The larger the relative change in emissions, the less likely that the HDDM sensitivities will properly capture the change in O_3 that

would be predicted by a brute force model simulation. Several studies have reported reasonable performance of HDDM for O_3 up to 50% emission changes (Hakami et al., 2003; Cohan et al., 2005; Hakami et al., 2004), but the magnitude of change over which HDDM will give accurate estimates will depend on the specific modeling episode, size of the model domain, emissions and meteorological inputs, and the size of the emissions source to which the sensitivity is being calculated. In this work, we applied sensitivities derived from model simulations done under varying NO_x levels (see Section 4D-4D-3.2.1) and found that using this technique we were able to replicate brute force estimates using HDDM sensitivities for up to 90% NO_x reductions with a mean bias of less than 3 ppb and a mean error of less than 4 ppb.

4D-3. APPLYING HDDM/CMAQ TO ADJUST OZONE TO JUST MEET EXISTING AND ALTERNATIVE STANDARDS: METHODOLOGY

4D-3.1 Conceptual Framework

This section outlines the methodology from Simon et al. (2012) in which we apply CMAQ/HDDM to estimate hourly O_3 concentrations that might result from meeting the existing and potential alternative standards. As part of the methodology, photochemical modeling results are not used in an absolute sense, but instead are applied to modulate ambient measurements, thus tying estimated O_3 distributions to measured values. The basic steps are outlined below and in Figure 4D-1 Details are given in section 4D-4D-3.2. The inputs, set-up, and evaluation of the modeling system are described in Appendix 4B.

- **Step 1:** Run CMAQ simulation with HDDM to determine hourly O_3 sensitivities to NO_x emissions and VOC emissions for the grid cells containing monitoring sites in an urban area.
- **Step 2:** For each monitoring site, season, and hour of the day use linear regression to relate first order sensitivities of NO_x and VOC (S_{NOx} and S_{VOC}) to modeled O_3 and second order sensitivities to NO_x and VOC (S^2_{NOx} and S^2_{VOC}) to the first order sensitivities.
- **Step 3:** For each measured hourly O_3 value, calculate the first and second order sensitivities based on monitoring site-, season-, and hour-specific functions calculated in Step 2.
- **Step 4:** Adjust measured hourly 2006-2010 O_3 concentrations for incrementally increasing levels of emissions reductions using assigned sensitivities and then recalculate 2006-2008 and 2008-2010 design values until all monitors in an urban area just meet the existing and potential alternative levels of the standard.

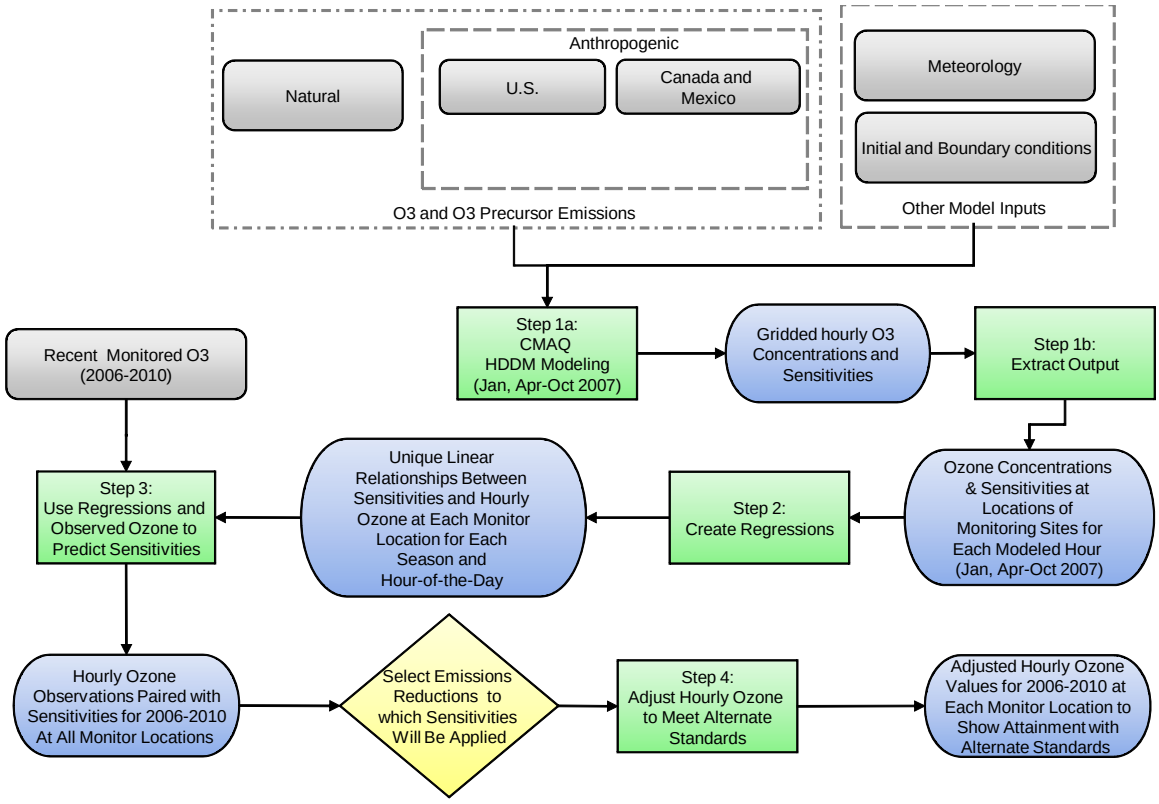

Figure 4D-1. Flow diagram demonstrating DDM model-based O_3 adjustment approach.

4D-3.2 Application to Measured O_3 Concentrations in 15 Urban Areas

In this analysis, we apply the model-based adjustment approach described above for just meeting the existing standard and three potential alternative standards. The analysis covers the 15 urban study areas listed in HREA Chapter 4 using photochemical modeling for January, and April-October of 2007 and ambient data for the years 2006-2010. When running CMAQ with HDDM, additional information is required to designate model inputs for calculating sensitivities. In this analysis, HDDM was set up to calculate the sensitivity of O_3 concentrations to U.S. anthropogenic NO_x and VOC emissions.[2] US anthropogenic emissions were defined as all emissions in the following sectors: commercial marine and rail, onroad mobile, offroad mobile, Electric Generating Unit (power plant) point sources, non-EGU point, and non-point area. These sectors accounted for 17.6 million of the total domain-wide 23.6 million tons per year of NO_x emissions and 13.8 million of the total domain-wide 68.1 million tons per year of VOC emissions. Sensitivities were not determined for biogenic, fire, Canadian, or Mexican emissions. In addition, sensitivities were not calculated for any emissions originating from outside the domain (i.e. entering through the use of boundary concentrations).

[2] Sensitivities only tracked U.S. emissions in the contiguous 48 states.

4D-3.2.1 Multi-step Application of HDDM Sensitivities

As discussed in Section 4D-4D-2.2 of this appendix, HDDM has been reported to reasonably replicate brute force emissions reductions up to a 50% change in emissions. For this analysis, it was desirable to have confidence that the HDDM sensitivities could replicate the entire range of emissions reductions. Evaluations of the HDDM estimates compared to brute force emissions reduction model runs confirm that the HDDM estimates of O_3 response to NO_x reductions are fairly comparable for a 50% change. However, HDDM and brute force estimates begin to diverge in comparisons under larger emissions changes (90%). Consequently four additional CMAQ/HDDM runs were performed under different levels of NO_x and VOC emissions reductions in order to characterize O_3 sensitivities to NO_x reductions over a larger range of emissions changes. One CMAQ/HDDM simulation was performed with U.S. anthropogenic NO_x cut by 50%. A second additional simulation was performed with a 90% NO_x reduction. Another set of CMAQ/HDDM simulations were performed for simultaneous NO_x and VOC cuts (50% NO_x and 50% VOC; 90% NO_x and 90% VOC). Emissions of other species were not modified from the base case in these four simulations. These additional HDDM simulations give O_3 sensitivities to NO_x and VOC under conditions with lower NO_x (or NO_x and VOC) emissions in the U.S. These sensitivities are used in a multistep adjustment approach.

Figure 4D-2 gives a conceptual picture of the multistep adjustment procedure using first-order sensitivities. Sensitivities from the base run are used to adjust O_3 concentrations for NO_x emissions reductions up to X%. Additional emission reductions beyond X% use sensitivities from the 50% NO_x cut run until reductions exceed (X+Y)%. Finally, sensitivities from the 90% NO_x cut run are applied for any emission reductions beyond (X+Y)%. In order to more closely approximate the non-linear O_3 response to any level of emissions reductions, 2nd order terms are added to the multistep approximation method in Equations (4D-4) to (4D-7). P represents the percentage NO_x cut for which the ΔO_3 values are being calculated, S and S^2 are the first and second order O_3 sensitivities to U.S. NO_x emissions, and X and Y are described above. Alternately, Equation (4D-8) can be used with Equations (4D-5) to (4D-7) if simultaneous NO_x and VOC_c cuts are being simulated. Note that the 50% and 90% cut sensitivities used in Equation (4D-8) come from model runs which cut both VOC and NO_x by these percentages in contrast to the NO_x cut only sensitivities that are used in Equation 4D-4. Consequently, Equation (4D-8) works only for equal percentage cuts in both NO_x and VOC emissions. In equations (4D-5) to (4D-8), we cap ΔO_3, so that O_3 never drops below zero due to emissions changes.

$$\Delta O_3 = -a \times S_{NOx_{base}} + \frac{a^2}{2} \times S^2_{NOx_{base}} - b \times S_{NOx_{50}\%cut} + \frac{b^2}{2} \times S^2_{NOx_{50}\%cut} - c \times S_{NOx_{90}\%cut} + \frac{c^2}{2} \times S^2_{NOx_{90}\%cut}$$

Equation (4D-4)

$$a = \begin{cases} \frac{P}{100} & for\ P \leq X \\ \frac{X}{100} & for\ P > X \end{cases}$$

Equation (4D-5)

$$b = \begin{cases} 0 & for\ P \leq X \\ \frac{2\times(P-X)}{100} & for\ X < P \leq (X+Y) \\ \frac{2\times Y}{100} & for\ P > (X+Y) \end{cases}$$

Equation (4D-6)

$$c = \begin{matrix} 0 & for\ P \leq (X+Y) \\ \frac{10\times(P-(X+Y))}{100} & for\ 100 \geq P > (X+Y) \end{matrix}$$

Equation (4D-7)

$$\Delta O_3 = -a \times S_{NOx_{base}} + \frac{a^2}{2} \times S^2_{NOx_{base}} - a \times S_{VOC_{base}} + \frac{a^2}{2} \times S^2_{VOC_{base}} + a^2 \times S^2_{NOx,VOC_{base}}$$
$$-b \times S_{NOx_{50}\%cut} + \frac{b^2}{2} \times S^2_{NOx_{50}\%cut} - b \times S_{VOC_{50}\%cut} + \frac{b^2}{2} \times S^2_{VOC_{50}\%cut} + b^2 \times S^2_{NOx,VOC_{50}\%cut}$$
$$-c \times S_{NOx_{50}\%cut} + \frac{c^2}{2} \times S^2_{NOx_{50}\%cut} - c \times S_{VOC_{50}\%cut} + \frac{c^2}{2} \times S^2_{VOC_{50}\%cut} + c^2 \times S^2_{NOx,VOC_{50}\%cut}$$

Equation (4D-8)

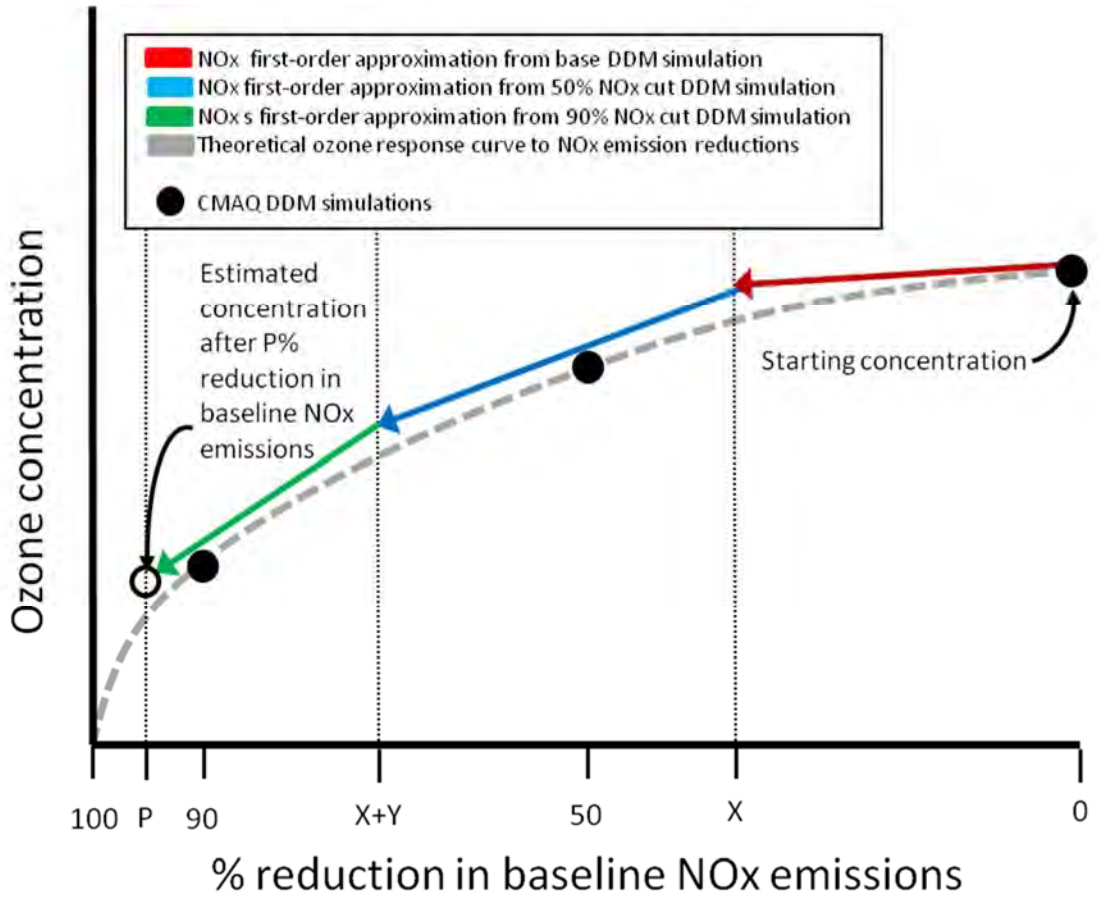

Figure 4D-2. Conceptual picture of 3-step application of HDDM sensitivities.

The ideal value for equation transition points, X and Y, are determined by minimizing the least square mean error between the adjusted concentrations using the multistep approach and modeled concentrations from brute force NO_x cut runs. We first determined the value of X which gave the lowest error compared to brute forces estimates at 50% NO_x cuts. Then holding X constant, we determined the value of Y which gave the lowest error compared to brute force estimates at 90% NO_x cuts. This process was performed independently for each of the 15 urban areas in this analysis.

Error in HDDM estimates of hourly O_3 is defined here as the difference between HDDM estimates and brute force O_3. Based on Equations (4D-4) to (4D-7), this can be calculated from Equations (4D-9) and (4D-10) for 50% NO_x cuts:

$$\varepsilon = \Delta Ozone_{HDDM,50} - \Delta Ozone_{BF,50}$$

Equation (4D-9)

$$\varepsilon = \frac{-X}{100} \times S_{NOx_base} + \frac{X^2}{2 \times 100^2} \times S^2_{NOx_base} - \frac{2(50-X)}{100} \times S_{NOx_{50}\%cut} + \frac{(2 \times (50-X))^2}{2 \times 100^2} \times S^2_{NOx_{50}\%cut} - \Delta Ozone_{BF,50}$$

Equation (4D-10)

Equation (4D-10) can be rearranged to appear in the form: $AX^2 + BX + C$:

$$\varepsilon = \left(\frac{S^2_{NOx_{base}}}{2 \times 100^2} + \frac{4 \times S^2_{NOx_{50}\%cut}}{2 \times 100^2}\right)X^2 + \left(\frac{-S_{NOx_{base}}}{100} + \frac{2 \times S_{NOx_{50}\%cut}}{100} - \frac{400 \times S^2_{NOx_{50}\%cut}}{2 \times 100^2}\right)X + \left(-S_{NOx_{50}\%cut} + \frac{S^2_{NOx_{50}\%cut}}{2} - \Delta Ozone_{BF,50}\right)$$

Equation (4D-11)

$$A = \left(\frac{S^2_{NOx_base}}{2 \times 100^2} + \frac{4 \times S^2_{NOx_{50}\%cut}}{2 \times 100^2}\right)$$

Equation (4D-12)

$$B = \left(\frac{-S_{NOx_base}}{100} + \frac{2 \times S_{NOx_{50}\%cut}}{100} - \frac{400 \times S^2_{NOx_{50}\%cut}}{2 \times 100^2}\right)$$

Equation (4D-13)

$$C = \left(-S_{NOx_{50}\%cut} + \frac{S^2_{NOx_{50}\%cut}}{2} - \Delta Ozone_{BF,50}\right)$$

Equation (4D-14)

Next, the error is squared, summed over all points (error can be calculated for each hourly O_3 value at each monitoring location), and the derivative is set to 0 to determine X which gives the least squares error (Equations (4D-15), (4D-16), and (4D-17)).

$$\varepsilon^2 = A^2X^4 + 2ABX^3 + (2AC + B^2)X^2 + 2BCX + C^2$$

Equation (4D-15)

$$\sum \varepsilon^2 = (\sum A^2)X^4 + (\sum 2AB)X^3 + (\sum 2AC + B^2)X^2 + (\sum 2BC)X + \sum C^2$$

Equation (4D-16)

$$(\sum \varepsilon^2)' = (4\sum A^2)X^3 + (3\sum 2AB)X^2 + (2\sum 2AC + B^2)X + (\sum 2BC) = 0$$

Equation (4D-17)

The value of X that gives the least squares error will occur at one of the 3 roots of the trinomial in Equation (4D-17) or at 0 or 50. All real roots, 0, and 50 were input into Equation (4D-16) and X was set to the value which resulted in the lowest error in each city. An analogous procedure was followed to determine Y using the 90% NO_x cut brute force simulation and Equations (4D-18) through (4D-24).

$$\varepsilon = \frac{-X}{100} \times S_{NOx_{base}} + \frac{X^2}{2 \times 100^2} \times S^2_{NOx_{base}} - \frac{2Y}{100} \times S_{NOx_{50}\%cut} + \frac{2^2Y^2}{2 \times 100^2} \times S^2_{NOx_{50}\%cut} - \frac{10\left(90 - (X+Y)\right)}{100} \times S_{NOx_{90}\%cut} + \frac{\left(10^2(90-(X+Y))\right)^2}{2 \times 100^2} \times S^2_{NOx_{90}\%cut} - \Delta Ozone_{BF,90}$$

Equation (4D-18)

$$\varepsilon^2 = A^2Y^4 + 2ABY^3 + (2AC + B^2)Y^2 + 2BCY + C^2$$

Equation (4D-19)

$$A = \left(\frac{4 \times S^2_{NOx_{50}\%cut}}{2 \times 100^2} + \frac{100 \times S^2_{NOx_{90}\%cut}}{2 \times 100^2}\right)$$

Equation (4D-20)

$$B = \left(\frac{-2 \times S_{NOx_{50}\%cut}}{100} + \frac{10 \times S_{NOx_{90}\%cut}}{100} - \frac{200 \times (90-X) S^2_{NOx_{90}\%cut}}{2 \times 100^2}\right)$$

Equation (4D-21)

$$C = \left(\frac{-X}{100} S_{NOx_base} + \frac{X^2}{2 \times 100^2} S^2_{NOx_base} - \frac{10 \times (90 - X)}{100} S_{NOx_{90}\%cut} + \frac{100 \times (90 - X)^2}{2 \times 100^2} S^2_{NOx_{90}\%cut} - \Delta Ozone_{BF,90}\right)$$

Equation (4D-22)

$$\sum \varepsilon^2 = (\sum A^2)Y^4 + (\sum 2AB)Y^3 + (\sum 2AC + B^2)Y^2 + (\sum 2BC)Y + \sum C^2$$

Equation (4D-23)

$$(\sum \varepsilon^2)' = (4 \sum A^2)Y^3 + (3 \sum 2AB)Y^2 + (2 \sum 2AC + B^2)Y + (\sum 2BC) = 0$$

Equation (4D-24)

This methodology can also be adjusted to calculate least squares error cut points for the combined NO_x and VOC emissions reduction case. X and Y cut points which have the least square error in each urban area are shown in Table 4D-1. This 3-step adjustment methodology was shown to be a robust method for minimizing error in the HDDM applications for larger percentage changes in emissions by Simon et al. (2012). Figure 4D-3 through Figure 4D-6 are density scatter plots that compare hourly O_3 estimates from brute force with hourly O_3 estimates from the 3-step HDDM adjustments at all monitor locations in each of the 15 urban areas evaluated in this study. The colors in these plots depict the percentage of points falling at any one location. Mean error for the 50% and 90% 3-step HDDM adjustment NO_x cut cases compared to brute force results are less than 1 ppb and 4 ppb respectively in all 15 case study areas.

Table 4D-1. X and Y cut points used in Equations (4D-4) and (4D-8). Note: the NO_x/VOC sensitivity case was only performed in two cities.

Urban Area	NO_x cuts only		NO_x and VOC combined cuts	
	X	Y	X	Y
Atlanta	40	46		
Baltimore	40	46		
Boston	39	45		
Chicago	38	45	40	46
Cleveland	42	45		
Dallas	37	46		
Denver	39	45	43	45
Detroit	38	45		
Houston	37	44		
Los Angeles	38	46		
New York	37	45		
Philadelphia	40	45		
Sacramento	38	45		
Saint Louis	39	45		
Washington D.C.	40	46		

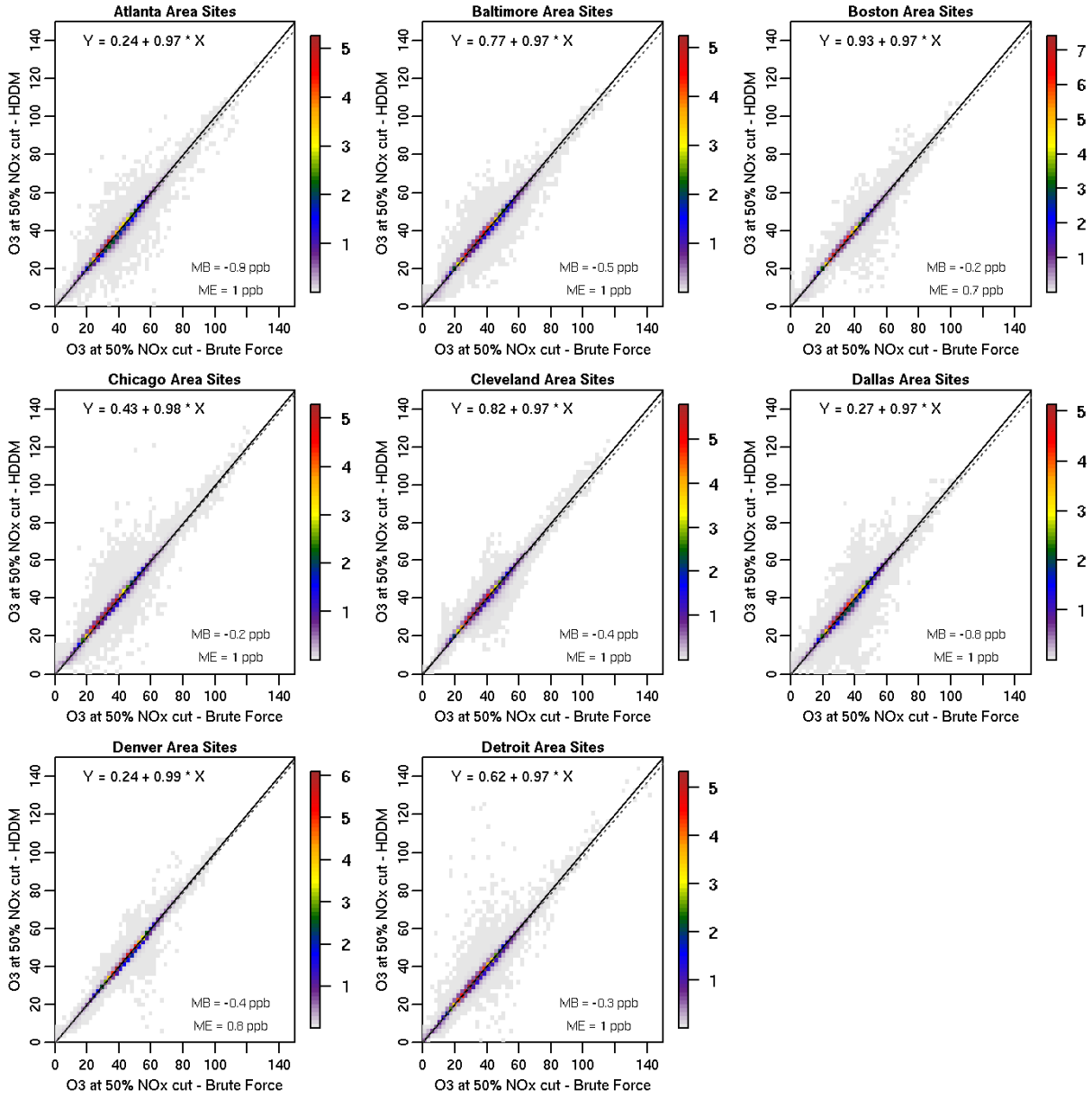

Figure 4D-3. Comparison of brute force and 3-step HDDM O_3 estimates for 50% NO_x cut conditions: Atlanta, Baltimore, Boston, Chicago, Cleveland, Dallas, Denver, and Detroit.

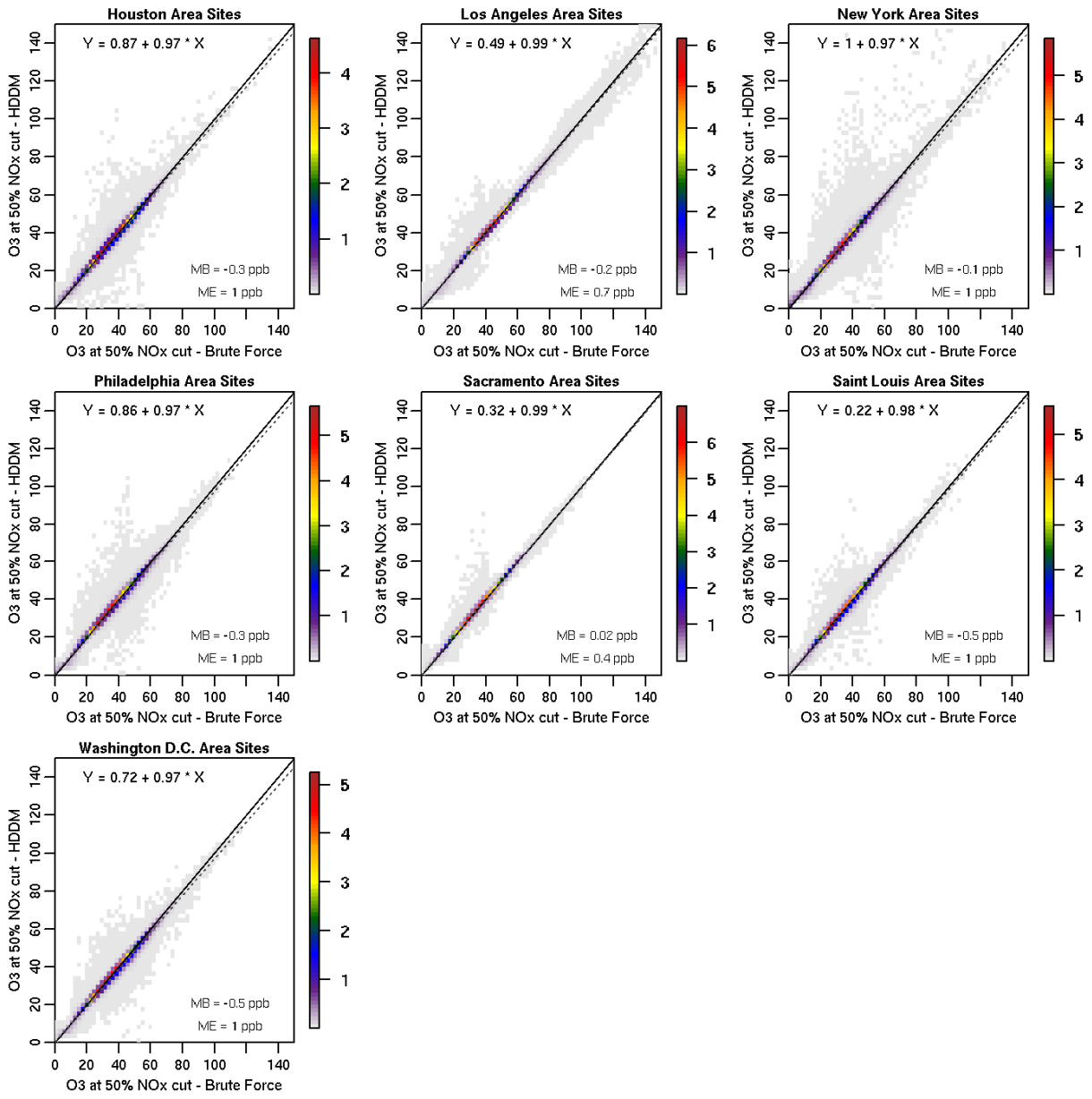

Figure 4D-4. Comparison of brute force and 3-step HDDM O_3 estimates for 50% NO_x cut conditions: Houston, Los Angeles, New York, Philadelphia, Sacramento, St. Louis, and Washington D.C.

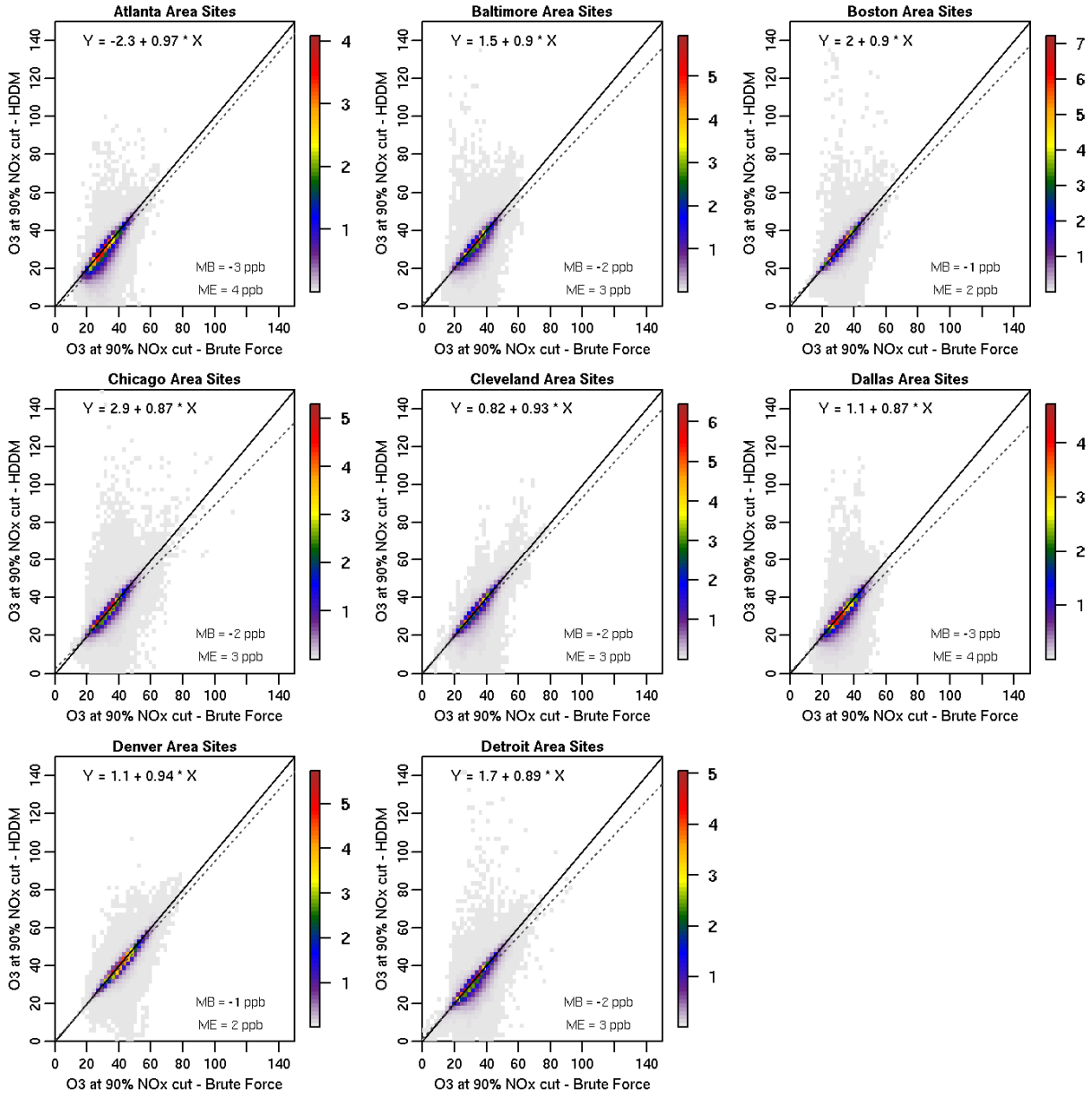

Figure 4D-5. Comparison of brute force and 3-step HDDM O_3 estimates for 90% NO_x cut conditions: Atlanta, Baltimore, Boston, Chicago, Cleveland, Dallas, Denver, and Detroit.

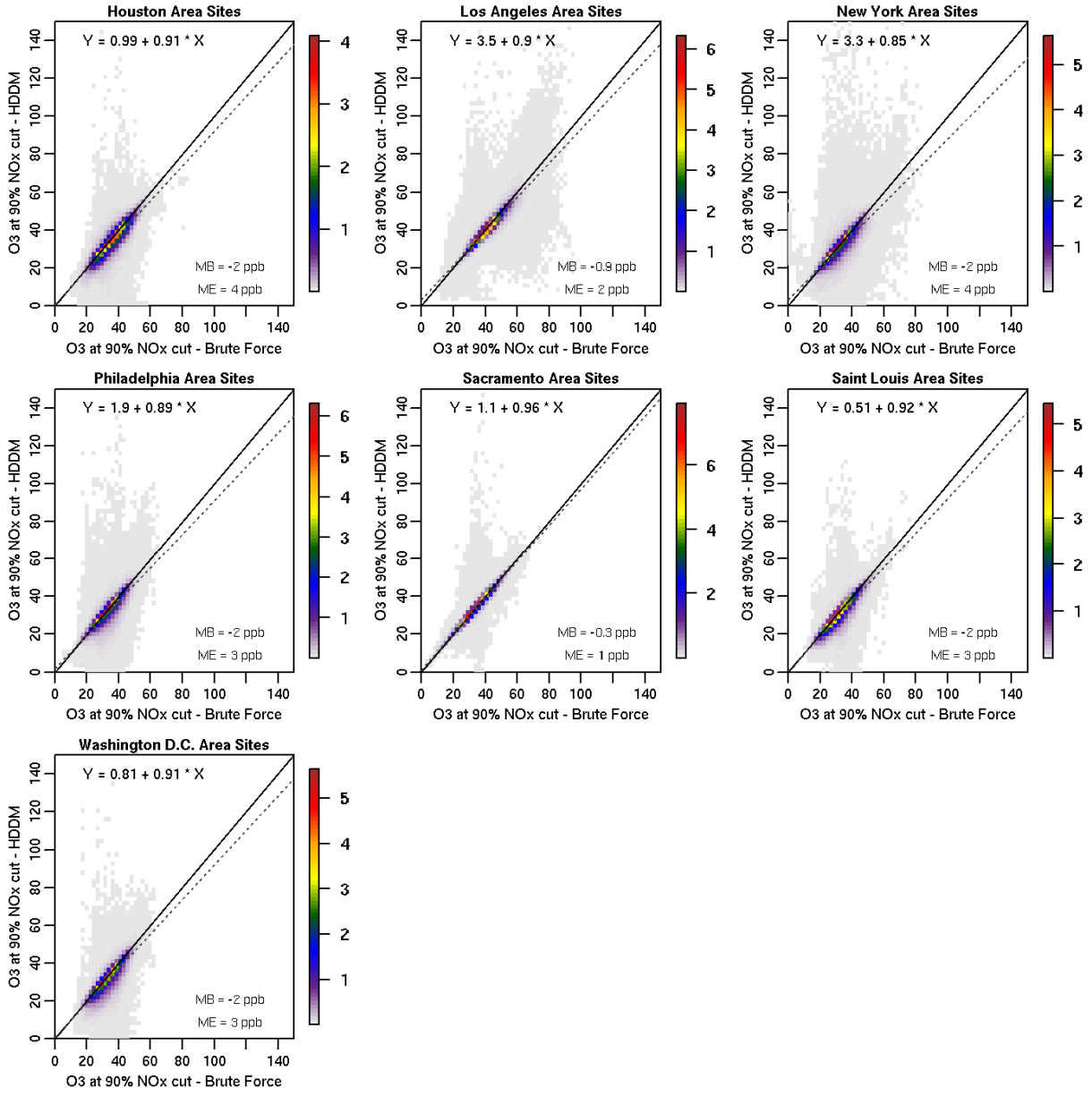

Figure 4D-6. Comparison of brute force and 3-step HDDM O_3 estimates for 90% NO_x cut conditions: Houston, Los Angeles, New York, Philadelphia, Sacramento, St. Louis, and Washington D.C.

4D-3.2.2 Relationships between HDDM Sensitivities and Modeled O_3 Concentrations

First and second order hourly O_3 sensitivities to VOC and NO_x were extracted from the HDDM simulation for model grid cells that contained the O_3 monitors in the 15 urban areas. Extracted data included modeled sensitivities at monitor locations for all modeled hours in 2007. These sensitivities cannot be applied directly to observed values for two reasons: 1) high

modeled O_3 days/hours do not always occur concurrently with high observed O_3 days/hours and 2) the modeling time period includes 8 months in 2007 but the time period we are analyzing in this HREA includes five full years of ambient data, 2006-2010. As to the first point, photochemical models are generally used in a relative sense for purposes of projecting design values to assess just meeting the NAAQS standard. In this manner, model predictions are "anchored" to measured ambient values. In general, the average response on high modeled days is used for this purpose. This allows for more confidence in calculated results when "less than ideal model performance [occurs] on individual days" (U.S. EPA, 2007). Similarly, for this analysis we believe it is appropriate to account for the fact the model does not always perfectly agree with measurements and that sensitivities from a low O_3 modeled day would not be appropriate to apply to a high O_3 measured day (and vice-versa) even if they occur on the same calendar day. For the second point, due to current resource and time constraints we were only able to model 8 months in 2007. However, the O_3 exposure analysis evaluates the effects of O_3 decreases for two 3-year periods in 2006-2008 and 2008-2010 most of which is outside the modeled time period. For both of these reasons, a method was developed to generalize the modeled site-, season-, and hour-specific sensitivities so that they could be applied to ambient data during 2006-2010.[3]

Simon et al. (2012) describe how first order sensitivities are generally well correlated with hourly modeled O_3 concentrations and second order sensitivities are well correlated to first order sensitivities. Based on their analysis, we create a separate linear regression for S_{NOx} and S_{VOC} as functions of hourly O_3 (i.e. $S_{NOx} = m \times O_3 + b$) for every site, season[4], and hour-of-the day examined in this analysis. For instance, for summer 8-am hours at Detroit Site 260990009, S_{NOx} and O_3 values from all 8 am hours in June-August 2007 are used to fit this relationship. Since only 8 months were modeled (Jan, April-October) regressions for summer season relationships include more data points (92) than those for winter (31), spring (61), and fall (61). Similarly, S^2_{NOx} and S^2_{VOC} were calculated as a function of S_{NOx} and S_{VOC} respectively and $S^2_{NOx,VOC}$ was calculated as a linear combination of both S_{NOx} and S_{VOC}. Figure 4D-7, Figure 4D-8, and Figure 4D-9 show examples of these regressions for first order NO_x sensitivities for a NO_x-limited site (summertime, downwind of Atlanta), a NO_x-saturated site (autumn, Queens NY), and a transitional site which switches between chemical regimes (spring, Long Island NY). Example

[3] The 8 months modeled covered a variety of conditions such that we can use the results from this modeled time period in conjunction with the ambient data from the longer 5-year period for estimating response and applying adjustments

[4] Here seasons are defined as follows:
For ambient data, Winter = December, January, February; Spring = March, April, May;
Summer = June, July, August; Fall = September, October, November.
For modeled data, Winter = January; Spring = April, May; Summer = June, July, August;
Fall = September, October

relationships are shown for four different times of day with different O_3 response behavior: nighttime (1:00 LST), mid-afternoon (15:00 LST), morning rush-hour (8:00 LST), and evening rush-hour (18:00 LST). The Atlanta area NO_x-limited site (Figure 4D-7) generally showed positive sensitivities which would lead to decreasing O_3 with decreasing emissions. However some limited O_3 increases with NO_x reductions from NOx (negative sensitivities) occurred at this site during nighttime and rush-hour times. The Queens site had negative sensitivities at these four hours on almost all days indicating strongly NO_x saturated conditions. The slopes from the regressions at the Queens site were negative indicating larger O_3 increases are high concentrations. Finally, the Long Island site had both positive and negative sensitivities but the slope was positive resulting in O_3 increases for low basecase concentrations but O_3 decreases at higher basecase concentrations. Correlations were strongest at the NO_x limited site and during rush-hour and nighttime periods for the other sites. Figure 4D-10, Figure 4D-11, and Figure 4D-12 show these regressions from the same sites and time-periods for second order sensitivities.

Comparisons between brute force and HDDM O_3 estimates shown in Figure 4D-5 and Figure 4D-6, demonstrate that for the vast majority of data points, HDDM replicates brute force with minimal errors. However, these figures show a small number of instances in which HDDM predicts very high hourly O_3 (> 100 ppb) while the brute force emissions simulations show much lower O_3 (< 40 ppb). In such cases, base modeled O_3 is low due to NO_x titration and increases occur with reductions of NO_x. The HDDM sensitivities for these few points appear to be too high to be applied over large emissions changes because of strongly nonlinear chemistry. While the brute force simulations predict modest increases in O_3 at these hours, the HDDM method predicts very large increase in O_3 at these hours. To avoid outlier sensitivities from biasing this analysis, we set a floor value for negative S_{NOx} values (O_3 increases) in each regression so that S_{NOx} never drops below the 5^{th} percentile modeled S_{NOx} (for each site, hour, season grouping) when negative S_{NOx} values are simulated (see dotted blue lines in Figure 4D-7, Figure 4D-8, and Figure 4D-9). In addition, S_{NOx} is prevented from dropping below 0 when all modeled S_{NOx} values were positive (i.e. no modeled increases in O_3). These floor values have the most influence when regressions with highly NO_x-saturated conditions, such as those shown for Queens NY, are applied to ambient O_3 values that are higher than the modeled range. For instance in Figure 4D-9, if there were any measured autumn 18:00 O_3 concentrations above 30 ppb at that site in 2006-2010, the floor would prevent the extrapolation of O_3 increases from the modeled time period to conditions that do not apply. This floor is necessary for O_3 increases which, if extrapolated, could unrealistically increase O_3 without a bound. In contrast, the O_3 decreases can never exceed the total measured O_3 so positive NO_x sensitivities have a built-in upper bound.

For the 50% and 90% emissions cut CMAQ/HDDM simulation, regressions were performed for first order NO_x and VOC sensitivities with modeled O_3 from the base HDDM simulation. The regression technique was performed for the first and second order NO_x and VOC sensitivities from the base run and the 50% emissions cut and 90% emissions cut simulations. The sensitivities from the emissions cut runs were fitted to hourly O_3 concentrations in the base simulation. Simon et al. (2012) found that correlation coefficients using for sensitivities from NO_x cut simulations to base case O_3 concentrations were similar to those with O_3 concentrations from the NO_x cut runs.

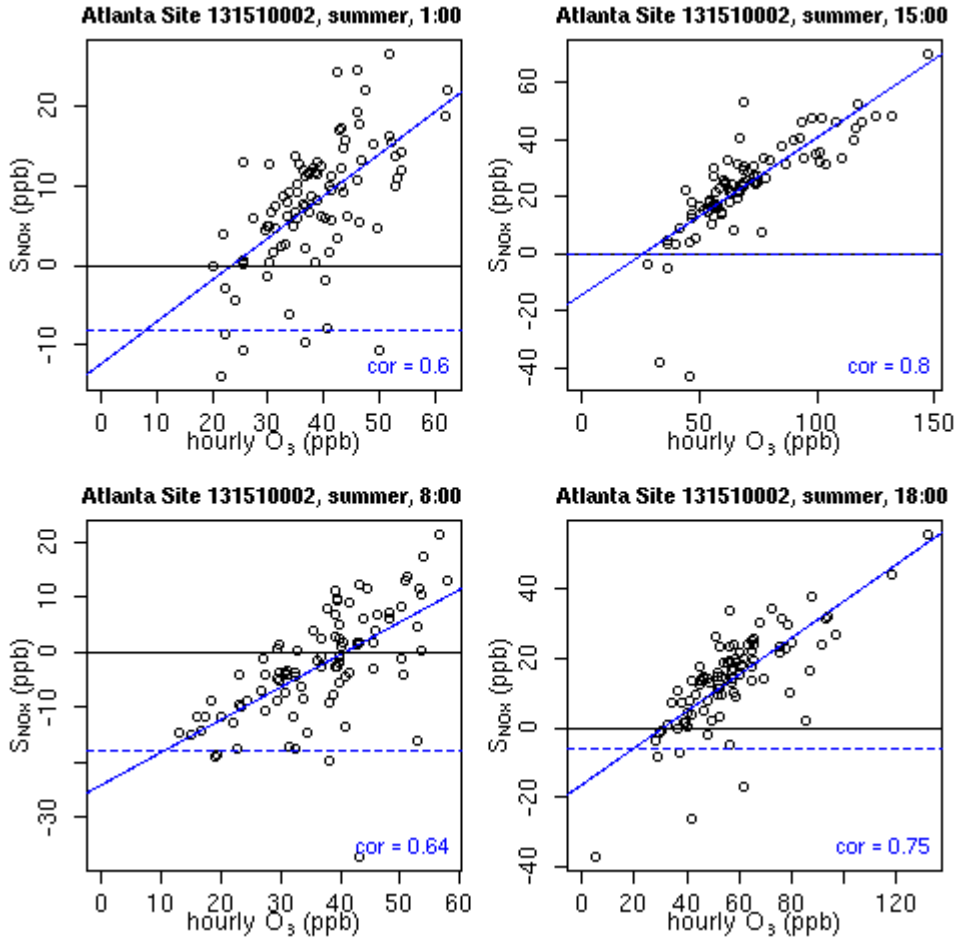

Figure 4D-7. Relationship between S_{NOx} and hourly O_3 at a NO_x-limited site downwind of Atlanta (summer). Relationships are shown for one nighttime hour, one morning rush-hour hour, one daytime hour, and one evening rush-hour hour. The solid blue line show the linear regression for these points and the dotted blue line shows the floor value used for S_{NOx} based on the 5th percentile modeled value.

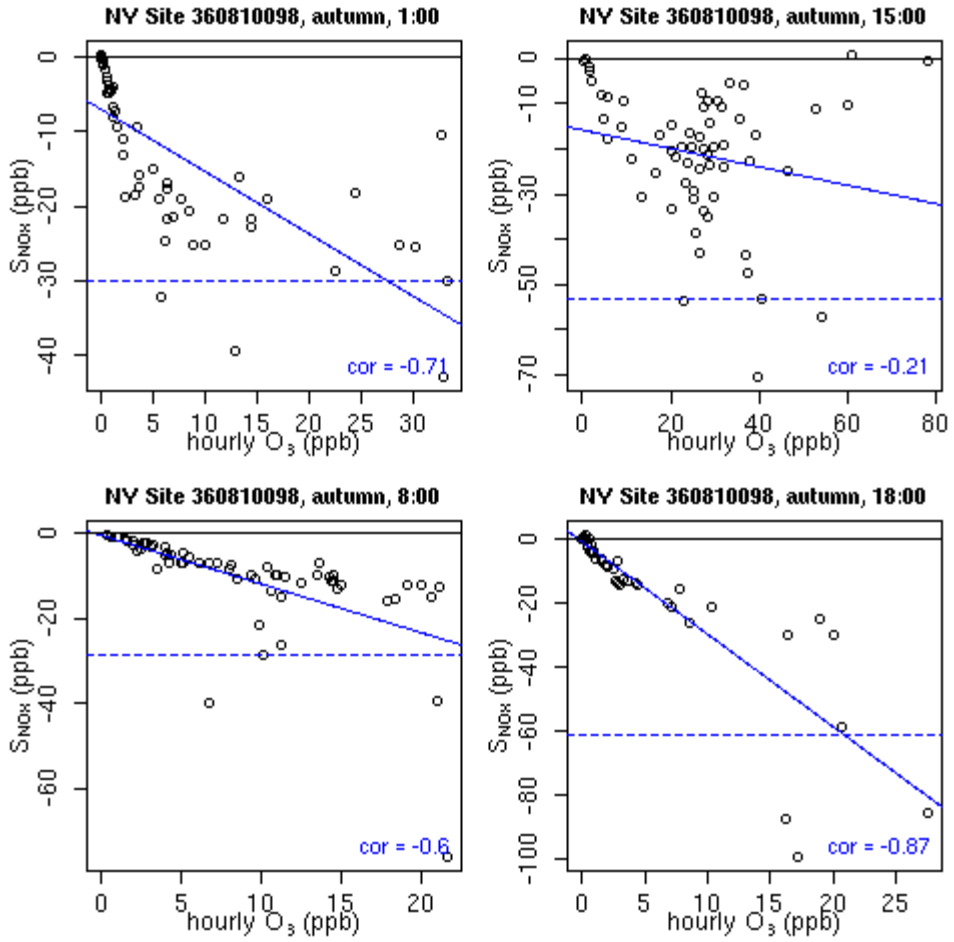

Figure 4D-8. Relationship between S_{NOx} and hourly O_3 at a NO_x-saturated site in Queens County, NY (autumn). Relationships are shown for one nighttime hour, one morning rush-hour hour, one daytime hour, and one evening rush-hour hour. The solid blue line show the linear regression for these points and the dotted blue line shows the floor value used for S_{NOx} based on the 5th percentile modeled value.

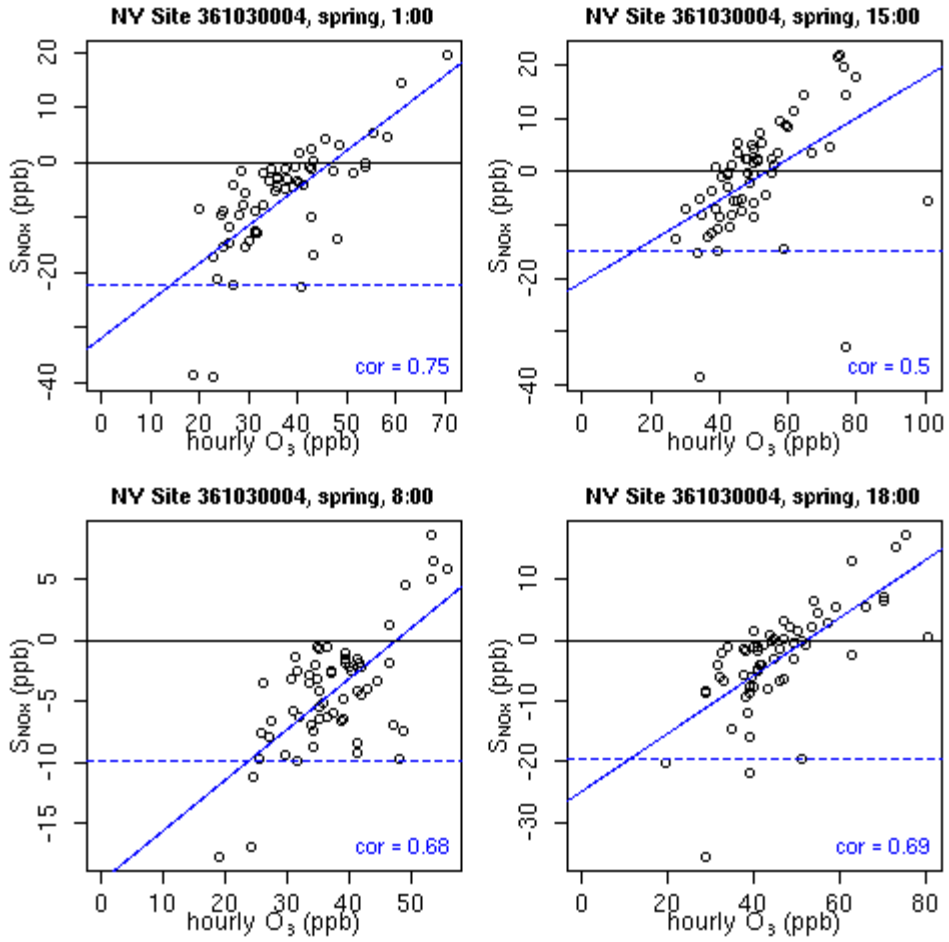

Figure 4D-9. Relationship between S_{NOx} and hourly O_3 at a NO_x-saturated site in Suffolk County, NY on Long Island (spring). Relationships are shown for one nighttime hour, one morning rush-hour hour, one daytime hour, and one evening rush-hour hour. The solid blue line show the linear regression for these points and the dotted blue line shows the floor value used for S_{NOx} based on the 5th percentile modeled value.

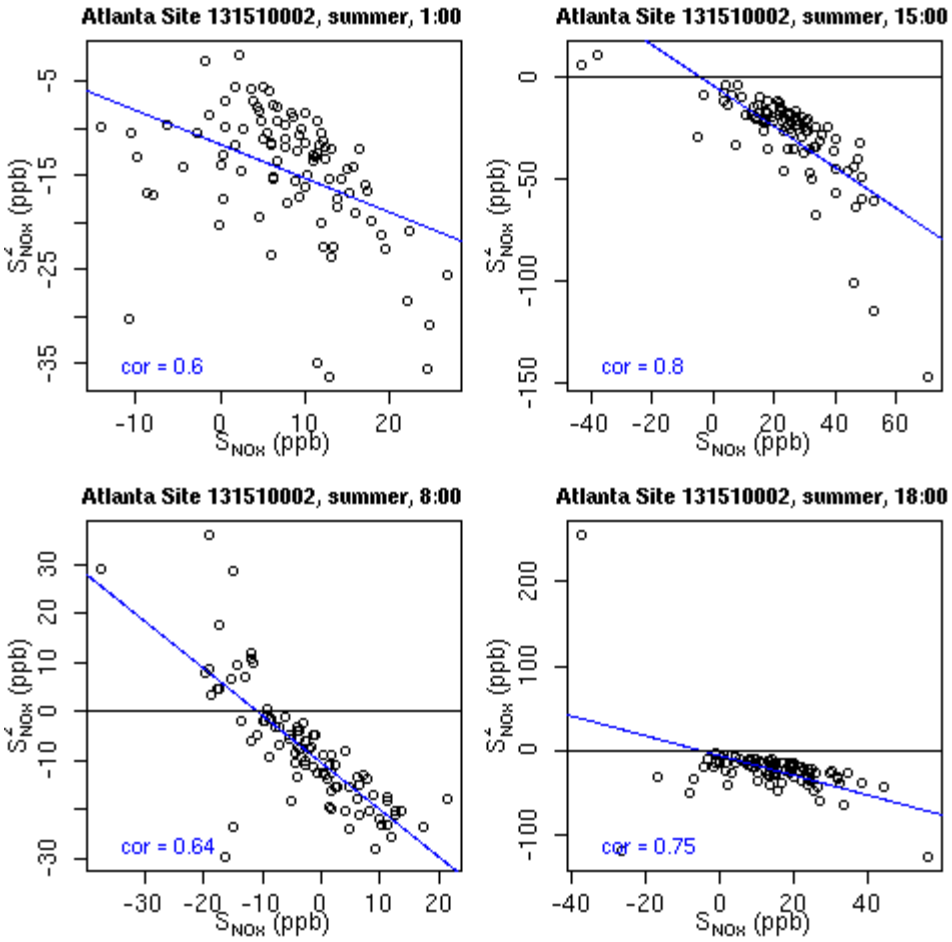

Figure 4D-10. Relationship between S^2_{NOx} and S_{NOx} at a NO_x-limited site downwind of Atlanta (summer). Relationships are shown for one nighttime hour, one morning rush-hour hour, one daytime hour, and one evening rush-hour hour. The solid blue line shows the linear regression for these points.

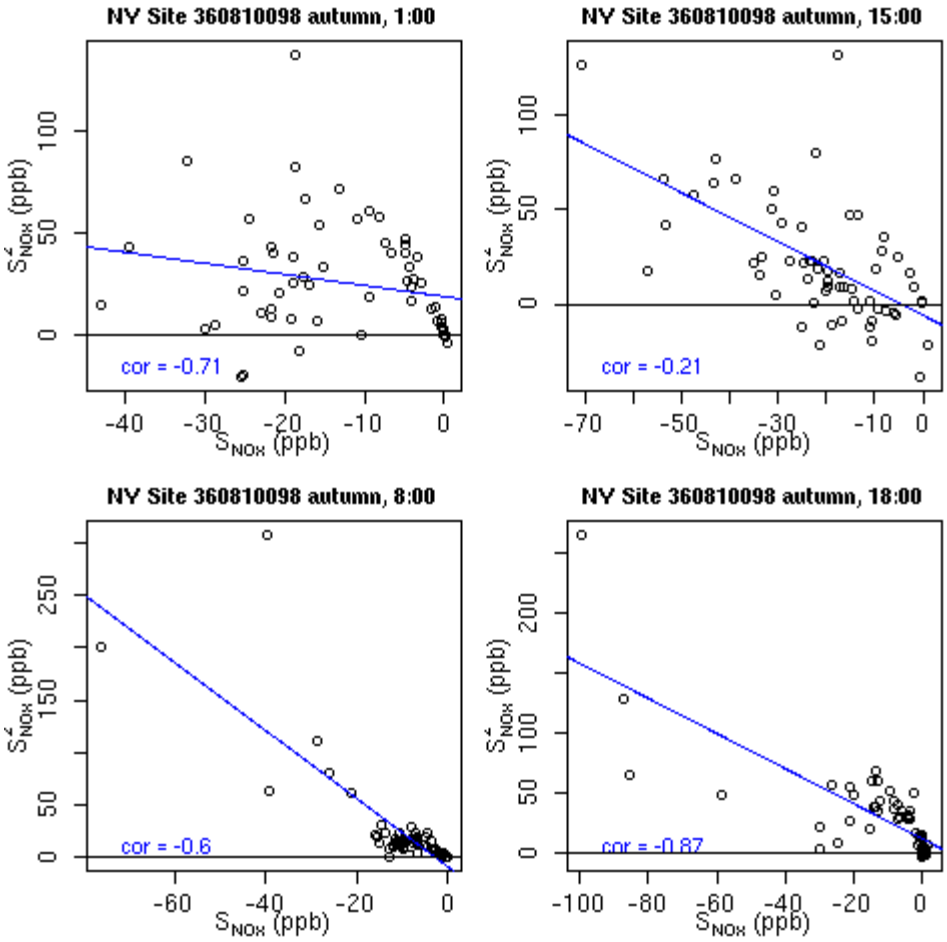

Figure 4D-11. Relationship between S^2_{NOx} and S_{NOx} at a NO_x-saturated site in Queens County, NY (autumn). Relationships are shown for one nighttime hour, one morning rush-hour hour, one daytime hour, and one evening rush-hour hour. The solid blue line shows the linear regression for these points.

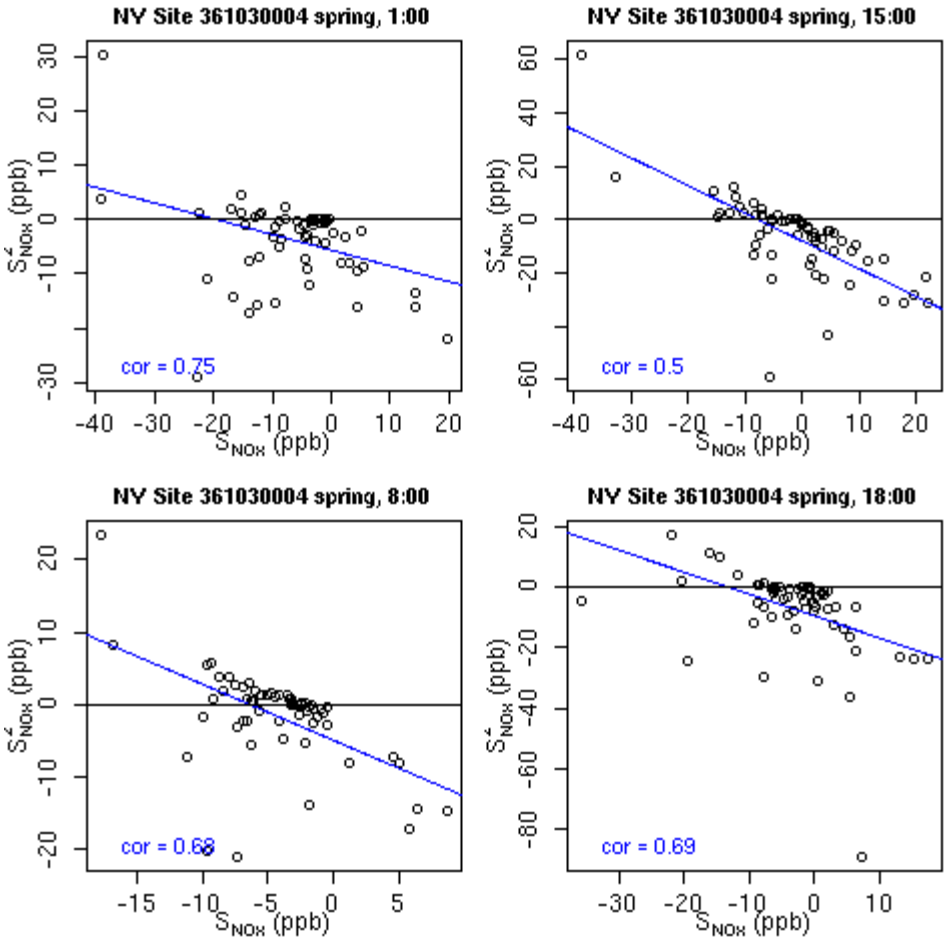

Figure 4D-12. Relationship between S^2_{NOx} and S_{NOx} at a NO_x-saturated site in Suffolk County, NY on Long Island (spring). Relationships are shown for one nighttime hour, one morning rush-hour hour, one daytime hour, and one evening rush-hour hour. The solid blue line shows the linear regression for these points.

4D-3.2.3 Application of Sensitivity Regressions to Ambient Data

To apply the HDDM adjustments to observed data, sensitivities must be determined for each hour from 2006-2010 at each site based on the linear relationship from the modeled data and the observed O_3 concentration. The linear regression model also allows us to quantify the standard error of each predicted sensitivity value at each hour and site.

Observed hourly O_3 from 2006-2010 at each monitor location was adjusted by applying incrementally increasing emissions reductions using Equations (4D-4) to (4D-8) and recalculating MDA8 values for incrementally increasing emissions reductions until an emissions level is reach for which all monitors in an urban area achieved design values at the standard level being evaluated (75, 70, 65, or 60 ppb). Therefore all monitors within an urban area were treated

as responding to the same percentage reduction in NO_x or NO_x/VOC emissions. The final emissions reductions that were applied in each urban study area are given in Table 4D-2.

The standard error associated with each predicted sensitivity from the linear model can be propagated through Equations (4D-4) and (4D-8) to quantify the standard error in the final predicted O_3 concentration. This gives a measure of uncertainty in the predicted mean sensitivity at any given O_3 concentration and allows us to quantify how much our predicted O_3 could change given that uncertainty. Further details on the standard error and uncertainty from the linear fits used in each of the urban study areas are provided in section 4D-4.44D-4.4.

4D-3.2.4 Alternate Methodologies

The methodology used for most of the 15 urban areas is described above. In most cases the O_3 response was calculated using Equation (4D-4) which represents a NO_x-only control strategy. In addition, sensitivities applied to observed data were based on the predicted sensitivity for that hourly O_3 from the site, season, and hour-specific regression. However, two alternate scenarios were used for a few cities as described below.

A combined NO_x/VOC control strategy was applied to two cities for which controlling monitors were sensitive to changes in VOC emissions: Chicago and Denver. These were the only urban study areas in which the addition of VOC reductions allowed adjusted air quality to just meet the targeted standard levels with smaller reductions in NO_x emissions than would be required if VOC emissions were held constant. In these cases, Equation (4D-8) was applied in place of Equation (4D-4) and the X,Y cut points described in Table 4D-1 were derived for the NO_x/VOC control case based on brute force runs that reduced the two O_3 precursors by equal percentages.

In two cities, New York and Los Angeles, results were affected by aberrant behavior at a few monitors which occurred during rush-hour and nighttime hours. At a few highly urbanized monitors during some seasons, the O_3 increases during highly titrated rush-hour and nighttime hours appear to be overestimated, leading to predictions that when NO_x was reduced O_3 would peak during rush-hour periods on the very highest O_3 days (compare outlier dots for 65 ppb standard at 9:00-17:00 to outlier dots for 65 ppb standard at 18:00-8:00 in Figure 4D-23). Even at these monitors, the majority of days did not have this problem as shown by the more normal diurnal pattern for the boxes (interquartile range) and whiskers (1.5 × interquartile range) in Figure 4D-23. As mentioned above, for each predicted hourly O_3 concentration we calculated a standard error based on the uncertainty in the fitted regressions representing the variability in modeled sensitivities which is not explained by hourly O_3 levels alone for each site, season, and hour. So, in addition to the predicted O_3, we can create alternate hourly O_3 datasets based on the standard error in these values. To address the aberrant behavior on the very highest O_3 days in

the adjustment scenarios in New York and Los Angeles, we took the 95th percentile confidence interval for each hourly O_3 prediction and used the lower bound value to determine the NO_x reductions required to meet the existing and potential alternative standards and to calculate the hourly O_3 that would occur under that reduced emission scenario. During most hours and at most monitors, the 95th percentile range was small (less than +/- 2.7 ppb) so the use of the lower-bound of the 95th percentile range made little difference in predicted O_3 concentrations (Table 4D-18 and Table 4D-19). However, using the lower bound of the 95th percent confidence interval allowed us to dampen the effect of over predicted O_3 increases during rush-hour times. Since the O_3 concentrations for each standard level were created using consistent methodology, these O_3 datasets can be used to compare between standards in these cities. In addition, at a single standard level (for instance 75 ppb) these O_3 values can be compared against those obtained using the base methodology in order to quantify uncertainty due to variability in modeled sensitivities. However, O_3 values for one standard obtained using the 95th percentile confidence interval lower bound are not contrasted against O_3 concentrations for a potential alternative standard which were obtained using the base methodology since these datasets are not directly comparable.

4D-4. APPLYING HDDM/CMAQ TO ADJUST OZONE TO JUST MEET EXISTING AND ALTERNATIVE STANDARDS: RESULTS

4D-4.1 Emission Reductions Applied to Meet Alternative Standards

Table 4D-2 reports the percentage reduction in domain-wide emissions that were used to reach the existing and potential alternative standard levels in each urban area. Percentages in Chicago and Denver represent reductions in anthropogenic NO_x and VOC. Percentages in all other cities represent reductions only in anthropogenic NO_x emissions. Percentages in New York and in Los Angeles were calculated based on air quality estimates at the lower end of the 95th percentile confidence interval as discussed above in section 4D-3.2.4. Please note that these reductions and broad nationwide emission cuts are not intended to represent recommended control scenarios since they would not be the most efficient method for achieving the standard in many localized areas.

Table 4D-2. Percent emissions reductions used for each urban area to obtain each standard.

Urban Area	Years	Standard Level*			
		75 ppb	70 ppb	65 ppb	60 ppb
Atlanta	2006-2008	50%	58%	64%	71%
	2008-2010	23%	43%	54%	62%
Baltimore	2006-2008	46%	54%	61%	69%
	2008-2010	44%	52%	60%	67%
Boston	2006-2008	40%	49%	61%	70%
	2008-2010	13%	40%	53%	65%
Chicago	2006-2008	19%	52%	66%	80%
	2008-2010	N/A	27%	55%	70%
Cleveland	2006-2008	48%	61%	73%	88%
	2008-2010	50%	64%	77%	88%
Dallas	2006-2008	50%	57%	65%	72%
	2008-2010	50%	58%	64%	71%
Denver	2006-2008	51%	65%	78%	87%
	2008-2010	15%	46%	64%	87%
Detroit	2006-2008	59%	69%	76%	84%
	2008-2010	N/A	54%	66%	78%
Houston	2006-2008	62%	68%	74%	82%
	2008-2010	42%	53%	63%	75%
Los Angeles	2006-2008	87.1%	89.3%	91.2%	93.2%
	2008-2010	87%	89%	91%	93%
New York	2006-2008	64%	74%	92%	N/A
	2008-2010	52%	67%	89%	N/A
Philadelphia	2006-2008	54%	61%	68%	74%
	2008-2010	42%	52%	61%	68%
Sacramento	2006-2008	63%	70%	76%	84%[5]
	2008-2010	64%	71%	77%	84%
Saint Louis	2006-2008	45%	56%	66%	75%
	2008-2010	10%	34%	50%	63%
Washington D.C.	2006-2008	53%	60%	67%	74%
	2008-2010	31%	50%	60%	71%

* N/A values for the 75 ppb standard level mean that a particular urban area did not have any design values above 75 for that 3-year period so no controls were needed. N/A values for the 60 ppb standard level mean that this adjustment methodology was not able to bring design values down to 60 for that particular city and 3-year period.

[5] An error was discovered in the Sacramento adjustment to 60 ppb for the 2006-2008 design value period in which 84% NO_x cuts were applied instead of 85% NO_x cuts. The 84% NO_x cuts thus simulate meeting a standard of 61 ppb for Sacramento for those years. Results for the 85% NO_x cut case are not expected to be substantially different from the 84% NO_x cut case that was analyzed.

4D-4.2 Design Values

Table 4D-3 through Table 4D-17 report the design values for sites in each of the urban areas for recent years (2006-2008 and 2008-2010) and for adjusted O_3 levels representing just meeting standards of 75, 70, 65, and 60 ppb. In each table, the highest design value for each scenario is displayed in bold text. These tables demonstrate that in some urban areas high O_3 values at monitors in different locations have different magnitudes of response to reductions in NO_x (and VOC) emissions. Atlanta monitor 132470001, a downwind monitor, had the highest design value for 2006-2008. With the NO_x reduction scenarios to meet various standard levels, the two downtown monitors (131210055 and 130890002) switch to being the highest monitors in the area. These downtown locations which have large amounts of spatially concentrated NO_x emissions are expected to be more VOC limited and therefore less responsive to NO_x emission reductions than surrounding rural and suburban areas. This phenomenon occurs to varying degrees in each of the 15 urban areas included in this analysis. For instance, the difference in response between monitors on high days is very pronounced in Cleveland and in New York. In Cleveland, a downwind monitor located east of the city along Lake Erie was the high monitor for both 2006-2008 and 2008-2010 (39071001). That monitor responded more dramatically to NO_x cuts than another monitor (390850003) which was closer to the city. As a result of adjusting air quality to just meet a 60 ppb standard level at monitor 390850003, the design value at monitor 390071001 was lowered to 45 ppb for the 2006-2008 data and 44 ppb for the 2008-2010 data. Similarly in the New York area, the highest measured O_3 values occurred at downwind sites in Connecticut and on Long Island. Two highly urbanized sites (360050110 in the Bronx and 360610135 in Manhattan) have lower observed design values but become the controlling monitors in the adjustment scenarios for 75, 70, and 65 ppb. In contrast, several cities do not show this change in location of the highest monitor after adjustments to just meet potential alternative standard levels. For example, the highest monitor for the 2008-2010 design value period in the Dallas area (484393009, located on the North side of Fort Worth) remained the highest monitor through all adjustment scenarios for that time period. Similarly, the controlling monitor in Sacramento (060670012, a downwind suburban site) remained the highest or second highest site for all adjustment scenarios. However, in Sacramento, another downwind monitor (060610006) which did not have as high of an observed design value, responded less to emissions changes and essentially "caught up" to the controlling monitor in the 65 and 60 ppb scenarios.

It is important to note that a model-based adjustment technique is uniquely capable of capturing this type of spatial heterogeneity in response to emissions reductions. The quadratic rollback technique used in the first draft HREA forces O_3 at all monitoring sites in an urban area to respond identically.

Table 4D-3. Design values for the Atlanta area regulatory monitors from observed data and for adjustments to meet the existing and potential alternative standards in 2006-2008 and 2008-2010.

Monitor	2006-2008					2008-2010				
	obs	75 ppb	70 ppb	65 ppb	60 ppb	obs	75 ppb	70 ppb	65 ppb	60 ppb
132470001	**95**	72	66	61	55	78	71	64	59	55
132230003	80	62	58	55	51	70	64	59	55	52
131510002	94	72	65	61	55	79	73	66	60	55
131350002	88	71	67	63	58	74	71	66	61	58
131210055	91	**75**	**70**	**65**	59	**80**	**75**	**70**	**65**	**60**
131130001	86	67	61	57	53	N/A	N/A	N/A	N/A	N/A
130970004	87	68	63	59	54	75	69	64	59	55
130890002	93	**75**	**70**	**65**	**60**	79	**75**	**70**	64	**60**
130850001	77	59	55	53	49	71	66	60	56	52
130770002	84	65	60	56	52	68	63	58	54	51
130670003	85	68	63	59	53	76	72	66	62	57

The highest DV for each scenario is shown in **bold**. N/A values indicate that there was not enough ambient data to compute a design value for that monitor during a specific 3-year period.

Table 4D-4. Design values for the Baltimore area regulatory monitors from observed data and for adjustments to meet the existing and potential alternative standards in 2006-2008 and 2008-2010.

Monitor	2006-2008					2008-2010				
	obs	75 ppb	70 ppb	65 ppb	60 ppb	obs	75 ppb	70 ppb	65 ppb	60 ppb
240030014	87	72	66	61	56	79	67	63	58	54
240051007	80	68	63	59	53	77	68	64	60	56
240053001	85	74	69	**65**	**60**	78	69	65	62	58
240130001	83	68	63	59	53	76	64	60	56	53
240251001	**91**	**75**	**70**	**65**	59	**89**	**75**	**70**	**65**	**60**
240259001	89	75	69	65	59	78	68	64	60	56
245100054	66	61	58	56	52	67	62	59	55	53

The highest DV for each scenario is shown in **bold.**

Table 4D-5. Design values for the Boston area regulatory monitors from observed data and for adjustments to meet the existing and potential alternative standards in 2006-2008 and 2008-2010.

Monitor	2006-2008					2008-2010				
	obs	75 ppb	70 ppb	65 ppb	60 ppb	obs	75 ppb	70 ppb	65 ppb	60 ppb
250010002	79	70	67	62	58	73	72	68	63	58
250051002	80	70	67	62	57	75	73	67	62	57
250070001	**83**	74	**70**	**65**	**60**	**78**	**75**	69	**65**	**60**
250092006	81	73	69	62	57	74	72	68	63	56
250094004	78	72	68	63	58	N/A	N/A	N/A	N/A	N/A
250095005	79	72	68	62	56	71	69	66	62	56
250170009	75	68	64	58	52	68	66	62	58	53
250171102	78	70	66	59	53	71	69	64	58	53
250213003	82	73	68	62	56	73	72	68	62	57
250250041	74	72	69	63	58	72	72	**70**	**65**	**60**
250250042	67	66	64	60	56	62	63	63	60	57
250270015	82	**75**	**70**	63	58	76	74	**70**	**65**	58

The highest DV for each scenario is shown in **bold**. N/A values indicate that there was not enough ambient data to compute a design value for that monitor during a specific 3-year period.

Table 4D-6. Design values for the Chicago area regulatory monitors from observed data and for adjustments to meet the existing and potential alternative standards using NO_x and VOC emissions reductions in 2006-2008 and 2008-2010.

Monitor	2006-2008					2008-2010				
	obs	75 ppb	70 ppb	65 ppb	60 ppb	obs	75 ppb	70 ppb	65 ppb	60 ppb
170310001	76	73	65	59	53	69	69	66	60	54
170310032	74	74	**70**	**65**	58	68	68	69	**65**	**60**
170310064	71	70	66	62	56	64	64	65	61	57
170310076	73	72	67	62	56	67	67	65	60	56
170311003	73	73	**70**	**65**	**60**	66	66	66	63	**60**
170311601	75	72	66	60	53	70	70	67	60	55
170314002	62	63	61	58	54	65	65	65	62	58
170314007	66	66	62	58	53	59	59	59	57	53
170314201	71	70	66	62	56	69	69	68	63	59
170317002	70	68	63	58	53	63	63	62	58	53
170436001	63	63	59	54	49	60	60	58	54	51
170890005	66	63	57	53	47	66	66	62	56	51
170971002	71	69	63	58	54	64	64	61	56	52
170971007	72	71	64	59	54	73	73	**70**	64	59
171110001	64	61	55	51	47	64	64	61	55	51

171971011	66	63	55	50	46	62	62	59	52	49
180890022	73	70	64	59	53	61	61	59	54	50
180890030	77	**75**	**70**	**65**	**60**	64	64	63	60	56
180892008	73	71	66	62	56	67	67	65	62	57
180910005	69	66	58	53	47	65	65	61	55	51
180910010	70	67	58	53	47	65	65	61	54	49
181270024	74	72	65	60	56	67	67	64	59	55
181270026	70	67	59	54	50	62	62	58	53	49
550590019	**78**	**75**	68	62	56	**74**	**74**	**70**	64	59

The highest DV for each scenario is shown in **bold**.

Table 4D-7. Design values for the Cleveland area regulatory monitors from observed data and for adjustments to meet the existing and potential alternative standards in 2006-2008 and 2008-2010.

	2006-2008					2008-2010				
Monitor	**obs**	**75 ppb**	**70 ppb**	**65 ppb**	**60 ppb**	**obs**	**75 ppb**	**70 ppb**	**65 ppb**	**60 ppb**
390071001	**84**	69	62	55	45	**77**	64	58	50	44
390350034	78	74	69	64	57	75	72	67	62	57
390350064	74	67	61	56	47	68	62	57	51	45
390355002	81	74	68	61	50	75	68	62	55	48
390550004	73	61	55	49	42	**77**	63	55	48	42
390850003	78	**75**	**70**	**65**	**60**	76	**75**	**70**	**65**	**60**
390850007	76	72	67	62	55	72	70	66	60	56
390930018	74	65	59	53	44	70	62	56	49	43
391030003	72	61	55	49	41	70	58	52	47	41
391331001	73	62	56	50	42	67	57	51	46	41
391530020	82	69	62	54	44	75	64	57	50	44

The highest DV for each scenario is shown in **bold.**

Table 4D-8. Design values for the Dallas area regulatory monitors from observed data and for adjustments to meet the existing and potential alternative standards in 2006-2008 and 2008-2010.

Monitor	2006-2008					2008-2010				
	obs	75 ppb	70 ppb	65 ppb	60 ppb	obs	75 ppb	70 ppb	65 ppb	60 ppb
480850005	83	70	66	61	57	77	66	62	57	54
481130069	74	67	63	59	56	67	63	59	56	54
481130075	80	71	68	63	59	78	71	67	63	58
481130087	82	65	63	59	55	78	65	61	58	54
481210034	**91**	73	68	62	56	80	67	62	57	53
481211032	81	65	62	57	53	78	65	60	55	51
481390016	75	62	59	55	51	72	61	57	54	50
481391044	N/A	N/A	N/A	N/A	N/A	68	56	53	50	47
482311006	70	56	54	51	47	64	54	50	47	45
482510003	83	69	66	61	56	80	69	65	59	55
482570005	73	59	57	53	50	67	56	53	50	47
483670081	84	66	62	57	52	75	61	57	54	50
483970001	75	61	57	53	49	74	62	57	53	49
484390075	89	**75**	**70**	64	58	85	74	69	63	58
484391002	83	71	68	64	**60**	79	70	66	62	58
484392003	87	**75**	**70**	**65**	**60**	**86**	**75**	**70**	**65**	**60**
484393009	87	73	68	63	57	82	71	66	61	55
484393011	79	64	61	58	54	79	66	61	58	54

The highest DV for each scenario is shown in **bold**. N/A values indicate that there was not enough ambient data to compute a design value for that monitor during a specific 3-year period.

Table 4D-9. Design values for the Denver area regulatory monitors from observed data and for adjustments to meet the existing and potential alternative standards using NO_x and VOC emissions reductions in 2006-2008 and 2008-2010.

Monitor	2006-2008					2008-2010				
	obs	75 ppb	70 ppb	65 ppb	60 ppb	obs	75 ppb	70 ppb	65 ppb	60 ppb
080013001	71	69	66	**65**	**60**	70	70	69	**65**	**60**
080050002	71	65	61	58	54	67	66	63	59	52
080130011	81	70	65	60	55	73	71	66	61	53
080310014	73	70	67	64	**60**	68	68	67	64	**60**
080310025	N/A	N/A	N/A	N/A	N/A	65	64	62	59	56
080350004	82	72	67	61	56	76	74	69	64	54
080590002	78	73	69	64	58	73	72	**70**	65	56
080590005	78	70	65	61	56	72	71	67	61	54
080590006	**86**	**75**	**70**	64	58	**77**	**75**	**70**	**65**	55
080590011	81	**75**	**70**	**65**	59	72	72	**70**	**65**	57
080690011	82	70	65	59	55	74	72	65	60	52
080691004	71	61	57	53	50	65	63	57	53	48
081230009	76	66	62	57	53	71	69	63	59	52

The highest DV for each scenario is shown in **bold**. N/A values indicate that there was not enough ambient data to compute a design value for that monitor during a specific 3-year period.

Table 4D-10. Design values for the Detroit area regulatory monitors from observed data and for adjustments to meet the existing and potential alternative standards in 2006-2008 and 2008-2010.

Monitor	2006-2008					2008-2010				
	obs	75 ppb	70 ppb	65 ppb	60 ppb	obs	75 ppb	70 ppb	65 ppb	60 ppb
260490021	74	61	56	52	49	68	68	59	54	49
260492001	76	58	54	50	46	68	68	56	51	47
260990009	81	69	64	61	57	74	74	66	61	57
260991003	80	**75**	**70**	**65**	**60**	73	73	**70**	**65**	**60**
261250001	76	70	65	60	55	72	72	69	64	57
261470005	78	63	58	55	51	71	71	60	56	51
261610008	74	61	56	53	49	66	66	58	54	49
261630001	71	64	59	56	51	66	66	62	58	53
261630019	**82**	74	69	64	59	**75**	**75**	**70**	**65**	59

The highest DV for each scenario is shown in **bold**.

Table 4D-11. Design values for the Houston area regulatory monitors from observed data and for adjustments to meet the existing and potential alternative standards in 2006-2008 and 2008-2010.

Monitor	2006-2008					2008-2010				
	obs	75 ppb	70 ppb	65 ppb	60 ppb	obs	75 ppb	70 ppb	65 ppb	60 ppb
480391004	85	63	59	55	50	**85**	73	67	61	54
480391016	76	56	53	51	47	74	63	60	55	50
481671034	N/A	N/A	N/A	N/A	N/A	75	65	61	57	52
482010024	83	64	60	56	51	83	**75**	69	63	55
482010026	80	61	57	54	50	78	68	63	58	52
482010029	85	63	58	54	47	81	72	66	59	51
482010046	75	60	57	54	49	72	66	61	56	51
482010047	76	61	58	54	49	76	73	68	62	55
482010051	80	63	59	56	51	77	71	66	61	55
482010055	**91**	70	65	60	53	82	75	69	64	57
482010062	81	62	58	55	50	72	65	62	57	52
482010066	89	**75**	**70**	**65**	**60**	75	**75**	**70**	**65**	59
482010070	74	66	64	61	59	73	71	68	64	**60**
482010075	76	66	64	62	59	74	73	69	65	**60**
482010416	89	70	65	62	56	77	72	67	62	57
482011015	74	57	55	52	48	73	65	61	57	52
482011034	80	63	60	57	53	76	71	66	62	55
482011035	73	59	56	53	49	75	69	64	59	53
482011039	87	63	59	56	51	81	68	65	59	53
482011050	80	61	58	55	51	75	67	62	58	53
483390078	80	56	52	49	45	71	61	56	50	45

The highest DV for each scenario is shown in **bold**. N/A values indicate that there was not enough ambient data to compute a design value for that monitor during a specific 3-year period.

Table 4D-12. Design values for the Los Angeles area regulatory monitors from observed data and for adjustments to meet the existing and potential alternative standards using the lower bound of the 95th percent confidence interval of estimated hourly O_3 in 2006-2008 and 2008-2010.

	2006-2008					2008-2010				
Monitor	**obs**	**75 ppb**	**70 ppb**	**65 ppb**	**60 ppb**	**obs**	**75 ppb**	**70 ppb**	**65 ppb**	**60 ppb**
060370002	96	63	60	56	53	89	63	60	56	52
060370016	107	64	60	57	53	103	65	61	57	53
060370113	69	54	52	50	48	72	55	53	50	48
060371002	92	69	64	59	54	84	69	64	59	54
060371103	73	68	64	61	56	70	68	64	60	56
060371201	97	54	52	50	47	91	53	51	49	47
060371301	58	56	54	52	50	N/A	N/A	N/A	N/A	N/A
060371602	78	71	67	63	59	69	68	64	61	57
060371701	103	63	59	55	52	90	62	58	55	51
060372005	92	**75**	**70**	**65**	**60**	87	**75**	**70**	**65**	**60**
060374002	59	54	52	52	50	61	55	54	53	52
060375005	64	56	54	53	51	61	56	54	52	50
060376012	105	57	54	51	47	97	57	54	50	47
060379033	94	55	52	49	47	91	54	52	50	48
060590007	73	58	56	54	51	68	58	55	53	51
060591003	66	52	51	50	48	66	53	52	51	49
060592022	87	55	52	50	48	81	54	52	50	47
060595001	83	61	57	54	51	74	60	57	54	51
060650004	N/A	N/A	N/A	N/A	N/A	97	60	56	53	49
060650008	79	55	53	52	51	81	55	54	53	52
060650012	102	58	55	52	49	102	58	55	52	49
060651010	N/A	N/A	N/A	N/A	N/A	78	52	51	49	48
060651016	105	60	57	54	51	102	59	56	53	50
060651999	N/A	N/A	N/A	N/A	N/A	77	52	51	49	48
060652002	86	55	54	52	51	85	55	53	52	50
060655001	97	56	54	52	50	95	55	54	52	49
060656001	107	57	54	51	47	102	55	52	50	47
060658001	107	63	59	55	51	97	60	56	53	49
060658005	N/A	N/A	N/A	N/A	N/A	93	58	55	51	48
060659001	102	55	52	49	46	96	53	51	48	46
060659003	63	48	47	46	45	63	48	47	47	46
060710001	86	57	56	54	53	80	54	52	51	50
060710005	**119**	70	65	61	55	**112**	68	64	59	55
060710012	96	60	57	56	54	99	60	57	55	54
060710306	89	60	57	56	54	87	58	56	53	52

060711004	110	67	62	57	52	100	65	61	56	52
060711234	80	56	55	54	53	75	54	53	52	51
060712002	112	68	63	58	53	101	65	61	56	51
060714001	96	60	56	53	50	96	60	57	53	50
060714003	116	68	63	59	54	103	65	61	56	51
060719004	116	67	62	58	53	102	64	60	55	50
061110007	75	47	46	44	43	78	48	46	45	44
061110009	80	47	46	44	43	79	47	46	45	43
061111004	83	49	48	46	45	79	47	46	45	44
061112002	88	49	48	46	44	86	49	48	46	44
061112003	64	48	47	46	46	63	47	46	46	45
061113001	61	47	46	46	45	63	47	46	45	44

The highest DV for each scenario is shown in **bold**. N/A values indicate that there was not enough ambient data to compute a design value for that monitor during a specific 3-year period.

Table 4D-13. Design values for the New York area regulatory monitors from observed data and for adjustments to meet the existing and potential alternative standards using the lower bound of the 95th percent confidence interval of estimated hourly O_3 in 2006-2008 and 2008-2010.

	2006-2008				2008-2010			
Monitor	**obs**	**75 ppb**	**70 ppb**	**65 ppb**	**obs**	**75 ppb**	**70 ppb**	**65 ppb**
090010017	99	**75**	67	39	91	74	65	43
090011123	102	60	50	36	91	64	54	37
090013007	102	70	61	40	89	68	60	42
090019003	106	66	58	39	91	70	61	41
090070007	104	62	53	37	86	63	54	40
090090027	90	61	54	37	77	61	53	39
090093002	**108**	64	56	40	88	64	55	41
340030006	N/A	N/A	N/A	N/A	84	71	63	46
340170006	92	69	64	60	91	71	64	60
340190001	94	54	45	38	88	59	49	39
340210005	101	59	50	36	87	63	53	39
340230011	100	59	50	37	86	64	53	39
340250005	94	58	51	37	87	65	55	39
340273001	94	51	42	38	87	56	46	40
340315001	86	53	45	37	83	60	50	37
360050110	89	74	**70**	**65**	76	70	66	60
360050133	87	70	66	54	82	72	65	54
360610135	N/A	N/A	N/A	N/A	80	**75**	**70**	**65**
360715001	97	49	41	35	88	54	45	36
360790005	91	53	46	35	87	59	50	37

360810124	88	65	58	44	85	70	61	46
360850067	95	61	55	45	90	66	59	47
361030002	98	65	58	40	90	71	61	43
361030004	102	61	53	40	84	61	54	42
361030009	104	65	58	41	**92**	70	61	44
361192004	104	64	56	37	87	67	57	38

The highest DV for each scenario is shown in **bold**. N/A values indicate that there was not enough ambient data to compute a design value for that monitor during a specific 3-year period.

Table 4D-14. Design values for the Philadelphia area regulatory monitors from observed data and for adjustments to meet the existing and potential alternative standards in 2006-2008 and 2008-2010.

	2006-2008					2008-2010				
Monitor	**obs**	**75 ppb**	**70 ppb**	**65 ppb**	**60 ppb**	**obs**	**75 ppb**	**70 ppb**	**65 ppb**	**60 ppb**
100031007	80	60	57	53	50	75	64	59	55	51
100031010	83	65	60	56	51	76	67	62	57	53
100031013	78	64	60	56	53	75	67	63	59	56
240150003	90	68	63	58	52	80	68	63	58	54
340010006	N/A	N/A	N/A	N/A	N/A	74	64	60	56	52
340070003	87	**75**	**70**	**65**	**60**	N/A	N/A	N/A	N/A	N/A
340071001	86	65	60	55	52	80	69	63	59	54
340110007	81	61	57	52	49	76	63	59	54	51
340150002	87	70	65	60	55	81	72	67	62	57
340290006	87	67	62	57	53	81	69	64	59	55
420170012	**92**	**75**	**70**	64	58	**83**	74	69	64	**60**
420290100	82	63	59	54	50	76	65	60	56	52
420450002	83	68	64	59	55	74	68	64	59	55
420910013	84	67	62	57	53	78	71	66	61	56
421010004	67	59	56	53	50	66	62	59	55	52
421010024	89	74	69	63	58	82	**75**	**70**	**65**	**60**

The highest DV for each scenario is shown in **bold**. N/A values indicate that there was not enough ambient data to compute a design value for that monitor during a specific 3-year period.

Table 4D-15. Design values for the Sacramento area regulatory monitors from observed data and for adjustments to meet the existing and potential alternative standards in 2006-2008 and 2008-2010.

Monitor	2006-2008					2008-2010				
	obs	75 ppb	70 ppb	65 ppb	60 ppb	obs	75 ppb	70 ppb	65 ppb	60 ppb
060170010	96	71	66	63	56	90	67	63	59	54
060170012	76	66	64	63	60	71	61	60	59	57
060170013	70	61	59	58	57	N/A	N/A	N/A	N/A	N/A
060170020	98	74	69	64	58	89	68	64	60	55
060570005	91	69	66	62	57	84	63	60	57	53
060570007	87	66	63	60	56	81	63	59	57	54
060571001	70	61	59	58	57	N/A	N/A	N/A	N/A	N/A
060610002	90	69	65	61	56	87	66	62	58	54
060610004	89	67	63	60	55	78	59	56	53	49
060610006	90	73	68	64	59	90	73	69	**65**	**60**
060670002	78	64	61	58	54	75	62	58	55	52
060670006	87	71	66	62	56	85	69	65	61	56
060670010	79	65	62	59	55	75	62	59	56	53
060670011	82	65	61	58	53	77	61	57	54	51
060670012	**99**	**75**	**70**	**65**	59	**99**	**75**	**70**	**65**	59
060670013	78	64	61	59	54	N/A	N/A	N/A	N/A	N/A
060670014	N/A	N/A	N/A	N/A	N/A	57	51	49	47	45
060675003	95	72	68	64	58	92	70	65	61	55
060950004	60	57	56	55	53	63	59	58	56	54
060950005	68	57	55	52	49	69	58	55	53	50
060953003	75	59	55	53	49	70	56	53	51	49
061010003	72	59	56	53	48	66	54	51	49	46
061010004	85	69	66	64	**61**	76	62	60	58	56
061130004	76	59	55	52	48	72	56	53	50	47
061131003	76	59	56	53	49	72	56	53	50	47

The highest DV for each scenario is shown in **bold**. N/A values indicate that there was not enough ambient data to compute a design value for that monitor during a specific 3-year period.

Table 4D-16. Design values for the Saint Louis area regulatory monitors from observed data and for adjustments to meet the existing and potential alternative standards in 2006-2008 and 2008-2010.

Monitor	2006-2008					2008-2010				
	obs	75 ppb	70 ppb	65 ppb	60 ppb	obs	75 ppb	70 ppb	65 ppb	60 ppb
170831001	73	61	57	52	48	69	67	62	57	52
171170002	70	58	54	50	46	66	64	60	55	51
171190008	76	67	62	57	52	71	70	67	61	56
171191009	78	67	62	57	52	72	70	66	61	56
171193007	77	68	63	57	52	68	67	63	59	53
171630010	72	65	60	55	51	68	67	64	59	55
290990019	N/A	N/A	N/A	N/A	N/A	72	70	67	62	56
291130003	81	67	62	56	51	72	70	65	60	55
291831002	N/A	N/A	N/A	N/A	N/A	**77**	**75**	**70**	**65**	59
291831004	N/A	N/A	N/A	N/A	N/A	74	72	66	61	54
291890004	78	71	66	60	55	N/A	N/A	N/A	N/A	N/A
291890005	76	65	60	55	50	65	64	59	55	51
291890014	**82**	73	68	62	57	71	70	66	62	57
295100085	N/A	N/A	N/A	N/A	N/A	68	68	69	65	**60**
295100086	81	**75**	**70**	**65**	**60**	N/A	N/A	N/A	N/A	N/A

The highest DV for each scenario is shown in **bold**. N/A values indicate that there was not enough ambient data to compute a design value for that monitor during a specific 3-year period.

Table 4D-17. Design values for the Washington D.C. area regulatory monitors from observed data and for adjustments to meet the existing and potential alternative standards in 2006-2008 and 2008-2010.

Monitor	2006-2008					2008-2010				
	obs	75 ppb	70 ppb	65 ppb	60 ppb	obs	75 ppb	70 ppb	65 ppb	60 ppb
110010025	80	62	58	53	48	75	68	60	55	49
110010041	86	73	69	64	59	77	74	69	**65**	**60**
110010043	**87**	**75**	**70**	**65**	**60**	79	**75**	**70**	**65**	**60**
240090011	79	61	57	54	49	77	69	61	56	49
240170010	82	63	59	55	50	75	68	61	56	50
240210037	82	65	61	56	52	75	69	63	58	52
240313001	84	68	63	59	54	74	68	63	59	53
240330030	83	68	64	60	54	79	74	67	62	55
240338003	**87**	65	60	56	52	77	70	62	57	51
510130020	85	70	66	62	56	79	74	68	63	57
510590005	79	61	58	54	50	67	62	57	53	50
510590018	86	68	64	60	56	73	68	62	58	52

The highest DV for each scenario is shown in **bold**.

510590030	85	69	64	60	55	**81**	**75**	68	63	55
510591005	83	68	64	59	54	68	65	60	57	54
510595001	83	66	61	57	52	66	62	58	54	51
510610002	70	54	51	48	45	65	59	53	50	45
510690010	72	55	52	49	46	68	61	55	51	46
511071005	82	62	58	53	49	75	68	60	56	50
511530009	78	58	54	49	46	70	61	55	51	46
511790001	81	60	56	52	48	70	63	57	53	48
515100009	81	65	61	56	53	74	68	61	56	51

4D-4.3 Distribution of Hourly O_3 Concentrations

Figure 4D-13 through Figure 4D-27 display diurnal boxplots of hourly O_3 concentrations at monitor locations in each urban area for observed air quality, air quality adjusted to meet the existing standard, and an example of air quality adjusted to meet a potential alternative standard (65 ppb), for 2006-2008 and 2008-2010. Note that these plots include data from multiple monitoring sites within each urban area so they generally encompass the overall distribution of O_3 at both the urban core sites and the downwind suburban sites. The hourly plots show similar patterns in most cities for which O_3 concentrations during daytime hours decrease from observed air quality (black) to air quality adjusted to meet the existing standard (red), and decrease further when adjusted to meet a potential alternative standard of 65 ppb (blue). These daytime decreases are generally seen most on high O_3 days represented by outlier dots. In some cities the mid-range O_3 days, represented by the 25^{th} – 75^{th} percentile boxes, remained fairly constant (Boston) and in other cities, mid-range O_3 days decreased (Atlanta). Although daytime O_3 decreases, concentrations during morning rush-hour generally increase. These increases are associated with VOC-limited and NO_x titration conditions near NO_x sources during rush-hour periods. Reducing NO_x under those conditions results in less O_3 titration and thus increases O_3 concentrations. Nighttime increases in O_3 are often seen to a lesser extent than morning rush-hour increases. These phenomena generally lead to a flattening of the diurnal O_3 pattern with smaller differences between daytime and nighttime concentrations as NO_x emissions are reduced. Cases that required more substantial NO_x cuts to reach 75 and 65 ppb standards generally have more pronounced patterns of decreases in daytime O_3 and increases in nighttime O_3 leading to a flatter diurnal O_3 pattern (e.g. Los Angeles in Figure 4D-22). Two cities, Houston and New York, do not follow this general pattern. In Houston (Figure 4D-21), mid-range O_3 values increase during daytime hours as the highest O_3 concentrations decrease. This pattern is consistent with NO_x-limited conditions on high O_3 days but VOC-limited conditions on mid-range O_3 days or potentially NO_x-limited conditions at high O_3 sites and VOC limited conditions at mid-range O_3 sites. Therefore NO_x reductions, which are applied on all days, increase O_3 on mid-range O_3

days. Note that mid-range O_3 days in Houston start out quite low (20-30 ppb) and increase modestly. The changes in O_3 from observed air quality to the existing standard in New York look similar to the trends shown for other cities, but the diurnal O_3 pattern for the 65 ppb potential alternative standard has some unrealistic features which were previously discussed in section 4D-4D-3.2.4 of this appendix. The steep NO_x cuts (~90%) applied to meet a 65 ppb standard in New York result in a very flat diurnal pattern for mid-range values (see boxes from Figure 4D-23) but the outliers represented by dots in Figure 4D-23 show an inverse diurnal pattern with lower O_3 concentrations during the day and higher values at night. This is a result of the modeled sensitivities showing that nighttime O_3 does not respond to NO_x emissions changes on high O_3 nights while daytime O_3 does respond to NO_x emission changes during those same days. Thus the daytime values drop substantially while the nighttime values show no change. These results are not seen when the sensitivities are applied for the more modest cuts (50-65%) to reach 75 ppb. The diurnal pattern in New York for the 65 ppb case for the highest days is clearly unrealistic as there is no chemical process expected to result in daytime values lower than values at night, rather it appears to be an artifact of applying this model-based methodology to extremely large emissions reductions in a location where relationships derived under 3 discrete conditions (base, 50% NO_x cut, 90% NO_x cut) cannot fully characterize sensitivities over the entire range of possible reductions. As discussed previously in section 4D-4D-3.2.4, the use of the lower bound from the 95^{th} percentile confidence interval can mitigate some of this behavior, but in the case of New York some unrealistic outliers still remain. It should be noted, however that this unrealistic diurnal pattern is only seen in the outlier points, and is not seen the box and whiskers which represent 1.5 times the interquartile range (most of the data).

Figure 4D-28 through Figure 4D-42 display the same information as Figure 4D-13 through Figure 4D-27 but for monthly rather than hourly distributions. Note that missing months in these plots indicate that there was no monitor data available for those months and years. Similar to the diurnal plots, the seasonal distributions become flatter when meeting 75 and 65 ppb standard levels especially for the highest O_3 days. This is due to more O_3 decreases during summer months and more O_3 increases in winter months. The O_3 increases in the winter are consistent with the understanding that solar insolation rates are lower in the winter reducing total photochemical activity and shifting the net effect of NO_x emissions on O_3 which can both create O_3 through photochemical pathways and destroy O_3 through titration. In addition, the decreases on the highest O_3 days and increases on the lowest O_3 days show a visible compression of the O_3 distribution in these plots similar to what was seen in the diurnal plots. The changes for mid-range O_3 days also show a pattern of shifting higher mid-range O_3 earlier in the year. While in most cities, the highest interquartile O_3 concentrations in the recent conditions occur in the

summer months (June-August), in many areas the highest interquartile O_3 concentrations shift to spring months (April-May) for the adjustment scenarios of meeting 75 and 65 ppb standard levels. This pattern can be seen most dramatically in Atlanta, Baltimore, Boston, Denver, Los Angeles, New York, Philadelphia, Sacramento, and Washington D.C. This pattern is consistent with higher contribution from non-U.S. anthropogenic sources at lower standard levels than under recent observed conditions. Many of these non-U.S. anthropogenic sources such as stratospheric intrusions and international transport have been shown to peak during spring months as discussed in the Integrated Science Assessment (EPA, 2013).

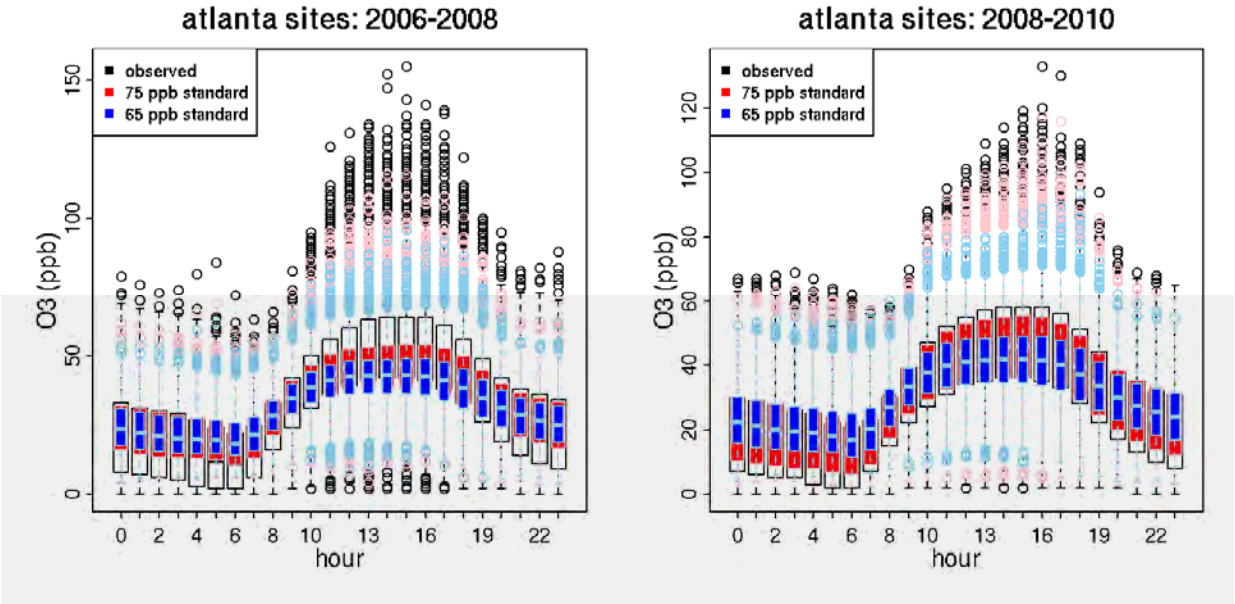

Figure 4D-13. Hourly O_3 distributions at Atlanta area regulatory monitoring sites for observed air quality, and air quality adjusted to meet the existing (75 ppb) and alternative (65 ppb) standards for 2006-2008 (left) and 2008-2010 (right). White boxes (black whiskers/dots) show the observed distribution of hourly O_3 concentrations, red boxes (pink whiskers/dots) show the predicted distribution of hourly O_3 concentrations for the 75 ppb adjustment scenarios and blue boxes (light blue whiskers/dots) show the predicted distribution of hourly O_3 concentrations for the 65 ppb adjustment scenario. Boxes show the interquartile range, whiskers extend to 1.5 × the interquartile range and dots depict outlier values.

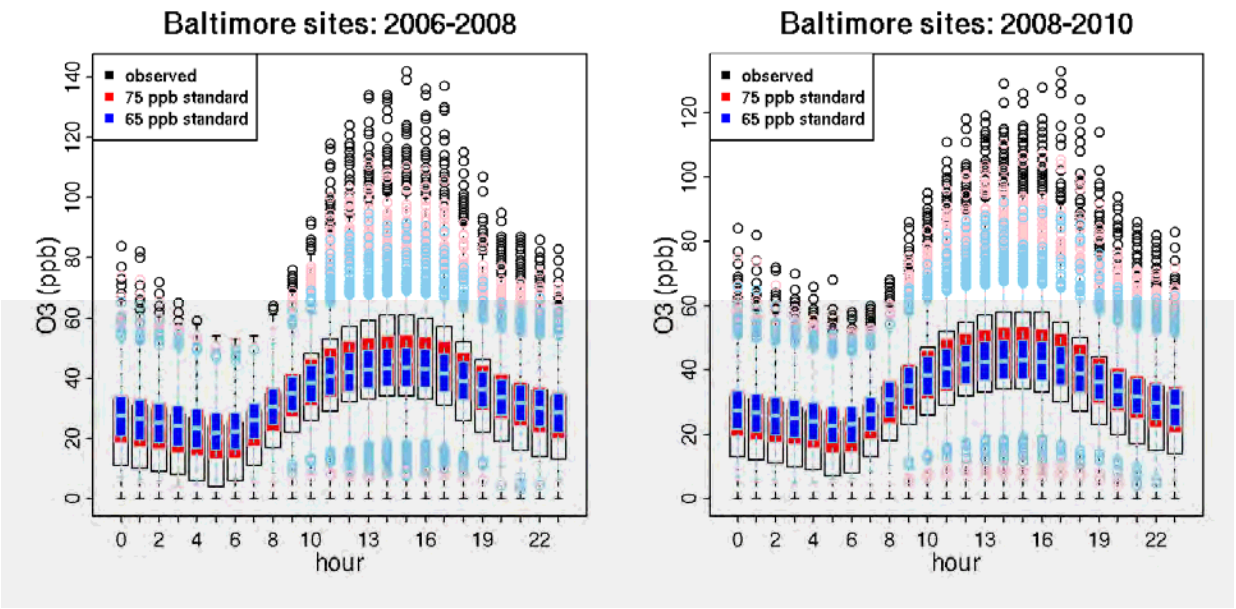

Figure 4D-14. Hourly O_3 distributions at Baltimore area regulatory monitoring sites for observed air quality, and air quality adjusted to meet the existing (75 ppb) and alternative (65 ppb) standards for 2006-2008 (left) and 2008-2010 (right). White boxes (black whiskers/dots) show the observed distribution of hourly O_3 concentrations, red boxes (pink whiskers/dots) show the predicted distribution of hourly O_3 concentrations for the 75 ppb adjustment scenarios and blue boxes (light blue whiskers/dots) show the predicted distribution of hourly O_3 concentrations for the 65 ppb adjustment scenario. Boxes show the interquartile range, whiskers extend to 1.5 × the interquartile range and dots depict outlier values.

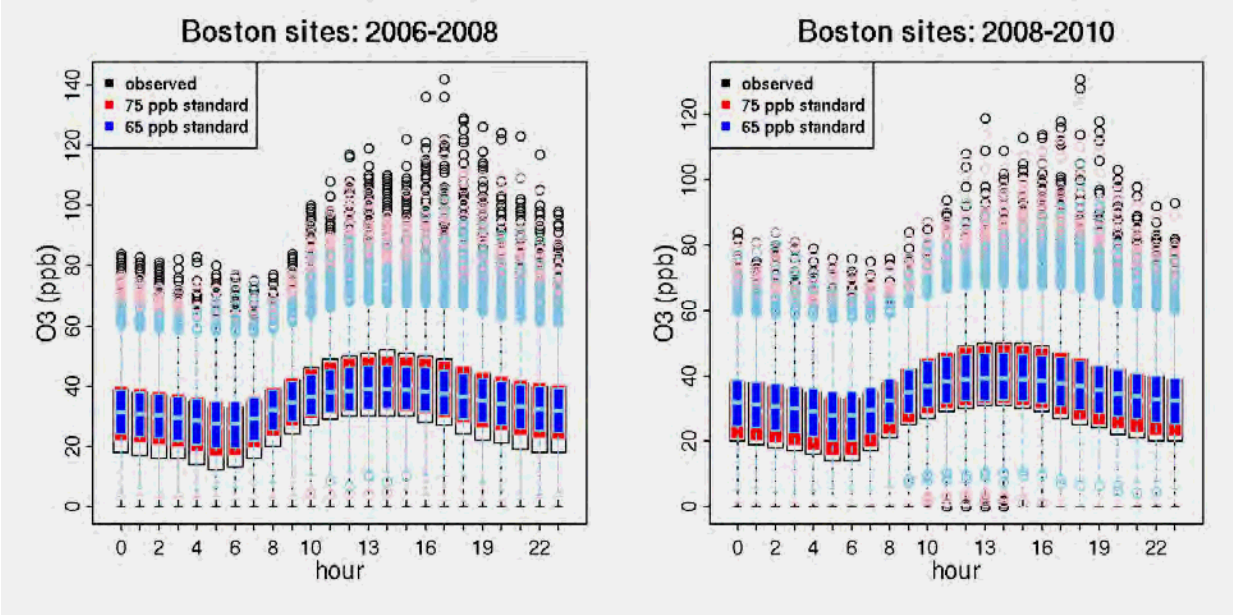

Figure 4D-15. Hourly O_3 distributions at Boston area regulatory monitoring sites for observed air quality, and air quality adjusted to meet the existing (75 ppb) and alternative (65 ppb) standards for 2006-2008 (left) and 2008-2010 (right). White boxes (black whiskers/dots) show the observed distribution of hourly O_3 concentrations, red boxes (pink whiskers/dots) show the predicted distribution of hourly O_3 concentrations for the 75 ppb adjustment scenarios and blue boxes (light blue whiskers/dots) show the predicted distribution of hourly O_3 concentrations for the 65 ppb adjustment scenario. Boxes show the interquartile range, whiskers extend to 1.5 × the interquartile range and dots depict outlier values.

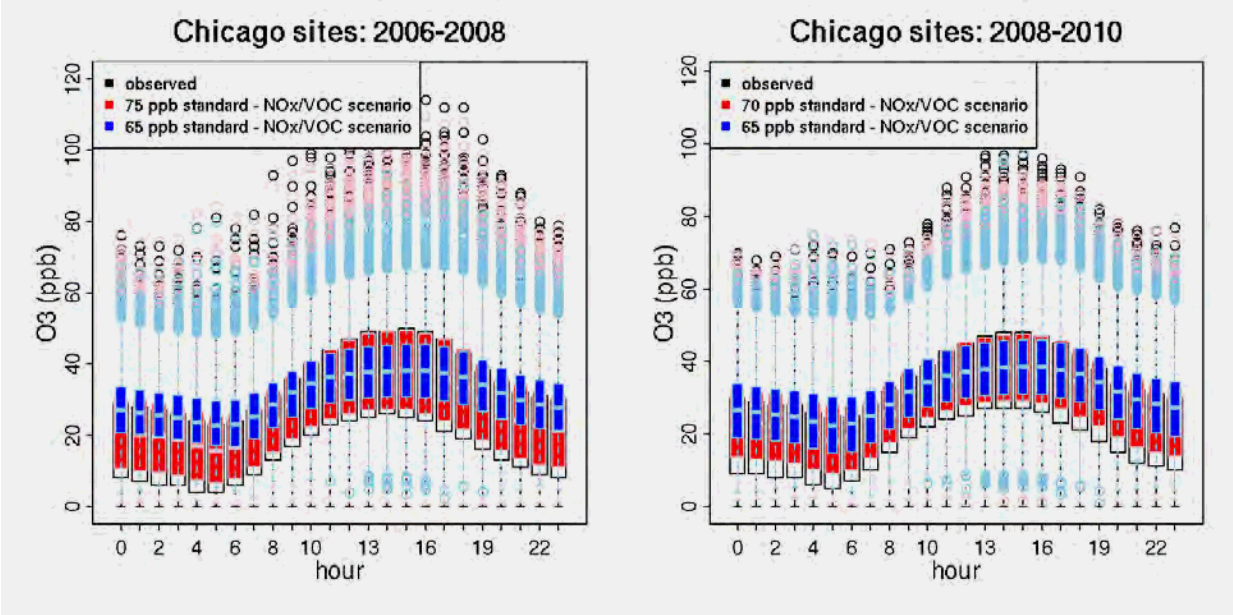

Figure 4D-16. Hourly O_3 distributions at Chicago area regulatory monitoring sites for observed air quality, and air quality adjusted to meet the existing (75 ppb) and alternative (65 ppb) standards for 2006-2008 (left) and 2008-2010 (right). White boxes (black whiskers/dots) show the observed distribution of hourly O_3 concentrations, red boxes (pink whiskers/dots) show the predicted distribution of hourly O_3 concentrations for the 75 ppb adjustment scenarios and blue boxes (light blue whiskers/dots) show the predicted distribution of hourly O_3 concentrations for the 65 ppb adjustment scenario. Boxes show the interquartile range, whiskers extend to 1.5 × the interquartile range and dots depict outlier values.

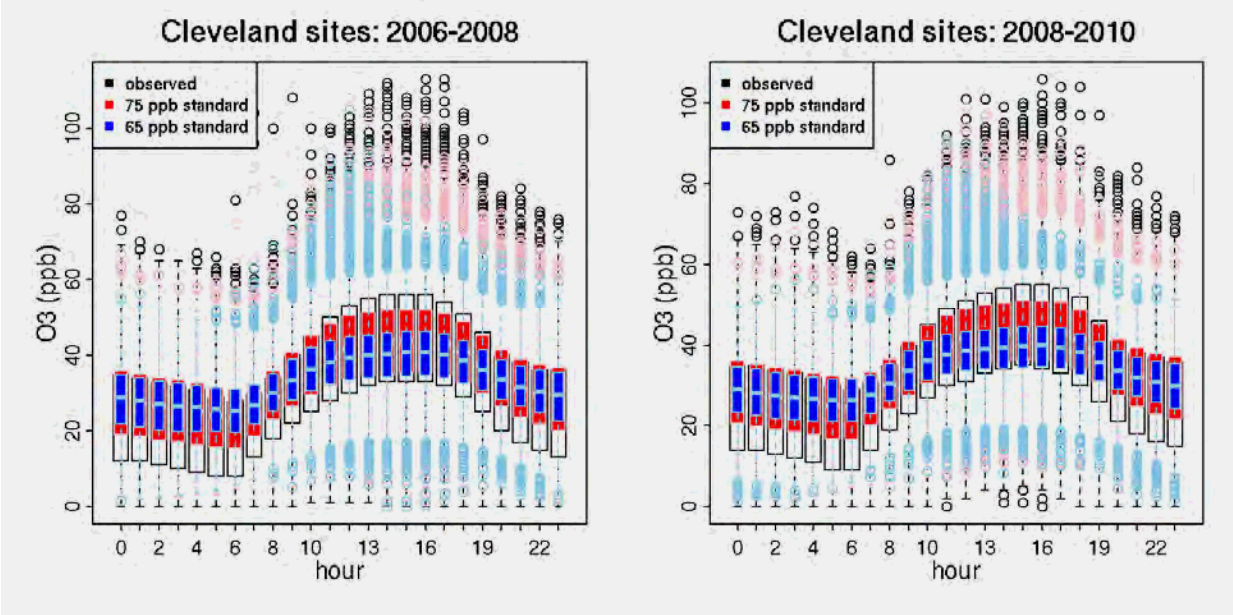

Figure 4D-17. Hourly O_3 distributions at Cleveland area regulatory monitoring sites for observed air quality, and air quality adjusted to meet the existing (75 ppb) and alternative (65 ppb) standards for 2006-2008 (left) and 2008-2010 (right). White boxes (black whiskers/dots) show the observed distribution of hourly O_3 concentrations, red boxes (pink whiskers/dots) show the predicted distribution of hourly O_3 concentrations for the 75 ppb adjustment scenarios and blue boxes (light blue whiskers/dots) show the predicted distribution of hourly O_3 concentrations for the 65 ppb adjustment scenario. Boxes show the interquartile range, whiskers extend to 1.5 × the interquartile range and dots depict outlier values.

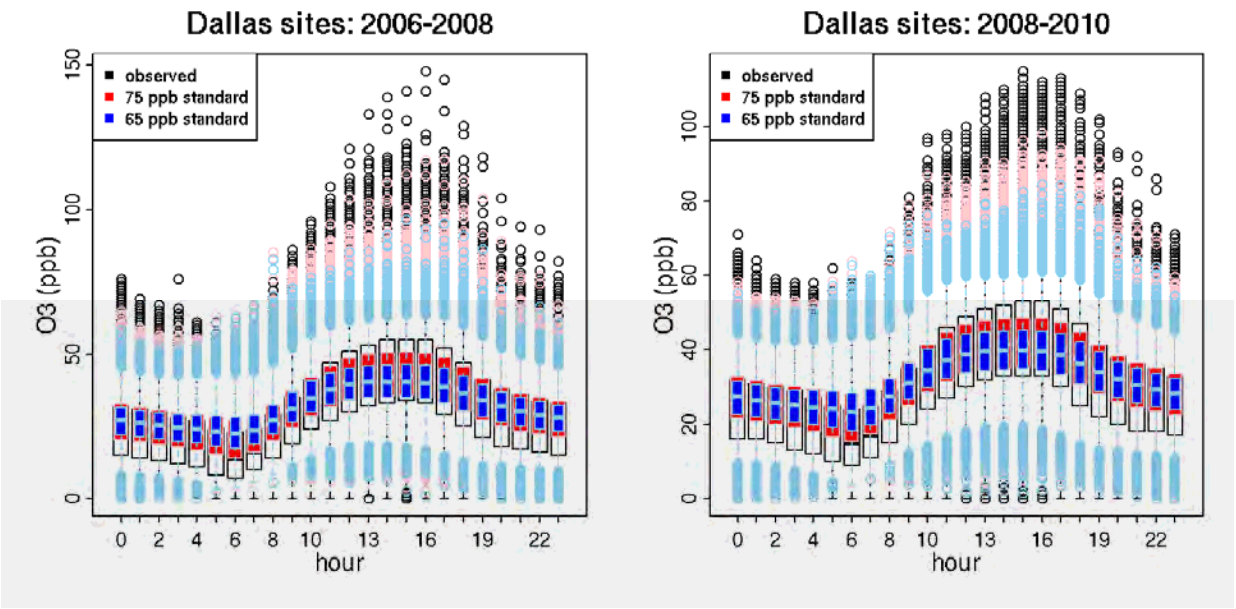

Figure 4D-18. Hourly O_3 distributions at Dallas area regulatory monitoring sites for observed air quality, and air quality adjusted to meet the existing (75 ppb) and alternative (65 ppb) standards for 2006-2008 (left) and 2008-2010 (right). White boxes (black whiskers/dots) show the observed distribution of hourly O_3 concentrations, red boxes (pink whiskers/dots) show the predicted distribution of hourly O_3 concentrations for the 75 ppb adjustment scenarios and blue boxes (light blue whiskers/dots) show the predicted distribution of hourly O_3 concentrations for the 65 ppb adjustment scenario. Boxes show the interquartile range, whiskers extend to 1.5 × the interquartile range and dots depict outlier values.

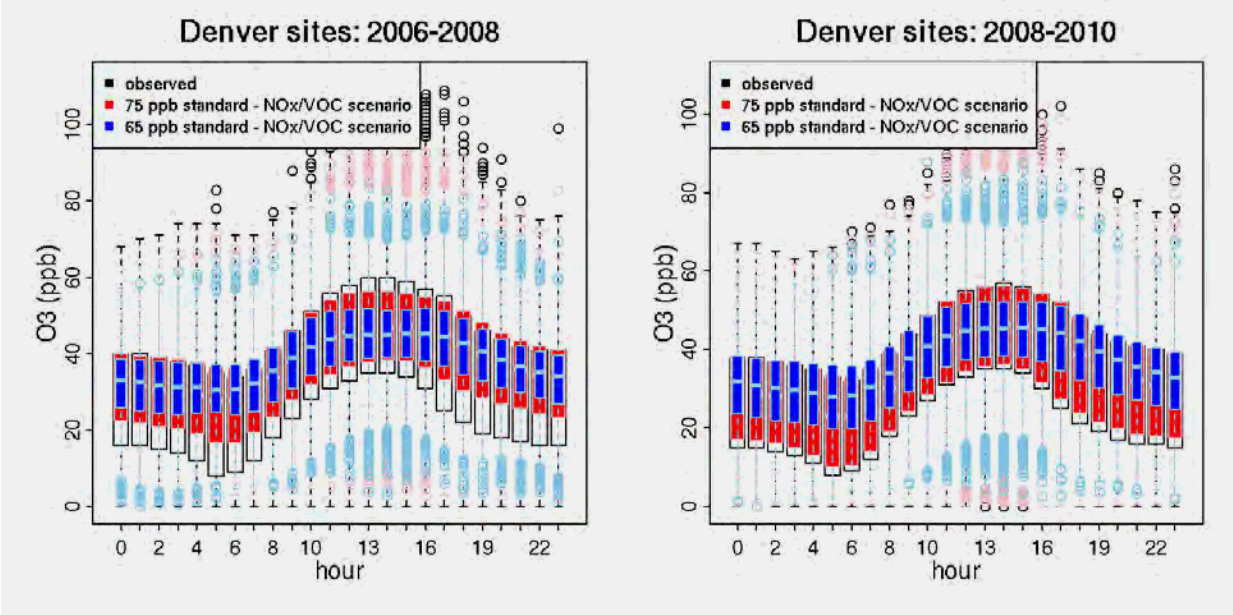

Figure 4D-19. Hourly O_3 distributions at Denver area regulatory monitoring sites for observed air quality, and air quality adjusted to meet the existing (75 ppb) and alternative (65 ppb) standards for 2006-2008 (left) and 2008-2010 (right). White boxes (black whiskers/dots) show the observed distribution of hourly O_3 concentrations, red boxes (pink whiskers/dots) show the predicted distribution of hourly O_3 concentrations for the 75 ppb adjustment scenarios and blue boxes (light blue whiskers/dots) show the predicted distribution of hourly O_3 concentrations for the 65 ppb adjustment scenario. Boxes show the interquartile range, whiskers extend to 1.5 × the interquartile range and dots depict outlier values.

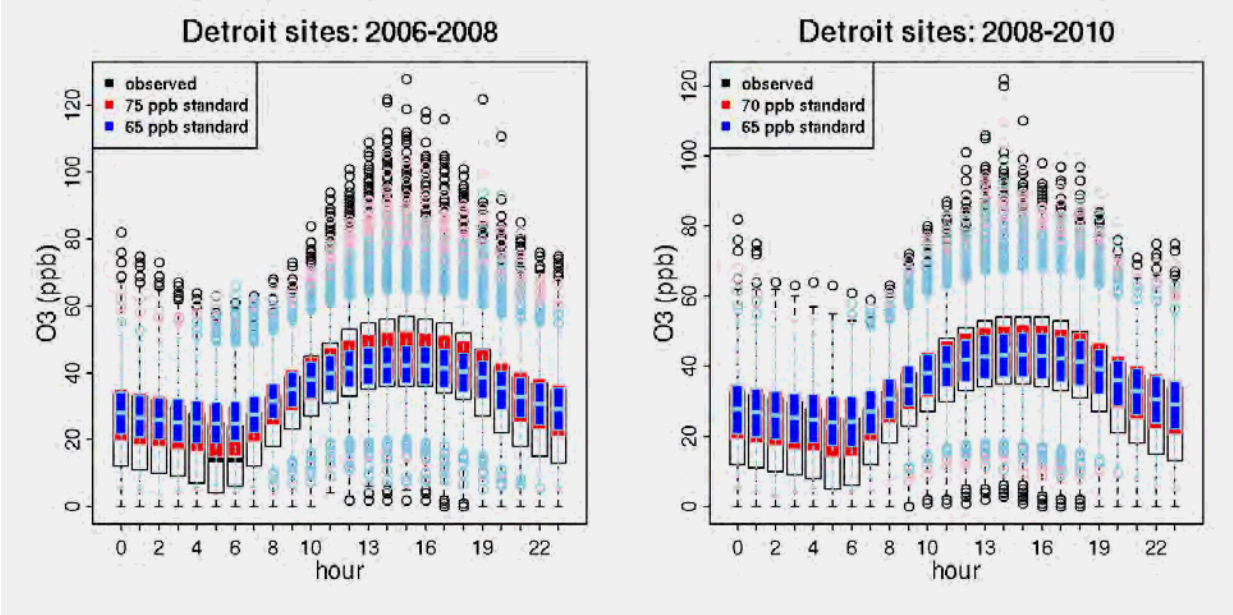

Figure 4D-20. Hourly O_3 distributions at Detroit area regulatory monitoring sites for observed air quality, and air quality adjusted to meet the existing (75 ppb) and alternative (65 ppb) standards for 2006-2008 (left) and 2008-2010 (right). White boxes (black whiskers/dots) show the observed distribution of hourly O_3 concentrations, red boxes (pink whiskers/dots) show the predicted distribution of hourly O_3 concentrations for the 75 ppb adjustment scenarios and blue boxes (light blue whiskers/dots) show the predicted distribution of hourly O_3 concentrations for the 65 ppb adjustment scenario. Boxes show the interquartile range, whiskers extend to 1.5 × the interquartile range and dots depict outlier values.

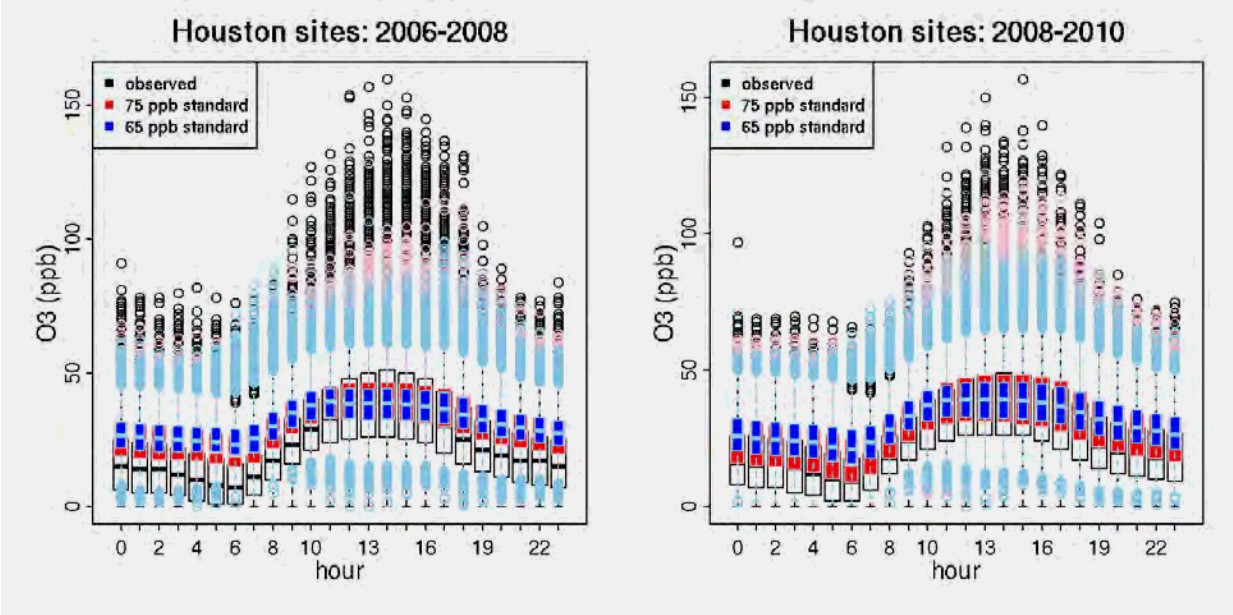

Figure 4D-21. Hourly O_3 distributions at Houston area regulatory monitoring sites for observed air quality, and air quality adjusted to meet the existing (75 ppb) and alternative (65 ppb) standards for 2006-2008 (left) and 2008-2010 (right). White boxes (black whiskers/dots) show the observed distribution of hourly O_3 concentrations, red boxes (pink whiskers/dots) show the predicted distribution of hourly O_3 concentrations for the 75 ppb adjustment scenarios and blue boxes (light blue whiskers/dots) show the predicted distribution of hourly O_3 concentrations for the 65 ppb adjustment scenario. Boxes show the interquartile range, whiskers extend to 1.5 × the interquartile range and dots depict outlier values.

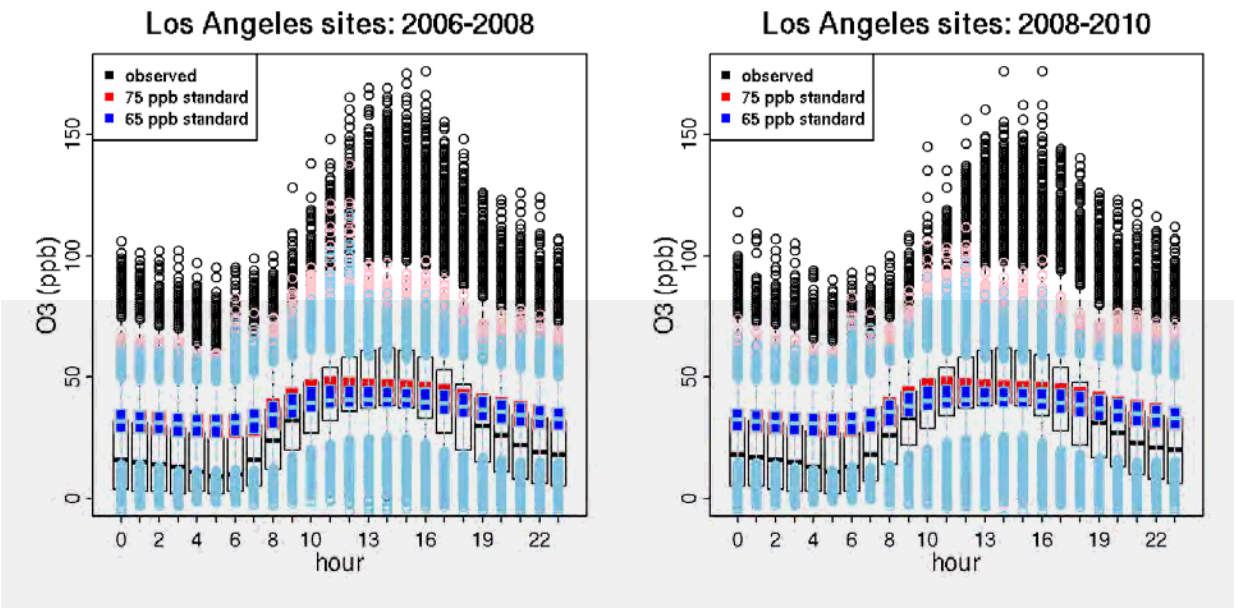

Figure 4D-22. Hourly O_3 distributions at Los Angeles area regulatory monitoring sites for observed air quality, and air quality adjusted to meet the existing (75 ppb) and alternative (65 ppb) standards for 2006-2008 (left) and 2008-2010 (right). White boxes (black whiskers/dots) show the observed distribution of hourly O_3 concentrations, red boxes (pink whiskers/dots) show the predicted distribution of hourly O_3 concentrations for the 75 ppb adjustment scenarios and blue boxes (light blue whiskers/dots) show the predicted distribution of hourly O_3 concentrations for the 65 ppb adjustment scenario. Boxes show the interquartile range, whiskers extend to 1.5 × the interquartile range and dots depict outlier values.

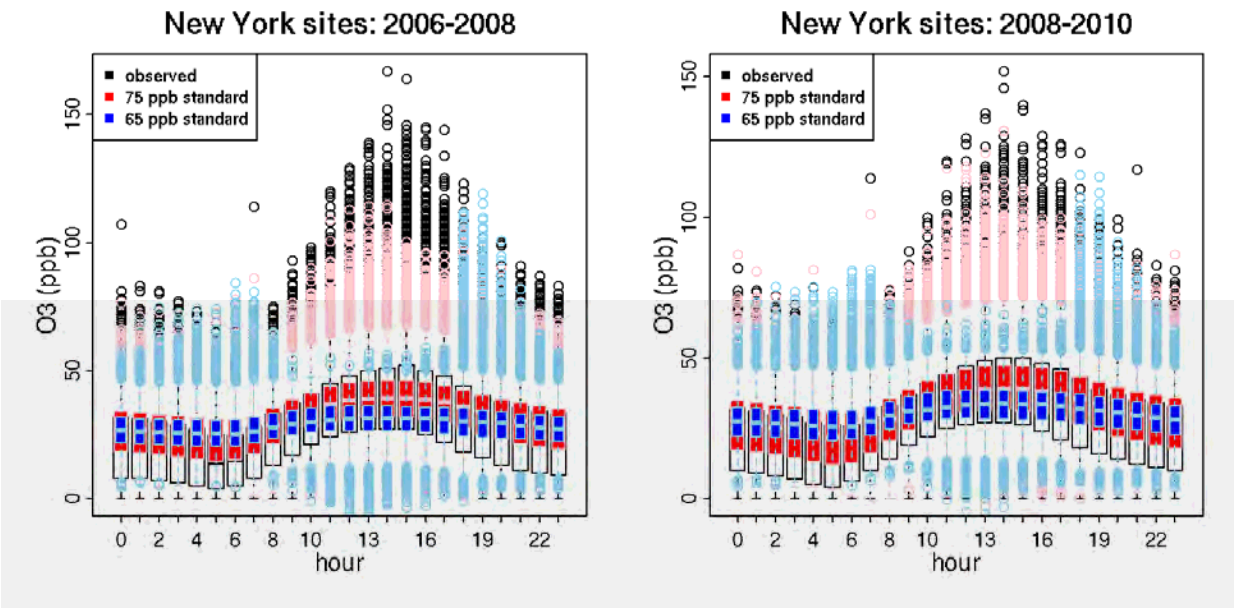

Figure 4D-23. Hourly O_3 distributions at New York area regulatory monitoring sites for observed air quality, and air quality adjusted to meet the existing (75 ppb) and alternative (65 ppb) standards for 2006-2008 (left) and 2008-2010 (right). White boxes (black whiskers/dots) show the observed distribution of hourly O_3 concentrations, red boxes (pink whiskers/dots) show the predicted distribution of hourly O_3 concentrations for the 75 ppb adjustment scenarios and blue boxes (light blue whiskers/dots) show the predicted distribution of hourly O_3 concentrations for the 65 ppb adjustment scenario. Boxes show the interquartile range, whiskers extend to 1.5 × the interquartile range and dots depict outlier values.

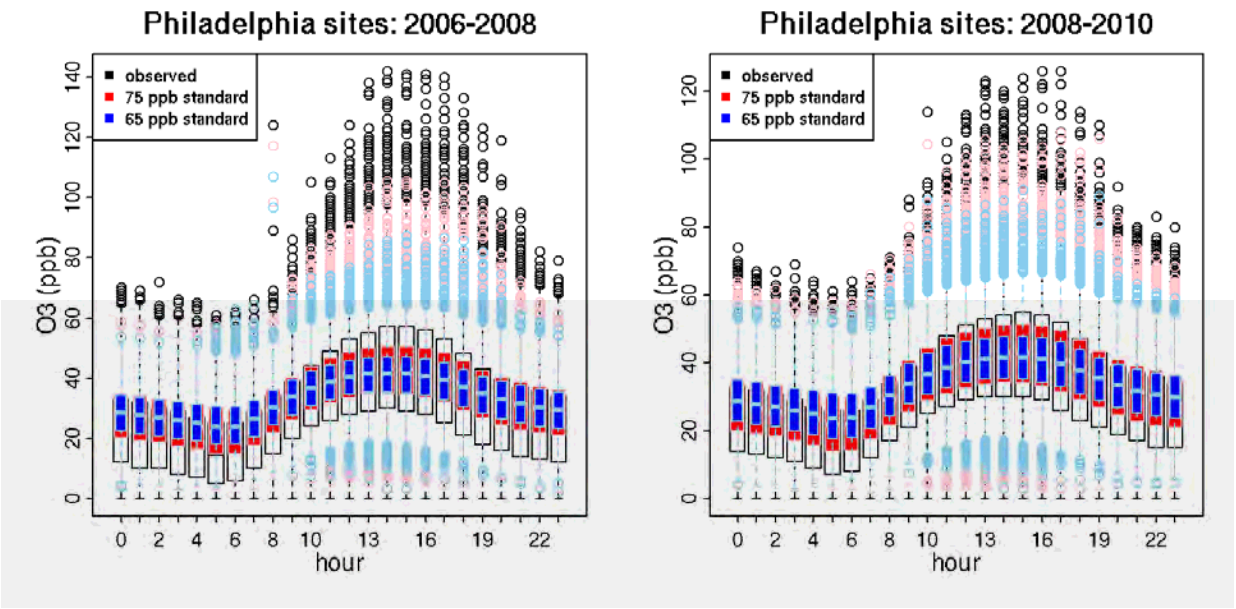

Figure 4D-24. Hourly O_3 distributions at Philadelphia area regulatory monitoring sites for observed air quality, and air quality adjusted to meet the existing (75 ppb) and alternative (65 ppb) standards for 2006-2008 (left) and 2008-2010 (right). White boxes (black whiskers/dots) show the observed distribution of hourly O_3 concentrations, red boxes (pink whiskers/dots) show the predicted distribution of hourly O_3 concentrations for the 75 ppb adjustment scenarios and blue boxes (light blue whiskers/dots) show the predicted distribution of hourly O_3 concentrations for the 65 ppb adjustment scenario. Boxes show the interquartile range, whiskers extend to 1.5 × the interquartile range and dots depict outlier values.

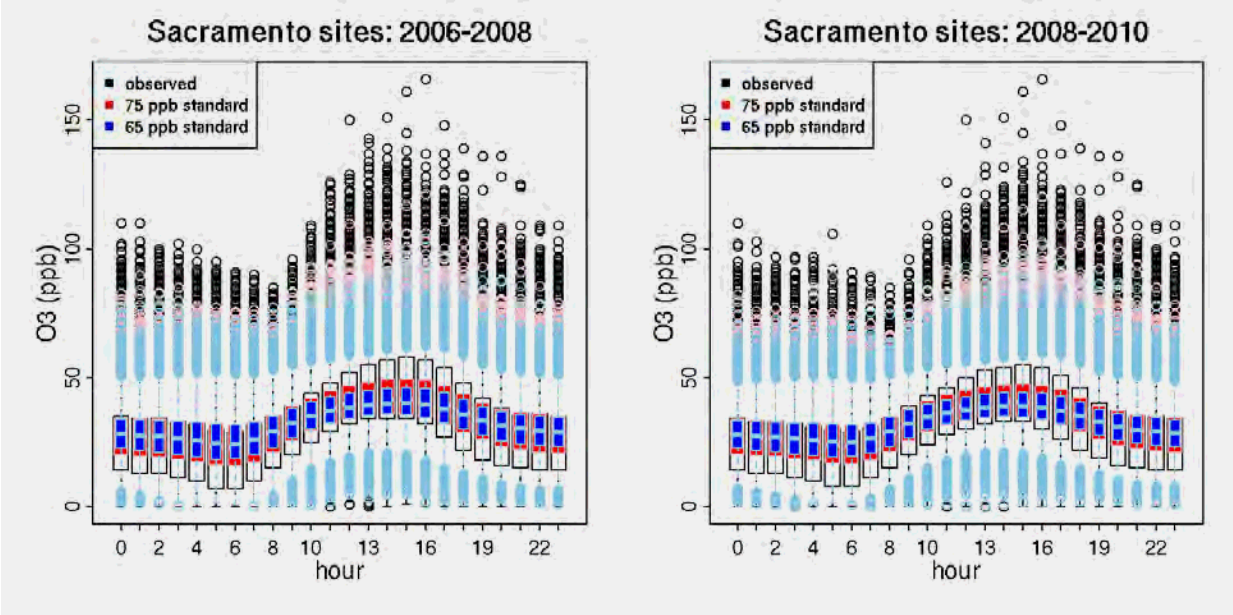

Figure 4D-25. Hourly O_3 distributions at Sacramento area regulatory monitoring sites for observed air quality, and air quality adjusted to meet the existing (75 ppb) and alternative (65 ppb) standards for 2006-2008 (left) and 2008-2010 (right). White boxes (black whiskers/dots) show the observed distribution of hourly O_3 concentrations, red boxes (pink whiskers/dots) show the predicted distribution of hourly O_3 concentrations for the 75 ppb adjustment scenarios and blue boxes (light blue whiskers/dots) show the predicted distribution of hourly O_3 concentrations for the 65 ppb adjustment scenario. Boxes show the interquartile range, whiskers extend to 1.5 × the interquartile range and dots depict outlier values.

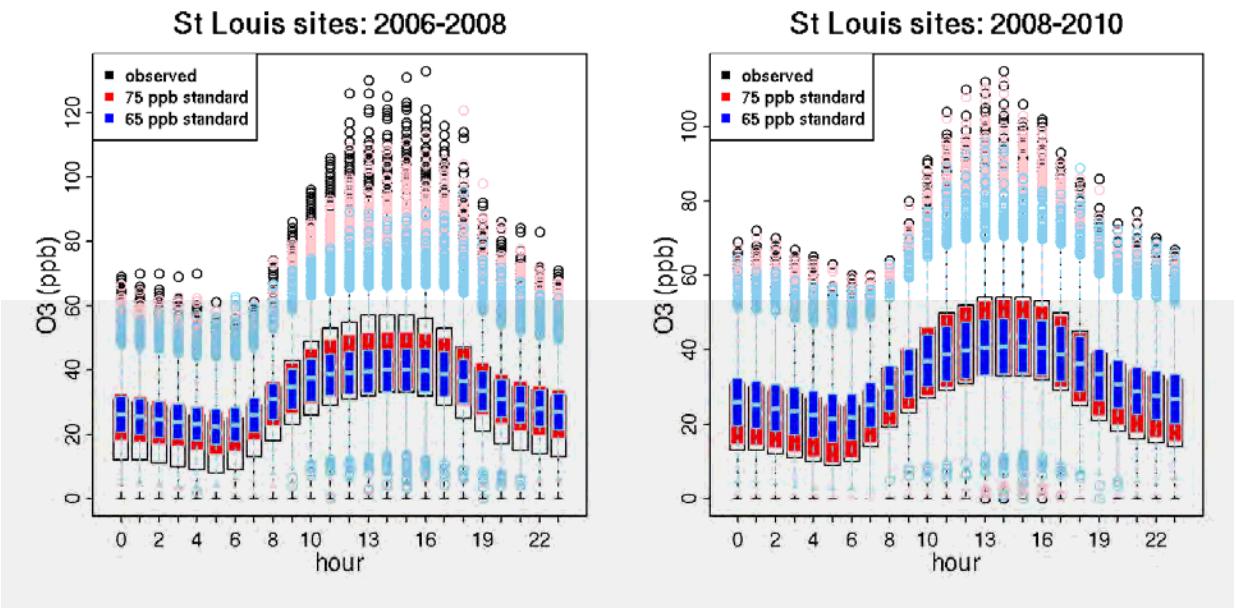

Figure 4D-26. Hourly O_3 distributions at St. Louis area regulatory monitoring sites for observed air quality, and air quality adjusted to meet the existing (75 ppb) and alternative (65 ppb) standards for 2006-2008 (left) and 2008-2010 (right). White boxes (black whiskers/dots) show the observed distribution of hourly O_3 concentrations, red boxes (pink whiskers/dots) show the predicted distribution of hourly O_3 concentrations for the 75 ppb adjustment scenarios and blue boxes (light blue whiskers/dots) show the predicted distribution of hourly O_3 concentrations for the 65 ppb adjustment scenario. Boxes show the interquartile range, whiskers extend to 1.5 × the interquartile range and dots depict outlier values.

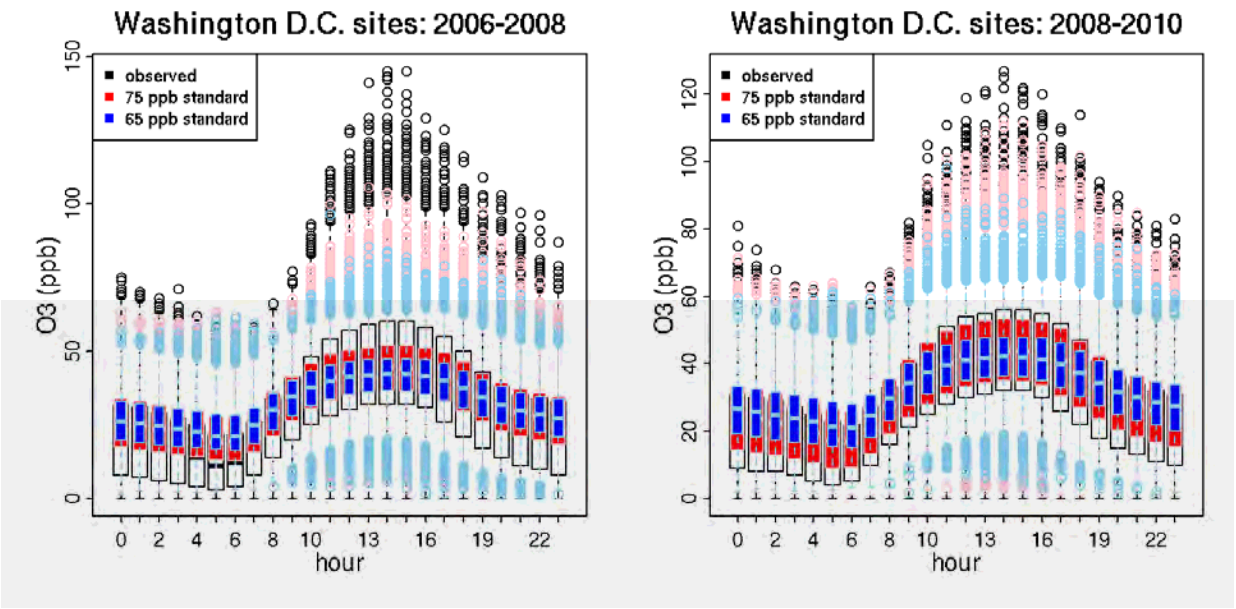

Figure 4D-27. Hourly O_3 distributions at Washington, D.C. area regulatory monitoring sites for observed air quality, and air quality adjusted to meet the existing (75 ppb) and alternative (65 ppb) standards for 2006-2008 (left) and 2008-2010 (right). White boxes (black whiskers/dots) show the observed distribution of hourly O_3 concentrations, red boxes (pink whiskers/dots) show the predicted distribution of hourly O_3 concentrations for the 75 ppb adjustment scenarios and blue boxes (light blue whiskers/dots) show the predicted distribution of hourly O_3 concentrations for the 65 ppb adjustment scenario. Boxes show the interquartile range, whiskers extend to 1.5 × the interquartile range and dots depict outlier values.

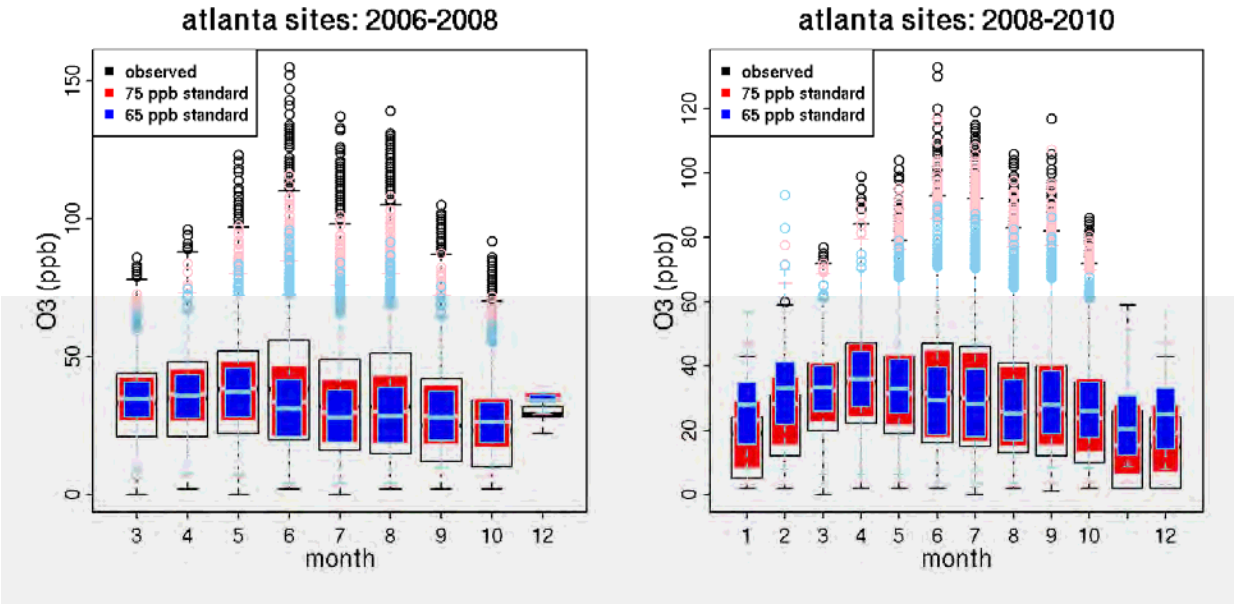

Figure 4D-28. Monthly O_3 distributions at Atlanta area regulatory monitoring sites for observed air quality, and air quality adjusted to meet the existing (75 ppb) and alternative (65 ppb) standards for 2006-2008 (left) and 2008-2010 (right). White boxes (black whiskers/dots) show the observed distribution of hourly O_3 concentrations, red boxes (pink whiskers/dots) show the predicted distribution of hourly O_3 concentrations for the 75 ppb adjustment scenarios and blue boxes (light blue whiskers/dots) show the predicted distribution of hourly O_3 concentrations for the 65 ppb adjustment scenario. Boxes show the interquartile range, whiskers extend to 1.5 × the interquartile range and dots depict outlier values.

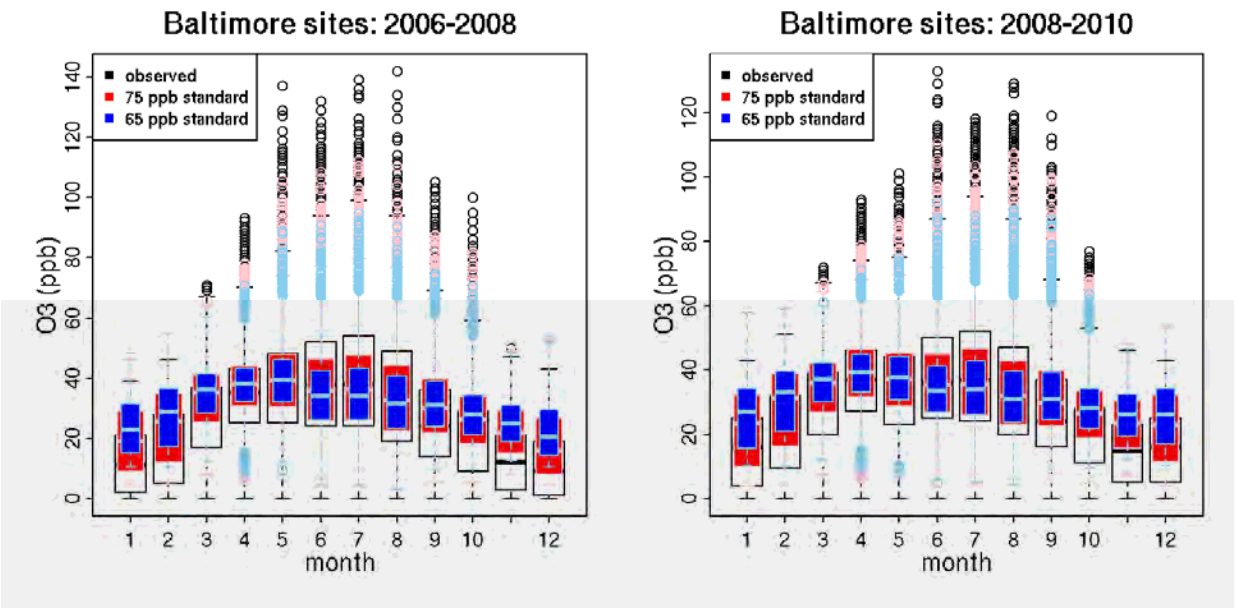

Figure 4D-29. Monthly O_3 distributions at Baltimore area regulatory monitoring sites for observed air quality, and air quality adjusted to meet the existing (75 ppb) and alternative (65 ppb) standards for 2006-2008 (left) and 2008-2010 (right). White boxes (black whiskers/dots) show the observed distribution of hourly O_3 concentrations, red boxes (pink whiskers/dots) show the predicted distribution of hourly O_3 concentrations for the 75 ppb adjustment scenarios and blue boxes (light blue whiskers/dots) show the predicted distribution of hourly O_3 concentrations for the 65 ppb adjustment scenario. Boxes show the interquartile range, whiskers extend to 1.5 × the interquartile range and dots depict outlier values.

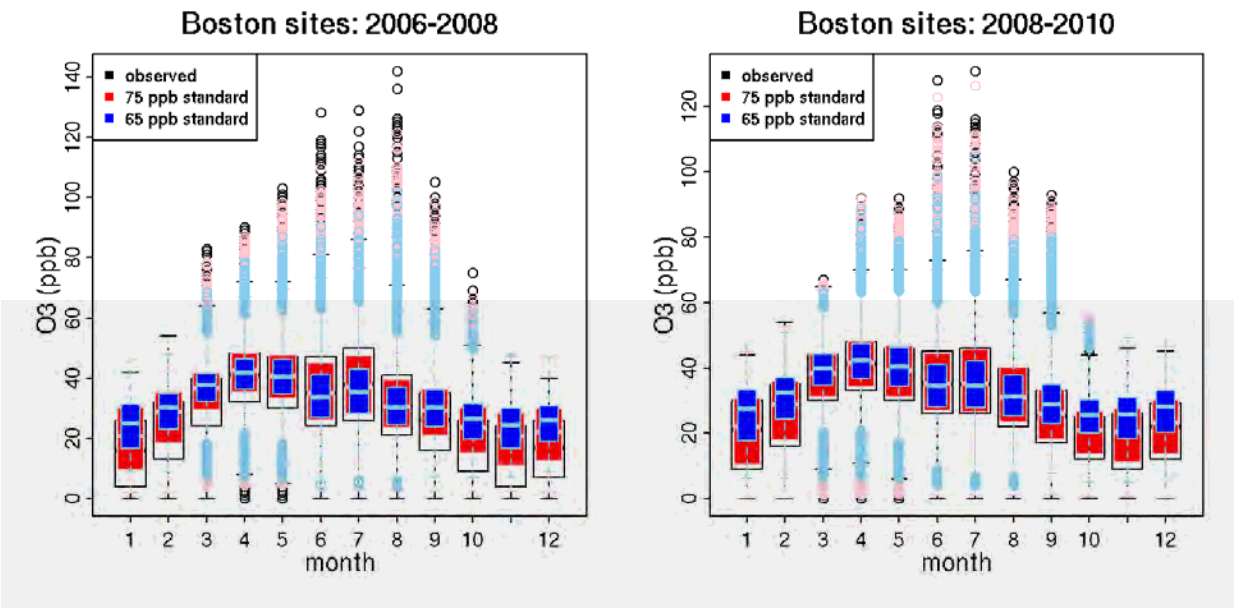

Figure 4D-30. Monthly O_3 distributions at Boston area regulatory monitoring sites for observed air quality, and air quality adjusted to meet the existing (75 ppb) and alternative (65 ppb) standards for 2006-2008 (left) and 2008-2010 (right). White boxes (black whiskers/dots) show the observed distribution of hourly O_3 concentrations, red boxes (pink whiskers/dots) show the predicted distribution of hourly O_3 concentrations for the 75 ppb adjustment scenarios and blue boxes (light blue whiskers/dots) show the predicted distribution of hourly O_3 concentrations for the 65 ppb adjustment scenario. Boxes show the interquartile range, whiskers extend to 1.5 × the interquartile range and dots depict outlier values.

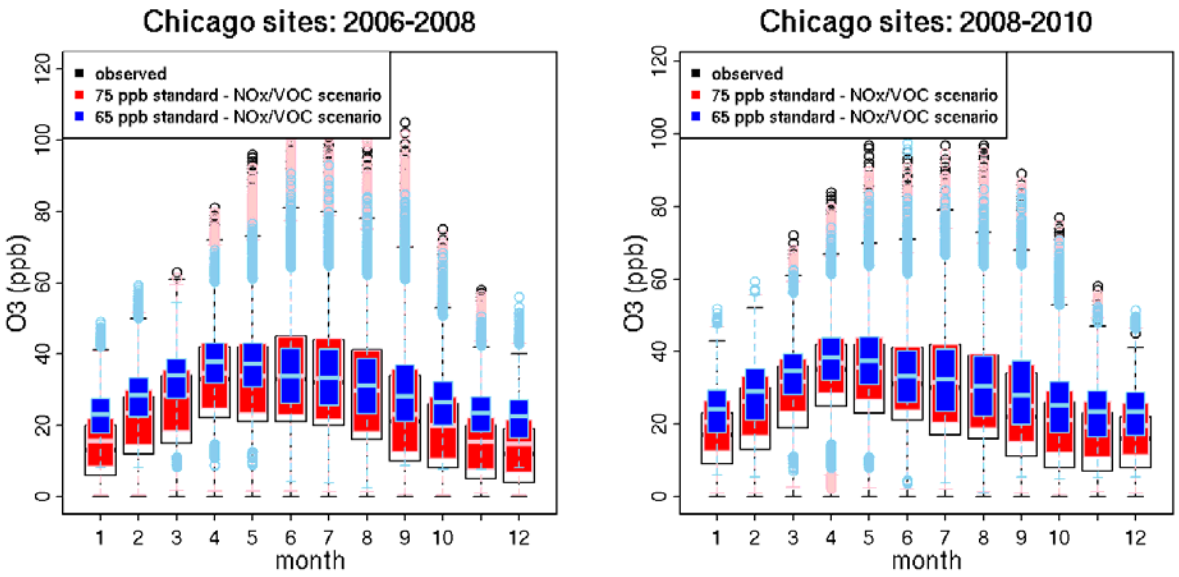

Figure 4D-31. Monthly O_3 distributions at Chicago area regulatory monitoring sites for observed air quality, and air quality adjusted to meet the existing (75 ppb) and alternative (65 ppb) standards for 2006-2008 (left) and 2008-2010 (right). White boxes (black whiskers/dots) show the observed distribution of hourly O_3 concentrations, red boxes (pink whiskers/dots) show the predicted distribution of hourly O_3 concentrations for the 75 ppb adjustment scenarios and blue boxes (light blue whiskers/dots) show the predicted distribution of hourly O_3 concentrations for the 65 ppb adjustment scenario. Boxes show the interquartile range, whiskers extend to 1.5 × the interquartile range and dots depict outlier values.

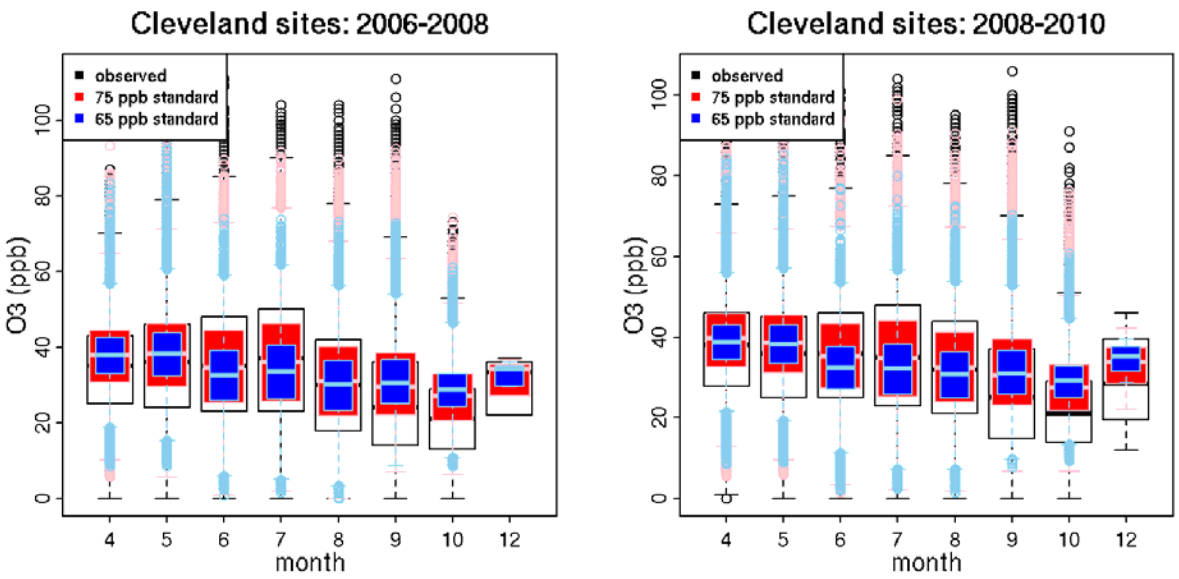

Figure 4D-32. Monthly O_3 distributions at Cleveland area regulatory monitoring sites for observed air quality, and air quality adjusted to meet the existing (75 ppb) and alternative (65 ppb) standards for 2006-2008 (left) and 2008-2010 (right). White boxes (black whiskers/dots) show the observed distribution of hourly O_3 concentrations, red boxes (pink whiskers/dots) show the predicted distribution of hourly O_3 concentrations for the 75 ppb adjustment scenarios and blue boxes (light blue whiskers/dots) show the predicted distribution of hourly O_3 concentrations for the 65 ppb adjustment scenario. Boxes show the interquartile range, whiskers extend to 1.5 × the interquartile range and dots depict outlier values.

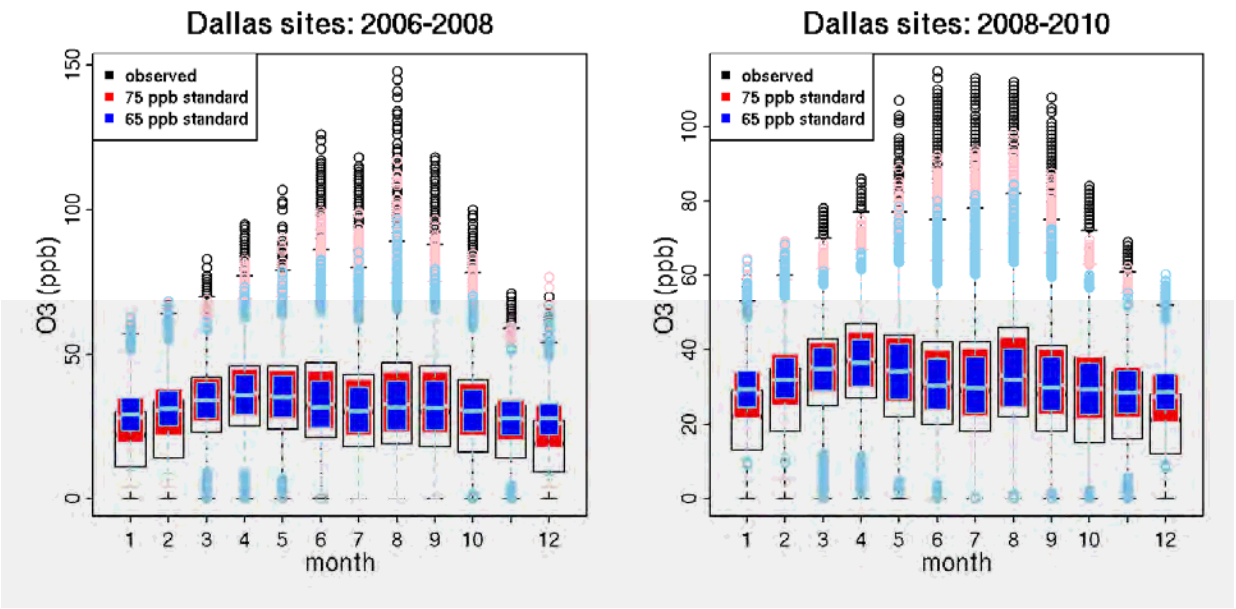

Figure 4D-33. Monthly O_3 distributions at Dallas area regulatory monitoring sites for observed air quality, and air quality adjusted to meet the existing (75 ppb) and alternative (65 ppb) standards for 2006-2008 (left) and 2008-2010 (right). White boxes (black whiskers/dots) show the observed distribution of hourly O_3 concentrations, red boxes (pink whiskers/dots) show the predicted distribution of hourly O_3 concentrations for the 75 ppb adjustment scenarios and blue boxes (light blue whiskers/dots) show the predicted distribution of hourly O_3 concentrations for the 65 ppb adjustment scenario. Boxes show the interquartile range, whiskers extend to 1.5 × the interquartile range and dots depict outlier values.

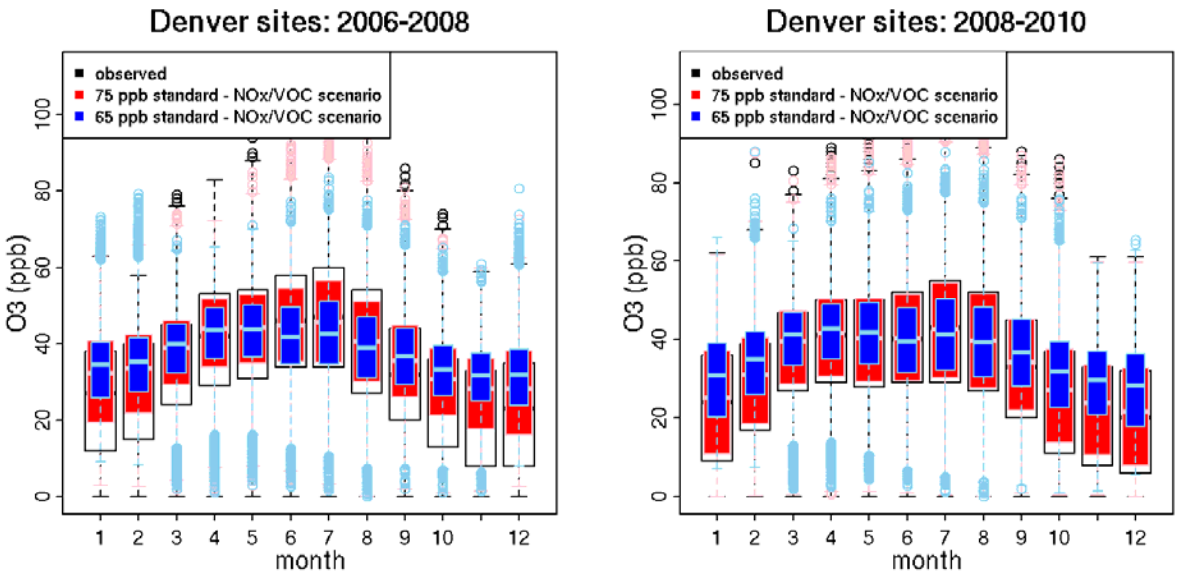

Figure 4D-34. Monthly O_3 distributions at Denver area regulatory monitoring sites for observed air quality, and air quality adjusted to meet the existing (75 ppb) and alternative (65 ppb) standards for 2006-2008 (left) and 2008-2010 (right). White boxes (black whiskers/dots) show the observed distribution of hourly O_3 concentrations, red boxes (pink whiskers/dots) show the predicted distribution of hourly O_3 concentrations for the 75 ppb adjustment scenarios and blue boxes (light blue whiskers/dots) show the predicted distribution of hourly O_3 concentrations for the 65 ppb adjustment scenario. Boxes show the interquartile range, whiskers extend to 1.5 × the interquartile range and dots depict outlier values.

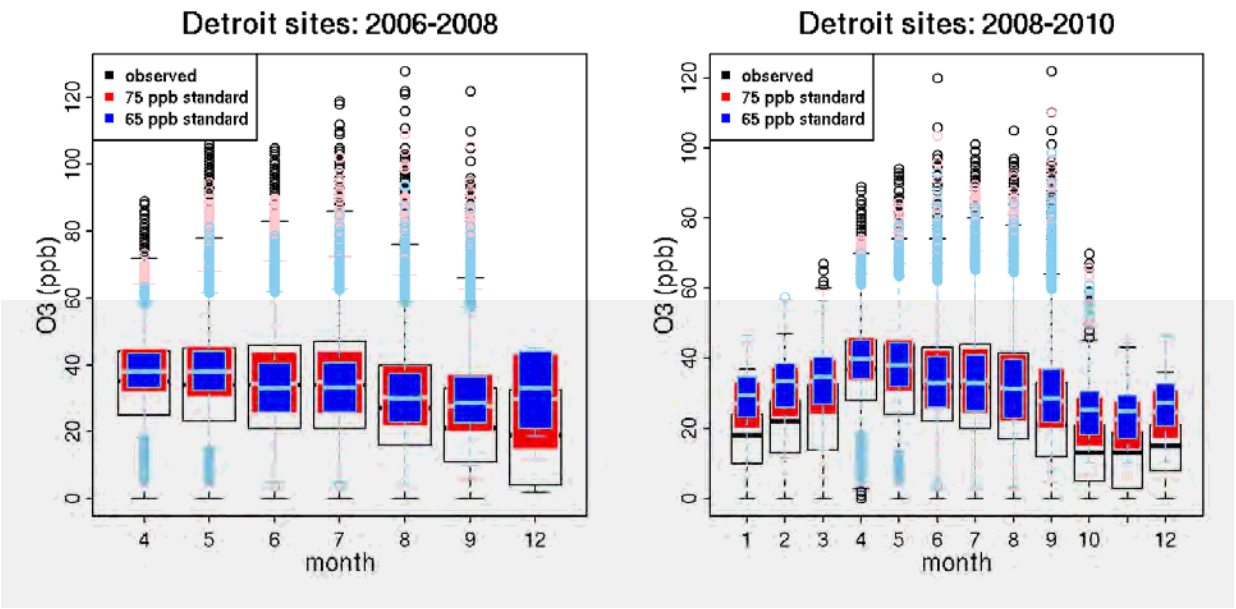

Figure 4D-35. Monthly O_3 distributions at Detroit area regulatory monitoring sites for observed air quality, and air quality adjusted to meet the existing (75 ppb) and alternative (65 ppb) standards for 2006-2008 (left) and 2008-2010 (right). White boxes (black whiskers/dots) show the observed distribution of hourly O_3 concentrations, red boxes (pink whiskers/dots) show the predicted distribution of hourly O_3 concentrations for the 75 ppb adjustment scenarios and blue boxes (light blue whiskers/dots) show the predicted distribution of hourly O_3 concentrations for the 65 ppb adjustment scenario. Boxes show the interquartile range, whiskers extend to 1.5 × the interquartile range and dots depict outlier values.

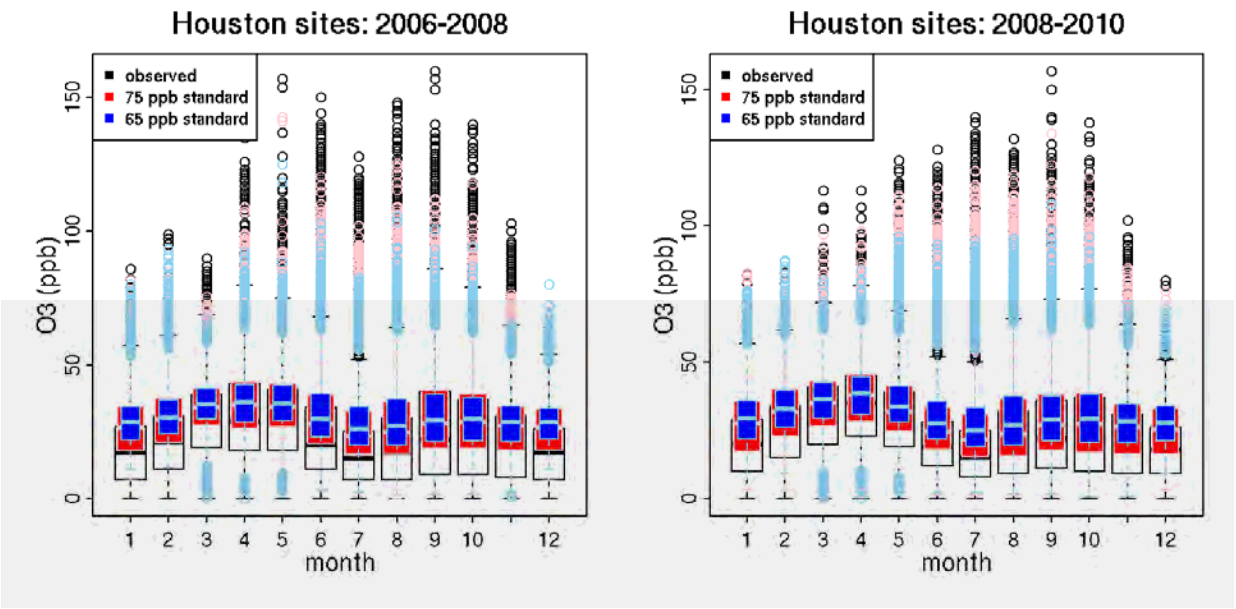

Figure 4D-36. Monthly O_3 distributions at Houston area regulatory monitoring sites for observed air quality, and air quality adjusted to meet the existing (75 ppb) and alternative (65 ppb) standards for 2006-2008 (left) and 2008-2010 (right). White boxes (black whiskers/dots) show the observed distribution of hourly O_3 concentrations, red boxes (pink whiskers/dots) show the predicted distribution of hourly O_3 concentrations for the 75 ppb adjustment scenarios and blue boxes (light blue whiskers/dots) show the predicted distribution of hourly O_3 concentrations for the 65 ppb adjustment scenario. Boxes show the interquartile range, whiskers extend to 1.5 × the interquartile range and dots depict outlier values.

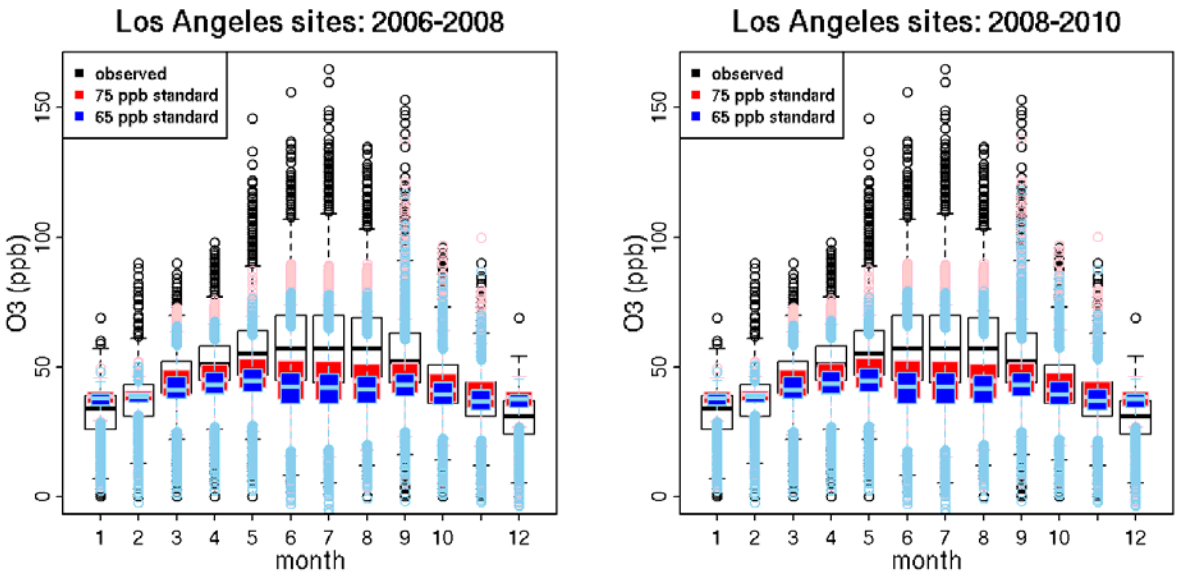

Figure 4D-37. Monthly O_3 distributions at Los Angeles area regulatory monitoring sites for observed air quality, and air quality adjusted to meet the existing (75 ppb) and alternative (65 ppb) standards for 2006-2008 (left) and 2008-2010 (right). White boxes (black whiskers/dots) show the observed distribution of hourly O_3 concentrations, red boxes (pink whiskers/dots) show the predicted distribution of hourly O_3 concentrations for the 75 ppb adjustment scenarios and blue boxes (light blue whiskers/dots) show the predicted distribution of hourly O_3 concentrations for the 65 ppb adjustment scenario. Boxes show the interquartile range, whiskers extend to 1.5 × the interquartile range and dots depict outlier values.

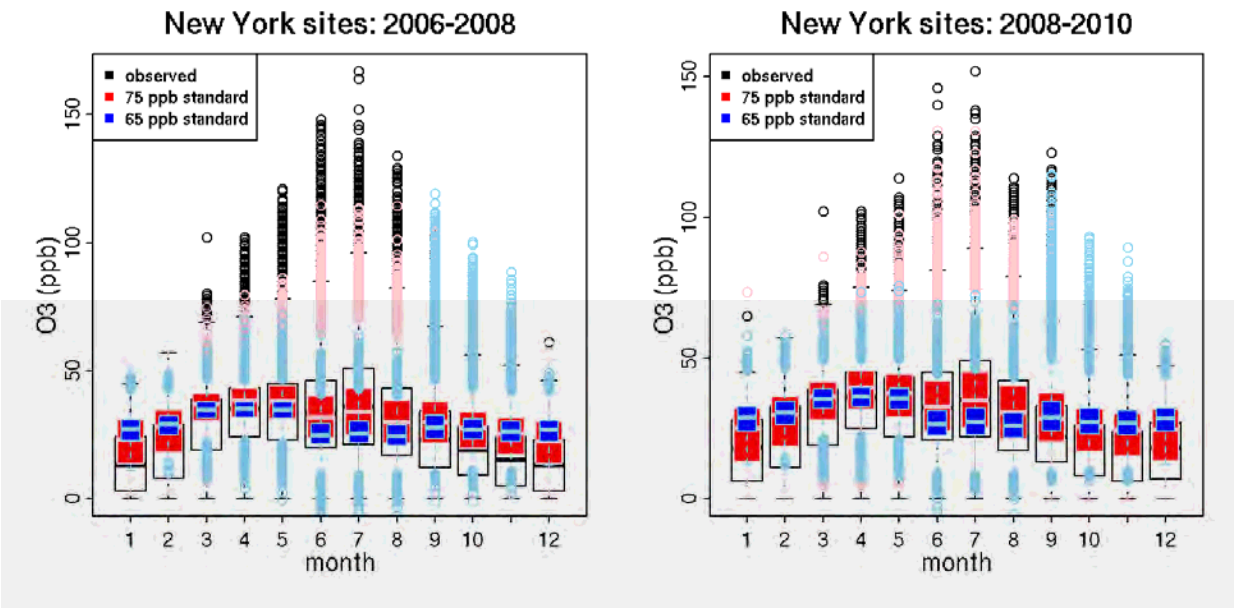

Figure 4D-38. Monthly O_3 distributions at New York area regulatory monitoring sites for observed air quality, and air quality adjusted to meet the existing (75 ppb) and alternative (65 ppb) standards for 2006-2008 (left) and 2008-2010 (right). White boxes (black whiskers/dots) show the observed distribution of hourly O_3 concentrations, red boxes (pink whiskers/dots) show the predicted distribution of hourly O_3 concentrations for the 75 ppb adjustment scenarios and blue boxes (light blue whiskers/dots) show the predicted distribution of hourly O_3 concentrations for the 65 ppb adjustment scenario. Boxes show the interquartile range, whiskers extend to 1.5 × the interquartile range and dots depict outlier values.

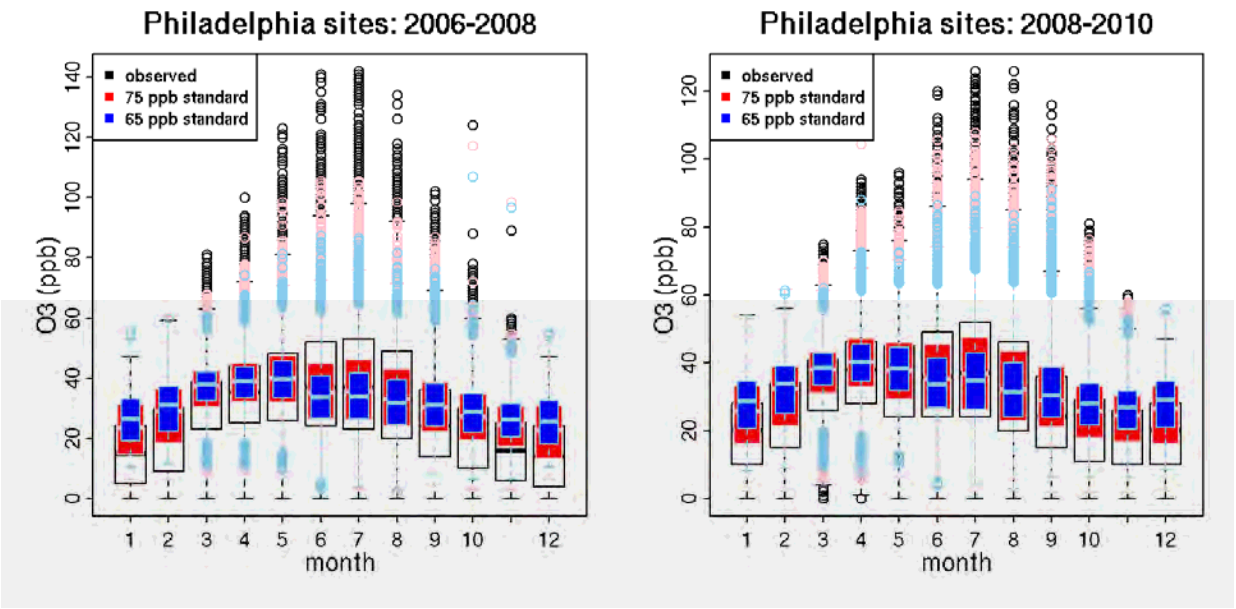

Figure 4D-39. Monthly O_3 distributions at Philadelphia area regulatory monitoring sites for observed air quality, and air quality adjusted to meet the existing (75 ppb) and alternative (65 ppb) standards for 2006-2008 (left) and 2008-2010 (right). White boxes (black whiskers/dots) show the observed distribution of hourly O_3 concentrations, red boxes (pink whiskers/dots) show the predicted distribution of hourly O_3 concentrations for the 75 ppb adjustment scenarios and blue boxes (light blue whiskers/dots) show the predicted distribution of hourly O_3 concentrations for the 65 ppb adjustment scenario. Boxes show the interquartile range, whiskers extend to 1.5 × the interquartile range and dots depict outlier values.

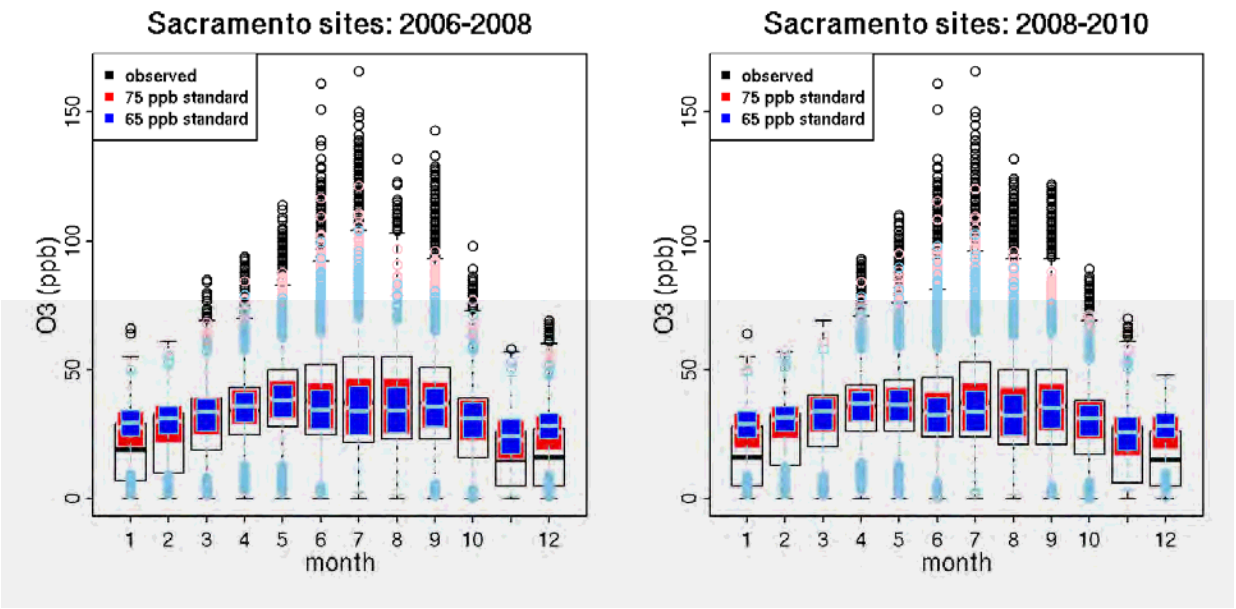

Figure 4D-40. Monthly O_3 distributions at Sacramento area regulatory monitoring sites for observed air quality, and air quality adjusted to meet the existing (75 ppb) and alternative (65 ppb) standards for 2006-2008 (left) and 2008-2010 (right). White boxes (black whiskers/dots) show the observed distribution of hourly O_3 concentrations, red boxes (pink whiskers/dots) show the predicted distribution of hourly O_3 concentrations for the 75 ppb adjustment scenarios and blue boxes (light blue whiskers/dots) show the predicted distribution of hourly O_3 concentrations for the 65 ppb adjustment scenario. Boxes show the interquartile range, whiskers extend to 1.5 × the interquartile range and dots depict outlier values.

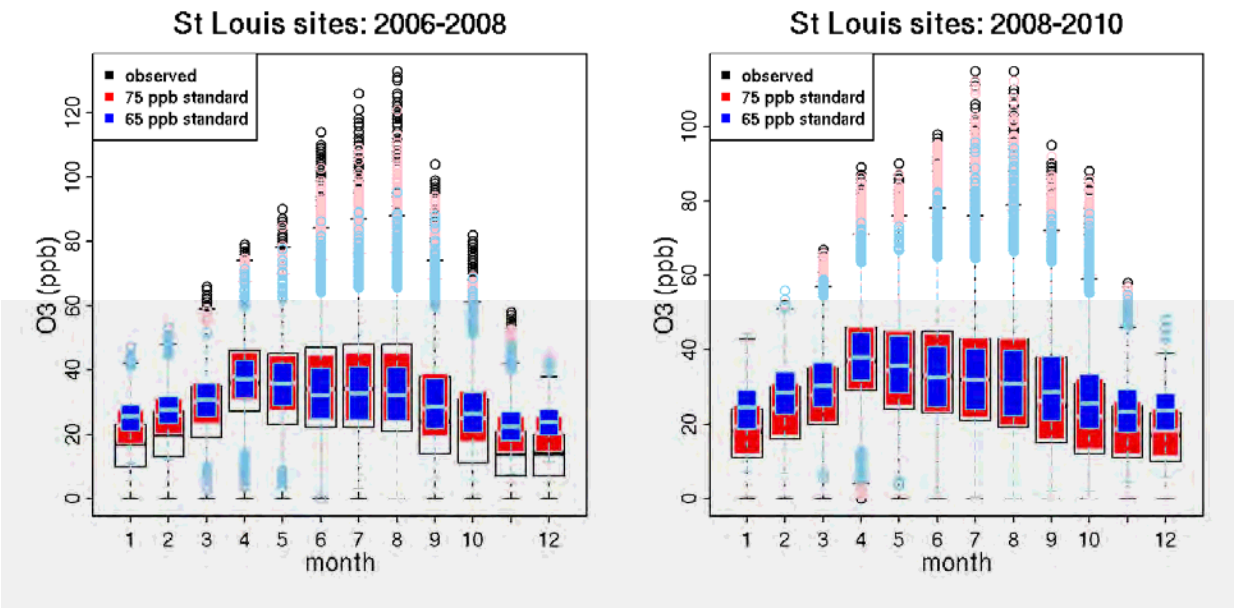

Figure 4D-41. Monthly O_3 distributions at St. Louis area regulatory monitoring sites for observed air quality, and air quality adjusted to meet the existing (75 ppb) and alternative (65 ppb) standards for 2006-2008 (left) and 2008-2010 (right). White boxes (black whiskers/dots) show the observed distribution of hourly O_3 concentrations, red boxes (pink whiskers/dots) show the predicted distribution of hourly O_3 concentrations for the 75 ppb adjustment scenarios and blue boxes (light blue whiskers/dots) show the predicted distribution of hourly O_3 concentrations for the 65 ppb adjustment scenario. Boxes show the interquartile range, whiskers extend to 1.5 × the interquartile range and dots depict outlier values.

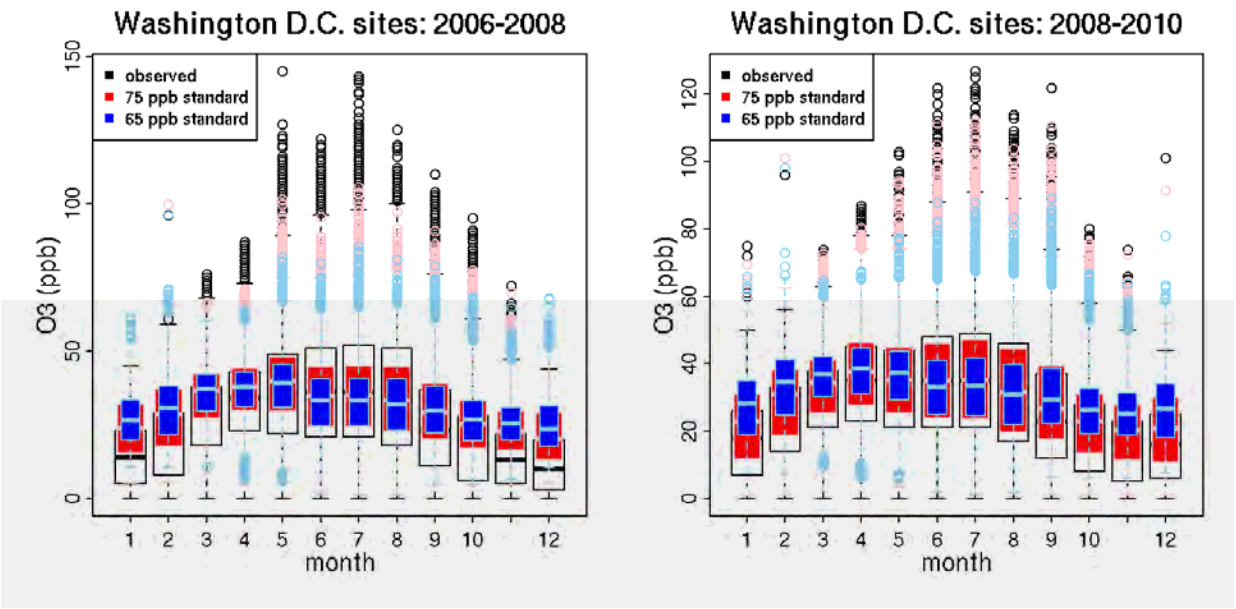

Figure 4D-42. Monthly O_3 distributions at Washington, D.C. area regulatory monitoring sites for observed air quality, and air quality adjusted to meet the existing (75 ppb) and alternative (65 ppb) standards for 2006-2008 (left) and 2008-2010 (right). White boxes (black whiskers/dots) show the observed distribution of hourly O_3 concentrations, red boxes (pink whiskers/dots) show the predicted distribution of hourly O_3 concentrations for the 75 ppb adjustment scenarios and blue boxes (light blue whiskers/dots) show the predicted distribution of hourly O_3 concentrations for the 65 ppb adjustment scenario. Boxes show the interquartile range, whiskers extend to 1.5 × the interquartile range and dots depict outlier values.

4D-4.4 Standard Errors for Predicted Hourly and Daily 8-hr Maximum O_3 Concentrations

Standard error values, s^2, for the predicted sensitivity are calculated using Equations (4D-25) and (4D-26) as described by Wilks (2006):

$$MSE = \frac{\sum(Y_i - \hat{Y}_i)^2}{n-2}$$

Equation (4D-25)

$$s^2\{\hat{Y}_h\} = MSE\left[\frac{1}{n} + \frac{(X_h - \overline{X})^2}{\sum(X_i - \overline{X})^2}\right]$$

Equation (4D-26)

In Equation (4D-25) mean standard error (MSE) is calculated as the sum of squared residual values from the linear model divided by n-2 to account for two degrees of freedom in the fit

(slope and intersect). In Equation (4D-26), the first term characterizes the uncertainty in estimating the true mean given a fixed sample size of n and the second term characterizes the uncertainty in the slope. Taken together, the standard error for each predicted sensitivity coefficient is impacted by the goodness of fit for the linear model (MSE), the sample size (n), and the distance of the x value from the bulk of the data. These standard error values represent the uncertainty in the predicted central tendency from the linear model.

The standard errors were propagated through Equations (4D-4) to (4D-8) to derive a standard error in hourly O_3 concentrations. These hourly O_3 standard errors are thus impacted both by the standard error in the sensitivity and by the amount of emissions reduction applied (i.e. standard error increases with larger emissions changes and thus at lower O_3 standard levels). These hourly O_3 standard errors represent uncertainty in predicted O_3 concentrations due to uncertainty in predicting the central tendency with the linear regression. Standard error values for predicted hourly O_3 were generally small relative to total predicted hourly O_3 concentrations. This indicates that even when regression fits had somewhat lower correlation coefficients, the resulting uncertainty from the use of the regression line does not substantially affect predicted O_3 concentrations.

Table 4D-18 and Table 4D-19 show the mean and 95th percentile standard error for all hourly O_3 values (2006-2010) in each urban area for the existing standard of 75 ppb and the potential alternative standards of 70 ppb, 65 ppb, and 60 ppb.

To further put this uncertainty into a context relevant to the form of the O_3 standard and the metric used in health analyses, we propagated standard errors for hourly O_3 to uncertainties in 8-hr daily maximum O_3 concentrations using Equation (4D-27):

$$\widehat{SE}(\bar{Y}) = \sqrt{\frac{\sum_{i=1}^{8}\left(\widehat{SE}(Y_i)\right)^2}{64}} = \frac{\sqrt{\sum_{i=1}^{8}\left(\widehat{SE}(Y_i)\right)^2}}{8}$$

Equation (4D-27)

Boxplots showing the range of 8-hr daily maximum O_3 standard errors calculated for each cases study area are shown in the chapter 4 of the HREA. Maps of mean standard error in 8-hr daily maximum O_3 concentration at each monitoring location are shown in Figure 4D-43 through Figure 4D-57. These figures generally show that 8-hr daily maximum O_3 mean standard error is small (less than 0.4 ppb) with slightly higher values up to 1.3 ppb in the most NO_x limited areas at the lower standard levels.

Table 4D-18. Mean standard error (ppb) in adjusted hourly O_3 concentration in each urban area for each standard.

Urban Area	Years	Standard Level			
		75 ppb†	70 ppb	65 ppb	60 ppb‡
Atlanta	2006-2008	0.65	0.69	0.74	0.81
	2008-2010	0.37	0.68	0.71	0.77
Baltimore	2006-2008	0.62	0.65	0.70	0.78
	2008-2010	0.62	0.64	0.69	0.75
Boston	2006-2008	0.51	0.53	0.59	0.69
	2008-2010	0.16	0.51	0.54	0.63
Chicago*	2006-2008	0.29	0.66	0.77	0.99
	2008-2010	N/A	0.41	0.68	0.83
Cleveland	2006-2008	0.60	0.65	0.76	0.96
	2008-2010	0.60	0.66	0.80	0.95
Dallas	2006-2008	0.59	0.64	0.74	0.86
	2008-2010	0.57	0.63	0.72	0.84
Denver*	2006-2008	0.51	0.62	0.77	0.85
	2008-2010	0.17	0.48	0.58	0.82
Detroit	2006-2008	0.60	0.70	0.80	0.92
	2008-2010	N/A	0.56	0.65	0.81
Houston	2006-2008	0.73	0.83	0.95	1.11
	2008-2010	0.52	0.55	0.62	0.76
Los Angeles*	2006-2008	1.15	1.17	1.18	1.21
	2008-2010	1.14	1.15	1.17	1.19
New York*	2006-2008	0.84	1.06	1.39	N/A
	2008-2010	0.69	0.92	1.34	N/A
Philadelphia	2006-2008	0.66	0.72	0.80	0.90
	2008-2010	0.62	0.65	0.71	0.79
Sacramento	2006-2008	0.49	0.55	0.61	0.81
	2008-2010	0.49	0.56	0.62	0.70
Saint Louis	2006-2008	0.57	0.61	0.70	0.81
	2008-2010	0.13	0.48	0.58	0.66
Washington D.C.	2006-2008	0.67	0.71	0.78	0.87
	2008-2010	0.49	0.66	0.72	0.84

*Values are from the standard NO_x reduction scenario for all cities except Chicago and Denver, for which value are from the standard NO_x/VOC reduction scenario and New York and Los Angeles, for which values based on reductions required when using the lower bound of the 95th percentile confidence interval.
†N/A values for the 75 ppb standard level mean that a particular urban area did not have any design values above 75 for that 3-year period so adjustments were made to ambient data.
‡N/A values for the 60 ppb standard level mean that this adjustment methodology was not able to bring design values down to 60 for that particular city and 3-year period.

Table 4D-19. 95th percentile standard error (ppb) in adjusted hourly O_3 concentration in each urban area for each standard.

Urban Area	Years	Standard Level			
		75 ppb†	70 ppb	65 ppb	60 ppb‡
Atlanta	2006-2008	1.28	1.34	1.42	1.56
	2008-2010	0.72	1.33	1.38	1.47
Baltimore	2006-2008	1.22	1.26	1.34	1.49
	2008-2010	1.21	1.26	1.33	1.46
Boston	2006-2008	1.02	1.05	1.19	1.41
	2008-2010	0.33	1.03	1.09	1.29
Chicago*	2006-2008	0.54	1.22	1.43	1.89
	2008-2010	N/A	0.78	1.27	1.56
Cleveland	2006-2008	1.13	1.19	1.35	1.69
	2008-2010	1.13	1.22	1.42	1.69
Dallas	2006-2008	1.16	1.26	1.48	1.79
	2008-2010	1.12	1.24	1.45	1.75
Denver*	2006-2008	1.14	1.35	1.70	1.89
	2008-2010	0.38	1.07	1.28	1.84
Detroit	2006-2008	1.12	1.28	1.46	0.69
	2008-2010	N/A	1.05	1.20	1.48
Houston	2006-2008	1.45	1.66	1.96	2.41
	2008-2010	0.98	1.04	1.15	1.39
Los Angeles*	2006-2008	2.84	2.86	2.89	2.93
	2008-2010	2.78	2.80	2.83	2.86
New York*	2006-2008	1.64	2.15	2.87	N/A
	2008-2010	1.34	1.87	2.98	N/A
Philadelphia	2006-2008	1.29	1.39	1.56	1.78
	2008-2010	1.25	1.29	1.41	1.58
Sacramento	2006-2008	1.10	1.22	1.35	1.54
	2008-2010	1.11	1.24	1.38	1.55
Saint Louis	2006-2008	1.07	1.14	1.29	1.51
	2008-2010	0.26	0.90	1.07	1.21
Washington D.C.	2006-2008	1.29	1.35	1.46	1.63
	2008-2010	0.94	1.27	1.36	1.57

*Values are from the standard NO_x reduction scenario for all cities except Chicago and Denver, for which value are from the standard NO_x/VOC reduction scenario and New York and Los Angeles, for which values based on reductions required when using the lower bound of the 95th percentile confidence interval.
†N/A values for the 75 ppb standard level mean that a particular urban area did not have any design values above 75 for that 3-year period so adjustments were made to ambient data.
‡N/A values for the 60 ppb standard level mean that this adjustment methodology was not able to bring design values down to 60 for that particular city and 3-year period.

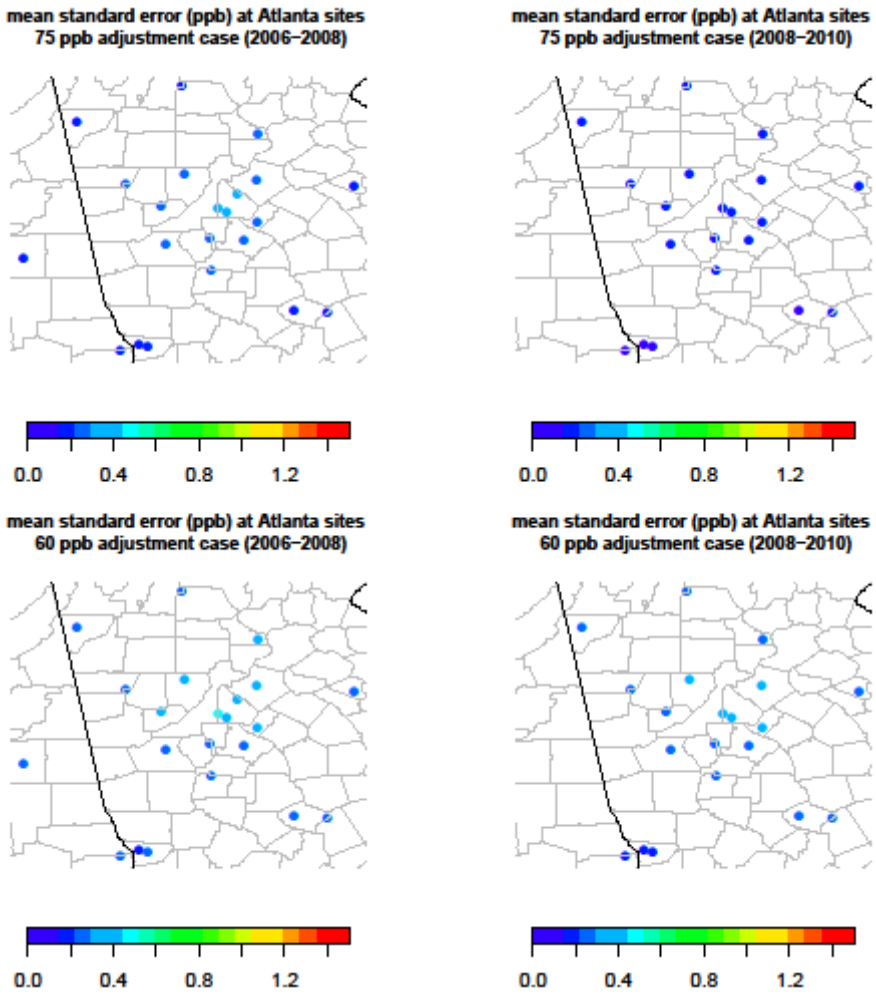

Figure 4D-43. Mean standard error in maximum daily 8-hr O_3 concentrations at each monitoring location in Atlanta for the 75 ppb adjustment scenario (top row) and the 60 ppb adjustment scenario (bottom row) for the 2006-2008 time period (left column) and the 2008-2010 time period (right column).

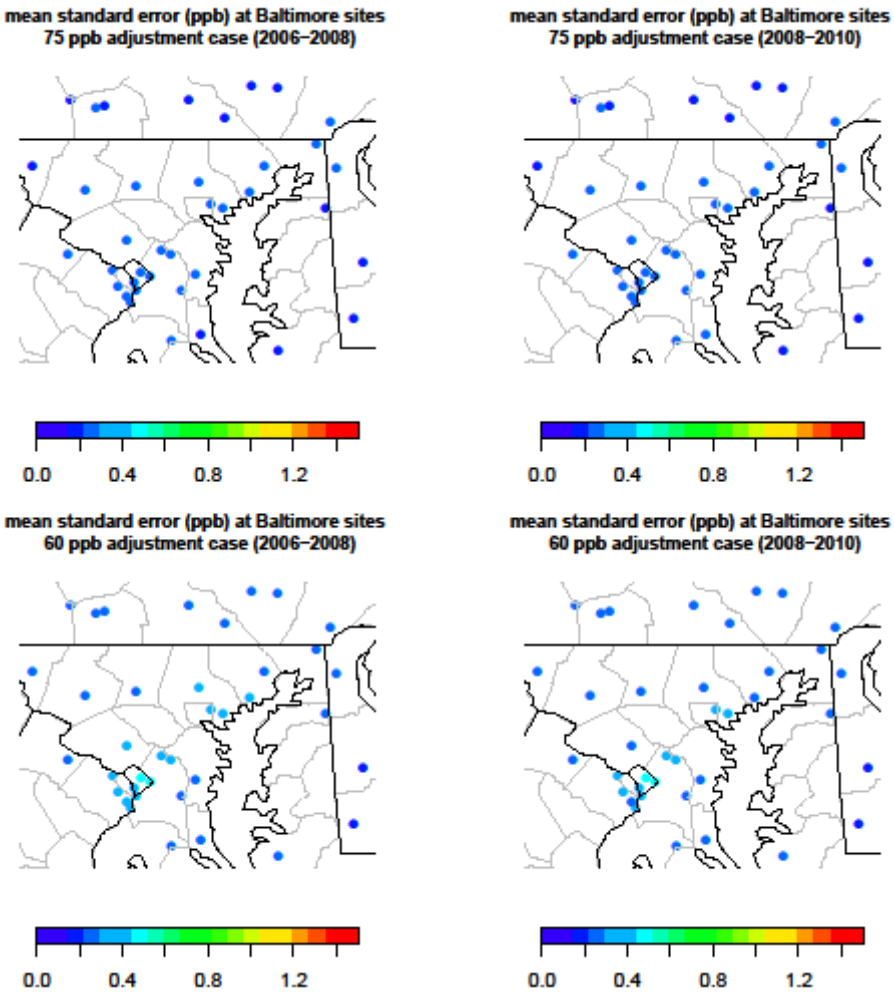

Figure 4D-44. Mean standard error in maximum daily 8-hr O_3 concentrations at each monitoring location in Baltimore for the 75 ppb adjustment scenario (top row) and the 60 ppb adjustment scenario (bottom row) for the 2006-2008 time period (left column) and the 2008-2010 time period (right column).

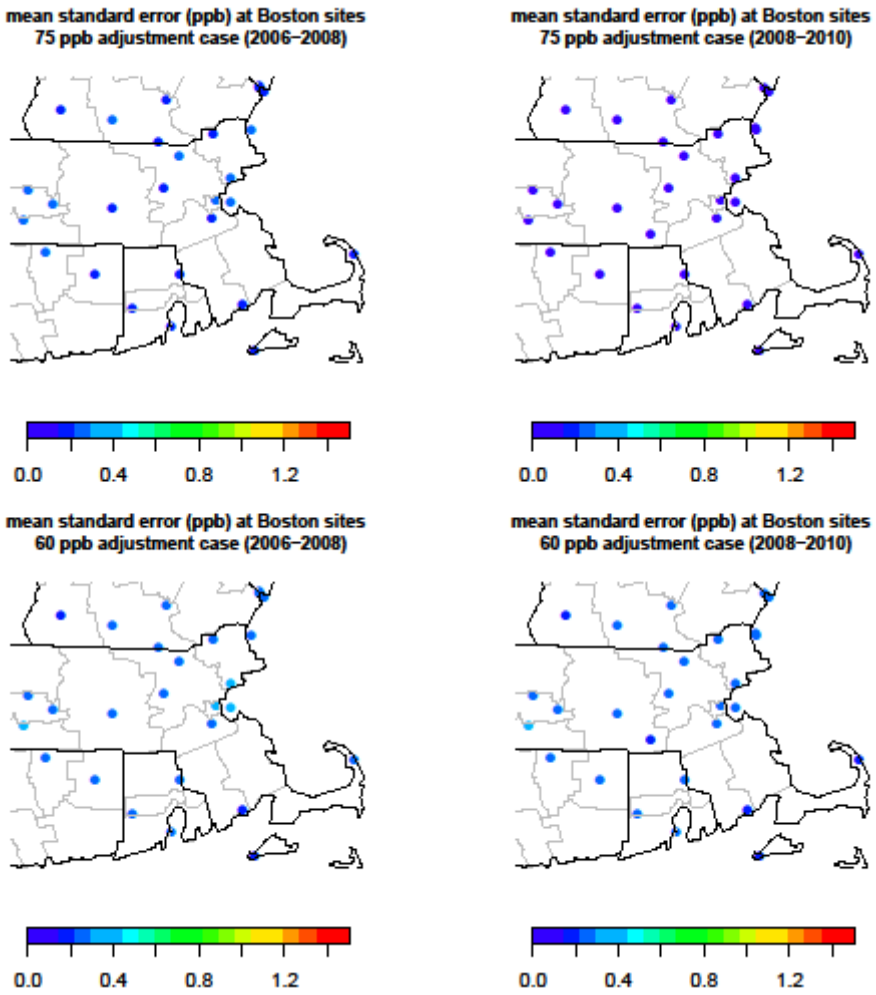

Figure 4D-45. Mean standard error in maximum daily 8-hr O_3 concentrations at each monitoring location in Boston for the 75 ppb adjustment scenario (top row) and the 60 ppb adjustment scenario (bottom row) for the 2006-2008 time period (left column) and the 2008-2010 time period (right column).

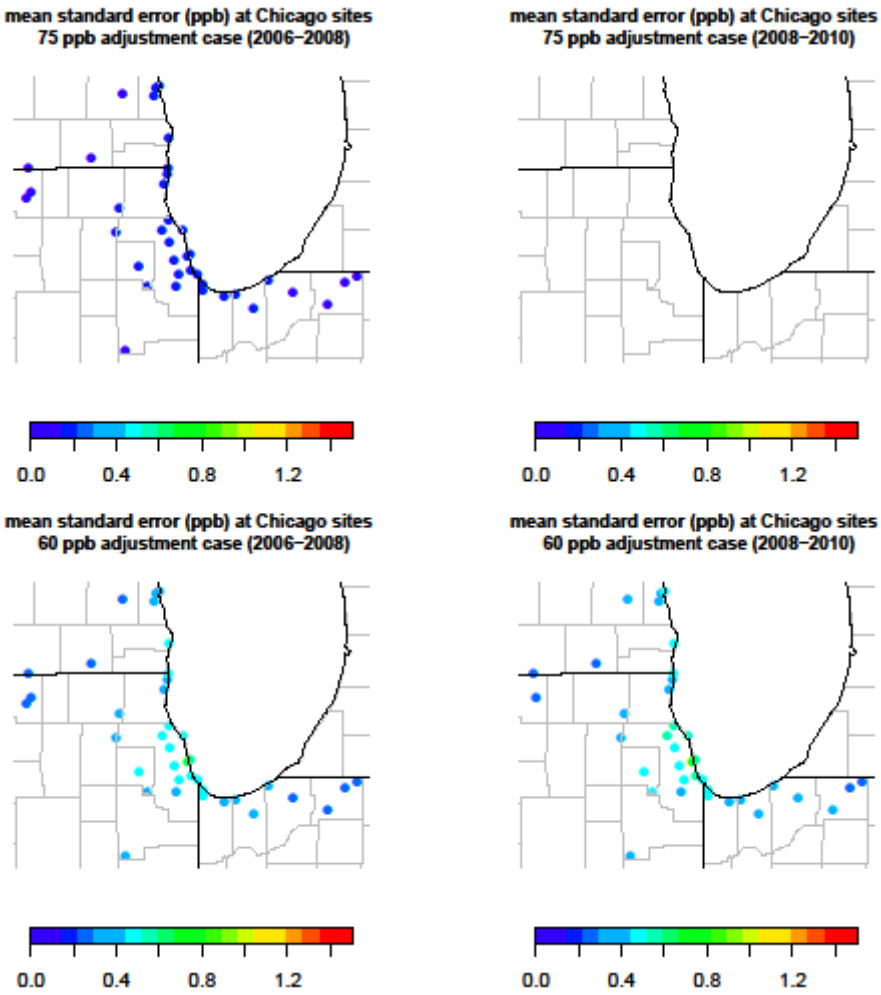

Figure 4D-46. Mean standard error in maximum daily 8-hr O_3 concentrations at each monitoring location in Chicago for the 75 ppb adjustment scenario (top row) and the 60 ppb adjustment scenario (bottom row) for the 2006-2008 time period (left column) and the 2008-2010 time period (right column).

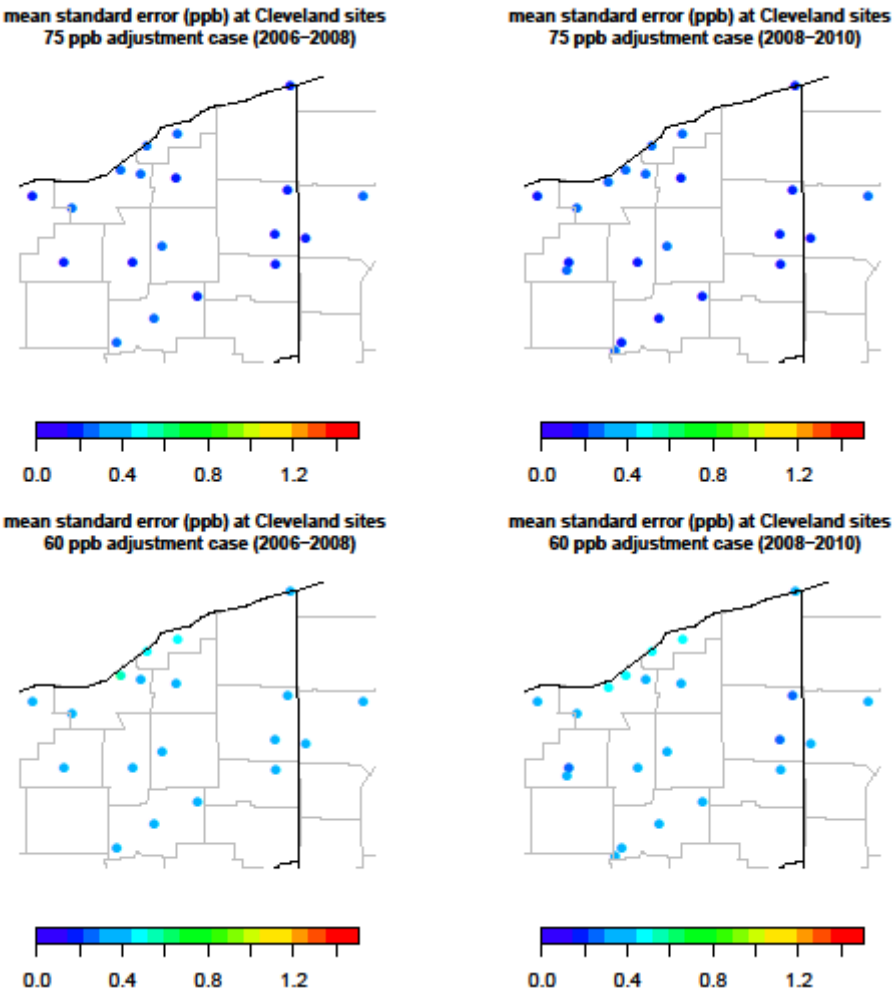

Figure 4D-47. Mean standard error in maximum daily 8-hr O_3 concentrations at each monitoring location in Cleveland for the 75 ppb adjustment scenario (top row) and the 60 ppb adjustment scenario (bottom row) for the 2006-2008 time period (left column) and the 2008-2010 time period (right column).

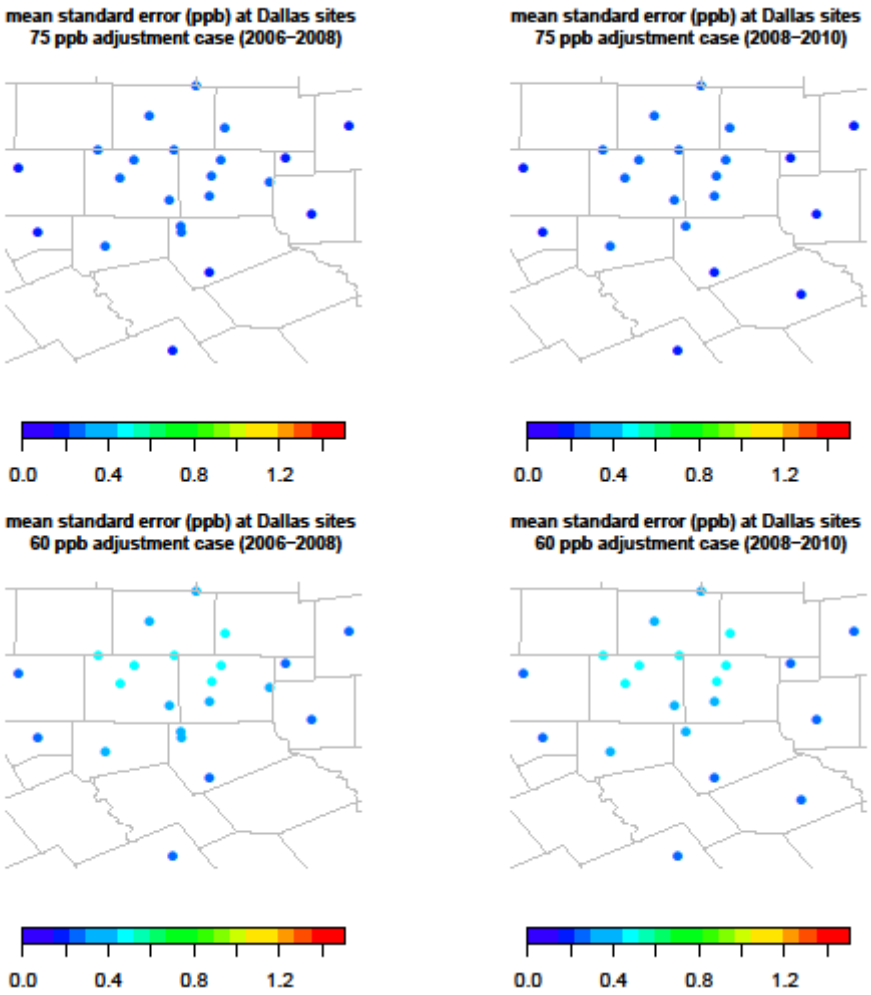

Figure 4D-48. Mean standard error in maximum daily 8-hr O_3 concentrations at each monitoring location in Dallas for the 75 ppb adjustment scenario (top row) and the 60 ppb adjustment scenario (bottom row) for the 2006-2008 time period (left column) and the 2008-2010 time period (right column).

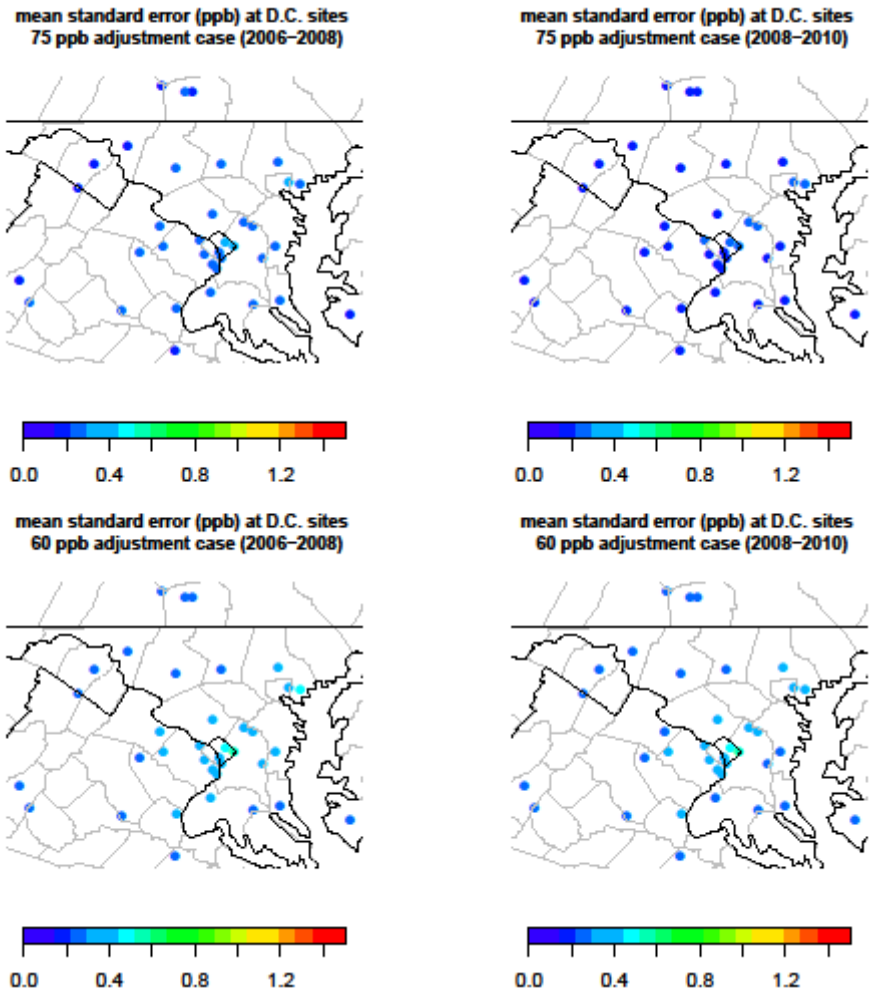

Figure 4D-49. Mean standard error in maximum daily 8-hr O_3 concentrations at each monitoring location in Washington D.C. for the 75 ppb adjustment scenario (top row) and the 60 ppb adjustment scenario (bottom row) for the 2006-2008 time period (left column) and the 2008-2010 time period (right column).

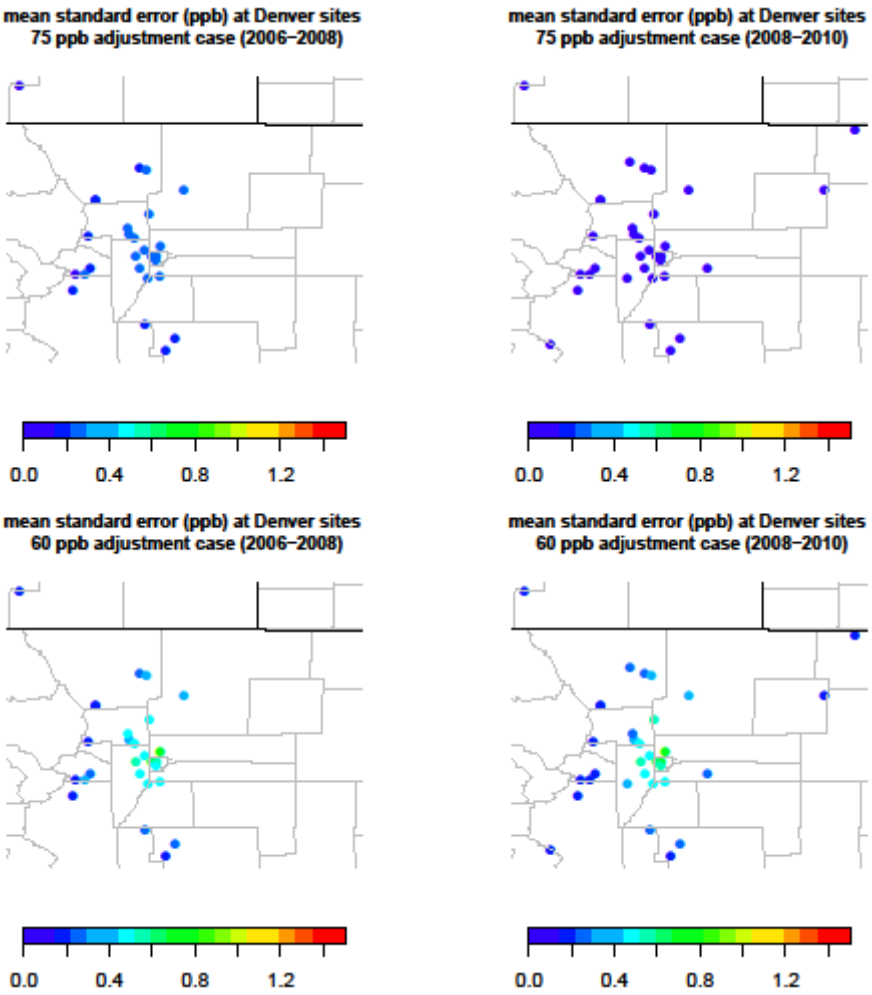

Figure 4D-50. Mean standard error in maximum daily 8-hr O_3 concentrations at each monitoring location in Denver for the 75 ppb adjustment scenario (top row) and the 60 ppb adjustment scenario (bottom row) for the 2006-2008 time period (left column) and the 2008-2010 time period (right column).

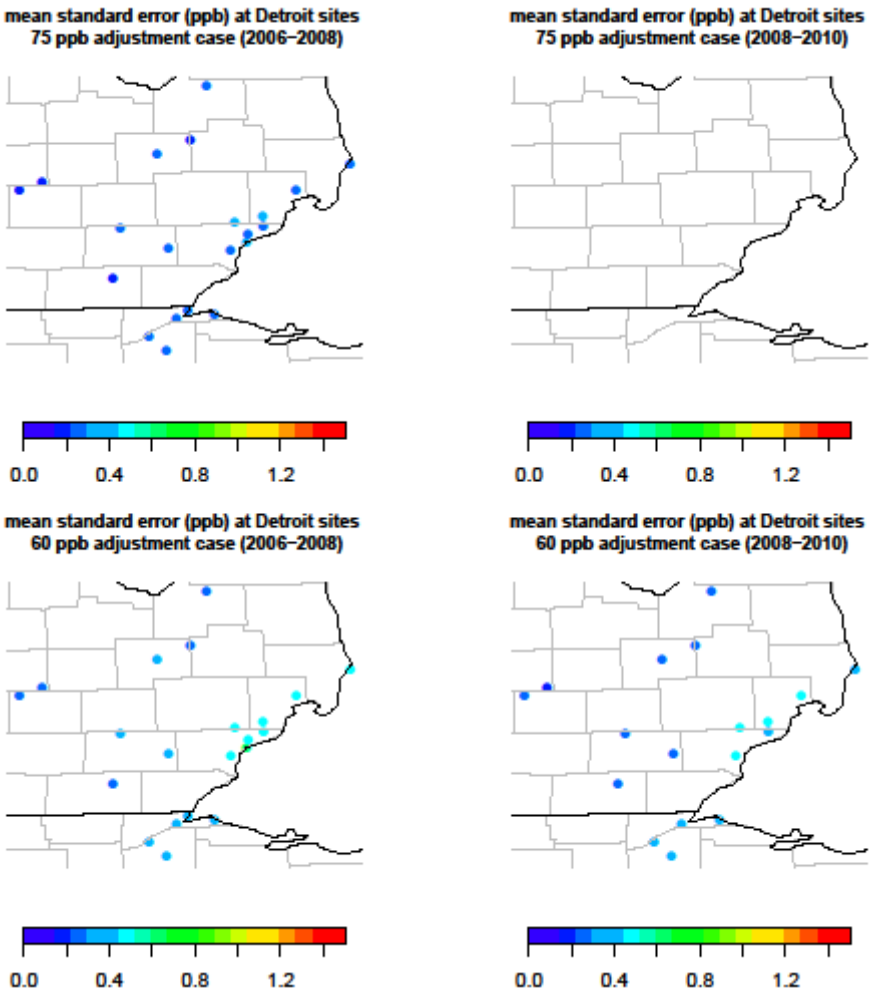

Figure 4D-51. Mean standard error in maximum daily 8-hr O_3 concentrations at each monitoring location in Detroit for the 75 ppb adjustment scenario (top row) and the 60 ppb adjustment scenario (bottom row) for the 2006-2008 time period (left column) and the 2008-2010 time period (right column).

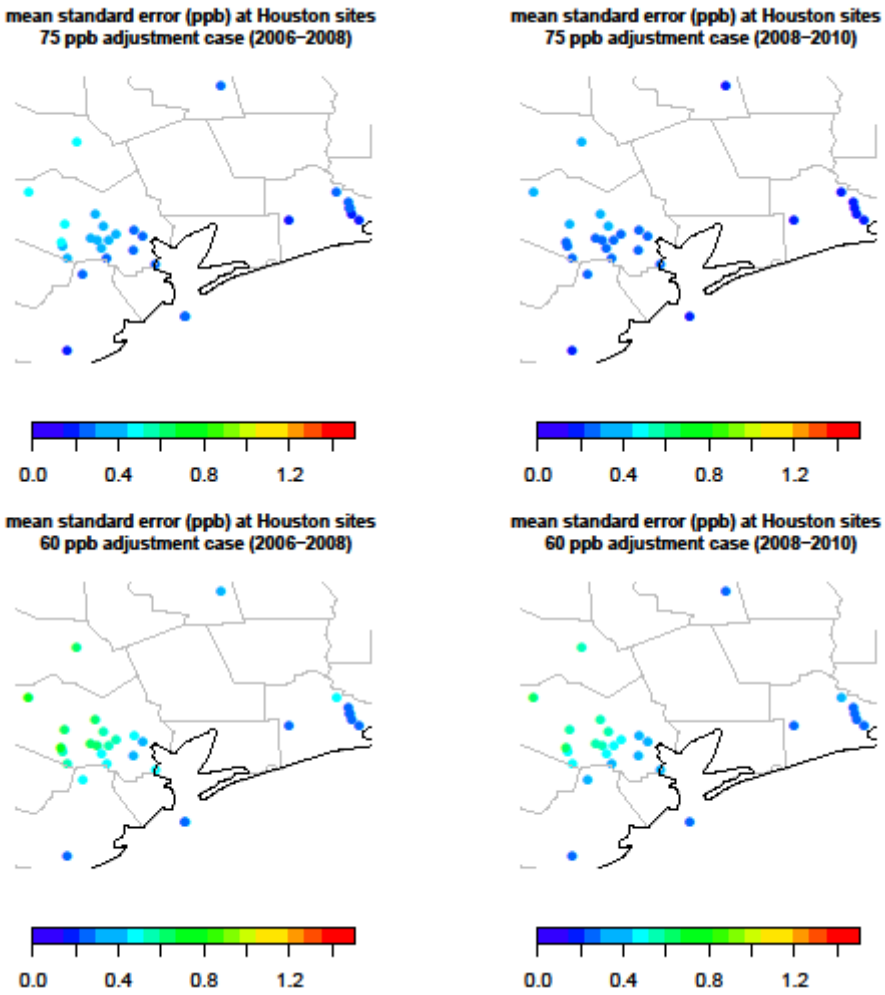

Figure 4D-52. Mean standard error in maximum daily 8-hr O_3 concentrations at each monitoring location in Houston for the 75 ppb adjustment scenario (top row) and the 60 ppb adjustment scenario (bottom row) for the 2006-2008 time period (left column) and the 2008-2010 time period (right column).

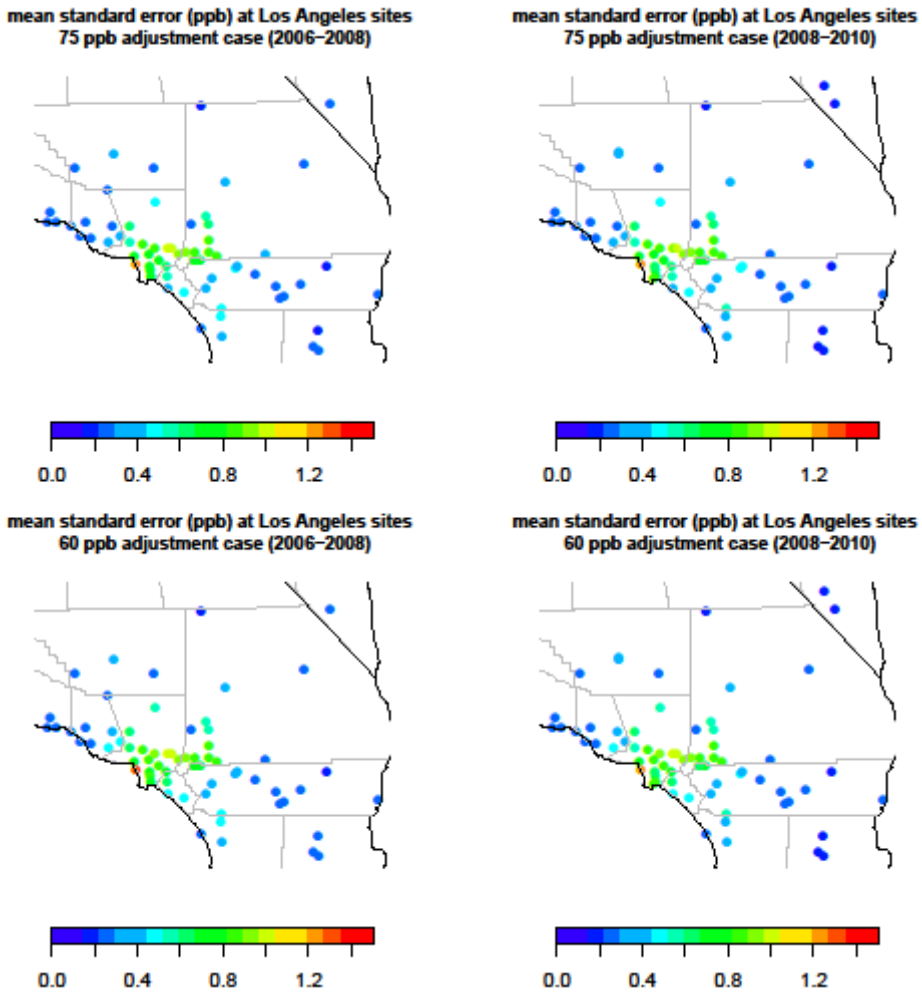

Figure 4D-53. Mean standard error in maximum daily 8-hr O_3 concentrations at each monitoring location in Los Angele for the 75 ppb adjustment scenario (top row) and the 60 ppb adjustment scenario (bottom row) for the 2006-2008 time period (left column) and the 2008-2010 time period (right column).

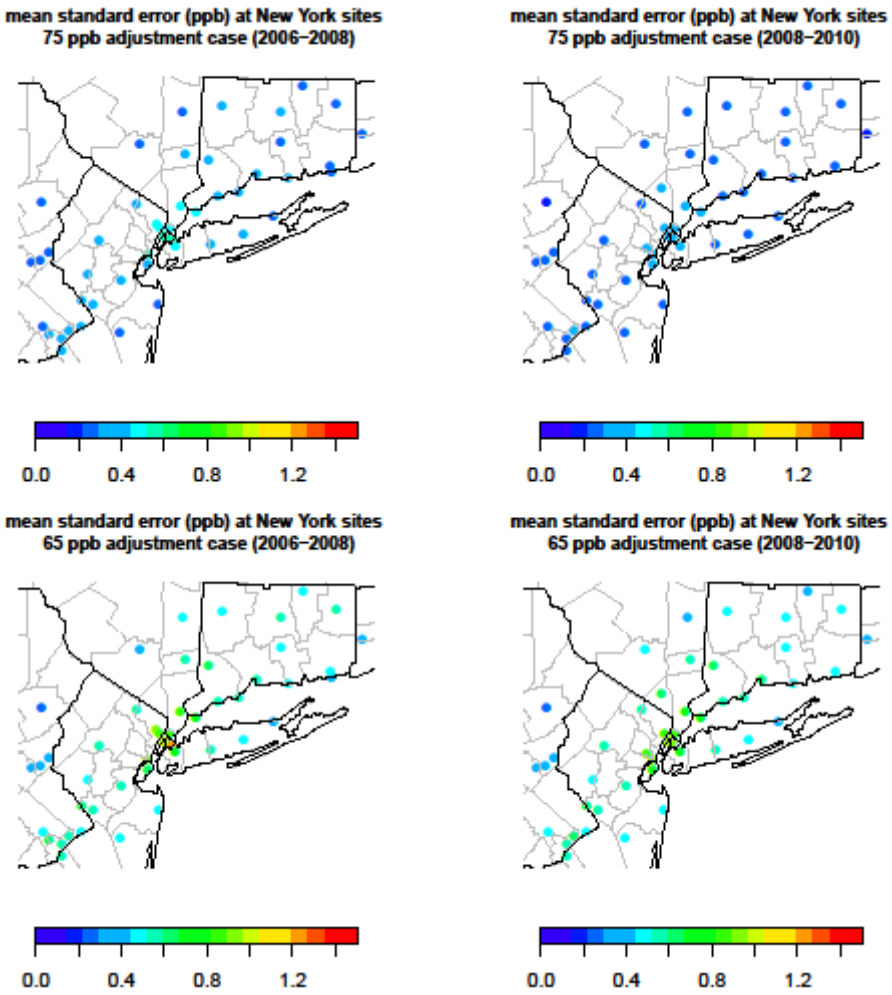

Figure 4D-54. Mean standard error in maximum daily 8-hr O_3 concentrations at each monitoring location in New York for the 75 ppb adjustment scenario (top row) and the 60 ppb adjustment scenario (bottom row) for the 2006-2008 time period (left column) and the 2008-2010 time period (right column).

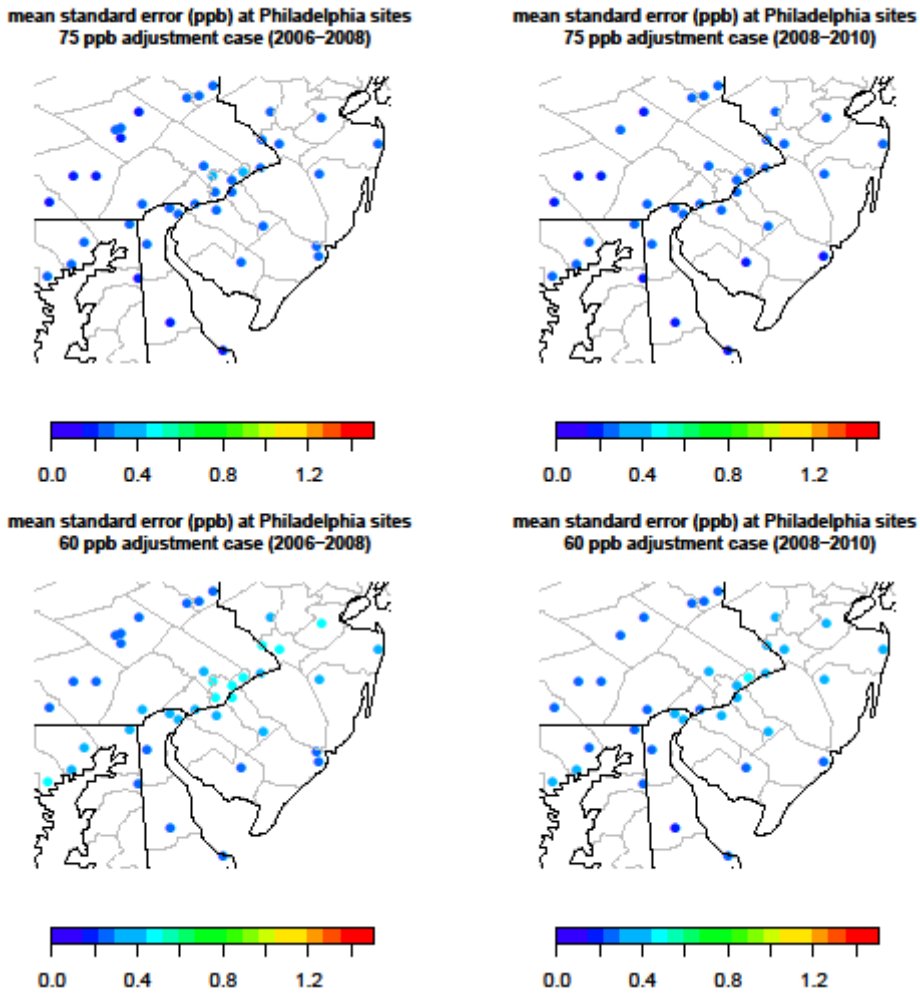

Figure 4D-55. Mean standard error in maximum daily 8-hr O_3 concentrations at each monitoring location in Philadelphia for the 75 ppb adjustment scenario (top row) and the 60 ppb adjustment scenario (bottom row) for the 2006-2008 time period (left column) and the 2008-2010 time period (right column).

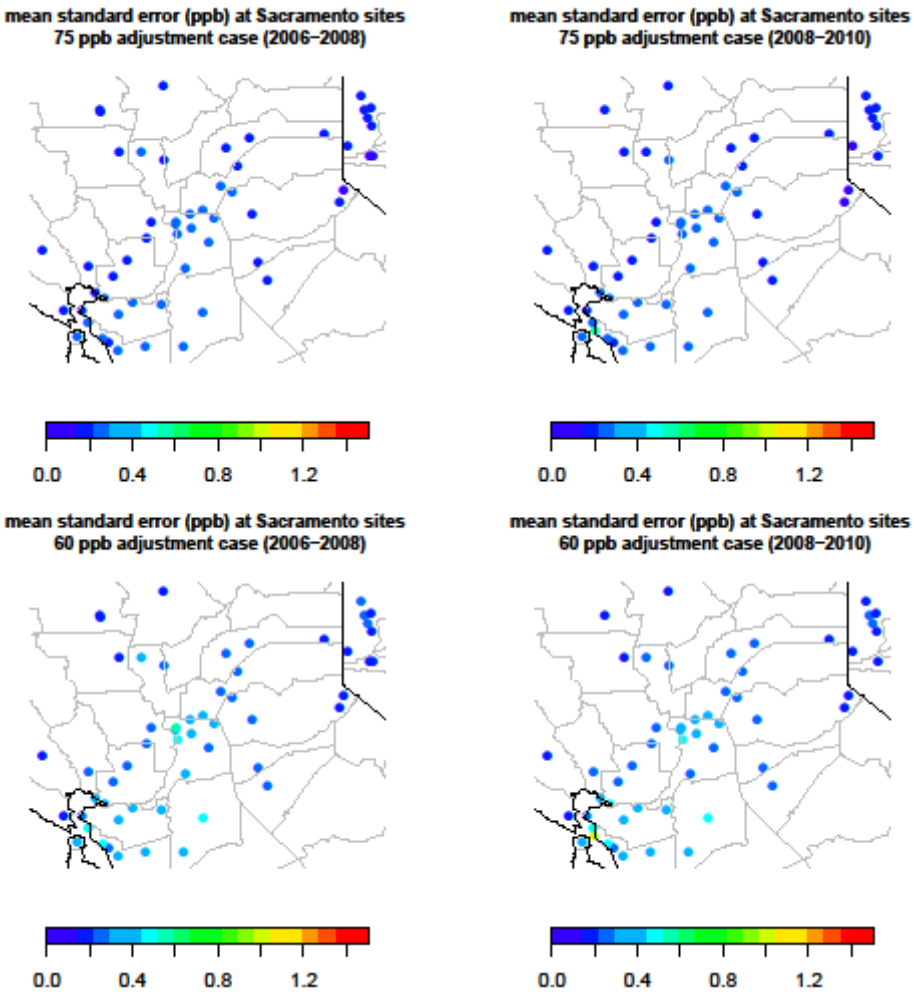

Figure 4D-56. Mean standard error in maximum daily 8-hr O_3 concentrations at each monitoring location in Sacramento for the 75 ppb adjustment scenario (top row) and the 60 ppb adjustment scenario (bottom row) for the 2006-2008 time period (left column) and the 2008-2010 time period (right column).

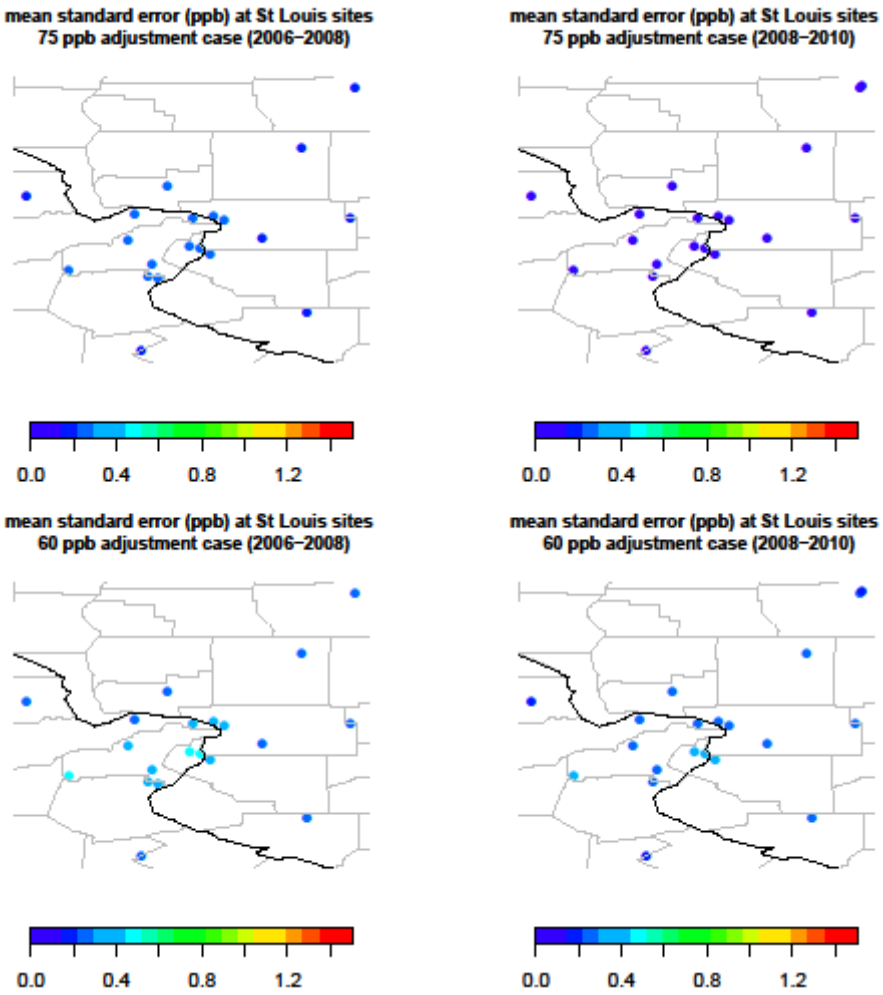

Figure 4D-57. Mean standard error in maximum daily 8-hr O_3 concentrations at each monitoring location in St. Louis for the 75 ppb adjustment scenario (top row) and the 60 ppb adjustment scenario (bottom row) for the 2006-2008 time period (left column) and the 2008-2010 time period (right column).

4D-4.5 Air Quality Inputs for the Epidemiology-Based Risk Assessment

The air quality inputs to the epidemiology-based risk assessment discussed in HREA Chapter 7 were spatially averaged "composite monitor[6]" values for 12 of the 15 urban study areas. The procedure for calculating these values is described in Appendix 4A. Figure 4D-58 through Figure 4D-69 show boxplots of the composite monitor daily maximum 8-hour values for observed air quality, air quality adjusted to meet the existing standard, and the potential alternative standards of 70 ppb, 65 ppb, and 60 ppb in the 12 urban areas in the epidemiology-

[6] Composite monitor values are calculated as the average of all monitors within each CBSA. See Appendix 4A for more details.

based risk assessment. There are eight panels in each figure. The panels are designed to show contrasts based on three factors:

1. Spatial extent of the urban study area: the top row of panels in each figure are based on the smaller areas from the Zanobetti and Schwartz (2008) study (Z & S), , while the bottom row of panels are based on the larger Core Based Statistical Areas (CBSAs). Length of the O_3 season: the 1st and 3rd columns of panels in each figure are based on a shorter June – August O_3 season, which was used in Z & S, while the 2nd and 4th columns of panels are based on a longer April – October O_3 season. The Smith et al. (2009) study was based on the required O_3 monitoring season, which varied by area but often encompassed the April-October period.
2. Year: the two left-hand columns of panels in each figure are based on 2007, while the two right-hand columns of panels in each figure are based on 2009. The epidemiology-based risk assessment focused on these two years: 2007, to represent a year with higher O_3 concentrations, and 2009, to represent a year with lower O_3 concentrations.

There are a few properties common to nearly all of the figures. First, the highest composite monitor values represented by the top whiskers decrease when air quality is adjusted to meet the existing standard, and continue to decrease as air quality is further adjusted to meet lower alternative standard levels. By contrast, the lowest composite monitor values represented by the bottom whiskers increase when air quality is adjusted to meet the existing standard, and continue to increase as air quality is further adjusted to meet lower alternative standard levels. The behavior of the 25th percentile, median, mean, and 75th percentile values making up the boxes varies by urban area and across the three contrasting factors.

The spatial extent contrasts show that the base composite monitor values based on the smaller Z & S study areas tend to be slightly lower than the base composite monitor values based on the CBSAs. This is because the highest O_3 concentrations are often located downwind of the urban area's population center, and the smaller Z & S areas often do not capture the highest observed concentrations. Two notable exceptions to this tendency are Atlanta and Sacramento, where the highest monitored concentrations are located near the population center. The spatial extent contrasts also show that when air quality is adjusted, the highest composite monitor values tend to decrease more quickly for the CBSAs than for the Z & S areas, and conversely the lowest composite monitor values tend to increase more slowly for the CBSAs than for the Z & S areas. This is consistent with observed air quality patterns, which show that as NO_x emissions decrease, O_3 concentrations decrease more quickly downwind of the urban population center, and may increase near the population center due to less titration. This phenomenon also affects the center of the distribution, where we see that the 25th percentile, median, mean, and 75th percentile of the composite monitor values decrease more quickly for the CBSAs than for the Z & S areas. In

cases where we see increases in these values, the values tend to increase more quickly for the Z & S areas than for the CBSAs.

The seasonal contrasts show that the composite monitor values based on observed air quality tend to be lower in the spring and fall months than in the summer months. The highest composite monitor values tend to occur in the June-August period, so the upper tail of the distribution often does not change, but the center and lower tail values are usually lower for the April-October period. One notable exception is Houston, where the highest O_3 concentrations are often observed in the spring and fall months. When O_3 concentrations are adjusted to meet the existing standard, there are many cases where net decreases in the 25th percentile, median, and mean composite monitor values for the June-August period turn into net increases in these values for the April-October period. When air quality is further adjusted to meet the potential alternative standards, initial increases in these values for the April–October period often persist, and in a few cases the increases grow larger as the level of the standard decreases. By contrast, initial increases in the 25th percentile, median, and mean composite monitor values are often reversed when air quality is further adjusted to meet the potential alternative standards.

Finally, the year contrasts are meant to show the effects of changes in emissions and meteorology on the composite monitor values. Precursor emissions were generally higher in 2007 than in 2009, and meteorological conditions were generally more favorable to O_3 formation in 2007 than in 2009. Thus, the composite monitor values based on observed air quality are generally higher in 2007 than in 2009, with the exception of Houston, where the climate regime was the reverse of most of the rest of the U.S. during those two years. When air quality are adjusted to meet the existing and potential alternative standards, the decreases in the 2007 composite monitor values tend to be larger than in 2009, and there tend to be fewer increases. However, it is worth noting that since the emissions and meteorological inputs used in the CMAQ/HDDM modeling for the air quality adjustments were based on 2007 data, we tend to have more confidence in the adjusted values for 2007 than for 2009.

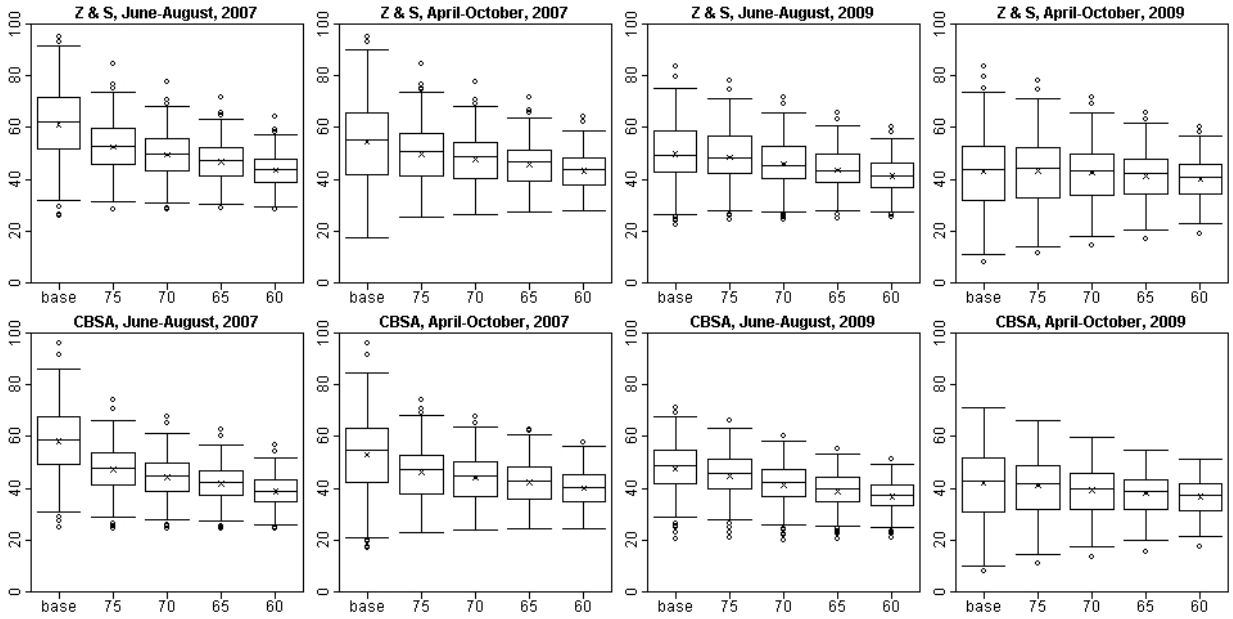

Figure 4D-58. Composite monitor daily maximum 8-hour O_3 values for Atlanta based on observed and adjusted air quality. Boxes represent the median and quartiles, x's represent mean values, whiskers extend up to 1.5x the inter-quartile range from the boxes, and circles represent outliers.

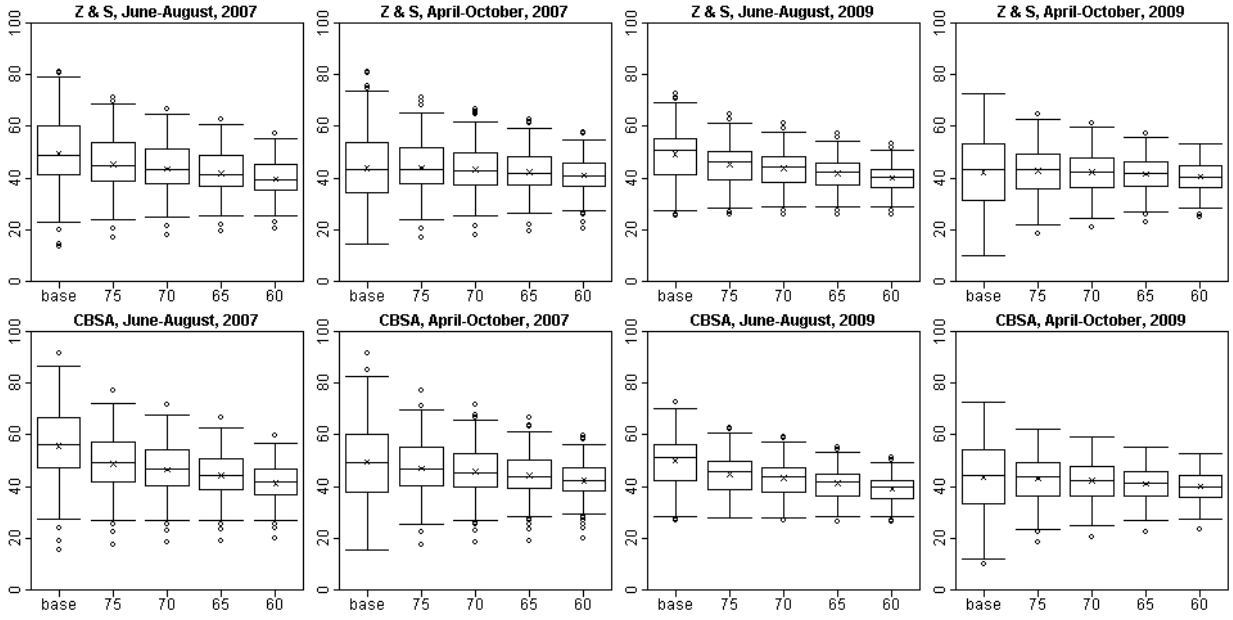

Figure 4D-59. Composite monitor daily maximum 8-hour O_3 values for Baltimore based on observed and adjusted air quality. Boxes represent the median and quartiles, x's represent mean values, whiskers extend up to 1.5x the inter-quartile range from the boxes, and circles represent outliers.

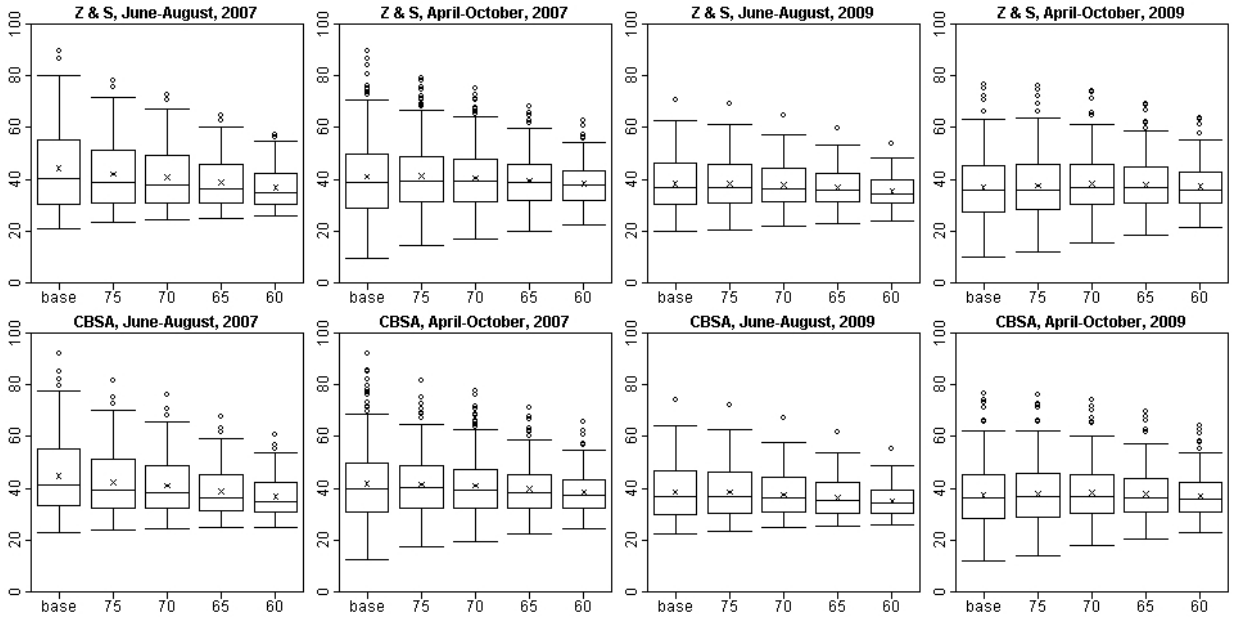

Figure 4D-60. Composite monitor daily maximum 8-hour O_3 values for Boston based on observed and adjusted air quality. Boxes represent the median and quartiles, x's represent mean values, whiskers extend up to 1.5x the inter-quartile range from the boxes, and circles represent outliers.

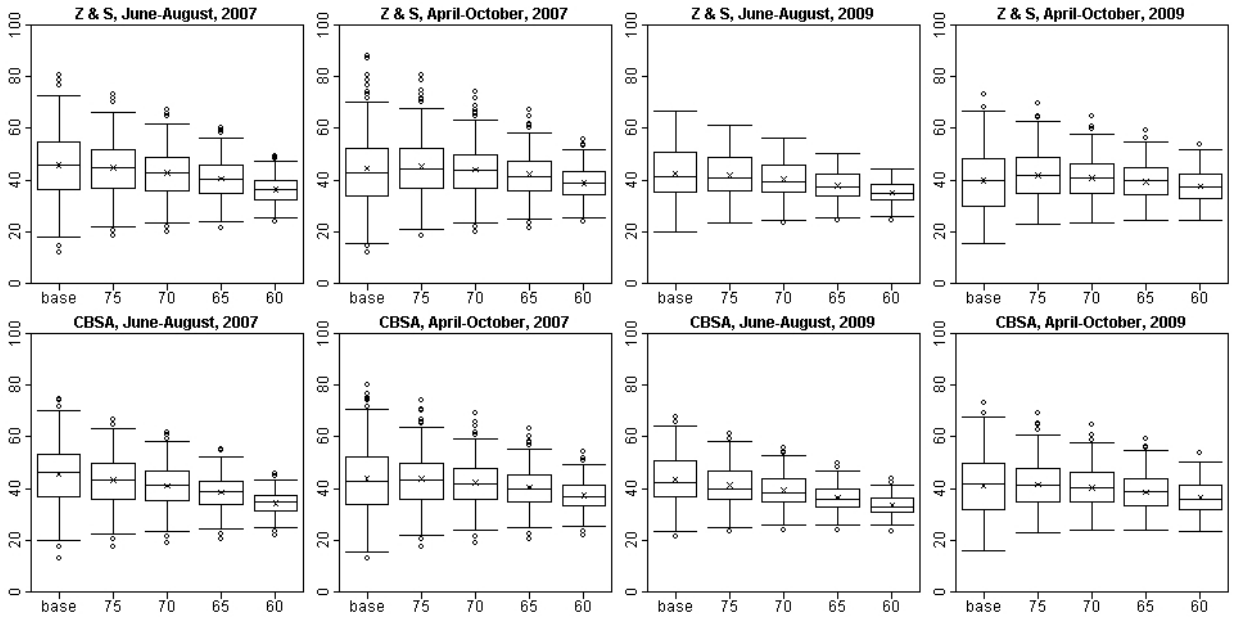

Figure 4D-61. Composite monitor daily maximum 8-hour O_3 values for Cleveland based on observed and adjusted air quality. Boxes represent the median and quartiles, x's represent mean values, whiskers extend up to 1.5x the inter-quartile range from the boxes, and circles represent outliers.

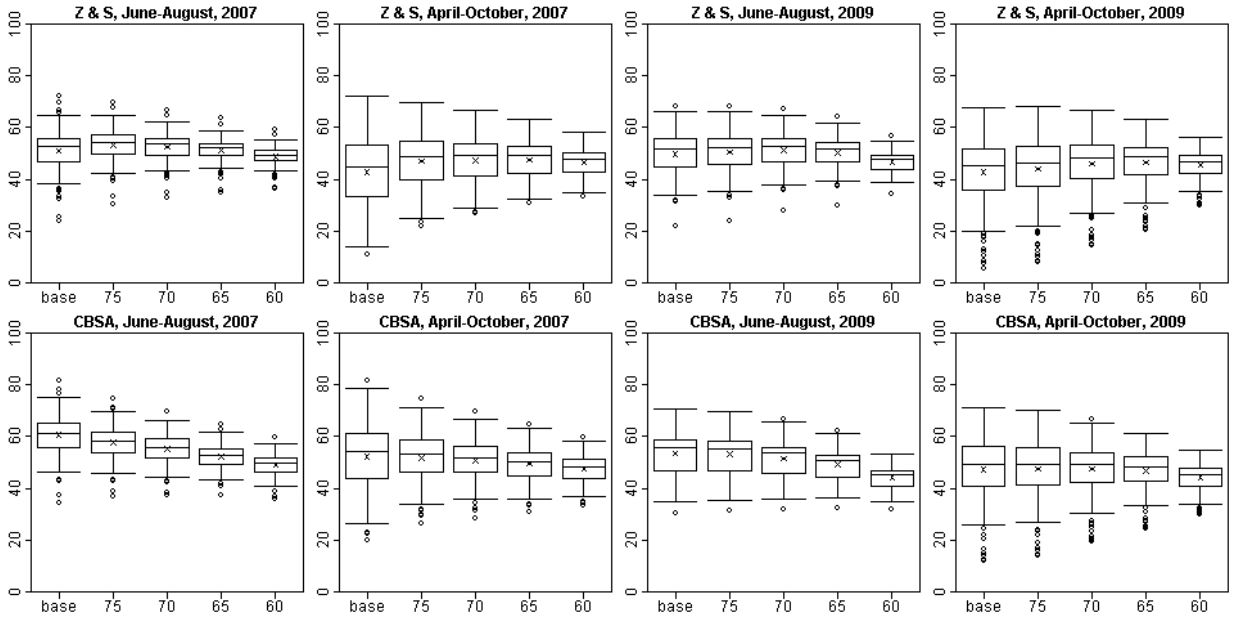

Figure 4D-62. Composite monitor daily maximum 8-hour O_3 values for Denver based on observed and adjusted air quality. Boxes represent the median and quartiles, x's represent mean values, whiskers extend up to 1.5x the inter-quartile range from the boxes, and circles represent outliers.

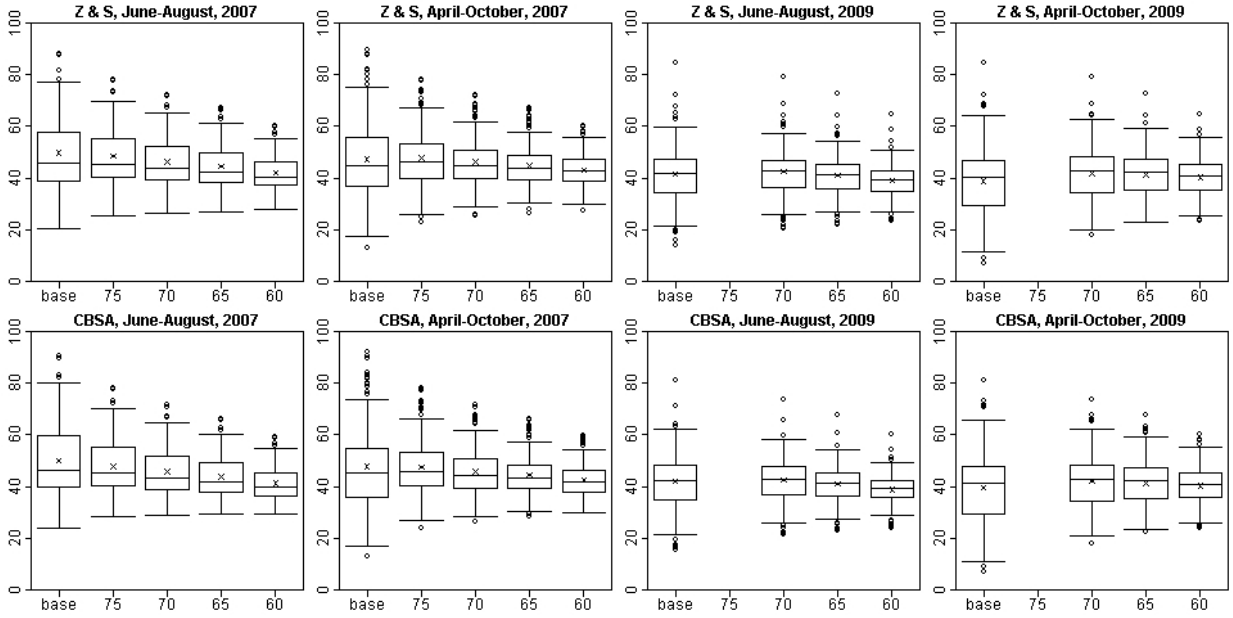

Figure 4D-63. Composite monitor daily maximum 8-hour O_3 values for Detroit based on observed and adjusted air quality. Boxes represent the median and quartiles, x's represent mean values, whiskers extend up to 1.5x the inter-quartile range from the boxes, and circles represent outliers.

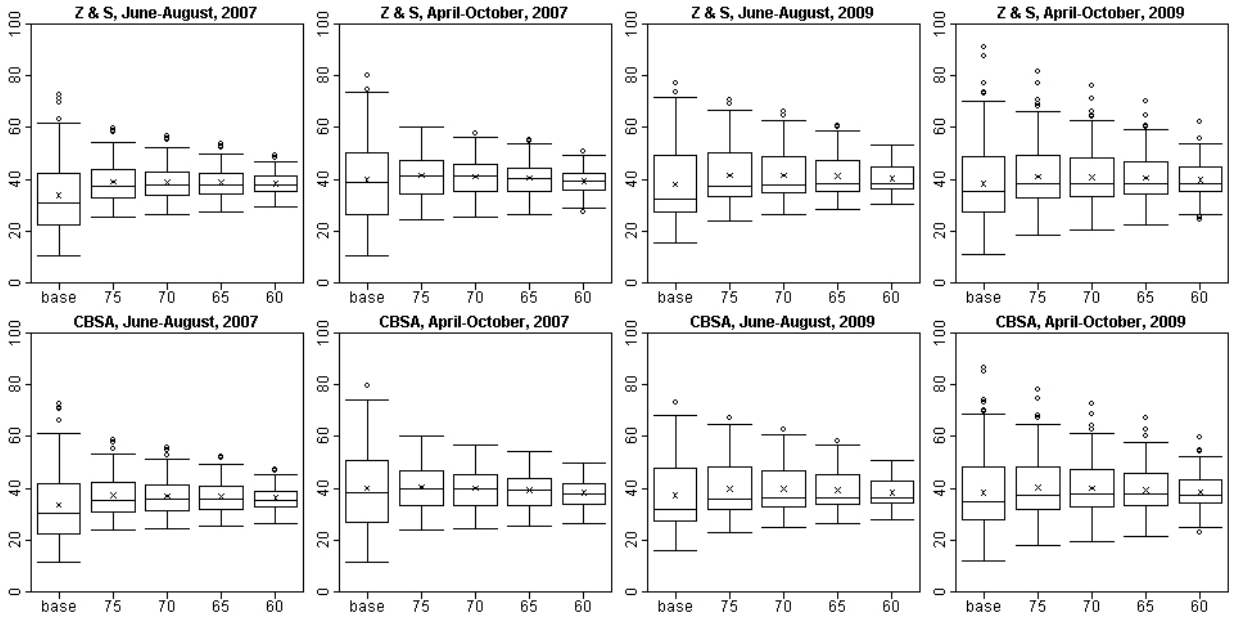

Figure 4D-64. Composite monitor daily maximum 8-hour O_3 values for Houston based on observed and adjusted air quality. Boxes represent the median and quartiles, x's represent mean values, whiskers extend up to 1.5x the inter-quartile range from the boxes, and circles represent outliers.

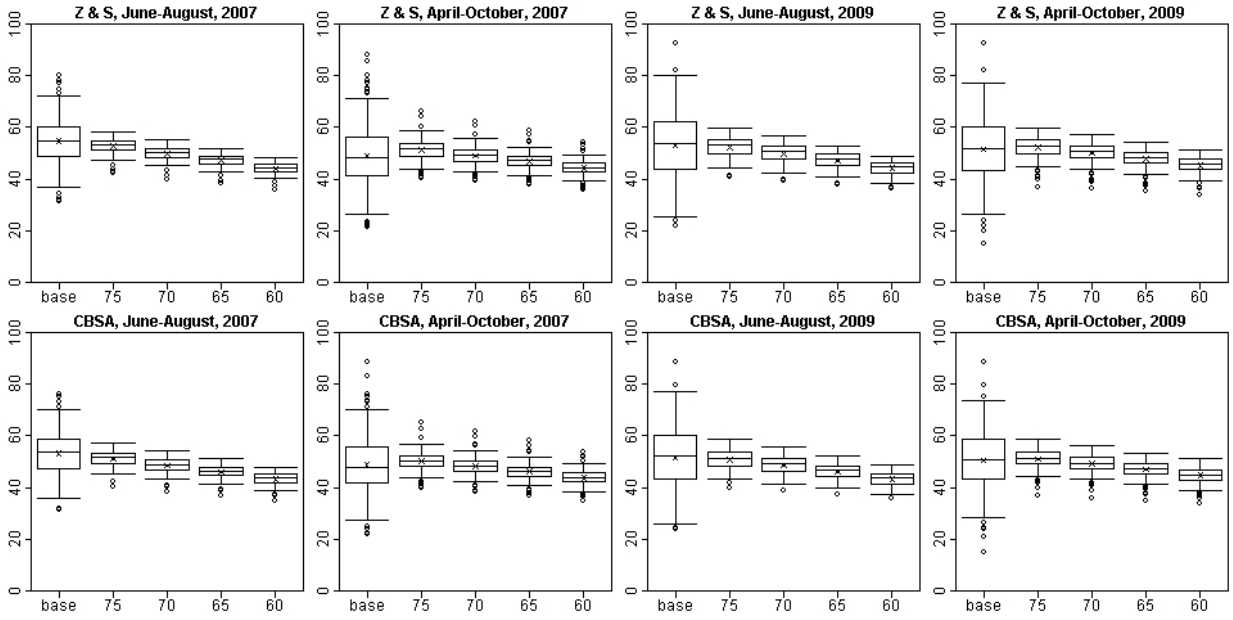

Figure 4D-65. Composite monitor daily maximum 8-hour O_3 values for Los Angeles based on observed and adjusted air quality. Boxes represent the median and quartiles, x's represent mean values, whiskers extend up to 1.5x the inter-quartile range from the boxes, and circles represent outliers.

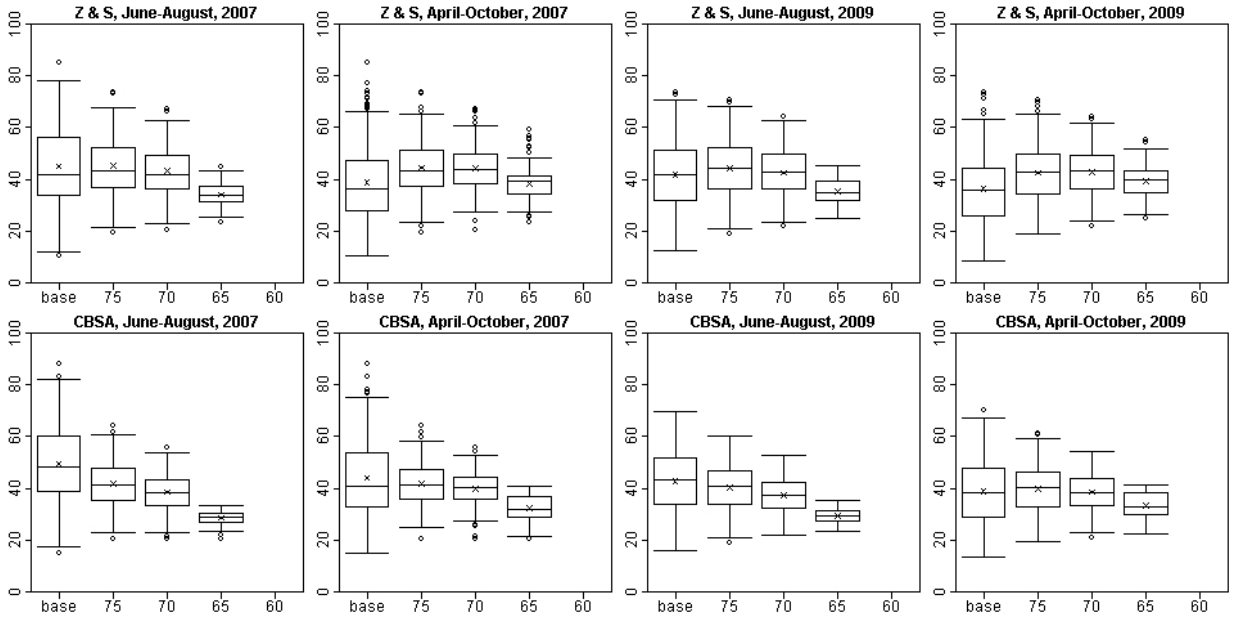

Figure 4D-66. Composite monitor daily maximum 8-hour O_3 values for New York based on observed and adjusted air quality. Boxes represent the median and quartiles, x's represent mean values, whiskers extend up to 1.5x the inter-quartile range from the boxes, and circles represent outliers.

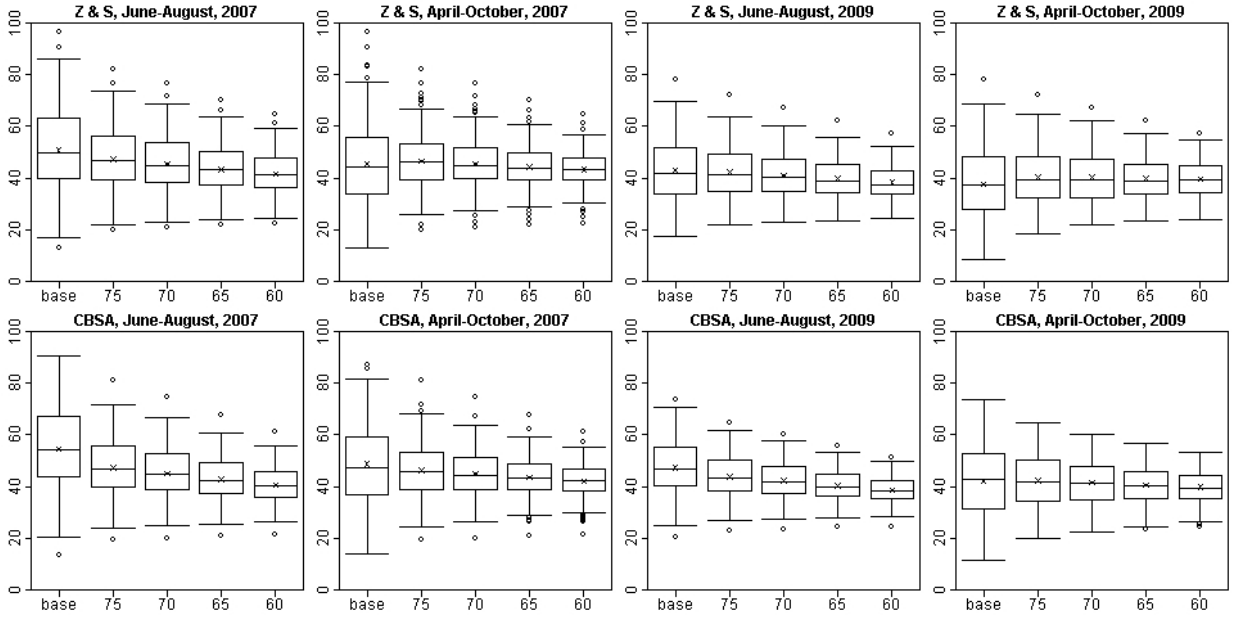

Figure 4D-67. Composite monitor daily maximum 8-hour O_3 values for Philadelphia based on observed and adjusted air quality. Boxes represent the median and quartiles, x's represent mean values, whiskers extend up to 1.5x the inter-quartile range from the boxes, and circles represent outliers.

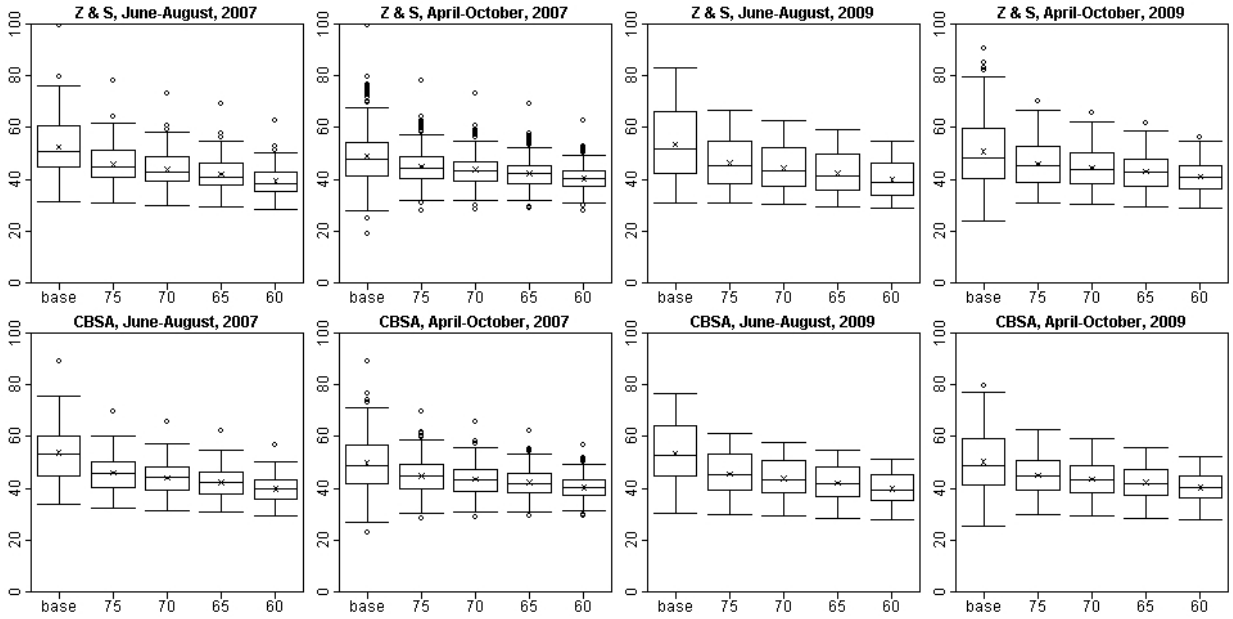

Figure 4D-68. Composite monitor daily maximum 8-hour O_3 values for Sacramento based on observed and adjusted air quality. Boxes represent the median and quartiles, x's represent mean values, whiskers extend up to 1.5x the inter-quartile range from the boxes, and circles represent outliers.

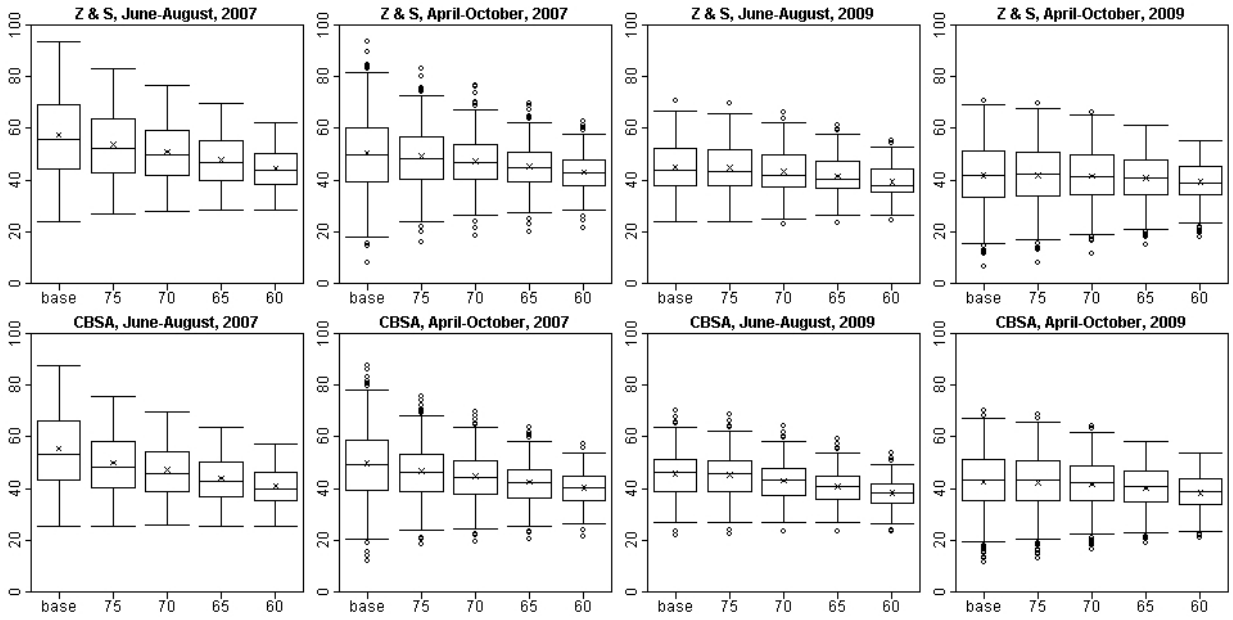

Figure 4D-69. Composite monitor daily maximum 8-hour O_3 values for St. Louis based on observed and adjusted air quality. Boxes represent the median and quartiles, x's represent mean values, whiskers extend up to 1.5x the inter-quartile range from the boxes, and circles represent outliers.

4D-4.6 Air Quality Inputs for the Exposure and Clinical Risk Assessment

The air quality inputs for the exposure and clinical-based risk assessments discussed in HREA Chapters 5 and 6 include spatial surfaces of hourly O_3 concentrations estimated for each census tract in the 15 urban study areas using Voronoi Neighbor Averaging (VNA). The VNA technique and its application to ambient concentrations is described in Appendix 4A. In this section, we present three types of figures that summarize the data from the hourly VNA surfaces (1) observed air quality, (2) air quality adjusted to meet the existing standard,[7] and (3) air quality adjusted to meet the potential alternative standard of 65 ppb.

Figure 4D-70 through Figure 4D-84 show density scatter plots of the change in daily maximum 8-hour average (MDA8) O_3 concentrations versus the observed concentration based on the hourly VNA estimates in each area. In each of these figures, the left-hand panels show the observed MDA8 values (x-axis) versus the change in those values that occur when air quality is adjusted to meet the existing standard (y-axis). The right-hand panels show the MDA8 values for air quality adjusted to meet the existing standard[7] (x-axis) versus the additional change in those values that occur when air quality is further adjusted to meet the alternative standard of 65 ppb (y-axis). The top panels show values based on 2006-2008, while the bottom panels show values based on 2008-2010. Within each panel, the x and y values are rounded to the nearest integer and colored to show the relative frequency of each 1 ppb x 1 ppb square within the plot region. Values falling outside of the plot region were set to the nearest value within the plot region, and frequencies above the range in the color bar were set to the highest value within the color bar.

Figure 4D-85 through Figure 4D-114 show maps of the changes in design values (3-year average of the annual 4th highest MDA8 values) and May – September average MDA8 values based on the ambient data and the hourly VNA surfaces. There are two figures for each of the 15 urban study areas, one based on 2006-2008 and one based on 2008-2010 air quality. In each figure, the panels on the left show the changes in these values that occur when air quality is adjusted to meet the existing standard,[7] and the panels on the right show the additional changes in these values that occur when air quality is further adjusted to meet the alternative standard of 65 ppb. The top panels show the changes in the design values, while the bottom panels show the changes in the May – September average MDA8 values. Within each panel, squares show values based on observed data at ambient O_3 monitoring sites while circles show values based on VNA estimates at census tract centroids. Regions shaded pink indicate counties in either the Z & S or Smith study areas (for the 12 urban study areas in the epidemiology-based risk assessment). The Z & S and Smith study areas had a few counties in common in all 12 areas, and were identical in

[7] Chicago and Detroit were already meeting the existing standard in 2008-2010. The 2008-2010 figures for those areas are based on air quality adjusted to meet the 70 ppb alternative standard instead of the existing standard.

6 of the areas. Regions shaded gray indicate additional counties in the CBSA, and regions shaded peach indicate any additional counties in the study areas for the exposure and clinical-based risk assessment. The maps also show monitors that are located outside of the exposure study areas. These monitors were adjusted along with the other monitors and used in the VNA estimates, but were not used when determining the emissions reductions necessary to meet standard levels.

Figure 4D-115 through Figure 4D-129 show changes in design values (3-year average of the annual 4th highest MDA8 values) and May – September average MDA8 values in the 15 urban study areas versus population and population density. The population counts and population density information for each census tract were obtained from the U.S. Census Bureau based on the 2010 U.S. Census. Within each figure, the top panels show histograms of the total population stratified by the change in design value or seasonal average, while the bottom panels show scatter plots of population density (x-axis) versus change in design value or seasonal average (y-axis). The left-hand panels are based on 2006-2008, while the right-hand panels are based on 2008-2010. The first and third rows of panels show changes in design values, while the second and fourth rows of panels show changes in May-September average values. Finally, the first and third columns show the changes that occur when air quality is adjusted to meet the existing standard,[7] while the second and fourth columns show the additional changes that occur when air quality is further adjusted to meet the alternative standard of 65 ppb. Within each panel, values associated with census tracts falling within the epidemiology study areas as defined previously are colored pink, values associated with additional census tracts falling within the CBSA are colored gray, and values associated with any additional census tracts falling within the exposure study areas are colored peach. Population density is shown on a logarithmic scale, with values falling outside of the plot region set to the nearest values within the plot region.

In general, the density scatter plots show that the HDDM adjustment procedure predicts increases in MDA8 O_3 at low ambient concentrations, and decreases in MDA8 O_3 at high concentrations. The vast majority of the increases in MDA8 O_3 occur at ambient concentrations below 50 ppb. The relationship between the starting concentrations and the changes in these values based on the HDDM adjustments is fairly linear with strong negative correlation in all 15 urban areas. In some areas, such as Baltimore and Philadelphia, there is a bimodal pattern near the center of the distribution that could indicate a differing behavior in the urban population center versus the surrounding suburban areas.

The maps reveal several trends in the spatial pattern of changes in O_3 in the urban study areas. The design values decreased almost universally when air quality was adjusted to meet the existing standard with a few exceptions,[8] and continued to decrease when air quality was further

[8] All design values from the VNA surfaces decreased when adjusted from recent conditions to the 75 ppb level except for the following: small areas in Boston where design values increased by up to 1 ppb (2008-2010),

adjusted to meet the 65 ppb alternative standard. The design values also tended to decrease more quickly in suburban and rural areas than in the urban population centers. The May-September "seasonal" average MDA8 values also followed this trend to some extent. However, the decreases in the seasonal average values were nearly universal in the suburban and rural areas, while the behavior in the urban population centers varied amongst the cities. The seasonal average values in the urban population centers followed one of three distinct patterns:

1. The seasonal average values decreased when air quality was adjusted to meet the existing standard, and continued to decrease when air quality was further adjusted to meet the 65 ppb alternative standard. (Atlanta, Sacramento, Washington D.C.)
2. The seasonal average values increased or remained constant when air quality was adjusted to meet the existing standard, then decreased when air quality was adjusted to meet the 65 ppb alternative standard. (Baltimore, Cleveland, Dallas, Detroit, Los Angeles, New York, Philadelphia, St. Louis)
3. The seasonal average values increased when air quality was adjusted to meet the existing standard, and continued to increase or remained constant when air quality was further adjusted to meet the 65 ppb alternative standard. (Boston, Chicago, Houston, Denver)

The population plots show a clear and consistent trend regarding the population living in areas associated with various changes in design values and seasonal average concentrations. In almost every figure, there is a positive correlation between population density and change in design value or seasonal average concentration. This suggests that in almost every scenario, when NO_x emissions were reduced, the suburban areas surrounding the urban population center experience more O_3 reductions than in the urban population center. For the 12 urban areas examined in the epidemiology-based risk assessment, the majority of the areas associated with increases in the seasonal average concentration occurred within the epidemiology study area, which tended to be focused on the urban population center.

These figures show that using the HDDM adjustment methodology, peak O_3 concentrations are reduced in urban areas with large domain-wide reductions in U.S. anthropogenic NO_x emissions. In most cases, seasonal average O_3 concentrations also decreased with large domain-wide reductions in U.S. anthropogenic NO_x emissions. However, there were a few cases, such as Chicago and Houston, where current NO_x emissions were high enough to cause titration in the urban population centers so that seasonal average O_3 concentrations were below regional background levels.

Chicago where design values increased by up to 2 ppb (2006-2008) and 4 ppb (2008-2010) and New York where design values increased by up to 3 ppb (2008-2010). All areas where design values increases started with very low design values based on recent air quality conditions.

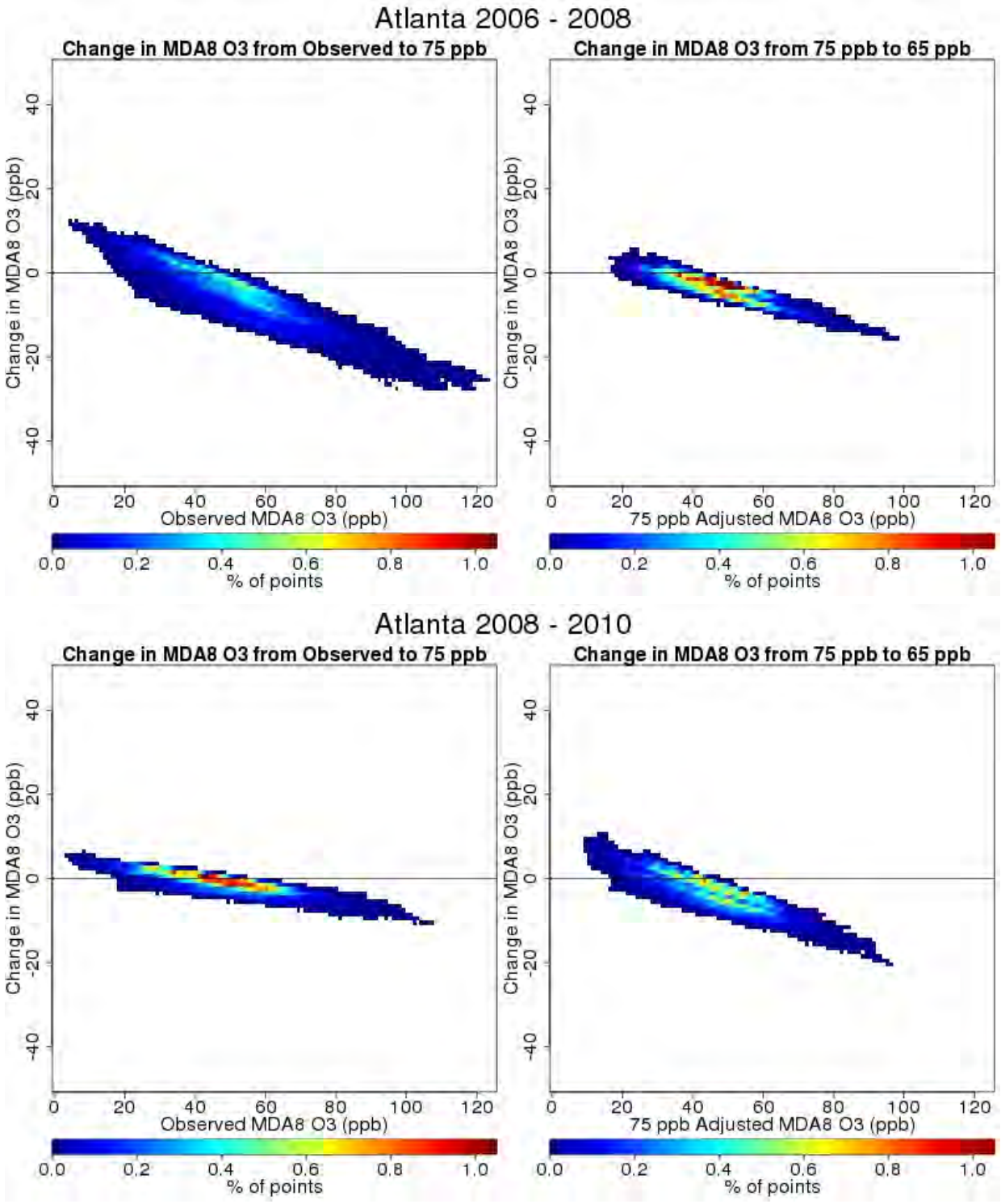

Figure 4D-70. Change in VNA estimates of the daily maximum 8-hour average (MDA8) O_3 concentrations based on HDDM adjustments in Atlanta.

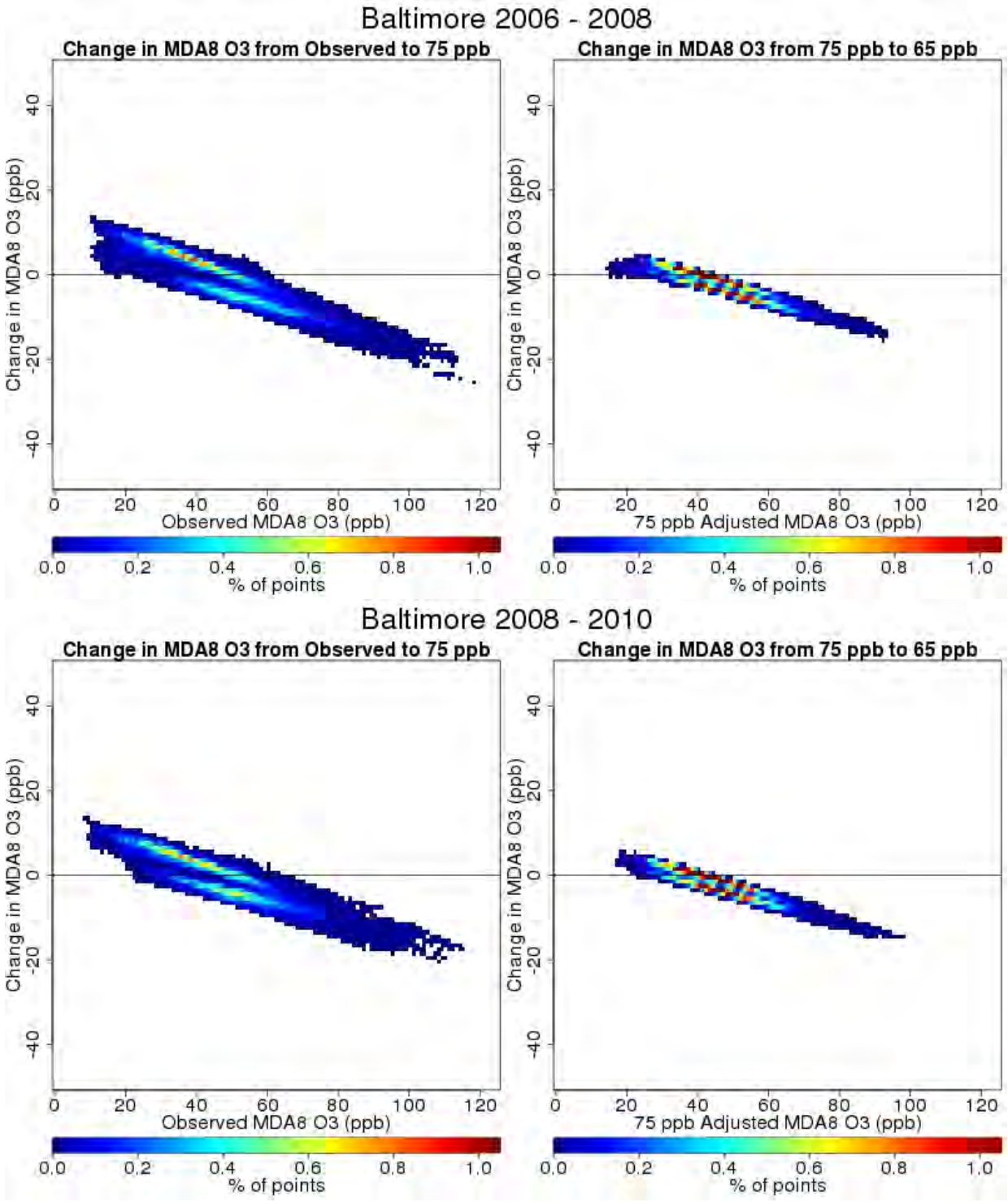

Figure 4D-71. Change in VNA estimates of the daily maximum 8-hour average (MDA8) O_3 concentrations based on HDDM adjustments in Baltimore.

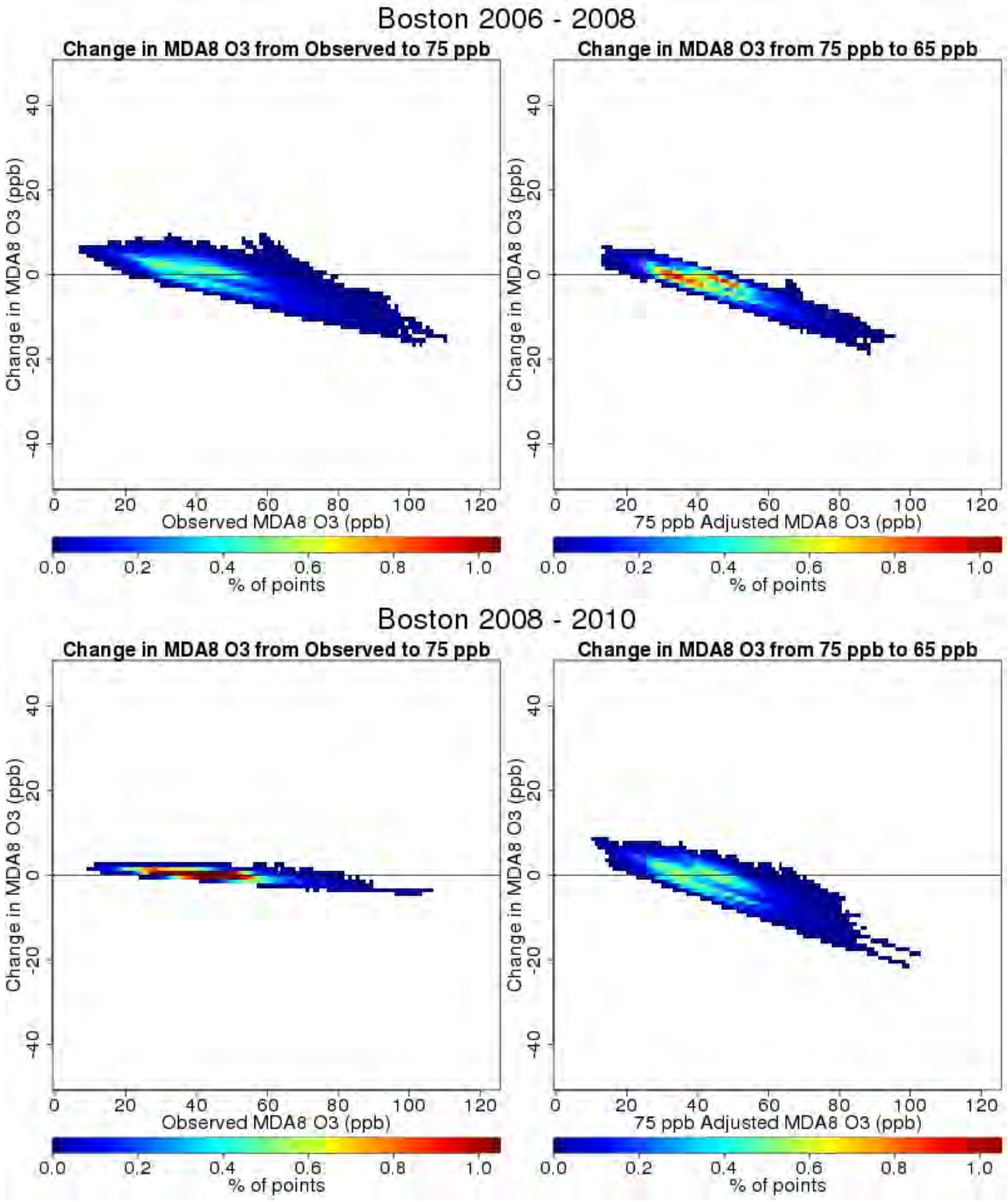

Figure 4D-72. Change in VNA estimates of the daily maximum 8-hour average (MDA8) O_3 concentrations based on HDDM adjustments in Boston.

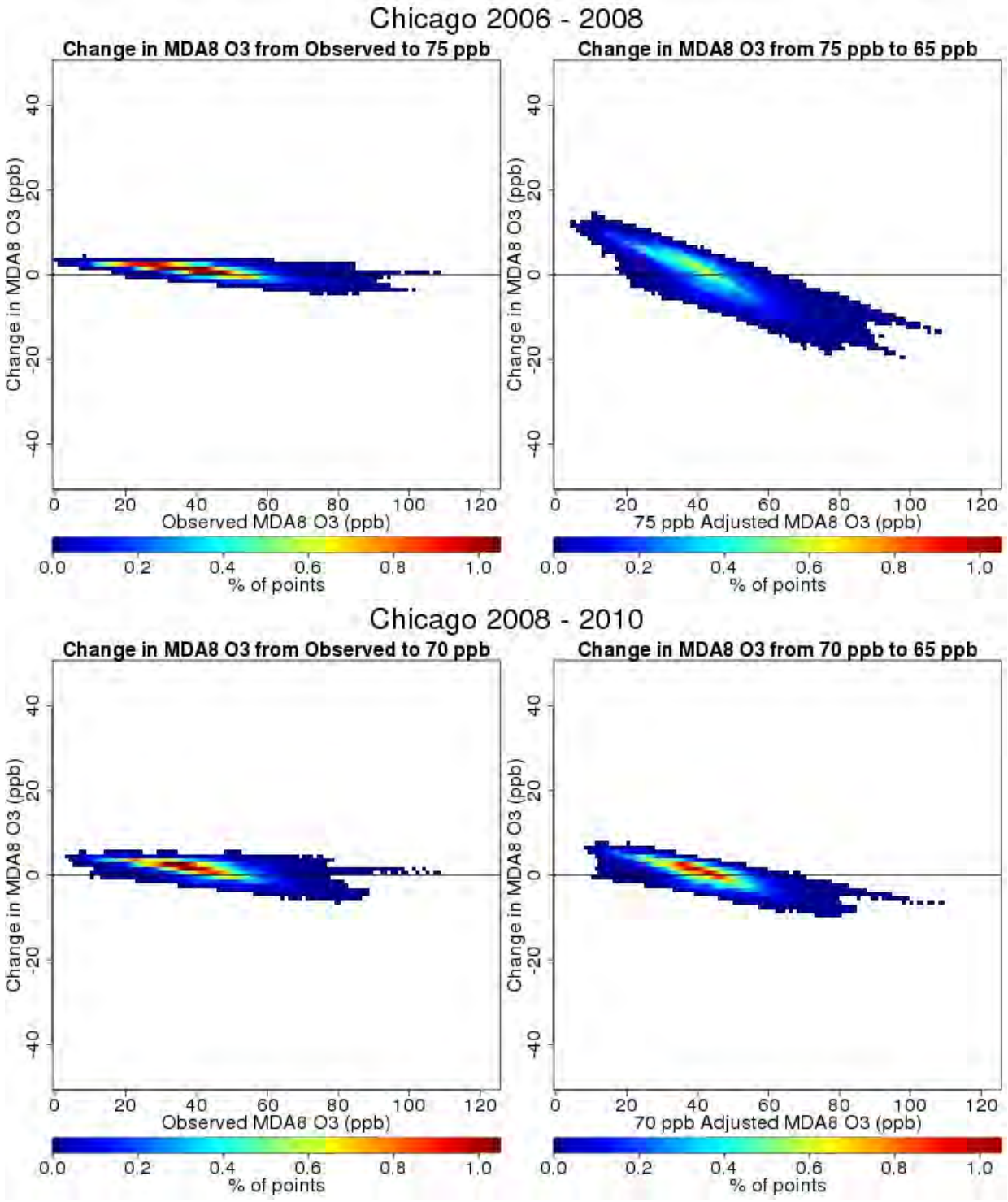

Figure 4D-73. Change in VNA estimates of the daily maximum 8-hour average (MDA8) O_3 concentrations based on HDDM adjustments in Chicago.

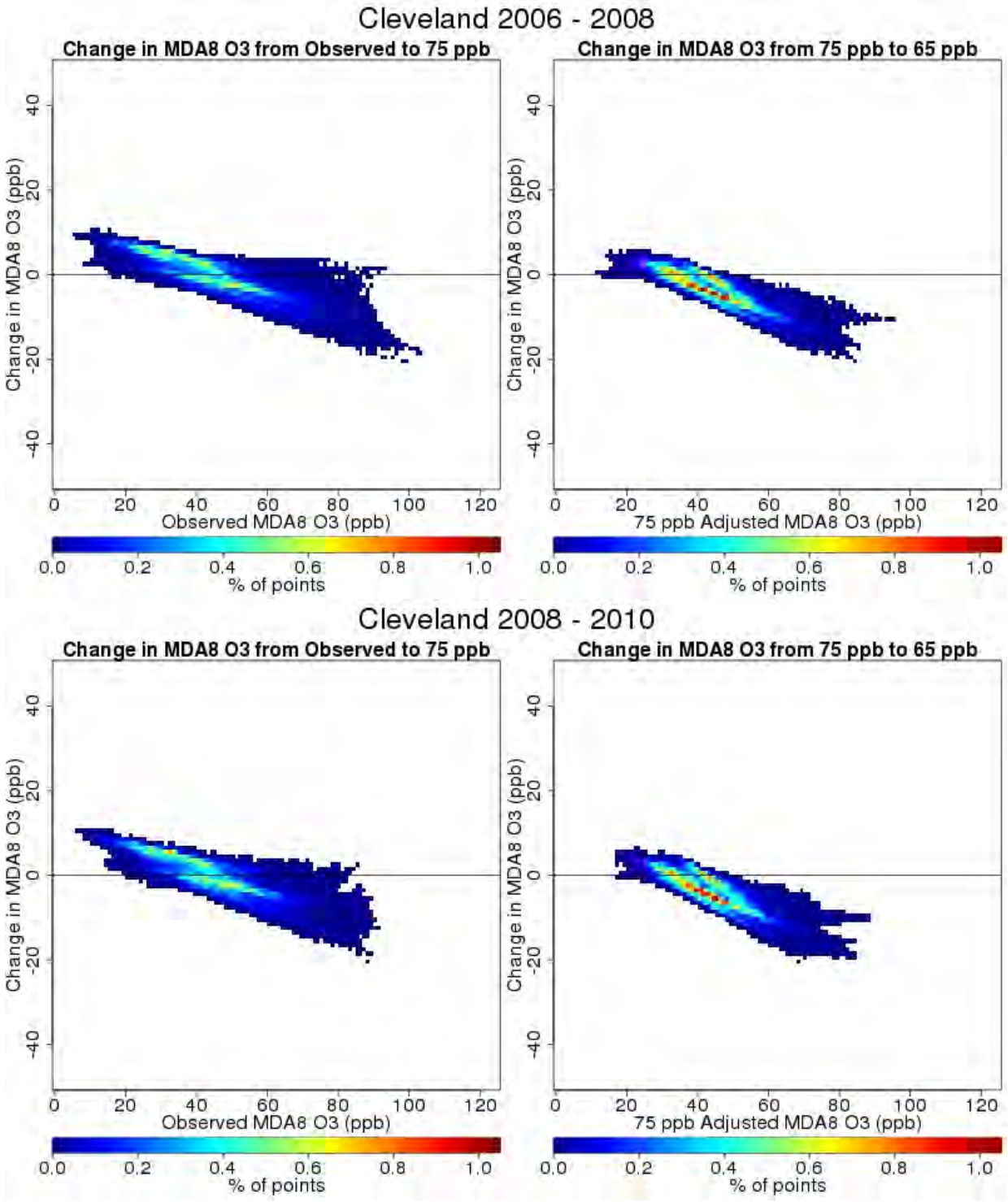

Figure 4D-74. Change in VNA estimates of the daily maximum 8-hour average (MDA8) O_3 concentrations based on HDDM adjustments in Cleveland.

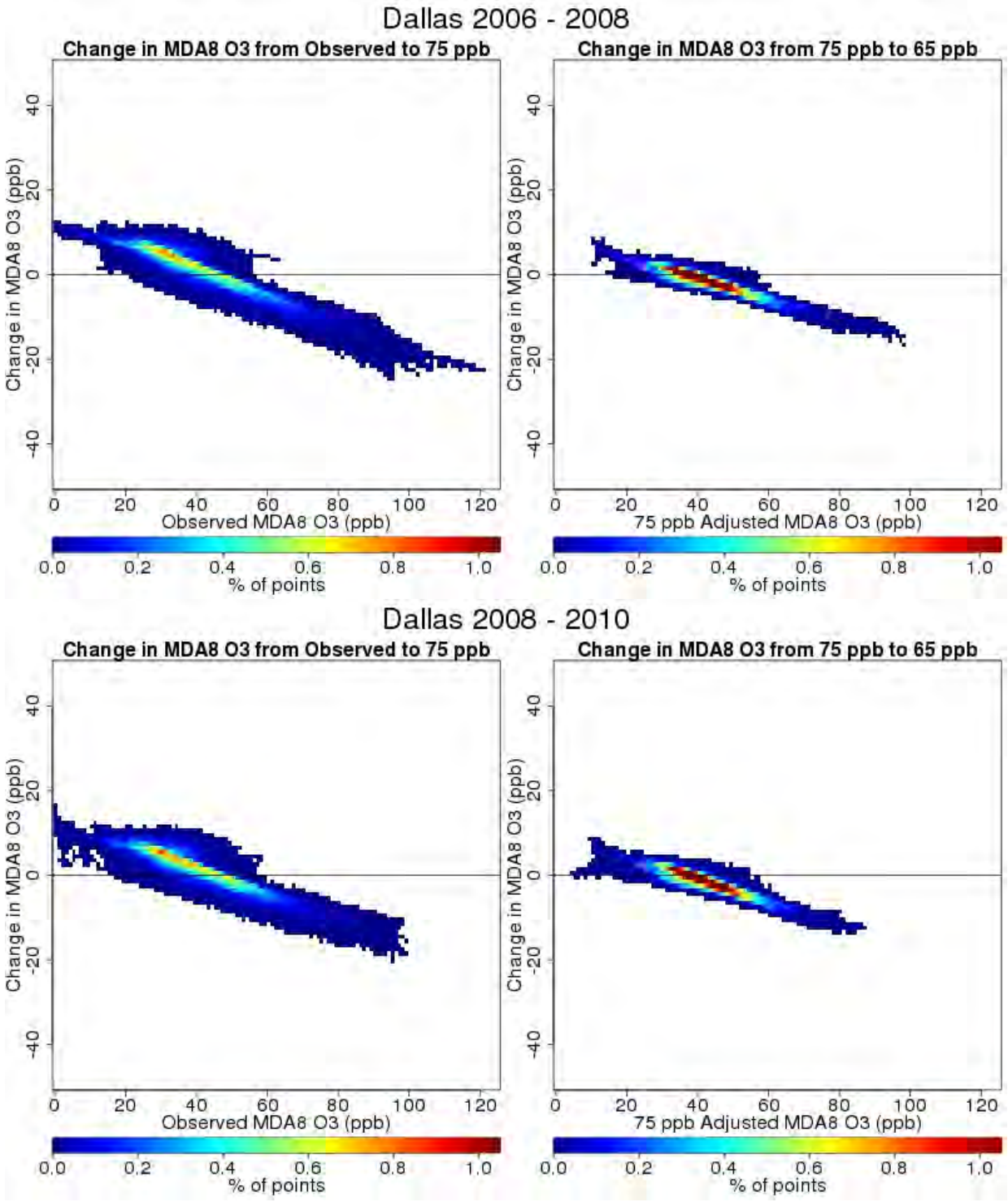

Figure 4D-75. Change in VNA estimates of the daily maximum 8-hour average (MDA8) O_3 concentrations based on HDDM adjustments in Dallas.

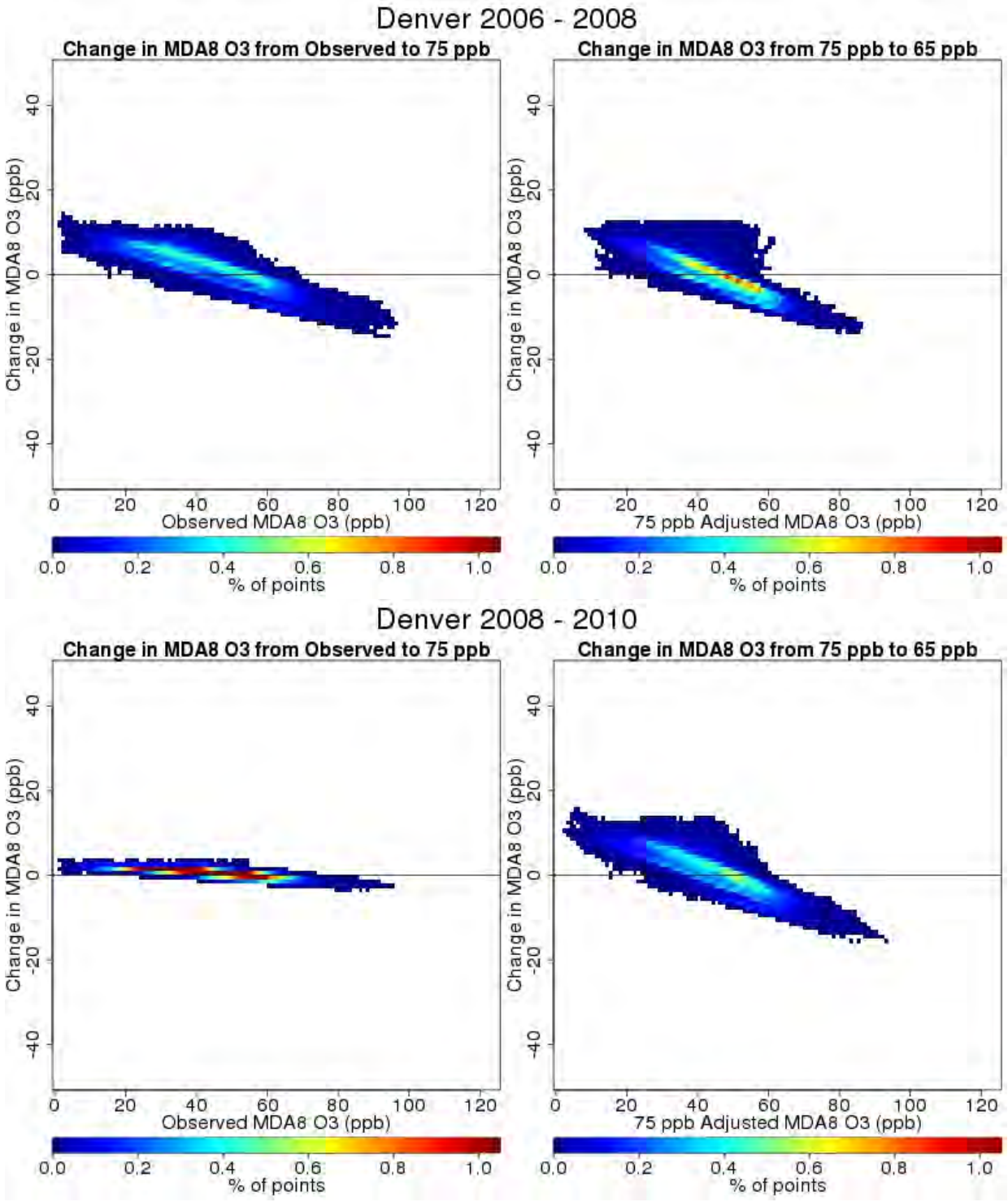

Figure 4D-76. Change in VNA estimates of the daily maximum 8-hour average (MDA8) O_3 concentrations based on HDDM adjustments in Denver.

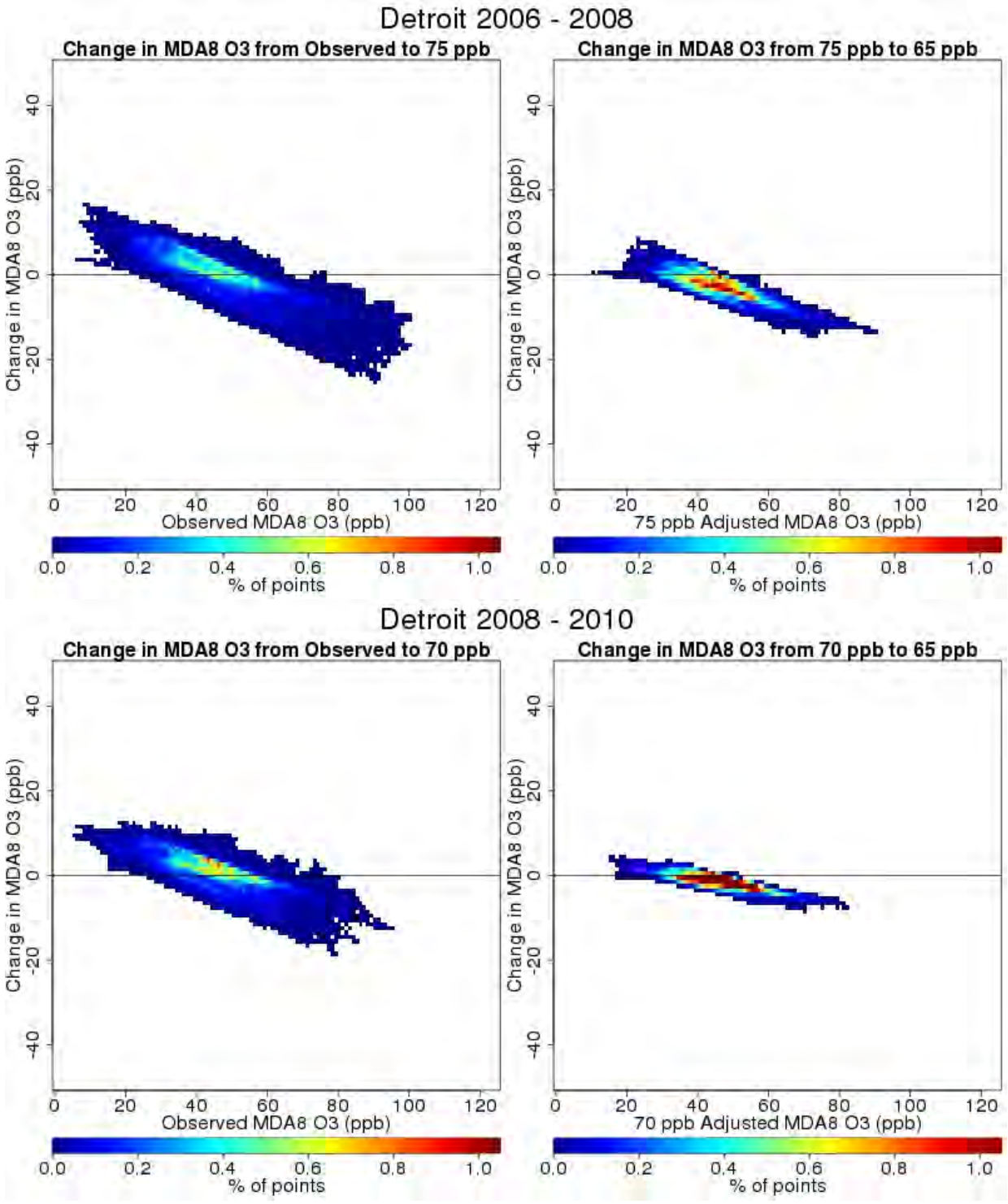

Figure 4D-77. Change in VNA estimates of the daily maximum 8-hour average (MDA8) O_3 concentrations based on HDDM adjustments in Detroit.

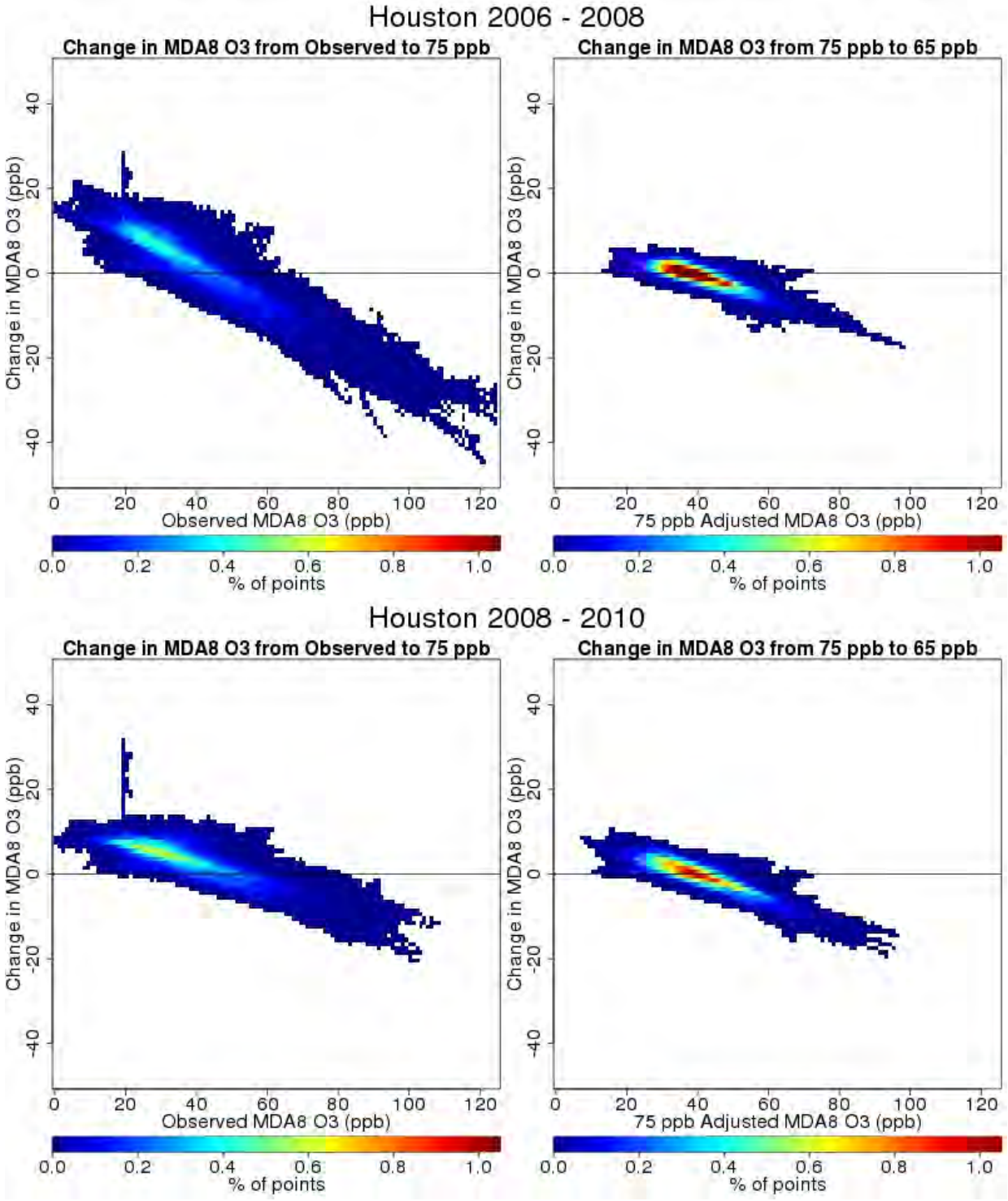

Figure 4D-78. Change in VNA estimates of the daily maximum 8-hour average (MDA8) O_3 concentrations based on HDDM adjustments in Houston.

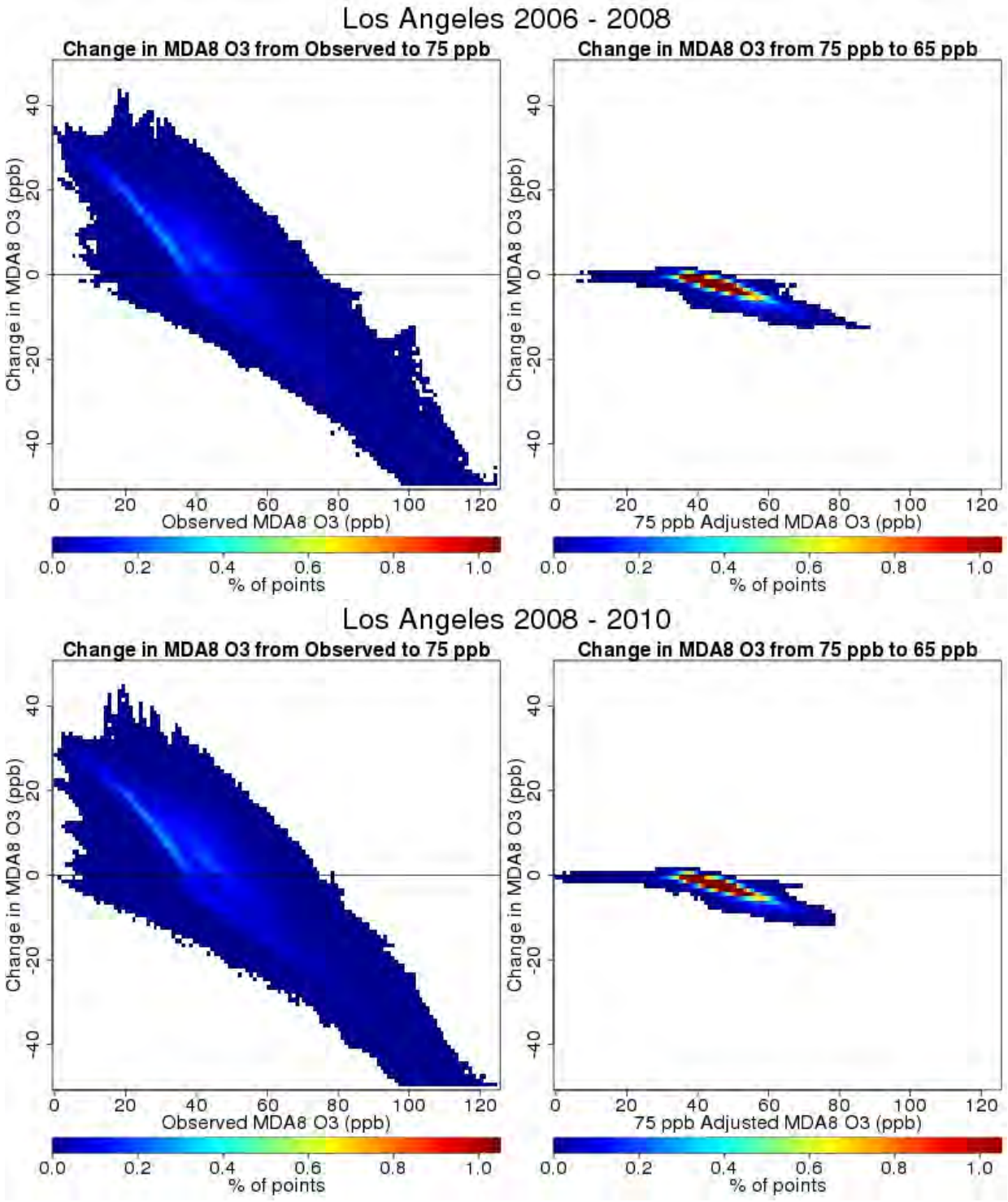

Figure 4D-79. Change in VNA estimates of the daily maximum 8-hour average (MDA8) O_3 concentrations based on HDDM adjustments in Los Angeles.

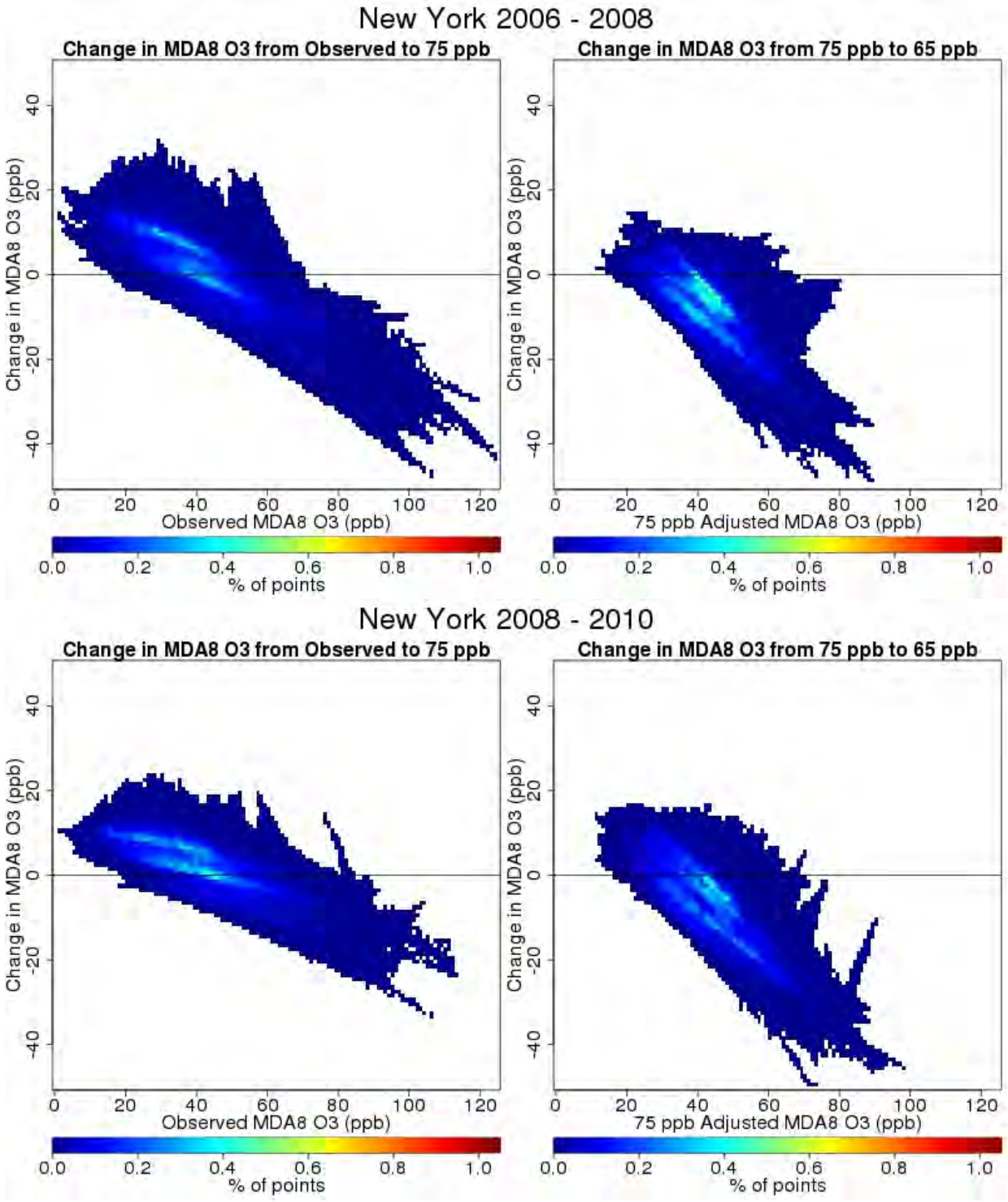

Figure 4D-80. Change in VNA estimates of the daily maximum 8-hour average (MDA8) O_3 concentrations based on HDDM adjustments in New York.

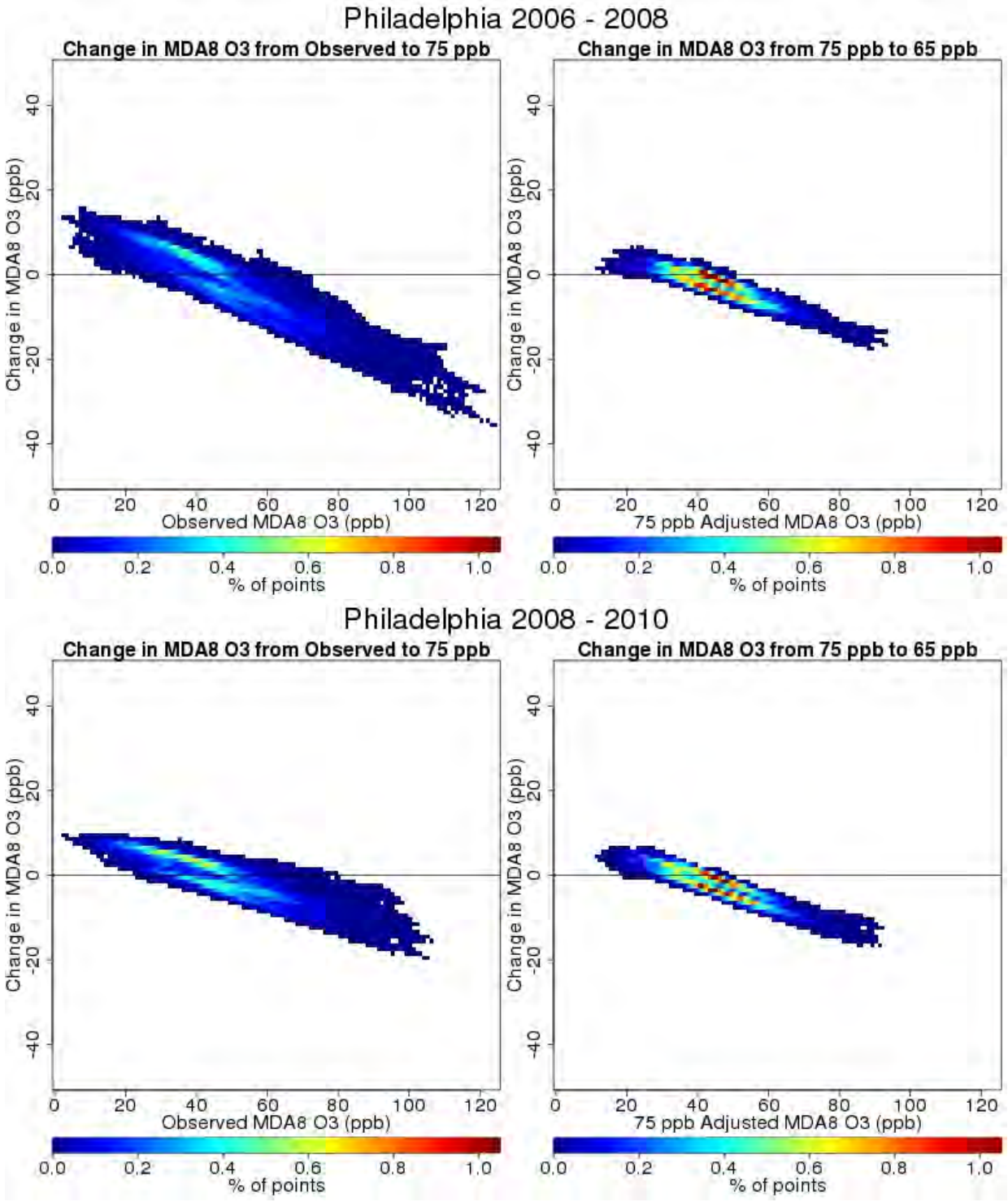

Figure 4D-81. Change in VNA estimates of the daily maximum 8-hour average (MDA8) O_3 concentrations based on HDDM adjustments in Philadelphia.

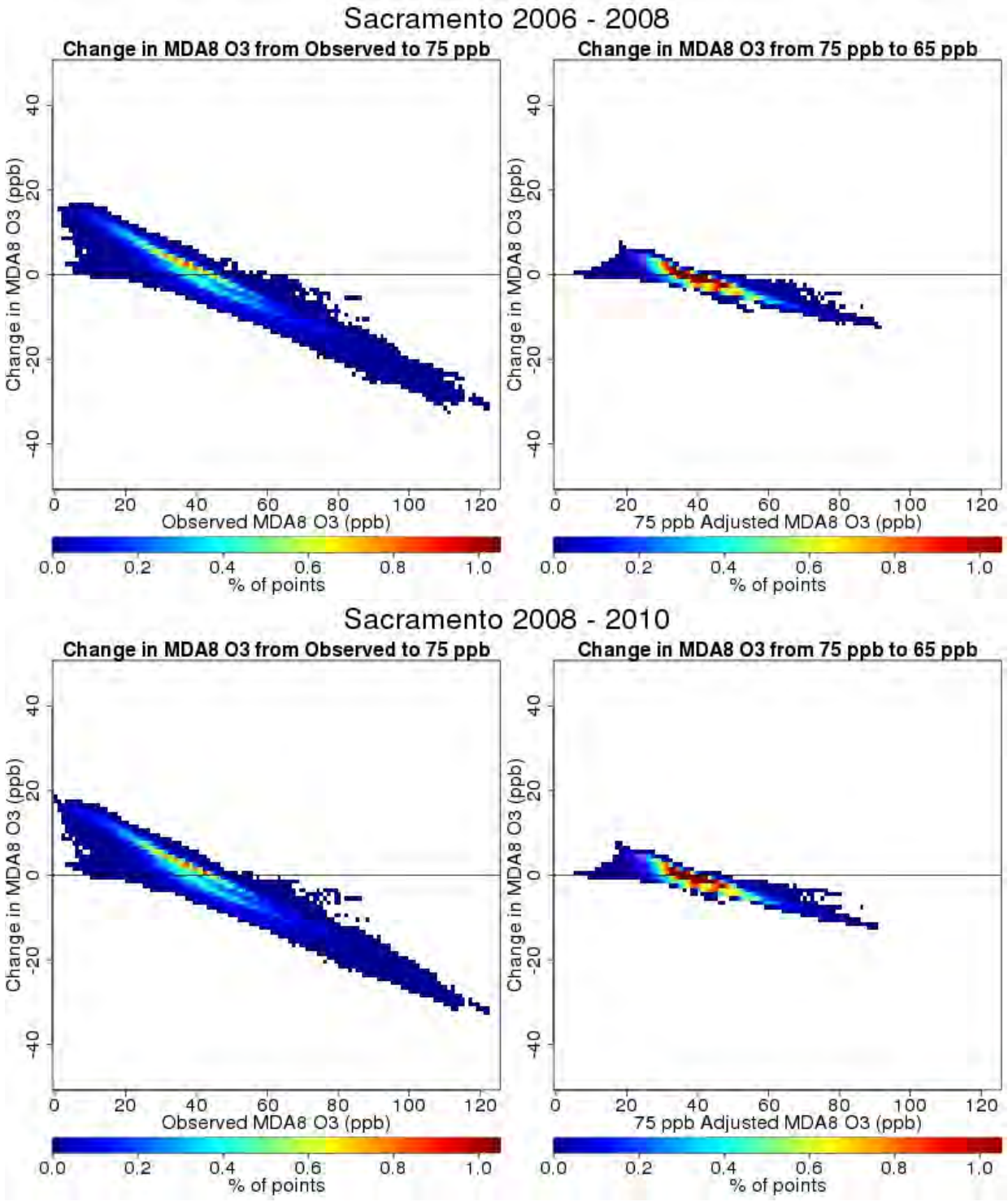

Figure 4D-82. Change in VNA estimates of the daily maximum 8-hour average (MDA8) O_3 concentrations based on HDDM adjustments in Sacramento.

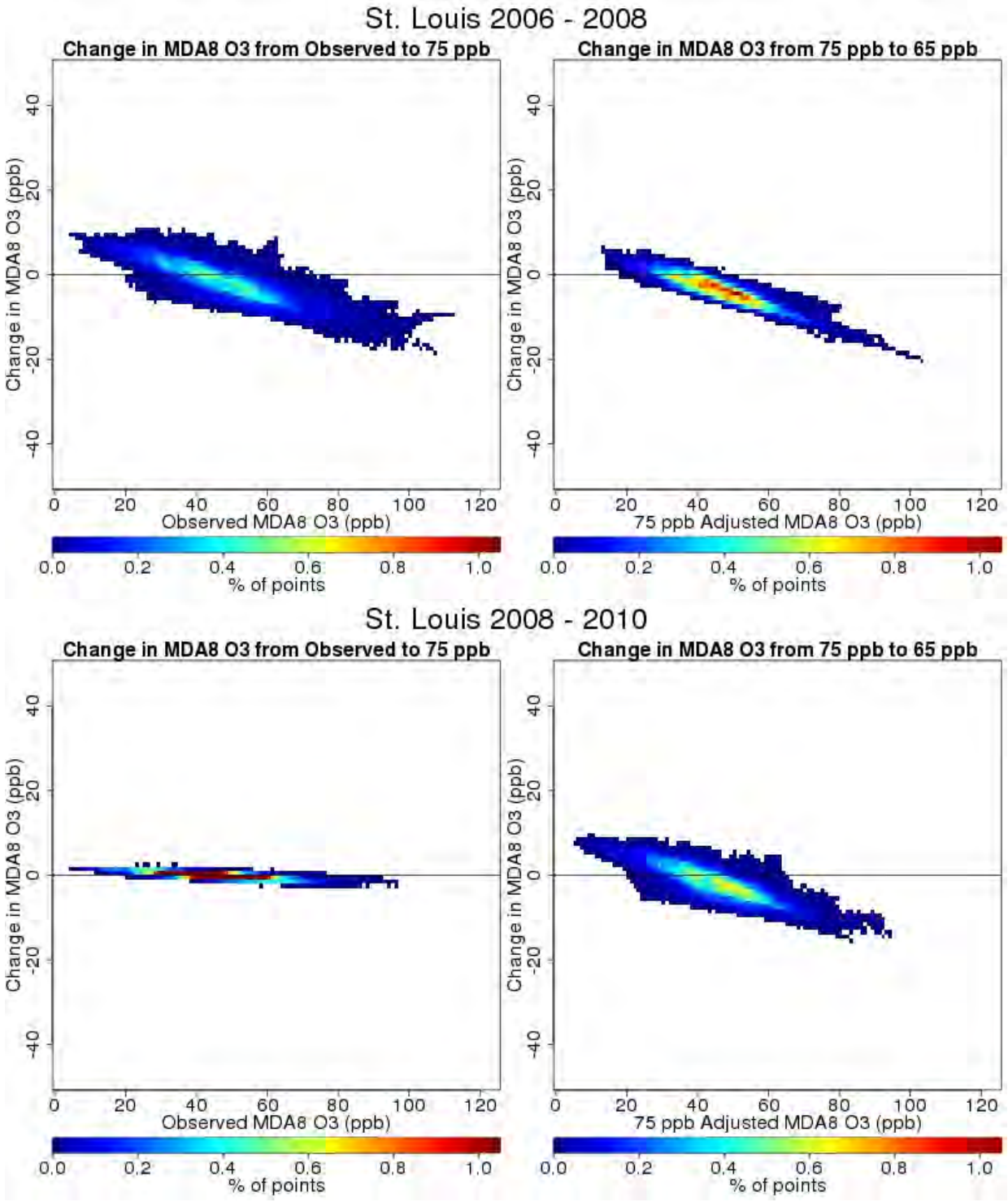

Figure 4D-83. Change in VNA estimates of the daily maximum 8-hour average (MDA8) O_3 concentrations based on HDDM adjustments in St. Louis.

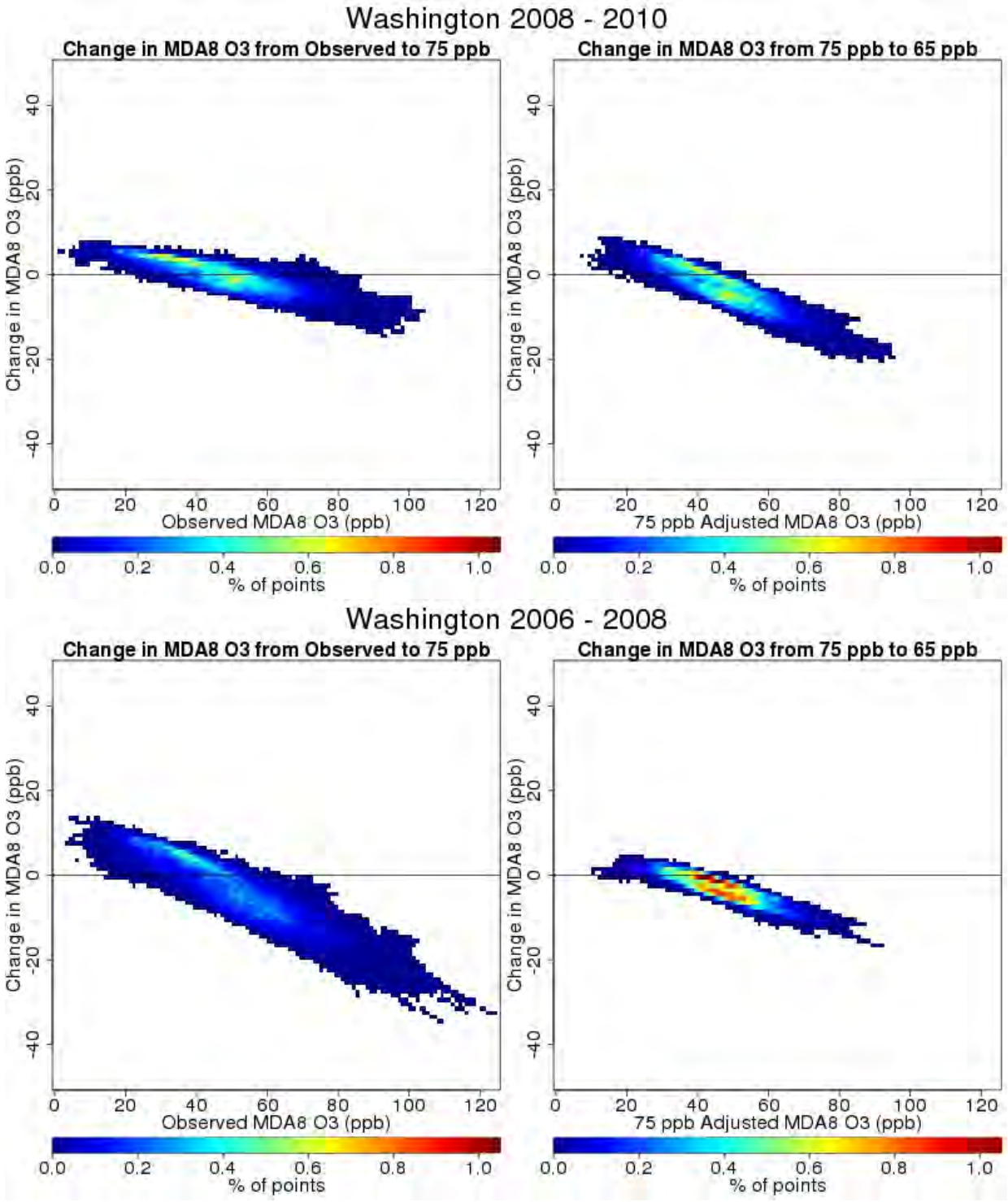

Figure 4D-84. Change in VNA estimates of the daily maximum 8-hour average (MDA8) O3 concentrations based on HDDM adjustments in Washington, D.C.

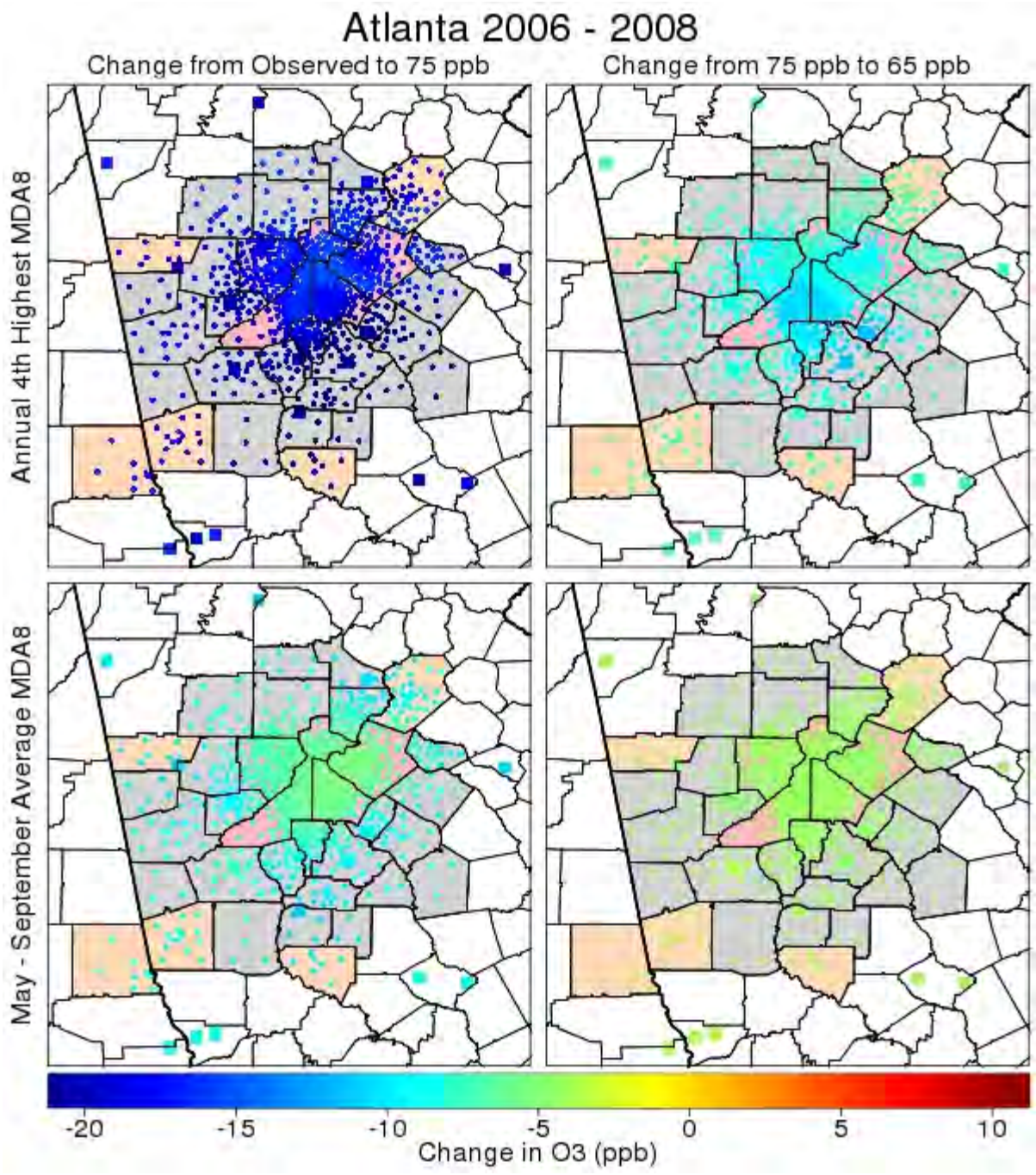

Figure 4D-85. Changes in annual 4th highest MDA8 and May-September average MDA8 values based on HDDM adjustments for Atlanta, 2006-2008. The points are colored according to the change in ppb, and values falling outside the range in the color bar were set to the nearest value within the color bar.

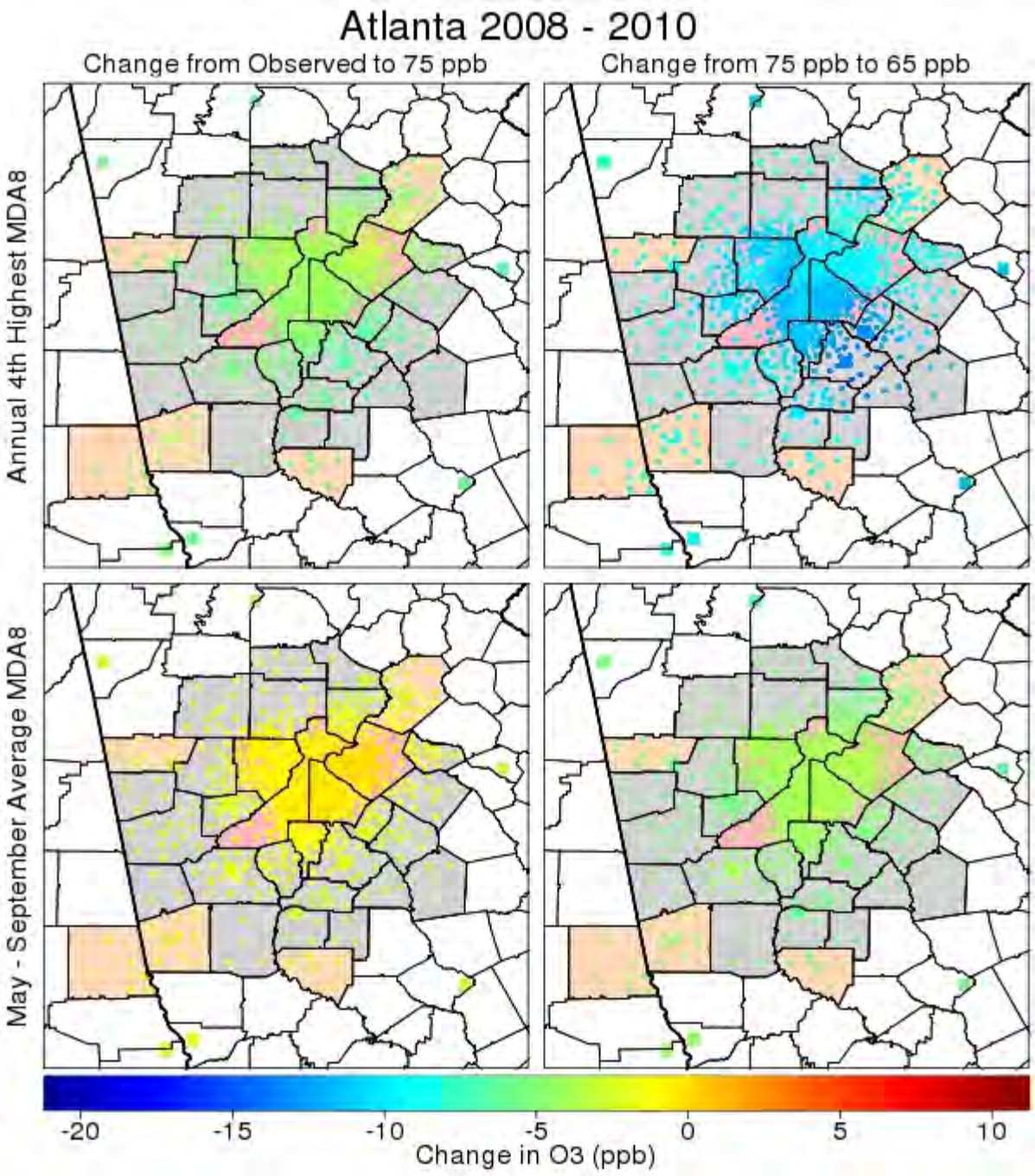

Figure 4D-86. Changes in annual 4th highest MDA8 and May-September average MDA8 values based on HDDM adjustments for Atlanta, 2008-2010. The points are colored according to the change in ppb, and values falling outside the range in the color bar were set to the nearest value within the color bar.

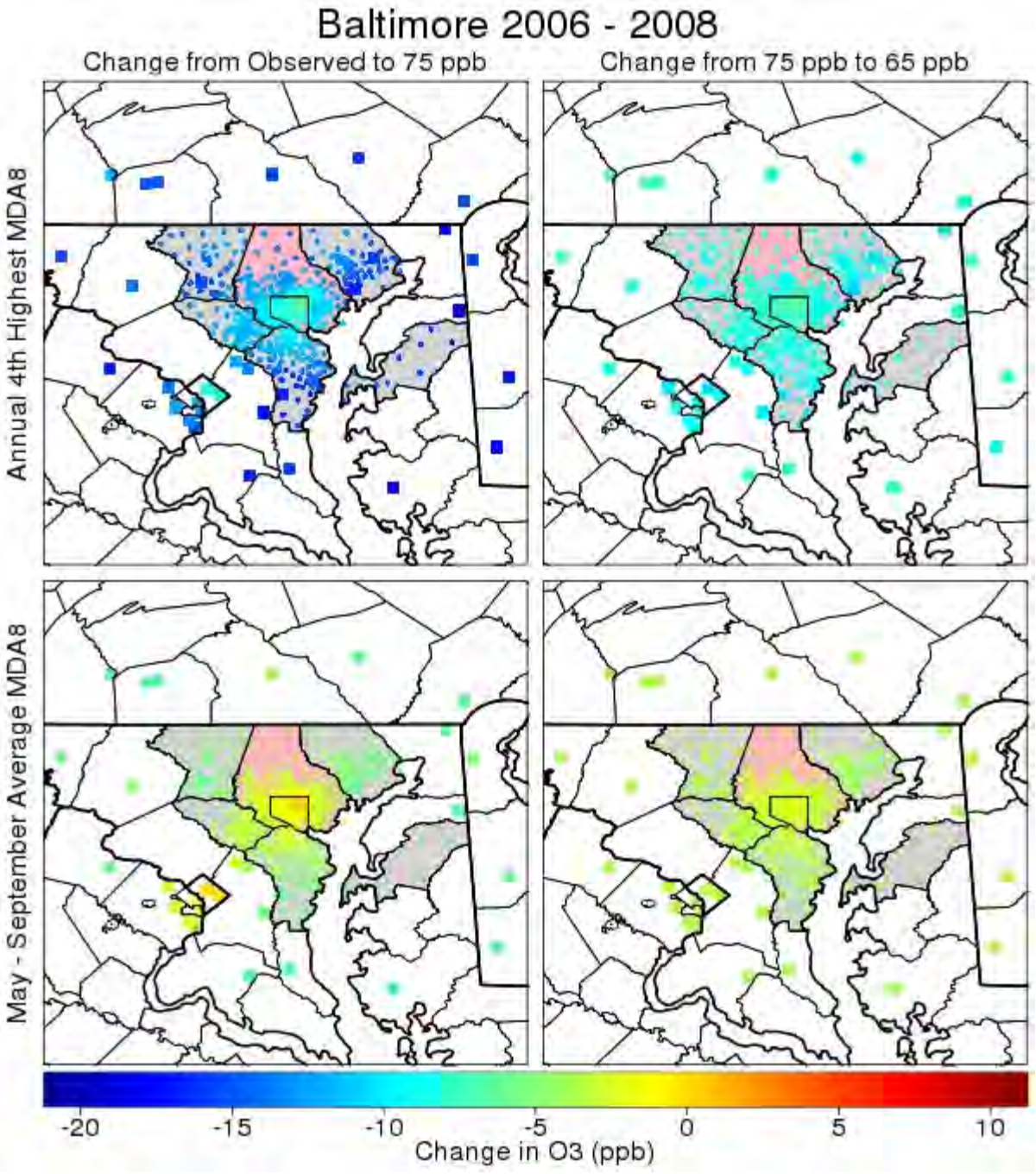

Figure 4D-87. Changes in annual 4th highest MDA8 and May-September average MDA8 values based on HDDM adjustments for Baltimore, 2006-2008. The points are colored according to the change in ppb, and values falling outside the range in the color bar were set to the nearest value within the color bar.

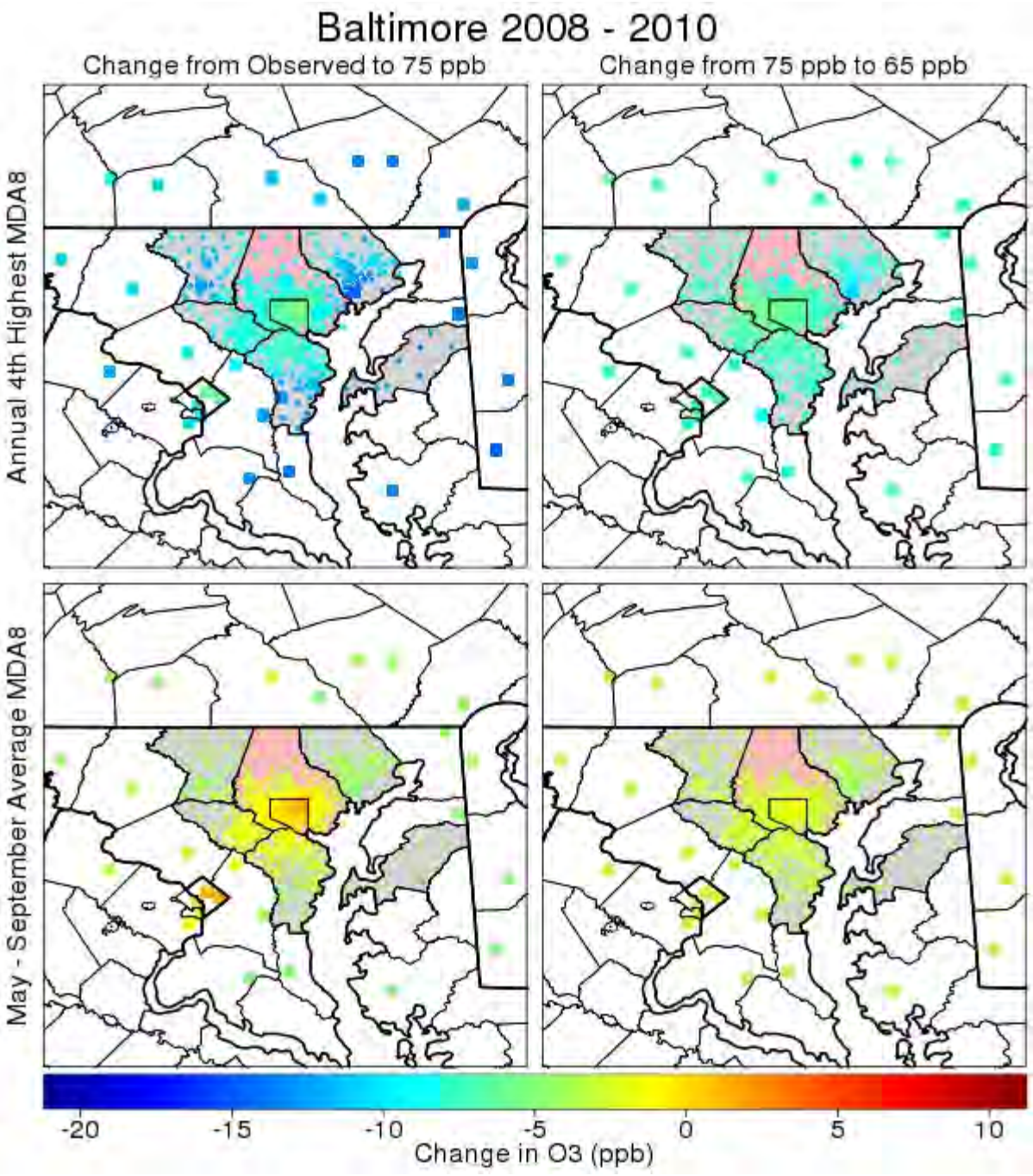

Figure 4D-88. Changes in annual 4th highest MDA8 and May-September average MDA8 values based on HDDM adjustments for Baltimore, 2008-2010. The points are colored according to the change in ppb, and values falling outside the range in the color bar were set to the nearest value within the color bar.

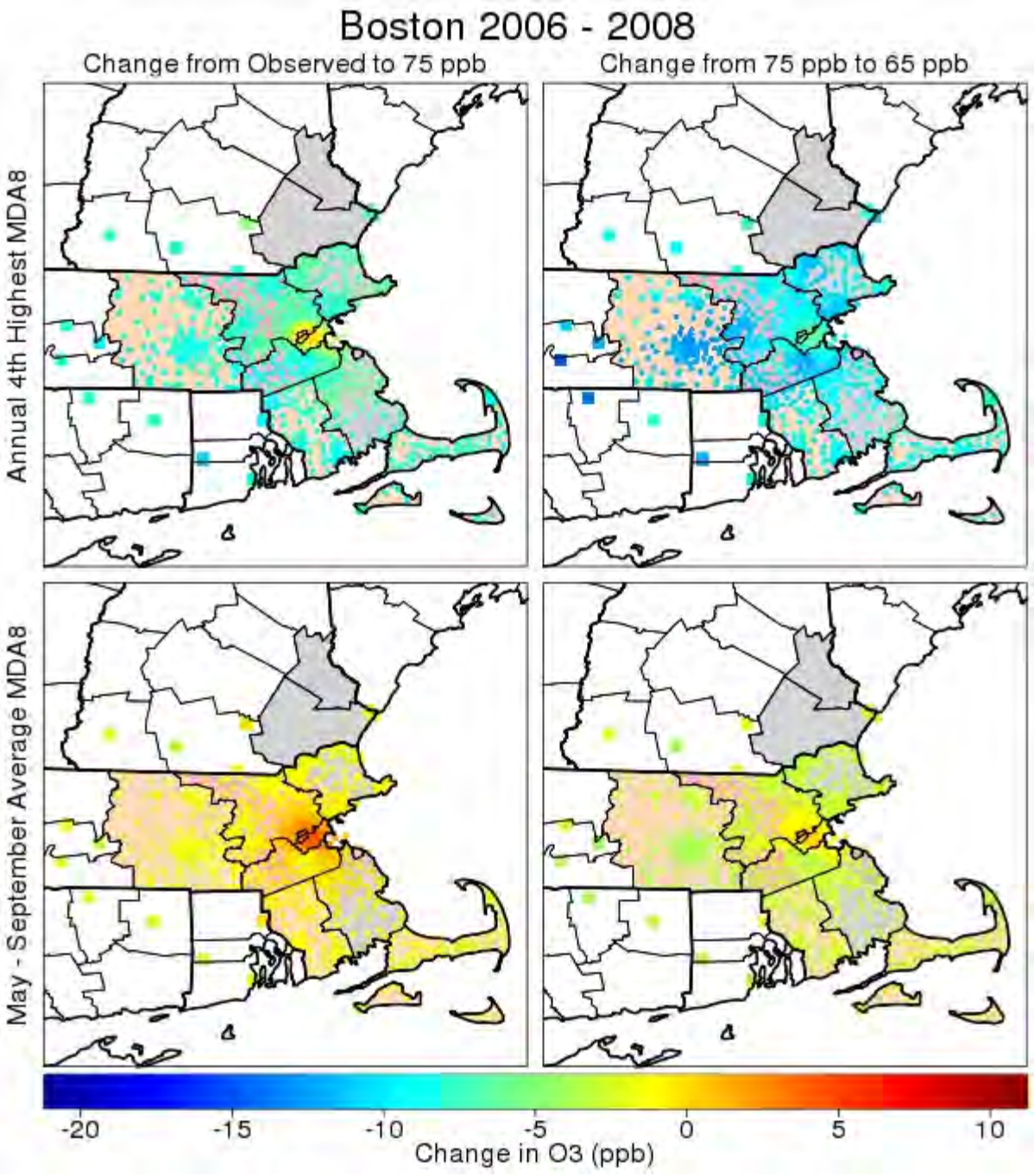

Figure 4D-89. Changes in annual 4th highest MDA8 and May-September average MDA8 values based on HDDM adjustments for Boston, 2006-2008. The points are colored according to the change in ppb, and values falling outside the range in the color bar were set to the nearest value within the color bar.

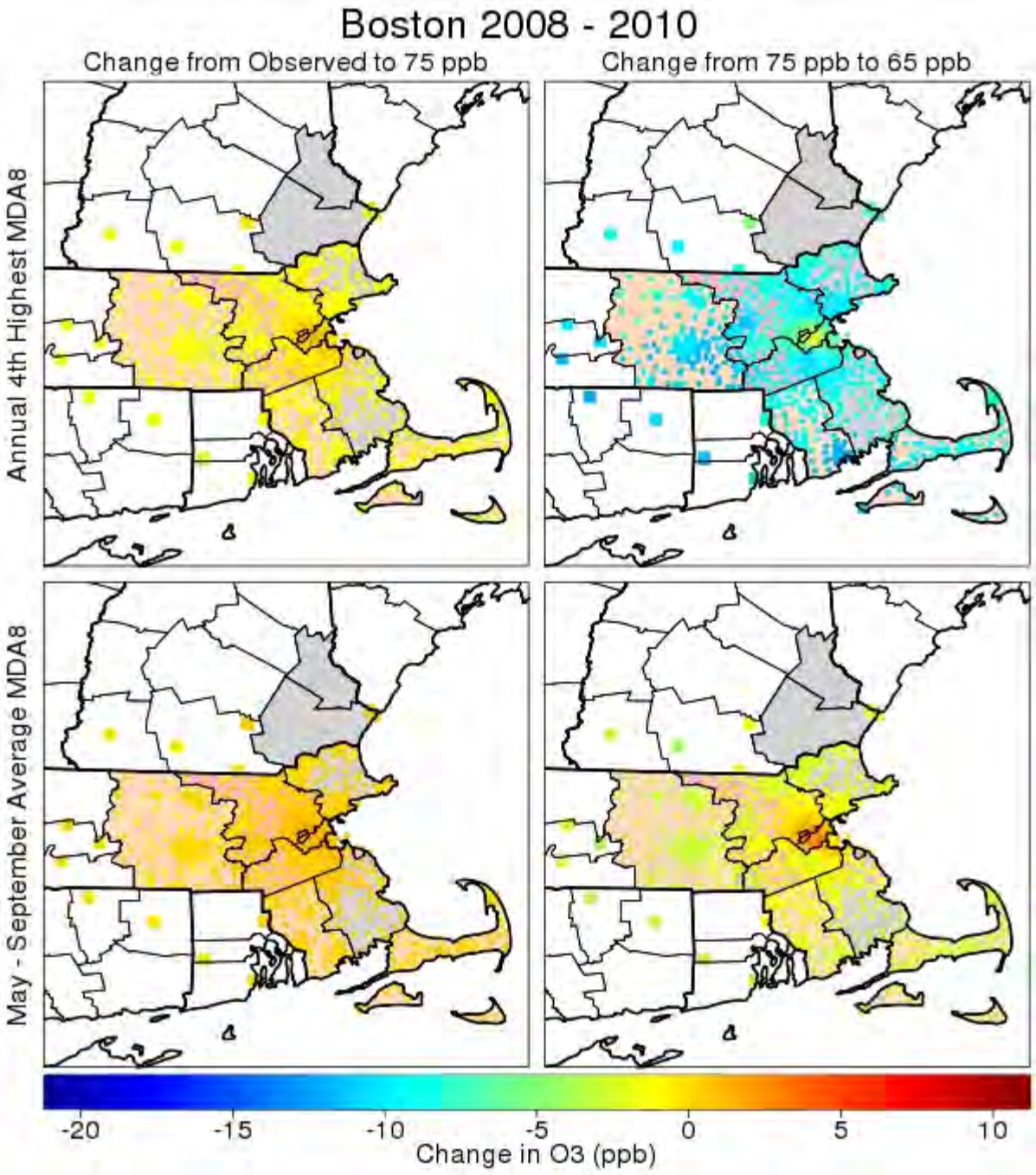

Figure 4D-90. Changes in annual 4th highest MDA8 and May-September average MDA8 values based on HDDM adjustments for Boston, 2008-2010. The points are colored according to the change in ppb, and values falling outside the range in the color bar were set to the nearest value within the color bar.

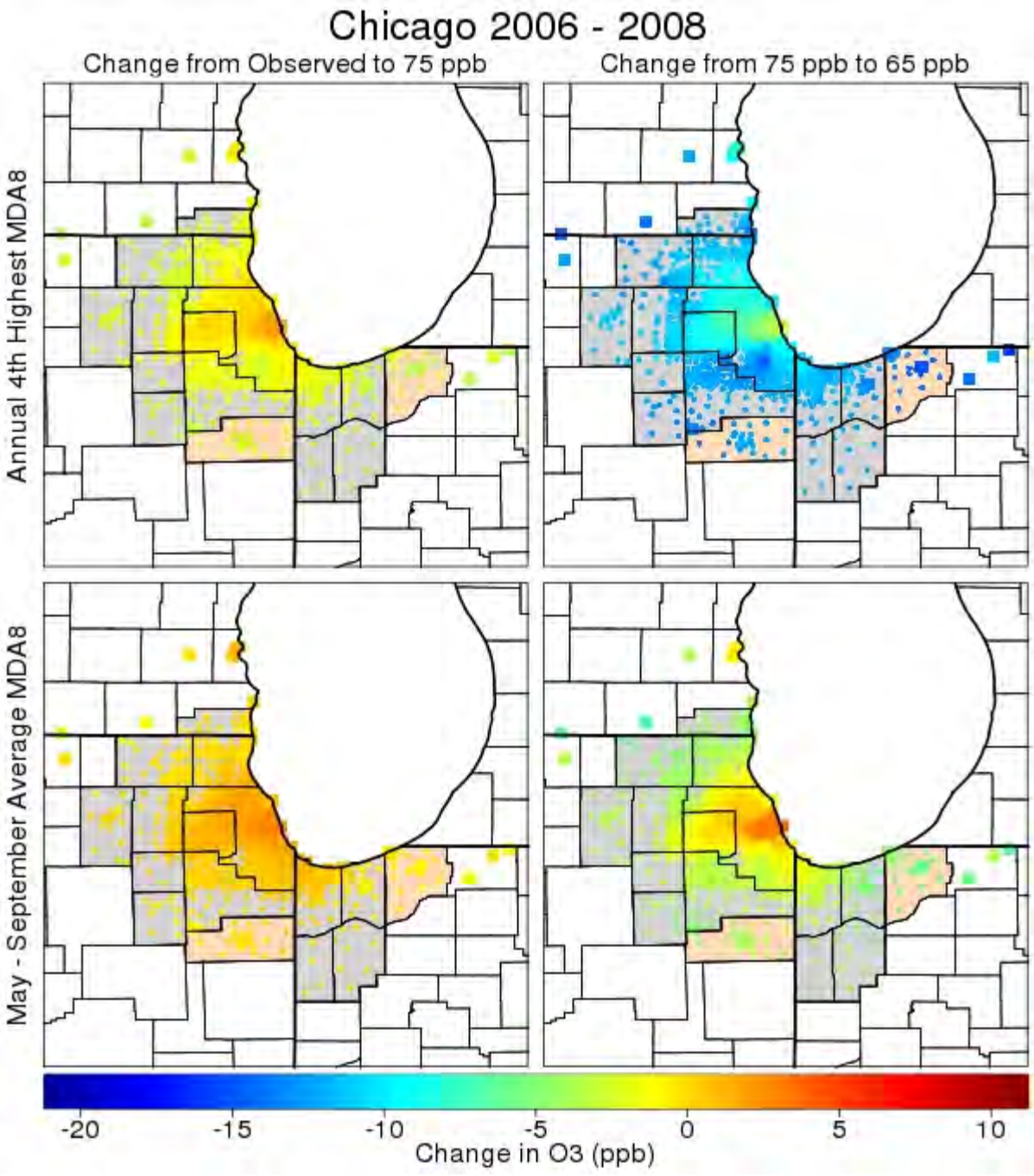

Figure 4D-91. Changes in annual 4th highest MDA8 and May-September average MDA8 values based on HDDM adjustments for Chicago, 2006-2008. The points are colored according to the change in ppb, and values falling outside the range in the color bar were set to the nearest value within the color bar.

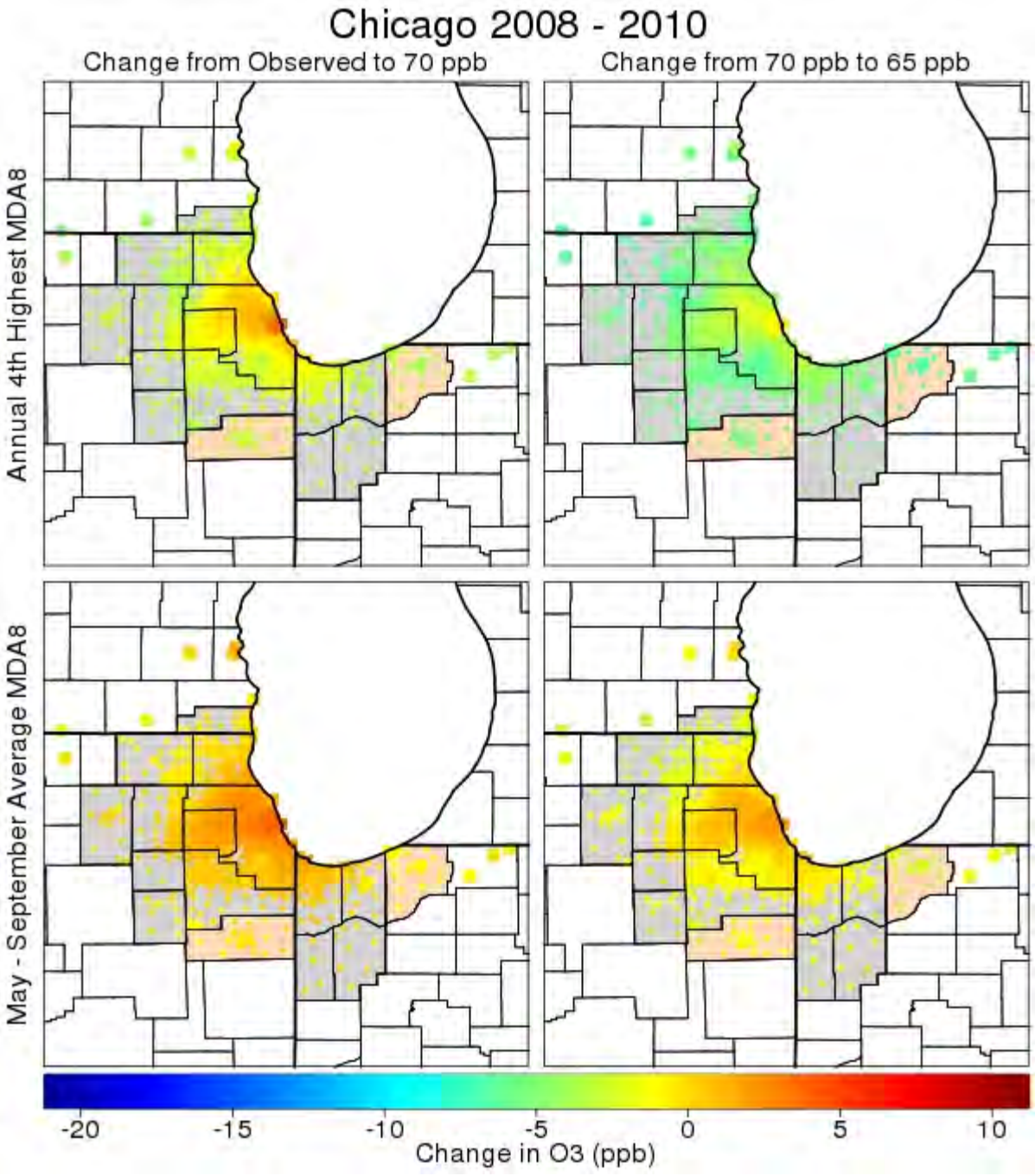

Figure 4D-92. Changes in annual 4th highest MDA8 and May-September average MDA8 values based on HDDM adjustments for Chicago, 2008-2010. The points are colored according to the change in ppb, and values falling outside the range in the color bar were set to the nearest value within the color bar.

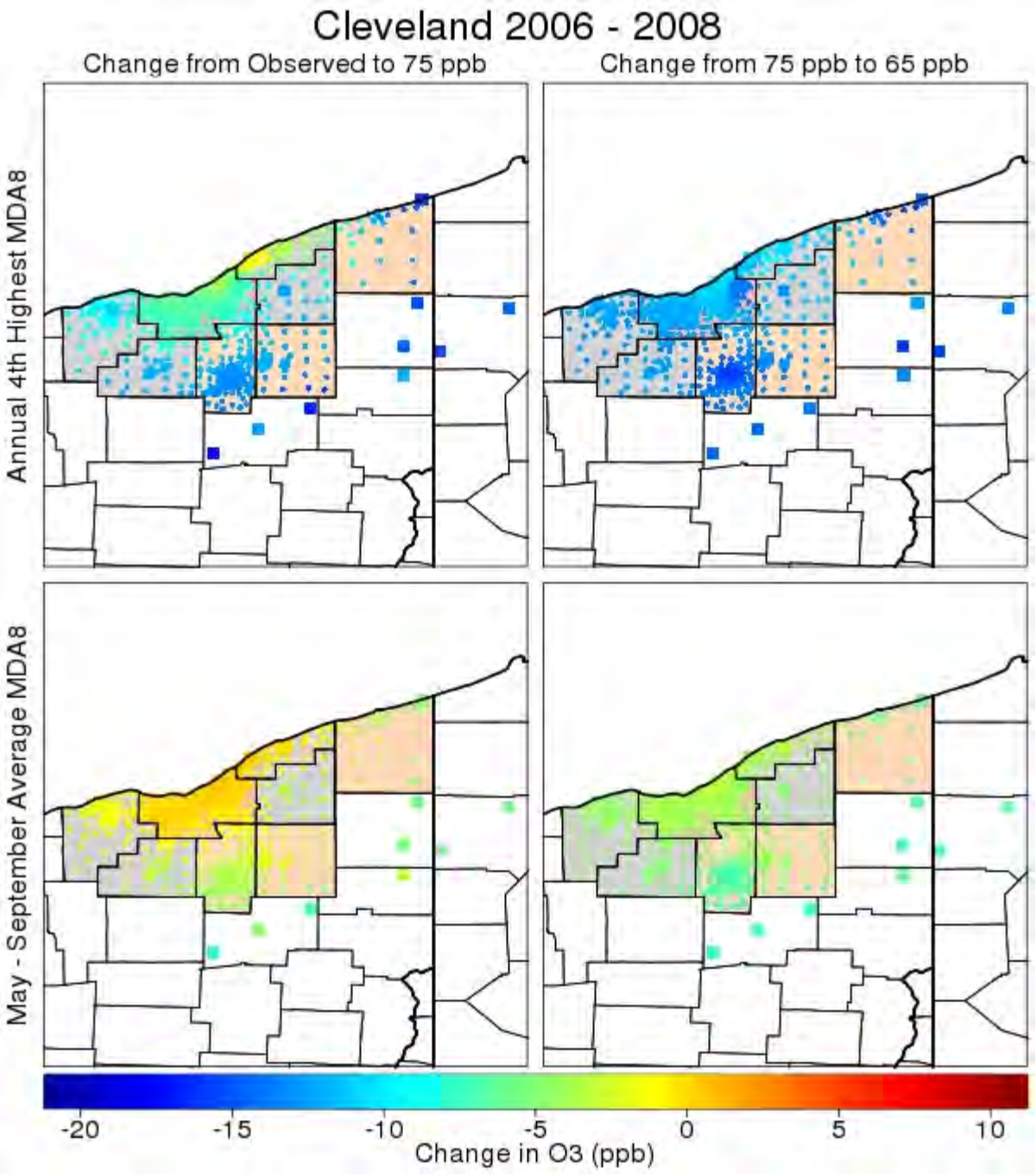

Figure 4D-93. Changes in annual 4th highest MDA8 and May-September average MDA8 values based on HDDM adjustments for Cleveland, 2006-2008. The points are colored according to the change in ppb, and values falling outside the range in the color bar were set to the nearest value within the color bar.

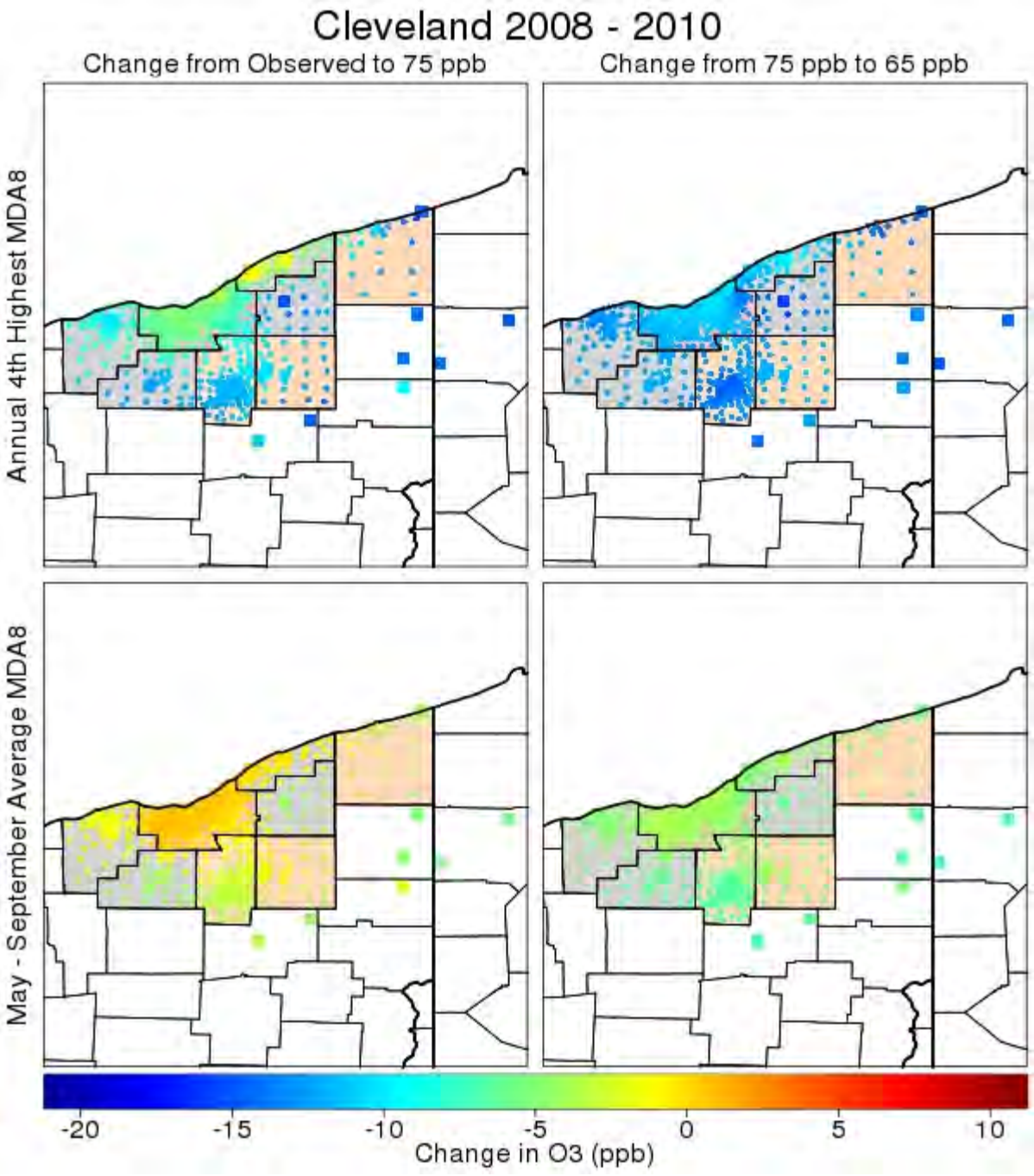

Figure 4D-94. Changes in annual 4th highest MDA8 and May-September average MDA8 values based on HDDM adjustments for Cleveland, 2008-2010. The points are colored according to the change in ppb, and values falling outside the range in the color bar were set to the nearest value within the color bar.

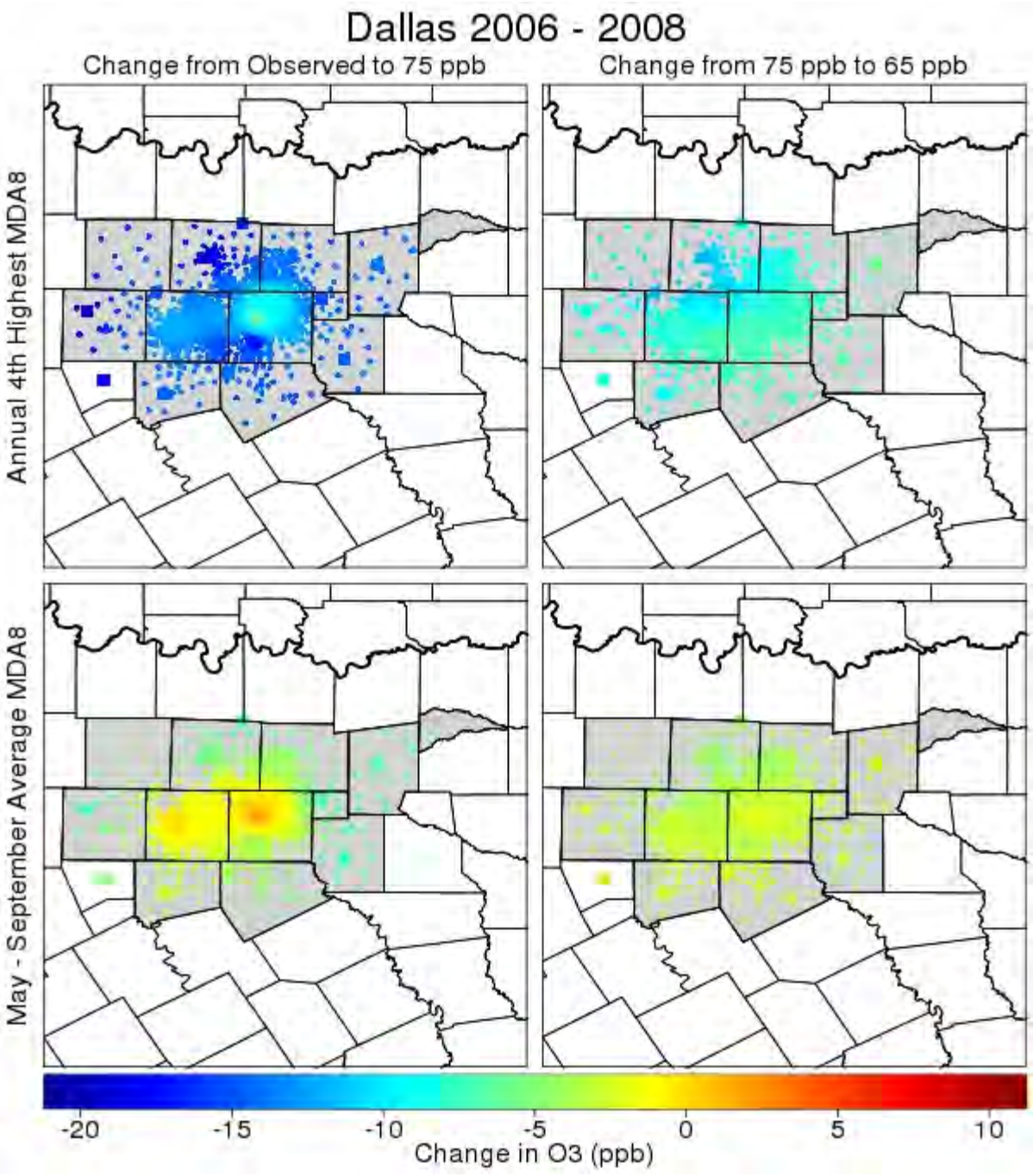

Figure 4D-95. Changes in annual 4th highest MDA8 and May-September average MDA8 values based on HDDM adjustments for Dallas, 2006-2008. The points are colored according to the change in ppb, and values falling outside the range in the color bar were set to the nearest value within the color bar.

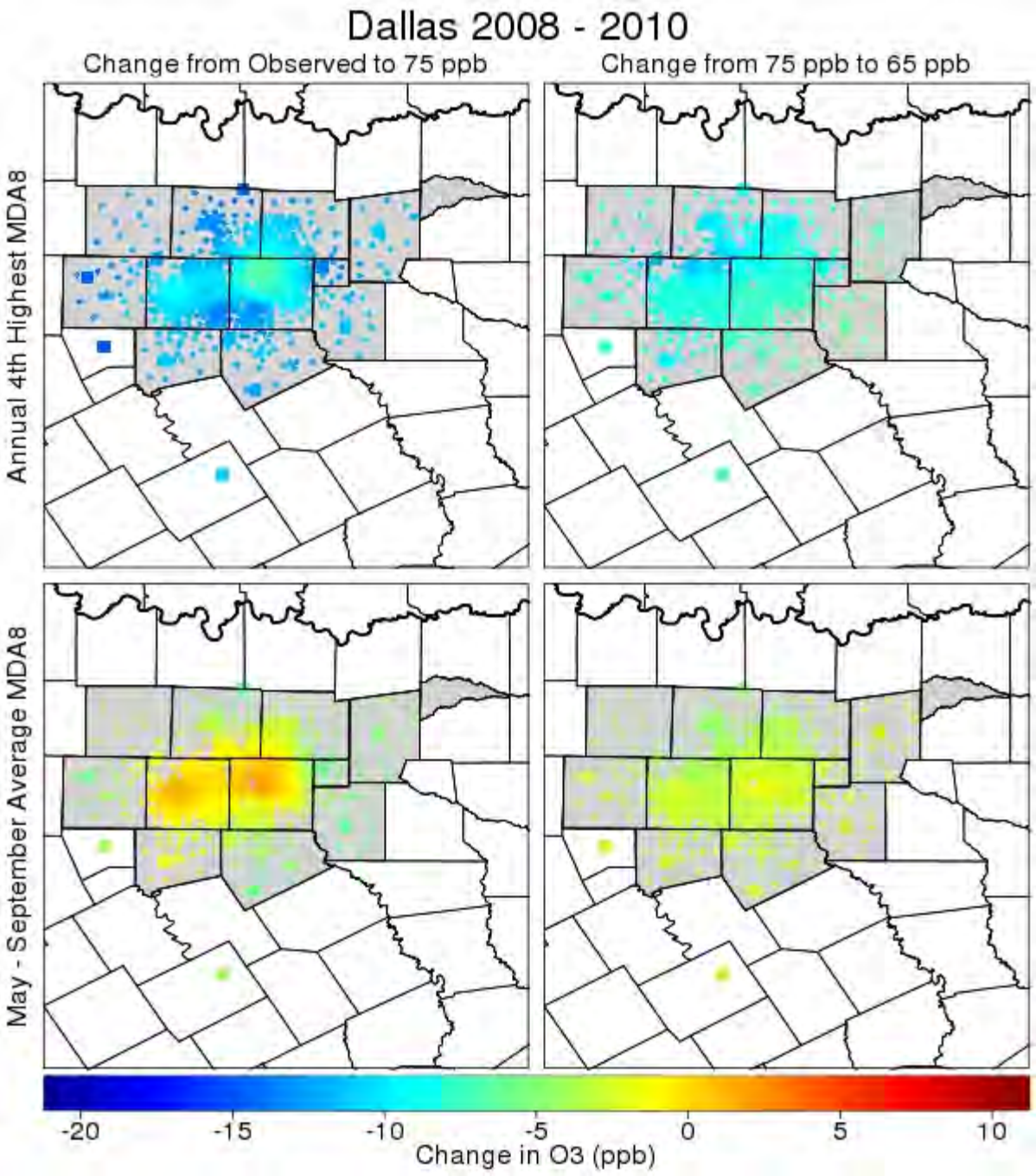

Figure 4D-96. Changes in annual 4th highest MDA8 and May-September average MDA8 values based on HDDM adjustments for Dallas, 2008-2010. The points are colored according to the change in ppb, and values falling outside the range in the color bar were set to the nearest value within the color bar.

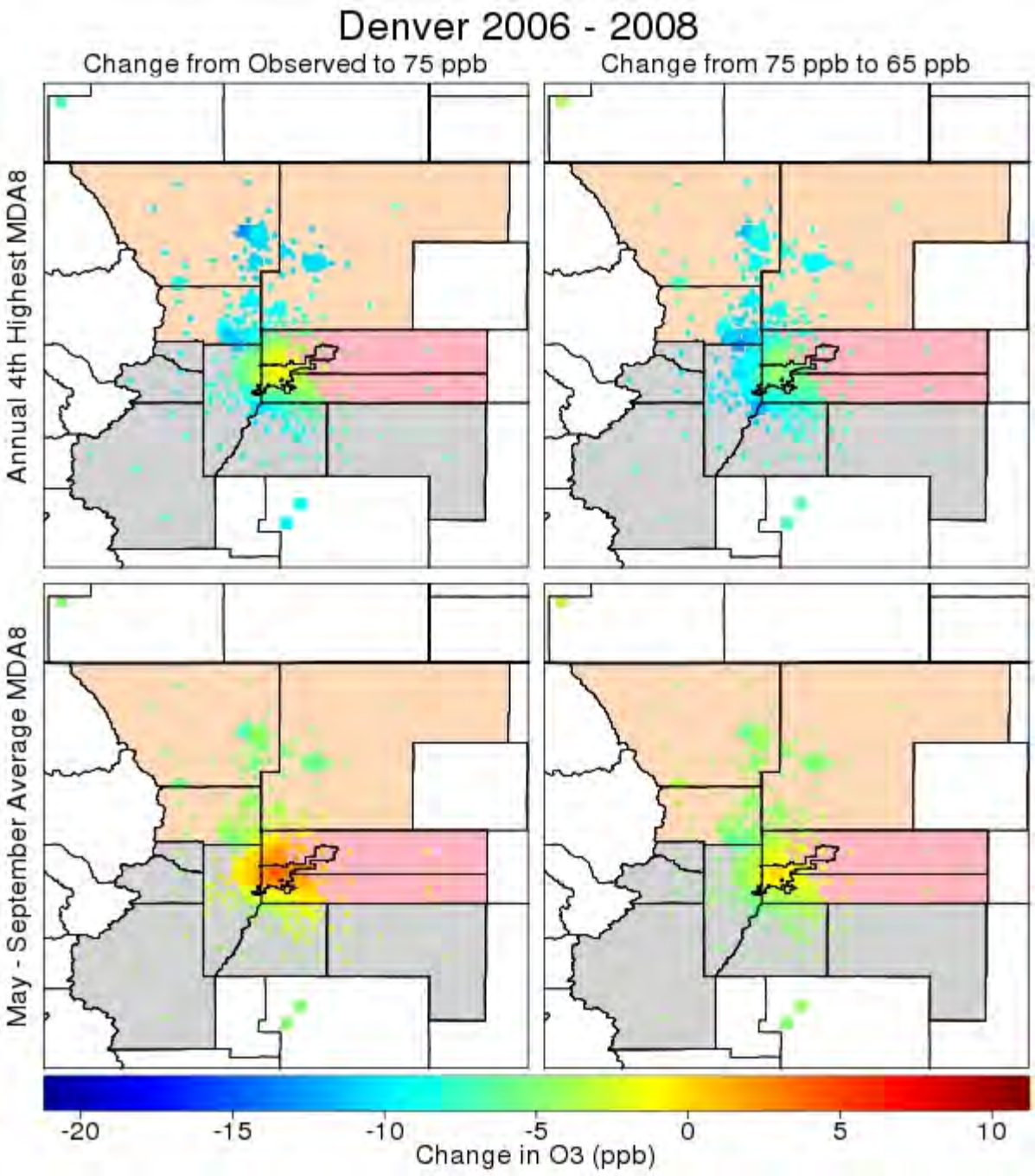

Figure 4D-97. Changes in annual 4th highest MDA8 and May-September average MDA8 values based on HDDM adjustments for Denver, 2006-2008. The points are colored according to the change in ppb, and values falling outside the range in the color bar were set to the nearest value within the color bar.

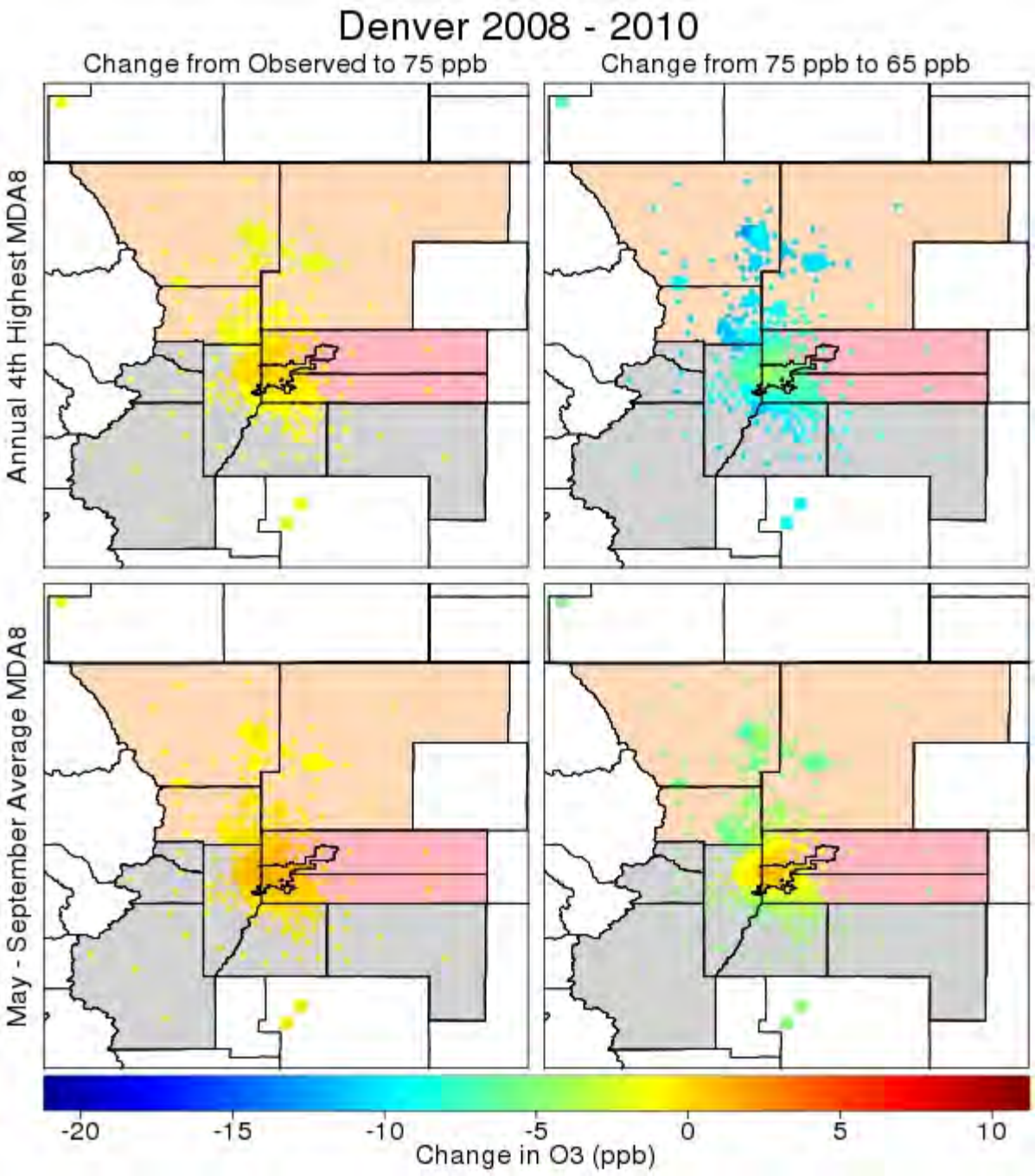

Figure 4D-98. Changes in annual 4th highest MDA8 and May-September average MDA8 values based on HDDM adjustments for Denver, 2008-2010. The points are colored according to the change in ppb, and values falling outside the range in the color bar were set to the nearest value within the color bar.

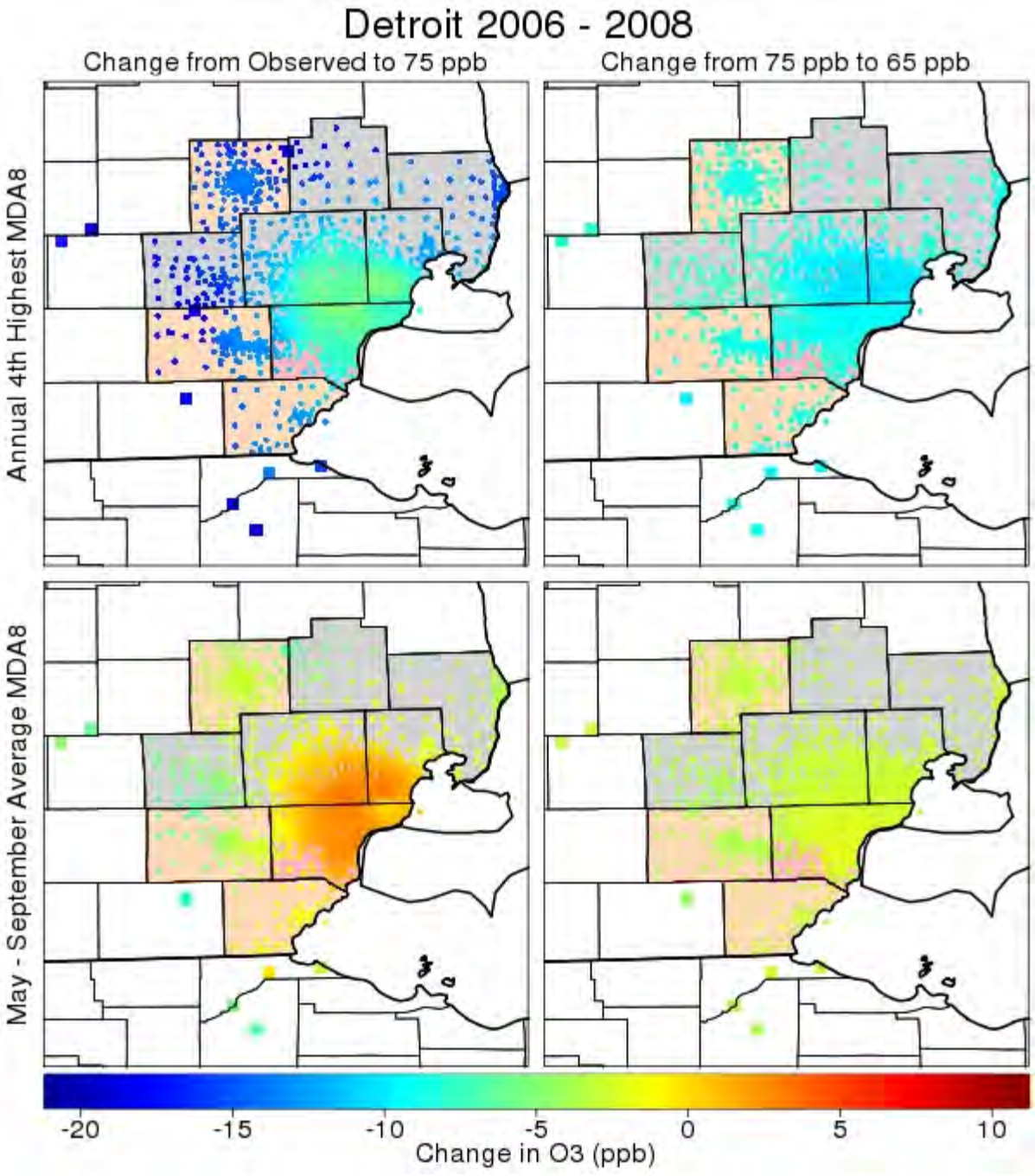

Figure 4D-99. Changes in annual 4th highest MDA8 and May-September average MDA8 values based on HDDM adjustments for Detroit, 2006-2008. The points are colored according to the change in ppb, and values falling outside the range in the color bar were set to the nearest value within the color bar.

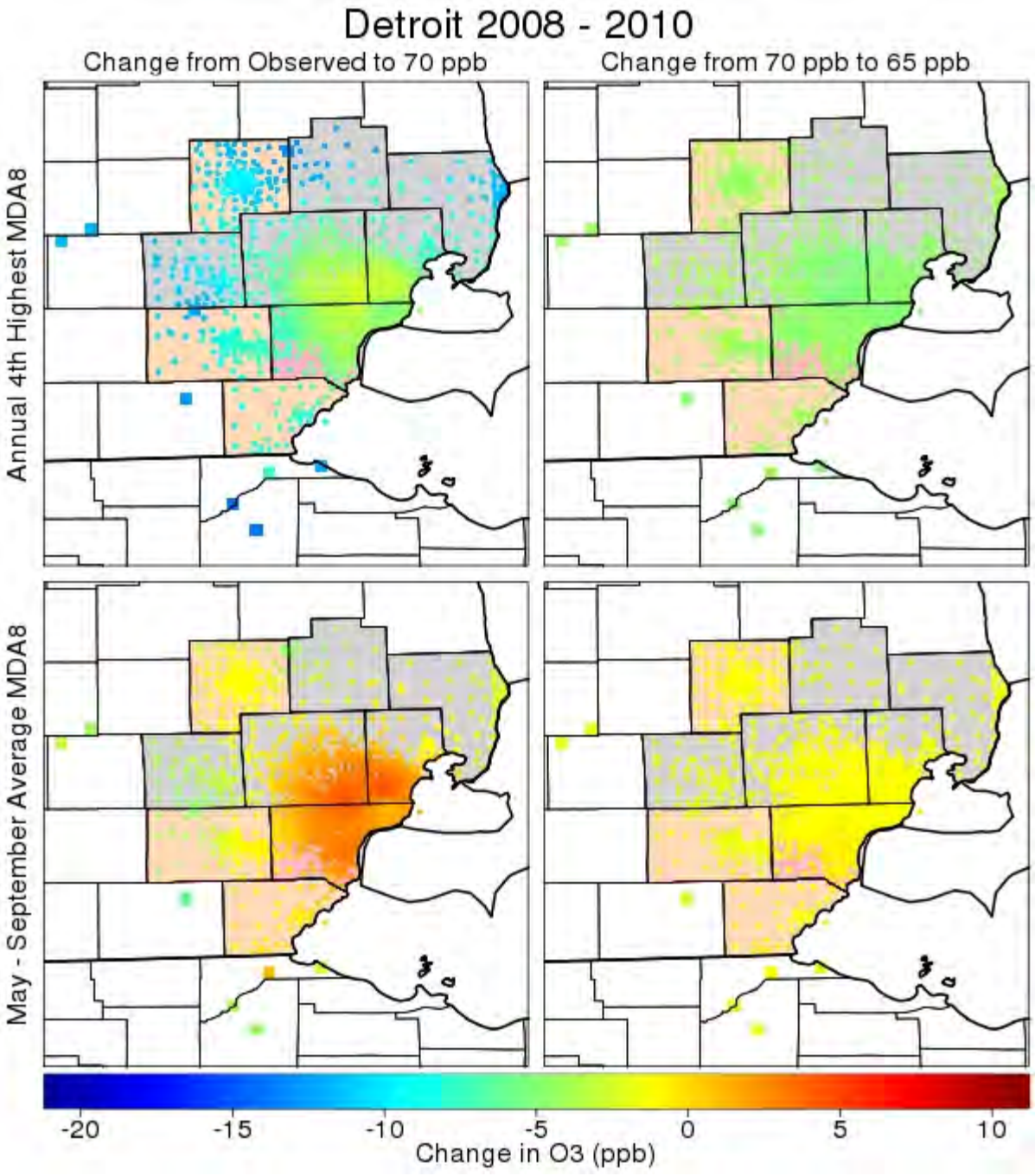

Figure 4D-100. Changes in annual 4th highest MDA8 and May-September average MDA8 values based on HDDM adjustments for Detroit, 2008-2010. The points are colored according to the change in ppb, and values falling outside the range in the color bar were set to the nearest value within the color bar.

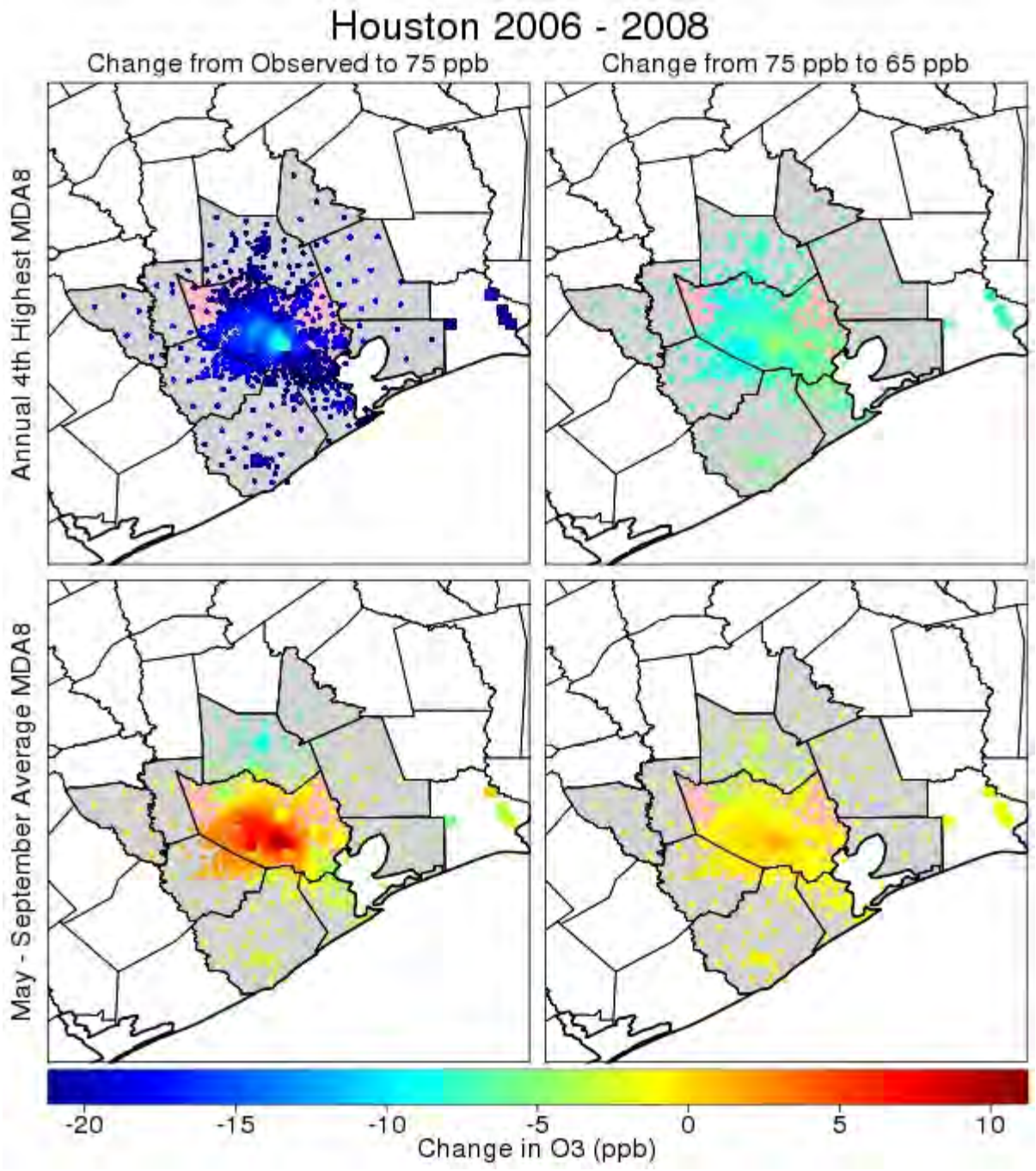

Figure 4D-101. Changes in annual 4th highest MDA8 and May-September average MDA8 values based on HDDM adjustments for Houston, 2006-2008. The points are colored according to the change in ppb, and values falling outside the range in the color bar were set to the nearest value within the color bar.

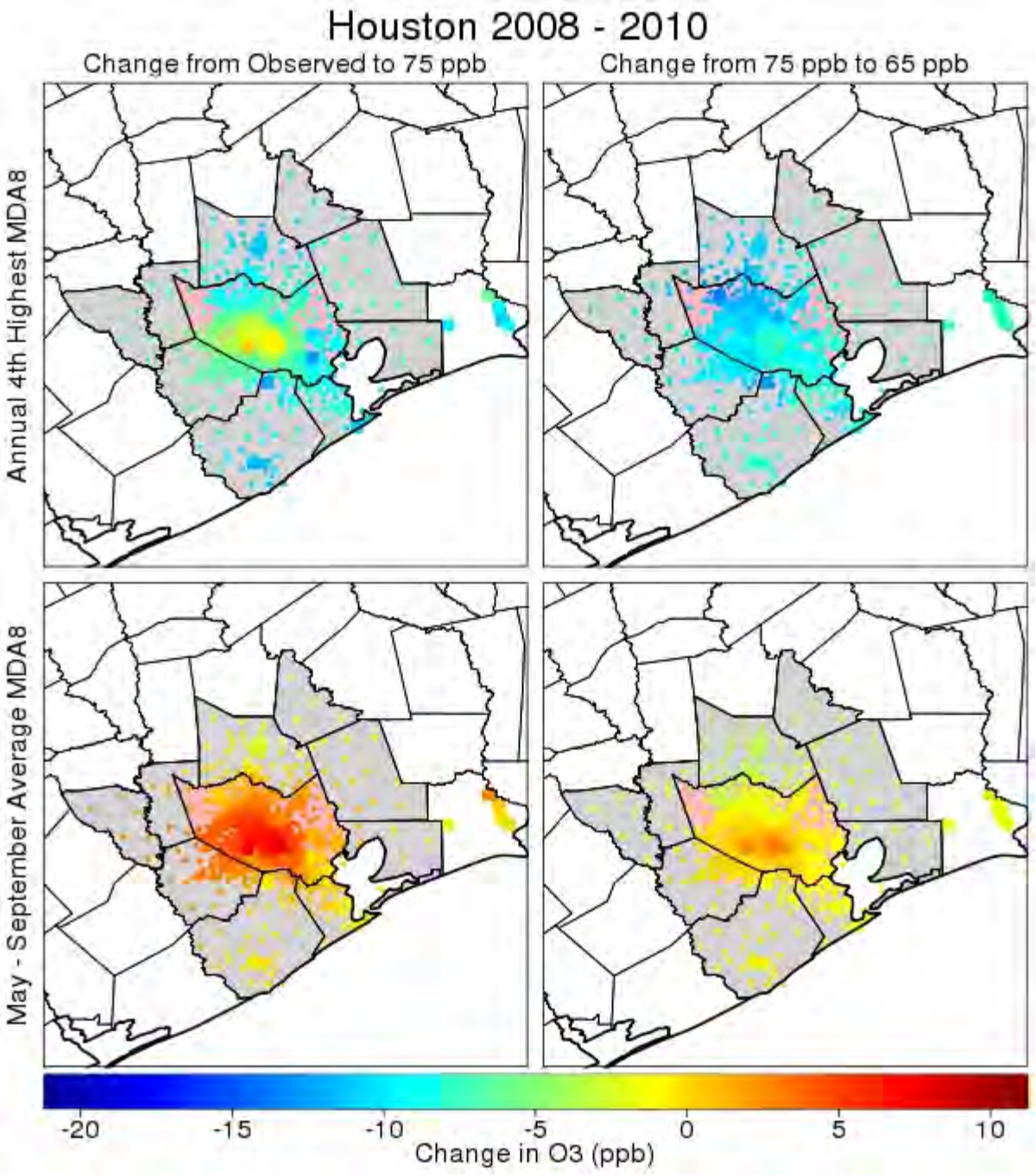

Figure 4D-102. Changes in annual 4th highest MDA8 and May-September average MDA8 values based on HDDM adjustments for Houston, 2008-2010. The points are colored according to the change in ppb, and values falling outside the range in the color bar were set to the nearest value within the color bar.

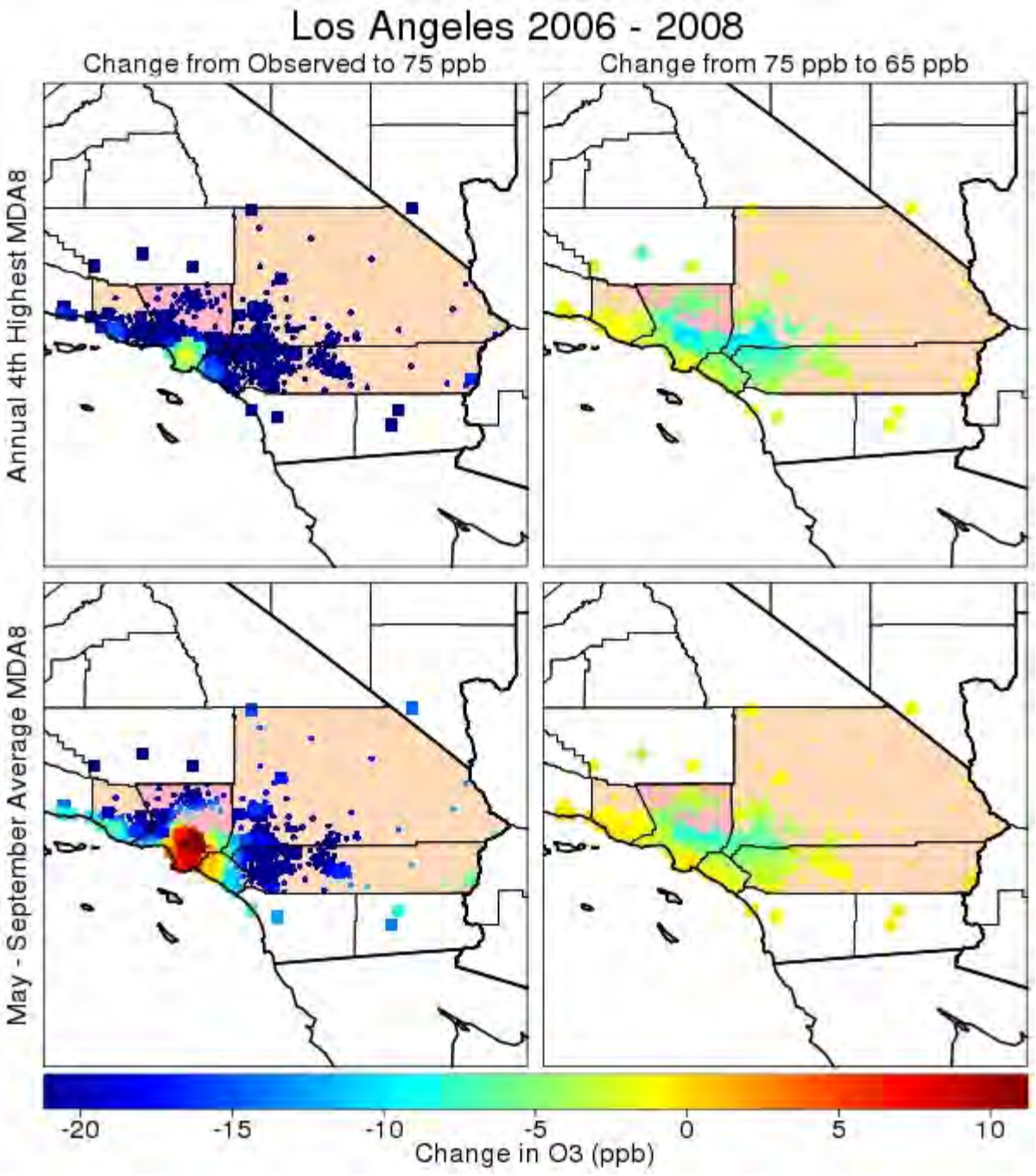

Figure 4D-103. Changes in annual 4th highest MDA8 and May-September average MDA8 values based on HDDM adjustments for Los Angeles, 2006-2008. The points are colored according to the change in ppb, and values falling outside the range in the color bar were set to the nearest value within the color bar.

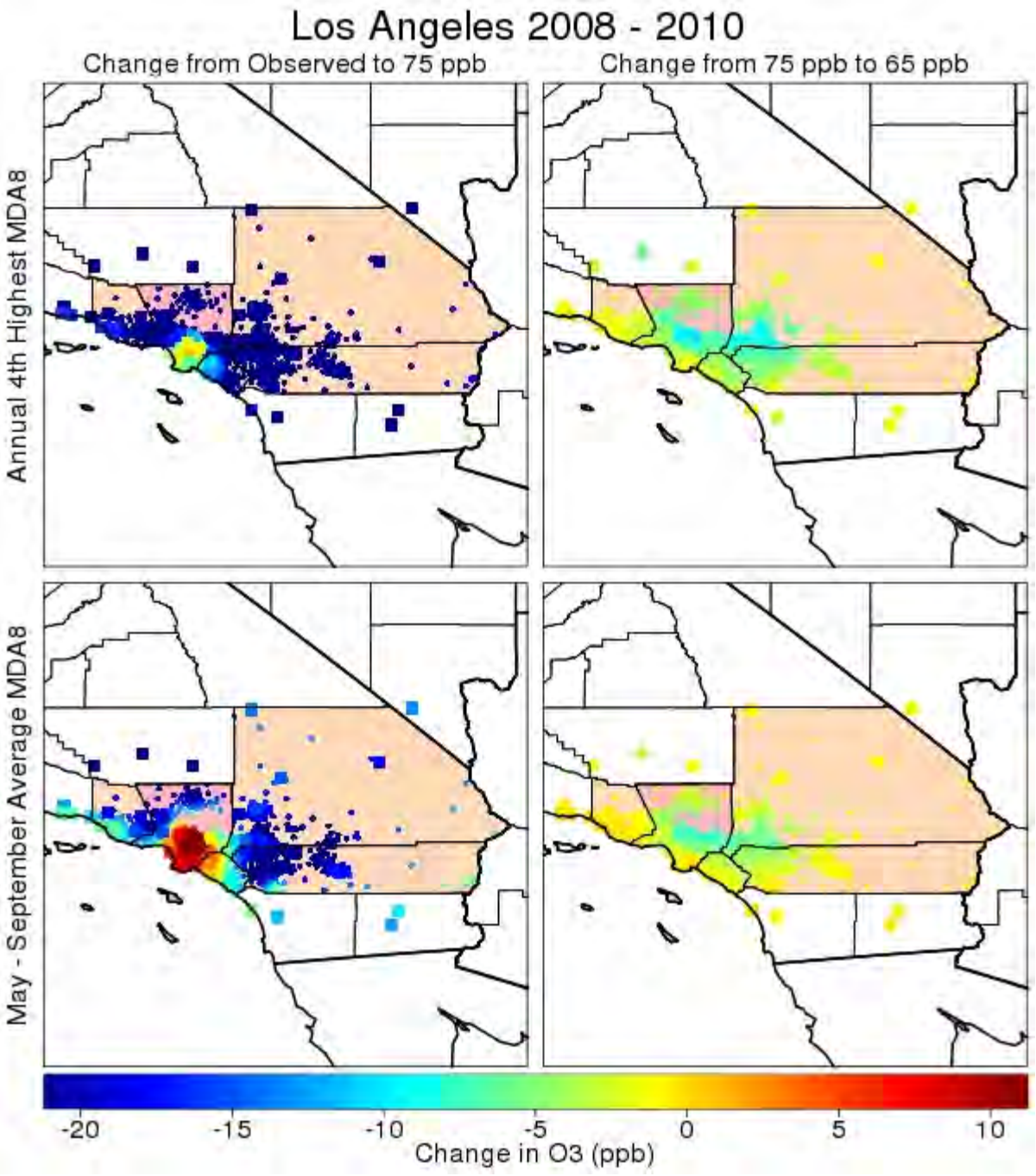

Figure 4D-104. Changes in annual 4th highest MDA8 and May-September average MDA8 values based on HDDM adjustments for Los Angeles, 2008-2010. The points are colored according to the change in ppb, and values falling outside the range in the color bar were set to the nearest value within the color bar.

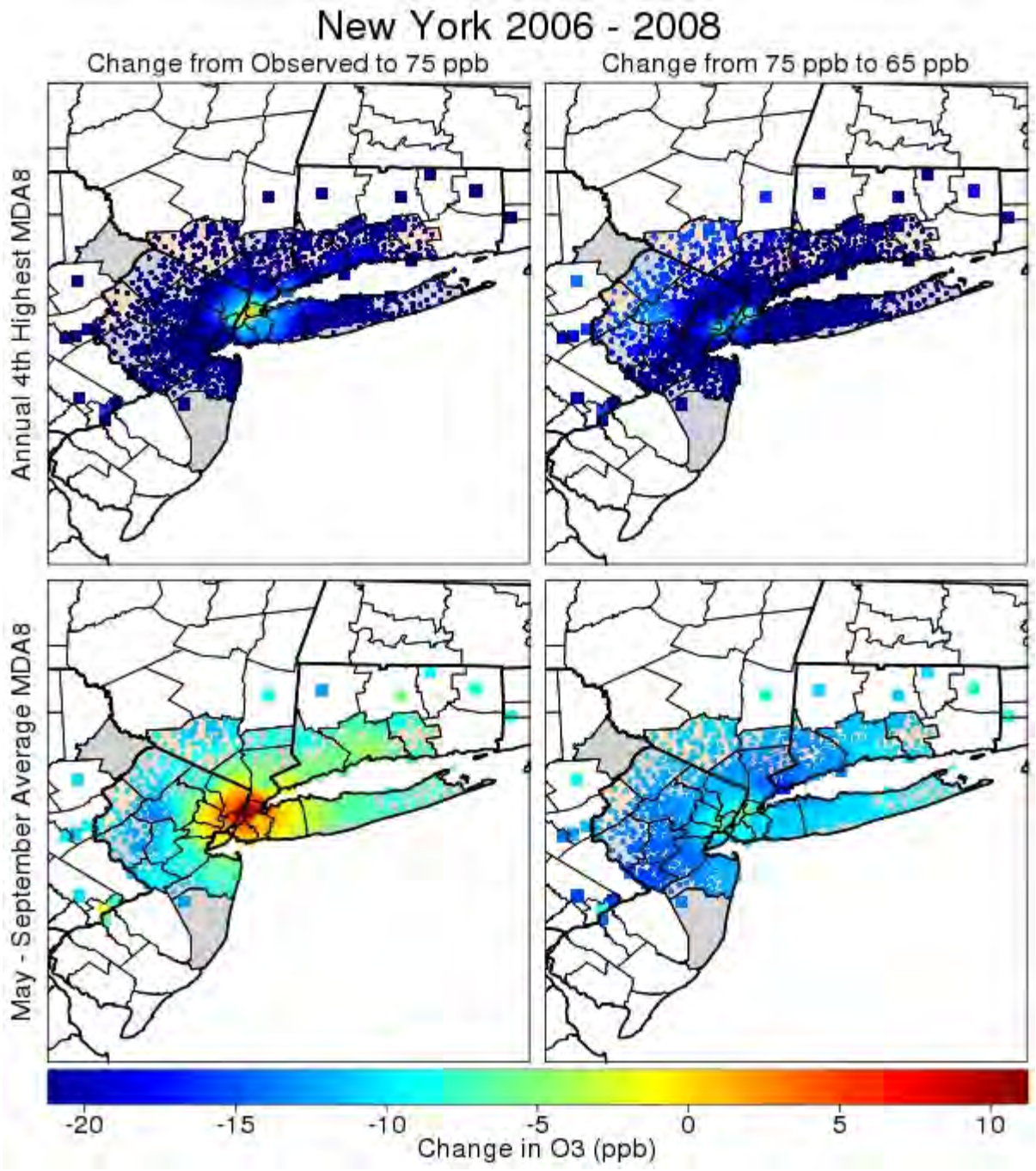

Figure 4D-105. Changes in annual 4th highest MDA8 and May-September average MDA8 values based on HDDM adjustments for New York, 2006-2008. The points are colored according to the change in ppb, and values falling outside the range in the color bar were set to the nearest value within the color bar.

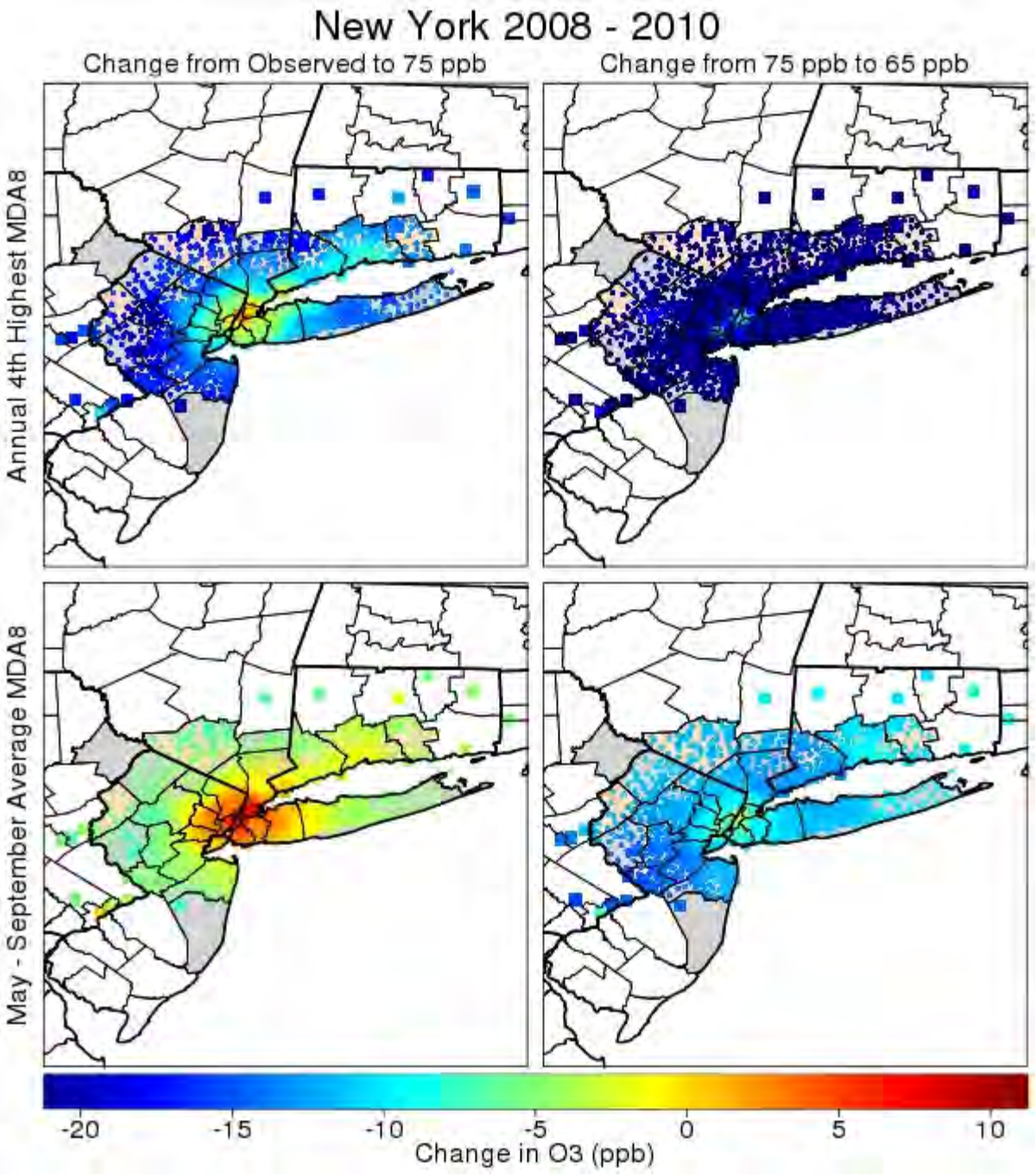

Figure 4D-106. Changes in annual 4th highest MDA8 and May-September average MDA8 values based on HDDM adjustments for New York, 2008-2010. The points are colored according to the change in ppb, and values falling outside the range in the color bar were set to the nearest value within the color bar.

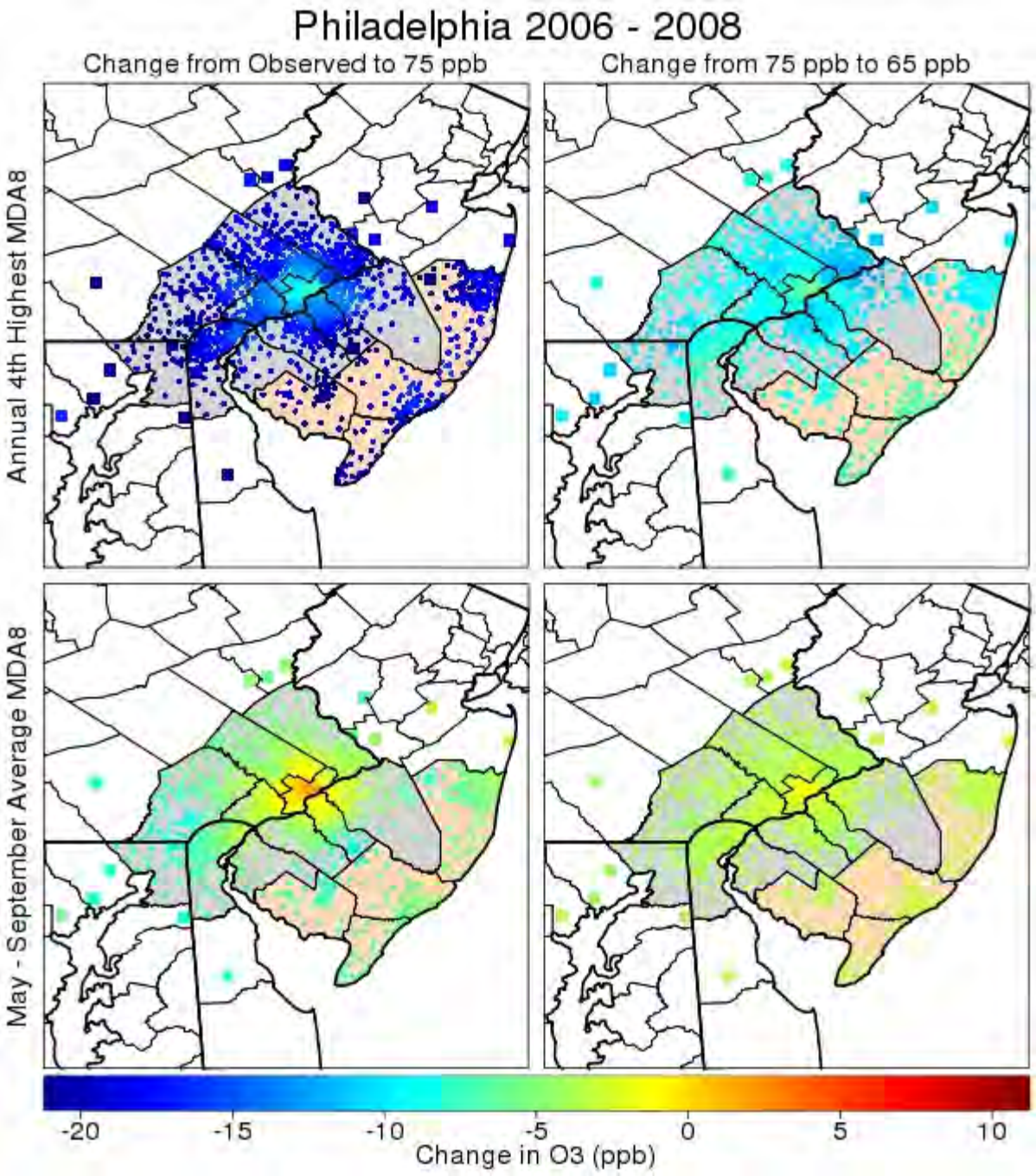

Figure 4D-107. Changes in annual 4th highest MDA8 and May-September average MDA8 values based on HDDM adjustments for Philadelphia, 2006-2008. The points are colored according to the change in ppb, and values falling outside the range in the color bar were set to the nearest value within the color bar.

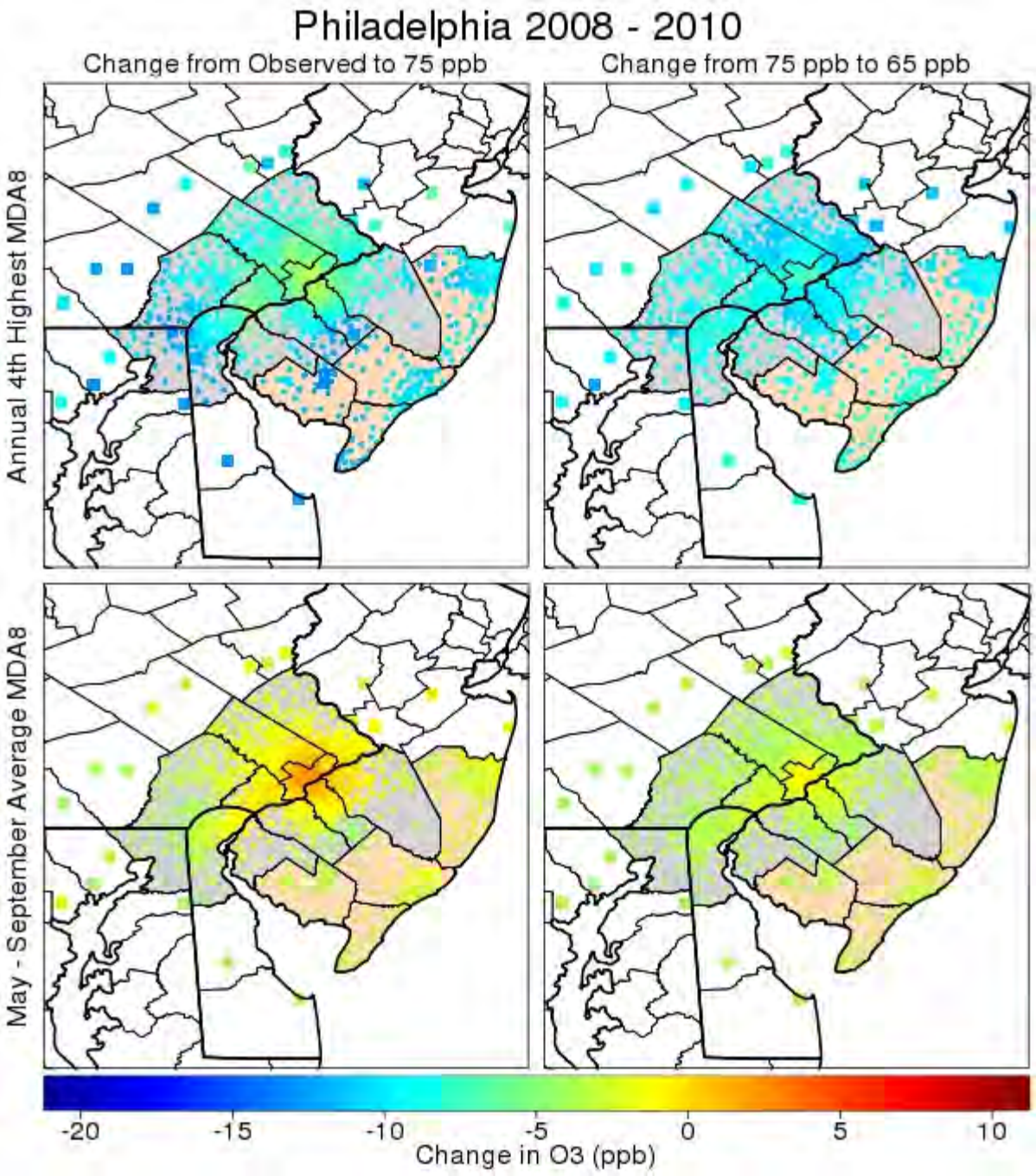

Figure 4D-108. Changes in annual 4th highest MDA8 and May-September average MDA8 values based on HDDM adjustments for Philadelphia, 2008-2010. The points are colored according to the change in ppb, and values falling outside the range in the color bar were set to the nearest value within the color bar.

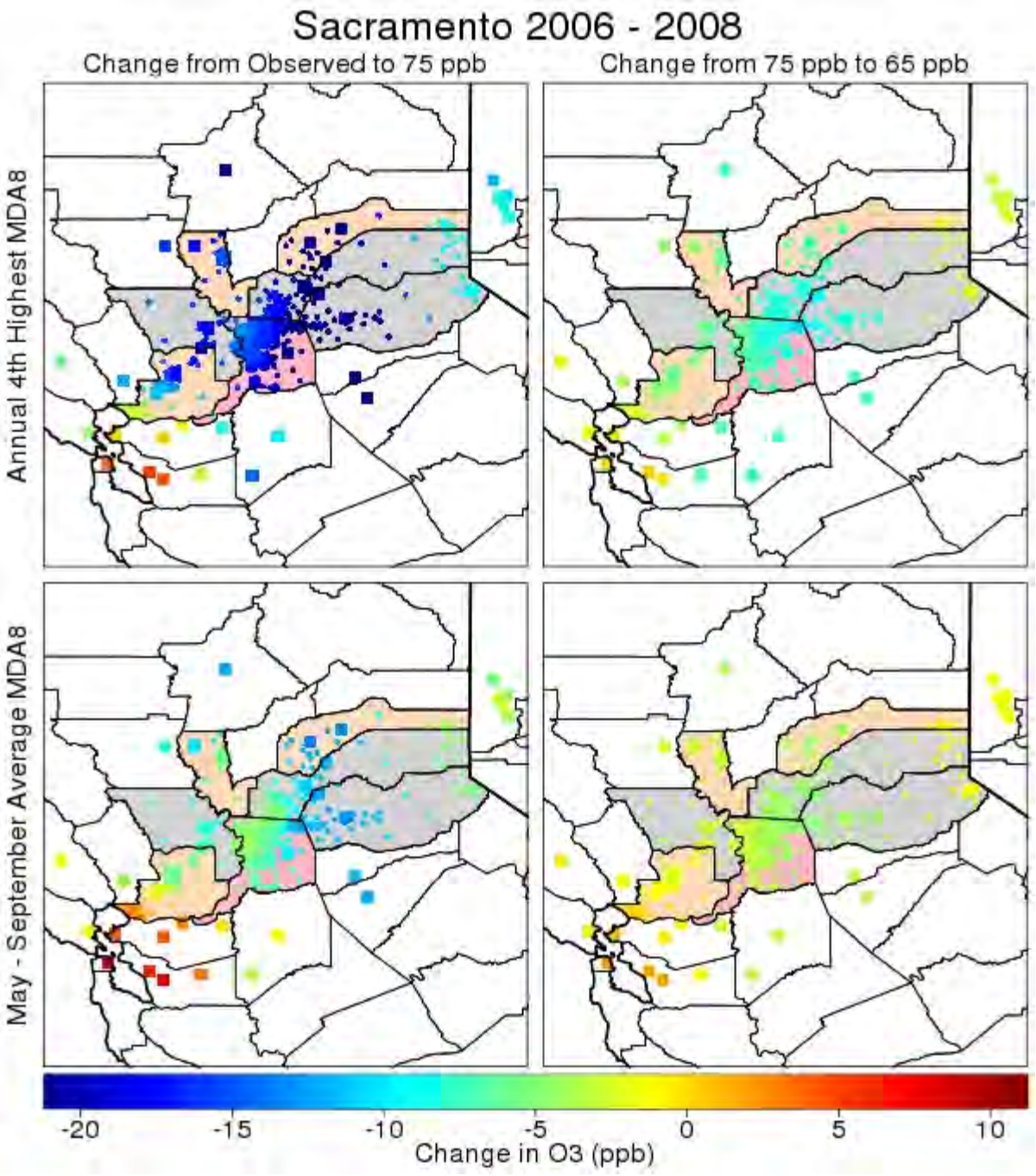

Figure 4D-109. Changes in annual 4th highest MDA8 and May-September average MDA8 values based on HDDM adjustments for Sacramento, 2006-2008. The points are colored according to the change in ppb, and values falling outside the range in the color bar were set to the nearest value within the color bar.

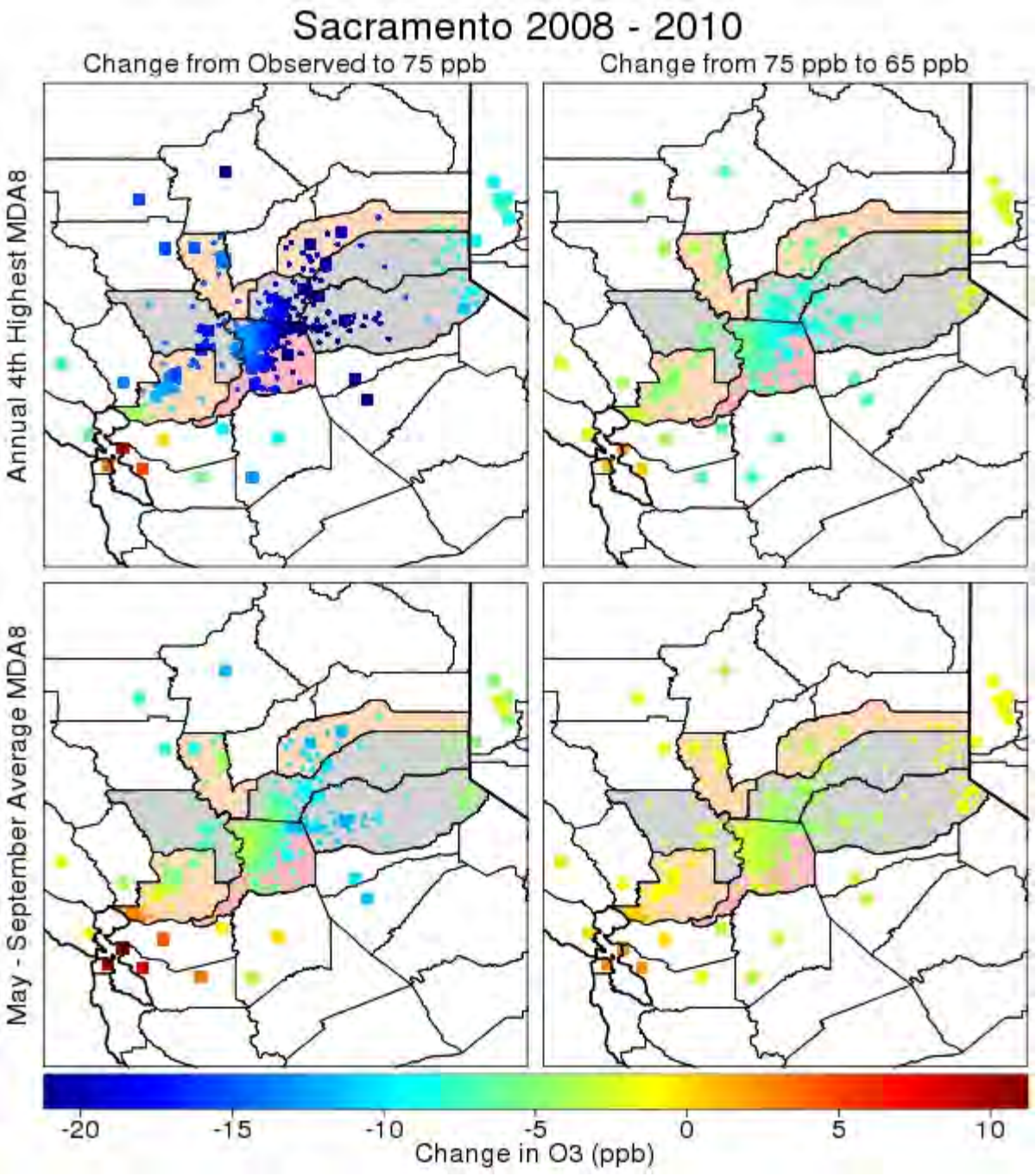

Figure 4D-110. Changes in annual 4th highest MDA8 and May-September average MDA8 values based on HDDM adjustments for Sacramento, 2008-2010. The points are colored according to the change in ppb, and values falling outside the range in the color bar were set to the nearest value within the color bar.

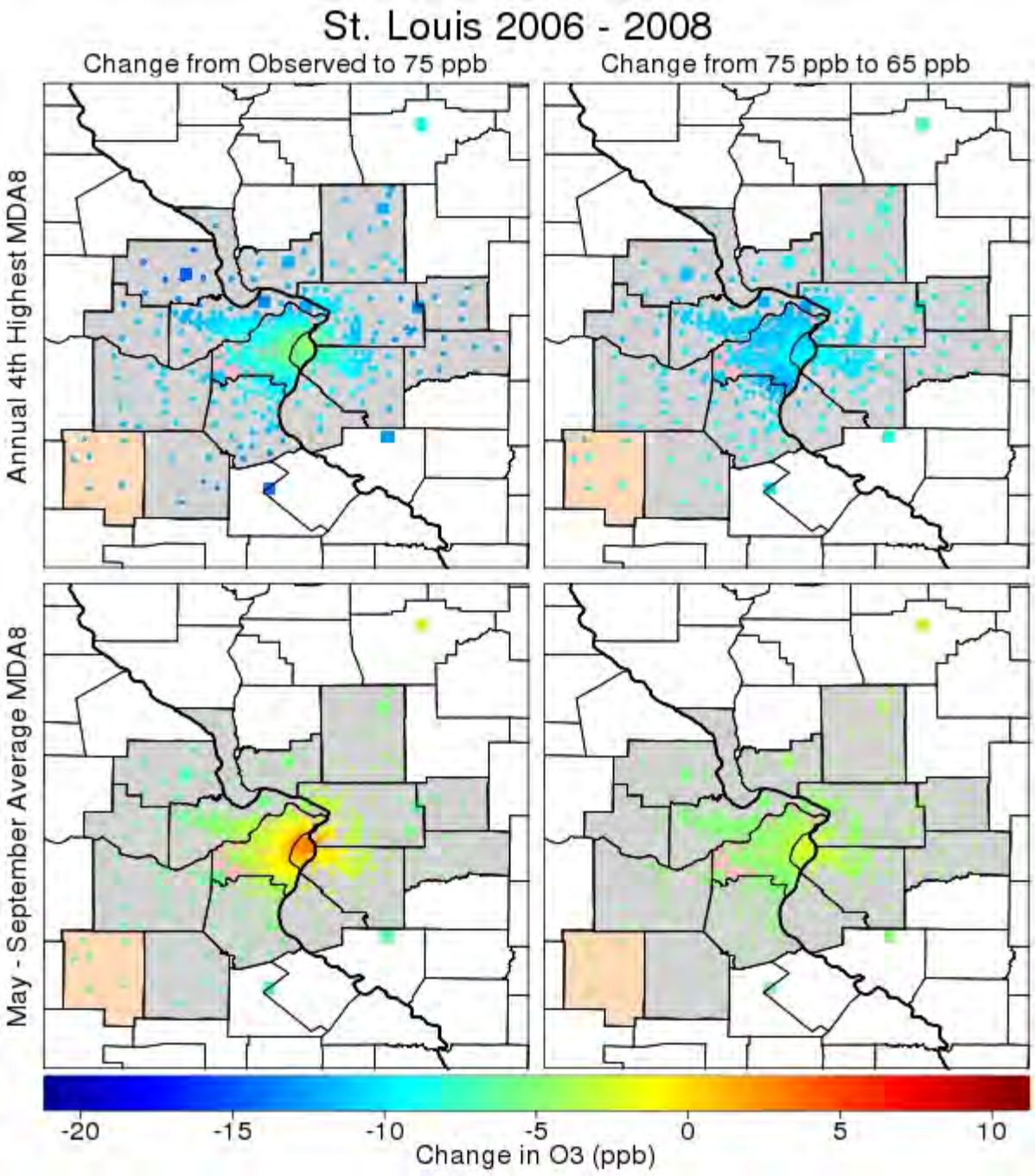

Figure 4D-111. Changes in annual 4th highest MDA8 and May-September average MDA8 values based on HDDM adjustments for St. Louis, 2006-2008. The points are colored according to the change in ppb, and values falling outside the range in the color bar were set to the nearest value within the color bar.

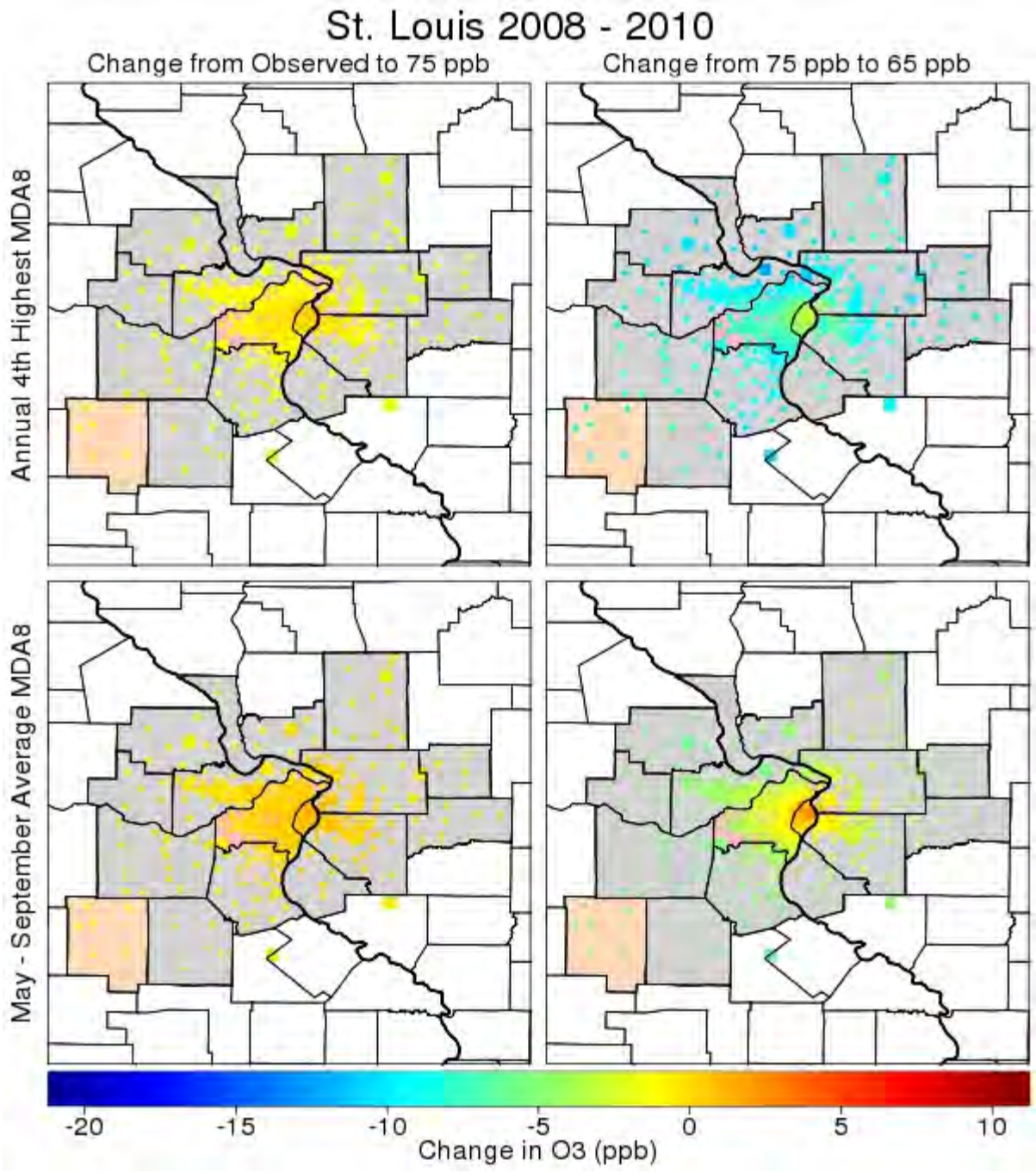

Figure 4D-112. Changes in annual 4th highest MDA8 and May-September average MDA8 values based on HDDM adjustments for St. Louis, 2008-2010. The points are colored according to the change in ppb, and values falling outside the range in the color bar were set to the nearest value within the color bar.

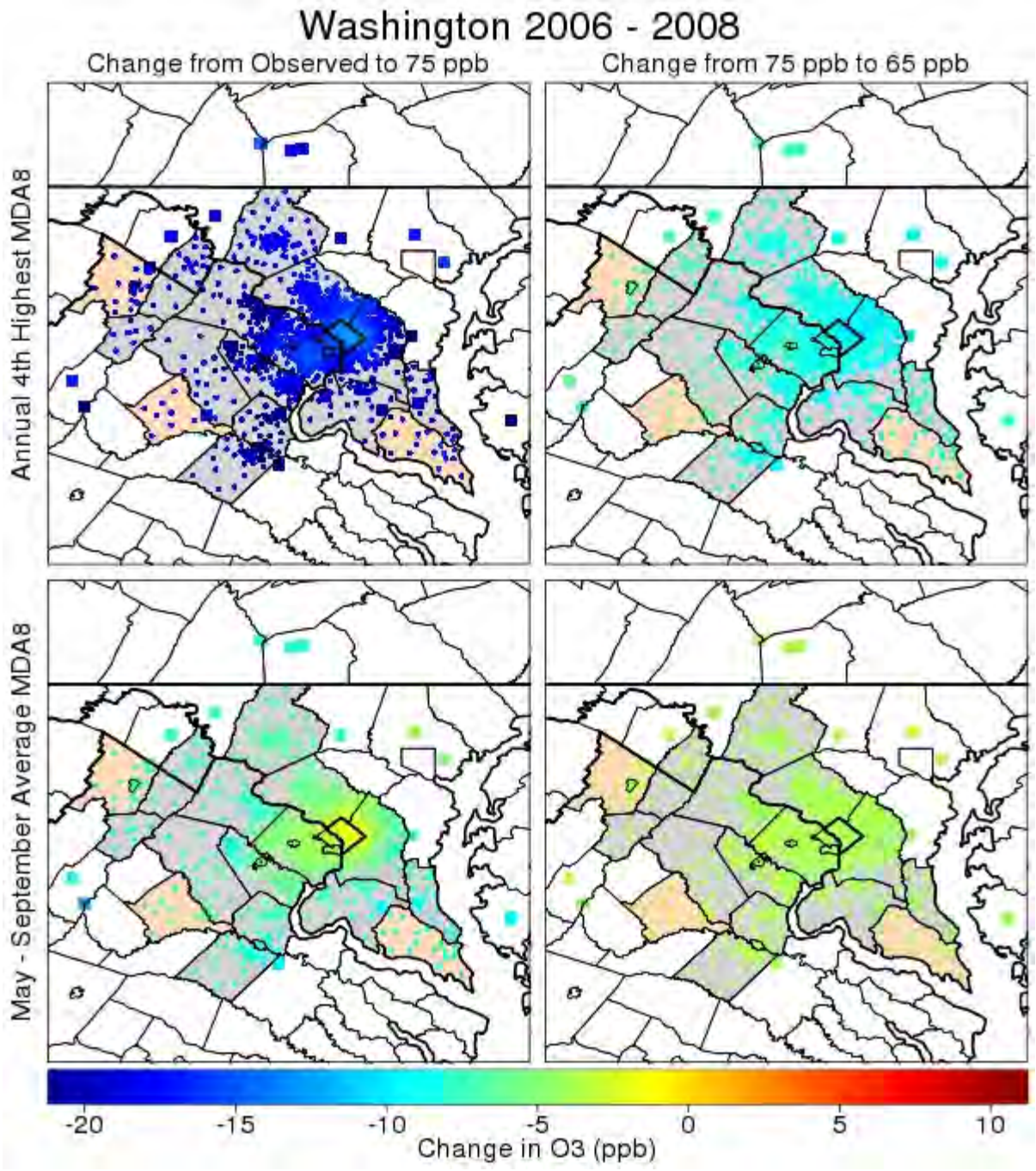

Figure 4D-113. Changes in annual 4th highest MDA8 and May-September average MDA8 values based on HDDM adjustments for Washington, D.C., 2006-2008. The points are colored according to the change in ppb, and values falling outside the range in the color bar were set to the nearest value within the color bar.

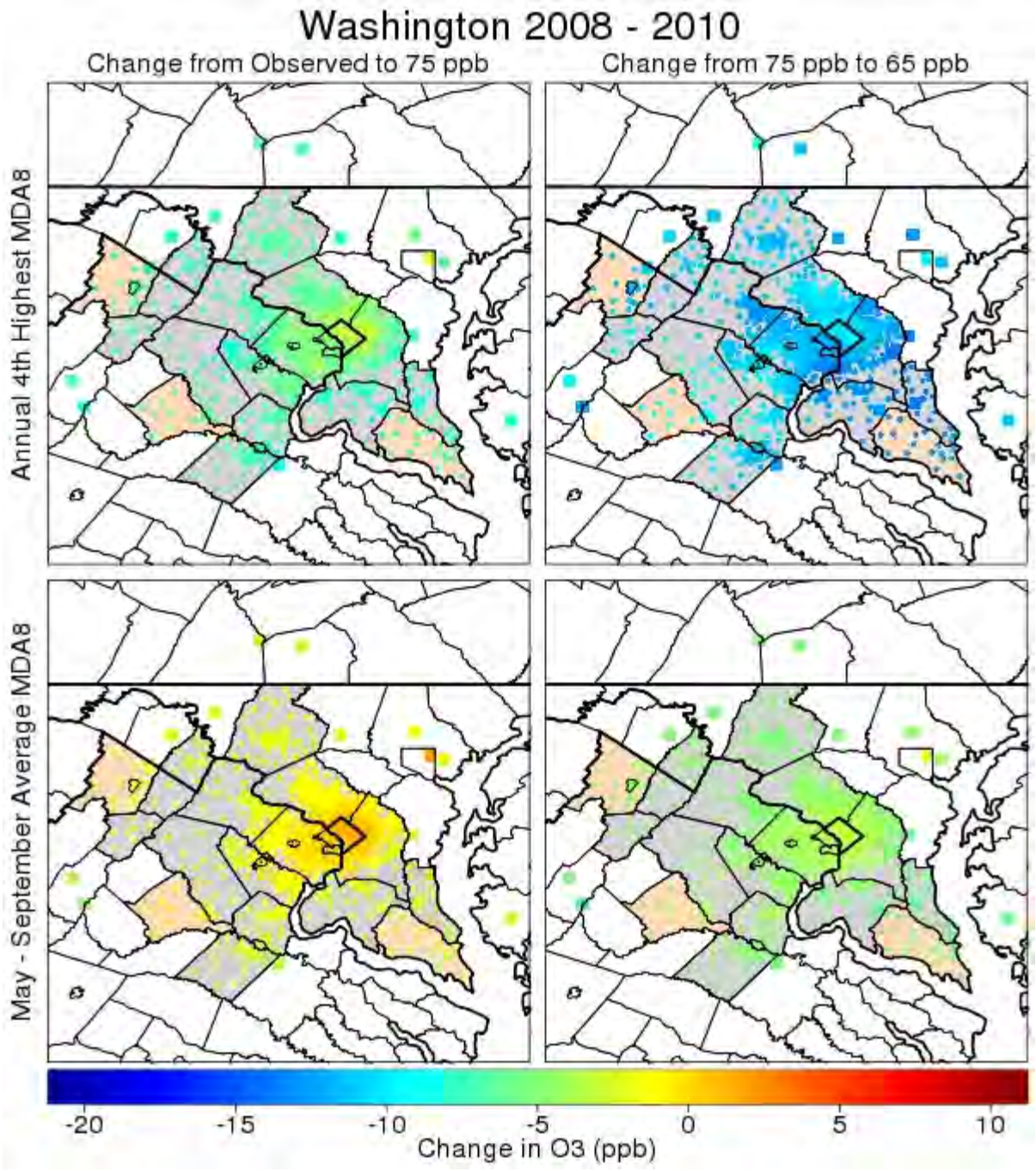

Figure 4D-114. Changes in annual 4th highest MDA8 and May-September average MDA8 values based on HDDM adjustments for Washington D.C., 2008-2010. The points are colored according to the change in ppb, and values falling outside the range in the color bar were set to the nearest value within the color bar.

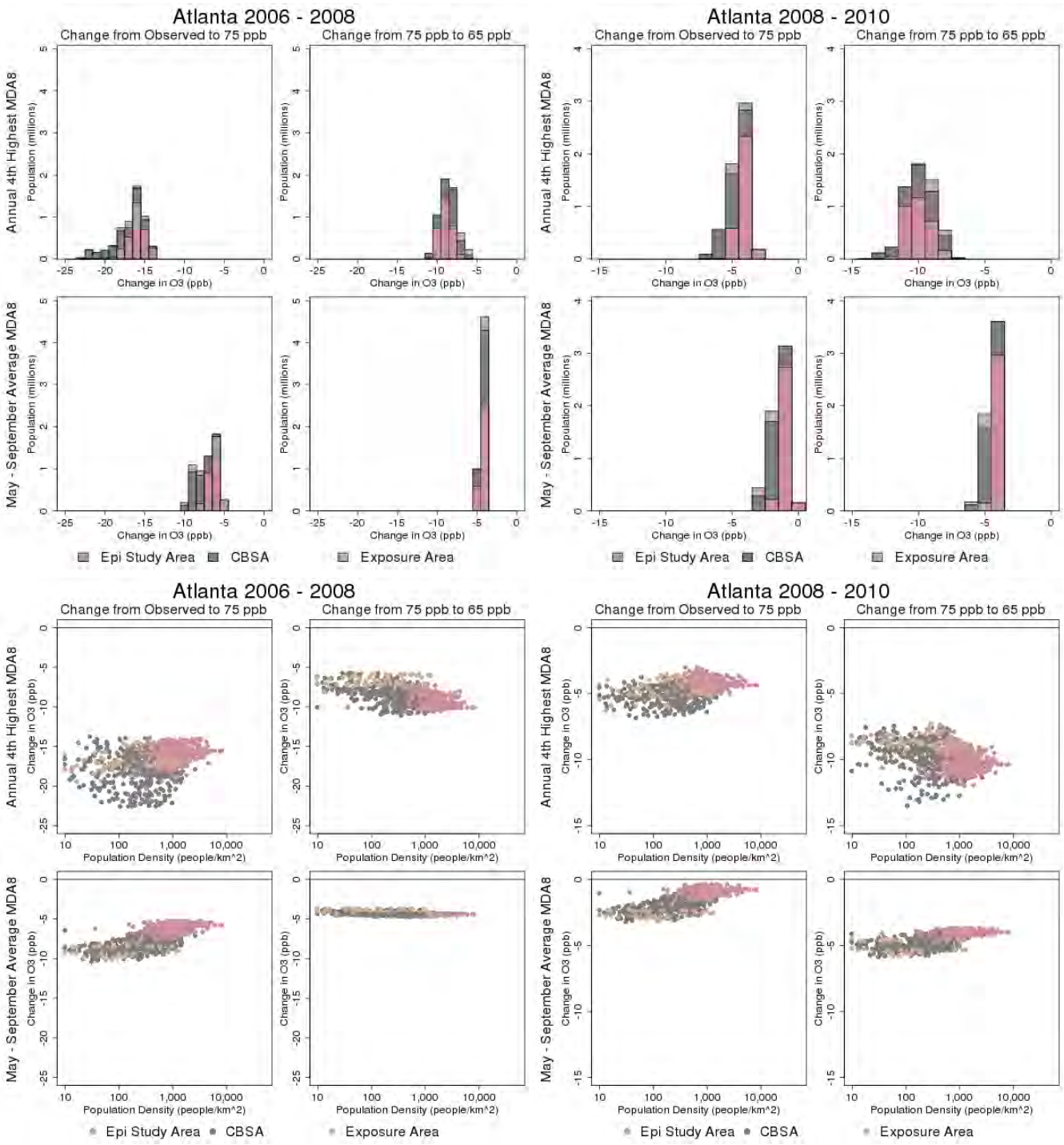

Figure 4D-115. Changes in VNA estimates of annual 4th highest MDA8 and May – September average MDA8 based on HDDM adjustments for Atlanta versus population and population density.

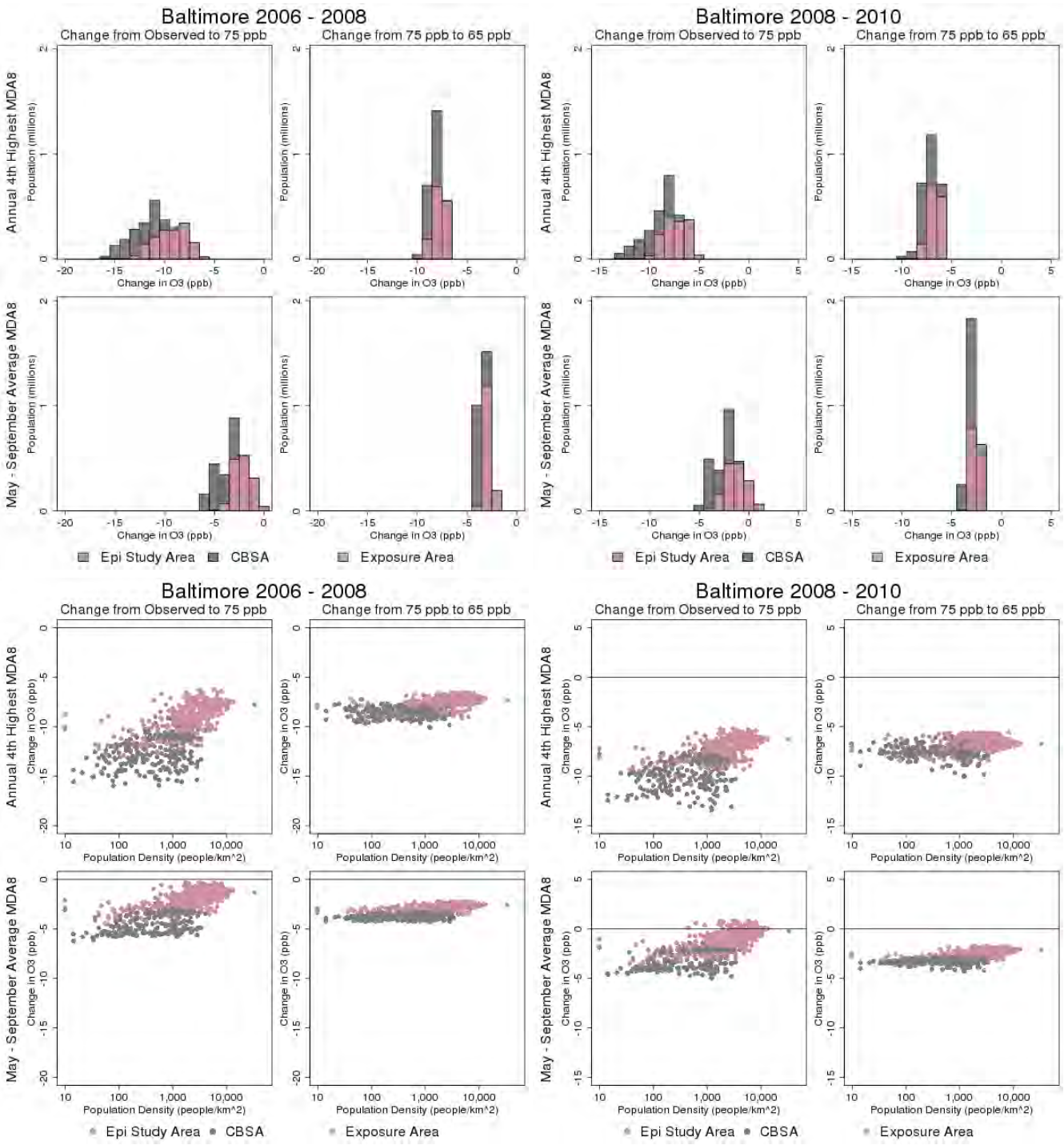

Figure 4D-116. Changes in VNA estimates of annual 4th highest MDA8 and May – September average MDA8 based on HDDM adjustments for Baltimore versus population and population density.

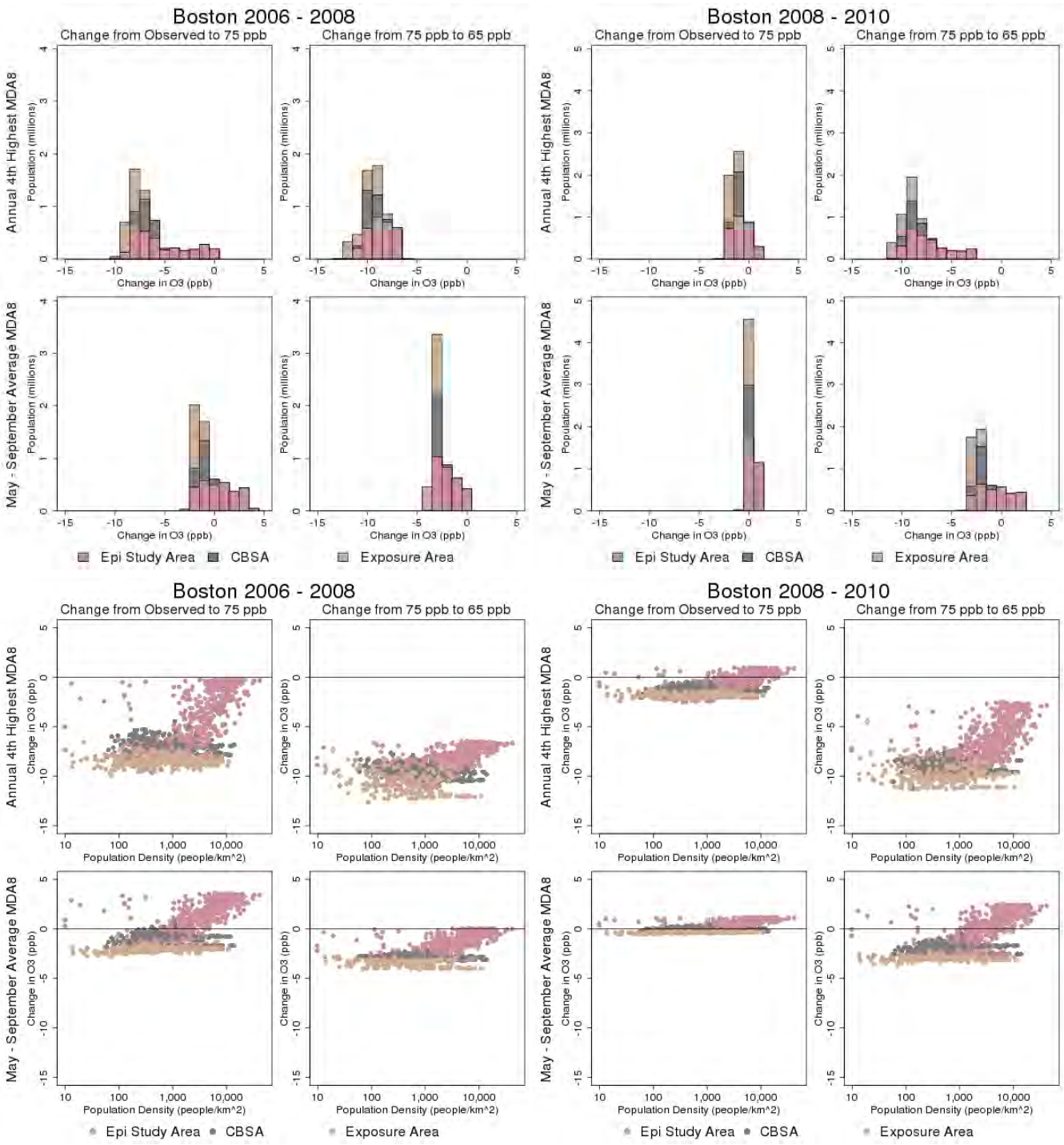

Figure 4D-117. Changes in VNA estimates of annual 4th highest MDA8 and May – September average MDA8 based on HDDM adjustments for Boston versus population and population density.

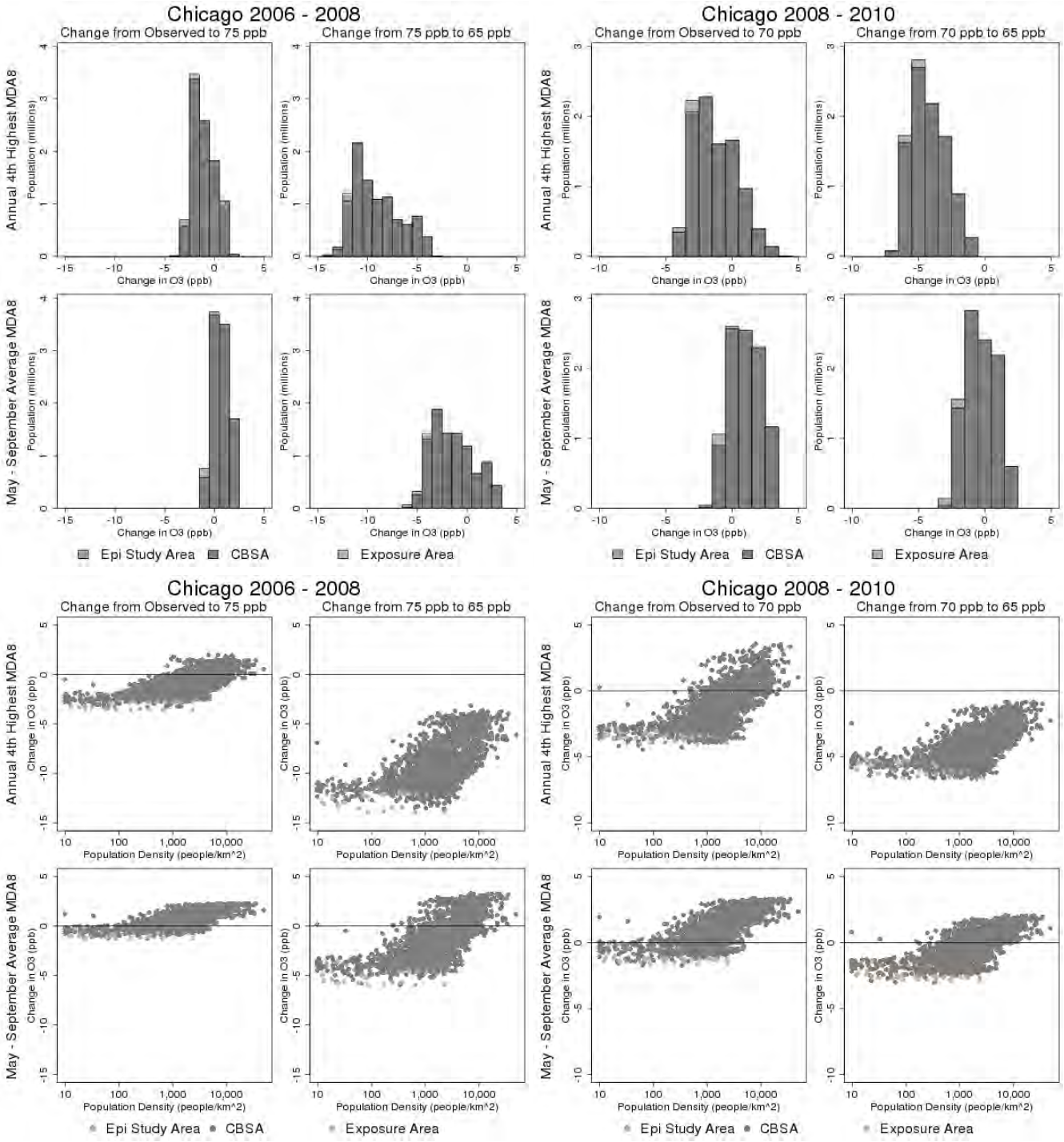

Figure 4D-118. Changes in VNA estimates of annual 4th highest MDA8 and May – September average MDA8 based on HDDM adjustments for Chicago versus population and population density.

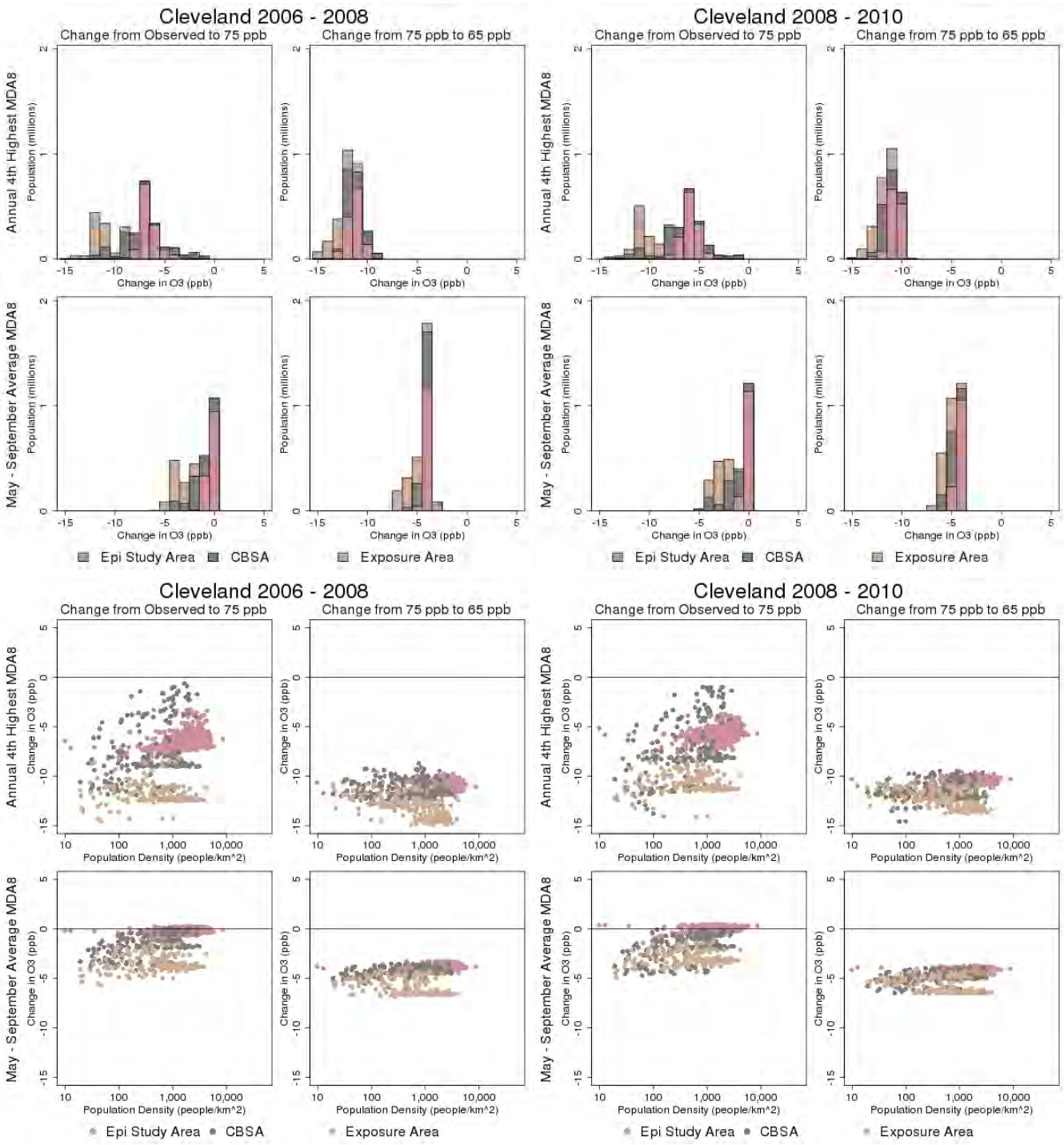

Figure 4D-119. Changes in VNA estimates of annual 4th highest MDA8 and May – September average MDA8 based on HDDM adjustments for Cleveland versus population and population density.

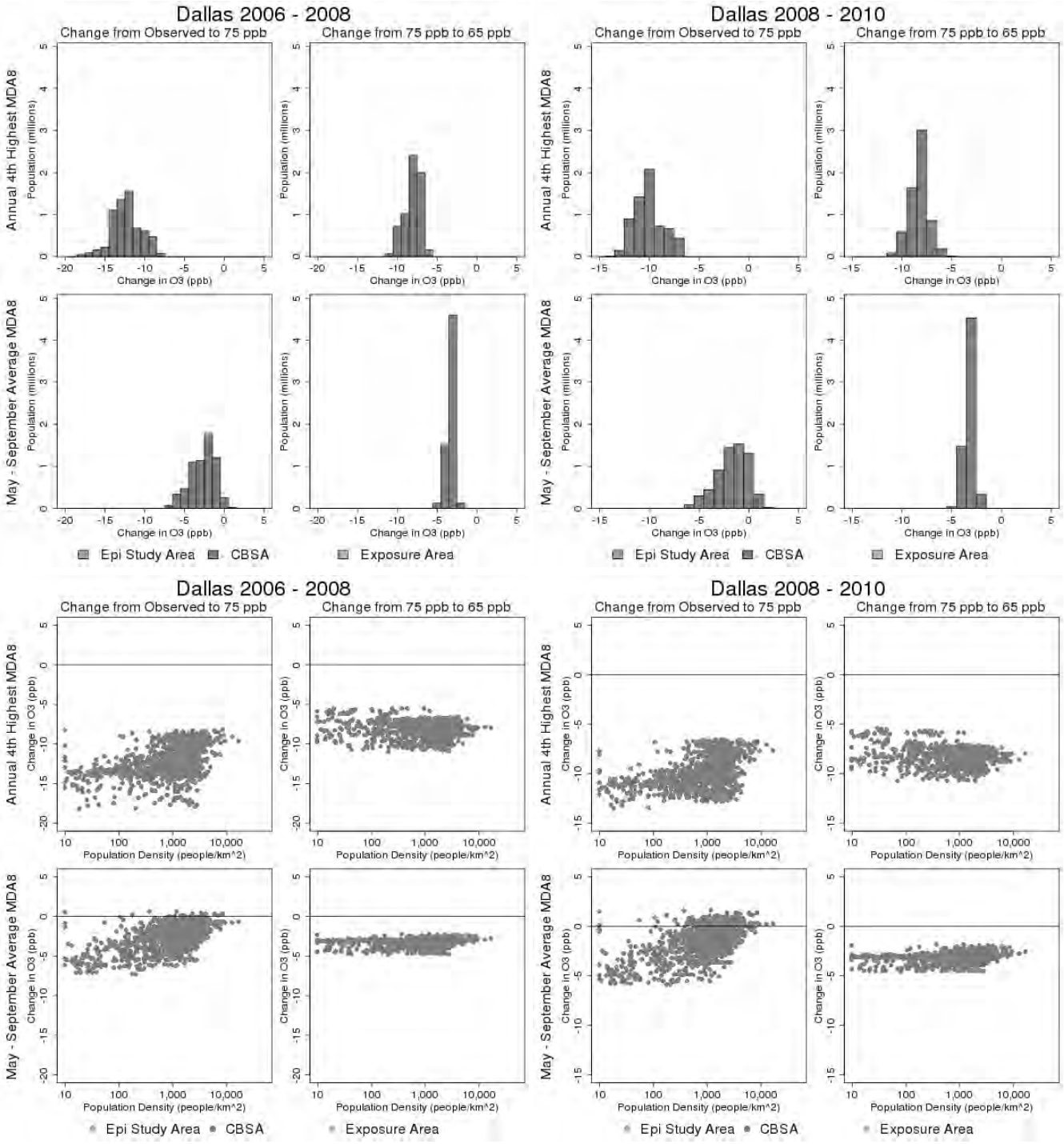

Figure 4D-120. Changes in VNA estimates of annual 4th highest MDA8 and May – September average MDA8 based on HDDM adjustments for Dallas versus population and population density.

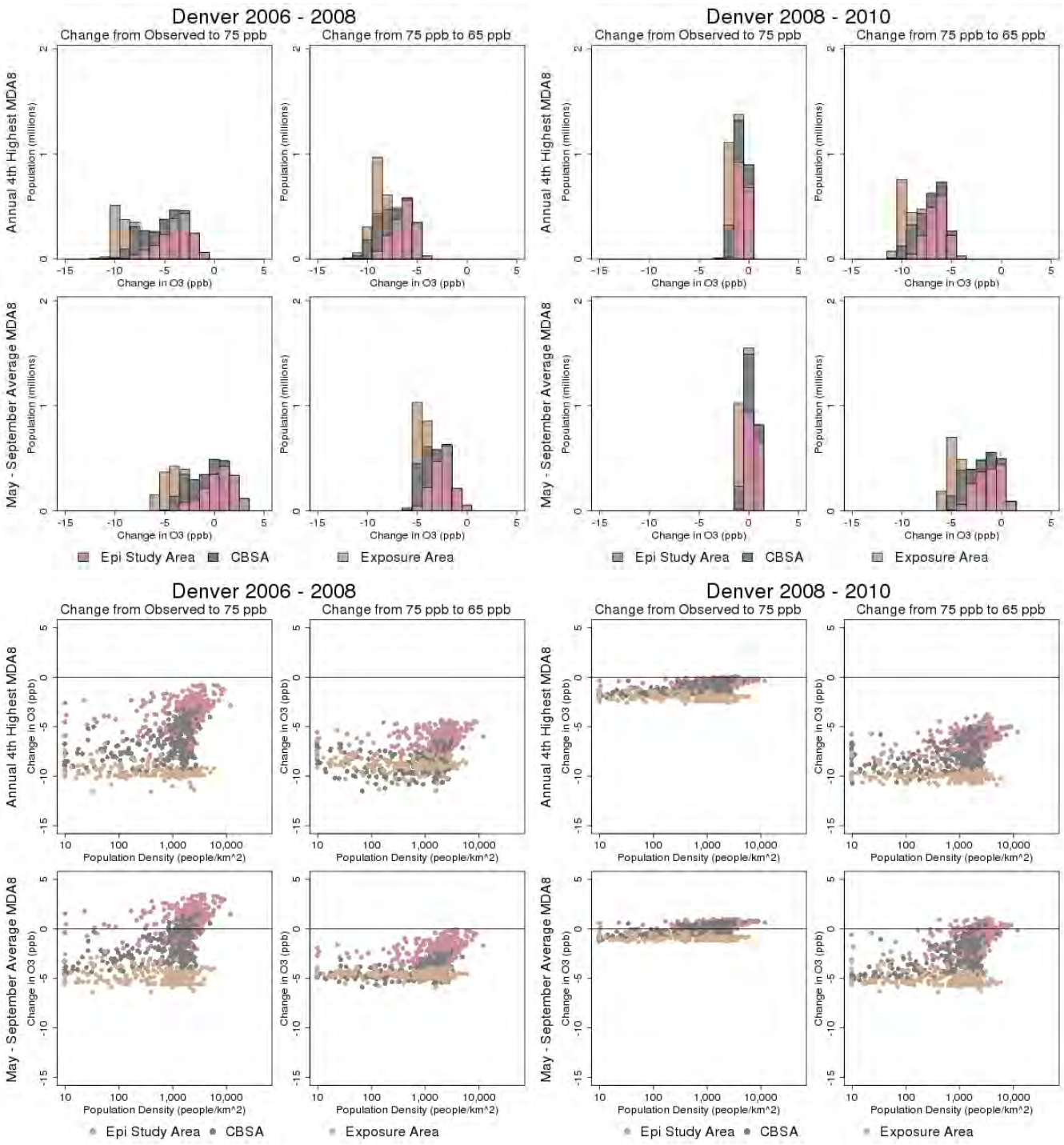

Figure 4D-121. Changes in VNA estimates of annual 4th highest MDA8 and May – September average MDA8 based on HDDM adjustments for Denver versus population and population density.

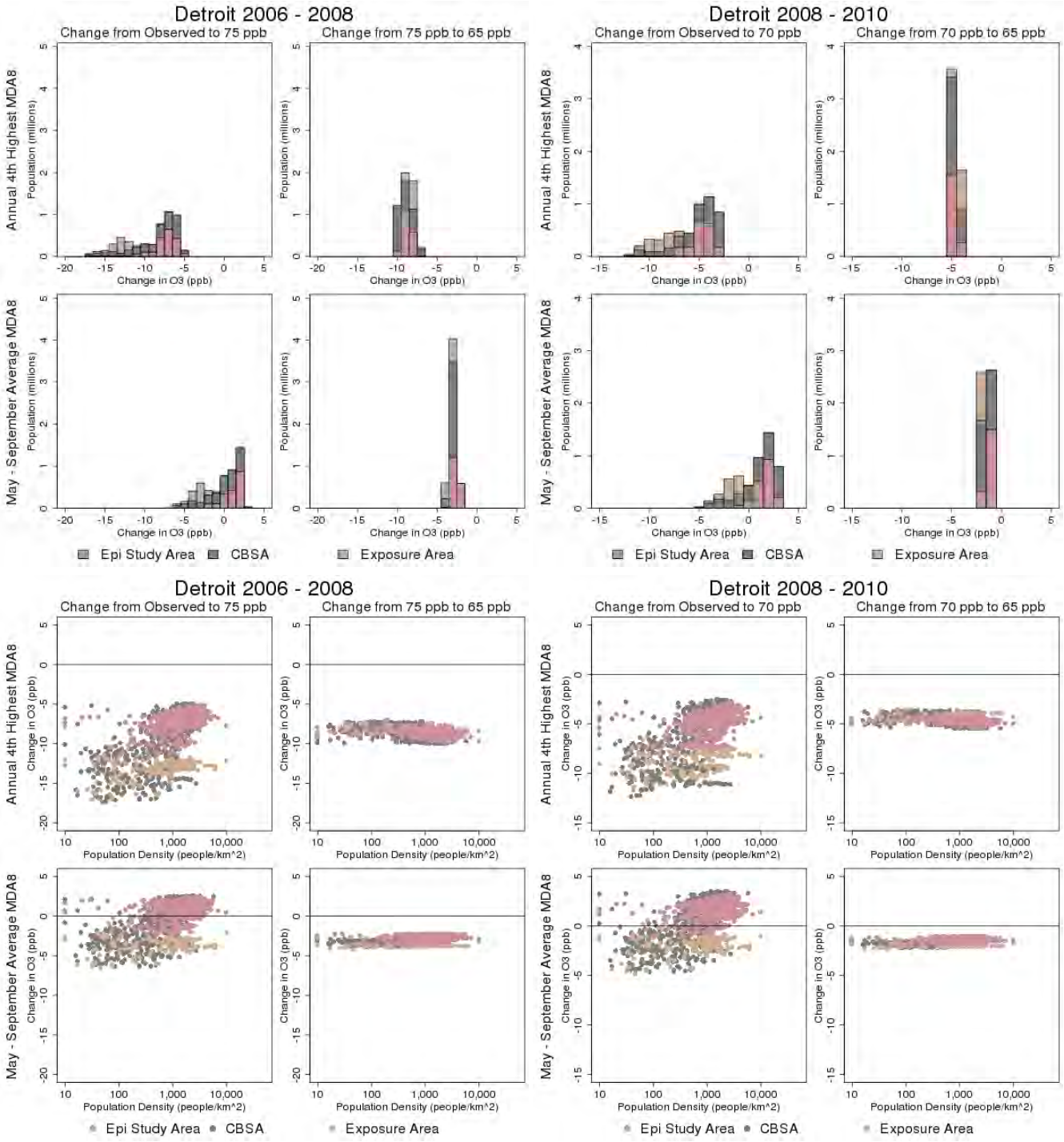

Figure 4D-122. Changes in VNA estimates of annual 4th highest MDA8 and May – September average MDA8 based on HDDM adjustments for Detroit versus population and population density.

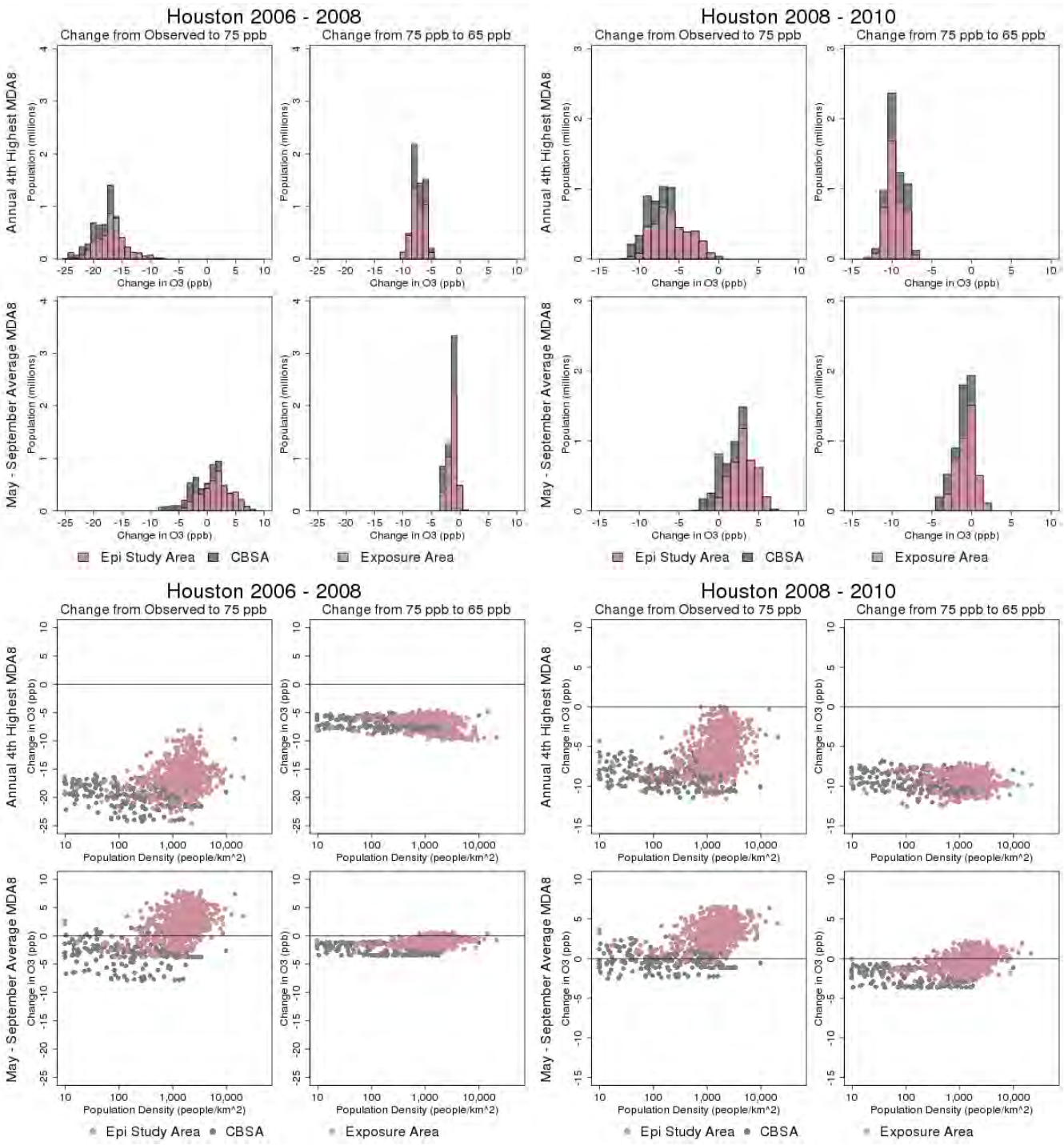

Figure 4D-123. Changes in VNA estimates of annual 4th highest MDA8 and May – September average MDA8 based on HDDM adjustments for Houston versus population and population density.

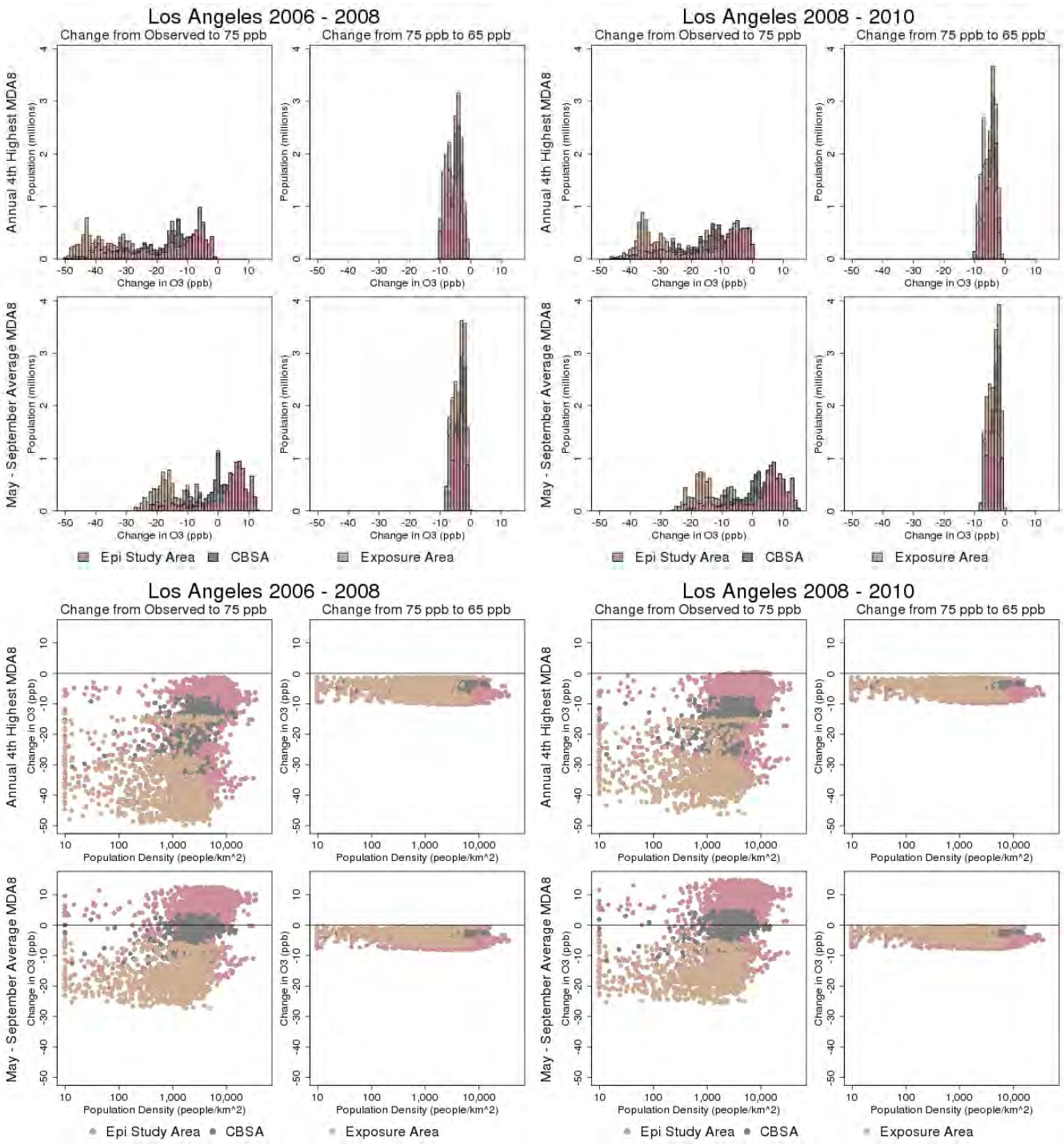

Figure 4D-124. Changes in VNA estimates of annual 4th highest MDA8 and May – September average MDA8 based on HDDM adjustments for Los Angeles versus population and population density.

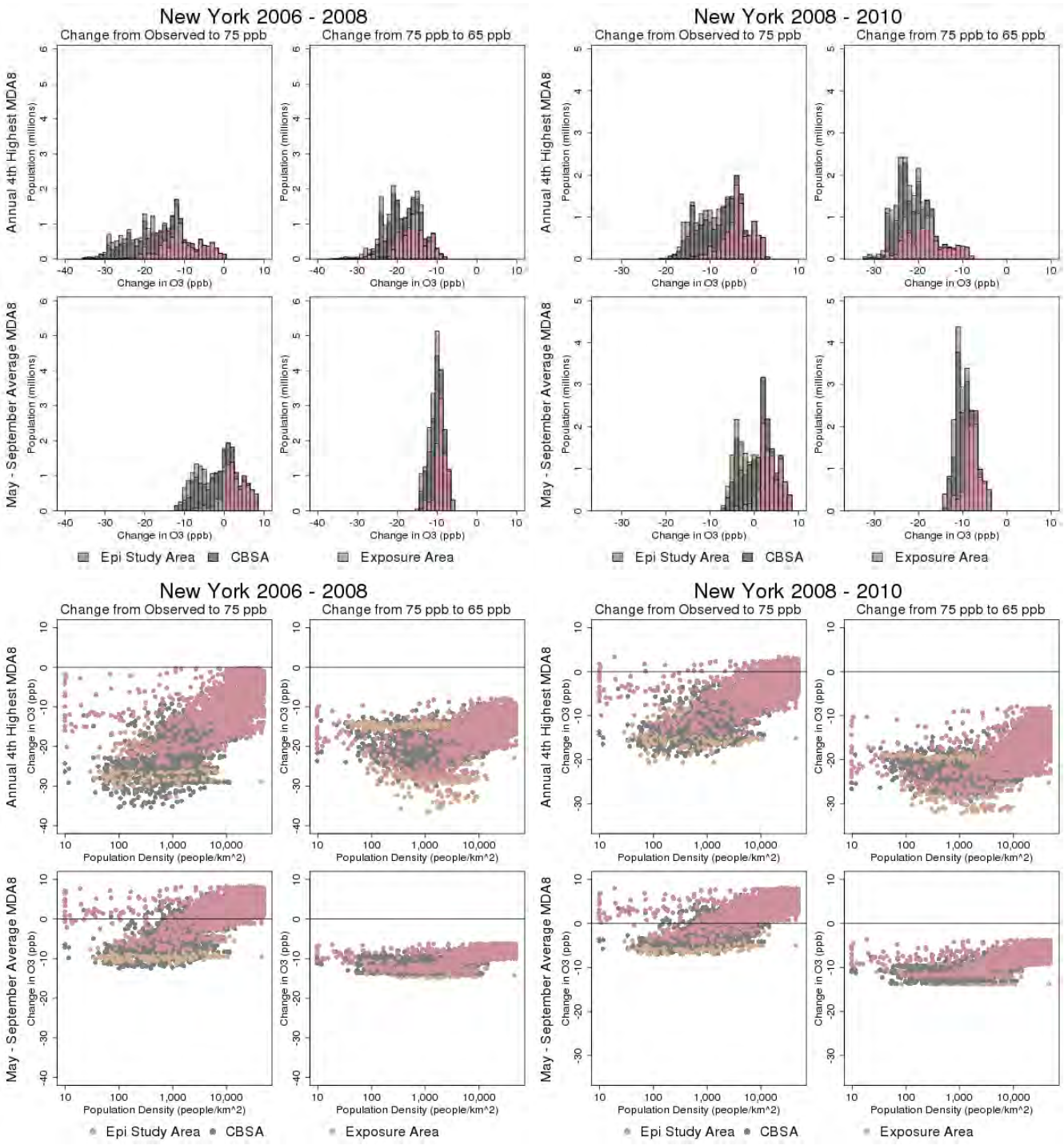

Figure 4D-125. Changes in VNA estimates of annual 4th highest MDA8 and May – September average MDA8 based on HDDM adjustments for New York versus population and population density.

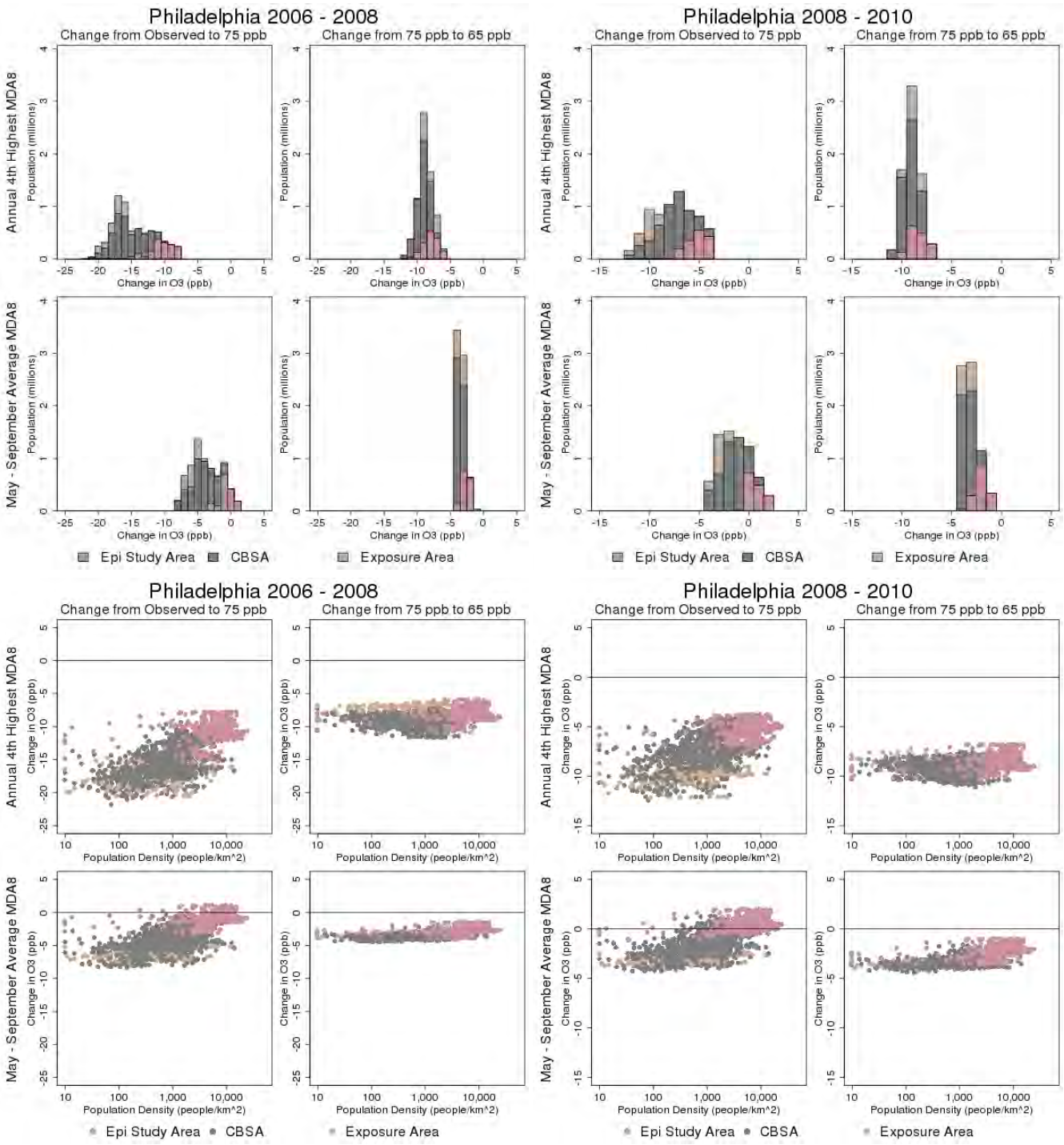

Figure 4D-126. Changes in VNA estimates of annual 4th highest MDA8 and May – September average MDA8 based on HDDM adjustments for Philadelphia versus population and population density.

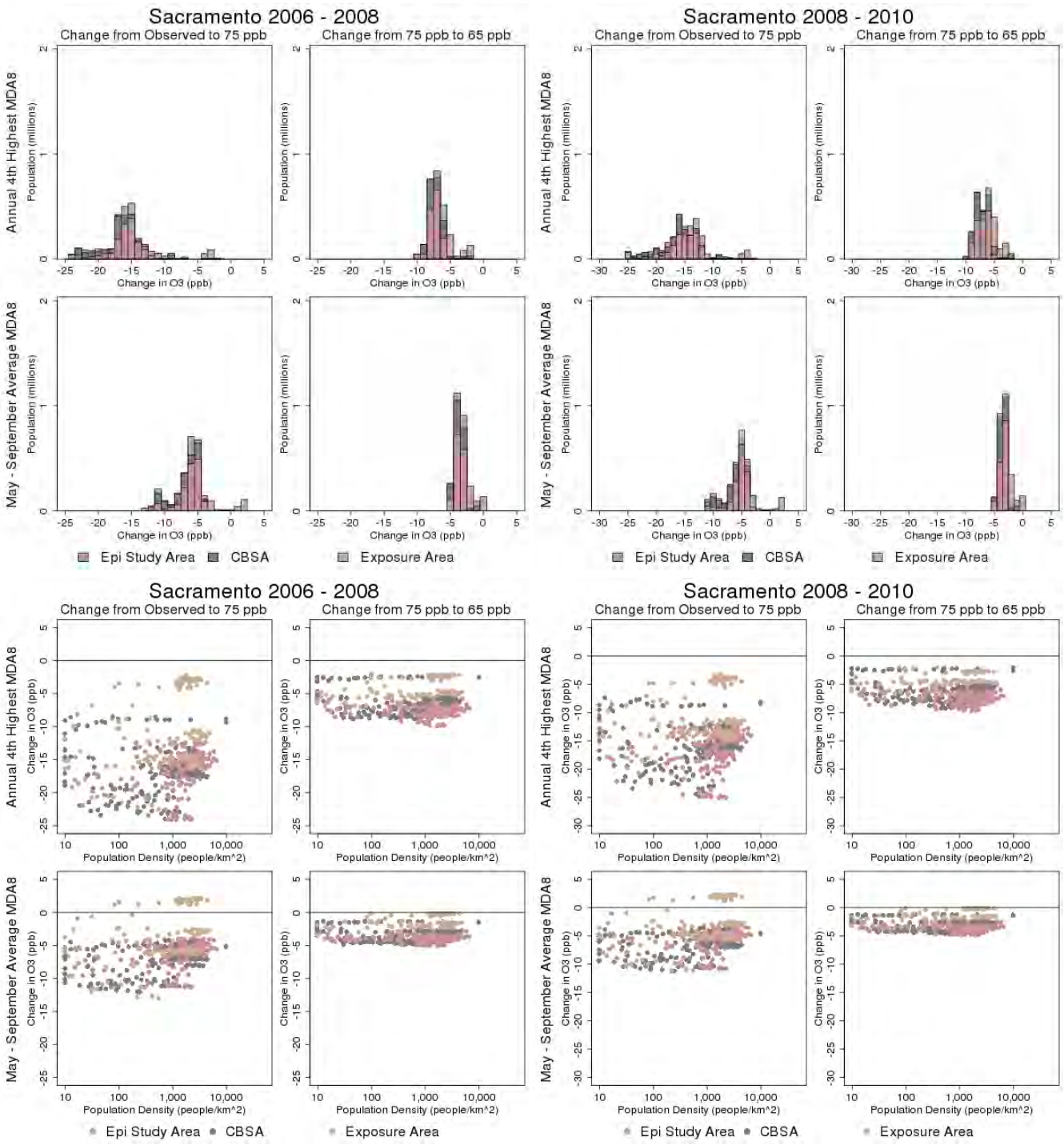

Figure 4D-127. Changes in VNA estimates of annual 4th highest MDA8 and May – September average MDA8 based on HDDM adjustments for Sacramento versus population and population density.

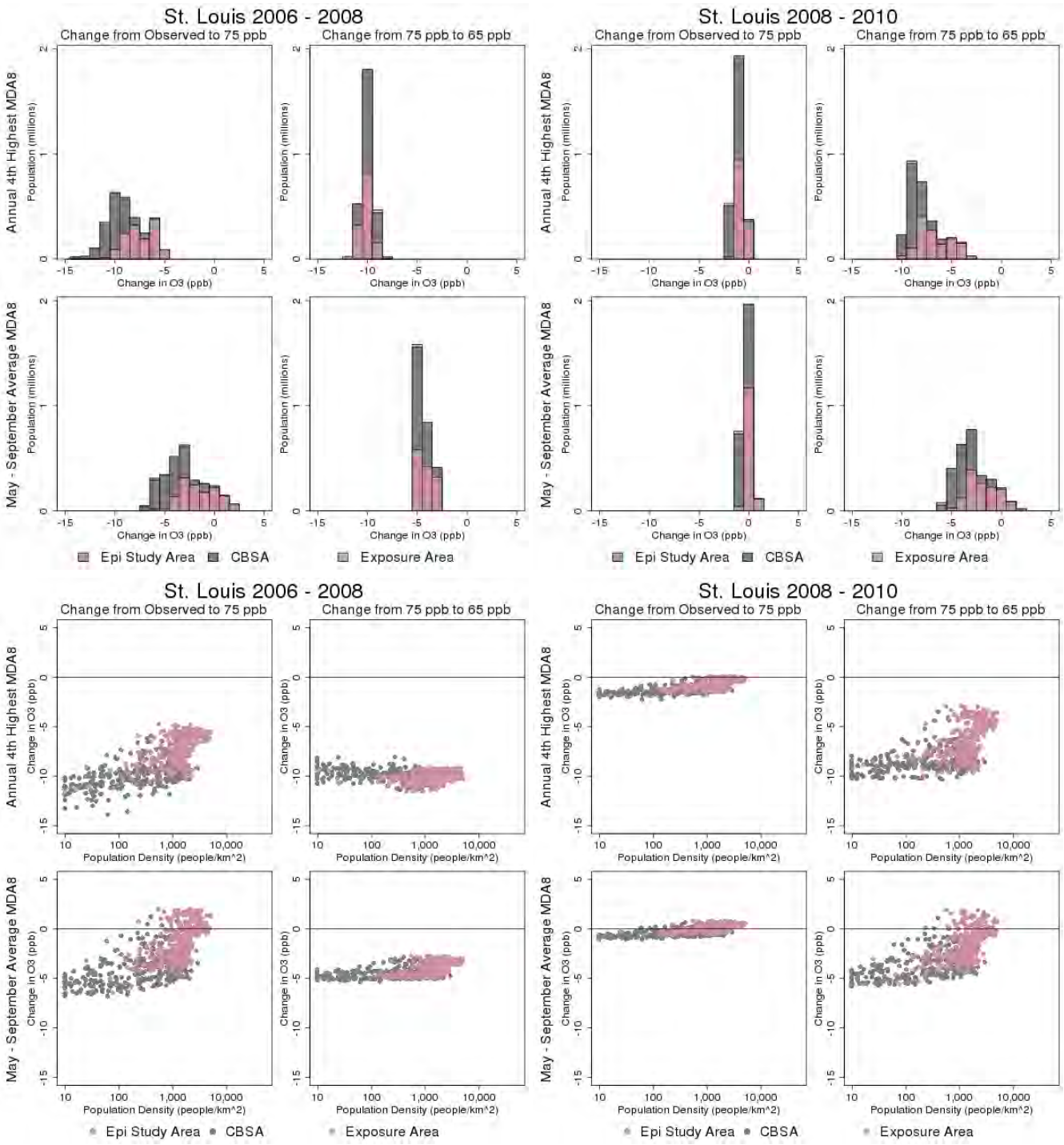

Figure 4D-128. Changes in VNA estimates of annual 4th highest MDA8 and May – September average MDA8 based on HDDM adjustments for St. Louis versus population and population density.

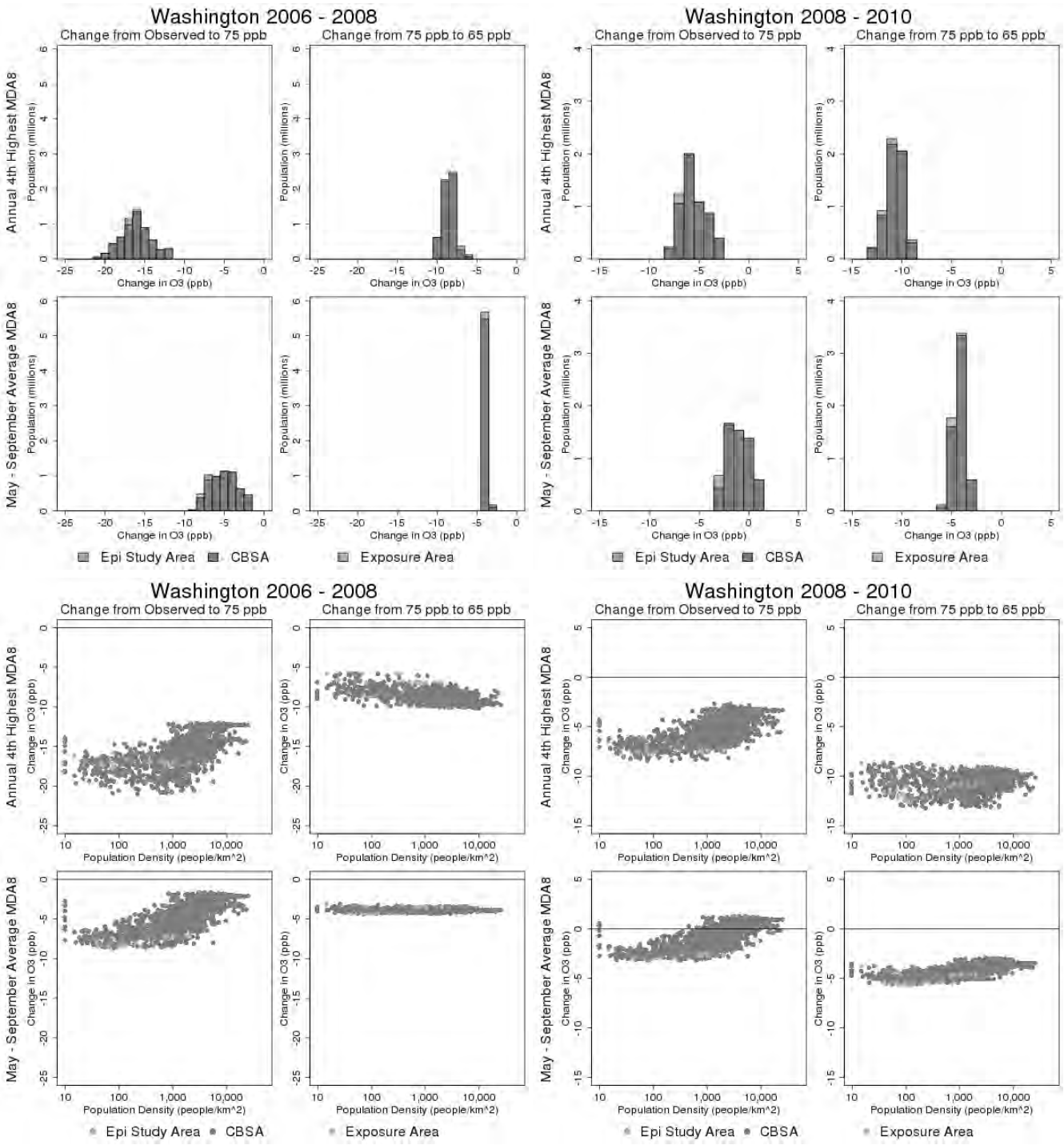

Figure 4D-129. Changes in VNA estimates of annual 4th highest MDA8 and May – September average MDA8 based on HDDM adjustments for Washington, D.C. versus population and population density.

4D-4.7 Comparing Air Quality Adjustments Based on NO_x Reductions Only to Air Quality Adjustments Based on NO_x and VOC Reductions

As mentioned in section 4D-4D-3, HDDM-adjustment scenarios could be carried out either by applying across-the-board reductions in U.S. anthropogenic NO_x emissions or by applying across-the-board reduction in U.S. anthropogenic NO_x and VOC emissions (with equal percentage reductions for the two precursors). The core analysis applied the NO_x-only reductions to all urban study areas except Chicago and Denver for which combined NO_x and VOC reductions were applied. However, in order to address the question of how the choice of NO_x-only emissions reductions affects estimated air quality distributions for adjustments to the existing and alternative standard levels we performed sensitivity analyses for seven cities: Denver, Detroit, Houston, Los Angeles, New York, Philadelphia, and Sacramento. For these seven cities, we performed both NO_x-only and N/VOC emissions reductions scenarios for all standard levels and compared the resulting air quality results. Although in six of these cities the additional VOC reductions did not result in needing lower percentage NO_x reductions, we recognize that some VOC reductions are likely to occur in future years due to on-the-books mobile source rules. However, the large VOC cuts applied here are larger than expected reductions from these rules. Several caveats need to be noted for this analysis. First, this is meant as a sensitivity test only and not as a potential realistic alternative control scenario. Second, because the methodology described in Section 4D-3 restricts the calculations to equal percentage cuts in NO_x and VOC, this sensitivity does not necessarily identify the optimal combination of NO_x and VOC reduction levels. Table 4D-20 shows the percentage reductions that were applied in each scenario for each of the seven cities.

Table 4D-20. Comparison of NO_x-only and NO_x/VOC emission reductions applied in sensitivity analyses for nine urban areas.

City	Years	NO_x-only				NO_x/VOC			
		75 ppb	70 ppb	65 ppb	60 ppb	75 ppb	70 ppb	65 ppb	60 ppb
Chicago	2006-2008	41%	54%	65%	75%	19%	52%	66%	80%
	2008-2010	N/A	42%	56%	67%	N/A	27%	55%	70%
Dallas	2006-2008	50%	57%	65%	72%	51%	60%	69%	77%
	2008-2010	50%	58%	64%	71%	50%	59%	68%	76%
Denver	2006-2008	54%	67%	76%	89%	51%	65%	78%	87%
	2008-2010	24%	53%	70%	89%	15%	46%	64%	87%
Detroit	2006-2008	59%	69%	76%	84%	60%	73%	85%	90%
	2008-2010	N/A	54%	66%	78%	N/A	53%	69%	85%
Houston	2006-2008	62%	68%	74%	82%	65%	73%	81%	87%
	2008-2010	42%	53%	63%	75%	40%	52%	65%	85%
Los Angeles (95% LB)	2006-2008	87%	89%	91%	93%	95%	96%	98%	99%
	2008-2010	87%	89%	91%	93%	93%	95%	97%	98%
New York (95% LB)	2006-2008	64%	74%	92%	N/A	60%	71%	89%	N/A
	2008-2010	52%	67%	89%	N/A	41%	55%	86%	N/A
Philadelphia	2006-2008	54%	61%	68%	74%	57%	65%	71%	79%
	2008-2010	42%	52%	61%	68%	37%	52%	62%	72%
Sacramento	2006-2008	63%	70%	76%	84%	65%	73%	80%	88%
	2008-2010	64%	71%	77%	84%	65%	74%	81%	88%

Figure 4D-130 through Figure 4D-136 show boxplots of composite monitor daily maximum 8-hr O_3 values for recent conditions (base) and each of the eight adjustment scenarios (NO_x-only and NO_x/VOC for 75, 70, 65, and 60 ppb standard levels) in the seven cities evaluated. A range of results can be seen in different urban areas. Denver, Houston, Los Angeles, and New York showed the largest difference between O_3 concentrations in NO_x-only versus NO_x/VOC scenarios while Detroit, Philadelphia and Sacramento had relatively less difference in the O_3 distributions estimated in two types of scenarios. In all cities, the NO_x-only and NO_x/VOC scenarios had very similar O_3 concentrations at the upper end of the distribution (top whiskers and outlier dots in the boxplots). This is not surprising since the adjustment scenarios were implemented to obtain identical 4th high O_3 concentrations. Mid-range O_3 concentrations (25th-75th percentiles) were generally lower in the NO_x/VOC adjustment scenarios than the NO_x-only adjustment scenarios for the same standard level with the exception of New York.

The reduction of mid-range O_3 concentrations in the NO_x/VOC scenarios compared to the NO_x-only scenarios tended to be larger in 2007 than in 2009 and tended to be larger at lower alternate standard levels. In most urban study areas the reduction in mid-level O_3 in the NO_x/VOC scenario compared to the NO_x-only scenario was modest but in Los Angeles it was significant. The change in mid-range O_3 concentrations between the two sets of scenarios was so dramatic in Los Angeles that in many cases the 75th percentile concentration in the NO_x/VOC scenario was lower than the 25th percentile concentration in the comparable NO_x-only scenario. The most dramatic differences between the NO_x-only and the NO_x/VOC scenarios occurred at the low end of the O_3 distribution. In all urban study areas, there were smaller increases in O_3 at low O_3 concentrations in the NO_x/VOC scenario when compared to the NO_x-only scenario for the same standard level. This is especially evident for extreme low concentrations (bottom whiskers for blue NO_x-only scenarios are much higher than bottom whiskers for red NO_x/VOC scenarios in the boxplots) but can also be seen in the 25th percentile O_3 values which are represented by the bottom of the boxes. The reductions were most apparent for Denver, Houston, Los Angeles, New York, and Philadelphia but were more modest in Detroit and Sacramento.

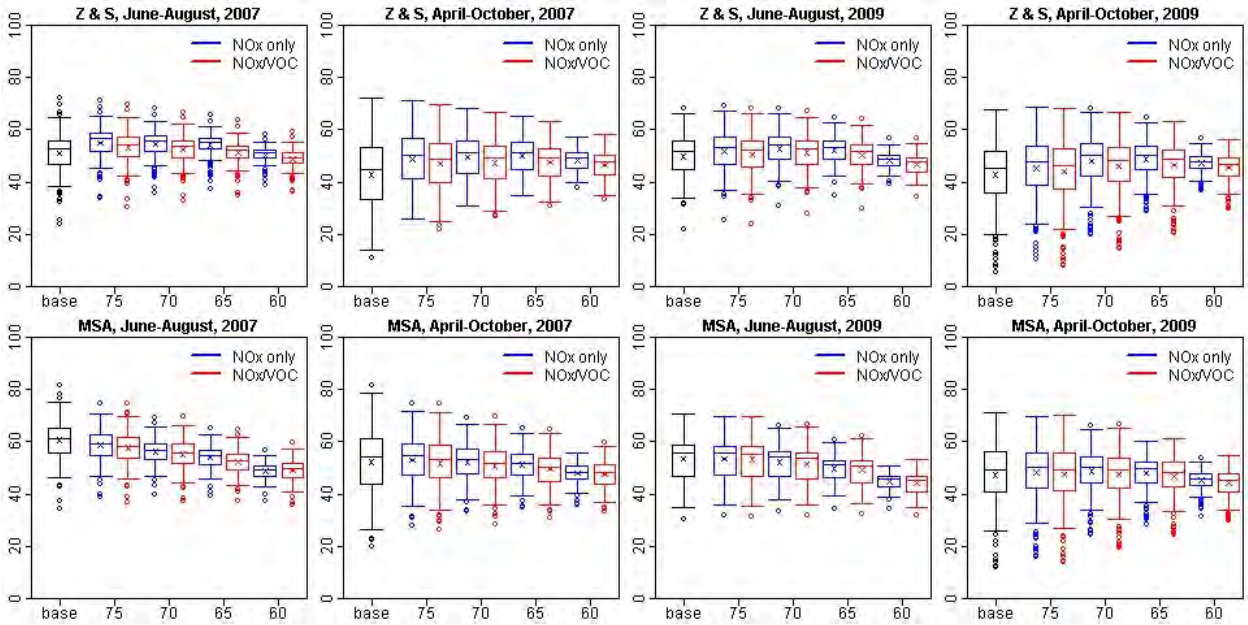

Figure 4D-130. Composite monitor daily maximum 8-hour O_3 values for Denver based on observed and adjusted air quality for the NO_x-only and NO_x/VOC scenarios. Boxes represent the median and quartiles, x's represent mean values, whiskers extend up to 1.5x the inter-quartile range from the boxes, and circles represent outliers.

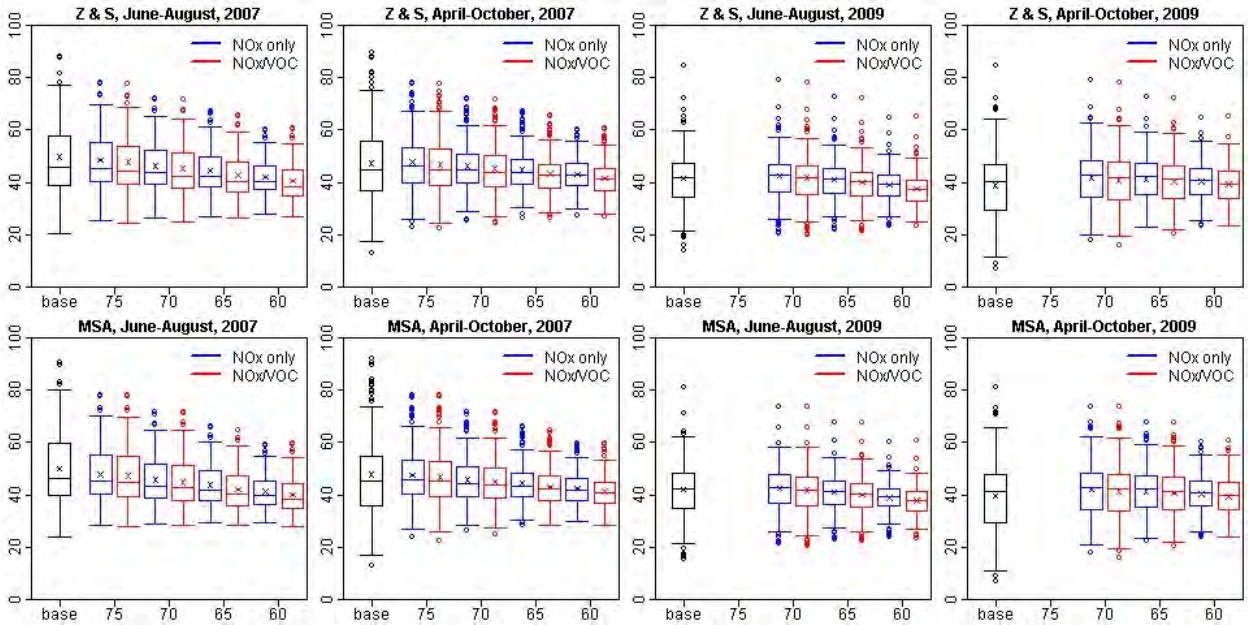

Figure 4D-131. Composite monitor daily maximum 8-hour O_3 values for Detroit based on observed and adjusted air quality for the NO_x-only and NO_x/VOC scenarios. Boxes represent the median and quartiles, x's represent mean values, whiskers extend up to 1.5x the inter-quartile range from the boxes, and circles represent outliers.

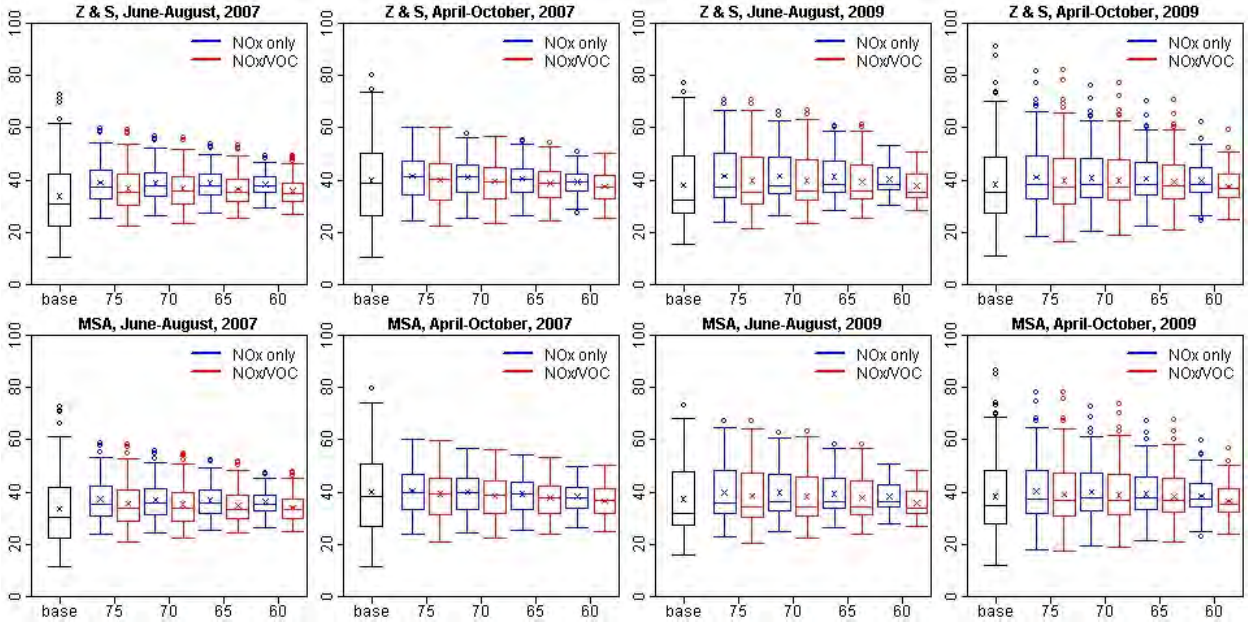

Figure 4D-132. Composite monitor daily maximum 8-hour O_3 values for Houston based on observed and adjusted air quality for the NO_x-only and NO_x/VOC scenarios. Boxes represent the median and quartiles, x's represent mean values, whiskers extend up to 1.5x the inter-quartile range from the boxes, and circles represent outliers.

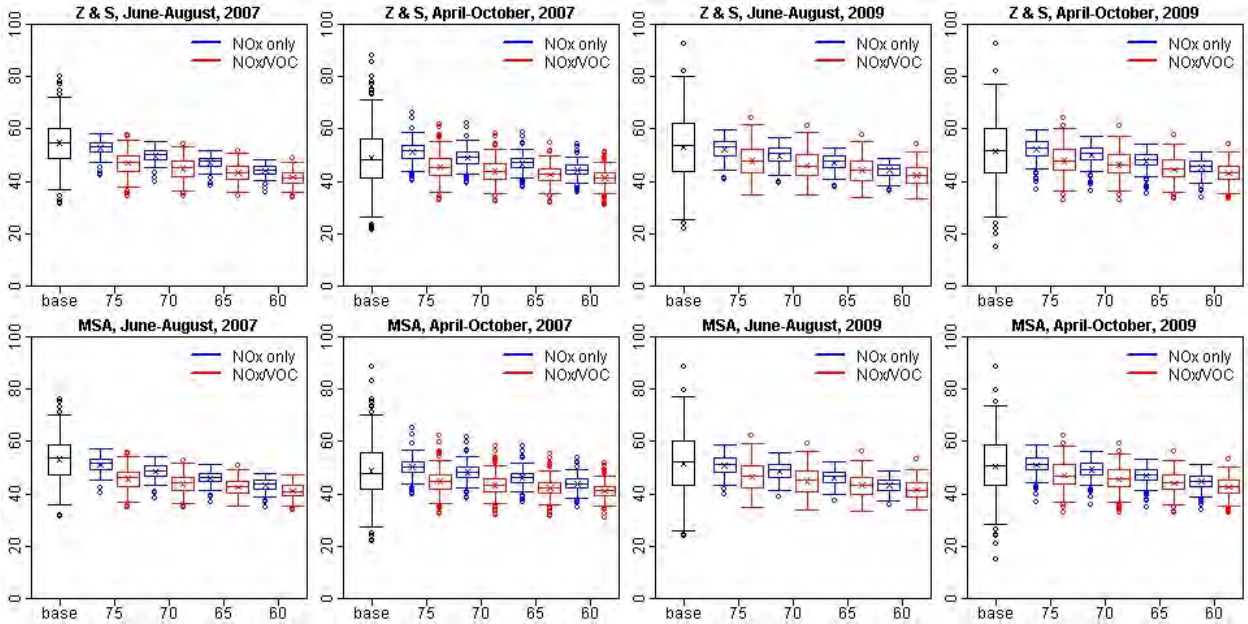

Figure 4D-133. Composite monitor daily maximum 8-hour O_3 values for Los Angeles based on observed and adjusted air quality for the NO_x-only and NO_x/VOC scenarios. Boxes represent the median and quartiles, x's represent mean values, whiskers extend up to 1.5x the inter-quartile range from the boxes, and circles represent outliers.

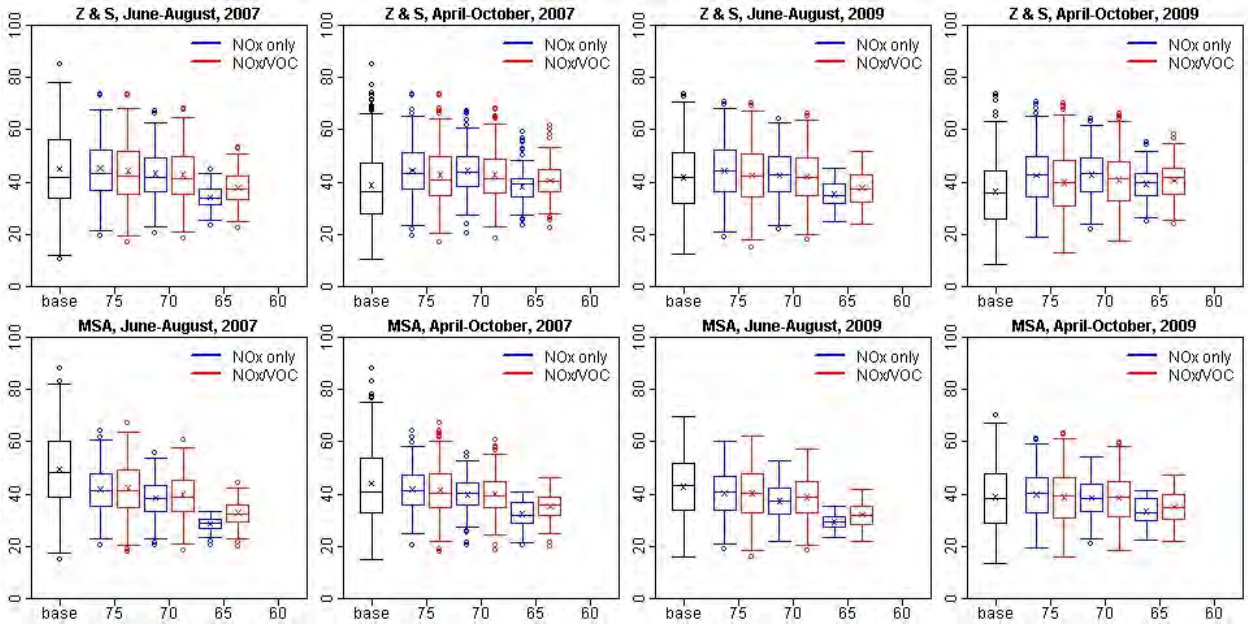

Figure 4D-134. Composite monitor daily maximum 8-hour O_3 values for New York based on observed and adjusted air quality for the NO_x-only and NO_x/VOC scenarios. Boxes represent the median and quartiles, x's represent mean values, whiskers extend up to 1.5x the inter-quartile range from the boxes, and circles represent outliers.

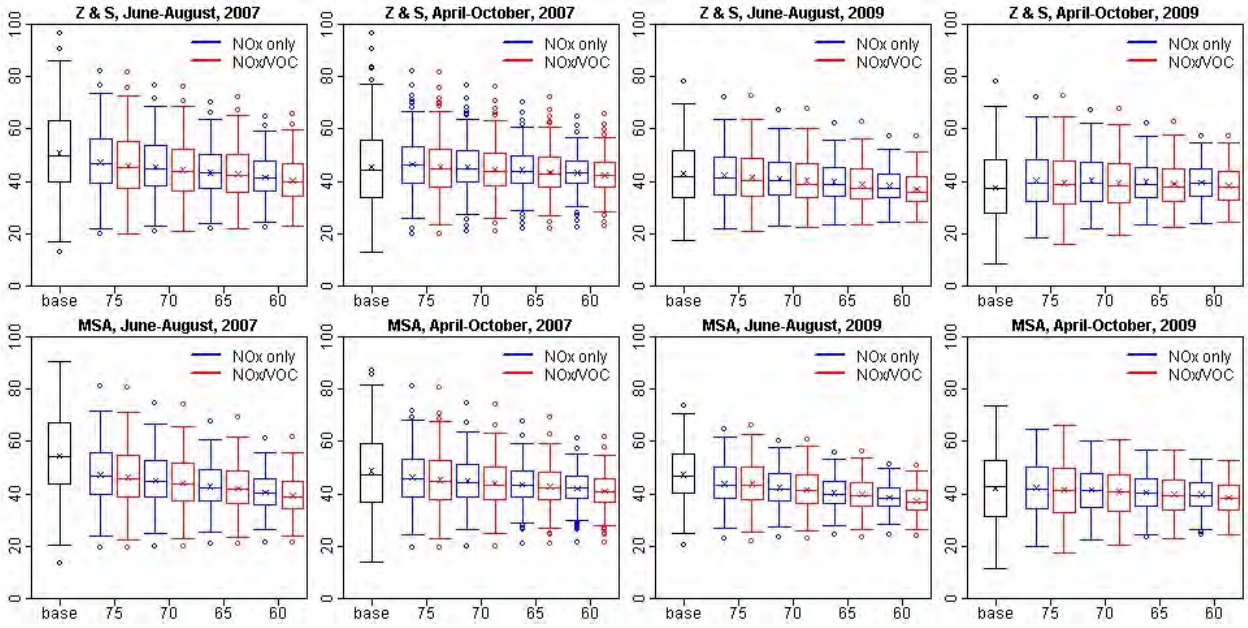

Figure 4D-135. Composite monitor daily maximum 8-hour O_3 values for Philadelphia based on observed and adjusted air quality for the NO_x-only and NO_x/VOC scenarios. Boxes represent the median and quartiles, x's represent mean values, whiskers extend up to 1.5x the inter-quartile range from the boxes, and circles represent outliers.

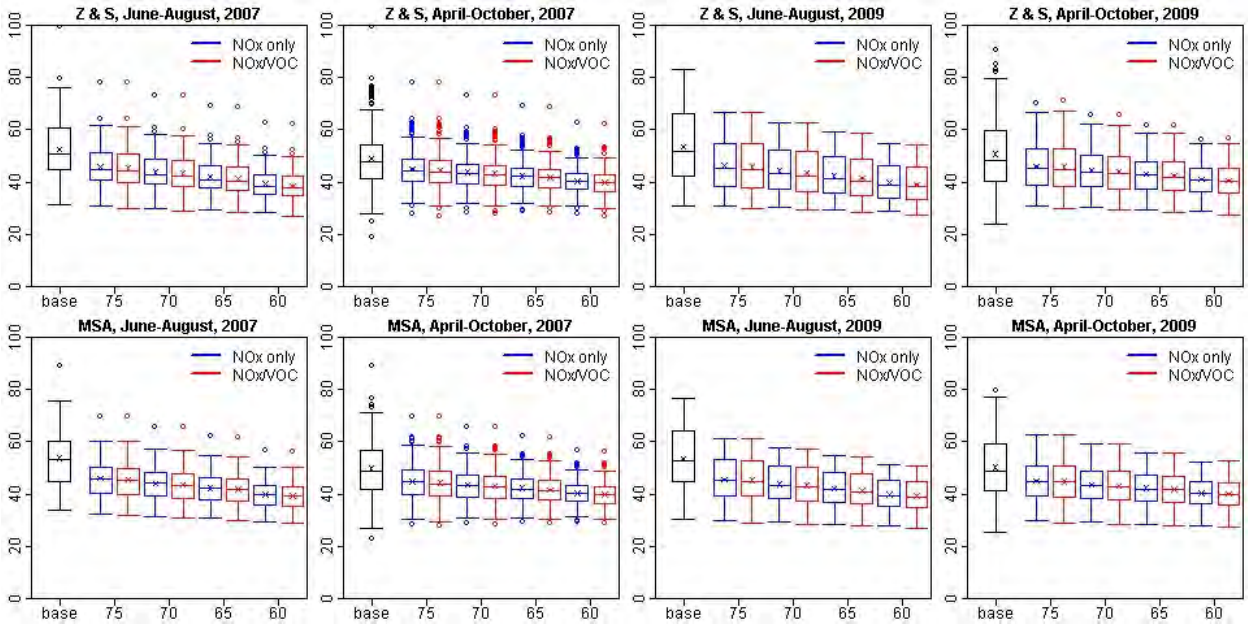

Figure 4D-136. Composite monitor daily maximum 8-hour O_3 values for Sacramento based on observed and adjusted air quality for the NO_x-only and NO_x/VOC scenarios. Boxes represent the median and quartiles, x's represent mean values, whiskers extend up to 1.5x the inter-quartile range from the boxes, and circles represent outliers.

Figure 4D-137 through Figure 4D-143 show maps of the 2006-2008 observed and adjusted April-October seasonal mean of the daily maximum 8-hr O_3 value at monitor locations in each of the urban study areas. Adjusted values are shown for the 75 ppb and 65 ppb NO_x-only and NO_x/VOC adjustment scenarios. As described earlier in this appendix and in HREA Chapter 4, these figures show that for observed 2006-2008 O_3 values, the seasonal mean of the daily maximum 8-hr O_3 concentration was suppressed in the highly urbanized areas compared to surrounding locations. In these figures, it is clear that O_3 concentrations are lower in the center city areas for all cities except Sacramento. The NO_x-only adjustment scenarios resulted in three types of behavior as demonstrated by the top panels on these maps. First, in Denver, Houston, Los Angeles, and New York the NO_x-only adjustment cases resulted in increasing seasonal mean concentrations in center city locations where O_3 was suppressed in observations and decreasing seasonal mean concentrations in outlying areas where O_3 was higher in the observations. This trend is so dramatic in Los Angeles and New York that the spatial gradient becomes inverted in the adjustment cases compared to the observed values (i.e. highest concentrations in urban core areas and lower concentrations in surrounding areas). The second type of response occurred in Detroit where there was little change at the monitor in the center of Wayne County but seasonal mean O_3 at the outlying monitors decreased in the NO_x-only adjustment cases. Finally, in Sacramento and Philadelphia, the NO_x-only adjustment cases cause relatively small decreases in

seasonal mean O_3 throughout the area. When comparing the NO_x-only to the NO_x/VOC adjustment scenarios three types of patterns emerge. In Denver and Los Angeles, the NO_x/VOC adjustment scenarios lead to lower seasonal mean O_3 concentrations than the equivalent NO_x-only adjustment scenarios in the urban core areas but looked similar to the NO_x-only adjustment scenario in the outlying areas. In Houston, Detroit, Philadelphia, and Sacramento, seasonal mean O_3 concentrations in equivalent NO_x-only and NO_x/VOC adjustment scenarios were very similar at monitors throughout the areas although the NO_x/VOC adjustment scenarios lead to slightly lower concentrations. Finally, in New York the 75 ppb adjustment scenarios were similar for the NO_x/VOC and NO_x-only cases but for the 65 ppb adjustment scenarios the NO_x/VOC case actually lead to higher seasonal mean O_3 concentration in the urban core area than the NO_x-only case.

An evaluation of the composite monitor and spatial plot maps leads to several general conclusions for this sensitivity analysis. First, the NO_x/VOC reduction scenarios tended to mitigate increases that occurred in the NO_x-only scenario at the lower end of the O_3 distribution. Second the effect on the NO_x/VOC scenario versus the NO_x-only scenario was less dramatic for mid-range O_3 concentrations and varied from city to city. The NO_x/VOC scenarios lead to lower mid-range O_3 concentrations than the NO_x-only scenarios except in the case of New York. Third, the high end O_3 concentrations at various standard levels were similar in the NO_x-only and the NO_x/VOC scenarios. Finally, the VOC reductions tended to have more impact in urban core areas and relatively little impact in outlying areas. The effects of these air quality sensitivity analyses on risk are evaluated and discussed in HREA Chapter 7.

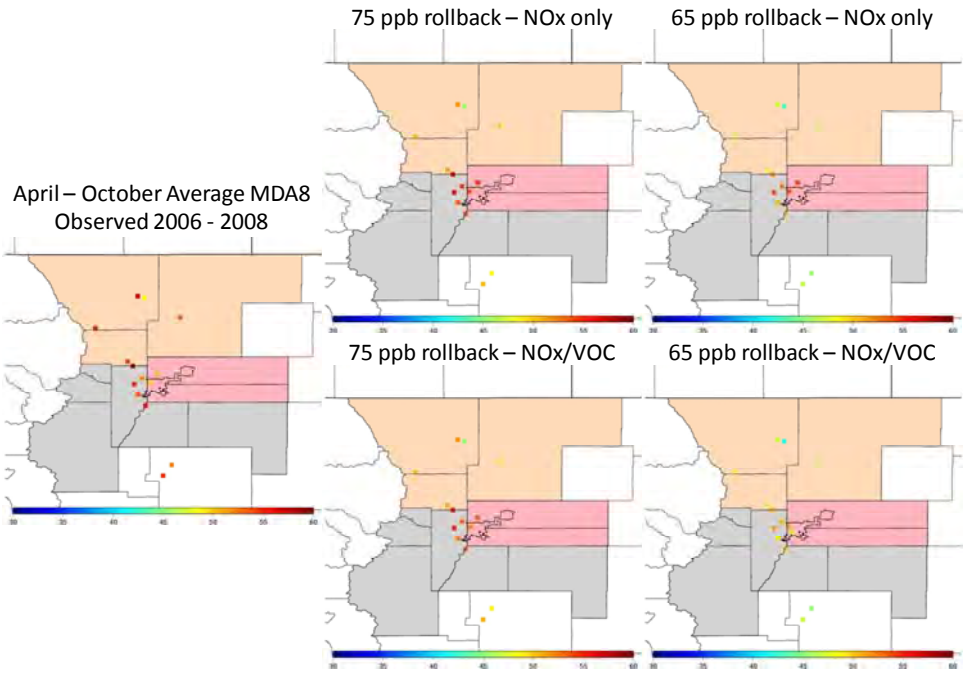

Figure 4D-137. April-October seasonal average of daily maximum 8-hour O_3 values at Denver area monitor locations for observed 2006-2008 conditions (left panel), 75 ppb adjustment scenarios (middle panels), and 65 ppb adjustment scenarios (right panels). NO_x-only adjustments are shown in top panels, NO_x/VOC adjustments are shown in bottom panels.

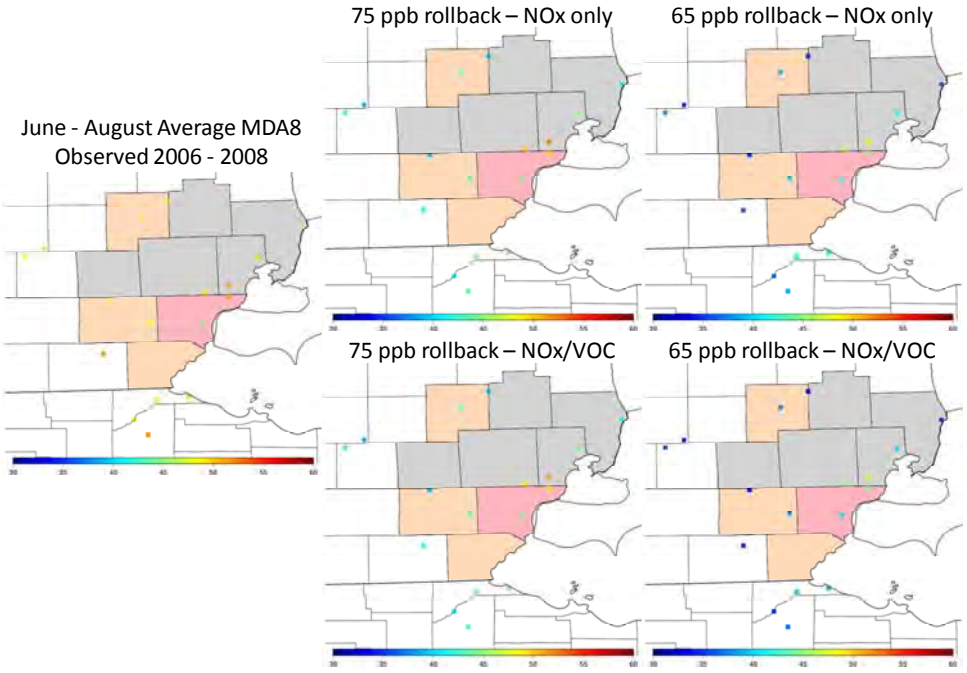

Figure 4D-138. April-October seasonal average of daily maximum 8-hour O_3 values at Detroit area monitor locations for observed 2006-2008 conditions (left panel), 75 ppb adjustment scenarios (middle panels), and 65 ppb adjustment scenarios (right panels). NO_x-only adjustments are shown in top panels, NO_x/VOC adjustments are shown in bottom panels.

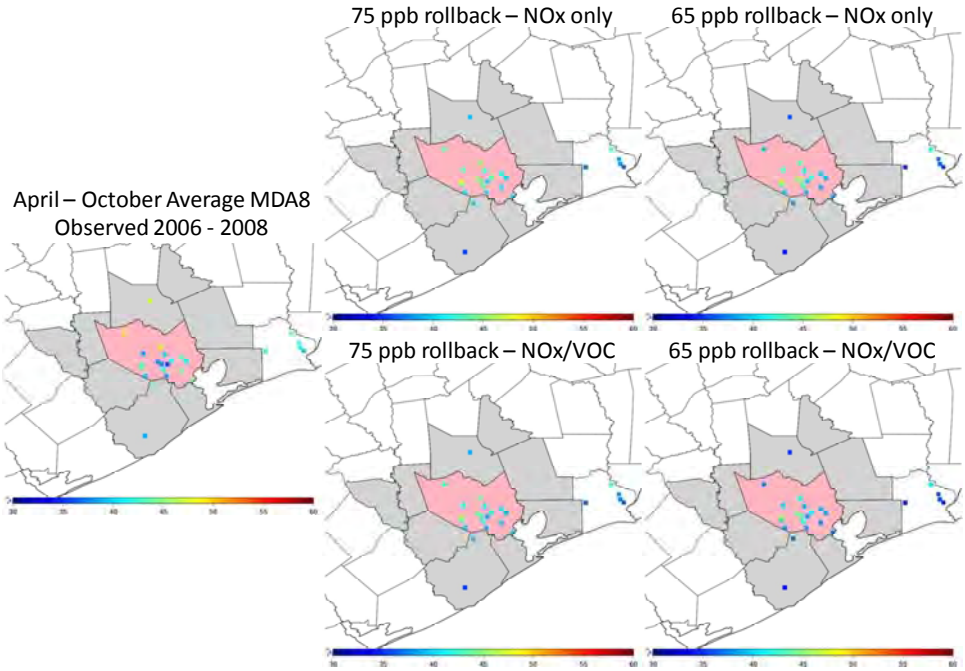

Figure 4D-139. April-October seasonal average of daily maximum 8-hour O_3 values at Houston area monitor locations for observed 2006-2008 conditions (left panel), 75 ppb adjustment scenarios (middle panels), and 65 ppb adjustment scenarios (right panels). NO_x-only adjustments are shown in top panels, NO_x/VOC adjustments are shown in bottom panels.

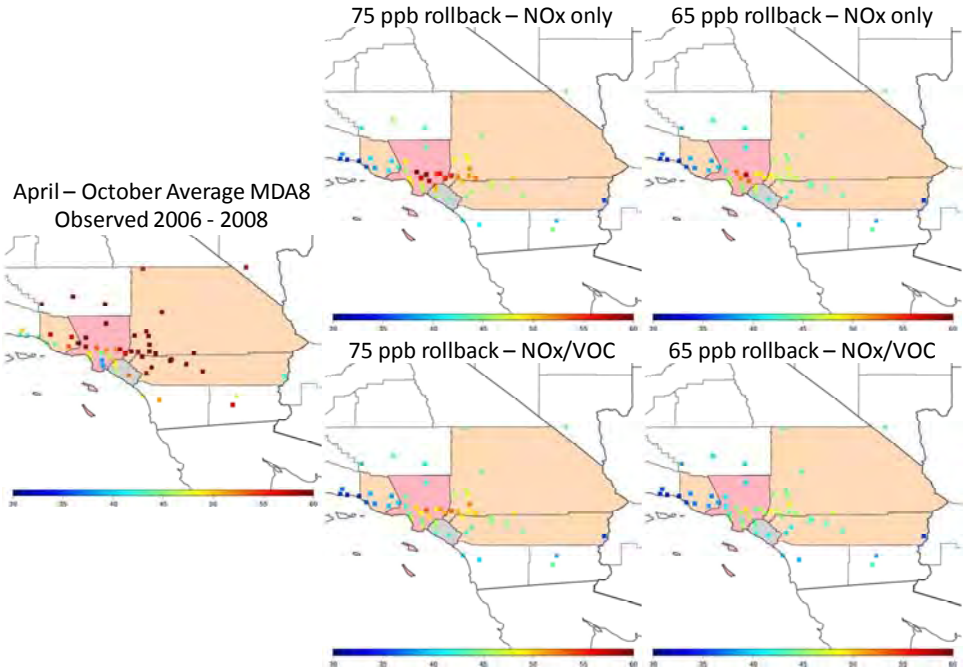

Figure 4D-140. April-October seasonal average of daily maximum 8-hour O_3 values at Los Angeles area monitor locations for observed 2006-2008 conditions (left panel), 75 ppb adjustment scenarios (middle panels), and 65 ppb adjustment scenarios (right panels). NO_x-only adjustments are shown in top panels, NO_x/VOC adjustments are shown in bottom panels.

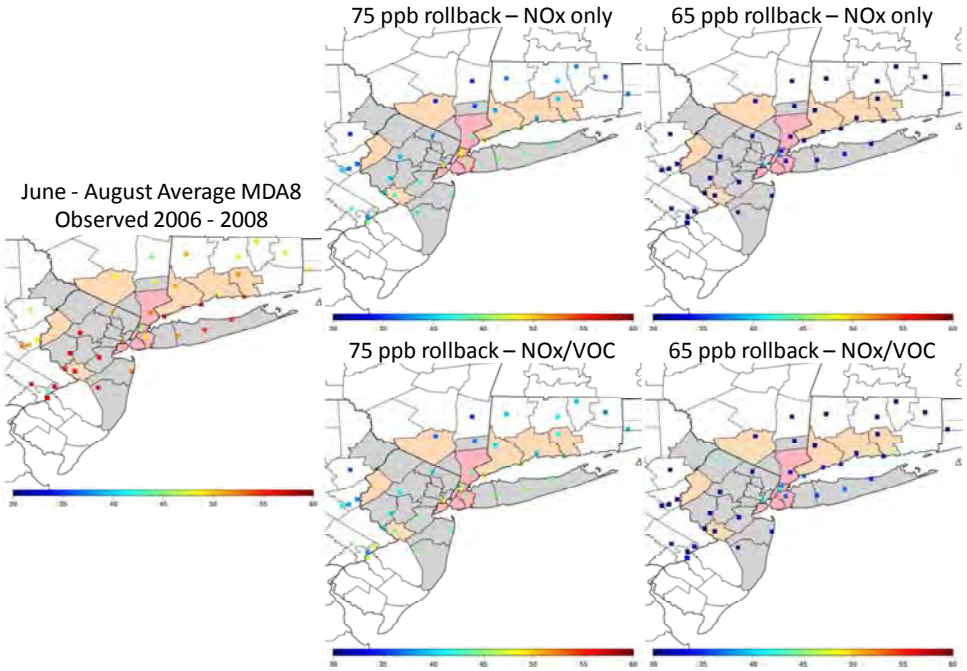

Figure 4D-141. April-October seasonal average of daily maximum 8-hour O_3 values at New York area monitor locations for observed 2006-2008 conditions (left panel), 75 ppb adjustment scenarios (middle panels), and 65 ppb adjustment scenarios (right panels). NO_x-only adjustments are shown in top panels, NO_x/VOC adjustments are shown in bottom panels.

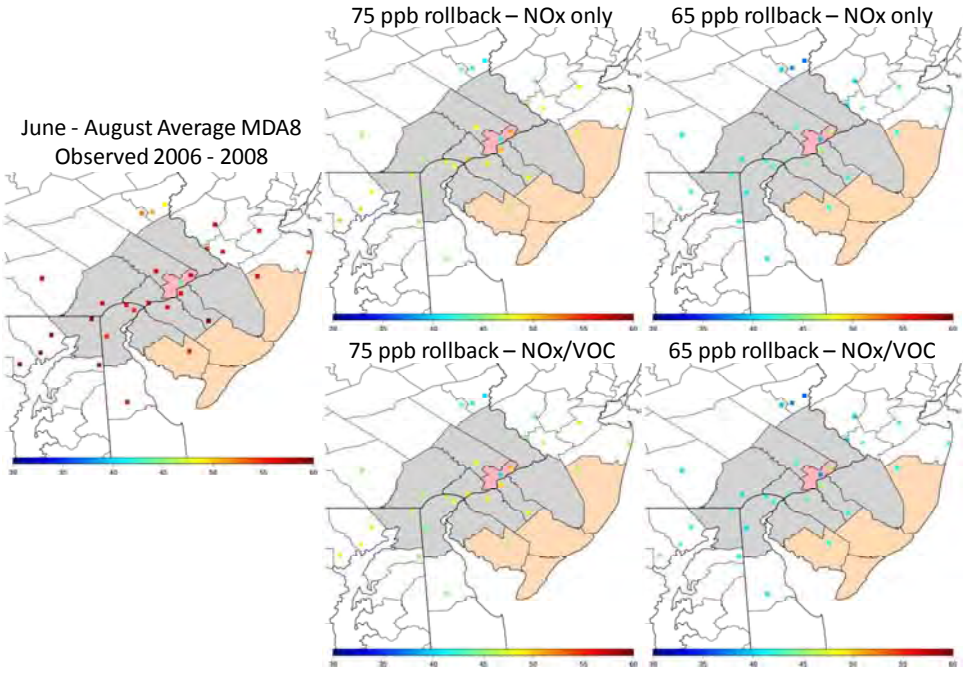

Figure 4D-142. April-October seasonal average of daily maximum 8-hour O_3 values at Philadelphia area monitor locations for observed 2006-2008 conditions (left panel), 75 ppb adjustment scenarios (middle panels), and 65 ppb adjustment scenarios (right panels). NO_x-only adjustments are shown in top panels, NO_x/VOC adjustments are shown in bottom panels.

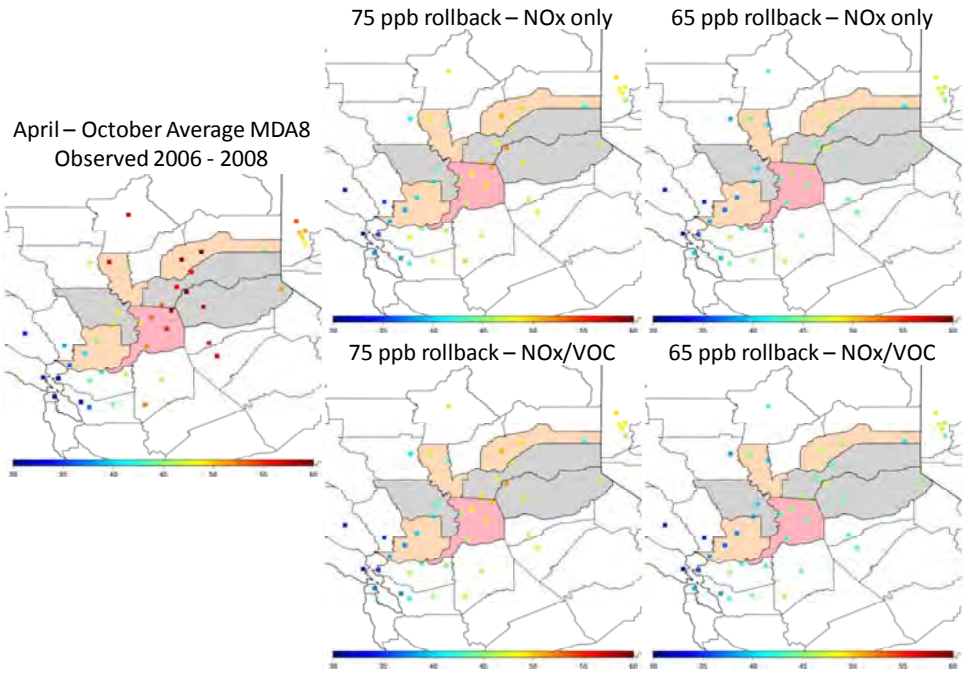

Figure 4D-143. April-October seasonal average of daily maximum 8-hour O_3 values at Sacramento area monitor locations for observed 2006-2008 conditions (left panel), 75 ppb adjustment scenarios (middle panels), and 65 ppb adjustment scenarios (right panels). NO_x-only adjustments are shown in top panels, NO_x/VOC adjustments are shown in bottom panels.

4D-5. REFERENCES

Appel, K.W., Gilliland, A.B., Sarwar, G., Gilliam, R.C. (2007). Evaluation of the Community Multiscale Air Quality (CMAQ) model version 4.5: Sensitivities impacting model performance Part I - Ozone. Atmospheric Environment, 41: 9603-9615.

Appel, K.W., Bhave, P.V., Gilliland, A.B., Sarwar, G., Roselle, S.J. (2008). Evaluation of the community Multiscale air quality (CMAQ) model version 4.5: Sensitivities impacting model performance; Part II - particulate matter. Atmospheric Environment, 42: 6057-6066.

Baker, K. and P. Dolwick. Meteorological Modeling Performance Evaluation for the Annual 2005 Eastern U.S. 12-km Domain Simulation, USEPA/OAQPS, February 2, 2009.

Baker, K. and P. Dolwick. Meteorological Modeling Performance Evaluation for the Annual 2005 Continental U.S. 36-km Domain Simulation, USEPA/OAQPS, February 2, 2009.

Byun, D.W., and Ching, J.K.S., eds., 1999. Science algorithms of EPA Models-3 Community Multiscale Air Quality (CMAQ modeling system, EPA/600/R-99/030, Office of Research and Development).

Byun, D., Schere, K.L. (2006). Review of the governing equations, computational algorithms, and other components of the models-3 Community Multiscale Air Quality (CMAQ) modeling system. Applied Mechanics Reviews, 59: 51-77.

Cohan, D.S., Hakami, A., Hu, Y., Russell, A.G. (2005). Nonlinear response of ozone to emissions: Source apportionment and sensitivity analysis. Environmental Science & Technology, 39: 6739-6748.

Cohan, D.S., Napelenok, S.L. (2011). Air quality response modeling for decision support. Atmosphere, 2: 407-425; doi:10.3390/atmos2030407.

Dunker, A.M. (1984). The decoupled direct method for calculating sensitivity coefficients in chemical kinetics. Journal of Chemical Physics, 81; 2385-2393.

Foley, K.M., Roselle, S.J., Appel, K.W., Bhave, P.V., Pleim, J.E., Otte, T.L., Mathur, R., Sarwar, G., Young, J.O., Gilliam, R.C., Nolte, C.G., Kelly, J.T., Gilliland, A.B., Bash, J.O. (2010). Incremental testing of the Community Multiscale Air Quality (CMAQ) modeling system version 4.7, Geoscientific Model Development, 3: 205-226.

Grell, G., J. Dudhia, and D. Stauffer (1994). A Description of the Fifth-Generation Penn State/NCAR Mesoscale Model (MM5), NCAR/TN-398+STR., 138 pp, National Center for Atmospheric Research, Boulder CO.

Hakami, A., Odman, M.T., Russell, A.G. (2003). High-order direct sensitivity analysis of multidimensional air quality models. Environmental Science & Technology, 37: 2442-2452.

Hakami, A., Odman, M.T., Russell, A.G. (2004). Nonlinearity in atmospheric response: A direct sensitivity analysis approach. Journal of Geophysical Research, 109: D15303; doi:10.1029/2003JD004502.

Houyoux, M.R., Vukovich, J.M., Coats, C.J., Wheeler, N.J.M., Kasibhatla, P.S. (2000). Emission inventory development and processing for the Seasonal Model for Regional Air Quality (SMRAQ) project. Journal of Geophysical Research-Atmospheres, 105: 9079-9090.

Koo, B., Dunker, A.M., Yarwood, G. (2007). Implementing the decoupled direct method for sensitivity analysis in a particulate matter air quality model. Environmental Science & Technology, 41: 2847-2854.

Napelenok, S.L., Cohan, D.S., Hu, Y., Russell, A.G. (2006). Decoupled direct 3D sensitivity analysis for particulate matter (DDM-3D/PM). Atmospheric Environment, 40: 6112-6121.

National Research Council of the National Academies (2008). Estimating Mortality Risk Reduction and Economic Benefits from Controlling Ozone Air Pollution. The National Academies Press, Washington, D.C

Pierce, T.; Geron, C.; Bender, L.; Dennis, R.; Tonnesen, G. Guenther, A. (1998). Influence of increased isoprene emissions on regional ozone modeling. J. Geophys. Res., 103: 25611–25629.

Seinfeld, J.H. and S.N. Pandis. (1998). Atmospheric chemistry and physics from air pollution to climate change. John Wiley & Sons, Inc, New York, 1998.

Simon, H., Baker, K.B., Akhtar, F., Napelenok, S.L., Possiel, N., Wells, B., Timin, B. (2013) A direct sensitivity approach to predict hourly ozone resulting from compliance with the national ambient air quality standard, Environmental Science and Technology, 47, 2304-2313.

U.S. EPA, 2007. Guidance on the Use of Models and Other Analyses for Demonstrating Attainment of Air Quality Goals for Ozone, PM2.5, and Regional Haze, Research Triangle Park. EPA-454/B-07-002: http://www.epa.gov/ttn/scram/guidance/guide/final-03-pm-rh-guidance.pdf.

U.S. EPA, Emissions Modeling for the Final Mercury and Air Toxics Standards Technical Support Document, 2011a, EPA-45A/R-11-011: http://epa.gov/ttn/chief/emch/toxics/MATS_Final_Emissions_Modeling_TSD_9Dec2011.pdf.

U.S. EPA, Air Quality Modeling Technical Support Document: Final EGU NESHAP, 2011b, EPA-45A/R-11-009.

U.S. EPA, Health Risk and Exposure Assessment for Ozone: First External Review Draft, 2012, EPA 452/P-12-001.

U.S. EPA Integrated Science Assessment for Ozone and Related Photochemical Oxidants, 2013, EPA 600/R-10/076F

Wilks, D.S. Statistical Methods in the Atmospheric Sciences, Second Edition, Elsevier, Burlington, MA

Yang, Y.-J., Wilkinson, J.G., Russell, A.G. (1997). Fast, direct sensitivity analysis of multidimensional photochemical models. Environmental Science & Technology, 31: 2859-2868.

Zhang, W., Capps, S.L., Hu, Y., Nenes, A., Napelenok, S.L., Russell, A.G. (2012). Development of the high-order decoupled direct method in three dimensions for particulate matter: Enabling advanced sensitivity analysis in air quality models. Geoscientific Model Development, 5: 355-368.

This page left intentionally blank

APPENDIX 4E

Evaluation of Seattle Air Quality

List of Figures

Figure 4E-1. All-site maximum hourly O_3 (ppb) in Seattle by year and month. This figure combines all hourly O_3 data from 11 sites in the Seattle area and plots the highest-site value at each hour for Mar-Sep. Boxes represent the median and quartiles, whiskers extend up to 1.5x the inter-quartile range from the boxes, and circles represent outliers. 4E-1

Figure 4E-2. Map of Seattle area monitoring sites used to create the ozone surfaces for the exposure assessment. Dark brown site is the most urban location (in a residential area of downtown Seattle), orange sites are suburban, sites in the far northern and southern portions of the area are plotted in blue and green respectively, dark green site is a high elevation site. 4E-2

Figure 4E-3. Map with aerial photography overlay showing where monitors are located with respect to highly urbanized (gray) areas versus suburban and rural areas (green). Downtown Seattle site is circled in orange. 4E-3

Figure 4E-4. Example of a day with large spatial ozone gradients in the Seattle area. Maximum 8-hr daily maximum ozone value for July 11, 2007. ..... 4E-4

Figure 4E-5. Example of a day with large spatial ozone gradients in the Seattle area. Maximum 8-hr daily maximum ozone value for July 26, 2007. ..... 4E-5

Figure 4E-6. Example of a day with large spatial ozone gradients in the Seattle area. Maximum 8-hr daily maximum ozone value for August 29, 2007..... 4E-5

Figure 4E-7. Example of a day with large spatial ozone gradients in the Seattle area. Maximum 8-hr daily maximum ozone value for September 11, 2007. ..... 4E-6

Figure 4E-8. Cumulative distribution of population living within set distances of an ozone monitor in each urban study area. 4E-7

Investigation of the monitoring network and ambient data trends in Seattle raised serious concerns about the appropriateness of using 2006 data for the purpose of an exposure analysis. Seattle experienced some high ozone events in 2006 that were substantially higher than any measured ozone that occurred in the modeled time period (Jan, April-October 2007) (Figure 4E-1). The model generally predicted ozone disbenefits to NO_x reductions in Seattle on the low ozone days that were predominant in 2007. Because these conditions are not likely to occur on high ozone days, we had serious concerns about extrapolating 2007 sensitivities to 2006 high ozone days.

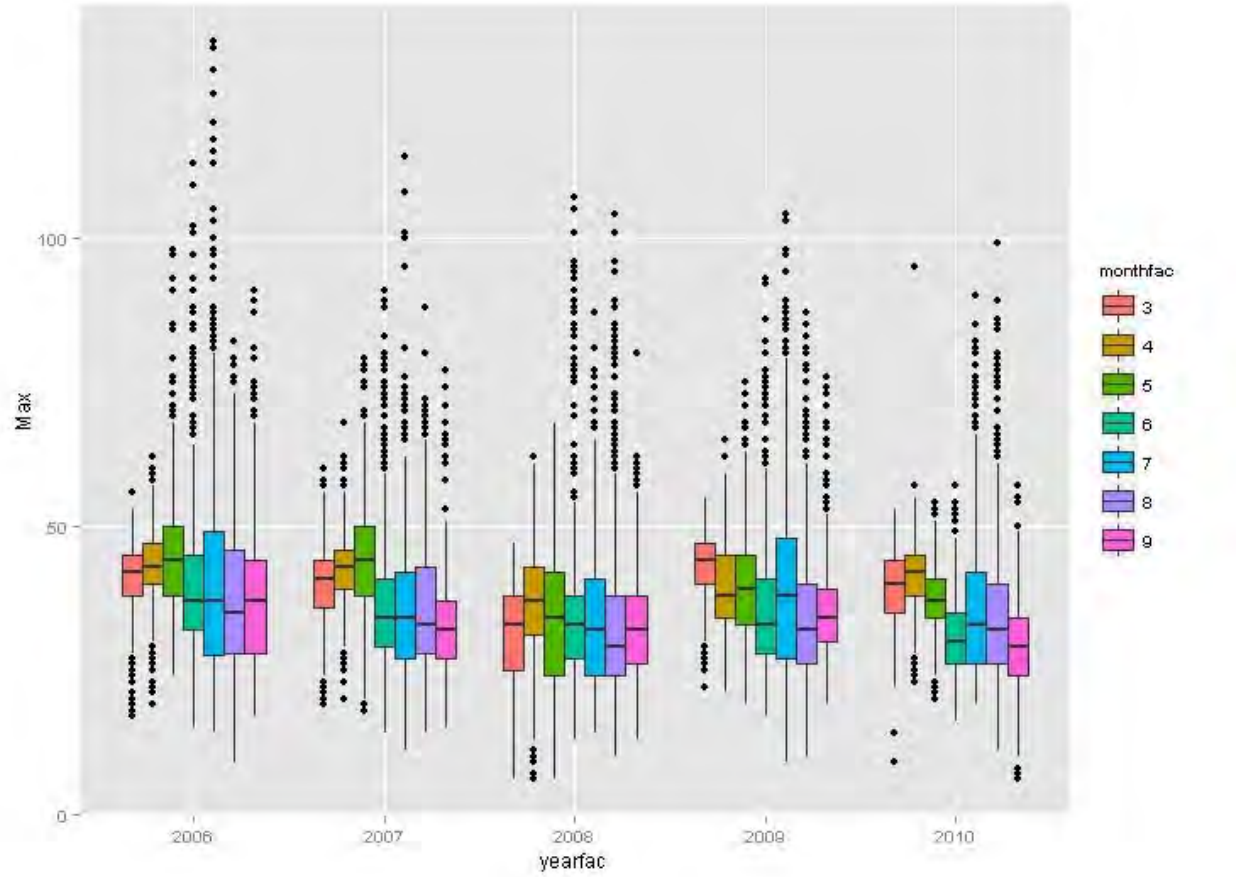

Figure 4E-1. All-site maximum hourly O_3 (ppb) in Seattle by year and month. This figure combines all hourly O_3 data from 11 sites in the Seattle area and plots the highest-site value at each hour for Mar-Sep. Boxes represent the median and quartiles, whiskers extend up to 1.5x the inter-quartile range from the boxes, and circles represent outliers.

Further concerns come from the lack of measured urban ozone concentrations in all years, but especially in 2006. The Seattle monitoring network is mainly focused on downwind and background areas. There is a single urban monitor in a residential area of downtown Seattle (Figure 4E-2 and Figure 4E-3). The urban monitor was not in operation from January-September of 2006, so no urban measurements were made during most of the 2006 ozone season. Performing a census-tract level exposure analysis for the Seattle and Tacoma urban areas would not be appropriate based solely on ozone values in outlying rural and suburban areas.

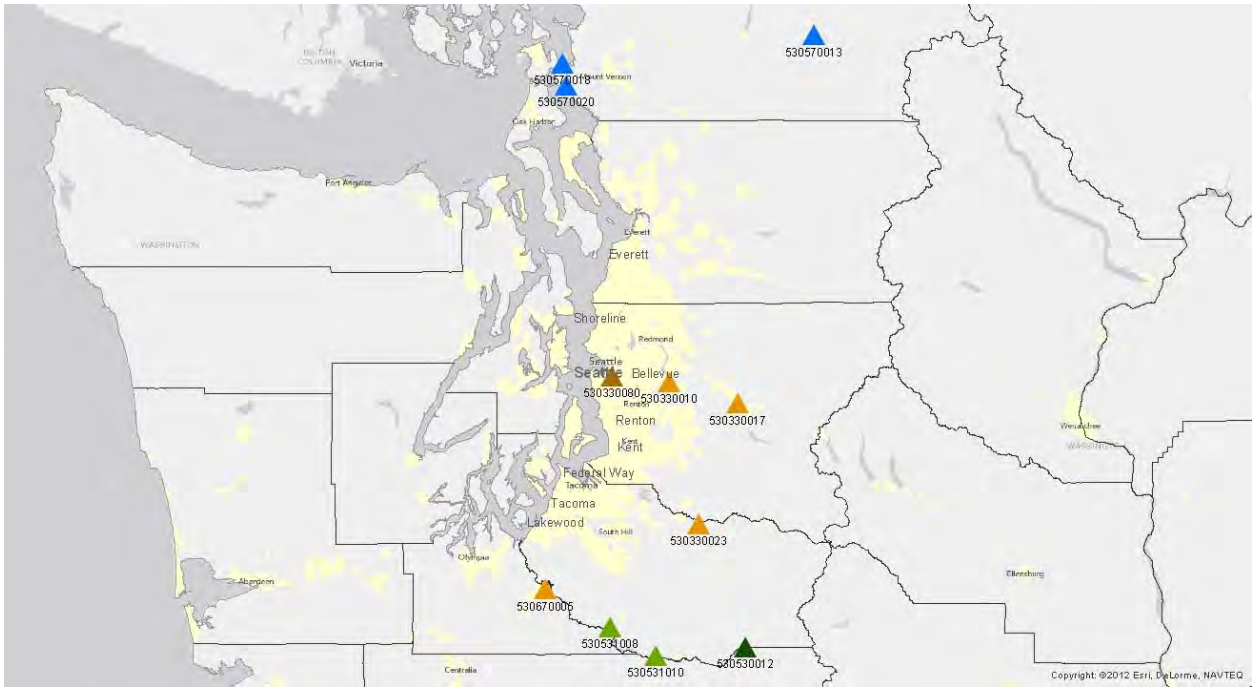

Figure 4E-2. Map of Seattle area monitoring sites used to create the ozone surfaces for the exposure assessment. Dark brown site is the most urban location (in a residential area of downtown Seattle), orange sites are suburban, sites in the far northern and southern portions of the area are plotted in blue and green respectively, dark green site is a high elevation site.

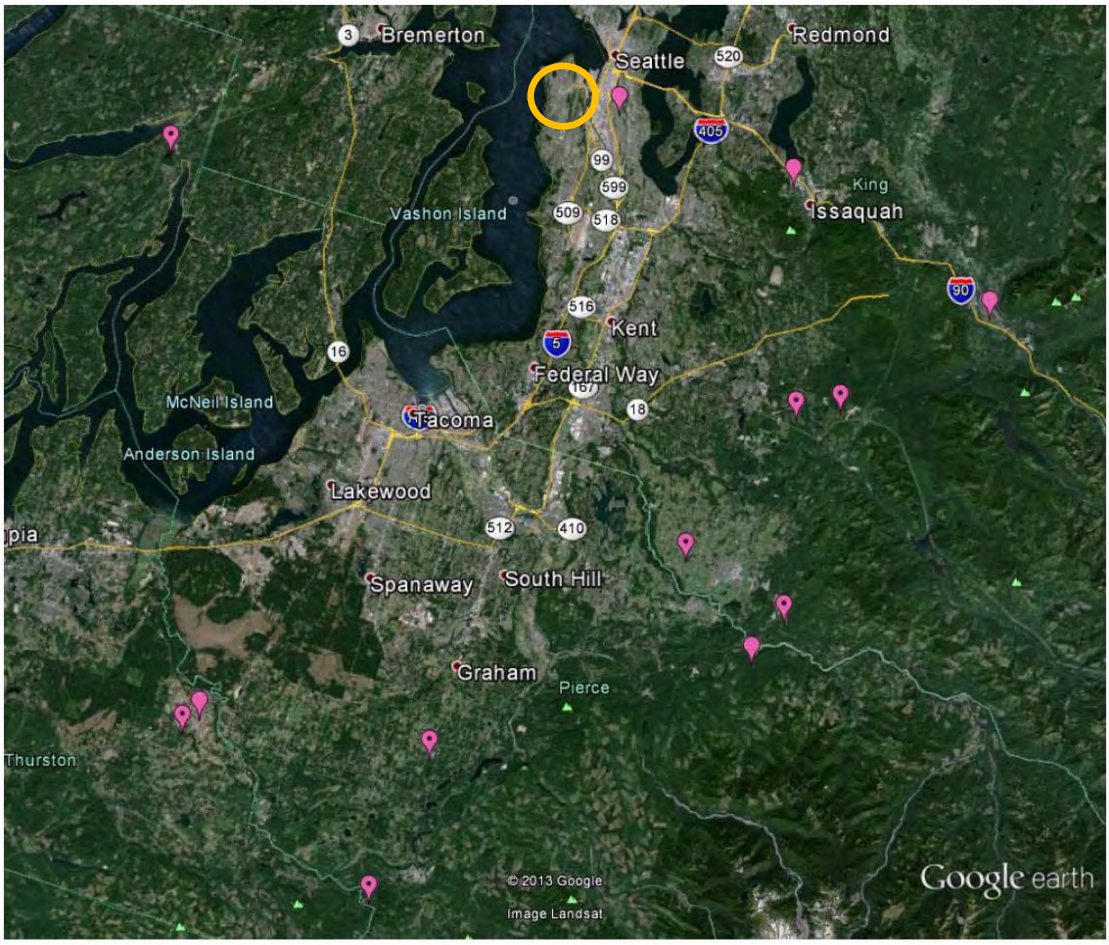

Figure 4E-3. Map with aerial photography overlay showing where monitors are located with respect to highly urbanized (gray) areas versus suburban and rural areas (green). Downtown Seattle site is circled in orange.

Additional concerns were raised about the potential insufficient density of the Seattle ozone monitoring network and subsequently its adequacy for use in a census-tract level exposure analysis beyond the concerns above for 2006. The Seattle area ozone monitoring network was designed primarily to address NAAQS compliance. For this purpose it is appropriate to focus on downwind suburban areas where ozone concentrations are expected to be highest. Modeling suggests that there are often large spatial gradients of ozone within the Seattle/Tacoma area. Figure 4E-4 through Figure 4E-7 show 8-hr daily maximum ozone concentration fields for the Seattle area from the 2007 CMAQ modeling described in Appendix 4A. Spatial fields for exposure modeling are created using interpolation of monitor data and do not capture any modeled spatial gradients. Therefore it is expected that at many times, interpolation of the single Seattle urban monitor with downwind suburban monitors will not adequately represent the ozone values in highly populated urban areas such a Tacoma. In addition, unlike most other urban areas, the Seattle monitoring network for the 2006-2010 time period did not include any upwind monitors (on the West side of Puget Sound).

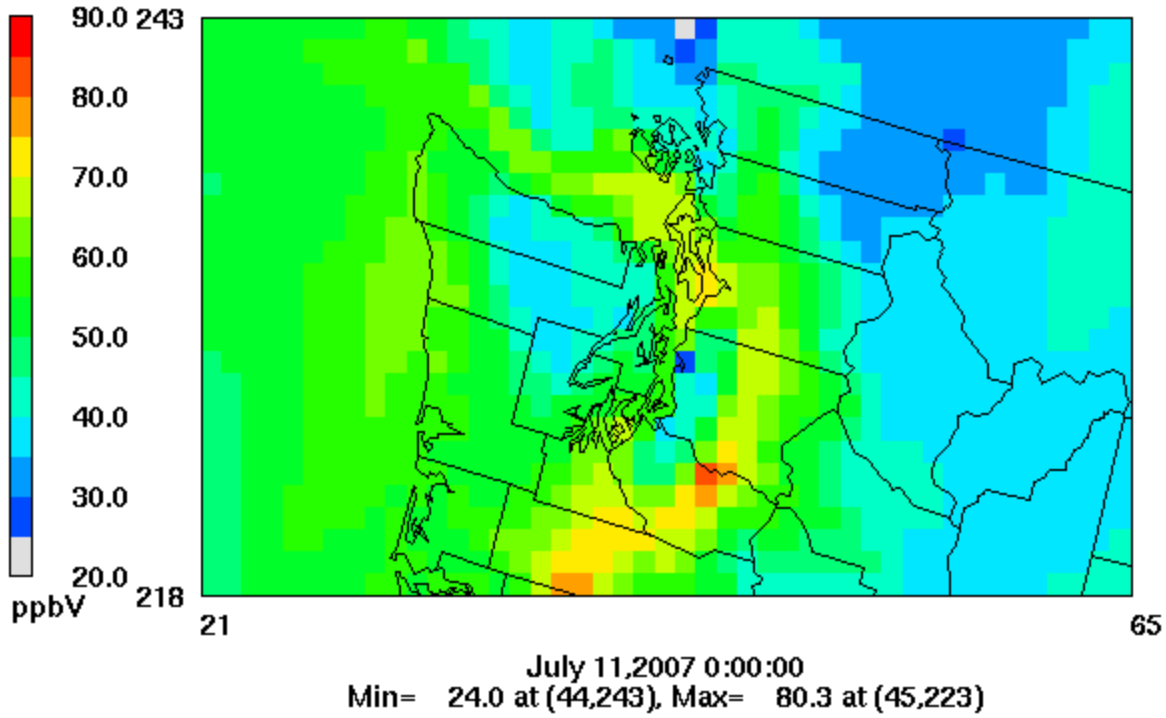

Figure 4E-4. Example of a day with large spatial ozone gradients in the Seattle area. Maximum 8-hr daily maximum ozone value for July 11, 2007.

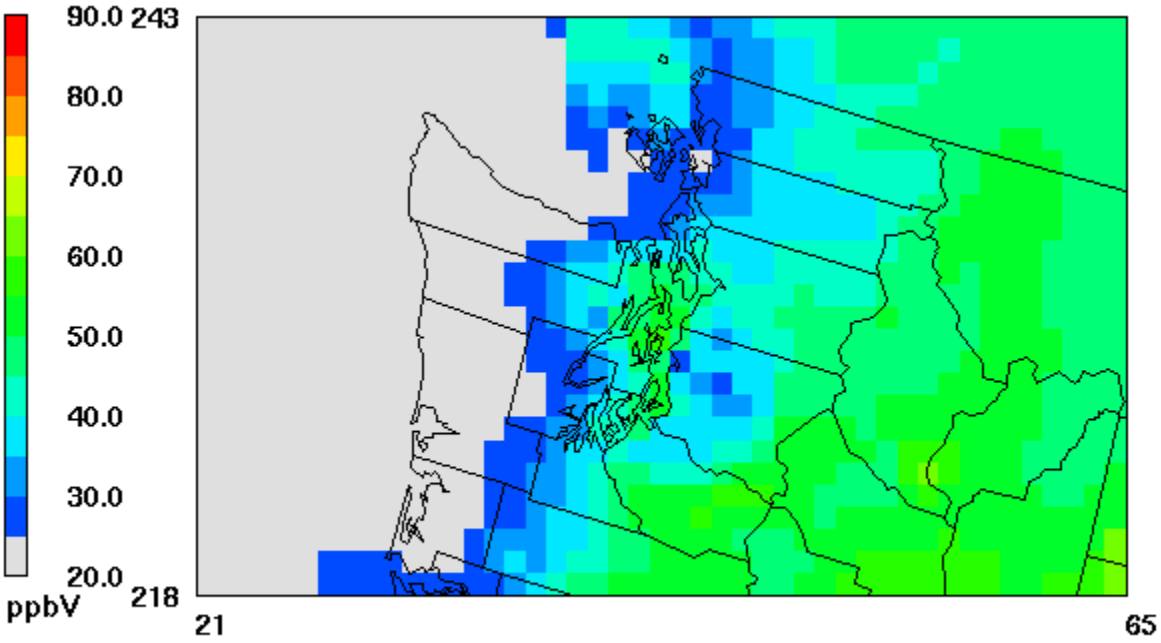

Figure 4E-5. Example of a day with large spatial ozone gradients in the Seattle area. Maximum 8-hr daily maximum ozone value for July 26, 2007.

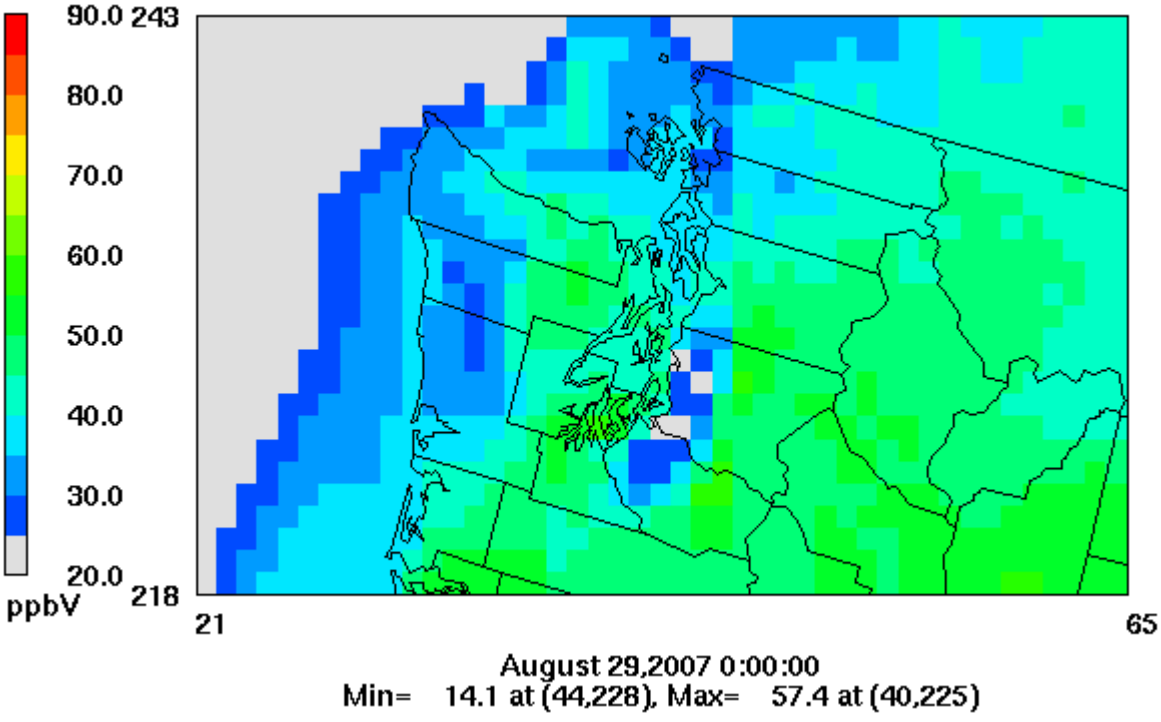

Figure 4E-6. Example of a day with large spatial ozone gradients in the Seattle area. Maximum 8-hr daily maximum ozone value for August 29, 2007.

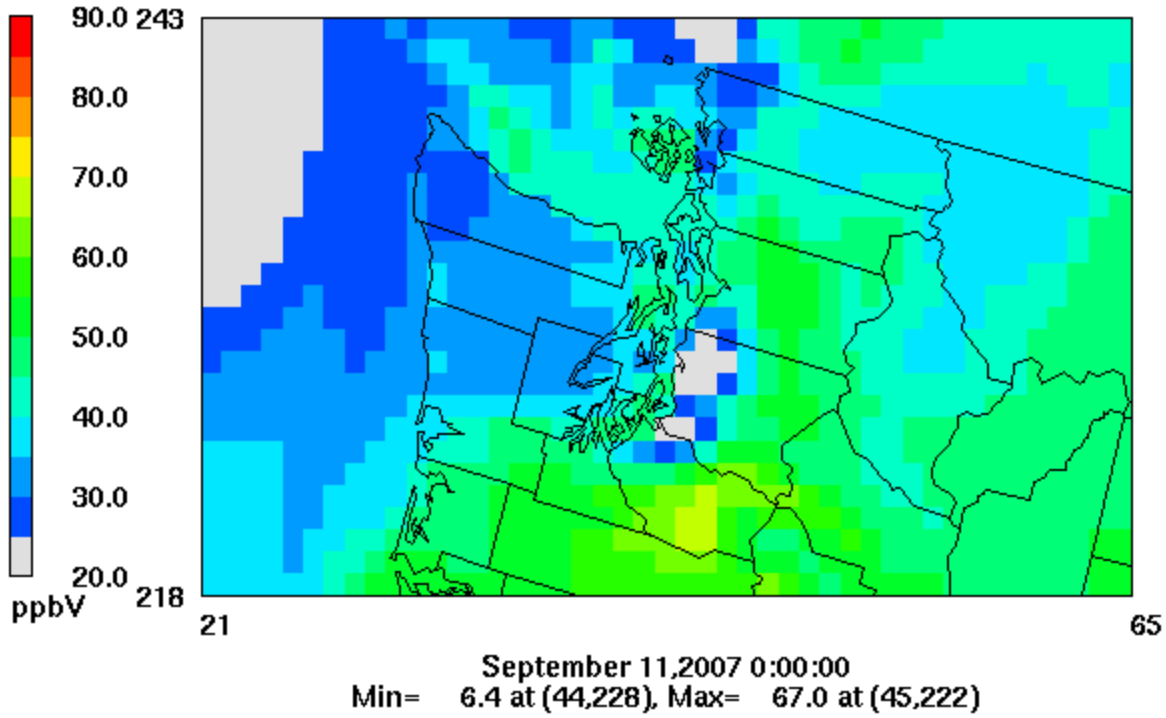

Figure 4E-7. Example of a day with large spatial ozone gradients in the Seattle area. Maximum 8-hr daily maximum ozone value for September 11, 2007.

To further analyze the appropriateness of the Seattle monitoring network for the purpose of performing an exposure assessment, the representativeness of the ozone monitoring network to total population in Seattle was compared to all other urban study areas (Figure 4E-8). This analysis showed that the Seattle monitoring network was much less representative of ozone concentrations where people live than the ozone networks in the other 15 urban study areas. For instance, while more than 75 % of the area-wide population lived within 20 km of an ozone monitor in each of the other 15 urban areas, in Seattle only about 55% of the population lives within 20 km of an ozone monitor. Furthermore, in 13 urban study areas, more than 50% of the population lives within 10 km of an ozone monitor, in 2 urban study areas more than 50% of the population lives within 13 km of an ozone monitor, yet in Seattle, more than 50% of the population lives within 18 km of an ozone monitor. Based on both the sharp spatial gradients predicted by the model and the much sparser monitor coverage in highly populated areas in Seattle compared to other urban study areas, it was determined that the monitoring network in Seattle likely does not capture ozone values representing levels to which large portions of the population are exposed and therefore it would not be appropriate to rely upon the currently available Seattle ozone monitors for the purpose of the exposure analysis which requires accurate fine scale estimates of ozone concentrations where people are exposed.

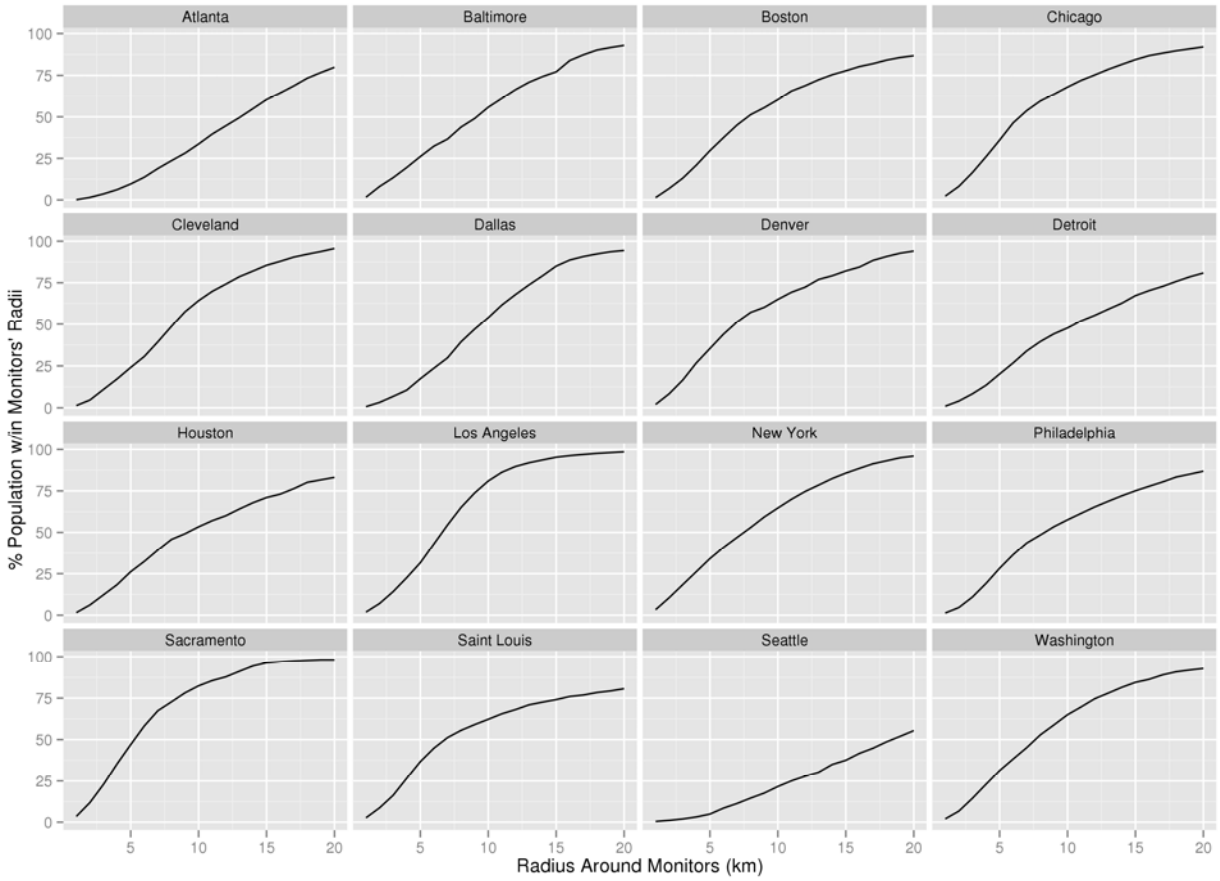

Figure 4E-8. Cumulative distribution of population living within set distances of an ozone monitor in each urban study area.

This page left intentionally blank

United States
Environmental Protection
Agency

Office of Air Quality Planning and Standards
Health and Environmental Impacts Division
Research Triangle Park, NC

Publication No. EPA-452/R-14-004b
August 2014